INFORMATION TO USERS

This manuscript has been reproduced from the microfilm master. UMI films the text directly from the original or copy submitted. Thus, some thesis and dissertation copies are in typewriter face, while others may be from any type of computer printer.

The quality of this reproduction is dependent upon the quality of the copy submitted. Broken or indistinct print, colored or poor quality illustrations and photographs, print bleedthrough, substandard margins, and improper alignment can adversely affect reproduction.

In the unlikely event that the author did not send UMI a complete manuscript and there are missing pages, these will be noted. Also, if unauthorized copyright material had to be removed, a note will indicate the deletion.

Oversize materials (e.g., maps, drawings, charts) are reproduced by sectioning the original, beginning at the upper left-hand corner and continuing from left to right in equal sections with small overlaps.

ProQuest Information and Learning
300 North Zeeb Road, Ann Arbor, MI 48106-1346 USA
800-521-0600

University of Alberta

Mesozoic to early Tertiary tectonic evolution of the Shuswap metamorphic complex in the Vernon area, southeastern Canadian Cordillera

by

Paul Manfred Glombick 

A thesis submitted to the Faculty of Graduate Studies and Research in partial fulfillment of the requirements for the degree of Doctor of Philosophy

Department of Earth and Atmospheric Sciences

Edmonton, Alberta
Fall 2005

Frontispiece

We have not known a single great scientist who could not discourse freely and interestingly with a child. Can it be that the haters of clarity have nothing to say, have observed nothing, have no clear picture of even their own fields? A dull man seems to be a dull man no matter what his field, and of course it is the right of the dull scientist to protect himself with feathers and robes, emblems and degrees, as do other dull men who are potentates and grand imperial rulers of lodges of dull men.

John Steinbeck, *The Log from the Sea of Cortez*

However, if I had waited long enough I probably never would have written anything at all since there is a tendency when you really begin to learn something about a thing not to want to write about it but rather to keep on learning about it always and at no time, unless you are very egotistical, which, of course, accounts for many books, will you be able to say: now I know all about this and will write about it.

Ernest Hemingway, *Death in the Afternoon*

The late Ken Daughtry pondering the wonder of it all.

Dedicated to the memory of Kenneth L. Daughtry

Mentor, colleague, teacher, friend

Abstract

Low-angle shear zones exposed near the western margin of the Shuswap metamorphic complex, part of the Okanagan Valley fault system, have been previously interpreted as crustal-scale shear zones. These shear zones are well-exposed in the Vernon area, where a semi-intact carapace of greenschist-facies superstructure extends across the width of the Shuswap metamorphic complex.

Detachment faults are absent in the Vernon area and the suprastructure has not been thinned by an array of extensional faults. Superstructure and infrastructure are juxtaposed by 1-2 km thick Paleocene to Early Eocene low-angle shear zones characterized by a well-developed stretching lineation and top to the west shear-sense indicators. To the east, in the Vidler Ridge-Pinnacles area, the transition from infrastructure to superstructure is characterized by a gradational, but attenuated metamorphic sequence; no shear zones are apparent.

Mineral assemblages and *P-T* estimates indicate peak metamorphic conditions of 8-10 kbar and 800-850°C for the infrastructure. Greenschist-facies mineral assemblages and conodont colour alteration index values indicate maximum temperatures of 440°C for the superstructure. Geochronological data (U-Pb zircon, titanite; chemical monazite dates) from infrastructure rocks exposed southeast of Vernon indicate a complex thermotectonic evolution. Metamorphic zircon growth occurred at 155-150, 100-90, and 70-50 Ma. Magmatism included emplacement of diorite at ~232 Ma, tonalite at 155-150 Ma, granodiorite at 102 Ma, and monzonite at 50 Ma. In contrast, greenschist-facies superstructure exposed west of Vernon records evidence of ductile deformation and emplacement of the Okanagan composite batholith between 170 and 155 Ma.

The minimal gaps in the superstructure, the lack of normal faults, and the lack of a regional detachment fault indicate that the infrastructure was not exhumed by removal of the suprastructure during motion on a low-angle detachment. On the basis of new and previously published mapping, geochronological, metamorphic, and geophysical data, and comparisons with thermal-mechanical modeling of large, hot orogens, exhumation of the infrastructure and the

formation of gneiss domes is hypothesized to have resulted from Late Cretaceous to Early Eocene channel flow of partially molten rocks. Exhumation is proposed to have occurred as the zone of channel flow encountered a crustal-scale ramp in the underlying Paleoproterozoic basement.

Acknowledgements

Foremost, I would like to thank my wife Jessica for your love and support. To my family, who supported me through my entire education, particularly during my medical treatment. To Philippe, for giving me the chance to jump in over my head, and supporting me to the end. To Bob T., for your patience, boundless enthusiasm, hospitality, and encouragement. Mat, no words are needed between us. Frenchie, your friendship, companionship, and creativity have always been a source of (sometimes competitive) inspiration. Ian, Jason, and Shaw, for your companionship during these past years. Kelly Franz: geologist, climber, fine human being.

I would also like to acknowledge the following people for a variety of things, including hospitality, assistance in the field, technical assistance, discussion, and friendship: Chris Böhm, Les and Joy Braden, Jenny Burgess, Tom Chacko, Katie Daughtry, Parm Dhesi, Richard Friedman, Stacey Hagan, Larry Heaman, Mark Labbe, Yvon Lemieux, Liz L'Heureux, Sergei Matveev, Roger Macleod, Don Resultay, Spike, and Tyler Ruks.

This work was supported through National Sciences and Engineering Research Council of Canada (NSERC) post-graduate scholarships PGS-A (1998-2000) and PGS-B (2000-2002), a Natural Resources Canada NSERC supplement (2001), a Walter H. Johns Graduate Fellowship (1998-2002), and a Canadian Association of Petroleum Producers Graduate Scholarship in Geology (1999-2000) awarded to P. Glombick, by an NSERC Discovery Grant awarded to P. Erdmer (University of Alberta), by funding through the southern component of the Geological Survey of Canada (GSC) Ancient Pacific Margin NATMAP project, and through contributions by Manfred and Linda Glombick.

Table of Contents

CHAPTER 1

Introduction

CHAPTER 2

A reappraisal of the tectonic significance of Late Paleocene to Early Eocene extensional shear zones in the Shuswap metamorphic complex near Vernon, southeast Canadian Cordillera

CHAPTER 3

Age of the Aberdeen gneiss complex and the thermal evolution of the Vernon antiform, southeast Canadian Cordillera

CHAPTER 4

Thermal and metamorphic evolution of the central Shuswap metamorphic complex in the Vernon area, southeast Canadian Cordillera

CHAPTER 5

Deflation of the middle crust: evidence from the Vernon area of the Shuswap metamorphic complex, southeast Canadian Cordillera

CHAPTER 6

Conclusions

APPENDIX A

Description of map units

APPENDIX B

Station location data

APPENDIX C

Fabric data

APPENDIX D

Representative electron microprobe data used in thermobarometric calculations

APPENDIX E

Monazite electron microprobe data from metapelitic rocks of the Vernon area

APPENDIX F

Monazite electron microprobe (EMP) chemical dating histograms, backscattered electron (BSE) images, and isochron plots from metapelitic rocks of the Vernon area

APPENDIX G

Selected backscattered electron (BSE) and cathodoluminescence (CL) images of zircon grains from geochronology samples

APPENDIX H

Thesis collection

List of Tables

CHAPTER 3

CHAPTER 4

List of Figures

CHAPTER 1

CHAPTER 2

CHAPTER 3

List of Figures (continued)

CHAPTER 4

List of Figures (continued)

CHAPTER 5

CHAPTER 6

APPENDIX A

APPENDIX C

List of Maps

(located within the cover pocket on the inside of the back cover)

List of Abbreviations

AGC	Aberdeen gneiss complex
BF	Beaven fault
CF	Cherry/Cherryville fault
CRF	Columbia River fault
FC	Frenchman Cap
GF	Granby fault
GFC	Grand Forks complex
GWF	Greenwood fault
KRF	Kettle River fault
MC	Monashee complex
MD	Monashee décollement
MG	Malton gneiss complex
OVF	Okanagan Valley fault
PTF	Purcell Trench fault
SLF	Slocan Lake fault
SMC	Shuswap metamorphic complex
TO	Thor-Odin dome
VC	Valhalla complex
VLZ	Valkyr shear zone

Ab	albite
Alm	almandine
Als	aluminosilicate
An	anorthite
Bt	biotite
Chl	chlorite
Cld	chloritoid
Crd	cordierite
Grt	garnet
Grs	grossular
Hbl	hornblende
Kfs	potassium-feldspar
Ky	kyanite
Ms	muscovite
Opx	orthopyroxene
Phl	phlogopite
Pl	plagioclase
Prp	pyrope
Qtz	quartz
Sil	sillimanite
Sps	spessartine
St	staurolite
L	liquid (melt)
V	volatile (fluid)

CHAPTER 1

Introduction

Background

The Shuswap metamorphic complex (SMC) remains an enigmatic feature of Canadian Cordilleran geology. The complexity of the SMC defies attempts at classification or definition; the term has been used in a variable manner to refer to a large region (greater than 100 km wide and 600 km long) in southern British Columbia and northern Washington underlain by high-grade metamorphic rocks (see reviews by Okulitch 1984 and Parrish et al. 1988). The SMC is located within the Omineca Belt, one of the five major orogen-parallel morpho-geological belts into which the Canadian Cordilleran has been sub-divided (Fig. 1-1). The crystalline Omineca Belt, which is composed dominantly of poly-deformed, amphibolite-facies metamorphic rocks and abundant intrusive rocks, forms the metamorphic hinterland to the Rocky Mountain Fold and Thrust (Foreland) Belt. Unlike the thin-skinned style of deformation that characterizes the Foreland Belt, rocks exposed within the Omineca Belt were deformed by penetrative ductile flow at mid-crustal levels from Middle Jurassic to Eocene time (e.g., Williams and Jiang 2005).

The SMC is the largest and northernmost of a series of normal fault-bounded exposures of high-grade metamorphic rocks, known as Cordilleran metamorphic core complexes (Crittenden et al. 1980), which occur within western North America (Fig. 1-2). Cordilleran metamorphic core complexes formed during the early to middle Tertiary within a belt of crust that was previously thickened during the Mesozoic Sevier orogeny (e.g., Coney and Harms 1984), but the underlying geodynamic causes of core complex formation remain debated (e.g., Sonder et al. 1987; Liu 1994; Bardoux and Mareschal 1994).

The SMC is cut, and in many places bounded by, a series of northerly-striking normal faults of early Tertiary age (Fig. 1-3). Early Tertiary extension faults range from gently dipping ductile shear zones, such as the Valkyr and Okanagan Valley shear zones, to steeply dipping cataclastic fault zones, such as the Granby, Kettle, and Beavan faults (Fig. 1-3). In many places, extension faults juxtapose rocks of markedly different metamorphic grades and thermal histories. High-grade metamorphic rocks exposed within the footwall of extension faults are characterized by Paleocene to Eocene K-Ar and $^{40}Ar/^{39}Ar$ dates (hornblende and micas), whereas lower-grade, predominantly greenschist-facies rocks, within the hanging wall record Middle Jurassic to Late Cretaceous dates (e.g., Mathews 1981; Parrish et al. 1988).

Prior to the 1980's, most workers within the SMC regarded the extension faults as relatively minor structures with only a few kilometres of displacement (Jones 1959; Read and

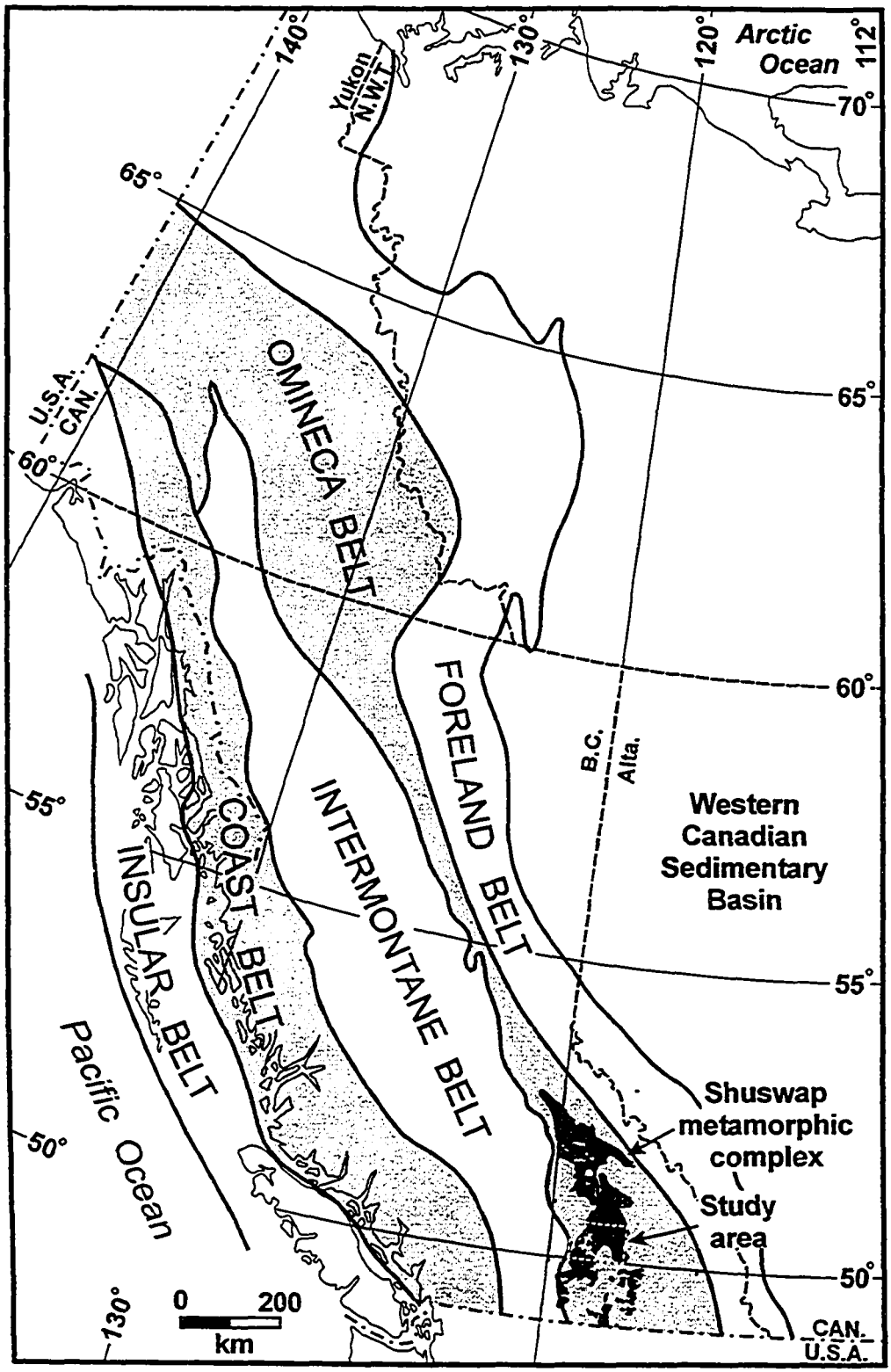

Fig. 1-1. Morpho-geological belts of the Canadian Cordillera and location of the Shuswap metamorphic complex (shaded black). Modified from Wheeler et al. (1991).

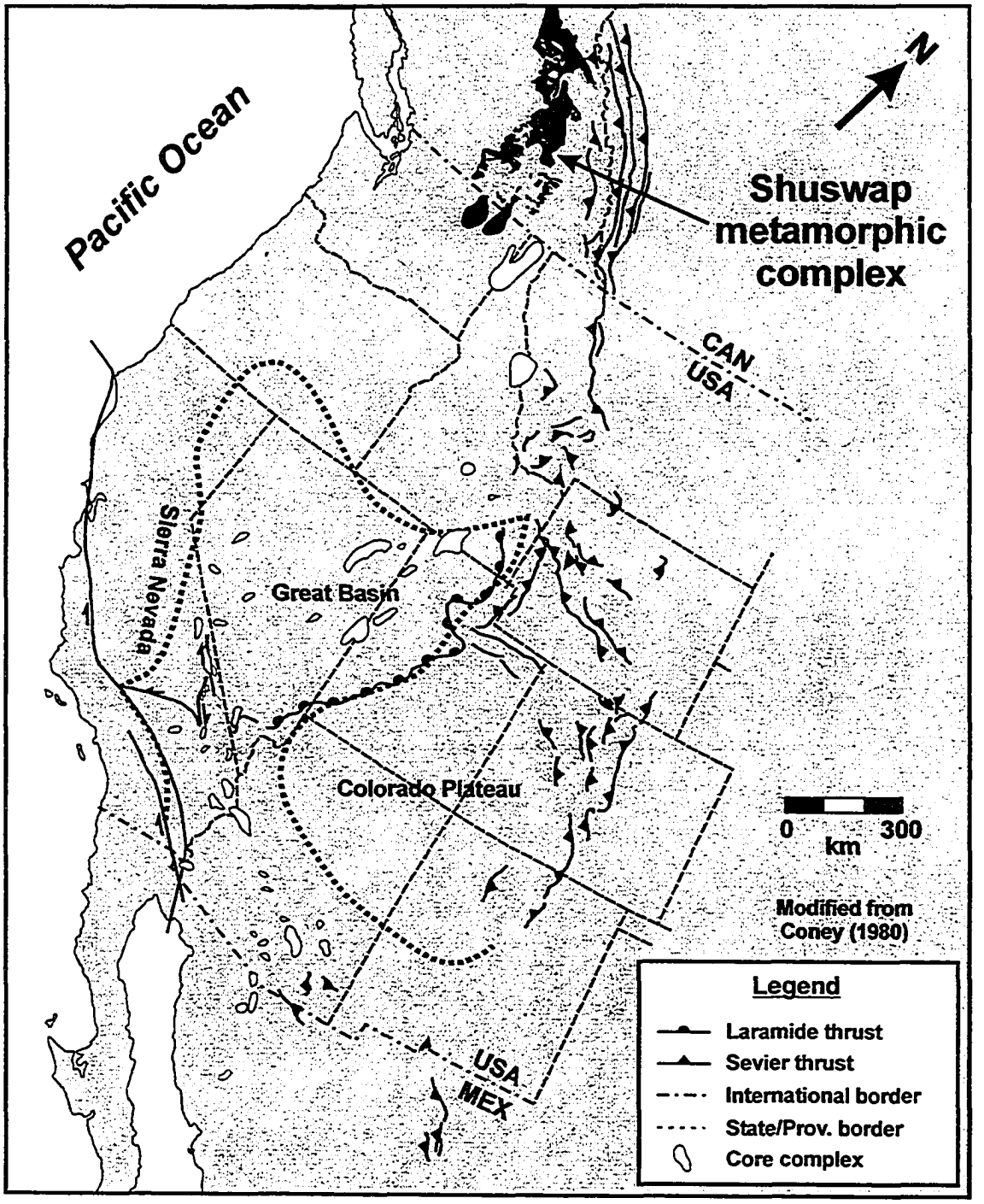

Fig. 1-2. Distribution of Cordilleran metamorphic core complexes within western North America (modified from Coney [1980]). The Shuswap metamorphic complex is shaded black.

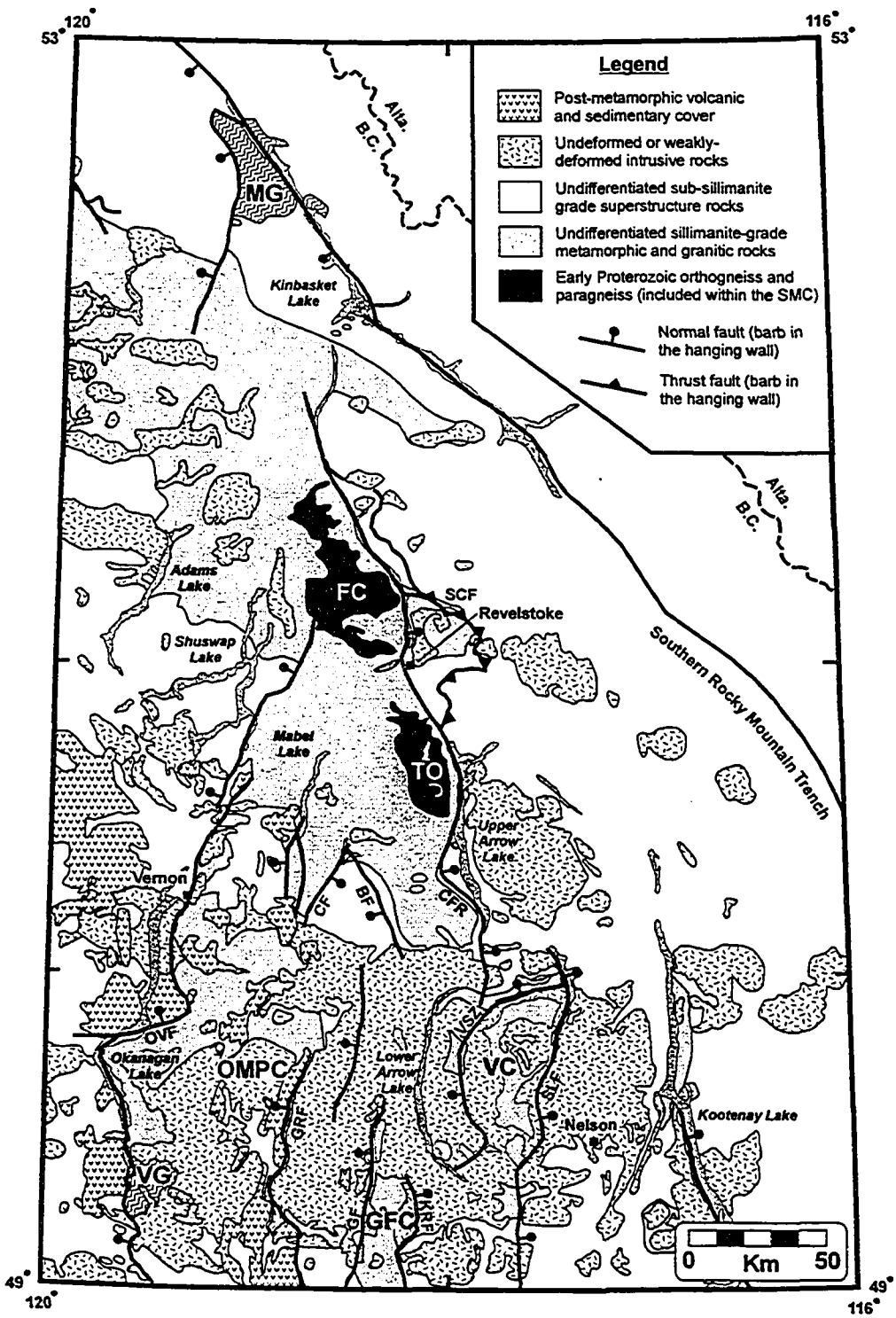

Fig. 1-3. Location and boundaries of the Shuswap metamorphic complex. *Faults*: BF - Beaven; CF - Cherry; CRF - Columbia River; GF - Granby; GRF - Greenwood; HF - Hope; KRF - Kettle River; NF - Newport; PTF - Purcell Trench; OVF - Okanagan Valley; SCF - Standfast Creek; SLF - Slocan Lake; VSZ - Valkyr shear zone. *Gneiss domes and structural complexes*: FC - Frenchman Cap; GFC - Grand Forks complex; KD - Kettle dome; MG - Malton gneiss complex; OD - Okanogan dome; PRC - Priest River complex; SD - Spokane dome; TO - Thor-Odin; VC - Valhalla complex; VG - Vaseaux gneiss. Modified from Read et al. (1991).

Brown 1981; Nielsen 1982; Brown and Read 1983; Okulitch 1984). This view began to change, however, as the tectonic significance of regionally extensive low-angle faults became clear in many metamorphic core complexes in the southwest United States (see Crittenden et al. 1980, and references therein). For example, Tempelman-Kluit and Parkinson (1986) suggested that the Okanagan Valley fault (OVF), a gently west-dipping mylonite zone exposed in the southern Okanagan Valley, was a crustal-scale shear that accommodated as much as 90 km of upper plate to the west displacement during the Middle Eocene. This type of large-displacement detachment fault model was later applied to many extension faults within the SMC, including the Columbia River, Kettle, Granby, Greenwood, and Slocan Lake faults, all of which have been interpreted to have accommodated 20 to 30 km of dip-slip displacement (Parrish et al. 1988). In this model, detachments cut the entire crust (Fig. 1-4).

The Okanagan Valley fault

The Okanagan Valley fault (OVF), a gently west-dipping, extensional shear zone with a strike length of more than 200 km, bounds the western margin of the SMC in the Vernon area (Fig. 1-3). Estimates of displacement on the OVF vary from 30-90 km on the basis of metamorphic omission and proposed hanging wall/footwall cut-offs (Tempelman-Kluit and Parkinson 1986; Parrish et al. 1988; Bardoux 1993; Johnson and Brown 1996).

The magnitude of displacement for the OVF has been questioned on the basis of geological relationships exposed in the Vernon area that appear to be inconsistent with the OVF being a crustal-scale detachment fault (Okulitch 1987; Thompson and Daughtry 1994, 1996). For instance, at the southern end of Wood Lake, a pluton of Middle Jurassic age, the Wood Lake pluton, is exposed on both sides of the fault trace (Thompson and Daughtry 1996). This relationship is inconsistent with the OVF having accommodated tens of kilometres of early Tertiary dip-slip displacement. A second observation that is inconsistent with current models is the occurrence of enclaves of amphibolite-grade gneiss within the Wood Lake pluton, *west* of the OVF fault trace (Thompson and Daughtry 1996). This places the high-grade (mid-crustal) rocks within the upper plate of the OVF, which should comprise low-grade, greenschist-facies upper-crustal rocks. Lastly, in the northern Okanagan Valley, south of Mara Lake, a distinctive lithostratigraphic succession as well as a belt of greenschist-facies rocks of the Slocan Group (included within the Quesnel Terrane) was mapped across the trace of the OVF with little (a few kilometres maximum) apparent stratigraphic offset, precluding the OVF from being a crustal-scale shear zone at this latitude (Okulitch 1987; Thompson and Daughtry 1996). All of these observations from the Vernon area are inconsistent with the OVF representing a crustal-scale

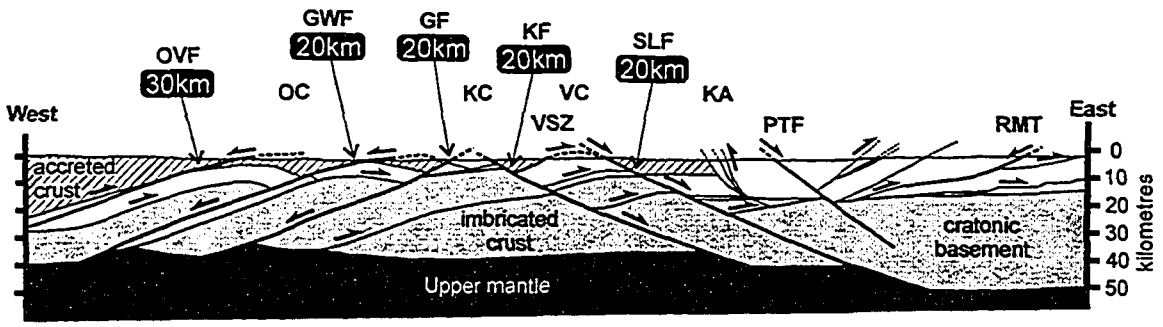

Fig. 1-4. Simplified interpreted present-day geological cross section through the southern Shuswap metamorphic complex (after Parrish et al. 1988) depicting early Tertiary extension faults as large-displacement, crustal-scale detachments that penetrate into the upper mantle. The amount of fault displacement (in km) for individual faults (as per Parrish et al. 1988) is indicated in the black boxes. Some estimates of displacement for the OVF are as high as 90 km (e.g., Tempelman-Kluit and Parkinson 1986). *Abbreviations*: GF - Granby fault; GWF - Greenwood fault; KA - Kootenay Arc; KC - Kettle complex; KF - Kettle fault; OC - Okanagan complex; OVF - Okanagan Valley fault; PTF - Purcell Trench fault; RMT - Rocky Mountain Trench; SLF - Slocan Lake fault; VC - Valhalla complex; VSZ - Valhalla shear zone. Early Tertiary extension faults are shown as heavy black lines. Early Proterozoic crust is shaded light grey. Middle Proterozoic to Jurassic pericratonic rocks are shaded white. Accreted rocks are shaded with horizontal striped pattern. Plutonic rocks have been omitted for clarity.

shear that juxtaposes upper and mid-crustal levels. Any viable tectonic model for the Vernon area needs to incorporate all of the available geological evidence; as such, current extensional models require revision.

Purpose

The primary goals of this study were:

1. To map the occurrence and distribution of extensional shear zones in the region between the Okanagan Valley and the Columbia River Valley between latitudes 50°00'N and 50°45'N at the scale of 1:20 000 (later compiled and published at 1:50 000), and to determine their tectonic significance by studying the kinematics, conditions of deformation, and constraining the amount of displacement of the shear zones.
2. To construct geological east-west cross sections from the Okanagan Valley to the Columbia River Valley consistent with new geological mapping and existing regional geological, geochronologic, and metamorphic constraints.
3. As part of the southern component of the ancient Pacific Margin NATMAP project (see Thompson et al. 2000), to further our understanding of the paleogeography, age, and metallogenic potential of the tectono-stratigraphic elements that comprised the Proterozoic to Paleozoic cratonic margin in the Vernon area.
4. To reconcile the geological relationships exposed in the Vernon area (Thompson and Daughtry 1994, 1996) with existing extension models.

During the course of this study, a previously unmapped migmatite complex, herein named the Aberdeen gneiss complex, was identified within the core of the Vernon antiform, an antiformal series of reflectors visible at upper to mid-crustal depths in east-west oriented seismic reflection profiles through the study area (e.g., Cook et al. 1992). Accordingly, the aim of the study was expanded to determine the emplacement age of the Aberdeen gneiss complex and to investigate the possibility that Paleoproterozoic crust may be exposed within the core of the Vernon antiform, similar to other Paleoproterozoic basement culminations within the southeastern Canadian Cordillera, such as the Monashee and Malton gneiss complexes (e.g., Armstrong et al. 1991; McDonough and Parrish 1991).

Methods

The following methods were utilized in order to achieve the study goals:

1. Geological mapping at 1:20 000 scale, compiled and published at 1:50 000 scale as Geological Survey of Canada Open File maps.
2. Construction of geological cross sections based on surface mapping, structural data, and seismic reflection data.
3. Metamorphic analysis: mapping the distribution of metamorphic isograds and metamorphic zones in the field, determining the relationship between metamorphic minerals and deformational fabrics in thin section, estimating (peak) pressure-temperature (*P-T*) conditions using thermobarometry, and estimating partial *P-T* paths using a combination of petrological data and Gibbs modelling (e.g., Spear and Selverstone 1983; Spear et al. 1984).
4. Geochronology: U-Pb isotopic dating of zircon, titanite, and monazite from metamorphic and igneous rocks using a combination of Isotope Dilution Thermal Ionization Mass Spectrometry (ID-TIMS) and Sensitive High Resolution Ion MicroProbe (SHRIMP) techniques. In addition, chemical dating of monazite was undertaken using the electron microprobe.
5. Structural analysis: field mapping of shear zones, construction of cross sections, structural and metamorphic analysis of upper and lower plate rocks, kinematic analysis of deformational fabrics, and constraining *P-T* conditions of deformation.

Presentation

The primary results of this study are summarized in paper format. The papers are supplemented by an introductory chapter (Chapter 1), a chapter of summary and conclusions (Chapter 6), and appendices, including: description of map units, station location data, structural data, electron microprobe data, monazite chemical isochron age calculations and monazite back-scattered electron (BSE) images, and zircon cathodoluminescence (CL) images.

Chapter 2 summarizes the results of a structural study of extensional shear zones that occur in the Vernon area and the nature of the contact between upper amphibolite-facies infrastructure and overlying greenschist-facies superstructure. The internal geometry and distribution of the superstructure was studied to provide constraints on the style and amount of early Tertiary upper crustal extension that occurred in the Vernon area.

Chapter 3 presents the results of a U-Pb geochronological study of the Aberdeen gneiss complex undertaken to determine the emplacement age and the thermotectonic evolution. The

Aberdeen gneiss complex is a complexly deformed assemblage of orthogneiss and paragneiss that is exposed within the core of the Vernon antiform, a antiformal series of reflectors visible at middle to upper crustal depths in existing east-trending seismic, crustal-scale reflection and refraction profiles through the Vernon area (e.g., Cook et al. 1992; Varsek and Cook 1994; Kanasewich et al. 1994).

Chapter 4 presents the results of a metamorphic study of the Vernon area that examines the nature of the contact between upper amphibolite-facies infrastructure and greenschist-facies superstructure. This chapter also contrasts the thermotectonic evolution of infrastructure and superstructure using thermobarometry, Gibbs modeling, chemical dating of metamorphic monazite from metapelitic rocks, and published U-Pb, K-Ar and $^{40}Ar/^{39}Ar$ dates.

Chapter 5 proposes a regional model for the Jurassic to Eocene tectonic evolution of the southeast Canadian Cordillera whereby partially molten rocks metamorphosed at mid-crustal depths (25-30 km) were exhumed primarily by ductile flow within a mid-crustal channel up a ramp in underlying Paleoproterozoic basement during the Late Cretaceous to Middle Eocene following radiogenic heating and widespread melting within the middle crust.

The final chapter, Chapter 6, summarizes the primary results of this study and highlights their implications for the Middle Jurassic to Middle Eocene tectonic evolution of the southeast Canadian Cordillera.

All chapters were formatted according to the style guidelines of the *Canadian Journal of Earth Sciences*. For punctuation, grammar, and spelling, *The St. Martin's Handbook for Canadians* by A. Lunsford, R. Connors, and J. Segal (St. Martin's Press, Scarborough, Ontario, 1989) and *Geoscience Reporting Guidelines* by B. Grant, PGeo (Victoria, B.C., 2003) were used.

Original contribution

This project was a collaborative effort with the Geological Survey of Canada under the auspices of the southern component of the Ancient Pacific Margin NATMAP project. The goal of the Ancient Pacific Margin NATMAP project was to further our understanding of the tectonic evolution and metallogenic potential of Paleozoic tectonostratigraphic elements that formed adjacent to the ancient Pacific cratonic margin (e.g., Thompson et al. 2000). R.I. Thompson spear-headed the southern component of the project, which concentrated on the Vernon area.

Due to the collaborative nature of the NATMAP project, many people made direct or indirect contributions to this study through their time, ideas, and support. The author was responsible for the majority of geological mapping and compilation of 1:50 000 (NTS) map sheets Oyama (82L03), Creighton Creek (82L02), and Eureka Mountain (82L01), which are

included in the map pocket, as well as significant portions of 82L01, 82L06, 82L07, 82L08, and 82L010 in conjunction with R.I. Thompson and Y. Lemieux. The areas mapped by the author during 1998 to 2001 are indicated in Fig. 1-5.

The author performed all steps of data gathering, sample preparation, and data analysis, except where otherwise indicated. The U-Pb geochronological data presented in Chapter 3 are an amalgamation of samples dated by the author at the University of Alberta and samples that were contracted to R.L. Friedman at the University of British Columbia and L. Heaman at the University of Alberta through the Geological Survey of Canada NATMAP project. For the samples that were dated as part of this thesis, all steps involved in mineral separation and chemical analyses were conducted by the author. The author was responsible for the compilation an interpretation of all isotopic data and calculation of ages. The electron microprobe data presented in Chapter 4 were collected by the author at the University of Alberta under the supervision of Lang Shi and Sergei Matveev. Finally, the author assumes all final responsibility for the data and interpretations presented in this work.

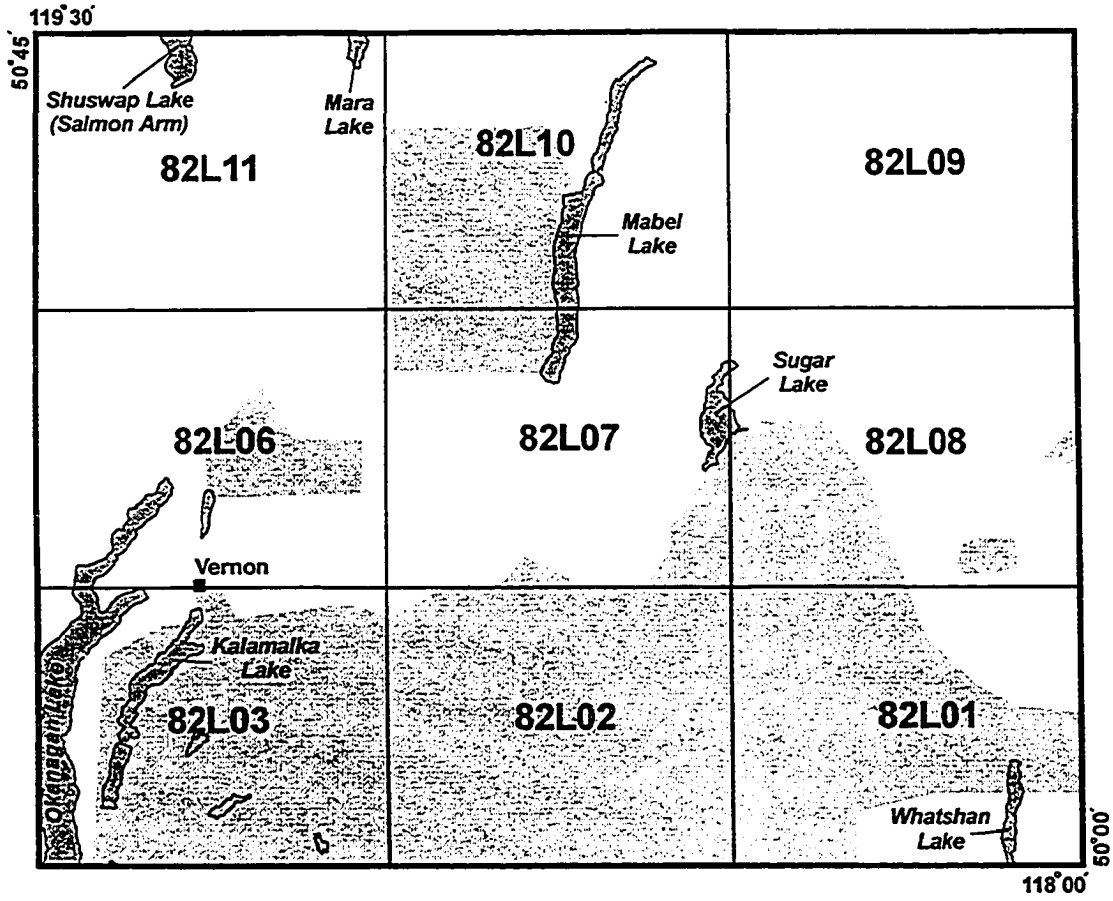

Fig. 1-5. Portions of NTS 1:50 000 topographic map sheets mapped by the author during the period of 1998 to 2001. The shaded areas were mapped in whole or in part by the author.

References

Armstrong, R.L., Parrish, R.R., Van der Heyden, P., Scott, K., Runkle, D., and Brown, R.L. 1991. Early Proterozoic basement exposures in the southern Canadian Cordillera: core gneiss of Frenchman Cap, Unit L of the Grand Forks Gneiss, and the Vaseaux Formation. Canadian Journal of Earth Sciences, **28**: 1169-1201.

Bardoux, M. 1993. The Okanagan Valley fault from Penticton to Enderby, south-central British Columbia. Ph.D. thesis, Carleton University, Ottawa.

Bardoux, M., and Mareschal, J.C. 1994. Extension in south-central British Columbia: mechanical and thermal controls. Tectonophysics, **238**: 451-470.

Brown, R.L., and Read, P.B. 1983. Shuswap terrane of British Columbia: a Mesozoic "core complex." Geology, **11**: 164-168.

Coney, P.B. 1980. Cordilleran metamorphic core complexes: an overview. *In* Cordilleran metamorphic core complexes. *Edited by* M.D. Crittenden, Jr., P.J. Coney, and G.H. Davis. Geological Society of America Memoir 153, pp. 7-31.

Coney, P.J., and Harms, T.A. 1984. Cordilleran metamorphic core complexes: Cenozoic extensional relics of Mesozoic compression. Geology, **12**: 550-554.

Cook, F.A., Varsek, J.L., Clowes, R.M., Kanasewich, E.R., Spencer, C.S., Parrish, R.R., Brown, R.L., Carr, S.D., Johnson, B.J., and Price, R.A. 1992. Lithoprobe crustal reflection cross section on the southern Canadian Cordillera, 1, Foreland Thrust and Fold Belt to Fraser River fault. Tectonics, **11**: 12-35.

Crittenden, M.D., Jr., Coney, P.J., and Davis, G.H. (eds). 1980. Cordillera Metamorphic Core Complexes. Geological Society of America Memoir 153.

Jones, A.G. 1959. Vernon map-area, British Columbia. Geological Survey of Canada Memoir 296.

Johnson, B.J., and Brown, R.L. 1996. Crustal structure and early Tertiary extensional tectonics of the Omineca belt at 51°N latitude, southern Canadian Cordillera. Canadian Journal of Earth Sciences, **33**: 1596-1611.

Kanasewich, E.R., Burianyk, M.J.A., Ellis, R.M., Clowes, R.M., White, D.J., Côté, Forsyth, D.A., Luetgert, J.H., and Spence, G.D. 1994. Crustal velocity structure of the Omineca Belt, southeastern Canadian Cordillera. Journal of Geophysical Research, **99 (B2)**: 2653-2670.

Lui, M.1994. Dynamic interactions between crustal shortening, extension, and magmatism in the North American Cordillera. Paleogeophysics, **146**: 447-467.

Mathews, W.H. 1981. Early Cenozoic resetting of potassium-argon dates and geothermal history of north Okanagan area, British Columbia. Canadian Journal of Earth Sciences, **18**: 1310-1319.

McDonough, M.R., and Parrish, R.R. 1991. Proterozoic gneisses of the Malton Complex, near Valemount, British Columbia: U-Pb ages and Nd isotopic signatures. Canadian Journal of Earth Sciences, **28**: 1202-1216.

Nielsen, N.K. 1982. Structural and metamorphic relations between the Mount Ida and Monashee groups at Mara Lake. British Columbia. Canadian Journal of Earth Sciences, **19**: 288-307.

Okulitch, A.V. 1984. The role of the Shuswap metamorphic complex in Cordilleran tectonism: a review. Canadian Journal of Earth Sciences, **21**: 1171-1193.

Okulitch, A.V. 1987. Comment and reply on "Extension across the Eocene Okanagan crustal shear in southern British Columbia." Geology, **15**: 187-188.

Parrish, R.R. 1995. Thermal evolution of the southeastern Canadian Cordillera. Canadian Journal of Earth Sciences, **32**: 1618-1642.

Parrish, R.R., Carr, S.D., and Parkinson, D.L. 1988. Eocene extensional tectonics and geochronology of the southern Omineca Belt, British Columbia and Washington. Tectonics, **7**: 181-212.

Read, P.B., and Brown, R.L. 1981. Columbia River fault zone: southeastern margin of the Shuswap and Monashee complexes, southern British Columbia. Canadian Journal of Earth Sciences, **18**: 1127-1145.

Read, P.B., Woodsworth, G.J., Greenwood, H.J., Ghent, E.D., and Evenchick, C.A. 1991. Metamorphic map of the Canadian Cordillera. Geological Survey of Canada, Map 1714A, scale 1:2 000 000.

Spear, F.S., and Selverstone, J. 1983. Quantitative P-T paths from zoned minerals: theory and tectonic applications. Contributions to Mineralogy and Petrology, **83**: 348-357.

Spear, F.S., Selverstone, J., Hickmott, D., Crowley, P., and Hodges, K.V. 1984. P-T paths from garnet zoning: a new technique for deciphering tectonic processes in crystalline terranes. Geology, **12**: 87-90.

Sonder, L.J., England, P.C., Wernicke, B., and Christiansen, R.L. 1987. A physical model for extension of western North America. *In* Continental Extensional Tectonics. *Edited by* M.P. Coward, J.F. Dewey, and P.L. Hancock. Geological Society Special Publication 28, pp. 187-201.

Tempelman-Kluit, D., and Parkinson, D. 1986. Extension across the Eocene Okanagan crustal shear in southern British Columbia. Geology, **14**: 318-321.

Thompson, R.I., and Daughtry, K.L. 1994. A new mapping project in Vernon map area, British Columbia. *In* Current Research 1994-A. Geological Survey of Canada, pp. 117-122.

Thompson, R.I., and Daughtry, K.L. 1996. New stratigraphic and tectonic interpretations, north Okanagan Valley, British Columbia. *In* Current Research 1996-A. Geological Survey of Canada, pp. 135-141.

Thompson, R.I., Nelson, J.L., Paradis, S., Roots, C.F., Murphy, D.C., Gordey, S.P., and Jackson, L.E. 2000. Ancient Pacific Margin NATMAP project, year one. Geological Survey of Canada, Current Research 2000-A1.

Varsek, J.L., and Cook, F.A. 1994. Three-dimensional crustal structure of the Eastern Cordillera, southwestern Canada and northwestern United States. Geological Society of America Bulletin, **106**: 803-823.

Wheeler, J.O., Brookfield, A.J., Gabrielse, H., Monger, J.W.H., Tipper, H.W., and Woodsworth, G.J. (compilers). 1991. Terrane map of the Canadian Cordillera. Geological Survey of Canada, Map 1713A, scale 1:2 000 000.

Williams, P.F., and Jiang, D. 2005. An investigation of lower crustal deformation: evidence for channel flow and its implications for tectonics and structural studies. Journal of Structural Geology, **27**: 1486-1504.

CHAPTER 2

A reappraisal of the tectonic significance of Late Paleocene to Early Eocene low-angle extensional shear zones in the Shuswap metamorphic complex near Vernon, southeast Canadian Cordillera[1]

[1] A version of this chapter has been submitted to the Canadian Journal of Earth Sciences for publication coauthored by P. Glombick, R. I. Thompson, P. Erdmer, and K. L. Daughtry†.

†deceased

Introduction

The Shuswap metamorphic complex (SMC) is a region within the hinterland of the southern Canadian Cordillera dominated by sillimanite-grade metamorphic rocks and granitic plutons (see, e.g., Okulitch 1984). The southern SMC is divided into normal-fault bounded structural culminations of amphibolite-facies rocks, such as the Valhalla, Grand Forks, and Okanagan complexes, whereas the central and northern parts of the SMC form a continuous region of sillimanite-grade rocks (Fig. 2-1).

The SMC is cut by a system of early Tertiary, northerly striking, gently to steeply dipping, brittle faults and shear zones with normal geometry (Fig. 2-1). The terms hanging wall and footwall are used in this paper when describing moderately to steeply dipping normal faults (30-90°), and upper plate and lower plate, for gently dipping (0-30°) faults or shear zones.

Many of the early Tertiary normal faults have been interpreted as gently dipping (0-30°), large-displacement (20-90 km) detachments that root in the middle to lower crust or upper mantle (e.g., Okanagan Valley fault, Tempelman-Kluit and Parkinson 1986; Slocan Lake fault, Parrish et al. 1988). According to these interpretations, motion on these faults resulted in the exhumation of mid-crustal rocks within the lower plate. It has been suggested more recently that ductile flow contributed to the exhumation of mid-crustal rocks and the formation of gneiss domes (e.g., Scammell 1993; Vanderhaeghe and Teyssier 1997; Johnston et al. 2000; Glombick et al. 2002). The relationship between detachment faulting and crustal flow, however, remains unclear.

As indicated by K-Ar dates, the metamorphic infrastructure of the SMC underwent rapid exhumation and cooling during the Late Paleocene to Middle Eocene (see, e.g., Parrish et al. 1988). In the present paper, the infrastructure includes rocks that were at temperatures above 500°C prior to the Late Paleocene (based on hornblende K-Ar data), and probably deforming by ductile flow, whereas rocks in the metamorphic superstructure cooled to less than 250°C before the Late Paleocene, and therefore were likely at upper crustal levels.

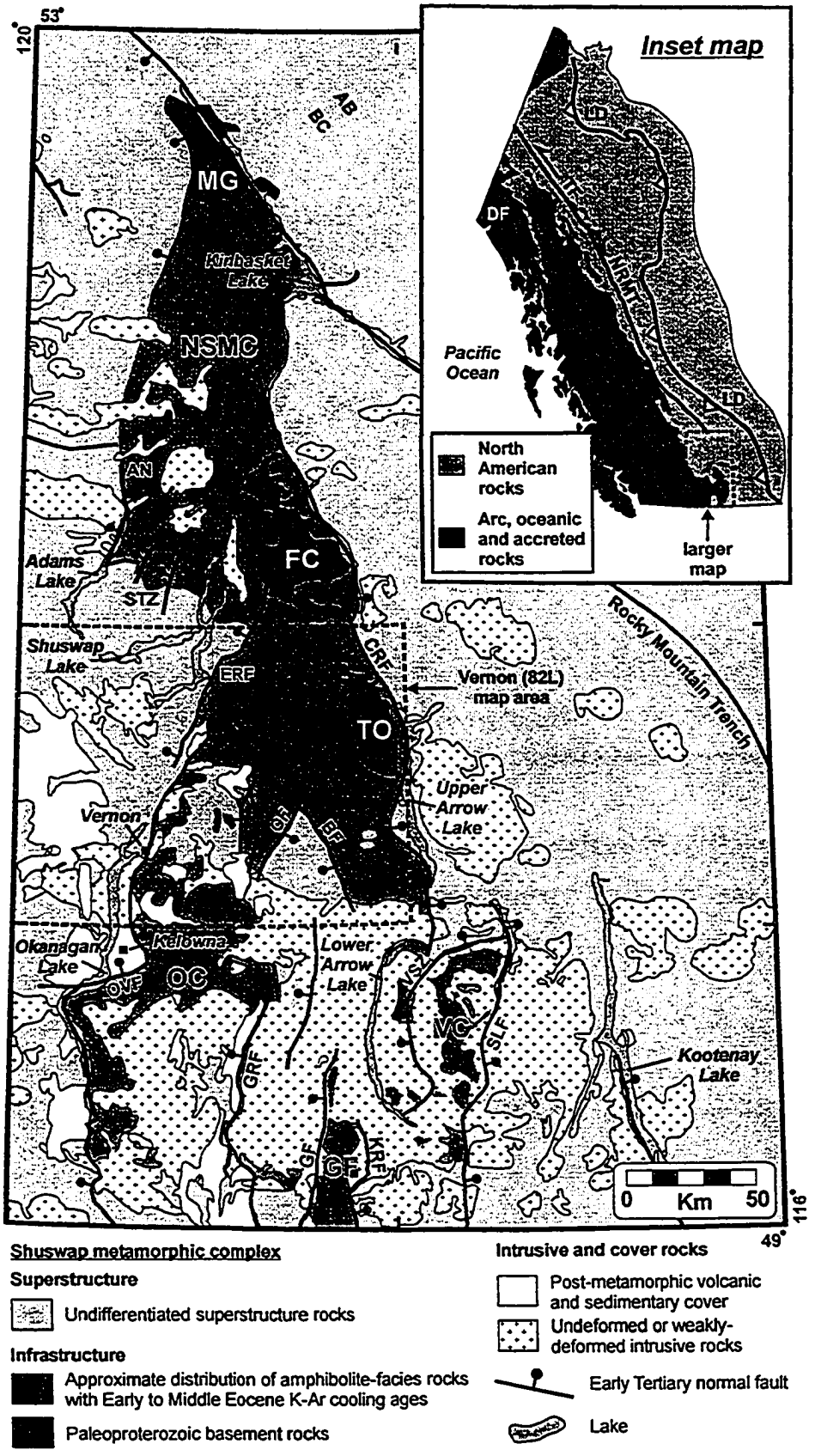

Fig. 2-1 (page 1 of 2). See next page for caption.

Fig. 2-1 (page 2 of 2). Generalized map of the southeast Canadian Cordillera showing the distribution of superstructure and infrastructure of the Shuswap metamorphic complex and the location of Late Paleocene to Middle Eocene extension faults. Modified from Wheeler and McFeely (1991) and Parrish et al. (1988). *Fault systems and shear zones*: AN - Adams Lake-North Thompson; BF - Beaven; CF - Cherry; CRF - Columbia River; ERF - Eagle River; GF - Granby; GRF - Greenwood; KRF - Kettle River; PTF - Purcell Trench; OVF - Okanagan Valley; SLF - Slocan Lake; STZ - Shuswap transfer zone; VSZ - Valkyr. Paleoproterozoic basement rocks: FC - Frenchman Cap dome (N. Monashee complex); MG - Malton gneiss complex; TO - Thor-Odin dome (S. Monashee complex). *Gneiss domes and structural complexes*: GF - Grand Forks; NSMC - Northern Shuswap metamorphic; OC - Okanagan; VC - Valhalla. ***Inset map***: Tectonic affinity of rocks within the Canadian Cordillera. Solid black lines outlines major fault systems. Dashed box outlines the area shown in the larger map. Abbreviations: DF - Denali fault; LD - limit of deformation (foreland folding and thrusting); NRMT - Northern Rocky Mountain Trench; TF - Tintina fault (modified from Erdmer et al. 2001).

The Vernon area is useful for studying the geometric and kinematic relationships between the superstructure and infrastructure, because a semi-continuous belt of superstructure is preserved across the SMC at this latitude (Figs. 2-1, 2-2). The belt of superstructure is noteworthy because: (1) in most other areas of the SMC it has been removed by faulting and/or post-Eocene erosion; (2) it yields information about the style and amount of extension that occurred during exhumation; and (3) the superstructure-infrastructure contact can be studied directly.

This paper summarizes the results of detailed geological mapping from the Okanagan Valley, on the west, to Whatshan Lake, on the east, between latitudes 50° 00' and 50° 45' N (Fig. 2-2). The three primary aims are: (1) to describe the transition from infrastructure to superstructure; (2) to document the distribution and internal structure of the superstructure; and (3) to determine the role of gently dipping early Tertiary extensional shear zones exposed at or near the contact.

Mapping indicates that the superstructure forms a nearly intact carapace across the SMC, with minimal internal thinning or removal by extensional faults. The evidence allows a new interpretation of the displacement, subsurface geometry, and the significance of gently dipping, Late Paleocene to Early Eocene shear zones in the Vernon area that does not require the existence of a crustal-scale, regional detachment fault.

Geological setting

The metamorphic infrastructure of the SMC consists of upper amphibolite-facies, polydeformed, Paleoproterozoic to Mesozoic metasedimentary and metavolcanic rocks that were deposited adjacent to the North American cratonic margin prior to being buried, metamorphosed, and deformed at mid-crustal depths during Mesozoic orogenesis (e.g., Parrish 1995). Geochronological and metamorphic data indicate a complex metamorphic and deformational history, with high-grade metamorphic events (6 to 10 Kb, 500 to 800°C) between the Middle Jurassic and the Paleocene (e.g., Parrish 1995; Crowley et al. 2000). The infrastructure is host to widespread syn- to postkinematic Late Paleocene to Early Eocene granitic rocks of the Ladybird suite (Carr et al. 1987; Carr 1992), the emplacement of which overlapped the onset of extension within the southeast Canadian Cordillera (Vanderhaeghe and Teyssier 1997).

The superstructure consists of greenschist to amphibolite-facies metamorphic and plutonic rocks flanking the SMC or locally preserved at upper structural levels or within structural depressions (Figs. 2-1, 2-2). North of approximately latitude 50°N, the superstructure is dominated by Late Proterozoic to Lower Jurassic metasedimentary and metavolcanic rocks of continental margin affinity. The superstructure south of 50°N is composed of Devonian to Lower

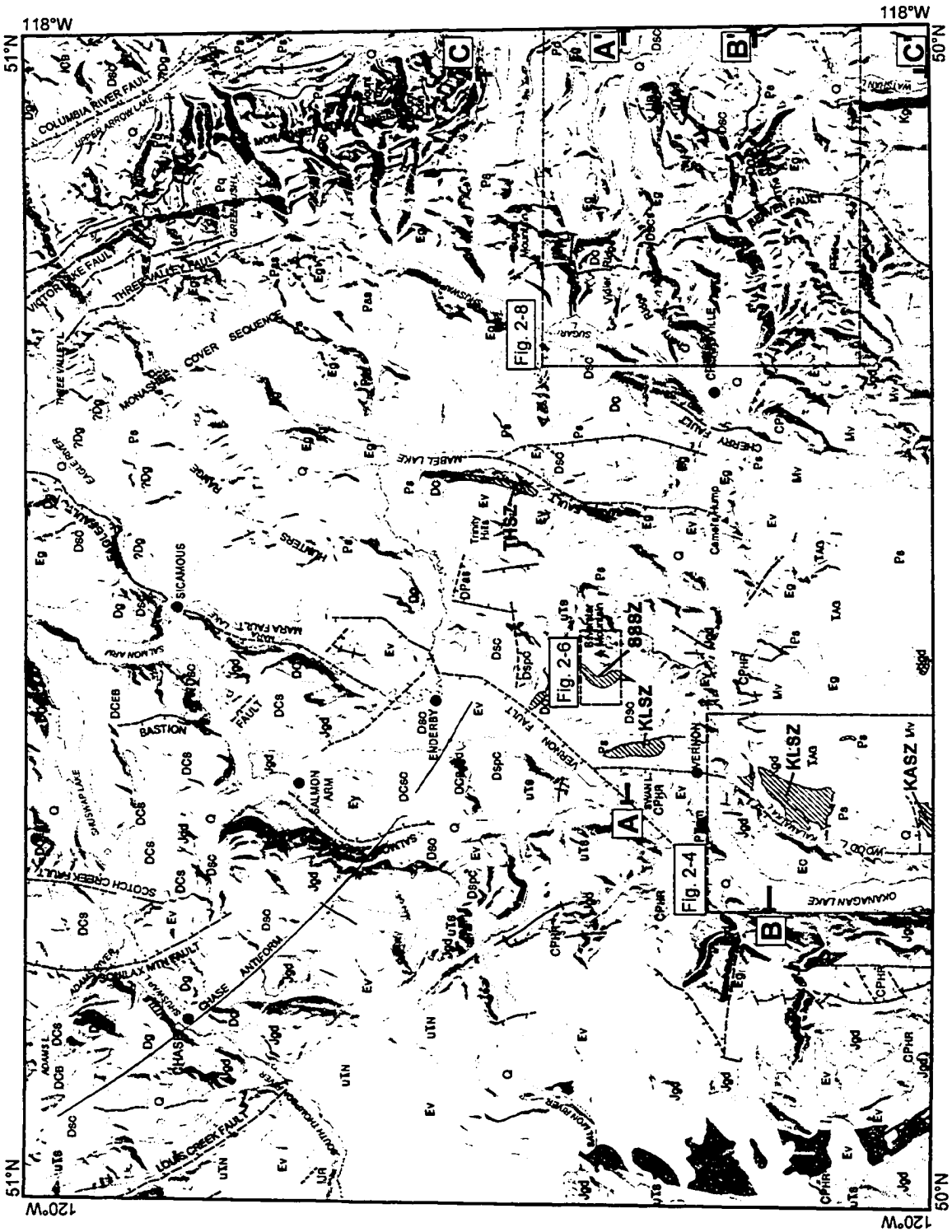

Fig. 2-2 (page 1 of 2). Geological map of the Vernon (NTS 82L, 1:250 000) map area. The location of detailed inset maps is indicated by dashed black boxes. End-points of cross section lines are indicated by letters in white boxes. *Abbreviations*: KASZ - Kelowna airport shear zone; KLSZ - Kalamalka Lake shear zone; SSSZ - Silver Star shear zone; THSZ - Trinity Hills shear zone.

Fig. 2-2 (page 2 of 2). Geological contacts modified from Daughtry and Thompson (2004*a*, 2004*b*), Glombick and Thompson (2004), Glombick et al. (2004), Thompson (2004*a*, 2004*b*, in press), Thompson and Glombick (2004*a*, 2004*b*), Thompson and Unterschutz (2004), and Thompson et al. (2004*a*, 2004*b*).

Jurassic metasedimentary and metavolcanic rocks of oceanic or arc affinity, intruded by weakly-deformed granitic rocks of Jurassic, Cretaceous and early Tertiary age (Fig. 2-2).

The superstructure was affected by Middle Jurassic regional metamorphism and deformation, synchronous with the emplacement of calcalkaline batholiths of the Nelson and Okanagan plutonic suites (170-155 Ma; e.g., Woodsworth et al. 1991). Middle Jurassic tectonism has been interpreted as reflecting the accretion of a large composite terrane (Intermontane Superterrane), comprising several Middle Paleozoic to Lower Jurassic oceanic and island arc terranes, to the cratonic margin following the closure of an ocean basin (e.g., Brown et al. 1986; Monger et al. 1991). The superstructure has yielded Middle Jurassic to Late Cretaceous cooling dates (K-Ar; hornblende and micas), indicating that it cooled below 250°C prior to the Paleocene (e.g., Mathews 1981).

Previous work on early Tertiary shear zones exposed along the western margin of the Shuswap metamorphic complex

The Okanagan Valley, a north-trending physiographic feature more than 300 km in length, has long been interpreted as the locus of a fault zone separating low-grade rocks on the west from higher grade rocks on the east (e.g., Jones 1959).

Tempelman-Kluit and Parkinson (1986) described a low-angle fault in the southern Okanagan Valley near Penticton, where fractured volcanic rocks of the Middle Eocene Marron Formation and Upper Paleozoic to Late Triassic greenschist-facies metasedimentary and metavolcanic rocks overlie brecciated and chloritized mylonitic gneiss. The correlation of three volcanic outliers in the upper plate with possible plutonic roots in the lower plate, as well as the metamorphic contrast across the valley, led them to propose 60 to 90 km of dip slip (top to the west displacement). Okulitch (1987) noted that such displacement on a top to the west detachment was incompatible with the existence of metamorphic superstructure near Vernon. Okulitch (1987) and Bardoux (1986) reported the occurrence of gneissic clasts in the basal conglomerate of Middle Eocene volcanic and sedimentary outliers, which Okulitch (1987) interpreted as evidence of a depositional contact. Bardoux (1993), however, proposed that Middle Eocene (52 ± 2 Ma) volcanic outliers east of the Okanagan Valley were situated within the upper plate of a west side down, gently dipping shear zone, which he correlated with the Okanagan Valley fault of Tempelman-Kluit and Parkinson (1986). On the basis of a palinspastically restored cross section at the latitude of Kelowna, he proposed a minimum of 45 km and a maximum of 70 km of displacement.

Mathews (1981) conducted a K-Ar study of the Vernon area. He obtained Middle Jurassic to Late Cretaceous dates from the greenschist to lower-amphibolite-facies superstructure (155-83 Ma; biotite, hornblende, and whole rock), and Late Paleocene to Middle Eocene dates from the underlying infrastructure (60-47 Ma; hornblende, muscovite, and biotite). Volcanic rocks from outliers in the Enderby Cliffs and Trinity Hills yielded Middle Eocene dates (42-49 Ma; biotite and whole rock). Mathews (1981) reported a depositional contact at the base of the Trinity Hills outlier that overlaps the (unexposed) contact between superstructure and infrastructure (Fig. 2-2).

Carr (1990), Bardoux (1993) and Vanderhaeghe et al. (1999) proposed that superstructure rocks and the Middle Eocene volcanic outliers in the Trinity Hills were situated within the upper plate of a detachment fault. A mylonitic granite with top to the west shear-sense indicators within the infrastructure, along the southwest margin of the Trinity Hills outlier, yielded dates between 56 and 60 Ma (U-Pb zircon; Bardoux 1993; Vanderhaeghe et al. 1999).

Exposures of mylonite have been reported east of Shuswap Lake, occurring between low-grade and higher-grade rocks (Journeay and Brown 1986). These authors proposed that the mylonite, which contained top to the west shear-sense indicators, was the northern extension of an Okanagan Valley fault system, which they named the Eagle River fault.

Johnson (1994) described a series of gently dipping, top to the west-directed, ductile shear zones cut by steeply dipping, west side down normal faults between Shuswap Lake and Adams Lake, which he interpreted as a west-stepping transfer zone linking the Eagle River fault of Journeay and Brown (1986) with the Adams Lake-North Thompson fault (Fig. 2-1). He estimated 32 km of displacement on the proposed Okanagan Valley-Eagle River fault system at the latitude of Sicamous (Johnson 1994; Johnson and Brown 1996).

On the basis of the continuity of lithostratigraphic units across the Okanagan Valley between Vernon and Mara Lake, Thompson and Daughtry (1996) inferred a stratigraphic offset of less than 5 km across the Okanagan Valley. Read and Okulitch (1977), Neilson (1982), and Erdmer et al. (1999) also mapped units across the Okanagan Valley at this latitude with minor apparent offset. Additional geological mapping related to this study showed that, although metamorphic grade is higher on the east side of the valley (sillimanite-potassium-feldspar-grade compared with garnet-grade on the west; Thompson 2004*a*; Thompson and Glombick 2004*b*), the Silver Creek and Chase formations are present on both sides of the Okanagan Valley, i.e., within both superstructure and infrastructure (Fig. 2-2).

New geological maps and cross sections of the Vernon area

As part of the Geological Survey of Canada's Ancient Pacific Margin NATMAP project, geological mapping was completed at 1:20 000 scale during the period 1998–2003, in the region between the Okanagan and the Columbia River valleys. The results have been published as Geological Survey of Canada Open File 1:50 000 scale geological maps (Fig. 2-2; Thompson 2004*a*, 2004*b*; Thompson and Glombick 2004*a*, 2004*b*; Thompson and Unterschutz 2004; Thompson et al. 2004*a*, 2004*b*; Glombick and Thompson 2004; Glombick et al. 2004).

In the present study, generalized east-west (A-A' and B-B') and north-south (C-C') cross sections were constructed through the area (Fig. 2-3), using the new maps together with Lithoprobe seismic reflection data (Lines 6-10, Southern Cordillera transect; Cook et al. 1992). In these cross sections, the structure of the upper 4 km of the crust was inferred from map data; below 4 km depth, the structure was inferred from seismic reflection data.

Kelowna-Kalamalka Lake area

In the region between Kelowna and Vernon, the western boundary of the SMC coincides with the valley containing Kalamalka and Wood lakes (Fig. 2-4).

Bedrock exposed on the west side of the valley includes greenschist-facies intermediate volcanic and sedimentary rocks of the Carboniferous and Permian Harper Ranch Group, weakly-deformed, medium to coarse-grained hornblende granodiorite of the Middle Jurassic Wood Lake pluton (164.4 ± 2.0 Ma, U-Pb titanite; Thompson and Daughtry 1996), and pink-weathering, pyroxene-bearing syenite of the Middle Eocene Coryell plutonic suite (Glombick et al. 2004). While metamorphic rocks are dominantly at greenschist grade, screens of amphibolite-facies quartzofeldspathic gneiss and marble tens to hundreds of metres across, locally known as the Wood Lake gneiss, occur within the Wood Lake pluton (Thompson and Daughtry 1996; Erdmer et al. 1998). A sample of the Wood Lake gneiss has yielded concordant zircon, dated at 171 Ma and interpreted as metamorphic in origin (U-Pb; Chapter 3).

Amphibolite-facies, variably retrogressed, mylonitic and cataclastic metamorphic rocks are exposed on the east side of the valley, from Kalamalka Lake to the southern limit of the study area (Fig. 2-4). Rock types include: potassium-feldspar augen gneiss, calcareous quartzite, pelitic schist, calcsilicate, and amphibolite. Less deformed exposures of augen gneiss (Fig. 2-5*a*) resemble the potassium-feldspar megacrystic Wood Lake granodiorite to the north.

At one location along the west shore of Kalamalka Lake, highly altered, retrogressed Wood Lake gneiss is in fault contact with syenite of the Coryell suite (Fig. 2-4). The fault is marked by a nearly vertical, north-northeast trending zone of breccia and gouge several metres

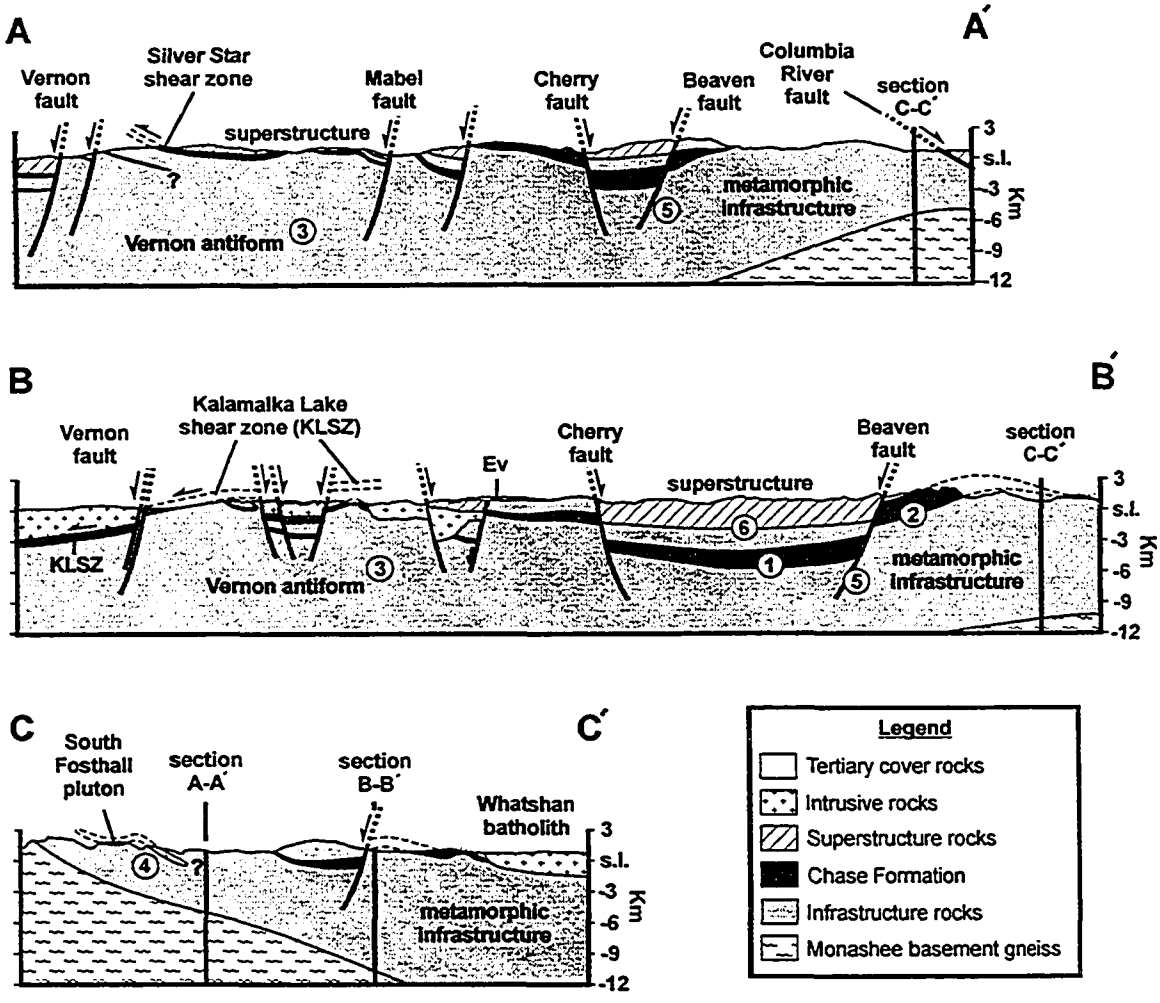

Fig. 2-3. Generalized geological cross sections through the study area. The large, capital bold letters in Fig. 2-2 indicate the location of cross section lines. No vertical exaggeration. *Abbreviations*: s.l. - sea level. *Notes*: (1) The Chase Formation is shown as a flat sheet in the subsurface on the basis of the orientation of reflectors in seismic reflection data (Cook et al. 1992) and of the observation that, at surface, the Chase Formation and its enclosing lithostratigraphy are not repeated at the map scale and form an open upright folded sheet with no structural repetition (Fig. 2-2). (2) This structure is interpreted as a broad, west-trending antiform, with the northern limb down-dropped by a steep normal fault, rather than a map-scale recumbent isoclinal fold (e.g., Carr 1990), based on detailed geological mapping in this area (see Lemieux et al. 2003; Thompson et al. 2004*a*). (3) The Vernon antiform is a domal series of reflectors visible at upper to mid-crustal depths near Vernon (Cook et al. 1992). (4) The geometry of the South Fosthall pluton in the subsurface is not well constrained. (5) The Beaven fault cuts the contact between infrastructure and superstructure, and therefore cannot be the "breakaway" of an Okanagan Valley-Eagle River fault system. Middle Eocene normal faults are inferred to root into the Middle Eocene brittle-ductile transition (not exposed). (6) While this line is shown as a discrete contact in the sections, it is transitional in the field (see text for description).

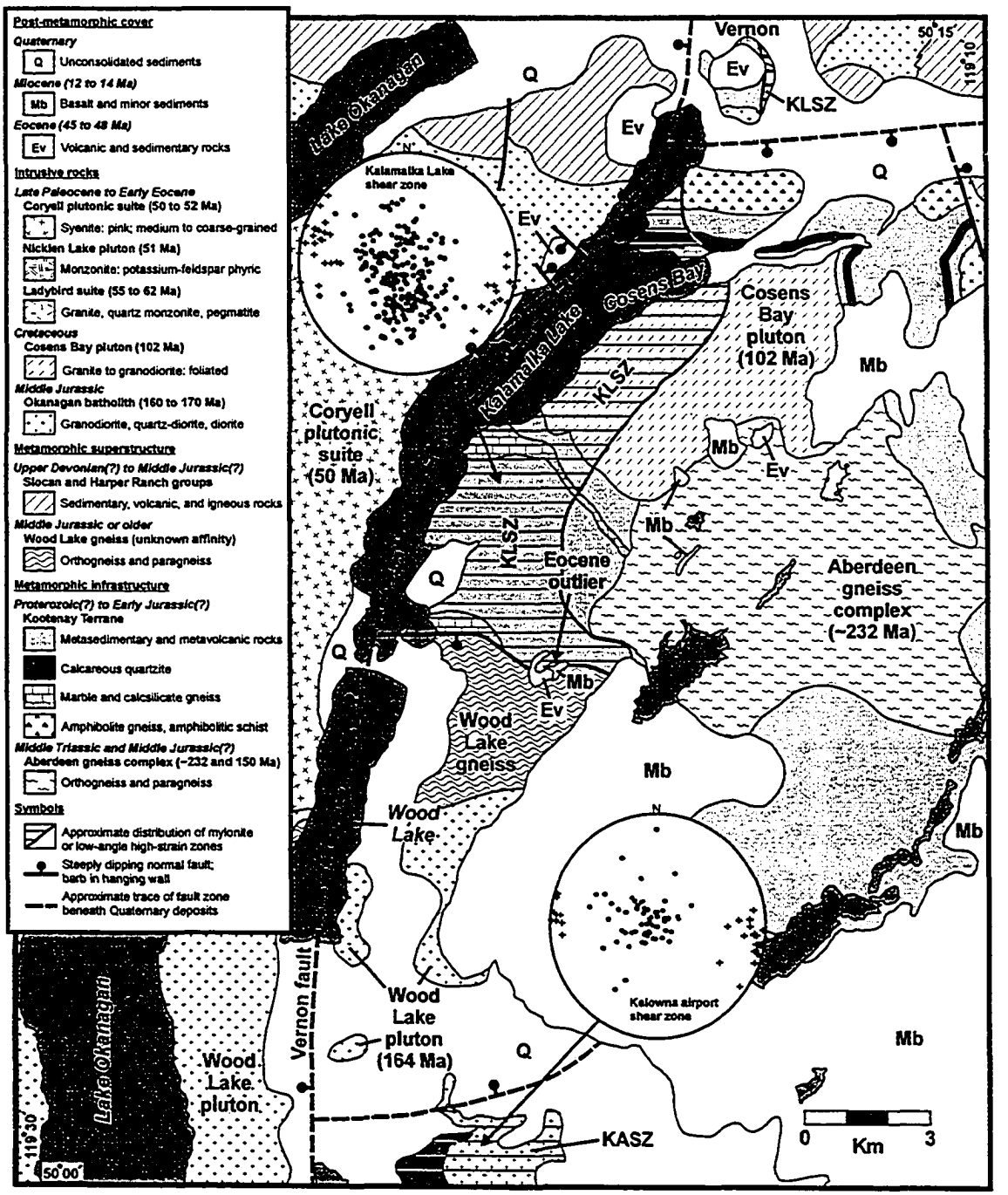

Fig. 2-4. Simplified geological map of the Kalamalka Lake area, showing the distribution of mylonite zones (striped pattern) and fabric data from the Kalamalka Lake shear zone (KLSZ) and the Kelowna airport shear zone (KASZ; Okanagan Valley fault, see also Bardoux 1993). Fabric data are plotted on lower hemisphere, equal-area projections. *Symbols*: solid circles - poles to mylonitic foliation; crosses - stretching lineations. Geological contacts modified from Glombick et al. (2004).

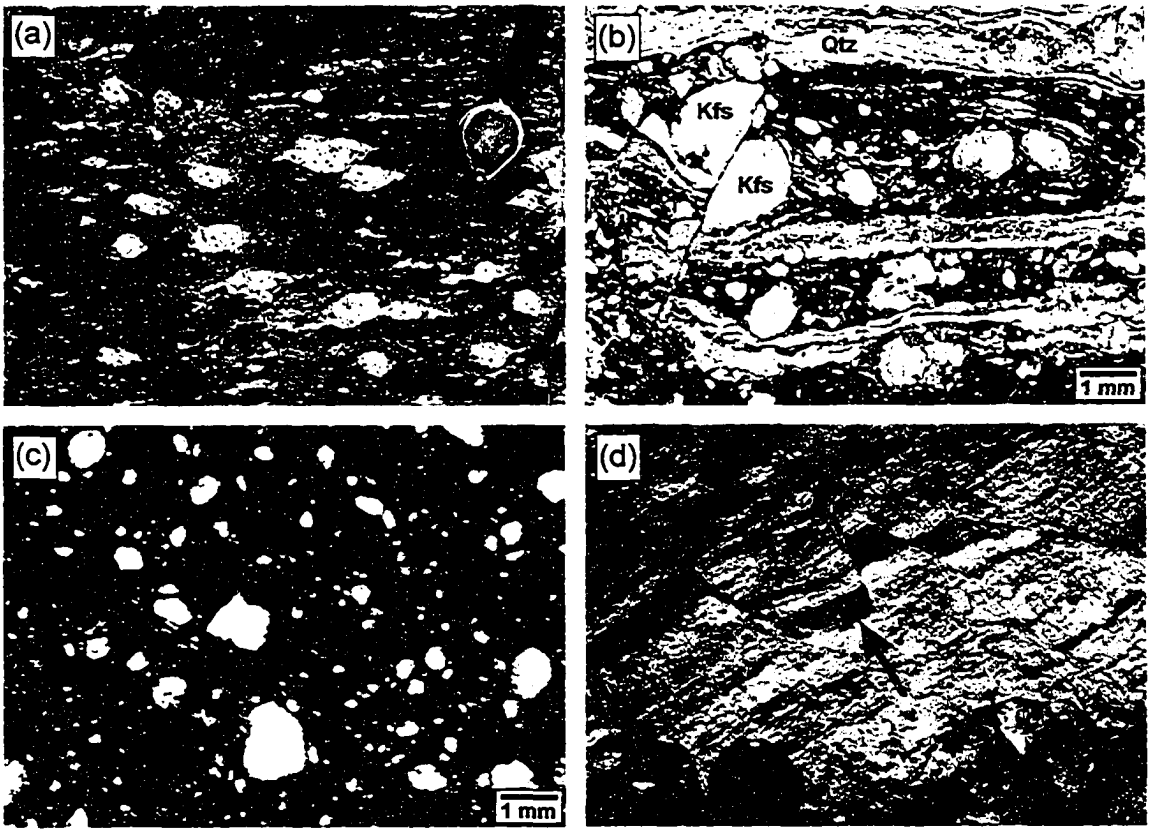

Fig. 2-5. Outcrop and thin section photographs of rocks exposed within shear zones adjacent to the Okanagan Valley. (a) Outcrop of potassium-feldspar augen orthogneiss. Hand lens for scale. (b) Thin-section photograph of mylonitic gneiss with late micro-fractures that cut the mylonitic fabric. The thin-section is oriented parallel to the stretching lineation and perpendicular to the foliation. Note the elongate quartz ribbons and fractured potassium-feldspar porphyroclast. Mineral abbreviations after Kretz (1983). (c) Thin-section photograph of cataclasite. Note quartz and feldspar fragments. (d) Outcrop of fractured and retrogressed cataclastic gneiss. Outcrop face is oriented sub-parallel to stretching lineation and approximately perpendicular to the foliation. Note minor faults that offset the dark band (indicated by black arrow). Lens cap is approximately 6 cm in diameter.

wide. It is interpreted to be a steeply dipping, west side down normal fault, underlying both Kalamalka and Wood lakes, named here the Vernon fault (Fig. 2-4).

At the southern limit of the map area, southeast of Wood Lake, a number of outcrops expose mylonite overprinted by brittle structures (Fig. 2-5*b*). Cataclastic layers, millimetres to centimetres across, occur locally (Fig. 2-5*c*). Fractures with centimetres of displacement cut the mylonitic foliation at angles between 45° and 60° (Fig. 2-5*d*). The rocks exhibit extensive alteration by fluids; primary mafic minerals have been retrogressed to chlorite and epidote; feldspars have been replaced by sericite. The mean orientation of the mylonitic foliation in this area (Fig. 2-4; Kelowna airport shear zone) is subhorizontal, and chlorite-coated quartz ribbons and grooves, interpreted as a stretching lineation, trend slightly south of east (100°/03°). Delta and sigma porphyroclasts yield a consistent top to the west vergence; the same vergence was reported in mylonitic rocks exposed several kilometres to the south (Bardoux 1993). The upper boundary is not exposed, but the zone has been interpreted to be 1-2 km thick near Kelowna (Bardoux 1993).

South of Wood Lake, scattered exposures of the Wood Lake pluton occur on both sides of the valley, straddling the trace of the proposed Okanagan Valley detachment (Fig. 2-4). Though not exposed, the contact between mylonitic gneiss and the Wood Lake pluton, approximately 5 km southeast of Wood Lake, was constrained to within 200 m. Near the contact, the pluton is extensively fractured and altered. The Wood Lake pluton is interpreted to be juxtaposed against the gneiss by a steep, north side down normal fault (Fig. 2-4).

East of Kalamalka Lake, upper-amphibolite facies Proterozoic to Devonian paragneiss is intruded by the Middle Triassic Aberdeen gneiss complex (Glombick et al. 2004). Near the lake, the paragneiss is overprinted by a gently dipping mylonite zone, the Kalamalka Lake shear zone (Fig. 2-4; Erdmer et al. 1998; Glombick et al. 1999; Glombick et al. 2004). Within the mylonite zone, foliation is openly folded at the outcrop scale; the mean orientation is subhorizontal, and a stretching lineation defined by quartz ribbons, elongated bundles of sillimanite and biotite, and tails of disaggregated feldspar porphyroclasts, trends approximately east or west (Fig. 2-4; mean orientation: 287°/17°). Shear-sense indicators, such as winged porphyroclasts, extensional shear bands, and back-rotated boudins (e.g., Hanmer and Passchier 1991), have consistently yielded top to the west sense (Erdmer et al. 1998; Glombick et al. 1999). Synkinematic sillimanite aligned with the stretching lineation and the absence of muscovite indicate that shearing occurred at pressure and temperature conditions above the second sillimanite isograd. Pods of leucosome are disaggregated, indicating that shearing post-dated migmatization. Muscovite and chlorite are

absent, except along late fractures. In contrast to mylonite farther south (Kelowna airport shear zone; Fig. 2-4), brittle overprinting and hydrothermal alteration are absent.

The upper boundary of the Kalamalka Lake shear zone is not exposed. The mylonite zone persists up the slope to the east, where its lower boundary is truncated by the present erosional surface (Figs. 2-3*b*, 2-4). West of Kalamalka Lake, the shear zone is cut by the Vernon fault, and its offset extension projects beneath the Wood Lake pluton and the Harper Ranch Group (Figs. 2-3*b*, 2-4).

The age of the Kalamalka Lake shear zone is constrained between 90 Ma, the time of migmatization within the Kalamalka Lake metamorphic assemblage (U-Pb concordant zircon and SHRIMP data; Chapter 3), and 47.1 ± 0.6 Ma, a preliminary date from an undeformed mafic dyke exposed along Kalamalka Lake (U-Pb zircon; Heaman et al. 1999). Fine-grained, weakly foliated biotite-bearing granite within the shear zone has been dated at 50.3 ± 0.4 Ma (U-Pb zircon; Heaman et al. 1999), indicating that a component of ductile deformation occurred between 47 and 50 Ma.

Three kilometres east of the south end of Kalamalka Lake, an erosional outlier of zeolite-facies volcanic flow and breccia units overlies upper amphibolite-facies mylonitic pelitic schist of the Kalamalka Lake shear zone (Fig. 2-4, labelled "Eocene outlier"; see also Glombick et al. 1999). Rocks in similar volcanic outliers in the Vernon area are Middle Eocene in age (48-42 Ma; Mathews 1981; Bardoux 1993; Breitsprecher 1998). Here, the predominant volcanic rock type is fine-grained, greenish-grey weathering dacite. The basal contact is well exposed in a road cut where dacite directly overlies an undulating, moderately dipping, 10 to 50 cm thick regolith developed in schist (Glombick et al. 1999). The regolith is a dark brown to reddish-brown zone of friable and weathered mylonitic pelite, less than a metre thick. There is no evidence of faulting between the dacite and the regolith. Approximately 100 m to the north, the contact is not exposed, but its location can be narrowed down to within 3 m. Randomly oriented clasts of schist and gneiss in the dacite occur up to 10 m above the contact (Glombick et al. 1999).

Exposures of mylonitic calcareous quartzite and schist occur immediately north of Vernon, adjacent to Swan Lake, along Highway 97A. The mylonite zone extends eastward (up slope) for several hundred metres, where it is interpreted as being cut by several steep normal faults (Thompson and Unterschutz 2004). The upper and lower boundaries of the mylonite zone are not exposed, and no age constraints are available. Similarly to the Kalamalka Lake shear zone, the mylonite formed at the approximate structural level of the Devonian Chase Formation, the shearing occurred under upper amphibolite-facies conditions, the mean mylonitic foliation is horizontal, and the mean stretching lineation trends west.

Silver Star Mountain area

On Silver Star Mountain, approximately 10 km northeast of Swan Lake (Fig. 2-2), a continuous section from infrastructure to superstructure is exposed. Previous authors have interpreted the contact to be an unconformity (Read and Okulitch 1977), or the westward extension of an Okanagan Valley-Eagle River detachment fault in this area (Carr 1990; Bardoux 1993; Vanderhaeghe et al. 1999).

The superstructure is composed of greenschist-facies (biotite zone) argillite, phyllite, marble, conglomerate, and augite porphyry of the Upper Triassic to Lower Jurassic(?) Slocan Group (Fig. 2-6; Read and Okulitch 1977; Unterschutz 2002; Thompson and Unterschutz 2004). Dark-grey weathering, carbonaceous argillite is the most abundant rock type. West of the Okanagan Valley, Late Triassic Slocan/Nicola rocks overlie older rocks of the Upper Paleozoic(?) Chapperon and Devonian to Permian Harper Ranch groups above a regional angular unconformity (cf. Read and Okulitch, 1977). On Silver Star Mountain, the contact between the Slocan Group and the underlying units has been overprinted by Middle Jurassic to Late Cretaceous deformation and regional amphibolite-facies metamorphism and Late Paleocene to Middle Eocene extension-related deformation.

The internal structure of the Slocan Group is complex. A strong cleavage defined by aligned platy metamorphic minerals is oriented subparallel or at low angles (0-30°) to transposed bedding, and is axial planar to tight to isoclinal folds. Both bedding and the strong cleavage are locally overprinted by a crenulation cleavage, and generally have moderate to steep dips (40°-70°).

Upper amphibolite-facies pelitic and semi-pelitic schist, quartzofeldspathic gneiss, amphibolite, and calcareous quartzite of the Devonian to Lower Carboniferous(?) Chase and Silver Creek formations underlie the western part of the Silver Star area (Fig. 2-6). Synkinematic, muscovite-bearing, lineated sills and lenses of granite and post-kinematic pegmatite dykes of inferred Late Paleocene to Early Eocene age occur near the sillimanite-in isograd, locally comprising 100% of exposed bedrock (Fig. 2-6). The dominant fabric within the Chase and Silver Creek formations is a gently dipping (0-30°) transposition foliation, defined by platy metamorphic minerals, compositional layering, and leucosome layers. The foliation is folded into tight to isoclinal folds, and locally refolded by closed to open folds and broad, post-metamorphic warps (see also Unterschutz 2002).

Detailed mapping in the Silver Star Mountain area revealed that the contact between greenschist-facies rocks of the Slocan Group and upper amphibolite-facies rocks of the Silver Creek Formation occurs across a ~2 km thick zone characterized by: (1) mylonitic rocks; (2) an

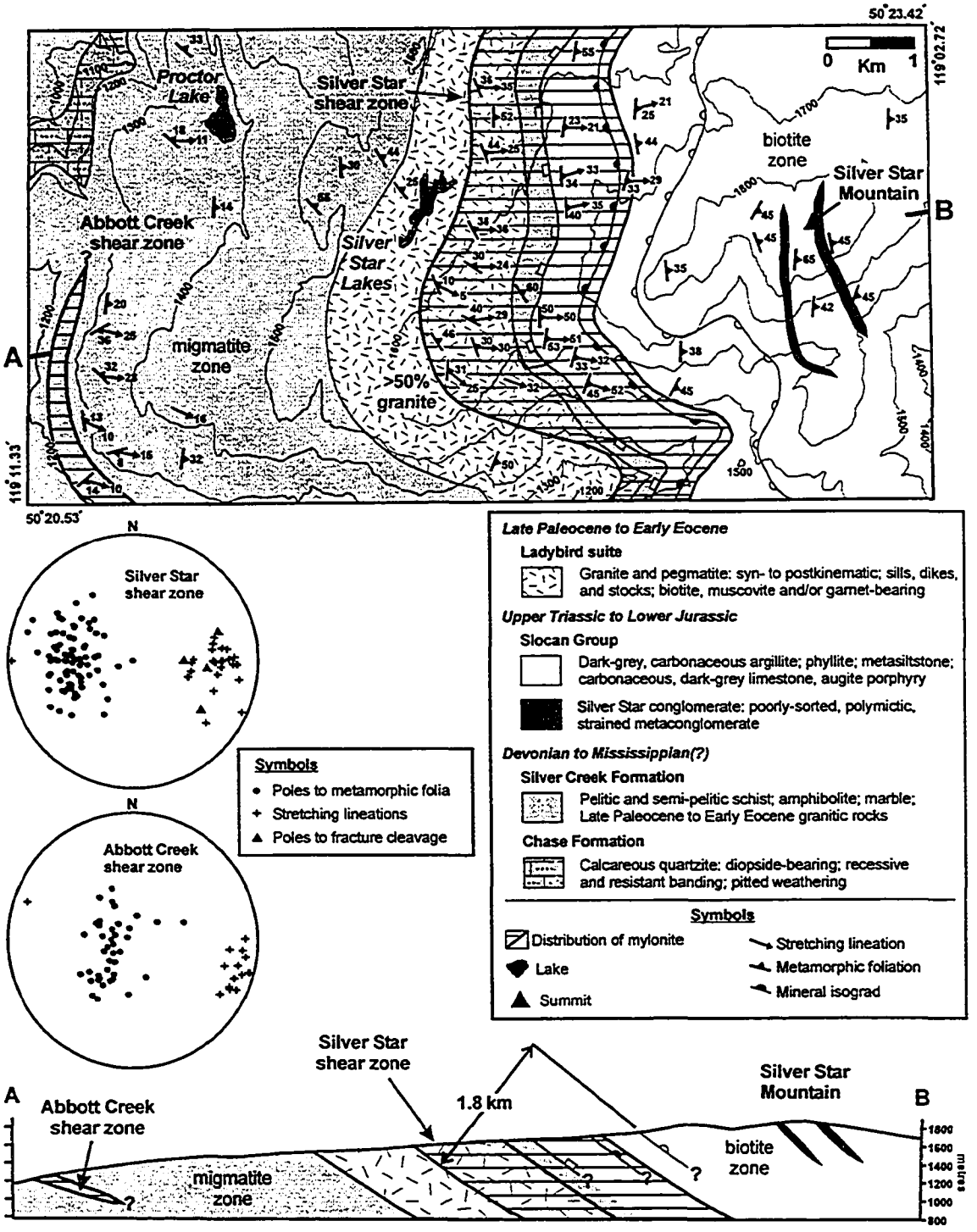

Fig. 2-6. Simplified geological map and cross section of the Silver Star Mountain area, showing the distribution of metamorphic isograds and the distribution of highly strained rocks (strain is heterogeneously distributed within this interval - see text). The contact between the Slocan Group and the Silver Creek Formation is arbitrarily placed at the sillimanite-in isograd (see text). Elevation contours are shown as thin dark-grey lines. Elevations are metres above sea level. Fabric data from the Silver Star and Abbott Creek shear zones are plotted on lower hemisphere, equal-area projections. *Mineral isograd symbols*: open half-circles - garnet-in; filled half-circles - staurolite-in; open rectangles - sillimanite-in. Mineral abbreviations after Kretz (1983).

increase in metamorphic grade; and (3) syn- to post-kinematic Late Paleocene to Early Eocene granitic rocks. The contact is difficult to locate precisely, because both units have similar protolith compositions. It is arbitrarily placed at the sillimanite-in isograd, which may not coincide with a stratigraphic contact. As a result of Middle Jurassic to Late Cretaceous metamorphic overprinting, it is possible that some parts of the Slocan Group are at amphibolite grade, and therefore may have been included with the Silver Creek Formation locally.

Within the zone of deformation, strain is heterogeneously distributed at all scales, and is concentrated in layers a few millimetres to several metres thick, separated by microlithon-sized or outcrop-sized domains of less deformed rock. Limited exposure did not permit the mapping of individual mylonite zone boundaries. Ductile strain is more pervasive where the metamorphic grade is higher (i.e., structurally lower in the zone), below the sillimanite-in isograd. Near the upper boundary of the high-strain zone, the metamorphic foliation dips moderately east (30°-45°). At the level of the garnet-in isograd, a weakly developed mineral lineation, defined by elongate clots of biotite on the foliation surface, plunges moderately to the east. A spaced fracture cleavage perpendicular to the mineral lineation is commonly filled with quartz and (or) calcite (Fig. 2-6). At this level of the deformation zone, evidence of non-coaxial deformation is restricted to millimetre-thick micaceous shear bands with elongate quartz grains parallel to the stretching lineation. Deeper in the zone, near the staurolite-in isograd, evidence of non-coaxial deformation includes quarter structures, and delta and sigma winged porphyroclasts (e.g., Hanmer and Passchier 1991). In sillimanite-grade rocks, high-strain zones include quartz ribbons with lattice preferred orientation and sub-grain development (Fig. 2-7*a*). A component of non-coaxial strain is indicated by C-S fabric, delta and sigma porphyroclasts, mica fish, and synthetic C' shear bands (Fig. 2-7*b*). Shear-sense indicators have yielded a consistent top to the west sense. Top to the east sense has been reported from metapelitic rocks in the Sovereign Lakes area (Unterschutz 2002), but was not confirmed in this study.

From east to west, structurally down-section, a gradual increase in metamorphic grade occurs, with garnet, staurolite-kyanite, and sillimanite-in isograds developed in pelitic and semi-pelitic rocks (Fig. 2-6). The second sillimanite isograd could not be accurately placed due to the abundance of granitic intrusions, but migmatitic rocks are present near Proctor Lake, indicating its proximity (Fig. 2-6).

Abundant synkinematic muscovite-bearing granite, which is absent in the superstructure, occurs near the sillimanite-in isograd (Fig. 2-6). Ductile strain is most evident in the granitic rocks, where rodded quartz grains and aggregates of micas are visible on the foliation surface, and C-S fabric and C' extensional shear bands are visible on surfaces oriented parallel to the

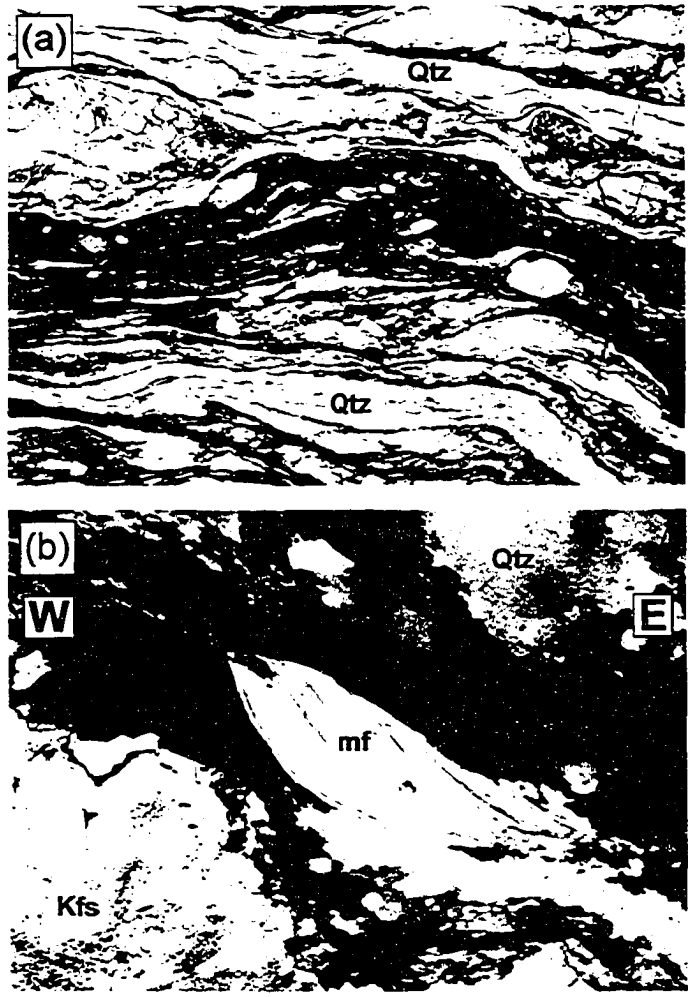

Fig. 2-7. Oriented thin-section photographs of mylonitic rocks from the Silver Star Mountain area. Both thin sections are oriented parallel to the stretching lineation and perpendicular to the mylonitic foliation. (a) Mylonitic semi-pelitic schist from the Sovereign Lakes ski area. Note the well-developed, elongate recrystallized quartz ribbons. Field of view is approximately 2.5 mm in the long dimension. (b) Mylonitic, muscovite-bearing, synkinematic granite of inferred Late Paleocene to Early Tertiary age from near Sovereign Lakes. The muscovite fish (mf) indicates a top to the west (sinistral) shear sense. Note undulose extinction, subgrains, and serrated grain boundaries of quartz grains (upper right). Field of view is approximately 1.0 mm in the long dimension. Photo taken with crossed polarizers.

stretching lineation and perpendicular to the foliation, both in outcrop and in thin section. The association of high-strain zones and granitic rocks of inferred Late Paleocene to Early Eocene age leads us to suggest that granitic rocks were instrumental in localizing high-strain zones during extension.

Farther west, deeper in the structural section, thin zones of mylonite (1-2 m) occur discontinuously along the Abbott Creek forest service road (Fig. 2-6, bottom left). Due to limited exposure, the extent of these high-strain zones is uncertain.

Farther north, a few kilometres east of Armstrong, exposures of mylonitic calcareous quartzite of the Chase Formation and muscovite-bearing granite occur along the south slope of Fortune Creek. The relationship of these mylonitic rocks to the strained rocks on the Abbott Creek forest service road and to the mylonite zone exposed near Swan Lake is not clear.

Trinity Hills area

The contact between infrastructure and superstructure was constrained to within several hundred metres near the Trinity Hills outlier of Middle Eocene volcanic and sedimentary rocks. At this locality, greenschist to lower amphibolite-facies metavolcanic rocks occur west of the contact, whereas upper amphibolite-facies to lower granulite-facies migmatitic pelitic schist, calcareous quartzite, and strained granitic rocks occur to the northeast. Map patterns indicate that the northern margin of the outlier overlaps the contact (Fig. 2-2, centre). Clast types within a poorly sorted, polymictic conglomerate, the lowest unit within the outlier, match the underlying rock units (Thompson and Glombick 2004*b*). No strain is apparent at the base of the outlier. Hence, as near Kalamalka Lake, Middle Eocene rocks are interpreted to lie unconformably above mylonitic schist and gneiss, and therefore could not be situated within the upper plate of a detachment.

To the southeast, a transition between greenschist-facies rocks and sillimanite-grade rocks is evident in scattered outcrops between the Trinity Hills and the Bobby Burns Mountain outliers (Fig. 2-2). Although exposure is poor, metamorphic grade increases progressively from west to east. Mylonitic granite that occurs near the sillimanite-in isograd, with well-developed C-S fabric recording top to the west shear-sense, has been dated at between 60 and 56 Ma (U-Pb zircon; Bardoux 1993; Vanderhaeghe et al. 1999). These data constrain the deformation of the granite as older than 48 Ma, the oldest undeformed volcanic rocks (Breitsprecher 1998), and younger than 60 Ma, the granite crystallization age. Thin zones of mylonite occur within rocks of the infrastructure along the western margin of the Trinity hills outlier, adjacent to Mabel Lake.

Silver Hills area

Southwest of Mabel Lake, in the Silver Hills, dark-grey, carbonaceous siliciclastic rocks and minor dark grey limestone of inferred Late Triassic age (Slocan Group) directly overlie rocks of the Chase and Silver Creek formations (Fig. 2-2; Thompson and Daughtry 2000; Thompson and Glombick 2004*a*). Detailed metamorphic or isotopic data have not been collected, but a dark grey, fine-grained siliceous unit, inferred to belong to the Slocan Group, truncates map patterns of the underlying Silver Creek and Chase formations (Fig. 2-2), consistent with either a low-angle fault or a transposed unconformity. In several localities, the contact between the carbonaceous, fine-grained, siliceous unit and underlying calcareous quartzite was constrained to within tens of metres. No strain is evident. It is not clear whether the apparent contrast in metamorphic grade results from a change in bulk composition, from a pelitic to a dominantly quartz-rich protolith, or from a structural and (or) metamorphic break. Due to the lack of isotopic age data, it is not clear where the infrastructure-superstructure contact is located, and whether it corresponds with the mapped base of the Slocan Group in this area (Fig. 2-2).

Vidler Ridge-Pinnacles area

The region southeast of Sugar Lake is underlain by a north-tapering salient of superstructure, bounded on the northwest by the Cherry fault, and on the northeast by the Beaven fault (Figs. 2-2, 2-8). The Cherry fault is inferred, from map unit offsets, to be a north-northeast striking (030°), east-southeast dipping (70-90°), east side down normal fault. The Beaven fault, where it is exposed on Vidler Ridge and near Cherry Creek, is characterized by 10-20 m of fractured rock and fault breccia (Carr 1990; this study). The Beaven fault strikes north-northwest (020°) and dips moderately to steeply west-southwest (60-80°; Fig. 2-8). It juxtaposes greenschist-facies (biotite grade) Slocan Group strata against amphibolite-facies rocks (staurolite-kyanite grade) of the Chase, Silver Creek, (and Tsalkom?) formations. The Beaven fault dies out approximately 5 km north of Sugar Lake, suggesting that it does not have significant displacement at this latitude (Fig. 2-8).

Near the northern margin of the salient, between Cherry and Vidler ridges, a transition from biotite-grade rocks of the Slocan Group to sillimanite-grade rocks occurs over a horizontal distance of approximately 2 km (Fig. 2-8). Transposed bedding and metamorphic foliation dip moderately to steeply (40°-80°) to the north and the existence of one or several faults cannot be ruled out due to poor exposure.

A progressive increase in metamorphic grade, from staurolite-kyanite to sillimanite-potassium-feldspar, also occurs over a horizontal distance of less than 2 km within the footwall of

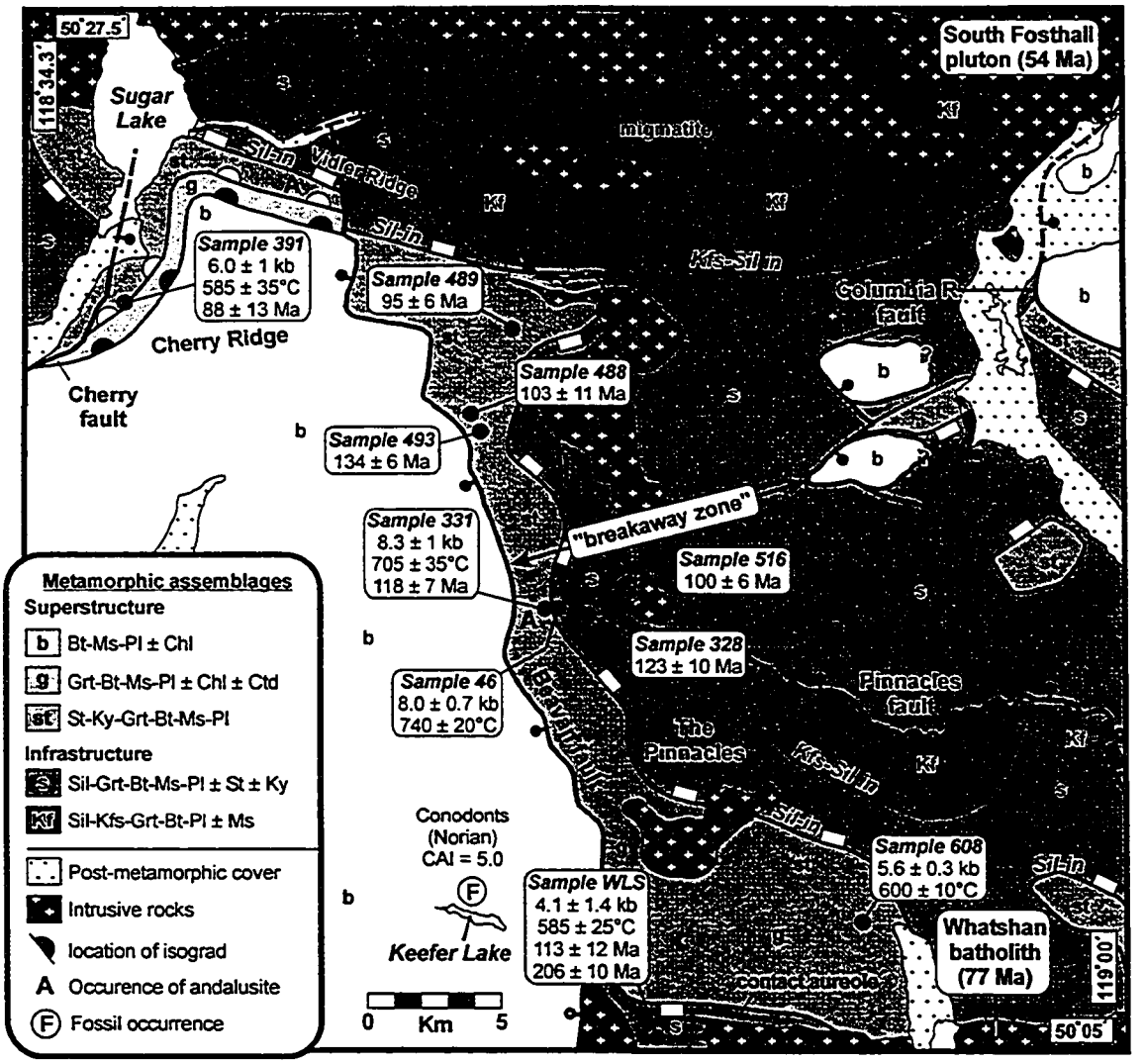

Fig. 2-8. Metamorphic map of the Vidler Ridge and Pinnacles areas, showing the distribution of mineral isograds in pelitic rocks. *Mineral isograd symbols*: open half-circles - garnet-in; filled half-circles - staurolite-in; open rectangles - sillimanite-in; filled rectangles - second sillimanite isograd. Note the distance between the Beaven fault and the Slocan Group outliers (center) and the closely-spaced isograds south of Vidler Ridge (upper left). The location of metamorphic isograds is modified from Reesor and Moore (1971), Carr (1990), and this study (Chapter 4).

the Beaven fault, on the south flank of Vidler Ridge (Fig. 2-8). Metamorphic foliation and compositional layering dip steeply (70°-90°) to the southwest or northeast. South of Vidler Ridge, the sillimanite-in isograd strikes south, flanking the western margin of the Pinnacles Peaks, then strikes eastward towards Whatshan Lake (Fig. 2-8).

A transposition foliation present within the footwall of the Beaven fault is tightly to isoclinally folded. A stretching lineation was not observed. Prismatic grains of amphibole and staurolite are oriented randomly on the foliation surface. Some porphyroblasts (garnet and staurolite) commonly have quartz-filled pressure shadows. Evidence of non-coaxial strain was not seen in outcrop or in thin section and no high-strain zones were observed.

Continuity of the superstructure: Okanagan Valley to Whatshan Lake

Between the Okanagan Valley and Whatshan Lake, the superstructure forms a nearly continuous cover of greenschist-facies rocks, overlying the amphibolite-facies infrastructure (Fig. 2-2). Metamorphic grade within the superstructure is consistent; pelitic rocks are dominantly at biotite grade, although garnet-grade was reached locally. Conodonts recovered from three localities in the superstructure have yielded CAI values of 5.0 to 5.5, compatible with peak temperatures of approximately 440°C (Harris 1979; Rejebian et al. 1987). Rocks in the superstructure cooled below 250°C by the late Cretaceous (e.g., Mathews 1981).

Steep to moderately dipping normal faults that cut the superstructure in the Vernon area also cut the underlying infrastructure (Fig. 2-2). The faults are, in places, overlapped by Middle Eocene volcanic rocks (e.g., Camel's Hump, Trinity Hills), while in other places they offset them (e.g., Enderby Cliffs). The faults thus appear to be synchronous with, or post-date, Middle Eocene volcanism (see also Lorencak et al. 2001). No internal thinning of the superstructure is apparent, such as through domino-style, parallel normal faulting. Structures within the superstructure are instead suggestive of horizontal shortening; they include mesoscopic upright chevron folds and crenulations which are likely Middle Jurassic in age (see Parrish 1995).

At the regional scale, the superstructure is nearly continuous as a map unit from the Okanagan Valley to Whatshan Lake. In the absence of significant internal thinning, a maximum amount of superstructure extension is provided by the exposure gaps in the belt. Such an estimate does not consider the effects of post-Eocene erosion (e.g., Heller et al. 1987), which would further reduce it. There is an exposure gap of approximately 10 km between the Mabel and Cherry faults (Fig. 2-2). The presence of superstructure in the hanging wall of these steep faults shows that the superstructure was continuous prior to faulting and has been eroded; the possible

horizontal extension is thus negligible at a regional scale. This conclusion is further supported by the occurrence of an outlier of greenschist-facies rocks to the north, in the Silver Hills (Fig. 2-2).

A gap of 12 km exists between the trace of the Beaven fault and two erosional outliers of Slocan Group rocks near the eastern margin of the SMC in the Pinnacles area (Fig. 2-8; see Read and Brown 1981; Lemieux et al. 2004). The base of the outliers has been interpreted as a flat section of the Columbia River fault zone (Read and Brown 1981; Carr 1990), or, alternatively, as an unconformity (Lemieux et al. 2004). The 12 km gap has been interpreted as the locus of a "breakaway zone" between the west-dipping Okanagan Valley-Eagle River fault system on the west and the east-dipping Columbia River fault zone on the east (Fig. 2-8; Carr 1990; Bardoux 1993). The present distance represents a maximum possible amount of extension of the superstructure, and it does not take into account any removal of superstructure by post-Eocene erosion. We conclude that, given the limited heave on steep normal faults of probable Middle Eocene age and the contribution of post-Eocene erosion to widening the resulting gaps, extension was minimal and the superstructure was essentially continuous from the Okanagan Valley eastward to at least the Beaven fault during the Late Paleocene to Early Eocene.

Discussion

Implications of superstructure continuity

Proposed estimates of displacement on Okanagan Valley-Eagle River detachment fault system are: 32 km (Sicamous area, Johnson and Brown 1996), 45 to 70 km (Kelowna area, Bardoux 1993), and 60 to 90 km (Penticton area, Tempelman-Kluit and Parkinson 1986). Our mapping of the superstructure in the Vernon area (Fig. 2-2) can be used to test these estimates.

The exposure gap in the superstructure between the proposed Okanagan Valley fault system (the Beaven fault), and the oppositely-dipping Columbia River fault is on the order of 12 km. Restoration of either the above displacements on the Okanagan Valley fault, and of 20 to 30 km of proposed top to the east displacement on the Columbia River fault (e.g., Parrish et al. 1988; Carr 1990; Bardoux 1993), causes the restored traces of the faults to overlap, by an amount between 40 and 100 km. Such an overlap is inconsistent with the observed maximum separation (~12 km), even assuming negligible post-Eocene erosion.

The proposed displacements could be accommodated if the superstructure had been internally thinned, for example, by a series of normal faults rooting into a master detachment at the base of the superstructure (Fig. 2-9*a*). That interpretation, however, is not compatible with the new mapping data (Fig. 2-2): normal faults are not confined to the superstructure, as they cut both superstructure and infrastructure (i.e., they are too young).

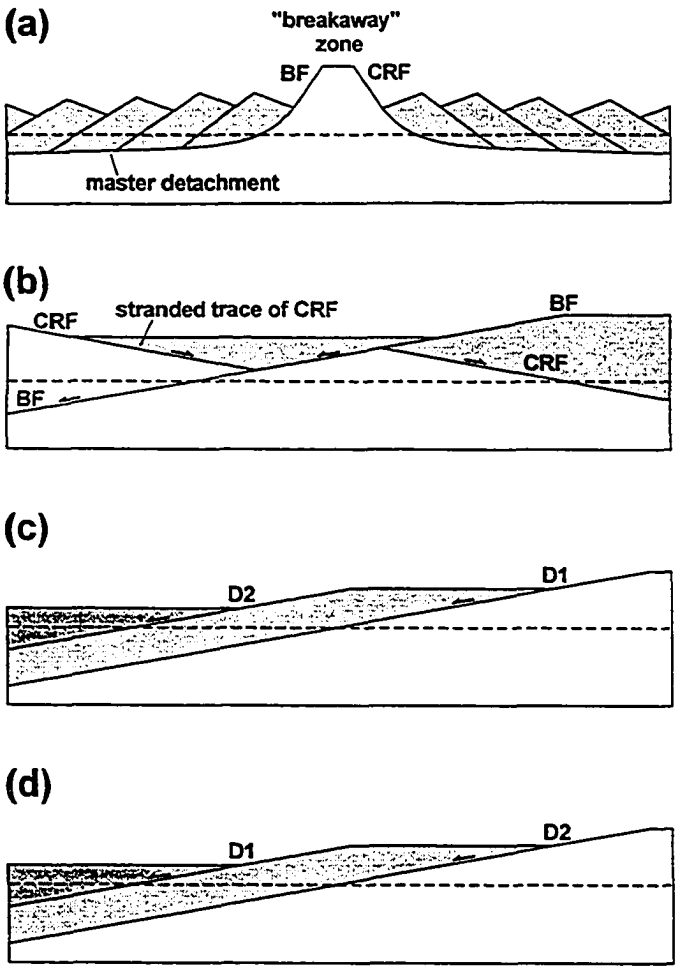

Fig. 2-9. Schematic two-dimensional block diagrams illustrating possible extension fault geometries. (a) Internal thinning of the suprastructure by domino-style faulting. Note that faults root into a basal detachment fault. (b) Oppositely-dipping extension faults active at different times. In this case, displacement on the CRF pre-dates displacement on the BF, stranding the trace of the CRF in the upper plate of the BF, where it should be exposed, unless the erosion level is deep enough to remove it (dashed horizontal line). (c) Detachment faults step up, into the upper plate, with time. (d) Detachment fault steps down, into the lower plate, with time. See text for discussion. *Faults*: BF - Beaven; CRF - Columbia River; D1 - first (oldest) detachment; D2 - second (younger) detachment.

A second possibility is that the proposed Columbia River and Okanagan Valley-Eagle River faults (Beaven fault on Fig. 2-2) were active at different times (e.g., Parrish et al. 1988). Geochronological data, however, show that shearing attributed to displacement on the Okanagan Valley and Columbia River faults was synchronous between 56 and 55 Ma (Carr 1992; Johnson 1994). Supposing that motion on the Columbia River fault, as Parrish et al. (1988) suggested, had preceded that on the Okanagan Valley fault, then a section of the Columbia River fault would be stranded in the upper plate of the younger Okanagan Valley fault, and would be recognizable today, unless it was eroded. The preservation of superstructure in the Vernon area does not support a deep erosion level, and field evidence of a stranded Columbia River fault is lacking (Fig. 2-9*b*).

A third possibility is that multiple generations of detachment faults are present, with successive detachments having either stepped up into the hanging wall with time (Fig. 2-9*c*), or down, into the footwall (cf. Lister and Davis 1989). As shown by the new mapping, however, extensional shear zones of only limited extent occur near the infrastructure-superstructure contact. There is little evidence that a regionally extensive detachment, consistently separating infrastructure from superstructure, was subsequently abandoned during the formation of deeper or shallower master detachment faults (Fig. 2-2).

We conclude, therefore, that previous estimates of displacement on an Okanagan Valley fault are incompatible with the continuity and internal structure of the superstructure in the Vernon area.

Late Paleocene to Middle Eocene exhumation of the infrastructure

To understand the tectonic significance of gently dipping Late Paleocene to Early Eocene extensional shear zones near Vernon, we require an estimate of how much exhumation occurred during this period.

The contrast in peak metamorphic conditions between infrastructure and superstructure, recorded by both mineral assemblages and thermobarometry, cannot be used to estimate the amount of infrastructure exhumation because metamorphism was diachronous, both regionally and with respect to structural level. For instance, U-Pb data from the Vernon area show that the superstructure attained peak metamorphic conditions in the Middle Jurassic (ca. 171 Ma), but the infrastructure experienced an episodic and complex thermal evolution, with high-grade events (sufficient to produce migmatite) in the Middle to Late Jurassic (160-150 Ma) and the Early to Late Cretaceous (100-90 Ma; Chapters 3 and 4).

It has been suggested that Late Paleocene to Middle Eocene K-Ar and $^{40}Ar/^{39}Ar$ dates (hornblende and mica) from infrastructure rocks in the Vernon area indicate rapid exhumation (Mathews 1981; Carr 1990; Vanderhaeghe et al. 2003). The data, however, only yield information about the cooling history of the rocks, and do not provide direct information about their burial depth. For example, the infrastructure is permeated with granitic intrusions of Late Paleocene to Middle Eocene age. These granites likely formed deeper in the crust before rising and crystallizing at shallower crustal levels (e.g., Holk and Taylor 1997). They would have raised the local geothermal gradient in two ways: (1) from heat advected by melt from deeper structural levels; and (2) from the heat supplied by crystallization of minerals from the melt. Continued regional high heat flow in the region during the Middle Eocene is indicated by widespread intrusive and volcanic activity (e.g., Mathews 1981; Parrish et al. 1988; Bardoux 1993). Hence, K-Ar cooling dates from the infrastructure do not constrain the amount of exhumation (relative to a fixed elevation), but indicate only when the rocks cooled from above 500°C to below 250°C. The K-Ar data from the Vernon area are consistent with: (1) rapid exhumation by erosion and (or) faulting, or (2) a widespread early Tertiary thermal event with a high geothermal gradient; or (3) a combination of these.

Both the superstructure and infrastructure are depositionally overlain by Middle Eocene rocks (~45 Ma); therefore, both were at surface at that time. If the infrastructure was at temperatures of approximately 500°C at 60 Ma (Mathews 1981; Vanderhaeghe et al. 2003), and the geothermal gradient was 35°C/km (consistent, for example, with present heat flow within the Cascadia back-arc; e.g., Currie 2004), then approximately 15 km of exhumation occurred between 60 and 45 Ma (1 km/ma). If a higher geothermal gradient of 50°C/km is assumed (e.g., Holder et al. 1990), then 10 km of exhumation occurred (0.67 km/ma). As the erosion rate of the hinterland during this interval is not known, it is unclear how much exhumation occurred by erosion, and how much was due to tectonic processes.

It is not certain, however, that the K-Ar data accurately reflect the cooling of the infrastructure, and their significance may thus be limited. In the Thor-Odin culmination of the southern Monashee complex (Fig. 2), Kuiper (2003) reported an empirical correlation between $^{40}Ar/^{39}Ar$ dates from hornblende and depletion in whole-rock $\delta^{18}O$ and hornblende δD values. She suggested that hornblende yielding $^{40}Ar/^{39}Ar$ dates younger than 75 Ma, which had previously been interpreted as cooling dates, experienced Ar-loss due to meteoric fluids ca. 50 Ma. Potassium-argon and $^{40}Ar/^{39}Ar$ dates from the Vernon area, which are primarily from the Trinity Hills area, near a sheared portion of the infrastructure-superstructure contact, may be influenced by such Ar-loss due to meteoric water circulating along shear zones (cf. Holk and Taylor 1997;

Fayon et al. 2004). Given the widespread Late Paleocene to Middle Eocene igneous event that affected the infrastructure and the possible Ar loss in other areas of the SMC, we conclude that amounts of exhumation estimated using K-Ar data and assumed geothermal gradients are potentially unreliable as indicators of rapid and significant exhumation.

The role of gently dipping Late Paleocene to Early Eocene ductile shear zones in exhumation and core complex formation

A comparison of the diffuse shear zones that occur in the Vernon area with the detachment faults bounding core complexes in the southwest United States reveals significant differences. Most conspicuous is the lack (in the Vernon area) of a regionally extensive, gently dipping master detachment separating infrastructure from superstructure. There are many examples of subhorizontal, regionally extensive, detachments separating high-grade mylonitic rocks (lower plate) from lower grade or unmetamorphosed rocks (upper plate) (e.g., Lister and Davis 1989; Davis et al. 2004; Braathen and Osmundsen 2004). Such a structure has not been found in the Vernon area: shear zones instead are discontinuous, have diffuse boundaries, and generally lack a brittle overprint.

It is possible that the various shear zones that occur in the Vernon area represent part of a detachment system deeper than the brittle-ductile transition. That interpretation, however, is inconsistent with several observations. First, the Silver Star shear zone separates superstructure from infrastructure, or low-grade from high-grade rocks, and therefore cannot have developed deep in the crust, below the brittle-ductile transition, because the upper plate was at a temperature of less than ~250°C when displacement occurred in the Late Paleocene to Eocene (Vanderhaeghe et al. 1999). Second, the shear zones are discontinuous, and none have been observed east of the Trinity Hills. Third, it has been stated, "The fundamental observation [of detachment faults] is that upper crustal faults either merge with, or are truncated by, the detachments." (Wernicke 1992, p. 557); that statement is not consistent with Vernon area map patterns, where normal faults cut both the superstructure and the infrastructure, as well as the shear zones developed locally between them. Fourth, it has also been stated that "The field observation most significant to the new conceptual framework [of Cenozoic extensional tectonism in the Cordillera] is the widespread occurrence of large subhorizontal faults...across which stratigraphic or structural succession is omitted..." (Wernicke 1992, p. 557). In the study area, the regional contact between infrastructure and superstructure (Figs. 2-2, 2-3) is essentially parallel to the underlying Chase Formation for approximately 85 km along the trend of the stretching lineation (100°/03°) – i.e. it does not cut across stratigraphic section for at least 85 km. Supposing an original dip of 30° to the

west of a hypothetical detachment fault (e.g., Johnson and Brown, 1996), later rotation to the present near horizontal is implied; western parts of the rotated upper plate should reflect progressively increasing burial (~40 km). Because metamorphic grade is uniformly low across the belt of superstructure, the interpretation of a rotated detachment is unlikely.

Thus, on the basis of all observations of gently dipping Late Paleocene to Early Eocene ductile shear zones within the study area, we conclude that they are not parts of a master detachment fault system, that would have exhumed the infrastructure by tectonically removing or "stripping" the superstructure. An alternative mechanism is needed to account for exhumation of the infrastructure between the times of peak metamorphism in the Cretaceous and the Middle Eocene.

Late Cretaceous to Early Eocene regional-scale channel flow of the middle crust in the southeast Canadian Cordillera?

Geochronological and metamorphic data have led to the suggestion that the metamorphic hinterland of the southern Canadian Cordillera was the locus of a crustal welt, or plateau, that was 50 to 60 km thick in the Late Cretaceous, prior to Paleocene collapse (e.g., Coney and Harms 1984; Parrish et al. 1988; Teyssier et al. 2005). Lowe and Ranalli (1993) constructed 1-D paleorheological profiles through the Cordillera. They suggested that, during the mid-Cretaceous to Paleocene, elevated temperatures in the hinterland (see also Spear and Parrish 1996; Lui and Furlong 1993) resulted in a three-layer (partially molten) rheologically layered crust consisting of a strong upper crust above 8 km depth, a weak middle crust between 8 and 30 km, and a relatively strong lower crust (the "dry" core gneiss of the Monashee complex). Recent evidence supporting this model includes preservation of Proterozoic fabric at deep structural levels of the northern Monashee complex, suggesting that Cordilleran tectonism was restricted to the upper and middle crust and the highest structural levels of the Monashee complex (Crowley et al. 2001). Structural, geochronological, and metamorphic data, as well as rheological modelling, suggest that during the Paleocene the melt-rich and hot middle crust (~8-30 km depth) had little strength compared to the superstructure (Lowe and Ranalli 1993; Lui and Furlong 1993; Vanderhaeghe and Teyssier 1997) and the underlying Monashee core gneiss (Crowley et al. 2001; Spark 2002).

Late Paleocene to Early Eocene granitic rocks within the infrastructure display shallowly plunging, east or west-trending stretching lineations. These fabrics are particularly well developed near the underlying Monashee complex (e.g., Reesor and Moore 1971; Journeay and Brown 1986; Spark 2002), and near the overlying superstructure, (i.e., at the upper and lower boundaries of the infrastructure (Fig. 2-10; see also Parrish et al. 1988). Paleocene granitic rocks

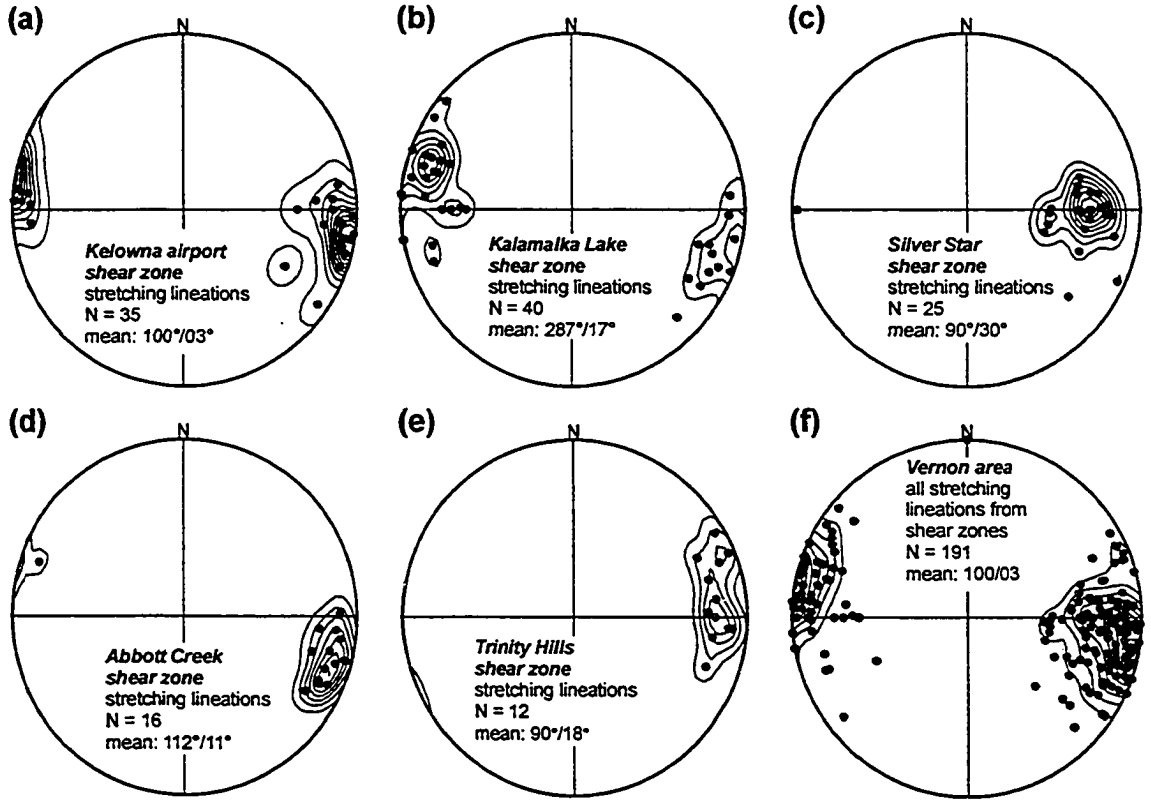

Fig. 2-10. Stretching lineations measured from gently-dipping, Late Paleocene to Early Eocene ductile shear zones plotted on equal-area, lower hemisphere projections. (a) Kelowna airport shear zone (Fig. 2-4). (b) Kalamalka Lake shear zone (Fig. 2-4). (c) Silver Star shear zone (Fig. 2-6). (d) Abbott Creek shear zone (Fig. 2-6). (e) Trinity Hills shear zone (Fig. 2-2). (f) Summary diagram showing all stretching lineations measured from early Tertiary low-angle shear zones exposed in the Vernon area. Contour intervals correspond to 0, 3, 6, 9, 12, 15, 18, 21, 24 % points per unit area. Regional variations in the mean orientation of the stretching lineation result, in part, from rotation resulting from Middle Eocene normal faulting.

(64.3 ± 0.3 Ma; U-Pb zircon) with moderately plunging, west-trending stretching lineation (288°/39°) occur in the Nicola Horst, a fault bounded uplift of amphibolite-facies rocks surrounded by greenschist-facies rocks of the Late Triassic Nicola Group, located approximately 80 km west of Vernon (Erdmer et al. 2002). The exposure of a Paleocene stretching fabric 80 km to the west of the SMC supports the notion that ductile flow of a partially molten, low viscosity middle crust was a regional-scale process, occurring across at least 200 km of the southern Canadian Cordillera during the Paleocene, beneath a thin (8-10 km) superstructure (see also Johnston et al. 2000; Kuiper 2003; Williams and Jiang 2005). Hence, the area of thickened crust (50-60 km) prior to orogenic collapse may have been broad across strike (Glombick et al. 2002; Teyssier et al. 2005).

We propose that a component of infrastructure exhumation occurred by ductile flow and thinning of a partially molten mid-crustal layer approximately 20 km thick. This process may have begun as early as the Cretaceous (Wells et al. 1990; Scammell 1993; Applegate and Hodges 1995), and may have accelerated during the Late Paleocene to Early Eocene as widespread partial melting of the middle crust (Vanderhaeghe and Teyssier 1997; Holk and Taylor 1997) drastically decreased its mechanical strength, forming a low viscosity, mid-crustal layer, or a channel (cf. Beaumont et al. 2004). Teyssier et al. (2005) have inferred mid-crustal flow in the Vernon area from anisotropy of magnetic susceptibility (AMS) and kinematic data in Late Paleocene to Early Eocene granitic rocks. They identified a zone of vergence reversal within the infrastructure, from top to the west shear west of Sugar Mountain, to dominantly coaxial deformation near Sugar Mountain, and to top to the east shear east of it. This kinematic pattern, which can account for the lack of non-coaxial strain observed in the Vidler Ridge-Pinnacles area in this study, is compatible with thinning and flow of the upper and middle crust away from the Sugar Mountain area, would have resulted in the exhumation and doming of the underlying Thor-Odin culmination of the Monashee complex (see also, Spark 2002). Such flow patterns can be produced by variation of a channel flow model, and this has been proposed for the exhumation of the Himalayan gneiss domes, such as the Kangmar and Mabja gneiss domes (Beaumont et al. 2004, their Fig. 12e).

We conclude that gently-dipping, Late Paleocene to Early Eocene extensional shear zones exposed in the study area are not crustal-scale, large-displacement detachment faults that removed the superstructure, but rather, discontinuous subhorizontal extensional shear zones that developed during differential displacement along a rheological interface between a rigid upper crust (superstructure) and a partially molten, "fluid" mid-crustal layer (infrastructure) that flowed in response to lateral pressure gradients during orogenic collapse (e.g., Wernicke 1990). The spatial association of Late Paleocene to Early Eocene granitic rocks and gently dipping shear

zones near Vernon (Vanderhaeghe and Teyssier 1997; this study) and elsewhere within the SMC (Valkyr shear zone; Simony and Carr 1997), leads us to suggest that granitic rocks localized ductile deformation during crustal flow. That interpretation is consistent with the hypothesis that low-angle faults can form if flow in the middle crust (e.g., Westaway 1998, see also Melosh 1990; Parsons and Thompson 1993). The transition between infrastructure and superstructure in the study area would represent the upper limit of crustal flow in the Late Paleocene to Early Eocene, within a partially molten, low viscosity channel (cf. Beaumont et al. 2004). Because the gently-dipping ductile shear zones exposed along the western margin of the SMC near Vernon are not crustal-scale extensional shears, they may be shear zones that formed along a transient, subhorizontal paleorheological boundary controlled by the structural level to which abundant Late Paleocene to Early Eocene granitic rocks rose within the crust.

References

Applegate, J.D.R., and Hodges, K.V. 1995. Mesozoic and Cenozoic extension recorded by metamorphic rocks in the Funeral Mountains, California. Geological Society of America Bulletin, **107**: 1063-1076.

Bardoux, M. 1986. Characteristics of the Okanagan Valley shear zone around Kelowna, south-central British Columbia. *In* Program with Abstracts, Geological Association of Canada, v. 11, p 43.

Bardoux, M. 1993. The Okanagan Valley fault from Penticton to Enderby, south-central British Columbia. Ph.D. thesis, Carleton University, Ottawa.

Beaumont, C., Jamieson, R.A., Nguyen, M.H., and Medvedev, S. 2004. Crustal channel flows: 1. Numerical models with applications to the tectonic of the Himalayan-Tibetan orogen. Journal of Geophysical Research, **109**: B06406.

Braathen, A., and Osmundsen, P.T. 2004. Dynamic development of fault rocks in a crustal-scale detachment: an example from Norway. Tectonics, **23**: TC4010, doi:1029/2003TC001558.

Breitsprecher, K. 1998. Volcanic stratigraphy, petrology and tectonic setting of the eastern margin of the Eocene Kamloops Group, south-central British Columbia. M.Sc. Thesis, Simon Fraser University, Vancouver.

Brown, R.L., Journeay, J.M., Lane, L.S., Murphy, D.C., and Rees, C. 1986. Obduction, backfolding and piggyback thrusting in the metamorphic hinterland of the southeast Canadian Cordillera. Journal of Structural Geology, **8**: 255-268.

Carr, S.D. 1990. Late Cretaceous-early Tertiary tectonic evolution of the southern Omineca Belt, Canadian Cordillera. Ph.D. thesis, Carleton University, Ottawa.

Carr, S.D. 1992. Tectonic setting and U-Pb geochronology of the early Tertiary Ladybird leucogranite suite, Thor-Odin-Pinnacles area, southern Omineca Belt, British Columbia. Tectonics **11**: 258-278.

Carr, S.D., Parrish, R.R., and Brown, R.L. 1987. Eocene structural development of the Valhalla complex, southeastern British Columbia. Tectonics, **6**: 175-196.

Coney, P.B., and Harms, T.A. 1984. Cordilleran metamorphic core complexes: Cenozoic extensional relics of Mesozoic compression. Geology, **12**: 550-554.

Cook, F.A., Varsek, J.L., Clowes, R.M., Kanasewich, E.R., Spencer, C.S., Parrish, R.R., Brown, R.L., Carr, S.D., Johnson, B.J., and Price, R.A. 1992. Lithoprobe crustal reflection cross section on the southern Canadian Cordillera, 1, Foreland Thrust and Fold Belt to Fraser River fault. Tectonics, **11**: 12-35.

Crowley, J.L., Ghent, E.D., Carr, S.D., Simony, P.S., and Hamilton, M.A. 2000. Multiple thermotectonic events in a continuous metamorphic sequence, Mica Creek area, southeastern Canadian Cordillera: Geological Materials Research, **2**: 1-45.

Crowley, J.L., Brown, R.L., and Parrish, R.R. 2001. Diachronous deformation and a strain gradient beneath the Selkirk allochthon, northern Monashee complex, southeastern Canadian Cordillera. Journal of Structural Geology **23**: 1103-1121.

Currie, C. A. 2004. The thermal structure of subduction zones and backarcs. Unpublished PhD dissertation, University of Victoria.

Daughtry, K.L., and Thompson, R.I. 2004*a*. Geology of the Shorts Creek map area, British Columbia (NTS 82L/04). Geological Survey of Canada Open File 4373, scale 1:50 000.

Daughtry, K.L., and Thompson, R.I. 2004*b*. Geology of the Westwold map area, British Columbia (NTS 82L/05). Geological Survey of Canada Open File 4374, scale 1:50 000.

Davis, G.H., Constenius, K.N., Dickinson, W.R., Rodríguez, E.P., and Cox, L.J. 2004. Fault and fault-rock characteristics associated with Cenozoic extension and core-complex evolution in the Catalina-Rincon region, southeastern Arizona. Geological Society of America Bulletin, **116**: 128-141.

Erdmer, P., Thompson R.I., and Daughtry, K.L. 1998. The Kalamalka Lake metamorphic assemblage, tectonic infrastructure in the Vernon map area, British Columbia. *In* Current Research 1998-A. Geological Survey of Canada, pp. 189-194.

Erdmer, P., Thompson, R.I., and Daughtry, K.L. 1999. Pericratonic Paleozoic succession in Vernon and Ashcroft map areas, British Columbia. *In* Current Research 1999-A. Geological Survey of Canada, pp. 205-215.

Erdmer, P., Heaman, L., Creaser, R.A., Thompson, R.I., and Daughtry, K.L. 2001. Eocambrian granite clasts in southern British Columbia shed light on Cordilleran hinterland crust. Canadian Journal of Earth Sciences, **38**: 1007-1016.

Erdmer, P., Moore, J.M., Heaman, L., Thompson, R.I., Daughtry, K.L., and Creaser, R.A. 2002. Extending the ancient margin outboard in the Canadian Cordillera: record of Proterozoic crust and Paleocene regional metamorphism in the Nicola horst, southern British Columbia. Canadian Journal of Earth Sciences, **39**: 1605-1623.

Fayon, A., Mulch, A., Teyssier, C., Person, M., and Vanderhaeghe, O. 2004. Fluid flow and heat transfer during exhumation of metamorphic core complexes. *In* Abstracts with Programs, Geological Society of America, 2002 annual meeting.

Glombick, P., and Thompson, R.I. 2004. Geology of the Creighton Creek map area, British Columbia (NTS 82L/02). Geological Survey of Canada Open File 4371, scale 1:50 000.

Glombick, P., Erdmer, P., Thompson, R.I., and Daughtry, K.L. 1999. Ductile shear zones and an Eocene unconformity between Kalamalka Lake and Oyama Lake, Vernon map area, British Columbia. *In* Current Research 1999-A. Geological Survey of Canada, pp. 193-198.

Glombick, P., Erdmer, P., Thompson, R.I., and Daughtry, K.L. 2000. Geology of the Oyama map sheet, Vernon map area, British Columbia. *In* Current Research 2000-A. Geological Survey of Canada.

Glombick, P., Thompson, R.I., and Erdmer, P. 2002. The role of a melt-rich middle crust layer in core complex formation; evidence from the Shuswap metamorphic complex, south-central British Columbia. *In* Abstracts with Programs, Geological Society of America, 2002 annual meeting, p. 109.

Glombick, P., Thompson, R.I., and Daughtry, K.L. 2004. Geology of the Oyama map area, British Columbia (NTS 82L/03). Geological Survey of Canada Open File 4372, scale 1:50 000.

Hanmer, S., and Passchier, C. 1991. Shear-sense indicators: a review. Geological Survey of Canada, Paper 90-17.

Harris, A.G. 1979. Conodont color alteration, an organo-mineral metamorphic index, and its application to Appalachian basin geology. *In* SEPM Special Publication No. 26, pp. 3-16.

Heaman, L.M., Erdmer, P., Thompson, R.I., and Daughtry, K.L. 1999. Preliminary U-Pb geochronology results from the Vernon area, British Columbia. *In* Proceedings, Lithoprobe Report No. 69: Cordilleran Tectonics Workshop, Calgary, Alberta, pp. 196-201.

Heller, P.L., Tabor, R.W., and Suczeck, C.A. 1987. Paleogeographic evolution of the Unites States Pacific northwest during Paleogene time. Canadian Journal of Earth Sciences, **24**: 1652-1667.

Holder, G.A.M., Holder, R.W., and Carlson, D.H. 1990. Middle Eocene dike swarms and their relation to contemporaneous plutonism, volcanism, core-complex mylonitization, and graben subsidence, Okanogan Highlands, Washington. Geology, **18**: 1082-1085.

Holk, G.J., and Taylor, H.P. Jr. 1997. $^{18}O/^{16}O$ homogenization of the middle crust during anatexis: the Thor-Odin metamorphic core complex, British Columbia. Geology, **25**: 31-34.

Johnson, B.J. 1994. Structure and tectonic setting of the Okanagan Valley fault system in the Shuswap Lake area, southern British Columbia. Unpublished Ph.D. thesis, Carleton University, Ottawa.

Johnson, B.J., and Brown, R.L. 1996. Crustal structure and early Tertiary extensional tectonics of the Omineca belt at 51°N latitude, southern Canadian Cordillera. Canadian Journal of Earth Sciences, **33**: 1596-1611.

Johnston, D.H., Williams, P.F., Brown, R.L., Crowley, J.L., and Carr, S.D. 2000. Northeastward extrusion and extensional exhumation of crystalline rocks of the Monashee complex, southeastern Canadian Cordillera. Journal of Structural Geology, **22**: 603-625.

Jones, A.G. 1959. Vernon map area, British Columbia. Geological Survey of Canada, Memoir 296.

Journeay, J.M., and Brown, R.L. 1986. Major tectonic boundaries of the Omineca belt in southern British Columbia: a progress report. *In* Current Research, Part A. Geological Survey of Canada Paper 86-1A, pp. 81-88.

Kuiper, Y. 2003. Geochronological, petrological and microstructural studies on the Thor-Odin dome, Monashee complex, southern Canadian Cordillera. Ph.D. thesis, University of New Brunswick, Fredericton.

Kretz, R. 1983. Symbols for rock-forming minerals. American Mineralogist, **68**: 277-279.

Lemieux, Y., Thompson, R.I., and Erdmer, P. 2003. Stratigraphy and structure of the Upper Arrow Lake area, southeastern British Columbia: new perspectives for the Columbia River fault zone. *In* Current Research 2003, Geological Survey of Canada, 2003-A7.

Lemieux, Y., Thompson, R.I., and Erdmer, P. 2004. Stratigraphic and structural relations across the Columbia River fault zone, Vernon and Lardeau map-areas. *In* Current Research, Geological Survey of Canada, 2004-A3.

Lister, G.S., and Davis, G.A. 1989. The origin of metamorphic core complexes and detachment faults during Tertiary continental extension in the northern Colorado River Region, U.S.A. Journal of Structural Geology, **11**: 65-94.

Lorencak, M., Seward, D., Vanderhaeghe, O., Teyssier, C., and Burg, J.P. 2001. Low-temperature cooling history of the Shuswap metamorphic core complex, British Columbia: constraints from apatite and zircon fission-track ages. Canadian Journal of Earth Sciences, **38**: 1615-1625.

Lowe, C., and Ranalli, G. 1993. Density, temperature, and rheological models for the southeastern Canadian Cordillera: implications for its geodynamic evolution. Canadian Journal of Earth Science, **30**: 77-93.

Lui, M., and Furlong, K. 1993. Crustal shortening and Eocene extension in the southeastern Canadian Cordillera: some thermal and rheological considerations. Tectonics, **12**: 776-786.

Mathews, W.H. 1981. Early Cenozoic resetting of potassium-argon dates and geothermal history of north Okanagan area, British Columbia. Canadian Journal of Earth Sciences, **18**: 1310-1319.

Melosh, H.J. 1990. Mechanical basis for low-angle normal faulting in the Basin and Range province. Nature, **343**: 331-335.

Monger, J.W.H., Wheeler, J.O., Tipper, H.W., Gabrielse, H., Harms, T., Struick, L.C., Campbell, R.B., Dodds, C.J., Gehrels, G.E., and O'Brien, J. 1991. Upper Devonian to Middle Jurassic assemblages. Part B. Cordilleran terranes, Chapter 8. *In* Geology of the Cordilleran orogen in Canada. *Edited by* H. Gabrielse and C.J. Yorath. Geological Survey of Canada, Geology of Canada no. 4, pp. 281-327.

Neilson, K.C. 1982. Structural and metamorphic relationships between the Mount Ida and Monashee Groups at Mara Lake, British Columbia. Canadian Journal of Earth Sciences, **19**: 288-307.

Okulitch, A.V. 1984. The role of the Shuswap metamorphic complex in Cordilleran tectonism: a review. Canadian Journal of Earth Sciences, **21**: 1171-1193.

Okulitch, A.V. 1987. Comment and reply on "Extension across the Eocene Okanagan crustal shear in southern British Columbia." Geology, **15**: 187-188.

Parrish, R.R. 1995. Thermal evolution of the southeastern Canadian Cordillera. Canadian Journal of Earth Sciences, **32**: 1618-1642.

Parrish, R.R., Carr, S.D., and Parkinson, D.L. 1988. Eocene extensional tectonics and geochronology of the southern Omineca Belt, British Columbia and Washington. Tectonics, 7: 181-212.

Parsons, T., and Thompson, G.A. 1993. Does magmatism influence low-angle normal faulting? Geology, **21**: 247-250.

Read, P.B., and Okulitch, A.V. 1977. The Triassic unconformity of south-central British Columbia. Canadian Journal of Earth Sciences, **14**: 606-638.

Read, P.B., and Brown, R.L. 1981. Columbia River fault zone: southeast margin of the Shuswap and Monashee complexes, southern British Columbia. Canadian Journal of Earth Sciences, **18**: 1127-1145.

Rejebian, V.A., Harris, A.J., and Huebner, J.S. 1987. Conodont colour and textural alteration: an index to regional metamorphism, contact metamorphism, and hydrothermal alteration. Geological Society of America Bulletin, **99**: 471-479.

Reesor, J.E., and Moore, J.M. 1971. Petrology and structure of the Thor-Odin gneiss dome, Shuswap metamorphic complex, British Columbia. Geological Survey of Canada Bulletin 195.

Scammell, R.J. 1993. Mid-Cretaceous to Tertiary thermotectonic history of former mid-crustal rocks, southern Omineca Belt, Canadian Cordillera. Ph.D. thesis, Queen's University, Kingston, Ontario.

Simony, P.S., and Carr, S.D. 1997. Large lateral ramps in the Eocene Valkyr shear zone: extensional ductile faulting controlled by plutonism in southern British Columbia. Journal of Structural Geology, **19**: 769-784.

Spark, R.N. 2002. Crustal thickening and tectonic denudation within the Thor-Odin culmination, Monashee complex, southern Canadian Cordillera. Ph.D. thesis, University of New Brunswick, Fredericton.

Spear, F.S. and Parrish, R.R. 1996. Petrology and cooling rates of the Valhalla complex, British Columbia, Canada. Journal of Petrology, **27**: 733-765.

Tempelman-Kluit, D., and Parkinson, D. 1986. Extension across the Eocene Okanagan crustal shear in southern British Columbia. Geology, **14**: 318-321.

Teyssier, C., Ferré, E., Whitney, D.L., Norlander, B., Vanderhaeghe, O., and Parkinson, D. (2005). Flow of partially molten crust and origin of detachments during collapse of the Cordilleran orogen. Geological Society of London, Special Publication on high strain zones.

Thompson, R.I. 2004*a*. Geology of the Salmon Arm map area, British Columbia (NTS 82L/11). Geological Survey of Canada Open File 4380, scale 1:50 000.

Thompson, R.I. 2004*b*. Geology of the Gates Creek map area, British Columbia (NTS 82L/09). Geological Survey of Canada Open File 4378, scale 1:50 000.

Thompson, R.I. (in press). Geology of the Monte Creek map area, British Columbia (NTS 82L/12). Geological Survey of Canada Open File 4381, scale 1:50 000.

Thompson, R.I. (in press). Geology of the Chase map area, British Columbia (NTS 82L/13). Geological Survey of Canada Open File 4382, scale 1:50 000.

Thompson, R.I. (in press). Geology of the Sorrento map area, British Columbia (NTS 82L/14). Geological Survey of Canada Open File 4383, scale 1:50 000.

Thompson, R.I. (in press). Geology of the Malakwa map area, British Columbia (NTS 82L/15). Geological Survey of Canada Open File 4384, scale 1:50 000.

Thompson, R.I. (in press). Geology of the Revelstoke map area, British Columbia (NTS 82L/16). Geological Survey of Canada Open File 4385, scale 1:50 000.

Thompson, R.I., and Daughtry, K.L. 1996. New stratigraphic and tectonic interpretations, north Okanagan Valley, British Columbia. *In* Current Research 1996-A. Geological Survey of Canada, pp. 135-141.

Thompson, R.I., and Daughtry, K.L. 2000. Stratigraphic linkage of carbonate-rich units across east-central Vernon map area, British Columbia: are Kingfisher (Colby) and Big Ledge zinc-lead occurrences part of the same regional marker succession? Geological Survey of Canada, Current Research 2000-A18.

Thompson, R.I. and Glombick, P. 2004*a*. Geology of the Shuswap Falls map area, British Columbia (NTS 82L/07). Geological Survey of Canada Open File 4376, scale 1:50 000.

Thompson, R.I., and Glombick, P. 2004*b*. Geology of the Mabel Lake map area, British Columbia (NTS 82L/10). Geological Survey of Canada Open File 4379, scale 1:50 000.

Thompson, R.I., and Unterschutz, J.L.E. 2004. Geology of the Vernon map area, British Columbia (NTS 82L/06). Geological Survey of Canada Open File 4375, scale 1:50 000.

Thompson, R.I. and Glombick, P., and Lemieux, Y. (compilers). 2004*a*. Geology of the Eureka Mountain map area, British Columbia (NTS 82L/01). Geological Survey of Canada Open File 4370, scale 1:50 000.

Thompson, R.I. and Glombick, P., and Lemieux, Y. (compilers). 2004*b*. Geology of the Mount Fosthall map area, British Columbia (NTS 82L/08). Geological Survey of Canada Open File 4377, scale 1:50 000.

Unterschutz, J. 2002. Geological and geochemical links between Quesnel "terrane" strata and ancestral North America, southern Canadian Cordillera. M.Sc. thesis, University of Alberta, Edmonton, Alberta.

Vanderhaeghe O. and Teyssier C. 1997. Role of partial melting during late-orogenic collapse: The Shuswap metamorphic core complex, British Columbia, Canada. Geodinamica Acta, **10**: 41-58.

Vanderhaeghe, O., Teyssier, C., and Wysoczanski, R. 1999. Structural and geochronological constraints on the role of partial melting during the formation of the Shuswap metamorphic core complex at the latitude of the Thor-Odin dome, British Columbia. Canadian Journal of Earth Sciences, **36**: 917-943.

Vanderhaeghe, O., Teyssier, C., McDougall, I., and Dunlap, W.J. 2003. Cooling and exhumation of the Shuswap Metamorphic Core Complex constrained by 40Ar/39Ar thermochronology. Geological Society of America Bulletin, **115**: 200-216.

Wells, M.L. 2001. Rheological control on the initial geometry of the Raft River detachment fault and shear zone, western United States. Tectonics **20**: 435-457.

Wells, M.L., Dallmeyer, R.D., Allmendinger, R.W. 1990. Late Cretaceous extension in the hinterland of the Sevier thrust belt, northwestern Utah and southern Idaho. Geology, **18**: 929-933.

Wernicke, B. 1990. The fluid crustal layer and its implications for continental dynamics. *In* Exposed cross-sections of the continental crust. *Edited by* M. Salisbury and D. Fountain. Kluwer Academic, Boston, Massachusetts, pp. 509-544.

Wernicke, B. 1992. Chapter 12. Cenozoic extensional tectonics of the U.S. Cordillera. *In* The Geology of North America Vol. G-3, The Cordilleran Orogen: Conterminous U.S. The Geological Society of America.

Westaway, R. 1998. Dependence of active normal fault dips on lower-crustal flow regimes. Journal of the Geological Society, **155**: 233-253.

Wheeler, J.O., and McFeely, P. (compilers). 1991. Tectonic assemblage map of the Canadian Cordillera and adjacent parts of the United States of America. Geological Survey of Canada, Map 1712A, scale 1:2 000 000.

Williams, P.F., and Jiang, D. 2005. An investigation of lower crustal deformation: evidence for channel flow and its implications for tectonics and structural studies. Journal of Structural Geology, **27**: 1486-1504.

Woodsworth, G.J., Anderson, R.G., and Armstrong, R.L. 1991. Plutonic regimes, Chapter 15. *In* Geology of the Cordilleran orogen in Canada. *Edited by* H. Gabrielse and C.J. Yorath. Geological Survey of Canada, Geology of Canada no. 4, pp. 491-531.

CHAPTER 3

Age of the Aberdeen gneiss complex and the thermal evolution of the Vernon antiform, southeast Canadian Cordillera[1]

[1] A version of this chapter has been submitted to the Canadian Journal of Earth Sciences for publication coauthored by P. Glombick, R. I. Thompson, P. Erdmer, L. Heaman, R. M. Friedman, M. Villeneuve, and K. L. Daughtry† (deceased).

Introduction

The Aberdeen gneiss complex is a heterolithic assemblage of migmatitic gneiss situated within the core of the Vernon antiform, a crustal-scale, dome-shaped reflector visible in seismic reflection data from the high-grade metamorphic and plutonic hinterland of the southern Canadian Cordillera (Cook et al. 1992). The Vernon antiform is situated at a key location within the southern Canadian Cordillera, as it corresponds to the boundary between variably metamorphosed Paleoproterozoic to Triassic aged rocks of probable North American affinity, included within the (pericratonic) Kootenay terrane, and Devonian to Jurassic volcanic and sedimentary rocks (Quesnellia and Slide Mountain terranes). The Quesnel Terrane has been interpreted as having formed within an intra-oceanic volcanic arc of Upper Triassic age (the Nicola arc) built on primitive Middle to Upper Paleozoic basement (e.g., Monger et al. 1991). The Quesnellia and Slide Mountain terranes are components of a larger composite terrane, the Intermontane Superterrane, proposed to have been tectonically assembled outboard of the continent prior to being accreted and thrust over the cratonic margin in Middle Jurassic time (e.g., Brown et al. 1986; Monger et al. 1991). North of latitude 50°30'N, the boundary between rocks included within the Intermontane Superterrane and rocks of the Kootenay terrane strikes north-northwest, parallel to the structural trend of the orogen (Fig. 3-1, inset). South of latitude 50°30'N, in the Vernon area, the boundary strikes eastward for approximately 150 kilometres, before turning to the south again, along the eastern margin of the Valhalla complex. That bend in the boundary between pericratonic rocks and rocks of the Intermontane Superterrane has been interpreted as reflecting the position of a southwest facing ramp in the pre-Middle Jurassic cratonic margin, the Vernon monocline (Price and Monger 2003).

The antiformal geometry visible in seismic reflection data at upper to mid-crustal depths in the Vernon area has been interpreted as an antiformal stack of tectonic slices of allochthonous North American rocks that have been thrust over North American cratonic basement during Cordilleran orogenesis (Fig. 3-2*b*; Cook et al. 1992). The western flank of the Vernon antiform corresponds with a moderately west-dipping panel of reflectors that continue into the lower crust where they flatten and become sub-horizontal at a depth of approximately twenty-four kilometres

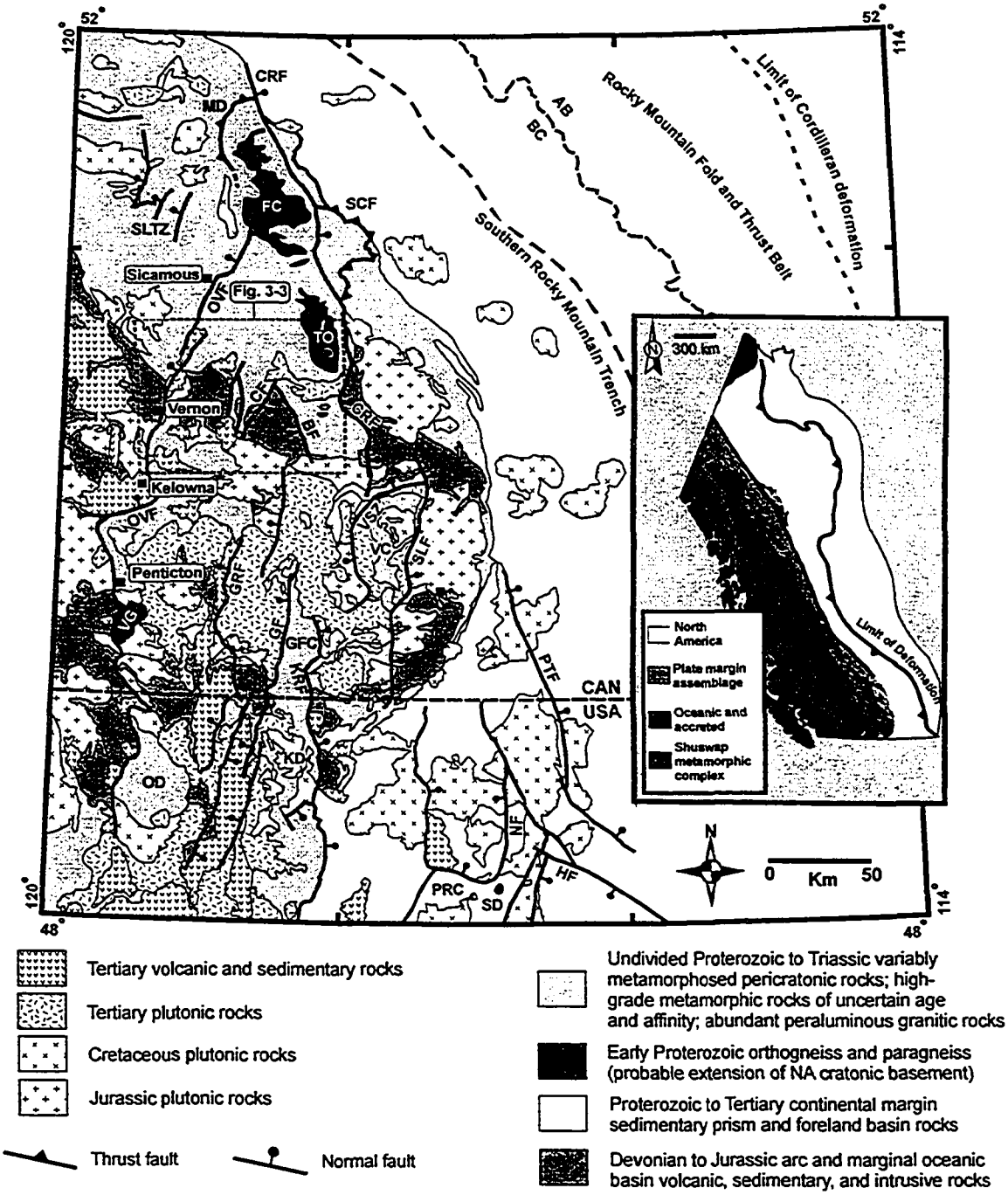

Fig. 3-1. Generalized tectonic assemblage map of the southeastern Canadian Cordillera indicating the location of the study area (modified from Wheeler and McFeely 1991). **Inset**: Tectonic elements of the Canadian Cordillera and the location of the Shuswap metamorphic complex (modified from Erdmer et al. 2001). *Faults*: BF - Beaven; CF - Cherry; CRF - Columbia River; GF - Granby; GRF - Greenwood; HF - Hope; KRF - Kettle River; MD - Monashee décollement; NF - Newport; PTF - Purcell Trench; OVF - Okanagan Valley-Eagle River; SCF - Standfast Creek; SLF - Slocan Lake; SLTZ - Shuswap Lake transfer zone; VSZ - Valkyr shear zone. *Gneiss complexes and culminations*: FC - Frenchman Cap culmination; GFC - Grand Forks complex; KD - Kettle dome; OD - Okanogan dome; PRC - Priest River complex; SD - Spokane dome; TO - Thor-Odin culmination; VC - Valhalla complex; VG - Vaseaux gneiss.

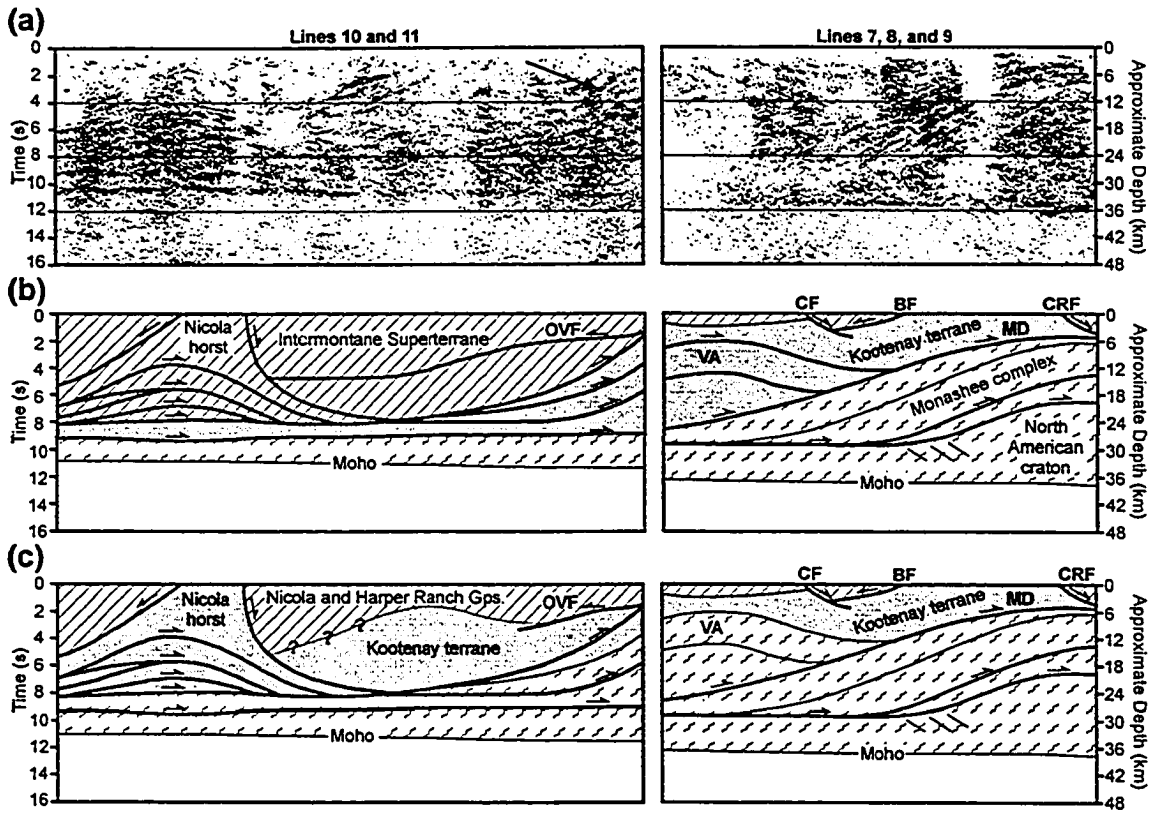

Fig. 3-2. Seismic reflection data and interpretations of lines 7, 8, 9, and 10 from the Lithoprobe southern Canadian Cordillera transect (see Cook et al. 1992). (a) Migrated data. No vertical exaggeration assuming an average seismic wave crustal velocity of 6 km/s. The location of lines are indicated in Fig. 3-1. The arrow shows the position of the west-dipping panel of reflectors on the western limb of the Vernon antiform. (b) Interpretation of Cook et al. (1992). *Structures*: BF - Beaven fault; CR - Cherry fault; MD - Monashee décollement; OVF - Okanagan Valley fault; VA - Vernon antiform. (c) An alternate interpretation of the seismic data, based on the interpretation of Erdmer et al. (2002), in which the Vernon antiform is cored by Paleoproterozoic North American basement rocks and the Quesnel and Slide Mountain Terranes are underlain by thick continental crust from west of the Okanagan Valley to the Fraser River fault.

(Fig. 3-2*a*). This ramp has been interpreted as corresponding to a drastic change in the thickness of the Intermontane Superterrane, from twenty-four kilometres west of the ramp, to a few kilometres thick east of the ramp (Fig. 3-2*b*). That interpretation has been questioned by Erdmer et al. (2002), who suggested, based on the presence of Proterozoic granitic clasts within a metasedimentary succession beneath the Nicola Group, that a large area of the southern Canadian Cordillera between the Okanagan Valley and the Fraser River fault might be underlain by thick continental crust. In that scenario, rocks presently included within the Intermontane Superterrane would comprise a thin veneer (three to six kilometres) of supracrustal cover resting unconformably above a thick succession of Proterozoic rocks of North American affinity, at least as far west as the Fraser River fault (Fig. 3-2*c*).

The domal geometry of the Vernon antiform suggests that deeper structural levels are more likely to be exposed within the core than on the flanks. Recent geological mapping southwest of Vernon, within the core of the Vernon antiform, has delineated a previously unstudied migmatite complex, the Aberdeen gneiss complex (AGC; Glombick et al. 2004*a*). The AGC resembles other domal migmatite culminations within the southern Canadian Cordillera, several of which, including the Monashee and Malton gneiss complexes, expose Paleoproterozoic crust interpreted to be North American cratonic basement (e.g., Parkinson 1991; McDonough and Parrish 1991). The possibility exists, therefore, that the Vernon antiform may be cored by autochthonous North American crust. Another possibility is that the core of the Vernon antiform consists of Proterozoic to Paleozoic pericratonic rocks of the Kootenay terrane. Knowing the age and tectonic affinity of rocks underlying the Vernon antiform would help greatly in reconstructing the Paleozoic paleogeography of the Pacific margin and interpreting existing seismic reflection data.

This paper presents the results of a U-Pb geochronological investigation of the AGC and surrounding rocks within the Vernon antiform. The primary goal was to determine the emplacement age of the Aberdeen gneiss complex in order to determine whether Paleoproterozoic crust is exposed at surface within the antiform. A secondary goal was to elucidate the thermal and tectonic evolution of rocks within the Vernon antiform to better understand their role in Cordilleran orogenesis.

Geology of the Aberdeen gneiss complex and the Vernon antiform

Within the hinterland of the southern Canadian Cordillera, sillimanite-grade rocks form a north-tapering metamorphic belt informally known as the Shuswap metamorphic complex (SMC; Okulitch 1984). High-grade, formerly mid-crustal rocks exposed within the SMC were exhumed

during early Tertiary extension synchronous with core complex formation (Parrish et al. 1988). Within the southern SMC, a series of sub-parallel, northerly-trending, brittle extension faults of Early to Middle Eocene age cut the complex, bounding the margins of structural culminations such as the Grand Forks and Valhalla complexes (Fig. 3-1). Within the northern SMC, early Tertiary extension faults are less abundant and have relatively minor displacements (< 2-6 km; e.g., Ghent et al. 1980; Pell 1984; Currie 1988; Digel 1988) compared to extensional faults exposed to the south. As a result, the contact between metamorphic infrastructure and low-grade superstructure rocks in the northern SMC is commonly gradational rather than a fault contact (e.g., Crowley et al. 2000).

The Vernon area is located between latitudes 50°00'N and 50°30'N near the western margin of the SMC (Fig. 3-1). The geology of the Vernon area is complex, resulting from the superposition of Paleocene to Eocene extensional deformation on earlier contraction structures of Middle Jurassic to Late Cretaceous age. Metamorphic rocks within the Vernon area can be separated into high-grade rocks, comprising the metamorphic infrastructure of the SMC, and low-grade superstructure rocks that flank the margins of the complex or locally overlie infrastructure rocks within a southeast-trending supracrustal belt that extends across the SMC in the Vernon area (Figs. 3-3, 3-4, 3-5).

A complexly deformed succession of upper amphibolite-grade metamorphic rocks is exposed in the southeast quadrant of the map area (Fig. 3-6). These high-grade rocks are the northern extension of an extensive region of metamorphic and plutonic rocks exposed between latitude 50°15'N and the 49th parallel, informally named the Okanagan metamorphic and plutonic complex (Okulitch 1984; designated "unassigned metamorphic rocks" by Wheeler and McFeely [1991]). Large areas of the Okanagan metamorphic and plutonic complex remain unstudied, and the age, affinity, and structure of these rocks remains poorly understood. Isotopic evidence from the Vaseaux gneiss, located approximately 200 km to the south of Vernon, suggests that the Okanagan metamorphic and plutonic complex may include protoliths of Paleoproterozoic age (Armstrong et al. 1991). In the Vernon area, a distinctive calcareous quartzite unit exposed at the northern end of Kalamalka Lake, correlated with the (Devonian) Chase Formation, suggests a stratigraphic linkage between the Okanagan metamorphic and plutonic complex and Proterozoic to Paleozoic rocks of the Kootenay terrane exposed to the north near Shuswap Lake (Thompson and Daughtry 1996).

South of Vernon, along the eastern shore of Kalamalka Lake, a heterolithic paragneiss succession is exposed (Erdmer et al. 1998; Glombick et al. 1999, 2000). Rock types within the succession include pelitic and semi-pelitic schist, quartzofeldspathic gneiss, calcsilicate gneiss,

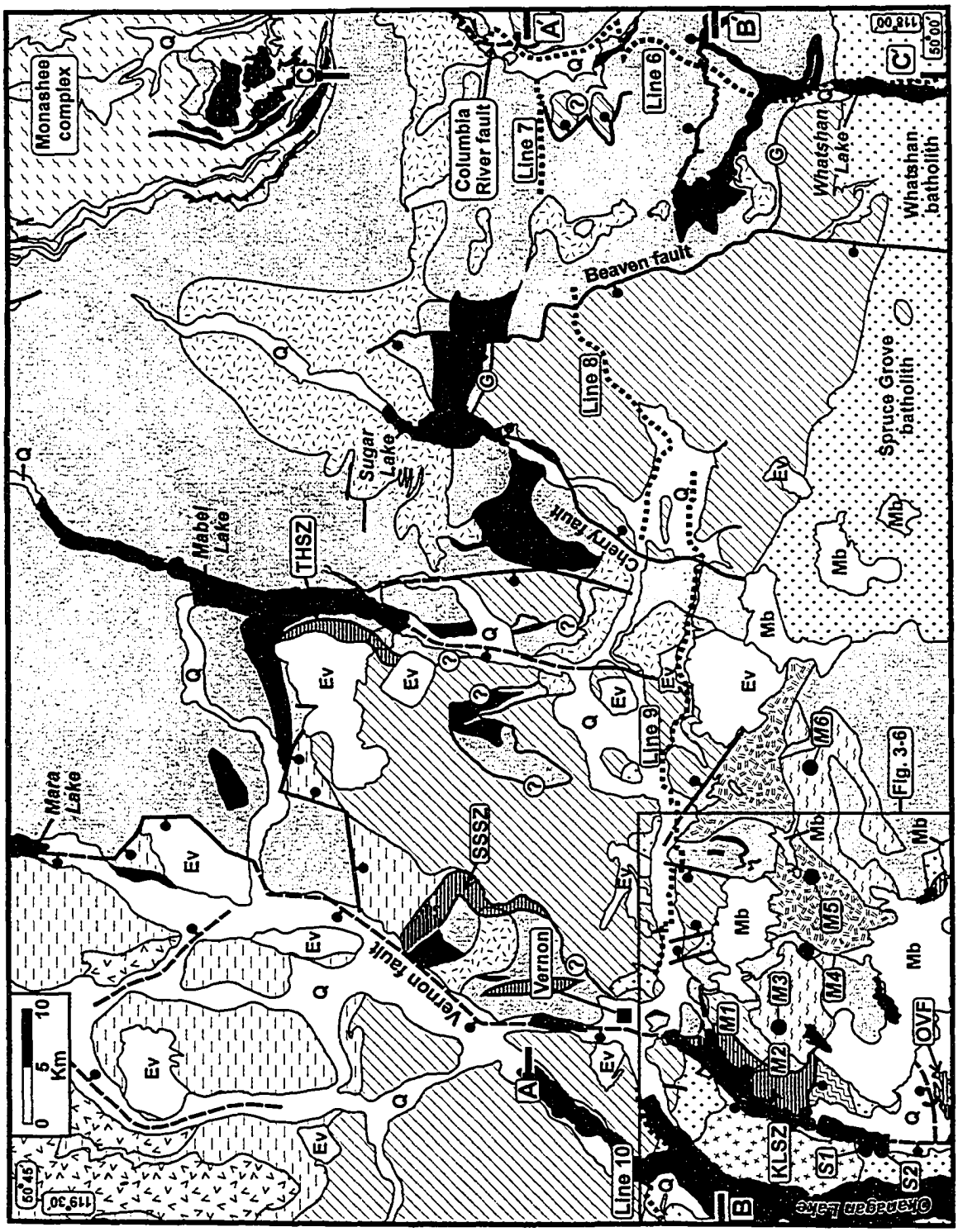

Fig. 3-3. Simplified geological map of the study area with sample locations indicated. Legend provided in Fig. 3-4. *Abbreviations*: KLSZ - Kalamalka Lake shear zone (Erdmer et al. 1998; Glombick et al. 1999); OVF - Okanagan Valley fault/Kelowna airport shear zone (Bardoux 1993; Glombick et al. 2004); SSSZ - Silver Star shear zone (Thompson and Unterschutz 2004); THSZ - Trinity Hills shear zone (Thompson and Glombick 2004*b*). Geological contacts modified from Glombick and Thompson (2004), Glombick et al. (2004), Thompson (2004*a*, 2004*b*), Thompson and Glombick (2004*a*, 2004*b*), Thompson and Unterschutz (2004), and Thompson et al. (2004*a*, 2004*b*).

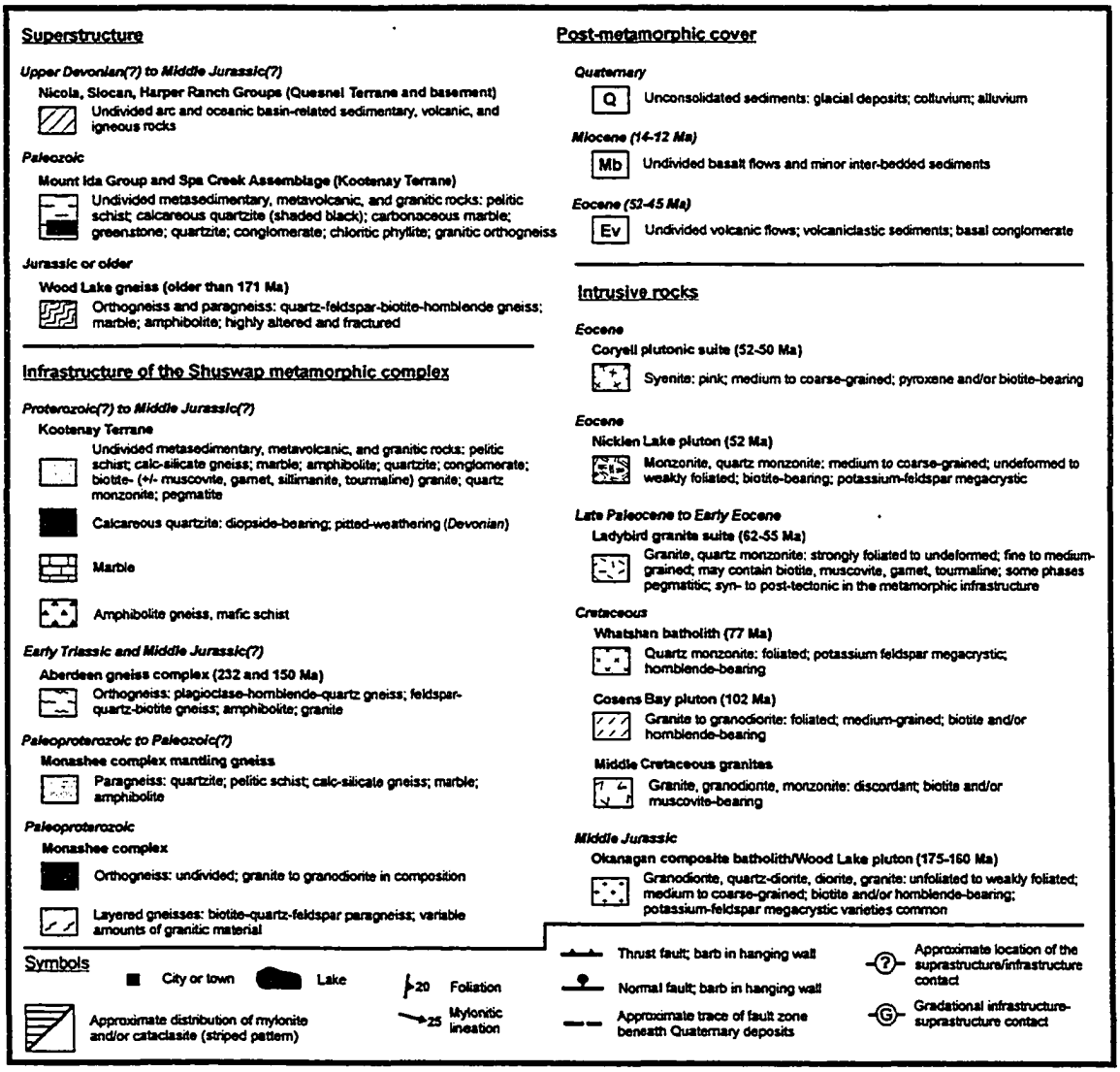

Fig. 3-4. Legend to accompany Figs. 3-3, 3-5, and 3-6.

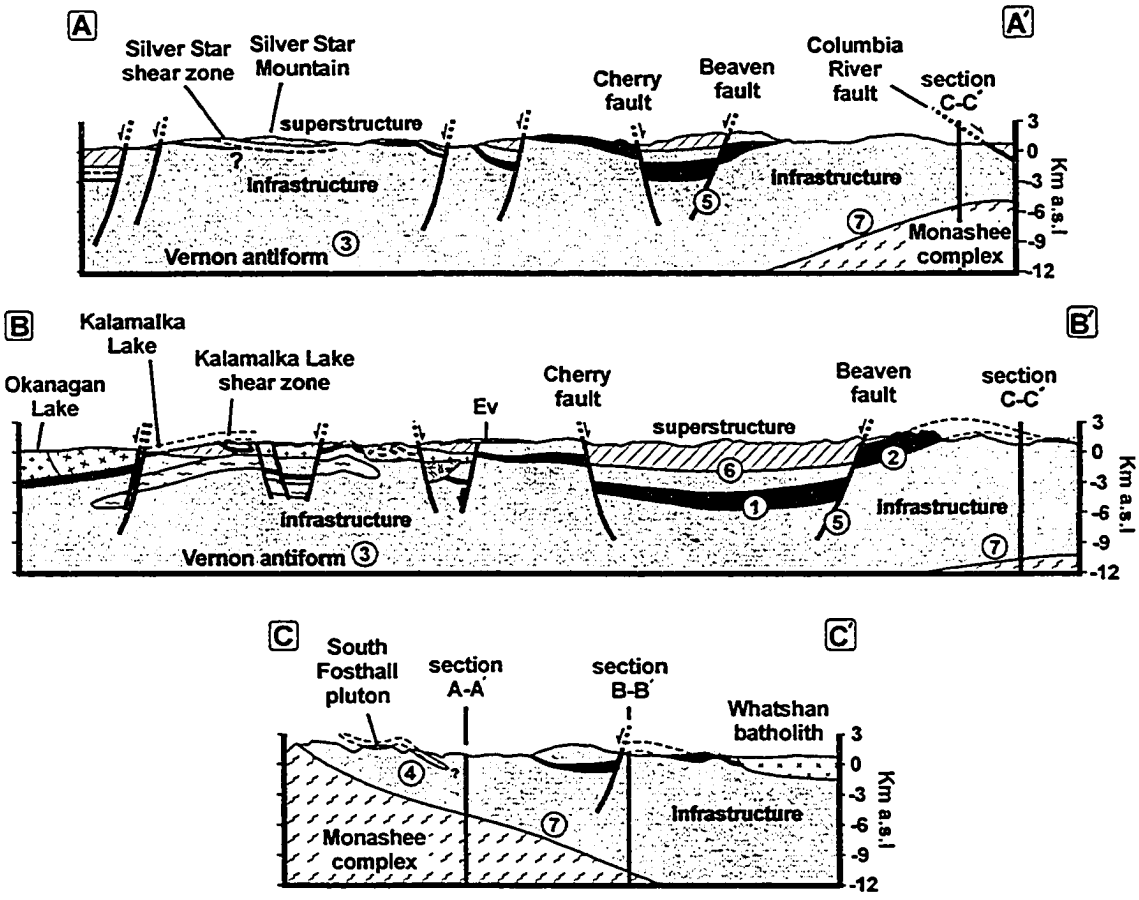

Fig. 3-5. Generalized geological cross sections through the study area. The endpoints of the section lines are indicated in Fig. 3-3. No vertical exaggeration. The subsurface geometry below 4 km is based on interpretation of LITHOPROBE seismic reflection profile data from lines 6-10 from the southern Canadian Cordilleran transect (see Cook et al. 1992). See Fig. 3-4 for legend. Notes: (1) The Devonian Chase Formation is interpreted as a gently-folded sheet in the subsurface on the basis of the orientation of reflectors in seismic reflection data (e.g., Cook et al. 1992) combined with the observation that the Chase Formation and other map units are not structurally repeated at the regional scale by folding or faulting (Fig. 3-3). (2) This structure is interpreted as a broad, gently east-plunging antiform, with the northern limb down-dropped by a steep normal fault, rather than a map-scale recumbent isoclinal fold (e.g., Carr 1990), on the basis of recent detailed geological mapping (e.g., Lemieux et al. 2003; Thompson et al. 2004*a*). (3) The Vernon antiform is defined by a series of antiformal-shaped reflectors visible at upper to mid-crustal depths (6-18 km) in E-W oriented seismic reflection lines through the Vernon area (Fig. 3-2*a*; see also, Cook et al. 1992). (4) The geometry of the South Fosthall pluton in the subsurface is not constrained, but is assumed to be approximately tabular on the basis of map patterns and the orientation of reflections in the upper 4 km. (5) The Beaven fault cuts the infrastructure-superstructure (transitional) contact near Vidler Ridge, and therefore cannot be the "breakaway" of an Okanagan Valley-Eagle River fault system in the Pinnacles area. Steeply dipping Middle Eocene normal faults are inferred to root into a Middle Eocene brittle-ductile transition not exposed at the present erosional level. (6) While the infrastructure-superstructure is drawn as a line in the cross sections, it is transitional over 1-2 km in the field and variable from region to region (see text for description). (7) The existence of the Monashee décollement as a discrete crustal-scale shear zone along the western margin of the southern Monashee complex has been questioned by Johnston et al. (2000) based on detailed geological mapping in the Joss Pass area and on theoretical grounds (Williams 1999; Williams and Jiang 2005), and is therefore not shown on the map and cross sections separating the southern Monashee complex from the overlying middle structural layer of the infrastructure.

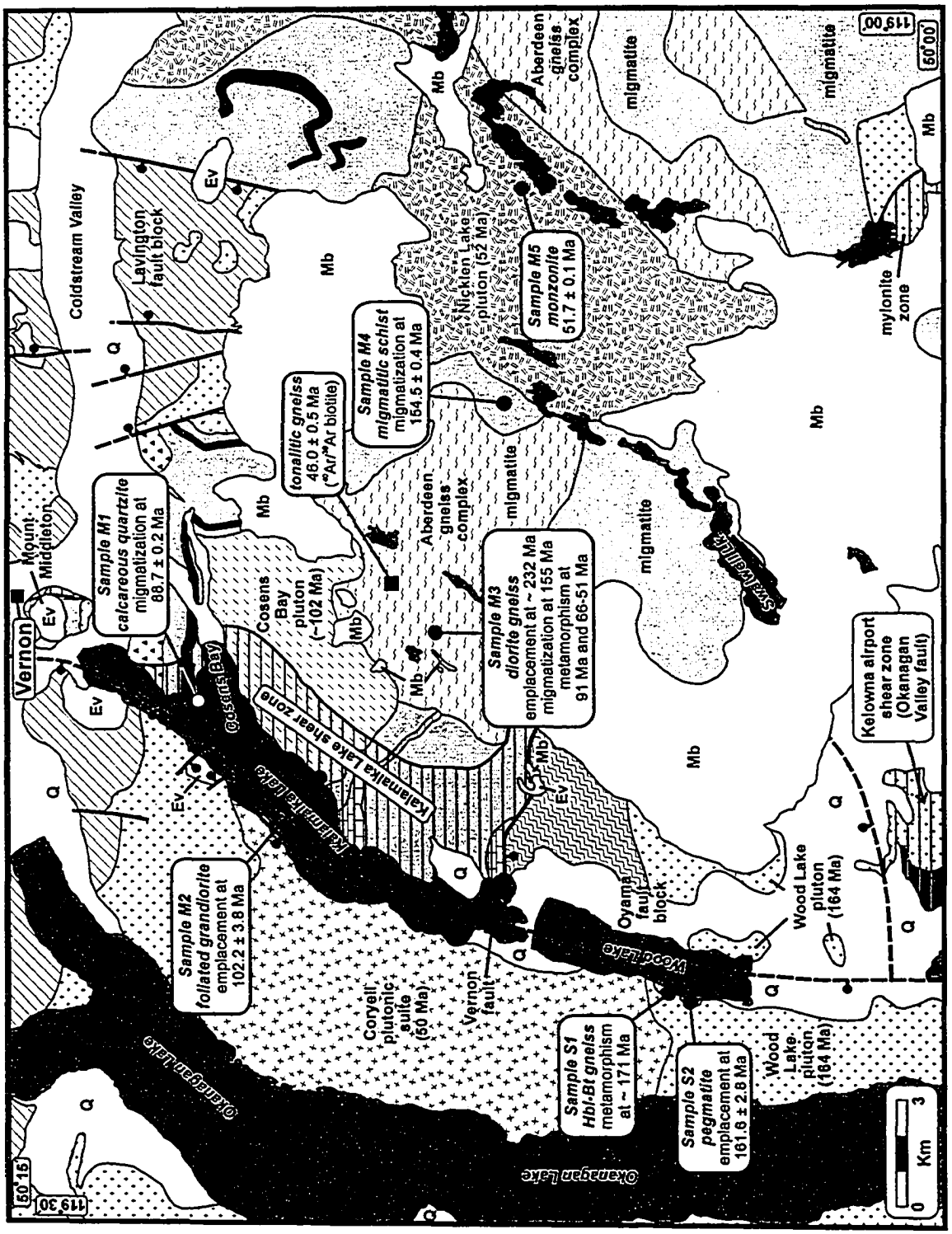

Fig. 3-6. Geological map of the Aberdeen gneiss complex (AGC) and surrounding region indicating the location and dates of U-Pb samples. Geological contacts modified from Glombick et al. (2004). See Fig. 3-4 for legend.

amphibolite, marble, and calcareous quartzite; semi-pelitic schist and quartzofeldspathic gneiss (meta-psammite) are the most abundant rock types. The paragneiss succession is host to, and deformed together with, large orthogneiss sheets of dioritic to tonalitic composition. This complexly deformed heterogeneous assemblage of migmatitic orthogneiss and paragneiss has been named the Aberdeen gneiss complex (AGC; Glombick et al. 2004*a*).

Internal contact relationships within the AGC are complex as a result of multiple intrusion phases, intense ductile deformation and migmatization. Several orthogneiss phases are present, ranging in composition from diorite to tonalite, with strongly foliated, biotite- and/or hornblende-bearing, medium-grained, tonalite gneiss being the most abundant. Late, post-kinematic granitic veins are common. Tonalite gneiss commonly hosts angular to rounded blocks, lenses, and/or layers of medium- to coarse-grained hornblende-diorite gneiss, ranging in size from centimetres to up to several metres across. Tonalitic to granitic veins commonly cut angular blocks of hornblende diorite gneiss, resembling agmatic migmatite (Ashworth 1985; Figs. 3-7*a*, 3-7*b*). Lenses and/or blocks of dioritic gneiss commonly preserve a foliation (S_1) that is discordant to the dominant foliation (S_2) within the enclosing tonalitic gneiss. Pegmatite-filled fractures and narrow shear zones within the diorite gneiss indicate that it behaved in a competent manner during ductile deformation of the surrounding tonalitic gneiss (Fig. 3-7*b*), possibly a result of its greater mafic mineral content. Elsewhere, the transition between diorite and tonalite phases is gradational and complex, suggesting that the diorite may constitute a paleosome or restite. Folds within the AGC are commonly ptygmatic and fabric elements have been overprinted during migmatization.

The AGC is host to several intrusive units. Along the eastern shore of Kalamalka Lake, a tabular body of foliated granodiorite, the Cosens Bay pluton (Erdmer et al. 1998), is exposed (Fig. 3-6). Enclaves of paragneiss are present at the pluton margin, indicating that the metamorphic layering within the paragneiss succession (S_2) predates the emplacement age of the pluton.

The AGC hosts several large intrusive bodies of weakly foliated to undeformed potassium feldspar megacrystic monzonite. The largest of these intrusive bodies is here named the Nicklen Lake pluton (Fig. 3-6). The Nicklen Lake pluton cuts all fabric within the enclosing gneiss. In addition, numerous small, post-kinematic granitic stocks and granite pegmatite dykes of probable Eocene age are scattered throughout the AGC.

A gently west-dipping mylonite zone, the Kalamalka Lake shear zone, is developed within the paragneiss succession exposed along the eastern shore of Kalamalka Lake (Erdmer et al. 1998; Glombick et al. 1999). The estimated structural thickness of the zone is at least eight

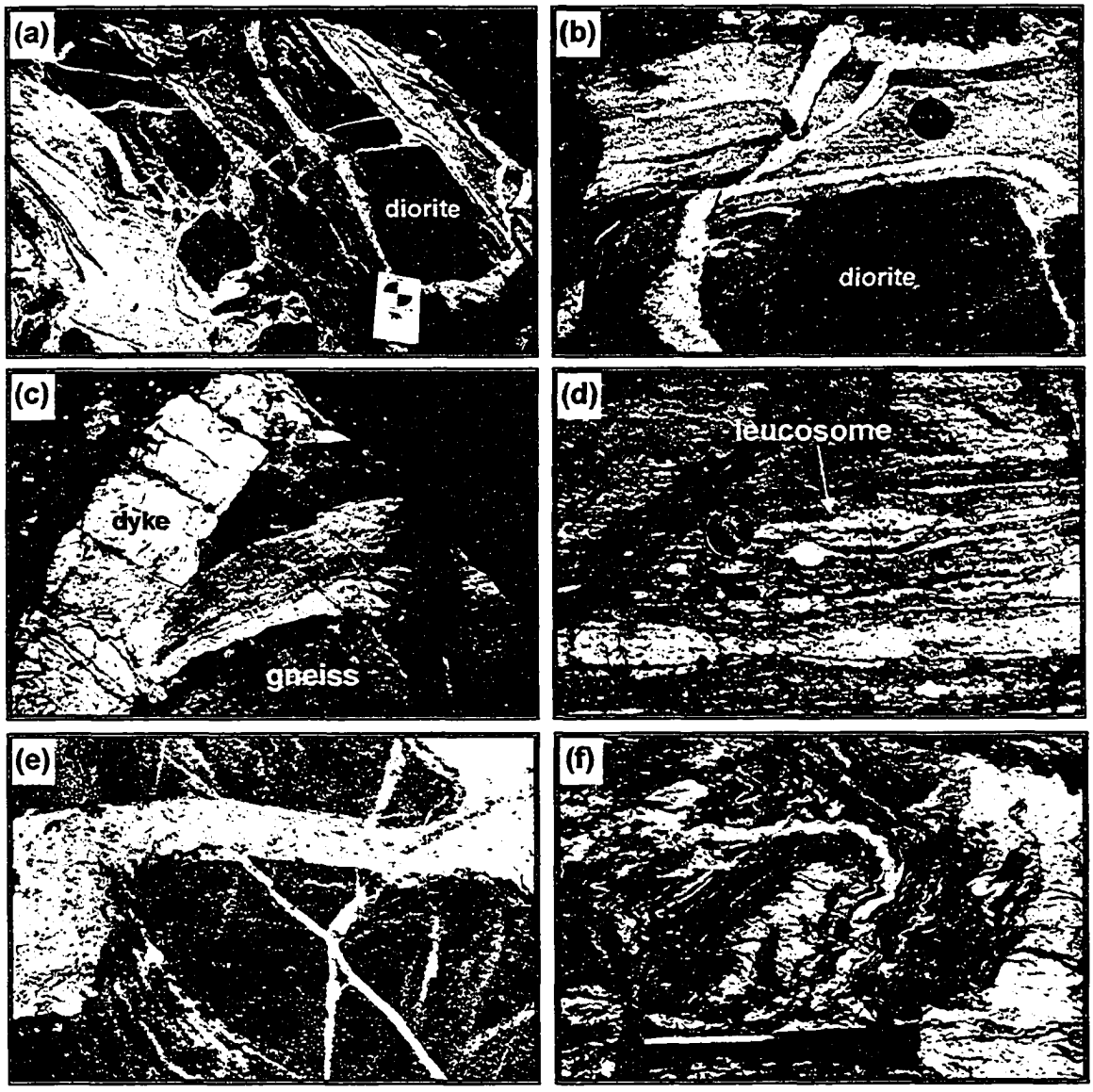

Fig. 3-7. Outcrop photographs of rocks from the Vernon area. (a) Layered, migmatitic orthogneiss exposed within the Aberdeen gneiss complex. Notebook is 17.5 cm long. (b) Diorite gneiss boudin cut by late granitic vein. Lens cap is 6.5 cm in diameter (c) Granite dyke cutting gneissic layering within the Wood Lake gneiss at a high angle. The length of the rock hammer shown in the picture (bottom right) is approximately 20 cm long. (d) Exposure of mylonitic calcareous quartzite within the Kalamalka Lake shear zone with discontinuous leucosome layers parallel to the mylonitic foliation. Exposure is oriented parallel to the mylonitic lineation and perpendicular to the foliation. Canadian quarter for scale. Arrow points to leucosome layer. (e) Medium-grained diorite cut by two generations of granitic veining. Lens cap for scale. (f) Complexly folded migmatitic pelitic schist (Sample M4) exposed within the Aberdeen gneiss complex. Rock hammer for scale.

hundred metres. The shear zone extends several kilometres eastward from Kalamalka Lake and approximately fifteen kilometres to the south, before being truncated by a steep brittle fault (Fig. 3-6). The eastward extension of the Kalamalka Lake shear zone projects above the present level of exposure, placing the AGC within the footwall (Fig. 3-5, section B-B'). A west-trending stretching lineation, defined by rodded quartz grains, aligned sillimanite needles, and elongated mineral aggregates is well-developed within the shear zone, where it is visible on the mylonitic foliation. A variety of shear-sense indicators within the shear zone, including winged porphyroclasts, C-S fabric and back-rotated boudins, consistently indicate a top-to-the-west (i.e., down dip) shear sense (Erdmer et al. 1998; Glombick et al. 1999). A small, strongly foliated, fine-grained, biotite-bearing granitic stock exposed within the shear zone has been dated at ca. 50 Ma (Heaman et al. 1999), indicating that a component of ductile deformation postdates 50 Ma. A lower age constraint is provided by a massive, undeformed mafic dyke exposed near Cosens Bay dated at 48 Ma.

South of the Vernon Creek fault, near the Kelowna airport, a gently-west-dipping ductile shear zone with a west-trending stretching lineation, inferred to be the southward continuation of the Kalamalka Lake shear zone, is developed in a heterogeneous gneiss succession that includes calcareous quartzite and orthogneiss of granodiorite composition (Fig. 3-6). This shear zone is continuous with a mylonite zone exposed in the Kelowna area that has been interpreted as part of the Okanagan Valley fault, a major, crustal scale extension fault (Bardoux 1993). Estimates of fault displacement on the Okanagan Valley fault and, by association, the Kalamalka Lake shear zone, range from a few kilometres in the Vernon area (Thompson and Daughtry 1996; Glombick et al. 2004*b*), to as much as ninety kilometres near Penticton, located two-hundred kilometres to the south (Tempelman-Kluit and Parkinson 1986; see discussion in Glombick et al. 2004*b*).

A number of steeply dipping, brittle normal faults of Middle Eocene age cut the Vernon area (Fig. 3-6). One of these faults, the Vernon fault, is exposed for several hundreds of metres along the western shore of Kalamalka Lake, where it faults massive, but highly altered rocks of the Coryell plutonic suite on the west against similarly altered gneiss on the east. As such, the Vernon fault is interpreted as a steeply dipping, west side down, brittle normal fault that underlies both Kalamalka and Wood lakes. On the east side of Wood Lake, near the southern end of the lake, a steeply-dipping structure, inferred to be a south side down normal fault, juxtaposes rocks of the weakly deformed Middle Jurassic Wood Lake pluton and its host, the Wood Lake gneiss (comprising the Oyama fault block), against amphibolite-grade mylonitic rocks of the Kalamalka Lake shear zone to the north (Fig. 3-6). Similarly, south of the Coldstream Valley, low-grade

volcanic and sedimentary rocks of the Harper Ranch Group are faulted against upper amphibolite grade gneiss of the AGC, forming the Lavington graben (Figs. 3-5, 3-6).

Low-grade superstructure rocks in the Vernon area consist mainly of Devonian to Permian volcanic and sedimentary rocks of the (Devonian to Permian?) Harper Ranch Group. Rock types within the Harper Ranch Group include intermediate to mafic, fine-grained to porphyritic volcanic rocks, volcanic breccia, agglomerate, augite porphyry, fine-grained, carbonaceous siliciclastic rocks and grey limestone. Metamorphic grade is generally low (chlorite-biotite zone) within the Harper Ranch Group, but garnet-grade rocks within the Lavington fault block and amphibolite-grade gneiss enclaves that occur within the Wood Lake pluton may be correlative. The Harper Ranch Group is host to large (>100 km^2) laccoliths of the Middle Jurassic Okanagan plutonic suite and smaller plutons of the Middle Eocene Coryell suite, as well as scattered, highly altered and deformed (pre-Triassic?) ultramafic stocks and dykes.

North of the Coldstream Valley, rocks of the Harper Ranch Group are largely absent; superstructure rocks are comprised of fine-grained, carbonaceous, siliciclastic rocks of the Upper Triassic to Lower Jurassic Nicola/Slocan Group. Collectively, the Nicola/Slocan and Harper Ranch Groups form the Quesnel Terrane, itself a component of the larger Intermontane Superterrane (e.g., Monger et al. 1991).

Samples locations, descriptions, and U-Pb results

Eight samples of intrusive and metamorphic rocks were selected for U-Pb dating: six samples from the core of the Vernon antiform (samples M1 to M6) and two samples from the western flank of the antiform, within the hanging wall of the Kalamalka Lake shear zone and the Vernon fault (samples S1 and S2) (Fig. 3-6). The samples were selected in order to constrain the emplacement age of the AGC and the timing of metamorphic and deformational events. All samples were analysed using standard isotope dilution thermal ionization mass spectrometry (ID-TIMS) techniques (Figs. 3-8, 3-9; Table 3-1). A sample of diorite gneiss (M3) that yielded scattered ID-TIMS results was further investigated by sensitive high-resolution ion microprobe (SHRIMP) (Fig. 3-9; Table 3-2). A description of analytical techniques is provided in the appendix.

Superstructure samples

Hornblende-biotite gneiss, Wood Lake (S1)

Within the Middle Jurassic Wood Lake pluton, several screens of amphibolite-facies paragneiss and orthogneiss crop out along Highway 97 adjacent to the western shore of Wood

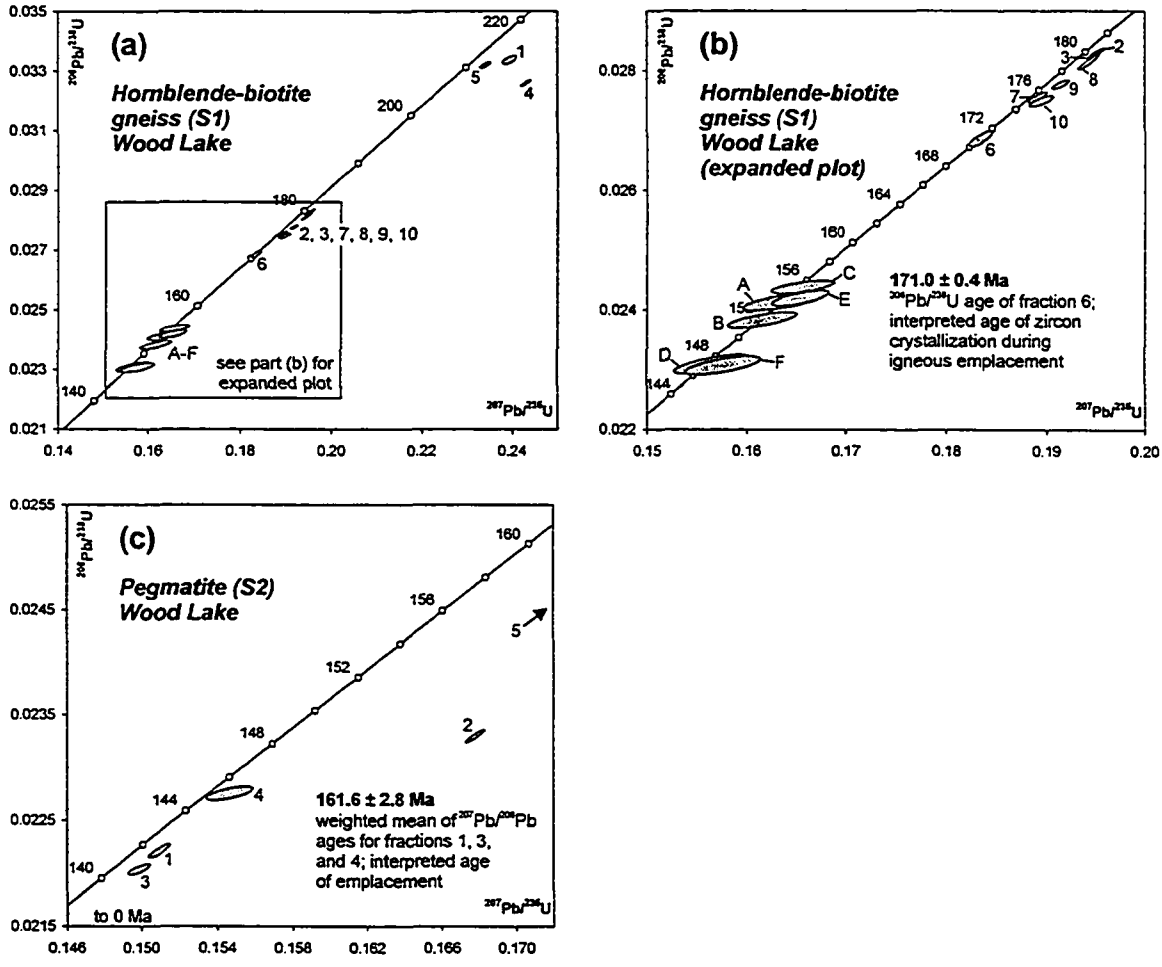

Fig. 3-8. Concordia diagrams displaying U-Pb data from supracrustal samples (S1, S2) within the hanging wall of the Kalamalka Lake shear zone. (a) Paragneiss, Wood Lake (S1); (b) Inset from part (a); (c) Pegmatite, Wood Lake (S2). Numbers and letters refer to zircon and titanite fractions, respectively. Fractions correspond to those listed in Table 3-1. Error ellipses plotted at the 2σ level.

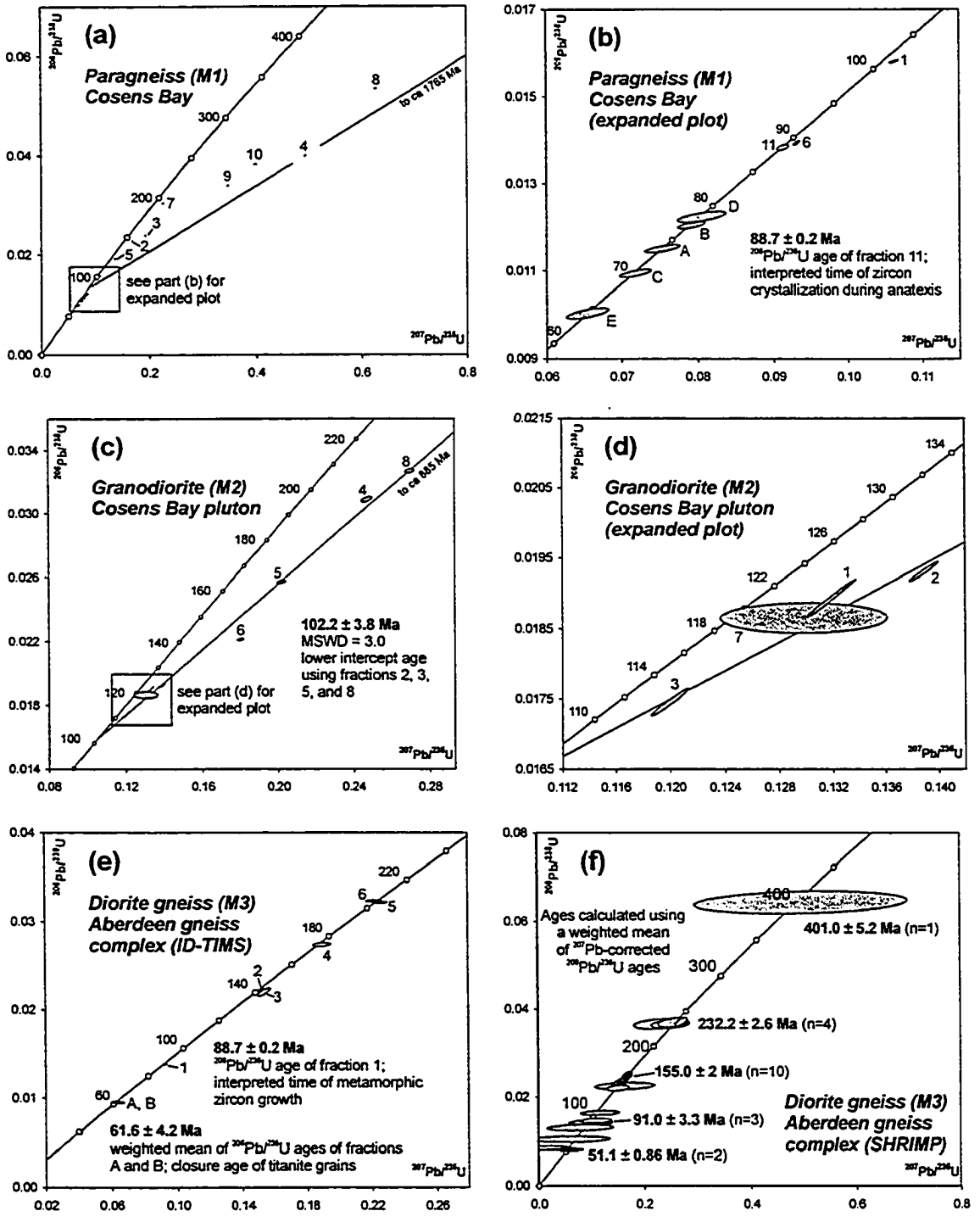

Fig. 3-9 (page 1 of 2). Concordia diagrams displaying U-Pb isotopic data from metamorphic infrastructure samples (M1-M6) from the core of the Vernon antiform. (a) Calcareous quartzite, Cosens Bay (M1); (b) Inset from part (a); (c) Foliated granodiorite, Cosens Bay pluton (M2); (d) Inset from part (c); (e) Diorite gneiss, Aberdeen gneiss complex (M3; ID-TIMS data); (f) Diorite gneiss, Aberdeen gneiss complex (M3; SHRIMP data). Numbers and letters refer to zircon and titanite fractions, respectively. Error ellipses are plotted at 2σ. Fraction labels correspond to those listed in Table 3-1 (ID-TIMS data) and Table 3-2 (SHRIMP data).

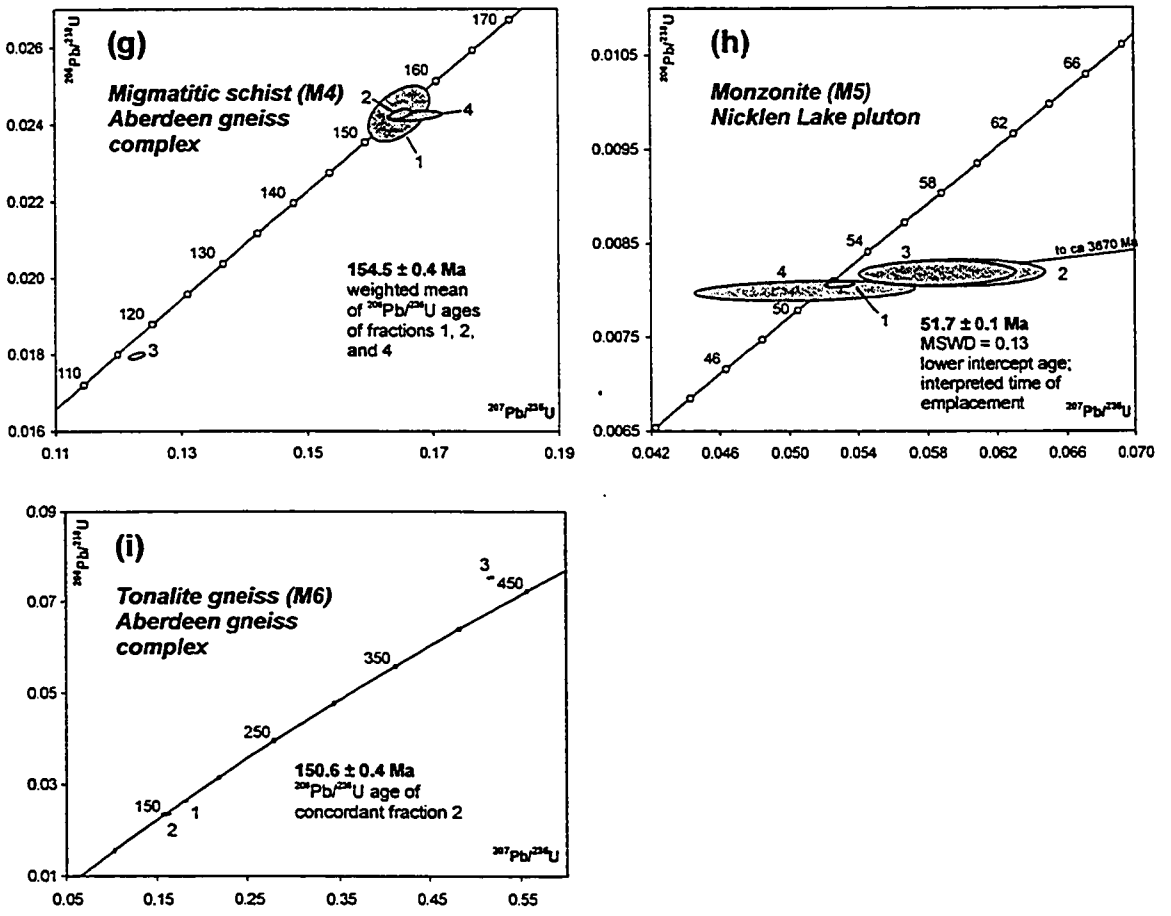

Figure 3-9 (page 2 of 2). (g) Migmatitic pelitic schist, Aberdeen gneiss complex (M4); (h) Monzonite, Nicklen Lake pluton (M5); (i) Tonalitic gneiss, Aberdeen gneiss complex (M6).

Table 3-1 (page 1 of 4). U-Pb (ID-TIMS) isotopic results for mineral fractions separated from Vernon area samples.

Frac.[a]	Description[b]	Wt. (µg)	Concentrations (ppm) U	Th	Pb	Th/U	TCPb (pg)	Atomic ratios[c,d] $^{206}Pb/^{204}Pb$	$^{206}Pb/^{238}U$	$^{207}Pb/^{235}U$	$^{207}Pb/^{206}Pb$	Apparent ages (Ma)[d] $^{206}Pb/^{238}U$	$^{207}Pb/^{235}U$	$^{207}Pb/^{206}Pb$	Disc. (%)
Superstructure samples															
Hornblende-biotite gneiss (S1)[e], west side of Wood Lake, UTM[f] 328148E 5549863N															
1	anh, cl, pr, rs, 5NM-1M (5)	20	588	362	21	0.62	4	5875	0.03322±4	0.2343±4	0.05115±6	210.7±0.3	213.7±0.4	247.8±2.8	15.2
2	anh, sl mky, pr, rs, 5NM-1M (20)	52	1607	851	48	0.53	15	9588	0.02833±3	0.1954±3	0.05002±4	180.1±0.2	181.2±0.3	196.1±1.9	8.3
3	anh, sl mky, pr, rs, 5NM-1M (20)	50	1396	696	41	0.50	12	9956	0.02827±3	0.1950±3	0.05002±4	179.7±0.2	180.9±0.3	195.8±2.0	8.3
4	anh, cl, pr, rs, 5NM-1M (30)	30	1051	569	36	0.54	8	8313	0.03261±4	0.2433±5	0.05411±5	206.8±0.3	221.1±0.4	375.5±2.1	45.6
5	sm, sbh, cl, pr, 5NM-1M (9)	10	650	361	23	0.56	1	10044	0.03338±6	0.2396±6	0.05204±11	211.7±0.4	218.1±0.6	287.3±4.8	26.8
6	lg, anh, mky, rs, 5NM-1M (3)	28	2360	834	63	0.35	46	2439	0.02688±5	0.1834±5	0.04950±8	171.0±0.4	171.0±0.4	171.4±3.8	0.3
7	lg, anh, mky, rs, 5NM-1M (7)	36	1709	1034	50	0.60	20	5464	0.02756±4	0.1892±4	0.04978±5	175.3±0.3	175.9±0.4	185.0±2.5	5.3
8	anh, sl mky, rs, 5NM-1M (8)	20	1867	1274	57	0.68	7	10099	0.02816±6	0.1945±5	0.05008±4	179.0±0.4	180.4±0.4	198.9±2.0	10.1
9	anh, mky, rs, 5NM-1M (18)	12	2107	1203	62	0.57	10	4398	0.02779±3	0.1916±4	0.05000±6	176.7±0.2	178.0±0.3	195.2±2.7	9.6
10	lg, anh, sl mky, rs, 5NM-1M (10)	8	2126	362	55	0.17	22	1345	0.02750±4	0.1896±5	0.05000±9	174.9±0.3	176.3±0.5	194.9±4.2	10.4
A	cl, yl, sbh, fr N20-M5	370	149	121	4	0.81	371	242	0.02416±6	0.1637±17	0.04916±42	153.9±0.8	154.0±1.5	155.4±20.2	1.0
B	cl, yl, sbh, fr N20-M5	355	150	104	4	0.69	367	234	0.02384±6	0.1615±14	0.04911±36	151.9±0.4	152.0±1.3	153.3±17.2	1.0
C	cl, yl, sbh, fr N20-M5	270	195	165	5	0.85	322	270	0.02439±5	0.1656±13	0.04923±33	155.4±0.3	155.6±1.2	158.7±15.8	2.1
D	cl, yl, sbh, fr N20-M5	220	152	95	4	0.63	246	218	0.02310±7	0.1564±16	0.04911±40	147.2±0.5	147.6±1.4	153.3±19.0	4.0
E	sm, cl, yl, sbh, fr N20-M5	240	171	96	4	0.56	224	295	0.02421±6	0.16539±12	0.04956±29	154.2±0.4	155.4±1.1	174.3±13.6	11.7
F	sm, cl, yl, sbh, fr N20-M5	220	158	107	4	0.68	231	235	0.02308±7	0.1576±16	0.04952±41	147.1±0.4	148.6±1.4	172.7±19.2	15.0
Pegmatite (S2)[e], west side of Wood Lake, UTM 328112E 5549726N															
1	euh, cl, tan, 2:1, pr, 2NM (30)	120	2848	163	58	0.06	252	1870	0.02221±3	0.1509±2	0.04928±4	141.6±0.2	142.7±0.2	161.3±1.8	12.3
2	euh, cl, 3:1, pr, 2NM (50)	96	3009	163	64	0.05	125	3314	0.02330±3	0.1679±2	0.05224±2	148.5±0.2	157.5±0.2	295.8±1.0	50.4
3	euh, cl, 3:1, pr, 2NM (40)	77	4486	151	90	0.03	366	1296	0.02204±2	0.1498±2	0.04931±5	140.5±0.2	141.8±0.2	162.4±2.5	13.6
4	euh, col, cl, 3:1, pr, 2NM (10)	5	2429	67	50	0.03	19	951	0.02276±3	0.1546±5	0.04928±13	145.1±0.2	146.0±0.5	161.3±6.2	10.2
5	col, cl, 2:1, pr, 2NM (16)	10	593	100	34	0.17	19	1135	0.05800±6	0.7675±17	0.09597±13	363.5±0.4	578.3±1.0	1547.2±2.6	78.6

Table 3-1 (page 2 of 4).

Frac.[a]	Description[b]	Wt. (µg)	Concentrations (ppm) U	Th	Pb	Th/U	TCPb (pg)	Atomic ratios[c,d] $^{206}Pb/^{204}Pb$	$^{206}Pb/^{238}U$	$^{207}Pb/^{235}U$	$^{207}Pb/^{206}Pb$	Apparent ages (Ma)[d] $^{206}Pb/^{238}U$	$^{207}Pb/^{235}U$	$^{207}Pb/^{206}Pb$	Disc. (%)
Metamorphic infrastructure samples															
Calcareous quartzite (M1)[e], Cosens Bay, UTM 336249E 5563487N															
1	cl, col, euh, 3.5:1, pr, 1 NM (1)	45	619	90	9	0.15	8	3407	0.01582±2	0.1063±2	0.04872±7	101.2±0.1	102.6±0.2	134.6±3.4	25.0
2	cl, col, euh, 2.5:1, pr, 1 NM (5)	180	1004	129	22	0.13	7	36318	0.02292±6	0.1664±4	0.05266±3	146.1±0.4	156.3±0.4	314.0±1.3	54.1
3	cl, col, euh, 3:1, pr, 1 NM (20)	287	913	135	21	0.15	5	73679	0.02394±2	0.1903±2	0.05764±1	152.5±0.2	176.9±0.2	516.3±0.4	71.3
4	cl, col, euh, 5:1, pr, 1 NM (50)	105	669	246	28	0.37	6	31598	0.04008±6	0.4917±7	0.08897±2	253.4±0.4	406.1±0.5	1403.6±0.5	83.5
5	cl, col, euh, 3:1, pr, 1 NM (1)	32	416	32	7	0.08	9	1790	0.01932±2	0.1336±3	0.05016±9	123.4±0.2	127.3±0.3	202.4±4.1	39.4
6	cl, col, euh, 3:1, pr, 1 NM (2)	54	2001	169	26	0.08	5	19894	0.01395±2	0.0931±2	0.04838±6	89.3±0.2	90.3±0.2	117.9±2.8	24.4
7	cl, col, euh, 3:1, pr, 1 NM (2)	16	275	51	8	0.19	4	1906	0.03045±3	0.2224±6	0.05296±10	193.4±0.2	203.9±0.5	327.1±4.3	41.5
8	cl, col, euh, 4:1, pr, 1 NM (10)	30	567	144	30	0.25	5	10242	0.05360±5	0.6263±10	0.08475±6	336.6±0.4	493.8±1.3	1309.8±1.5	76.2
9	cl, col, euh, 4:1, pr, 1 NM (30)	34	931	238	31	0.26	19	3452	0.03403±4	0.3458±6	0.07370±8	215.7±0.3	301.5±0.5	1033.1±2.1	80.4
10	cl, col, euh, 5:1, pr, 1 NM (50)	34	899	231	34	0.26	7	10189	0.03834±3	0.3966±6	0.07503±6	242.5±0.2	339.2±0.5	1069.2±1.6	78.7
11	cl, col, sbh, 2:1, pr, 1 NM (1)	10	603	41	8	0.07	2	2121	0.01385±3	0.0913±3	0.04780±14	88.7±0.2	88.7±0.3	89.5±7.0	0.9
A	cl, yl, sbh, loz, N20-M5 (40)	618	220	250	3	1.14	617	180	0.01151±4	0.0753±9	0.04744±49	73.8±0.3	73.7±0.9	71.3±24.5	-3.5
B	cl, yl, sbh, loz, N20-M5 (50)	715	199	242	3	1.22	649	186	0.01206±4	0.0792±7	0.04762±37	77.3±0.3	77.4±0.7	80.4±18.2	4.0
C	cl, yl, sbh, loz, N20-M5 (25)	370	270	299	4	1.11	436	179	0.01095±4	0.0718±9	0.04753±46	70.2±0.3	70.4±0.8	75.9±23.2	7.6
D	cl, yl, sbh, fr, N20-M5 (35)	540	220	261	3	1.19	832	130	0.01225±5	0.0805±13	0.04766±64	78.5±0.4	78.6±1.2	82.5±32.2	4.9
E	cl, yl, sbh, fr, N20-M5 (45)	680	269	197	3	0.73	1099	125	0.01004±5	0.0653±12	0.04720±70	64.4±0.4	64.3±1.1	59.3±35.3	-8.6
Granodiorite (M2)[f], Cosens Bay pluton, UTM 334280E 5559720N															
1	euh, 5:1, pr, col, 0NM (200)	230	558	50	11	0.09	12	13605	0.01894±11	0.13196±77	0.05054±3	120.9±0.7	125.9±0.7	220.0±1.6	45.5
2	col ndl, 0M (196)	223	330	25	6	0.08	12	7398	0.01932±6	0.13989±44	0.05217±4	123.4±0.4	132.1±0.4	293.1±1.7	58.5
3	sbh, pr, 0NM (200)	149	423	40	7	0.10	13	5351	0.01746±8	0.11994±57	0.04983±5	111.6±0.5	115.0±0.5	186.9±2.4	40.7
4	lg, col, mky cr, (1)	14	240	25	8	0.11	9	743	0.03092±7	0.24739±116	0.05802±23	196.3±0.4	224.5±0.9	530.7±8.7	64.0
5	el, pr, lt yl, sl rs, mky cr, 0M (1)	13	202	14	5	0.07	4	1147	0.02574±5	0.20181±88	0.05686±22	163.9±0.3	186.7±0.7	485.9±8.6	67.1
6	el, pr, rs, sl yl, inc-cr, 0M (1)	11	377	13	8	0.03	4	1458	0.02216±3	0.18024±61	0.05898±17	141.3±0.2	168.2±0.5	566.5±6.4	75.9
7	cl, pr, sl rs, lg cr 0M (1)	14	432	27	14	0.06	85	99	0.01866±9	0.12993±1974	0.05049±2013	119.2±0.6	124.0±2.3	217.7±45.9	45.7
8	el, pr, 3:1, sl rs, lt yl, 0M (1)	19	257	21	9	0.08	22	479	0.03273±6	0.26978±98	0.05978±20	207.6±0.3	242.5±0.8	595.6±7.3	66.2
A	ang fr, cl, 1A M (54)	324	437	229	5	0.52	448	176	0.00798±3	0.05241±51	0.04765±51	51.2±0.2	51.9±0.6	82.1±25.1	37.8

Table 3-1 (page 3 of 4).

Fr.[a]	Description[b]	Wt. (µg)	Concentrations (ppm) U	Th	Pb	Th/U	TCPb (pg)	Atomic ratios[c,d] $^{206}Pb/^{204}Pb$	$^{206}Pb/^{238}U$	$^{207}Pb/^{235}U$	$^{207}Pb/^{206}Pb$	Apparent ages (Ma)[d] $^{206}Pb/^{238}U$	$^{207}Pb/^{235}U$	$^{207}Pb/^{206}Pb$	Disc. (%)
Diorite gneiss (M3)[f], Aberdeen gneiss complex, UTM 338432E 5556169N															
1	lg, col, eq fr, 1NM (1)	10	522	24	7	0.05	4	1268	0.01386±3	0.09150±45	0.04789±20	88.7±0.2	88.9±0.4	93.8±10.1	5.4
2	col, pr, euh, 1NM (1)	5	843	115	18	0.14	3	1794	0.02237±4	0.15151±59	0.04913±16	142.6±0.3	143.3±0.5	154.2±7.4	7.6
3	lg, col, sl yl, pr, 1NM (1)	7	278	62	6	0.22	3	853	0.02206±20	0.15260±170	0.05017±34	140.7±1.2	144.2±1.5	203.0±15.6	31.1
4	el, sl yl, 3:1, rs, pr, 1NM (1)	5	191	45	5	0.24	4	500	0.02744±9	0.18893±236	0.04994±59	174.5±0.6	175.7±2.0	192.0±27.1	9.2
5	el, sl yl, 3:1, rs, pr, 1NM (1)	5	235	66	8	0.28	3	702	0.03221±5	0.22505±180	0.05067±39	204.4±0.3	206.1±1.5	225.8±17.6	9.7
6	el, sl yl, 3:1, rs, pr, 1NM (1)	6	184	67	6	0.36	4	603	0.03240±5	0.22124±200	0.04953±43	205.5±0.3	202.9±1.7	172.9±20.1	-19.2
A	cl, yl, ang fr, 1A M (54)	269	249	7633	4	30.69	256	176	0.00963±3	0.06121±68	0.04609±51	61.8±0.2	60.3±0.7	2.4±26.4	-
B	cl, yl loz, 1A M (48)	192	170	104	3	0.61	258	94	0.00952±5	0.06321±137	0.04815±106	61.1±0.3	62.2±1.3	106.7±51.2	43.0
Migmatite schist (M4)[f], Aberdeen gneiss complex, UTM 345013E 5553979N															
1	cl, col, el, pr, 1NM (1)	6	639	138	22	0.22	44	150	0.02430±7	0.16472±201	0.04917±61	154.6±0.5	154.8±1.8	155.9±28.8	0.7
2	fr, pr, sl rs, cl, col, 1 NM (1)	12	887	181	22	0.20	23	788	0.02428±5	0.16492±69	0.04927±18	154.6±0.3	155.0±0.6	160.6±8.6	3.8
3	mky cr, pr, rs, 2:1, 1 NM (1)	17	645	55	12	0.09	18	672	0.01798±4	0.12288±50	0.04956±17	114.9±0.2	117.7±0.5	174.4±8.1	34.4
4	col, mky, inc, fr, 1NM (1)	10	327	67	8	0.21	7	666	0.02424±5	0.16733±178	0.05007±50	154.4±0.3	157.1±1.6	198.3±23.0	22.4
Monzonite (M5)[f], Nicklen Lake pluton, UTM 351939E 5553138N															
1	cl, yl, rs, inc, 3:1, pr, 1NM (1)	31	252	201	3	0.80	9	469	0.00807±1	0.05290±36	0.04753±31	51.8±0.1	52.3±0.3	76.1±15.3	32.0
2	col, inc, euh, 2:1, pr, 1NM (1)	6	257	44	5	0.17	19	63	0.00819±6	0.05956±216	0.05272±194	52.6±0.4	58.7±2.1	316.8±81.5	83.7
3	col, inc, sbh, rs, eq, 1 NM (1)	8	395	74	7	0.19	30	73	0.00819±5	0.05857±185	0.05187±165	52.6±0.3	57.8±1.8	279.5±71.1	81.5
4	cl, col, pr, 3:1, rs, 1 NM (1)	6	134	1582	2	11.78	8	68	0.00800±4	0.05091±262	0.04615±233	51.4±0.3	50.4±2.5	5.6±100.0	-
Tonalite gneiss (M6)[f], Aberdeen gneiss complex, UTM 360806E 5553415N															
1	rs, col, 3:1, inc-cr, pr, 1NM (1)	10	513	98	13	0.19	5	1727	0.02641±4	0.18234±58	0.05008±14	168.02±0.3	170.07±0.5	198.73±6.4	15.7
2	el, rs, lt yl, 4:1, 1NM (1)	21	94	28	3	0.30	10	297	0.02364±7	0.15994±200	0.04908±58	150.6±0.4	150.65±1.8	151.47±27.5	0.6
3	euh, cl, yl, inc, 3:1, pr, 1NM (1)	16	988	190	74	0.19	82	905	0.07540±9	0.51775±115	0.04980±10	468.62±0.5	423.65±0.8	185.69±4.6	-

Table 3-1 (page 4 of 4).

[a] numbers denote zircon fractions; letters titanite fractions.

[b] euh: euhedral; sbh: subhedral; pr: prismatic; loz: lozenges; ndl: needle; col: colourless; cl: clear; el: elongate; lt: light; yl: yellow; mky: milky; sl: slightly; eq: equant; cr: core; inc-cr: inclusion-rich core; rs: resorbed; ang: angular; fr: fragment(s); lg: large; sm: small; 3:1: 3 to 1 length to width ratio; inc: inclusions; frac: fractured; ireg: irregular; 0NM: fraction chosen from 0 degrees; non-magnetic split at 1.8 A unless other current is indicated, alternately M denotes a magnetic split; A: Amperes; number in brackets refers to the number of grains in the analysis.

[c] Atomic ratios corrected for blank and initial common Pb. The isotopic composition of the common Pb in excess of blank was calculated using the model of Stacey and Kramers (1975).

[d] All errors reported at 1 sigma.

[e] Sample dated at the University of British Columbia.

[f] Samp

[g] All UTM co-ordinates cited using a NAD83 datum, UTM Zone 11.

Table 3-2. U-Pb (SHRIMP) isotopic results for diorite gneiss (M3), Aberdeen gneiss complex.

Spot[a]	Textural context	Interpreted origin	U (ppm)	Th (ppm)	Th/U	$^{206}Pb^*$ (ppm)	^{204}Pb (ppb)	$^{206}Pb/^{204}Pb$	$\pm^{206}Pb/^{204}Pb$[b]	$f(206)^{207}$[c,d]	$^{208}Pb^*/^{206}Pb^*$	$\pm^{208}Pb/^{206}Pb$	$^{206}Pb^*/^{238}U$	$\pm^{206}Pb/^{238}U$	Apparent ages (Ma) $^{206}Pb/^{238}U$	Apparent ages (Ma) $\pm^{206}Pb/^{238}U$
Infrastructure																
Diorite gneiss (M3), Aberdeen gneiss complex, UTM[e] 338452E 5556169N																
7631-36.1	low CL planar banded rim	metamorphic	419	48	0.12	3	2	4.0223E-04	5.7963E-04	0.20509	0.04925	0.00565	0.00791	0.00010	50.8	0.6
7631-45.1	low CL planar banded rim	metamorphic	2333	344	0.15	18	2	1.5936E-04	7.1220E-05	0.04441	0.04703	0.00209	0.00799	0.00009	51.3	0.6
7631-86.1	high CL cloudy rim	metamorphic	99	4	0.04	1	2	5.1788E-03	1.1151E-03	0.48392	-0.01108	0.01451	0.00868	0.00014	55.7	0.9
7631-3.2	cloudy rim	metamorphic	171	12	0.07	2	2	1.7538E-03	1.3443E-03	0.32212	0.03001	0.00772	0.01036	0.00016	66.4	1.0
7631-53.1	high CL rim/overlap	overlap?	316	10	0.03	4	16	4.5382E-03	8.4529E-04	0.60377	-0.00091	0.01540	0.01287	0.00025	82.5	1.6
7631-91.1	high CL cloudy rim	metamorphic	177	17	0.10	2	3	1.0000E-03	1.0000E-03	0.30343	0.03045	0.00768	0.01350	0.00016	86.4	1.0
7631-91.2	high CL cloudy rim	metamorphic	186	34	0.19	2	3	9.9309E-04	3.4279E-04	0.27871	0.05742	0.00865	0.01401	0.00016	89.7	1.0
7631-45.2	cloudy high CL core	metamorphic	240	22	0.10	3	2	2.7153E-04	3.7881E-04	0.18663	0.02405	0.00452	0.01435	0.00017	91.8	1.1
7631-47.1	high CL rim	metamorphic	87	2	0.02	1	3	6.5784E-03	1.2313E-03	0.46004	0.00445	0.01064	0.01437	0.00020	92.0	1.3
7631-67.1	cloudy high CL rim	metamorphic	198	2	0.01	3	2	6.5238E-04	4.0693E-04	0.22812	0.00703	0.00771	0.01612	0.00020	103.1	1.3
7631-7.1	high CL rim/overlap	overlap?	337	18	0.06	7	2	2.7435E-04	1.7285E-04	0.09905	0.01671	0.00257	0.02177	0.00024	138.8	1.5
7631-71.1	cloudy rim	recrystallized?	113	23	0.21	2	2	6.8868E-04	4.5155E-04	0.23648	0.07147	0.00745	0.02220	0.00029	141.5	1.8
7631-96.1	sector/oscillatory core	igneous	1361	53	0.04	28	3	4.1350E-05	4.9320E-05	0.04109	0.00808	0.00148	0.02240	0.00024	142.8	1.5
7631-75.1	oscillatory core	igneous	625	46	0.08	13	2	1.8926E-04	8.1930E-05	0.04507	0.02854	0.00207	0.02324	0.00027	148.1	1.7
7631-47.2	sector core	igneous	1494	78	0.05	32	2	4.0900E-05	5.2930E-05	0.02254	0.01706	0.00131	0.02339	0.00026	149.0	1.6
7631-42.1	sector/oscillatory core	igneous	1014	79	0.08	22	2	7.1290E-05	4.0490E-05	*0.03321*	*0.02391*	0.00186	0.02342	0.00025	149.2	1.6
7631-17.1	sector core	igneous	1002	35	0.04	22	2	1.3982E-04	5.4010E-05	0.03274	0.01117	0.00164	0.02364	0.00027	150.6	1.7
7631-82.1	sector/oscillatory core	igneous	1642	161	0.10	36	1	6.0220E-05	4.7660E-05	0.01387	0.03182	0.00236	0.02369	0.00026	151.0	1.6
7631-30.1	oscillatory	igneous	1454	64	0.05	32	4	6.0530E-05	4.1940E-05	0.03677	0.01382	0.00186	0.02382	0.00026	151.8	1.6
7631-56.1	sector core	igneous	1548	62	0.04	34	2	9.5690E-05	3.4850E-05	0.02401	0.01224	0.00132	0.02384	0.00025	151.9	1.6
7631-32.1	sector core	igneous	1927	144	0.08	43	2	6.7380E-05	2.6950E-05	0.01500	0.02640	0.00158	0.02388	0.00026	152.1	1.7
7631-2.1	sector core	*igneous*	*1924*	*71*	*0.04*	*42*	*2*	*6.8060E-05*	*3.3890E-05*	*0.01807*	*0.01265*	*0.00172*	*0.02394*	*0.00027*	*152.5*	*1.7*
7631-51.1	irregular core	igneous	2374	97	0.04	52	3	4.5990E-05	5.9430E-05	0.01740	0.01234	0.00103	0.02401	0.00030	153.0	1.9
7631-4.1	sector core	igneous	1147	43	0.04	25	3	6.4750E-05	3.5300E-05	0.03888	0.01092	0.00133	0.02436	0.00027	155.2	1.7
7631-12.1	sector core	igneous	1985	147	0.08	45	1	4.3840E-05	2.1780E-05	0.00861	0.02478	0.00127	0.02456	0.00029	156.4	1.8
7631-8.1	sector core	igneous	1783	93	0.05	40	2	7.6090E-05	2.9820E-05	0.01917	0.01614	0.00195	0.02471	0.00028	157.4	1.8
7631-86.2	sector/oscillatory core	igneous	2008	94	0.05	45	4	4.6660E-05	2.3920E-05	0.02836	0.01276	0.00114	0.02481	0.00027	158.0	1.7
7631-16.1	*sector core*	*igneous*	*2101*	*76*	*0.04*	*48*	*0*	*8.8460E-05*	*2.5320E-05*	*0.00329*	*0.01338*	*0.00102*	*0.02497*	*0.00030*	*159.0*	*1.9*
7631-73.2	oscillatory core	igneous	279	101	0.37	10	2	3.3055E-04	1.7430E-04	0.07456	0.12776	0.00386	0.03643	0.00039	230.7	2.4
7631-29.1	oscillatory core	igneous	306	128	0.43	12	1	4.5356E-04	1.2917E-04	0.02536	0.14459	0.01199	0.03667	0.00049	232.1	3.1
7631-64.1	oscillatory core	igneous	271	113	0.43	10	3	3.6180E-04	1.0219E-04	0.08996	0.12914	0.00531	0.03677	0.00045	232.8	2.8
7631-74.1	oscillatory core	igneous	417	201	0.50	16	2	1.0000E-03	1.0000E-03	0.04410	0.15505	0.00541	0.03689	0.00041	233.6	2.6
7631-3.1	irregular core	igneous	69	48	0.72	5	2	5.1164E-04	5.8057E-04	0.14736	0.22591	0.00737	0.06417	0.00086	401.0	5.2

[a] Digits before decimal refer to grain number, digit after decimal refers to spot number.
[b] Radiogenic Pb, corrected for common Pb using the $^{207}Pb/^{206}Pb$ method (Stern 1997).
[c] Uncertainties reported at 1s (absolute) and are calculated by numerical propagation of all known sources of error.
[d] $f206^{207}$ refers to mole fraction of total ^{207}Pb that is due to common Pb, calculated using the ^{207}Pb-method; common Pb composition used is that of Cumming and Richards (1975) at the $^{207}Pb/^{206}Pb$ age.
[e] All UTM co-ordinates cited using a NAD83 datum, UTM Zone 11.

Lake (Thompson and Daughtry 1996). Gneissic fabric within the enclaves is truncated near the contact with the Wood Lake pluton, which is massive to weakly deformed (Fig. 3-7*c*). A sample of hornblende-biotite (ortho?)gneiss was selected in order to determine the age of metamorphism and(or) igneous emplacement. The sample contained centimetre-scale compositional layering parallel to the metamorphic foliation. Leucocratic layers contained plagioclase, quartz, hornblende, biotite, and secondary chlorite. Mafic layers were dominated by hornblende and plagioclase with lesser biotite.

Both zircon and titanite were recovered from the sample. Zircon grains are generally translucent and milky, but a small proportion of clear grains were also recovered. A minority of grains are prismatic, but most are irregular in shape. Virtually all grains exhibit evidence of minor to significant resorption. All zircon fractions were abraded prior to dissolution. Two distinct types of titanite grains were recovered: clear, pale yellow discs and blocky, broken fragments.

The results from seven of the ten multigrain zircon fractions analyzed, consisting of slightly cloudy to turbid grains, define a quasi-linear array plotting near the concordia between 180 and 170 Ma (Figs. 3-8*a*, 3-8*b*). These fractions have relatively high U contents (1396–2360 ppm) and moderate to high Th/U (0.17–0.68). There is a quasi-linear inverse relationship between U content and the $^{206}Pb/^{238}U$ age of the fractions. Fraction 6 plots near the lower end of the array and has a concordant $^{206}Pb/^{238}U$ date of 171.0 ± 0.8 Ma. Three-multigrain zircon fractions (1, 4, and 5) composed of clear grains with lower U contents (588–1051 ppm) have more discordant results and older $^{207}Pb/^{206}Pb$ dates. A best-fit line constructed through fractions 2, 3, 5, 6, 7, 8, 9 and 10 yields a lower intercept of 171.1 +3/-4.7 Ma and a poorly-defined upper intercept of ~520 Ma (MSWD = 4.2). If all of the zircon in the Wood Lake gneiss is detrital in origin, then the age of the protolith is younger than 171 Ma. This is considered unlikely, however, because the oldest phase of the Okanagan plutonic suite, which is intrusive into the Wood Lake gneiss, was emplaced between 173 and 170 Ma (Carr 1991; R.I. Thompson, unpublished data) and the composition of the gneiss is suggestive of a plutonic or volcanic protolith. Given that the Wood Lake gneiss must be older than 170 Ma, a more likely interpretation is that the date from concordant fraction 6, which is similar to the lower intercept age, records either the igneous emplacement age of the protolith or metamorphic zircon growth at 171 Ma, resulting from either regional metamorphism related to the accretion of the Intermontane Superterrane or contact metamorphism associated with the emplacement of the Okanagan plutonic suite. In the latter scenario, fractions with older $^{207}Pb/^{206}Pb$ dates would be interpreted to contain a mixture of metamorphic zircon and older detrital zircon. Given the composition of the gneiss, the relatively high Th/U of most fractions (5 out of 7 above 0.50), and the local prevalence of magmatism of

this age, the $^{206}Pb/^{238}U$ date from fraction 6 (171.0 ± 0.8 Ma) is interpreted as the best estimate of the emplacement age for the protolith of the Wood Lake orthogneiss.

The results from six titanite fractions fall near the concordia curve between 155 and 147 Ma (Fig. 3-8*b*). There is no clear relationship between grain size and age. The dispersion of the titanite dates may reflect the mixing of two or more age populations or variable amounts of post-crystallization lead loss. One possibility is that lead loss or new titanite growth occurred during high heat flow associated with widespread, extension-related Middle Eocene igneous activity (e.g., Mathews 1981).

Pegmatite, Wood Lake (S2)

Along the western shore of Wood Lake, numerous, weakly deformed pegmatite veins cut enclaves of amphibolite-grade paragneiss that occur within the Wood Lake pluton (Fig. 3-7*c*). The age of the pegmatite veins constrains the minimum age of the gneissic fabric.

A sample of pegmatite yielded abundant clear to opaque, pale tan- to beige-coloured, metamict and euhedral prismatic zircon grains. Only high-clarity grains were selected for analysis; opaque grains and those with visible core and overgrowth relationships were avoided. Zircon grains were abraded prior to analysis.

Five-multigrain fractions were selected for analysis. Fractions 1 to 4 have high U contents (2429–4486 ppm) and low Th/U (0.03–0.06). Three of these fractions (1, 3 and 4) are collinear, defining a reference line between 0 and 162 Ma (Fig. 3-8*c*). A weighted mean age calculation using $^{207}Pb/^{206}Pb$ dates from these fractions yields a date of 161.6 ± 2.8 Ma, which is taken as the best estimate of the igneous crystallization age. Fractions 2 and 5, which have older $^{207}Pb/^{206}Pb$ dates, are interpreted to contain an older inherited zircon component. The discordance of fractions 1, 3, and 4 may result from leaching of lead from metamict portions of zircon grains by meteoric fluids. The upper intercept date agrees within error with a U-Pb titanite date of 164.4 ± 2.0 Ma from the Wood Lake pluton, sampled near the southern end of Wood Lake (Thompson and Daughtry 1996).

Metamorphic infrastructure samples

Calcareous quartzite, Cosens Bay (M1)

At the north end of Kalamalka Lake, a resistant-weathering, north-dipping panel of mylonitic, diopside bearing, calcareous quartzite several hundreds of meters thick is exposed. The calcareous quartzite contains abundant millimetre to centimetre scale, discontinuous quartzofeldspathic layers oriented sub-parallel to the mylonitic foliation. Due to the pervasive

nature of the overprinting mylonitic fabric, it is unclear whether these leucocratic layers were generated *in-situ* or were sourced from elsewhere, possibly the underlying migmatitic pelitic schist succession. In order to constrain the timing of metamorphism and the crystallization of the leucosome, a bulk sample of mylonitic feldspathic calcareous quartzite with abundant, thin leucocratic layers was sampled.

The sample yielded a single population of clear, colourless, euhedral prismatic zircon and clear, pale yellow discs and broken fragments of titanite. Eleven zircon fractions, both single and multigrain, were selected and abraded prior to dissolution.

The results from the eleven zircon fractions range from highly discordant, with Proterozoic $^{207}Pb/^{206}Pb$ dates, to concordant at 89 Ma (Figs. 3-9*a*, 3-9*b*). The concordant result was obtained from a single, elongate prismatic zircon with an aspect ratio of about 4:1 and a square euhedral cross section (fraction 11). This grain morphology is most consistent with an igneous origin, although a low Th/U (0.07) is commonly associated with zircon crystallized in the solid state (i.e., metamorphic). Our interpretation of this concordant date is that it records zircon crystallization from a melt (now represented by the attenuated leucocratic layers) that was generated or emplaced during high-grade metamorphism. It is unclear whether the leucocratic layer was sourced by impure calcareous quartzite (which contains a small feldspar component), or was derived from the underlying migmatitic schist succession.

The U-Pb results from five multigrain titanite fractions plot along the concordia line between 79 and 64 Ma (Fig. 3-9*b*). As in the case of the Wood Lake gneiss, there are several ways to interpret the data, including the mixing of different age components, variable amounts of post-crystallization lead loss, or a combination of the two. There is a weak correlation between the Th/U of the fractions and their $^{207}Pb/^{206}Pb$ ages, with the oldest fractions having the highest Th/U, supporting the interpretation that the dispersion represents mixing of two geochemically distinct age populations. As such, a reasonable interpretation is that the fractions contain a mixture of titanite that grew during high temperature metamorphism at ~90 Ma (fraction 11, and see sample M3) and younger titanite that grew during a later event, possibly at ~61 Ma.

Granodiorite, Cosens Bay pluton (M2)

The age of the Cosens Bay pluton, which has been mylonitized at its margins and contains enclaves of the enclosing paragneiss succession, provides a minimum age for the metamorphic layering within the Kalamalka Lake metamorphic assemblage and a maximum age for shear associated with the Kalamalka Lake shear zone. A sample of medium-grained, strongly foliated, biotite and hornblende bearing granodiorite was selected for analysis.

A variety of zircon types were recovered from the sample, ranging from clear, colourless, euhedral elongate prisms and needles, to variably resorbed, colourless to yellow prisms with turbid cores. Dark to pale yellow titanite rhomboids and irregular fragments were also recovered.

The results of eight zircon fractions, displayed in Fig. 3-9*c*, fall within a poorly defined array. The results of three-multigrain fractions (1 to 3), composed of approximately two hundred delicate elongate prisms and needles, plot near the lower end of the loose array (Fig. 3-9*d*). These fractions have low to moderate U contents (330–558 ppm) and low Th/U (0.08–0.1). The other zircon fractions, composed of larger, light yellow, slightly resorbed single prisms, have similar U contents and Th/U, but are characterized by older $^{207}Pb/^{206}Pb$ dates, with the exception of fraction 7, which has a $^{207}Pb/^{206}Pb$ date similar to fractions 1, 2, and 3. Four out of five of these single grain fractions have visible core and overgrowth relationships, with the cores defined by turbid regions or by a central region with abundant dark inclusions. Four fractions (2, 3, 5, and 8) are approximately collinear and yield a lower intercept age of 102.2 ± 3.8 Ma and an upper intercept of ~ 1765 Ma. (Fig. 3-9*d*).

There are two possible interpretations for these U-Pb zircon results. In the first, the upper intercept represents the igneous crystallization age and the lower intercept represents the timing of zircon crystallization or lead loss during metamorphism. Alternatively, the lower intercept may be interpreted as the time of igneous emplacement, with the older dates reflecting an inherited zircon component. The second interpretation is favoured for two reasons: (1) the hosting paragneiss of the Cosens Bay pluton is thought to be Paleozoic in age, and therefore could not host a Paleoproterozoic pluton; and (2) the morphology of the delicate, elongate zircon needles comprising fractions 1 to 3 (lying near the lower intercept of the reference line) is most consistent with an igneous origin, as metamorphic zircon grains are commonly rounded or ovoid in shape (e.g., Heaman and Parrish 1991). As such, the lower intercept date of 102.2 ± 3.8 Ma is considered the best estimate for the emplacement age of the Cosens Bay pluton. The scatter of the data may reflect variable ages of inherited zircon components.

A single titanite fraction selected from this sample, composed of approximately fifty clear, angular fragments, yielded discordant results with a $^{206}Pb/^{238}U$ date of 51.2 ± 0.2 Ma. The significance of this date, which is approximately fifty million years younger than the estimated igneous emplacement age of the pluton, is not clear; it may be related to high Eocene heat flow associated with regional extension.

Diorite gneiss, Aberdeen gneiss complex (M3)

A sample of diorite gneiss from the AGC was selected to determine the igneous emplacement age. As leucocratic veins were present within the diorite gneiss (Fig. 3-7*d*), the sample was broken into fist-sized fragments and all vein material was removed.

A modest amount of zircon and titanite was recovered from the diorite gneiss. The zircon population is quite heterogeneous. The dominant zircon type includes clear, colourless, resorbed prisms with length to width ratios of 2:1 to 3:1. Less abundant types include clear, colourless multifaceted equant balls, irregular fragments, and subhedral egg-shaped grains. A small amount of clear, light yellow, elongate, slightly resorbed prisms with dark inclusions is also present. Most grains are slightly to moderately resorbed and do not contain visible core and overgrowth relationships. Titanite grains are of two types: (1) light yellow, clear fragments; and (2) slightly darker yellow lozenges with dark inclusions.

The U-Pb results for six single grain zircon fractions are shown in Fig. 3-9*e*. All six fractions yield concordant to slightly discordant results with $^{207}Pb/^{206}Pb$ dates between 225.8 and 93.8 Ma. The U content of the fractions is low to moderate (181-843 ppm) with variable Th/U (0.05-0.36). There is no clear correlation between the $^{207}Pb/^{206}Pb$ date and U content or Th/U. The results of fractions 1 to 6 are consistent with a short mixing line between ~220 and ~90 Ma. This mixing line can be interpreted in variety of ways. One possibility is that the igneous crystallization age of the main protolith of the Aberdeen gneiss complex is ~220 Ma or older, and that new zircon growth or lead loss occurred at ~90 Ma. Another possibility is that the igneous emplacement age is ~90 Ma, and that the fractions contain a component of older inherited zircon. Fraction 1, consisting of a clear, colourless, equant fragment, has an ovoid morphology, a low Th/U (0.05), and the youngest $^{207}Pb/^{206}Pb$ date, consistent with a metamorphic origin.

The U-Pb results for two multigrain titanite fractions, one composed of light yellow fragments and the other of darker yellow lozenges, plot near concordia at ~61 Ma (Fig. 3-9*e*). A weighted mean of the similar $^{206}Pb/^{238}U$ dates yields a date of 61.6 ± 4.2 Ma. In the absence of additional information, the geological significance of this result is difficult to determine, but it may represent the time at which the titanite grains cooled below their closure temperature or, alternatively, the timing of titanite growth during a discrete thermal event.

To gain additional age information from this sample within a textural context, selected zircons were analyzed using the SHRIMP II instrument located at the Geological Survey of Canada geochronology facility in Ottawa. The SHRIMP U-Pb results are plotted in Fig. 3-9*f* and listed in Table 3-2. The isotopic data were initially corrected for common Pb using the ^{204}Pb method (Stern 1997). Due to the small amount of ^{207}Pb present in young samples, once the gross

concordance of the results is checked using the ^{204}Pb method (ellipses plotted in Fig. 3-9*f*), the ^{207}Pb data, which yield little age information due to the poor precision, are commonly used to correct for common lead by the ^{207}Pb method (Stern 1997). The resulting ^{207}Pb-corrected data (Table 3-2) were used to calculate the weighted mean $^{206}Pb/^{238}U$ dates.

The cathodoluminescence (CL; Fig. 3-10) and backscattered electron (BSE) images (Appendix G) of zircon from sample M-3 reveal a considerable degree of structure within individual grains. Based on their textural setting, zoning characteristics, and CL emission, six distinct zircon domain types were recognized: (1) rare, resorbed, variably-luminescent cores; (2) oscillatory-zoned cores; (3) sector-zoned cores; (4) highly-luminescent and cloudy, or planar-banded overgrowths; (5) low- to moderately-luminescent, unzoned or planar-banded overgrowths; and (6) highly-luminescent, patchy and irregular domains.

Type 1 domains, characterized by high luminescence and embayed margins, are mantled by domain types 2 and 3 (Fig. 3-10, grains 50 and 86), suggesting that type 1 domains represent grains that were incompletely resorbed in a melt. Type 2 zircon, which exhibits oscillatory zoning characteristic of igneous zircon (e.g., Hanchar and Millar 1993; Rubatto and Gebauer 2000), commonly occurs as large, prismatic grains that are mantled by thin overgrowths of zircon types 4 and/or 5 (Fig. 3-10, grains 29 and 50). Type 3 zircon is similar in occurrence to type 2 zircon (Fig. 3-10, grains 47 and 91) and is interpreted, based on its sector zoning and mode of occurrence, to be igneous. Type 4 zircon is rarely found in the centre of grains, where it is mantled by type 5 zircon (Fig. 3-10, grain 45). The most common occurrence of type 4, however, is as thin overgrowths on zircon types 2 and 3 (Fig. 3-10, grains 47, 50, 86, and 91). The inner margins of type 4 domains are commonly irregular and truncate zoning within the cores, suggesting that the cores were resorbed prior to the crystallization of the (type 4) overgrowth. The occurrence of type 4 zircon as thin shells mantling types 2 and 3 zircon, its high CL emission, and its unzoned or planar-banded zoning are compatible with a metamorphic origin (e.g., Rubatto and Gebauer 2000). Type 5 zircon, which occurs as thin overgrowths on all other types (Fig. 3-10, grains 36 and 45), is similarly interpreted to be metamorphic in origin. Type 6 zircon, which occurs as patchy zones that truncates zoning and domain boundaries (Fig. 3-10, grain 29), is interpreted to result from late alteration, possibly along fractures or zones of radiation damage.

The $^{206}Pb/^{238}U$ SHRIMP dates fall within five broad groups (Fig. 3-9*f*) and show a clear relationship to CL domain type (Table 3-3). A single data point from type 1 zircon yielded the oldest $^{206}Pb/^{238}U$ date of 401 Ma. The $^{206}Pb/^{238}U$ dates from zircon types 2 and 3 fall within two groups: (1) ~232 Ma; and (2) 159-143 Ma (Fig. 3-10; Tables 3-2 and 3-3). Zircon types 4 and 5 fall within two poorly defined age categories of 66-51 Ma and 103-82 Ma (Fig. 3-10; Table 3-2).

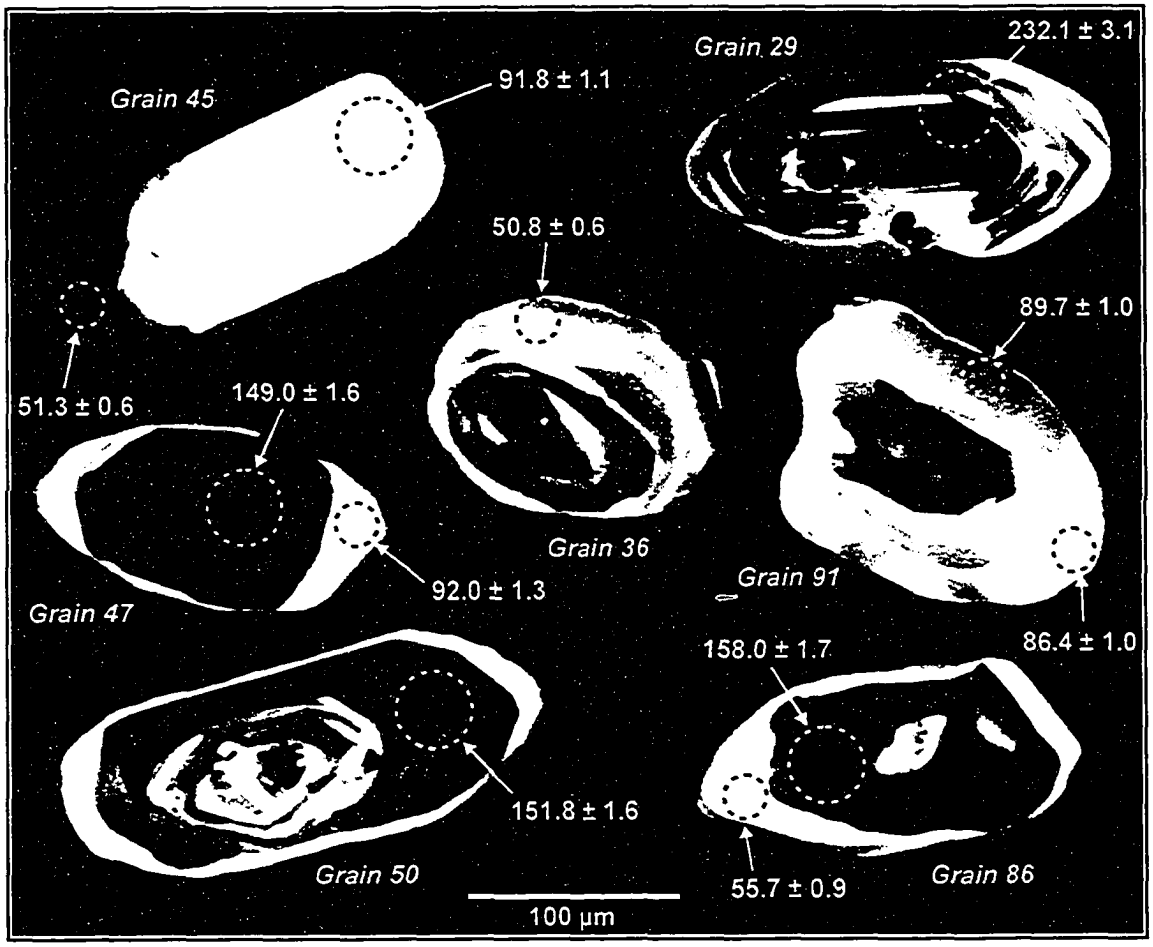

Fig. 3-10. Cathodoluminescence (CL) images of selected polished zircon grains separated from a diorite gneiss phase exposed within the Aberdeen gneiss complex (M3) indicating the approximate SHRIMP spot size and location (dashed circles). The $^{206}Pb/^{238}U$ ages and 1σ errors are shown for corresponding spot locations. Scale bar (bottom centre) is 100 microns long.

Table 3-3. Comparison of zircon characteristics and spot ages from diorite gneiss (M3), Aberdeen gneiss complex.

Domain	Textural context	Zoning	CL emission	Geochemical signature	$^{206}Pb/^{238}U$ ages (Ma)[a]
1	core	oscillatory	high	low U, high Th/U	**401** (1)
2	core	oscillatory	variable	moderate U, high Th/U	**143-159** (16), **231-234** (4)
3	core	sector	variable	high to moderate U, low Th/U	**143-159** (16), **231-234** (4)
4	core/overgrowth	cloudy	high	low U, low Th/U	**56-64** (2), **86-103** (5)
5	overgrowth	unzoned/planar-banded	low to moderate	low U, low Th/U	**51** (2)
6	patchy	unzoned	high	unknown	unknown

[a] The number in brackets refers to the number of individual spot analyses.

Some of the range in ages can be attributed to beam overlap between different domains during analysis, as the width of the overgrowths is commonly less than the 30 μm beam width.

The four age groups have distinctive geochemical characteristics. The 232 Ma group has low U content (271–417 ppm) and high Th/U (0.37–0.50), compatible with a magmatic origin. The 159-143 Ma group has extremely variable U content (625–2374 ppm) but relatively uniform and low Th/U (0.04–0.1). The two younger age groups generally have moderate to low U content and low Th/U, consistent with a metamorphic origin.

The data indicate that zircon types 2 and 3, interpreted as igneous in origin based on their mode of occurrence and zoning characteristics, grew within the diorite gneiss at 232 Ma and in the interval between 159 and 143 Ma. The latter age group has a considerable range in $^{206}Pb/^{238}U$ dates (~16 million years) that cannot be accounted for entirely by analytical error. The cause of this spread in ages is unclear.

There are several possible interpretations for these results. If the 232 Ma old zircon is inherited, the igneous emplacement age for the gneiss would be between 159 and 143 Ma. However, all four of the 230 Ma zircons were large, euhedral to subhedral prisms, lacking evidence of significant resorbtion or igneous overgrowths. Alternatively, the igneous emplacement age of the diorite may be 232 Ma, with the younger igneous zircon forming during migmatization of the gneiss. The second interpretation is most consistent with both the textural relationships and data from a nearby sample (M4), which suggest that migmatization of the pelitic units within the gneiss complex occurred at 155 Ma. Therefore, this sample of diorite gneiss is interpreted as having been emplaced at 232.2 ± 2.6 Ma (weighted mean of $^{206}Pb/^{238}U$ dates) and migmatized at 155.0 ± 2.0 Ma. The highly luminescent, cloudy, unzoned zircon overgrowths, interpreted to be metamorphic in origin, yielded $^{206}Pb/^{238}U$ dates of ~90 Ma. This age agrees well with the $^{206}Pb/^{238}U$ date (ID-TIMS) of 88.7 ± 0.2 Ma obtained from a single clear, colourless, ovoid zircon (#1), selected due to its characteristic metamorphic morphology. Both the morphology of the single zircon grain and the low Th/U (0.05) suggest a metamorphic origin.

Several lines of evidence indicate that the diorite gneiss was affected by a second, younger metamorphic event (see also, Fig. 3-11). A number of zircon rims, characterized by high luminescence and cloudy zoning (type 4), or low luminescence and planar-banded zoning (type 5), yielded ages between 51 and 66 Ma (Fig. 3-10, grains 36, 45, and 86). The range in ages may be due, in part, to beam overlap between domains, as the rims are often nominally wider than the beam width. The mode of occurrence and moderate to low Th/U of the zircon rims is consistent with a metamorphic origin. In addition, the weighted mean $^{206}Pb/^{238}U$ dates (ID-TIMS) of 61.6 ±

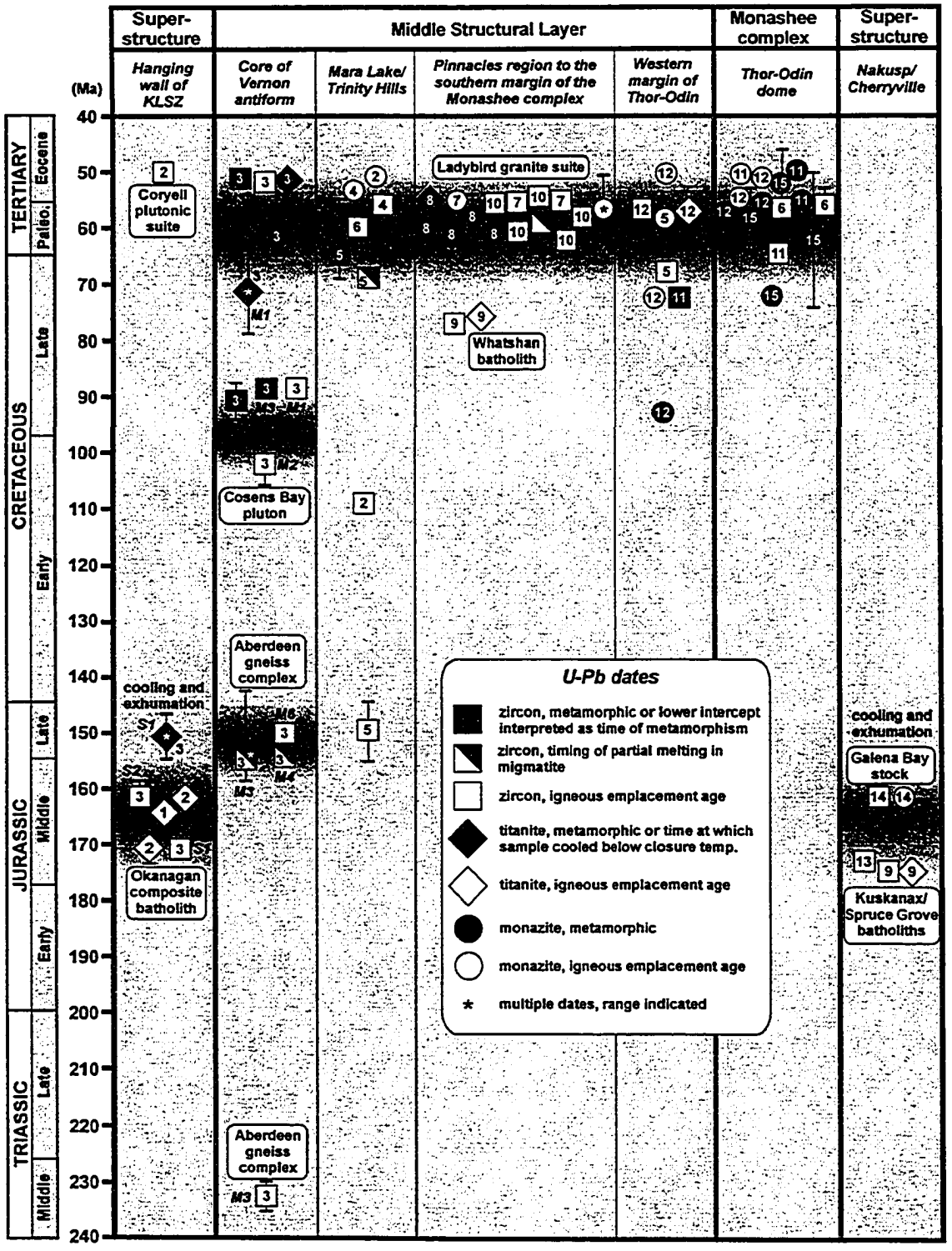

Fig. 3-11. Compilation diagram of Triassic to Eocene U-Pb age dates from the Shuswap metamorphic complex between latitudes 50° and 51° N. The structural level of the area is indicated at the top of the columns. Sources: 1 – Thompson and Daughtry (1996); 2 – R.I. Thompson, unpublished data; 3 – this study; 4 – Bardoux (1993); 5 – Johnson (1994); 6 – Vanderhaeghe et al. (1999); 7 – Parrish et al. (1988); 8 – Carr (1990); 9 – Carr (1991); 10 – Carr (1992); 11 – Parkinson (1992); 12 – Johnston et al. (2000); 13 – Parrish and Wheeler (1983); 14 – Parrish and Armstrong (1987); 15 – Kuiper (2003).

4.2 Ma from the two titanite fractions falls within this age range, suggesting that a metamorphic event during this time interval resulted in the crystallization of both zircon and titanite.

Migmatitic schist, Aberdeen gneiss complex (M4)

Pelitic rocks within the AGC are migmatitic with millimetre to centimetre scale, discontinuous leucosome layers oriented co-planar with the transposition foliation (stromatic migmatite; Fig 3-7*e*). The leucosome layers outline hinges of rare isoclinal (F_1) folds, suggesting that partial melting preceded D_2 folding. A sample of migmatitic pelitic schist was dated to determine the timing of migmatization.

A bulk sample of the migmatitic schist yielded abundant zircon of variable character, including colourless, clear to cloudy fragments, needles, anhedral blobs, multi-facetted spheres, and euhedral prisms.

Four single grain zircon fractions were selected for analysis. The results of three of the fractions cluster on or near the concordia curve at 155 Ma, while a single fraction (#3) is more discordant, with a lower Th/U (0.09 compared with 0.20–0.22) and a younger $^{207}Pb/^{207}Pb$ date (Fig. 3-5*g*). As the depositional age of the pelitic schist must be older than 232 Ma, the emplacement age of the diorite phase (M3) discussed above, the weighted mean of the $^{206}Pb/^{238}U$ dates of fractions 1, 2, and 4, is interpreted to reflect the timing of migmatization, rather than the age of detrital zircon from a single source. The significance of the discordant result is unclear; a reference line through fraction 3, anchored at 155 Ma, yields a negative intercept. One possibility is that this single grain fraction, in which a core and overgrowth relationship was observed in plain polarized light, contains a mixture of (metamorphic?) zircon younger than 155 Ma and a component of older detrital zircon inherited from the protolith.

Monzonite, Nicklen Lake pluton (M5)

The Aberdeen gneiss complex is intruded by the Nicklen Lake pluton, a massive to weakly deformed pluton of medium to coarse-grained, biotite-bearing, potassium feldspar megacrystic monzonite to quartz monzonite (Glombick et al. 2000; Fig. 3-6). The emplacement age of the pluton post-dates the fabric of the enclosing gneiss.

A sample of the Nicklen Lake pluton yielded a large amount of zircon. The dominant type of zircons are large, clear, colourless to light yellow, variably resorbed prisms with large, cloudy inclusions that are evenly distributed throughout the grains. A smaller number of clear, colourless, anhedral equant zircon grains and fragments were also recovered.

Four single grain zircon fractions were selected for analysis. The results lie near the concordia line at ~51 Ma (Fig. 3-9*h*). A best-fit line through all four analyses yields a lower intercept of 51.7 ± 0.1 Ma, the best estimate of the igneous emplacement age of the Nicklen Lake pluton.

Tonalite gneiss, Aberdeen gneiss complex (M6)

The most abundant orthogneiss phase present within the AGC is a hornblende and/or biotite-bearing, medium grained tonalitic gneiss. This phase contains blocks, wispy enclaves, and layers of the diorite, although, in places, the transition between the two is gradational (Fig. 3-7*a*, *b*). A sample of homogeneous, medium-grained, foliated hornblende bearing tonalitic gneiss was selected to determine the emplacement age.

The sample yielded abundant zircon with variable shapes, sizes, clarity, and colour. Elongate prisms with an aspect ratio of 2:1 to 3:1 are the most common grain shape; equant spheres, stubby fragments, and egg-shaped grains are also present. A large proportion of the prismatic grains have turbid, inclusion-rich cores and clear overgrowths. Colourless varieties are the most common, but elongate prisms may have a slightly yellowish tint.

Three single grain zircon fractions were analysed. The results from two of the fractions (1 and 2) plot near concordia between 175 and 150 Ma (Fig. 3-9*i*). The third fraction is reversely discordant, lying above concordia near 450 Ma. The significance of this result is not clear; it may reflect contamination during analysis, as the fraction contained a large amount of common Pb (82 pg) (Table 3-1). The other two results have low to moderate U content (94-513 ppm) and a Th/U consistent with a magmatic origin (0.19-0.30). The geological significance of the results is difficult to determine, but in the absence of additional information, the $^{206}Pb/^{238}U$ date of 150.6 ± 0.4 Ma from concordant fraction 2 is taken as the best estimate for the igneous emplacement age of the tonalitic gneiss.

Discussion

Emplacement age of the Aberdeen gneiss complex

Based on the U-Pb results, the AGC was emplaced during two magmatic episodes, a Middle Triassic (predominantly mafic?) magmatic pulse at 232 Ma, and a younger event at 155-150 Ma, synchronous with Middle to Late Jurassic regional high-grade metamorphism and anatexis within the Vernon antiform (Fig. 3-11). The relative volume of these two age components within the AGC is unclear, but the younger episode may have resulted in a large amount of (re)melting and mobilization of older protoliths within the complex, leaving dioritic

restite of Middle Triassic age. There is no evidence, at present, of a Paleoproterozoic age component exposed at surface within the AGC. Further Sm-Nd and U-Pb age dating may reveal evidence for a Paleoproterozoic basement at depth.

Magmatism of Middle Triassic age is rare within the southern Canadian Cordillera. To the west of the Vernon area, within the Upper Triassic Nicola Group, the oldest intrusive rocks are approximately 219 Ma old (Ghosh 1995, and references therein). An older date of 230.2 ± 0.8 Ma has been obtained from the Clark Creek metatonalite, a foliated pluton within the Nicola horst, itself a fault-bounded uplift of amphibolite-grade metamorphic rocks that underlie Upper Triassic rocks of the Nicola Group (Fig. 3-2) (Erdmer et al. 2002). A date of 225 ± 5 Ma has been obtained from highly altered, layered quartz-feldspar-epidote gneiss (Sample MV-82-176) from the Mount Lytton-Eagle plutonic complex, located adjacent to the Pasayten-Fraser River fault system (Parrish and Monger 1992). The gneiss is cut by massive biotite granodiorite dated at 212 ± 1 Ma, which is coeval with Nicola arc magmatism (Parrish and Monger 1992). The Eagle River complex contains Middle to Late Jurassic (157-148 Ma) tonalite gneiss and weakly foliated granodiorite of the Fallslake plutonic suite dated at 110.5 ± 2 Ma (Greig et al. 1991). Interestingly, the timing of magmatic events in the Mount Lytton-Eagle plutonic complex overlaps the timing of magmatic events in the Vernon antiform almost exactly (~232, 155-150, and 102 Ma).

The Clark Creek metatonalite intrudes a heterolithic metasedimentary succession (the Bob Lake assemblage) including metaconglomerate that has yielded a Proterozoic-aged granitic clast (1038 Ma) and Proterozoic detrital zircons. The relationship between the Bob Lake assemblage and rocks of the Nicola Group is unclear. A correlation between the metamorphic rocks exposed within the Nicola horst and similar rocks exposed to the north of Vernon (the Spa Creek assemblage) has been proposed previously based on lithological similarities (Erdmer et al. 1999). That correlation is supported by the occurrence of rare Middle Triassic tonalitic intrusive rocks in both areas. Because rocks of the Vernon area can be depositionally linked to the cratonic margin during Middle Paleozoic to Jurassic time (see review in Thompson et al. 2004), the occurrence of distinctive Middle Triassic deformed metatonalite bodies in both the Vernon antiform and the Nicola horst indicates that the basement of the Nicola Group, possibly exposed within the Nicola horst and Mount Lytton-Eagle River plutonic complex, may have been stratigraphically linked to the cratonic margin during the Middle Triassic, immediately prior to the initiation of Upper Triassic (Nicola) arc magmatism.

In light of the 232 Ma age obtained for the AGC, two previously unreported (U-Pb, zircon) results obtained from mafic gneiss exposed west of Mabel Lake with upper intercepts of

228 and 235 Ma are of potential significance. Both results, of three to four multigrain zircon fractions each, yielded discordant results with imprecise upper intercepts of 228 and 235 Ma and poorly constrained lower intercepts around 55 Ma (no errors reported; Okulitch 1979). These results, though inconclusive, may indicate that Middle Triassic mafic magmatism may have been more widespread in the Vernon area than has previously been recognized.

Thermotectonic evolution of the Vernon antiform

Rocks within the core of the Vernon antiform preserve evidence of a complex and episodic thermotectonic evolution (Fig. 3-11). The earliest recorded event within the AGC is the emplacement of diorite at ~232 Ma. That result is surprising, as that age is approximately ten million years older than the oldest known magmatism associated with the Nicola arc (e.g., Ghosh 1995).

The next oldest event recorded within the Vernon antiform is widespread migmatization during high-grade regional metamorphism at ~155 Ma. Evidence of this event includes leucosome within migmatitic pelitic rocks (sample M4), the formation of igneous zircon within diorite gneiss of the Aberdeen gneiss complex (sample M3) and the emplacement of homogenous tonalitic gneiss at ~150 Ma (sample M6). Pelitic schist within the AGC also experienced metamorphic monazite growth at this time (Fig. 3-11).

As Middle Triassic diorite gneiss within the AGC preserves gneissic layering (S_1) that is discordant to the foliation (S_2) within the enclosing tonalitic gneiss, the age of S_1 fabric must be between 150 and 232 Ma. Leucosome within stromatic migmatite, dated at 154.5 ± 0.5 Ma, is parallel to the metamorphic transposition foliation (S_2) that is folded by isoclinal (F_2) folds. The age of the metamorphic foliation (S_2) must therefore be between 154 Ma and 102 Ma, the age of the Cosens Bay pluton, and F_2 folds must be younger than 154 Ma.

The Cosens Bay pluton was emplaced at 102.2 ± 3.8 Ma. This is similar to the age of other deformed orthogneiss sheets of similar composition within the SMC (e.g., Ghosh 1995; Parrish 1995, and references therein). A similar deformed hornblende granodiorite sheet exposed within the footwall of the Okanagan Valley fault near Skaha Lake, approximately two hundred kilometres due south of Vernon, has been dated at 105 ± 11 Ma (Parkinson 1985). The Kalamalka Lake shear zone overprints the Cosens Bay pluton, constraining the age of the shear zone to be younger than 102 Ma.

Evidence of a second high-grade metamorphic event within the Vernon antiform ca. 90 Ma includes metamorphic zircon growth within diorite gneiss (sample M3) and crystallization of (igneous?) zircon within leucosome-bearing calcareous quartzite gneiss (sample M4). The

crystallization of igneous zircon suggests that this event was of sufficiently high temperature (>730°C) to induce dehydration melting within fertile rock types. Metamorphism of that age is common within the Shuswap metamorphic complex and has been reported from the Pinnacles (Fig. 3-11), Joss Pass (Johnston et al. 2000) and Mica Dam (Crowley et al. 2000) areas.

The final metamorphic event recorded within the Vernon antiform, which is poorly constrained between 66 and 51 Ma (Fig. 3-11), resulted in the crystallization of metamorphic zircon within diorite gneiss (M3). This event overlaps the timing of widespread igneous activity within the SMC, including the emplacement of the Nicklen Lake pluton and granitic rocks of the Ladybird plutonic suite (Parrish et al. 1988; Carr 1992; this study). The pressure and temperature conditions of this event are unclear, as the timing of this event coincides with cooling of metamorphic infrastructure rocks from 500°C through 250°C and widespread extension faulting and exhumation (Parrish et al. 1988).

The composition and emplacement age (51 Ma) of the undeformed Nicklen Lake pluton are similar to those of other extension-related Middle Eocene (51-48 Ma) intrusive rocks of granitic to alkalic composition, collectively known as the Coryell plutonic suite (e.g., Parrish et al. 1988).

The high-temperature cooling history of the Vernon antiform is poorly constrained. The titanite dates of approximately 62 Ma from the diorite gneiss (M3) suggest that the complex had cooled below the closure temperature of titanite before this time (~660-700°C; Scott and St-Onge 1995), in good agreement with Paleocene to Eocene K-Ar cooling dates from hornblende and mica from infrastructure rocks in the greater Vernon area (Mathews 1981; Vanderhaeghe et al. 2003). A sample of biotite-bearing tonalitic gneiss from the AGC has yielded a K-Ar (biotite) date of 46.9 ± 0.5 Ma (R. I. Thompson, unpublished data).

In contrast to the complex thermal evolution recorded by infrastructure rocks within the footwall of the Kalamalka Lake shear zone, superstructure rocks situated within the hanging wall record a simple thermal evolution with one high-temperature event at ~171 Ma (see sample M2) that overlapped the emplacement of the Middle Jurassic Okanagan plutonic suite (Fig. 3-11). That event is slightly older (fifteen to twenty million years) than the Late Jurassic event (~155-150 Ma) that is recorded in high-grade rocks within the core of the Vernon antiform. Middle to Late Jurassic potassium-argon cooling dates from superstructure rocks in the Vernon area support the interpretation that superstructure rocks cooled to below ~250°C within twenty to thirty million years after peak regional metamorphism and were not significantly heated after this time (Mathews 1981). The lack of evidence of Cretaceous (100-90 Ma) and Paleocene (65-50 Ma) metamorphic events within rocks of the hanging wall of the Kalamalka Lake shear zone suggests

that the hanging wall and footwall rocks were situated at significantly different structural levels during Cretaceous to Paleocene time.

A comparison of the thermotectonic evolution of the Vernon area with adjacent areas of the SMC reveals significant differences (Fig. 3-11). The metamorphic infrastructure in the Vernon area records three metamorphic events (occurring at 155-150, 90, and 65-50 Ma), with the two older events being of sufficient grade to cause migmatization and metamorphic zircon growth in a several different rocks types. The Trinity Hills area, northeast of Vernon (Fig. 3), records a similar three-stage metamorphic evolution (Fig. 3-11). Further to the east, in the Pinnacles area and along the western margin of the Monashee complex, there is evidence of a Cretaceous metamorphic event around 90 Ma, but no evidence of a Middle to Late Jurassic event. The Thor-Odin culmination of the southern Monashee complex, possibly the deepest structural level exposed at this latitude of the hinterland, does not record Cordilleran metamorphism prior to Paleocene time (Fig. 3-11).

Largely on the basis of geochronological data from the northern SMC, Parrish (1995) proposed that the age of tectonism and metamorphism varies with structural level within the southeast Canadian Cordillera. In his model, the highest structural levels are metamorphosed in the Middle Jurassic (170-160 Ma), with the age of tectonism becoming progressively younger with increasing structural depth, so that the lowermost structural levels, presently exposed within the Monashee complex, were not buried and metamorphosed until Paleocene to Eocene time. This younging pattern of tectonism has been interpreted in the context of a northeast-directed orogenic wedge that progressively overrode and buried rocks of the cratonic margin as it moved forward, continuously accreting rocks to its base (see also Brown 2004). The model predicts a relatively simple thermal history for rocks within the wedge. After being buried and metamorphosed beneath the advancing wedge, rocks are accreted into the wedge at its base when the basal shear zone steps down. Once within the wedge, rocks are progressively exhumed by extension faulting within the wedge and/or erosion of the upper wedge surface (Brown 2004). A particle following such a path would experience a single high-grade metamorphic event, before being gradually exhumed.

The data from the Vernon antiform and other areas of the Cordillera, where detailed geochronological data are available (e.g., Crowley et al. 2000), show that certain structural levels of the hinterland experienced a complex and episodic thermotectonic evolution; some areas preserve evidence of as many as five distinct metamorphic events. This complexity may indicate that current thermotectonic models are too simple and that the thermal evolution of the hinterland is inadequately accounted for. A major limitation of all thermotectonic studies within the SMC

remains the uncertainty in determining the metamorphic conditions (pressure and temperature) associated with the crystallization of accessory minerals in high-grade, polymetamorphic rocks.

References

Armstrong, R.L., Parrish, R.R., Van der Heyden, P., Scott, K., Runkle, D., and Brown, R.L. 1991. Early Proterozoic basement exposures in the southern Canadian Cordillera: core gneiss of Frenchman Cap, Unit L of the Grand Forks Gneiss, and the Vaseaux Formation. Canadian Journal of Earth Sciences, **28**: 1169-1201.

Ashworth, J.R. 1985. Migmatites. Chapman and Hall Ltd., New York.

Bardoux, M. 1993. The Okanagan Valley fault from Penticton to Enderby, south-central British Columbia. Ph.D. thesis, Carleton University, Ottawa.

Brown, R.L. 2004. Thrust belt accretion and hinterland underplating of orogenic wedges: an example from the Canadian Cordillera. *In* Thrust Tectonics and Petroleum Systems. *Edited by* K. McClay American Association of Petroleum Geologists, Memoir 82, pp. 1-14.

Brown, R.L., Journeay, J.M., Lane, L.S., Murphy, D.C., and Rees, C.J. 1986. Obduction, backfolding and piggyback thrusting in the metamorphic hinterland of the southeastern Canadian Cordillera. Journal of Structural Geology, **8**: 255-268.

Carr, S.D. 1990. Late Cretaceous-early Tertiary tectonic evolution of the southern Omineca Belt, Canadian Cordillera. Ph.D. thesis, Carleton University, Ottawa.

Carr, S.D. 1991. U-Pb zircon and titanite ages of three Mesozoic igneous rocks south of the Thor-Odin-Pinnacles area, southern Omineca Belt, British Columbia. Canadian Journal of Earth Sciences, **28**: 1877-1882.

Carr, S.D. 1992. Tectonic setting and U-Pb geochronology of the early Tertiary Ladybird leucogranite suite, Thor-Odin-Pinnacles area, southern Omineca Belt, British Columbia. Tectonics, **11**: 258-278.

Cook, F.A., Varsek, J.L., Clowes, R.M., Kanasewich, E.R., Spencer, C.S., Parrish, R.R., Brown, R.L., Carr, S.D., Johnson, B.J., and Price, R.A. 1992. Lithoprobe crustal reflection cross-section on the southern Canadian Cordillera, 1, Foreland Thrust and Fold Belt to Fraser River fault. Tectonics, **11**: 12-35.

Crowley, J.L., Ghent, E.D., Carr, S.D., Simony, P.S., and Hamilton, M.A. 2000. Multiple thermotectonic events in a continuous metamorphic sequence, Mica Creek area, southeastern Canadian Cordillera: Geological Materials Research, **2**: 1-45.

Cumming, G.L., and Richards, J.R. 1975. Ore lead in a continuously changing Earth. Earth and Planetary Science Letters, **28**: 155-171.

Currie, L.D. 1988. Geology of the Allen Creek area, Cariboo Mountains, British Columbia. M.Sc. thesis, University of Calgary, Calgary.

Digel, S.C., Ghent, E.D., Carr, S.D., and Simony, P.S. 1998. Early Cretaceous kyanite-sillimanite metamorphism and Paleocene sillimanite overprint near Mount Cheadle, southeastern British Columbia: geometry, geochronology, and metamorphic implications. Canadian Journal of Earth Sciences, **35**: 1070-1087.

Erdmer, P., Thompson R.I., and Daughtry, K.L. 1998. The Kalamalka Lake metamorphic assemblage, tectonic infrastructure in the Vernon map area, British Columbia. *In* Current Research 1998-A. Geological Survey of Canada, pp. 189-194.

Erdmer, P., Thompson, R.I., and Daughtry, K.L. 1999. Pericratonic Paleozoic succession in Vernon and Ashcroft map areas, British Columbia. *In* Current Research 1999-A. Geological Survey of Canada, pp. 205-215.

Erdmer, P., Heaman, L., Creaser, R.A., Thompson, R.I., and Daughtry, K.L. 2001. Eocambrian granite clasts in southern British Columbia shed light on Cordilleran hinterland crust. Canadian Journal of Earth Sciences, **38**: 1007-1016.

Erdmer, P., Moore, J.M., Heaman, L.M., Thompson, R.I., Daughtry, K.L., and Creaser, R.A. 2002. Extending the ancient margin outboard in the Canadian Cordillera; record of Proterozoic crust and Paleocene regional metamorphism in the Nicola horst, southern British Columbia. Canadian Journal of Earth Sciences, **39**: 1605-1623.

Ghent, E.D., Simony, P.S., and Knitter, C.C. 1980. Geometry and pressure-temperature significance of the kyanite-sillimanite isograd in the Mica Creek area, British Columbia. Contributions to Mineralogy and Petrology, **74**: 67-73.

Ghosh, D.K. 1995. Nd-Sr isotopic constraints on the interactions of the Intermontane Superterrane with the western edge of North America in the southern Canadian Cordillera. Canadian Journal of Earth Sciences, **32**: 1740-1758.

Glombick, P., and Thompson, R.I. 2004. Geology of the Creighton Creek map area, British Columbia (NTS 82L/02). Geological Survey of Canada Open File 4371, scale 1:50 000.

Glombick, P., Erdmer, P., Thompson, R.I., and Daughtry, K.L. 1999. Ductile shear zones and an Eocene unconformity between Kalamalka Lake and Oyama Lake, Vernon map area, British Columbia. *In* Current Research 1999-A. Geological Survey of Canada, pp. 193-198.

Glombick, P., Erdmer, P., Thompson, R.I., and Daughtry, K.L. 2000. Geology of the Oyama map sheet, Vernon map area, British Columbia. *In* Current Research 2000-A. Geological Survey of Canada.

Glombick, P., Thompson, R.I., and Daughtry, K.L. 2004*a*. Geology of the Oyama map area, British Columbia (NTS 82L/03). Geological Survey of Canada Open File 4372, scale 1:50 000.

Glombick, P., Thompson, R.I., Erdmer, P., and Daughtry, K.L. 2004*b*. Infrastructure to superstructure transition in the Vernon area of the Shuswap metamorphic complex, southeast Canadian Cordillera: implications for core complex formation. Submitted to the Canadian Journal of Earth Sciences.

Greig, C.J., Armstrong, R.L., Harakal, J.E., Runkle, D., and van der Heyden, P. 1992. Geochronometry of the Eagle plutonic complex and the Coquihalla area, southwestern British Columbia. Canadian Journal of Earth Sciences, **29**: 812-829.

Hanchar, J.M., and Millar, C.F. 1993. Zircon zonation patterns as revealed by cathodoluminescence and backscattered electron images: implications for interpretation of complex crustal histories. Chemical Geology, **110**: 1-13.

Heaman, L.M., and Parrish, R.R. 1991. U-Pb geochronology of accessory minerals. *In* Applications of Radiogenic isotopic systems to problems in geology. *Edited by* L. Heaman and J.N. Ludden. Mineralogical Association of Canada, pp. 59-102.

Heaman, L.M., Erdmer, P., Thompson, R.I., and Daughtry, K.L. 1999. Preliminary U-Pb geochronology results from the Vernon area, British Columbia. *In* Proceedings, Lithoprobe Report No. 69: Cordilleran Tectonics Workshop, Calgary, Alberta, pp. 196-201.

Heaman, L.M., Erdmer, P., and Owen, J.V. 2002. U-Pb geochronologic constraints on the crustal evolution of the Long Range Inlier, Newfoundland. Canadian Journal of Earth Sciences, **39**: 845-865.

Johnson, B.J. 1994. Structure and tectonic setting of the Okanagan Valley fault system in the Shuswap Lake area, southern British Columbia. Unpublished Ph.D. thesis, Carleton University, Ottawa.

Johnston, D.H., Williams, P.F., Brown, R.L., Crowley, J.L., and Carr, S.D. 2000. Northeastward extrusion and extensional exhumation of crystalline rocks of the Monashee complex, southeastern Canadian Cordillera. Journal of Structural Geology, **22**: 603-625.

Krogh, T.E. 1982. Improved accuracy of U-Pb zircon ages by the creation of more concordant systems using an air abrasion technique. Geochimica et Cosmochimica Acta, **46**: 637-649.

Ludwig, K.R. 1980. Calculation of uncertainties of U-Pb isotopic data. Earth and Planetary Science Letters, **46**: 212-220.

Ludwig, K.R. 2001. User's manual for Isoplot/Ex rev. 2.49: a Geochronological Toolkit for Microsoft Excel. Special Publication, 1a, Berkeley Geochronology Centre, Berkeley.

Mathews, W.H. 1981. Early Cenozoic resetting of potassium-argon dates and geothermal history of north Okanagan area, British Columbia. Canadian Journal of Earth Sciences, **18**: 1310-1319.

McDonough, M.R., and Parrish, R.R. 1991. Proterozoic gneisses of the Malton Complex, near Valemount, British Columbia: U-Pb ages and Nd isotopic signatures. Canadian Journal of Earth Sciences, **28**: 1202-1216.

Monger, J.W.H., Wheeler, J.O., Tipper, H.W., Gabrielse, H., Harms, T., Struick, L.C., Campbell, R.B., Dodds, C.J., Gehrels, G.E., and O'Brien, J. 1991. Part B: Cordilleran terranes. *In* Upper Devonian to Middle Jurassic assemblages, Chapter 8 of Geology of the Cordilleran orogen in Canada. *Edited by* H. Gabrielse and C.J. Yorath. Geological Survey of Canada, Geology of Canada no. 4, 281-327 (*also* Geological Society of America, The Geology of North America, v. G-2).

Okulitch, A.V. 1979. Thompson-Shuswap-Okanagan map area. Geological Survey of Canada, Open File 637.

Okulitch, A.V. 1984. The role of the Shuswap Metamorphic Complex in Cordillera tectonism: a review. Canadian Journal of Earth Sciences, **21**: 1171-1193.

Parkinson, D.L. 1985. U-Pb geochronology and regional geology of the southern Okanagan Valley, British Columbia: the western boundary of a metamorphic core complex. M.Sc. thesis, University of British Columbia, Vancouver.

Parkinson, D.L. 1991. Age and isotopic character of Early Proterozoic basement gneisses in the southern Monashee Complex, southeastern British Columbia. Canadian Journal of Earth Sciences, **28**: 1159-1168.

Parkinson, D.L. 1992. Age and tectonic evolution of the southern Monashee Complex, southeastern British Columbia: a window into the deep crust. Ph.D. thesis, University of California, Santa Barbara.

Parrish, R.R. 1995. Thermal evolution of the southeastern Canadian Cordillera. Canadian Journal of Earth Sciences, **32**: 1618-1642.

Parrish, R.R., and Armstrong, R.L. 1987. The ca. 162 Ma Galena Bay stock and its relationship to the Columbia River fault zone, southeast British Columbia. *In* Radiogenic Age and Isotopic Studies: Report 1. Geological Survey of Canada, Paper 87-2, pp. 25-32.

Parrish, R.R., and Monger, J.W.H. 1992. New U-Pb dates from southwestern British Columbia. *In* Radiogenic Age and Isotopic studies: Report 5. Geological Survey of Canada, Paper 91-2, pp. 87-108.

Parrish, R.R., and Wheeler, J.O. 1983. U-Pb zircon age of the Kuskanax batholith, southeastern British Columbia. Canadian Journal of Earth Sciences, **20**: 1751-1756.

Parrish, R.R., Roddick, J.C., Loveridge, W.D., and Sullivan, R.W. 1987. Uranium-Lead analytical techniques at the geochronology laboratory. *In* Radiogenic Age and Isotopic Studies: Report 1. Geological Survey of Canada, Paper 87-2, pp. 3-7.

Parrish, R.R., Carr, S.D., and Parkinson, D.L. 1988. Eocene extensional tectonics and geochronology of the southern Omineca Belt, British Columbia and Washington. Tectonics, 7: 181-212.

Parrish, R.R., Bellerive, D., and Sullivan, R.W. 1991. U-Pb chemical procedures for titanite and allanite in the Geochronology Laboratory, Geological Survey of Canada. *In* Radiogenic Age and Isotopic Studies: Report 5. Geological Survey of Canada, Paper 91-2, pp. 187-190.

Pell, J. 1984. Stratigraphy, structure and metamorphism of Hadrynian strata in the southeastern Cariboo Mountains, British Columbia. Ph.D. thesis, University of Calgary, Calgary.

Price, R.A., and Monger J.W.H. 2003. A transect of the Southern Canadian Cordillera from Calgary to Vancouver. Geological Association of Canada, fieldtrip guidebook.

Roddick, J.C. 1987. Generalized numerical error analysis with application to geochronology and thermodynamics. Geochimica et Cosmochimica Acta, **51**: 2129-2135.

Rubatto, D., and Gebauer, D. 2000. Use of cathodoluminescence for U-Pb zircon dating by ion microprobe: some examples from the western Alps. *In* Cathodoluminescence in the geosciences. *Edited by* M. Pagel, V. Barbin, P. Blanc, and D. Ohnenstetter. Springer, Berlin, pp. 373-400.

Stacey, J.S., and Kramers, S.D. 1975. Approximation of terrestrial lead isotope evolution by a two-stage model. Earth and Planetary Science Letters, **26**: 207-221.

Steiger, R.H., and Jäger, E. 1977. Subcommission on Geochronology. Convention on the use of decay constants in geo- and cosmochronology. Earth and Planetary Science Letters, **36**: 359-362.

Stern, R.A. 1997. The GSC Sensitive High Resolution Ion Microprobe (SHRIMP): analytical techniques of zircon U-Th-Pb age determinations and performance evaluation. *In* Radiogenic Age and Isotope Studies: Report 10. Geological Survey of Canada, Current Research 1997-F, pp. 1-31.

Stern, R.A., and Amelin, Y. 2003. Assessment of errors in SIMS zircon U-Pb geochronology using a natural zircon standard and NIST SRM 610 glass. Chemical Geology, **197**: 111-146.

Tempelman-Kluit, D., and Parkinson, D. 1986. Extension across the Eocene Okanagan crustal shear in southern British Columbia. Geology, **14**: 318-321.

Thompson, R.I. 2004*a*. Geology of the Salmon Arm map area, British Columbia (NTS 82L/11). Geological Survey of Canada Open File 4380, scale 1:50 000.

Thompson, R.I. 2004*b*. Geology of the Gates Creek map area, British Columbia (NTS 82L/09). Geological Survey of Canada Open File 4378, scale 1:50 000.

Thompson, R.I., and Daughtry, K.L. 1996. New stratigraphic and tectonic interpretations, north Okanagan Valley, British Columbia. *In* Current Research 1996-A. Geological Survey of Canada, pp. 135-141.

Thompson, R.I. and Glombick, P. 2004*a*. Geology of the Shuswap Falls map area, British Columbia (NTS 82L/07). Geological Survey of Canada Open File 4376, scale 1:50 000.

Thompson, R.I., and Glombick, P. 2004*b*. Geology of the Mabel Lake map area, British Columbia (NTS 82L/10). Geological Survey of Canada Open File 4379, scale 1:50 000.

Thompson, R.I., and Unterschutz, J.L.E. 2004. Geology of the Vernon map area, British Columbia (NTS 82L/06). Geological Survey of Canada Open File 4375, scale 1:50 000.

Thompson, R.I. and Glombick, P., and Lemieux, Y. (compilers). 2004*a*. Geology of the Eureka Mountain map area, British Columbia (NTS 82L/01). Geological Survey of Canada Open File 4370, scale 1:50 000.

Thompson, R.I. and Glombick, P., and Lemieux, Y. (compilers). 2004*b*. Geology of the Mount Fosthall map area, British Columbia (NTS 82L/08). Geological Survey of Canada Open File 4377, scale 1:50 000.

Thompson, R.I., Glombick, P., Erdmer, P., Daughtry, K.L., Heaman, L., and Friedman, R.L. (in prep). Evolution of the ancestral Pacific margin, southern Canadian Cordillera: Insights from new geologic maps. *In* Colpron, M., Nelson, J. L. and Thompson, R. I. (eds.), Paleozoic evolution and metallogeny of pericratonic terranes at the ancient Pacific margin of North America, Canadian and Alaskan Cordillera. Geological Association of Canada, Special Paper.

Todt, W., Cliff, R. Hanser, A. and Hofman, A.W. 1984. $^{202}Pb + ^{205}Pb$ double spike for lead isotopic analyses. Terra Cognita, **4**: 209.

Vanderhaeghe, O., Teyssier, C., and Wysoczanski, R. 1999. Structural and geochronological constraints on the role of partial meting during the formation of the Shuswap metamorphic complex at the latitude of Thor-Odin dome, British Columbia. Canadian Journal of Earth Sciences, **36**: 917-943.

Vanderhaeghe, O., Teyssier, C., McDougall, I., and Dunlap, W.J. 2003. Cooling and exhumation of the Shuswap Metamorphic Core Complex constrained by 40Ar/39Ar thermochronology. Geological Society of America Bulletin, **115**: 200-216.

Wheeler, J.O., and McFeely, P. (compilers). 1991. Tectonic assemblage map of the Canadian Cordillera and adjacent parts of the United States of America. Geological Survey of Canada, Map 1712A, scale 1:2 000 000.

Williams, P.F. 1999. Interpretation of thrust-like structures in middle and lower crustal rocks. *In* Tectonic and Magmatic Processes in Crustal Growth: a Pan-Lithoprobe Perspective. Lithoprobe Report 75, pp. 67-68.

Williams, P.F., and Jiang, D. 2005. An investigation of lower crustal deformation: evidence for channel flow and its implications for tectonics and structural studies. Journal of Structural Geology, **27**: 1486-1504.

Appendix 3*a*

ID-TIMS U-Pb analytical techniques

Uranium-bearing minerals were dated by the IDTIMS method at the geochronology laboratories at the University of Alberta (U of A) and the University of British Columbia (UBC). Zircon, titanite, and monazite were separated from approximately 10 kg of sample using conventional crushing, grinding and Wilfley Table techniques, followed by final concentration using heavy liquids and magnetic separation. Mineral fractions were selected for analysis based on grain morphology, quality, size and magnetic susceptibility. Zircon fractions analyzed at the UBC lab were abraded prior to dissolution to minimize the effects of post-crystallization Pb-loss, using the technique of Krogh (1982). All other fractions were not abraded to preserve core/overgrowth relationships. Fractions were washed in HNO_3, H_2O, and acetone and weighed using a Mettler UM2 microbalance (± 2 μg). Zircon and titanite samples were dissolved in concentrated HF and HNO_3 and monazite in 6.2 N HCl, in the presence of a mixed $^{233-235}U$-^{205}Pb isotopic tracer (UBC) and ^{235}U-^{205}Pb (U of A). Zircon fractions were dissolved in teflon microcapsules within Parr bombs for a minimum of 40 hrs. at 240°C (UBC) and TFE teflon minicapsules for 72 hours at 220°C (U of A). The HF solution was evaporated and fluorides were dissolved in 3.1N HCl in Parr bombs for 12 hrs. at 210 °C. Titanite fractions were dissolved in Savillex PFA beakers on a hot plate at 100 °C, for not less than 72 hours. HF was evaporated and fluorides were dissolved in 6.2N HCl on a hot plate for 24 hrs. This solution was evaporated to dryness and chlorides were dissolved on the hot plate for 24 hrs in 3.1 HCl. Monazites were dissolved in Savillex PFA beakers on a hot plate at 100 °C, for not less than 72 hours. HCl was evaporated and chlorides were dissolved on the hot plate for 24 hrs in 3.1 HCl. Separation and purification of Pb and U from zircon and monazite fractions employed ion exchange column techniques modified slightly from those described by Parrish et al. (1987) and Heaman et al.

(2002). Ion exchange chromatography techniques employed for titanite fractions were modified from those described by Parrish et al. (1991), Heaman et al. (2002) and from D. Davis (written communication, 1995). Pb and U for all mineral samples were eluted separately and loaded together on a single Re filament using a phosphoric acid-silica gel emitter. Isotopic ratios were measured using a modified single collector VG-54R (UBC) and VG354 (U of A) thermal ionization mass spectrometers, both equipped with a Daly photomultiplier detectors. Most measurements were in peak-switching mode on the Daly detector. U and Pb analytical blanks were in the range of 1 pg and 1-3 pg, respectively, during the course of this study. U fractionation was determined directly on individual runs using the $^{233\text{-}235}U$ tracer (UBC). A uranium fractionation correction of 0.16%/amu was used for data obtained at U of A. Pb isotopic ratios were corrected for a fractionation of 0.12% per amu (UBC) and 0.09% (U of A) and 0.43% per amu (UBC) for Faraday and Daly runs, respectively, based on replicate analyses of the NBS-981 Pb standard as compared to the values recommended by Todt et al. (1984). All analytical errors were propagated through the entire age calculation using the technique of Roddick (1987). Concordia intercept ages and associated errors were calculated using a modified version of the York-II-regression model (wherein the York-II errors are multiplied by the square root of the MSWD, when greater than 1) and the algorithm of Ludwig (1980). The decay constants recommended by Steiger and Jäger (1977) were used (^{238}U - 1.55125×10^{-10}; ^{235}U - 9.8485×10^{-10}; ^{232}Th - 0.49475×10^{-10}). Errors for Pb/U and Pb/Pb ages are quoted at the 1σ level in Table 3-1 and plotted at the 2σ level on concordia diagrams.

SHRIMP U-Pb analytical techniques

Zircons selected for SHRIMP analyses were separated at the University of Alberta using standard separating techniques. The grains selected for analysis were randomly selected from the least magnetic split from the sample. The zircons were mounted, imaged, and dated at the Geological Survey of Canada J.C. Roddick Ion Microprobe Laboratory in Ottawa. Approximately 80 to 100 grains from the sample were mounted in epoxy and polished to expose the centre of the grains. The mount was coated with Au (99.9999%), prior to imaging using back-scattered electron (BSE) and cathodoluminescence techniques to reveal the internal structure of the grains. The mount was then cleaned, the surface was evaporatively coated with 15 nm of high purity Au, and left in a vacuum for at least 24 hours prior to analysis.

SHRIMP analytical procedures followed those described by Stern (1997), with standards and U-Pb calibration methods following Stern and Amelin (2003). Analyses were conducted using an $^{16}O^-$ primary beam, projected onto the zircons at 10 kV. The sputtered area used for

analysis was ca. 30μm in diameter with a beam current of ca. 1.7 nA. The count rates of ten isotopes of Zr^+, U^+, Th^+, and Pb^+ in zircon were sequentially measured (7 scans) with a single electron multiplier and a pulse counting system with deadtime of 28 ns. Mass resolution was 5300 (1%). Off-line data processing was accomplished using customized in-house software. The 1σ external errors of $^{206}Pb/^{238}U$ ratios reported in Table 3-2 incorporate the error in calibrating the standard zircon (see Stern and Amelin 2003). No fractionation correction was applied to the Pb-isotope data; common Pb correction utilized the measured $^{207}Pb/^{206}Pb$ and compositions modelled after Cumming and Richards (1975). Isoplot v. 2.49 (Ludwig 2001) was used to generate concordia plots and calculate weighted means.

CHAPTER 4

Thermal and metamorphic evolution of the central Shuswap metamorphic complex in the Vernon area, southeast Canadian Cordillera[1]

[1] A version of this chapter is preparation for submission to the Journal of Metamorphic Geology coauthored by P. Glombick, T. Chacko, P. Erdmer, R.I. Thompson, and M.B. Mylod.

Introduction

The Shuswap metamorphic complex (SMC) is an informal term used to refer to a geologically complex region within southeastern British Columbia and northeastern Washington underlain dominantly by sillimanite-grade metamorphic rocks exhumed during early Tertiary extension (Fig. 4-1). The pre-Tertiary metamorphic evolution of the SMC remains incompletely understood, due, in part, to a pervasive early Tertiary thermal, magmatic, and deformational overprint.

The Vernon area, located within the central SMC, preserves a highly deformed belt of greenschist-facies Devonian to Early Jurassic metasedimentary and metavolcanic rocks that transects the complex, perpendicular to the strike of early Tertiary extension faults (Fig. 4-2). Greenschist-facies metamorphic rocks that comprise the belt are characterized by Middle Jurassic to Late Cretaceous cooling ages (K-Ar; hornblende and biotite), whereas underlying upper amphibolite-facies rocks of the metamorphic infrastructure have yielded Late Paleocene to Middle Eocene cooling ages (e.g., Mathews 1981; Vanderhaeghe et al. 2003).

This chapter reports the results of a metamorphic and geochronological study of greenschist to upper amphibolite-facies metamorphic rocks in the Vernon area. The aim is to determine the nature of the contact between the belt of greenschist-facies rocks and underlying amphibolite-facies rocks and to compare and contrast their metamorphic evolution. A multi-disciplinary approach is used to achieve this goal, involving: (1) detailed geological mapping; (2) thin section petrography; (3) thermobarometry and Gibbs modelling; and (4) electron microprobe (EMP) chemical dating of monazite. Based on new data and published metamorphic, geochronological, and structural data, I present a thermotectonic evolutionary model for the central SMC, from the Middle Jurassic to the Middle Eocene.

Geological setting

The SMC is located within the high-grade metamorphic and plutonic core zone of the southeast Canadian Cordillera (Fig. 4-1). The SMC straddles the boundary between Paleoproterozoic to Jurassic continental sedimentary prism rocks and pericratonic rocks known to have been depositionally linked to the ancestral cratonic margin, and Devonian to Jurassic

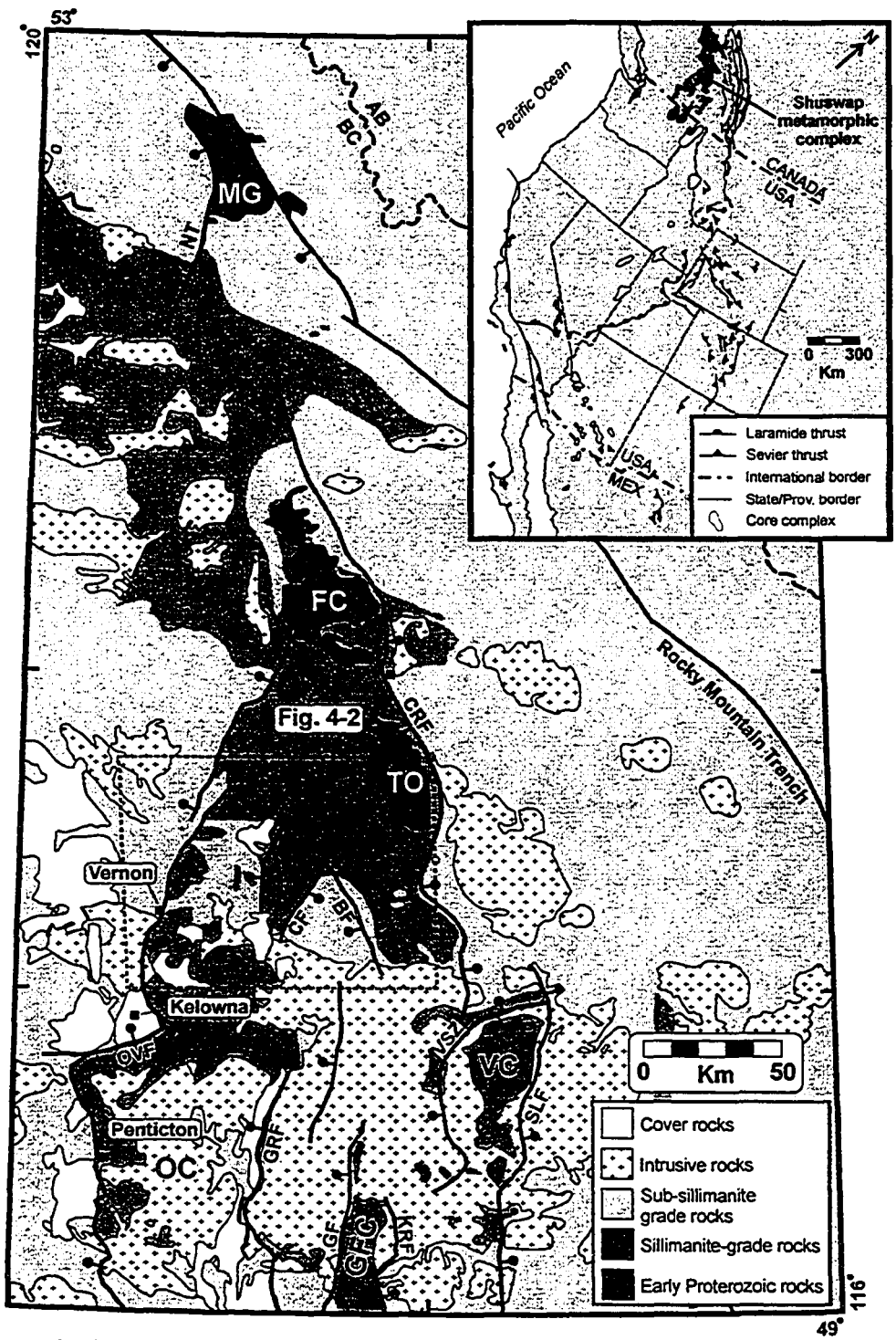

Fig. 4-1. Distribution of sillimanite-grade rocks and early Tertiary extension faults within the southeast Canadian Cordillera (modified from Read et al. 1991). *Fault systems*: BF – Beaven; CF – Cherry; CRF – Columbia River; GF – Granby; GRF – Greenwood; KRF – Kettle River; NT – North Thompson; OVF – Okanagan Valley; SLF – Slocan Lake; VSZ – Valkyr shear zone. *Gneiss domes and structural complexes*: FC – Frenchman Cap; GFC – Grand Forks complex; MG – Malton gneiss complex; OC – Okanagan complex; TO – Thor-Odin; VC – Valhalla complex. **Inset:** Location of the Shuswap metamorphic complex and other core complexes within western North America (modified from Coney 1980). Schuswap metamorphic complex shown in black

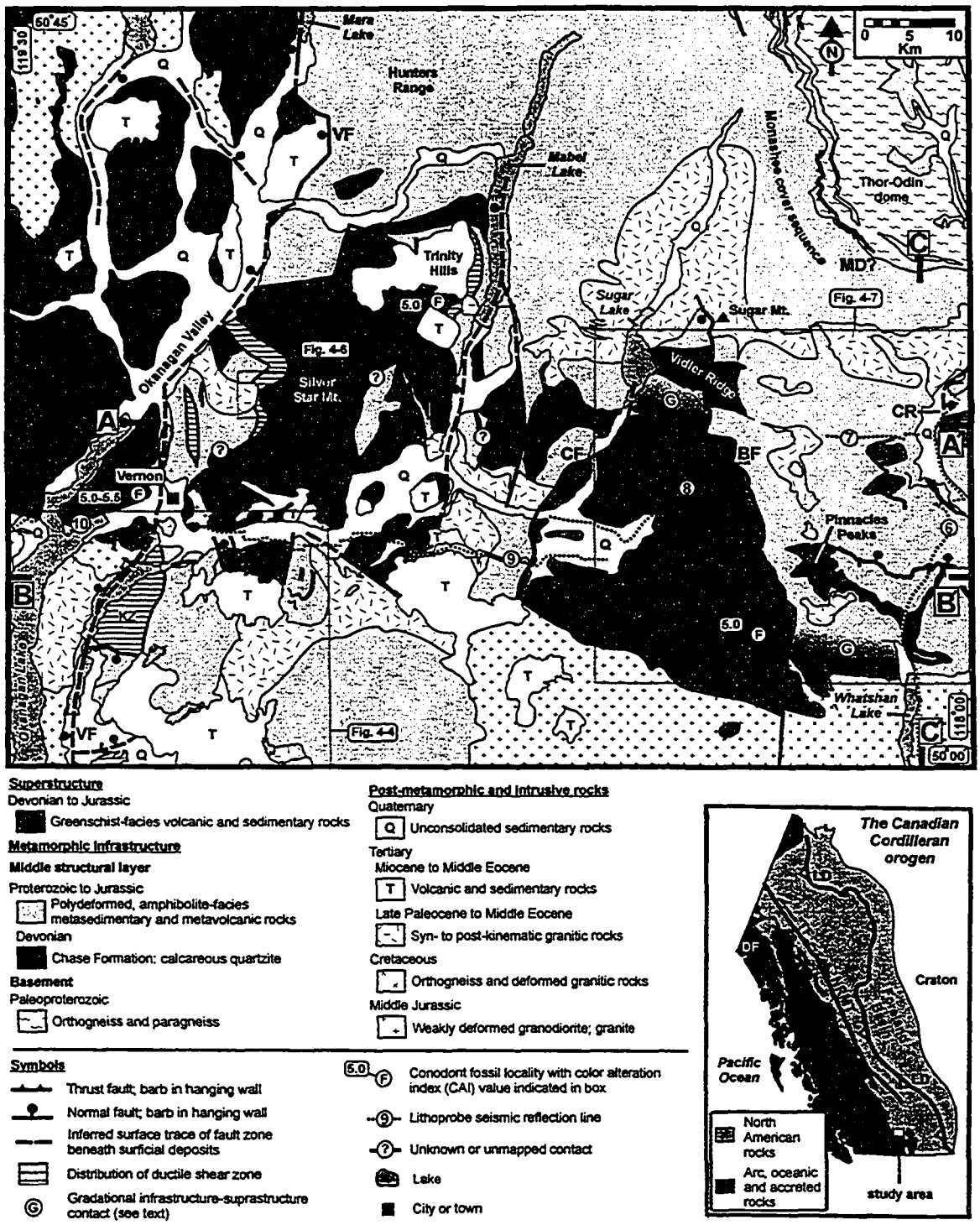

Fig. 4-2. Simplified geological map of the Vernon area of the central Shuswap metamorphic complex. *Abbreviations*: BF - Beaven fault; BZ -break-away zone discussed in text; CF - Cherry fault; CR - Columbia River fault; KZ - Kalamalka Lake shear zone; MD - Monashee décollement; VF - Vernon fault. Modified from Glombick and Thompson (2004), Glombick et al. (2004), Thompson (2004*a*, 2004*b*, in press), Thompson and Glombick (2004*a*, 2004*b*); Thompson and Unterschutz (2004); Thompson et al. (2004*a*, 2004*b*). **Lower right**: Tectonic elements of the Canadian Cordillera (modified from Wheeler et al. 1991).

metasedimentary and metavolcanic rocks of oceanic and (or) volcanic arc affinity with uncertain original paleogeography (Fig. 4-2, inset map). North of 50°N, the boundary between these two tectonostratigraphic sequences lies to the west of the SMC, whereas in the Vernon area the boundary bends to the southeast, striking across the SMC, perpendicular to orogenic strike, before striking to the south, east of the Valhalla complex. The nature of the original, pre-tectonic contact between these tectonostratigraphic sequences remains debated, with several workers favouring tectonic emplacement (e.g. Monger et al. 1982; Brown et al. 1986; Monger et al. 1991) and others a depositional contact (e.g., Klepacki 1985; Erdmer et al. 2001; Unterschutz et al. 2002).

The SMC is difficult to define. Traditionally, the term was used to refer to sillimanite-grade rocks located within the southeast Canadian Cordillera (see Okulitch 1984, for a historical review). Subsequently, the SMC has been reinterpreted as a composite metamorphic core complex, composed of a number of detachment fault-bounded structural culminations (see Parrish et al. 1988). In places though, the boundaries are gradational and detachments are absent (see Chapter 2) and the SMC does not conform to classic metamorphic core complex models (cf. Lister and Davis 1989).

For the purpose of this study, rocks referred to as superstructure are dominantly at greenschist-facies metamorphic grade with Middle Jurassic to Late Cretaceous K-Ar (hornblende and micas) dates. Superstructure rocks are situated at upper structural levels, within the hanging wall of early Tertiary extension faults, or flanking the margins of the complex. Metamorphic infrastructure includes upper amphibolite-facies metasedimentary and metavolcanic rocks with Late Paleocene to Middle Eocene K-Ar and $^{40}Ar/^{39}Ar$ dates situated within the footwall of early Tertiary extension faults (middle structural unit) and underlying Paleoproterozoic basement culminations. The infrastructure can be subdivided into Paleoproterozoic basement and an overlying middle structural unit composed of a Paleoproterozoic to Jurassic(?) complexly-deformed mantling gneiss sequence suffused with early Tertiary granitic rocks. The mantling gneiss is hereafter referred to as the middle structural layer (Figs. 4-2, 4-3).

At the lowest exposed structural level of the southeast Canadian Cordillera, Paleoproterozoic amphibolite-facies gneiss is present in the Malton and Monashee complexes (Fig. 4-1; Armstrong et al. 1991; McDonough and Parrish 1991). On the basis of age and isotopic similarities, Paleoproterozoic gneiss exposed within the core of these culminations is believed to be autochthonous North American basement (e.g., Armstrong et al. 1991; Parkinson 1991). Geochronological data (U-Pb; zircon, monazite, xenotime) from the deepest exposed structural levels of the northern Monashee complex (Fig. 4-1) suggest that Cordilleran tectonism did not affect the deepest levels of the complex until the Early Eocene (52-49 Ma), synchronous with

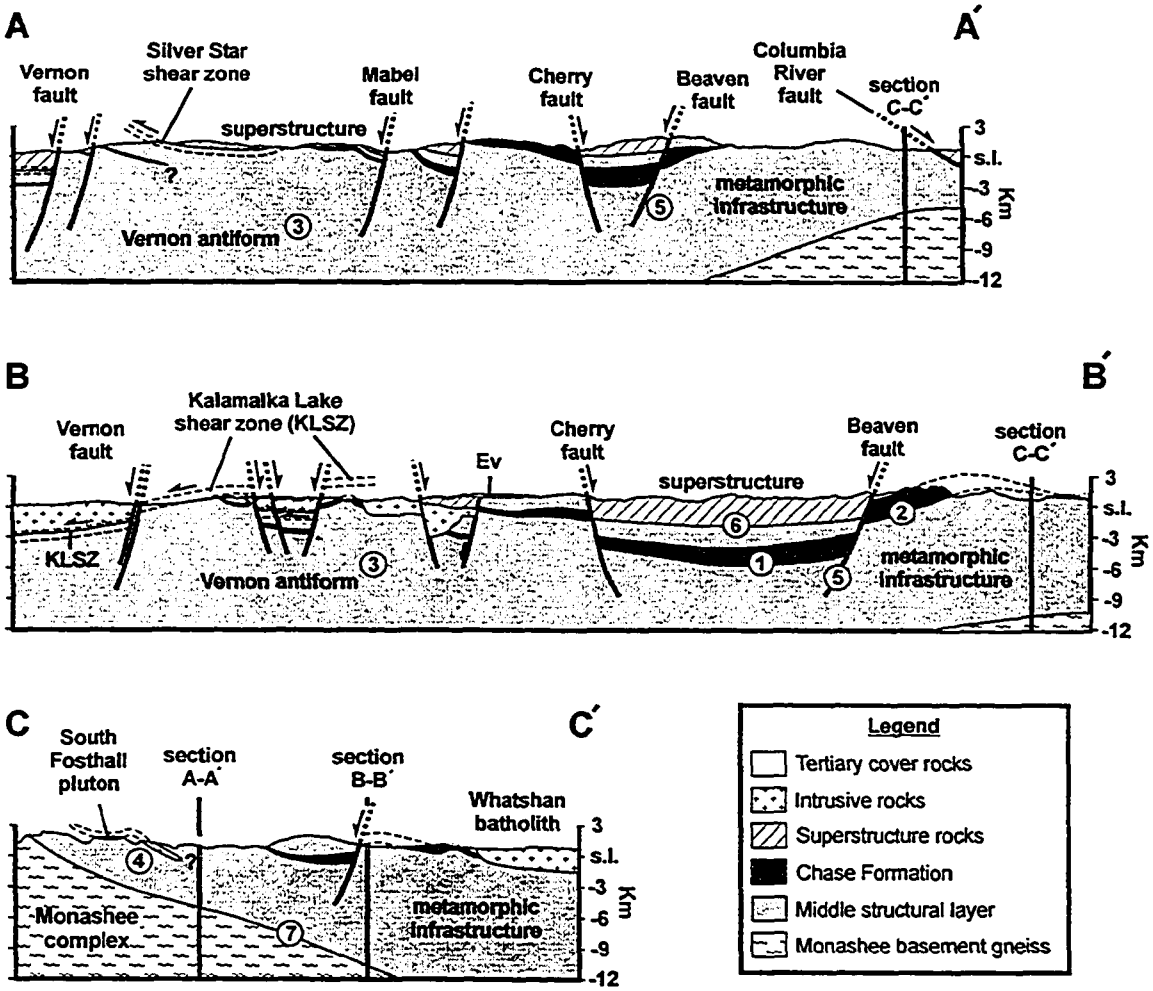

Fig. 4-3. Generalized geological cross sections through the study area. The large, capital bold letters in Fig. 4-2 indicates the endpoints of section lines. No vertical exaggeration. *Abbreviations*: s.l. - sea level. *Notes:* (1) The Chase Formation is shown as a gently-dipping sheet in the sub-surface on the basis of surface map patterns (Fig. 4-2). (2) This structure is interpreted as a broad, west-trending antiform, with the northern limb down-dropped by a steep normal fault, rather than a map-scale recumbent isoclinal fold (e.g., Carr 1990), on the basis of detailed geological mapping in this area (see Lemieux et al. 2003; Thompson et al. 2004*a*). (3) The Vernon antiform is a domal series of reflectors visible at upper to mid-crustal depths near Vernon (Fig. 4-20*b*; Cook et al. 1992). (4) The geometry of the South Fosthall pluton in the subsurface is not well constrained. (5) The Beaven fault cuts the contact between infrastructure and superstructure, and therefore cannot be the "breakaway" of an Okanagan Valley-Eagle River detachment fault system. Middle Eocene steeply-dipping normal faults are inferred to root into the Middle Eocene brittle-ductile transition. (6) While this line is shown as a sharp contact in the sections, it is transitional in the field, occurring over a structural thickness of 1-2 km (see text). (7) Basement-cover contact is drawn parallel to south-dipping reflectors are visible in Lithoprobe line 6 (see Cook et al. 1992).

cooling and exhumation of overlying rocks (e.g., Crowley et al. 2001), and motion on major extension faults at upper crustal levels (Parrish et al. 1988).

The Monashee and Malton gneiss complexes are unconformably overlain by the middle structural layer, a complexly deformed Paleoproterozoic to Jurassic (?) succession of metasedimentary and metavolcanic rocks 10-15 km thick intruded by abundant and widespread Late Paleocene to Early Eocene granitic rocks (e.g., Reesor and Moore 1971; Carr 1990; Scammell and Brown 1990; Johnson 1994; Crowley 1997). Rocks that comprise the middle structural layer are believed to have been deposited adjacent to the ancestral cratonic margin prior to being buried, deformed, and metamorphosed beneath an advancing orogenic wedge during the Middle Jurassic to Late Cretaceous (e.g., Parrish 1995). Geochronological data (U-Pb; zircon, monazite, titanite, allanite) suggest that the middle structural layer experienced a complex thermotectonic evolution that varies with structural level and region (e.g., Parrish 1995; Crowley et al. 2000). K-Ar ages (hornblende, micas) from infrastructure rocks suggest that widespread cooling, from above 500°C to below 250°C, of the infrastructure occurred during the Late Paleocene to Middle Eocene across the entire complex synchronous with the emplacement of granitic rocks into the middle structural layer (e.g., Mathews 1981; Carr 1992; Vanderhaeghe et al. 2003). The cooling ages, which overlap the timing of early Tertiary magmatism, have been interpreted as reflecting the timing of exhumation of mid-crustal rocks during displacement on a system of low-angle, crustal-scale north-striking detachments (e.g., Parrish et al. 1988).

The superstructure of the SMC, which forms the uppermost structural level, is preserved around the margins of the complex, or locally within normal fault bounded structural lows. The superstructure is composed of dominantly greenschist-facies, but locally lower amphibolite-facies, Proterozoic to Jurassic metasedimentary and metavolcanic rocks of continental, oceanic, and arc affinity. Geochronological data (U-Pb and K-Ar) indicate that regional deformation and metamorphism of the superstructure occurred in the Middle Jurassic (~175-160), followed by cooling to below 250°C by Late Jurassic to Late Cretaceous time (e.g., Mathews 1981; Archibald et al. 1984; Parrish 1995).

During the Late Paleocene to the Early Eocene, the hinterland of the southeast Canadian Cordillera experienced a transition from crustal thickening to extension. It has been proposed that Late Paleocene to Early Eocene exhumation of mid-crustal rocks occurred during displacement on a system of north-striking low-angle detachments (e.g., Parrish et al. 1988). Middle Eocene volcanic and sedimentary successions are locally preserved in fault-bounded basins (e.g., Mathews 1981). The relative importance of detachments versus mid-crustal ductile flow in the formation of the SMC continues to be debated (e.g., Vanderhaeghe et al. 1999; Johnston et al.

2000; Chapter 2). Proposed causes for the onset of extension include: (1) melt weakening of the middle to lower crust, leading to diapirism and upper crustal extension (Vanderhaeghe et al. 1999); (2) decompression melting of the middle crust as it was thrust up a crustal-scale ramp in a ductile shear zone called the Monashee décollement (e.g., Carr 1992); (3) convective removal of a lithospheric mantle root (Ranalli et al. 1989); (4) back-arc extension (Davis and Lewis 1984); (5) a change in far-field plate velocities (Price and Carmichael 1986; Bardoux and Mareschal 1994); and (6) mantle upwelling (Gough 1986).

Geology of the study area

The study area is bounded by latitudes 50° 00' and 50°45' N on the south and north and by longitudes 118°00' and 119°30' on the east and west, respectively (Fig. 4-2).

Late Paleocene to Early Eocene, gently-dipping shear zones exposed near the Okanagan Valley have been interpreted as part of a crustal-scale detachment, the proposed Okanagan Valley-Eagle River (OV-ER) fault system, with an estimated 30 to 90 km of top to the west displacement (Tempelman-Kluit and Parkinson 1986; Parrish et al. 1988; Carr 1990; Bardoux 1993; Johnson and Brown 1996). On the basis of continuity of lithostratigraphic units across the Okanagan Valley, several authors have questioned large-displacement models (Okulitch 1987; Thompson and Daughtry 1996; Erdmer et al. 1999). Low-angle ductile shear zones exposed in the Vernon area are locally cut by steep, brittle normal faults, which are locally overlain by Middle Eocene volcanic successions (Figs. 4-2, 4-3, 4-4).

The eastern margin of the SMC is bounded by the Columbia River Valley, the locus of a moderately to steeply east-dipping Late Paleocene to Early Eocene extensional fault known as the Columbia River fault (CRF; Lane 1984). Estimates of down-dip displacement range from 1-10 km (Lane 1984; Lemieux et al. 2003) to 30-40 km (Parrish et al. 1988; Parkinson 1992).

All three structural levels of the SMC are exposed within the study area. Upper amphibolite-facies Paleoproterozoic basement gneiss (~1960 Ma-1870) is exposed in the core of the Thor-Odin culmination, which is located in the northeast corner of the study area (Fig. 4-2; Parkinson 1992). The Paleoproterozoic basement gneiss of the Thor Odin culmination is unconformably overlain by a mantling gneiss succession of the middle structural layer. The mantling gneiss is bounded at the base by a regionally continuous orthoquartzite unit of variable thickness (Reesor and Moore 1971; Thompson et al. 2004*b*). Locally, the mantling gneiss is structurally interlayered with slivers of basement gneiss (Johnston et al. 2000). The middle structural layer, dominated at lower levels by quartzite, calcsilicate gneiss, marble, and amphibolite, grades upwards into a succession of pelitic and semi-pelitic schist with rare

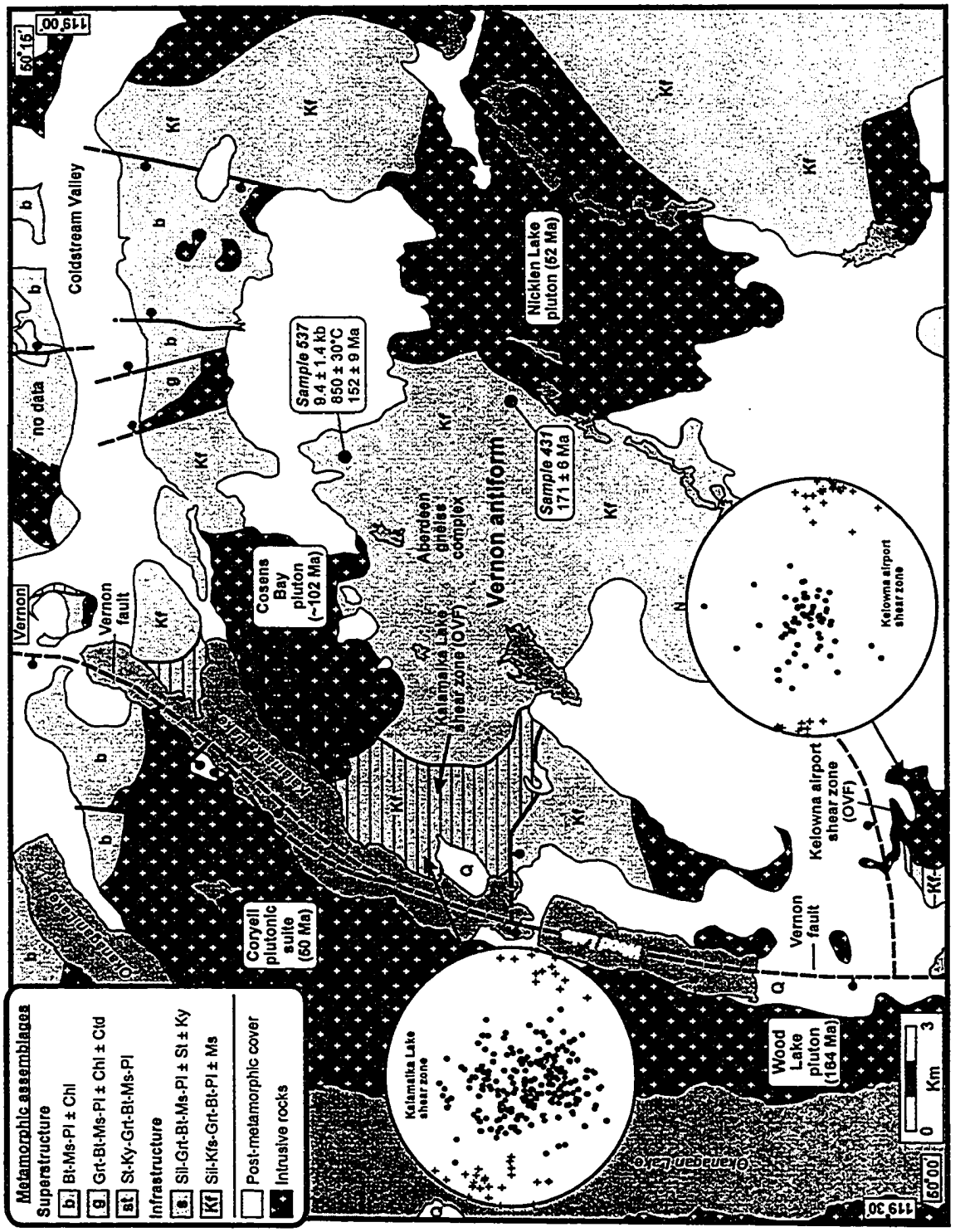

Fig. 4-4. Metamorphic map of the Aberdeen gneiss complex and surrounding areas, showing the location of samples used for thermobarometry and monazite EMP chemical dating. Symbols for lower hemisphere, equal-area projections: solid circles - poles to metamorphic foliation; crosses - stretching lineations.

amphibolite and calc-silicate layers (Reesor and Moore 1971; Johnston et al. 2000). Granitic rocks are common, particularly higher in the succession, locally comprising 100 percent of exposed bedrock (Reesor and Moore 1971; Carr 1992).

The infrastructure is locally overlain by greenschist-facies superstructure rocks, which are exposed in a 30 km wide belt, extending from the southeast corner of the study area eastwards, towards Vernon, where it broadens to the north and south (Fig. 4-2). Although the superstructure is locally cut by steep normal faults, it forms a semi-continuous cover across the entire SMC. The base of the superstructure belt within the study area is the topic of debate, and has been interpreted as: (1) a regional unconformity (Read and Okulitch 1977); or (2) a low-angle detachment fault, proposed to be the eastward extension of the OVF fault system (Carr 1990; Bardoux 1993; Vanderhaeghe et al. 1999).

The infrastructure (middle structural layer)

Within the study area, a highly deformed succession of upper amphibolite-facies metasedimentary and metavolcanic rocks of Proterozoic to Jurassic(?) age underlies the superstructure belt (Figs. 4-2, 4-3). Dominant rock types include: migmatitic pelitic and semi-pelitic schist, amphibolite, calcsilicate gneiss, marble, and calcareous quartzite. Granitic rocks of the Late Paleocene to Early Eocene (62-55 Ma) Ladybird suite (Carr 1992; Vanderhaeghe et al. 1999) are ubiquitous within the middle structural layer, occurring as plutons (e.g., South Fosthall pluton), stocks, sills, and dykes. Early phases of the Ladybird suite are synkinematic with respect to extension-related structures, but late (~50 Ma) pegmatitic dykes are undeformed (e.g., Carr 1992; Johnston et al. 2000).

The dominant structure is a metamorphic foliation (S_T), defined by transposed compositional layering, layering of leucosome in migmatitic rocks, and the alignment of platy metamorphic minerals. Isoclinal fold hinges are commonly observed at the outcrop scale. The dip of S_T is generally shallow (0 to 30°), but steeper dips occur locally. Near the contact with the superstructure and with the underlying Paleoproterozoic basement of the Thor-Odin culmination, a penetrative, gently plunging, east or west-trending stretching lineation is well developed in metamorphic rocks of the middle structural layer and Late Paleocene to Early Eocene granitic rocks (Reesor and Moore 1971; Carr 1992; Vanderhaeghe et al. 1999; Chapter 2).

The superstructure

The superstructure is composed dominantly of greenschist-facies siliciclastic rocks of the Upper Triassic to Lower Jurassic Slocan Group and metasedimentary and metavolcanic rocks of

the Upper Devonian to Upper Permian Harper Ranch Group (Monger et al. 1991), although only Permian and Mississippian equivalents have been identified in the Vernon area.

The Slocan Group is dominated by dark-grey to black, carbonaceous phyllite, argillite, and minor metasiltstone with rare beds (~1-3m) of dark-grey limestone. The Harper Ranch Group is composed primarily of intermediate metavolcanic breccias and flows, with subordinate amounts of argillite, carbonaceous phyllite, and folded sheets and pods (up to several kilometres long and hundreds of metres wide) of grey-weathering marble. The superstructure hosts Middle Jurassic (~171 Ma) granitic rocks of the Okanagan plutonic suite (Carr 1990) and Cretaceous plutons (e.g., Thompson 2004*a*).

Poor exposure and a paucity of marker units mask the internal structure of the Slocan and Harper Ranch groups. The dominant structure at the outcrop scale is a well-developed cleavage or schistosity (S_1), generally oriented sub-parallel or at a low angle (0-30°) to compositional layering (S_0). The S_1 cleavage is axial planar to tight to isoclinal outcrop and thin-section-scale folds. In many areas, S_0 and S_1 are overprinted by a closely spaced (1-5 mm) crenulation cleavage (S_2), generally oriented at a high angle to S_0 and S_1, which may be axial planar to map-scale folds. Locally, S_2 is crenulated by a second, poorly developed crenulation cleavage (S_3). The S_{0-2} foliations are generally moderately to steeply dipping (>45°) and strikes southeast, suggesting that the succession is likely folded by tight, upright to overturned folds with steeply to moderately southwest-dipping axial surfaces.

The infrastructure-superstructure contact

Based on new mapping and previous metamorphic studies (Reesor and Moore 1971; Carr 1990), we have compiled a metamorphic map of the Vernon area showing the distribution of the biotite, garnet, staurolite-kyanite, sillimanite, and potassium-feldspar-sillimanite zones (Figs. 4-4, 4-5).

The Thor-Odin culmination of the southern Monashee complex (Fig. 4-2, upper right) has been the subject of numerous structural and metamorphic studies (e.g., Reesor and Moore 1971; Ghent et al. 1977; Nyman et al. 1995; Johnston 1998; Spark 2002; Norlander 2002) and was not mapped during this study.

Most of the infrastructure is marked by homogenous metamorphic conditions that reached the upper amphibolite-facies (potassium-feldspar-sillimanite zone). Migmatite is common in metapelitic rocks, with 20-40 % (by volume) of leucosome locally present (e.g., Nyman et al. 1995). In certain areas, such as in the middle structural layer south of the Thor-Odin

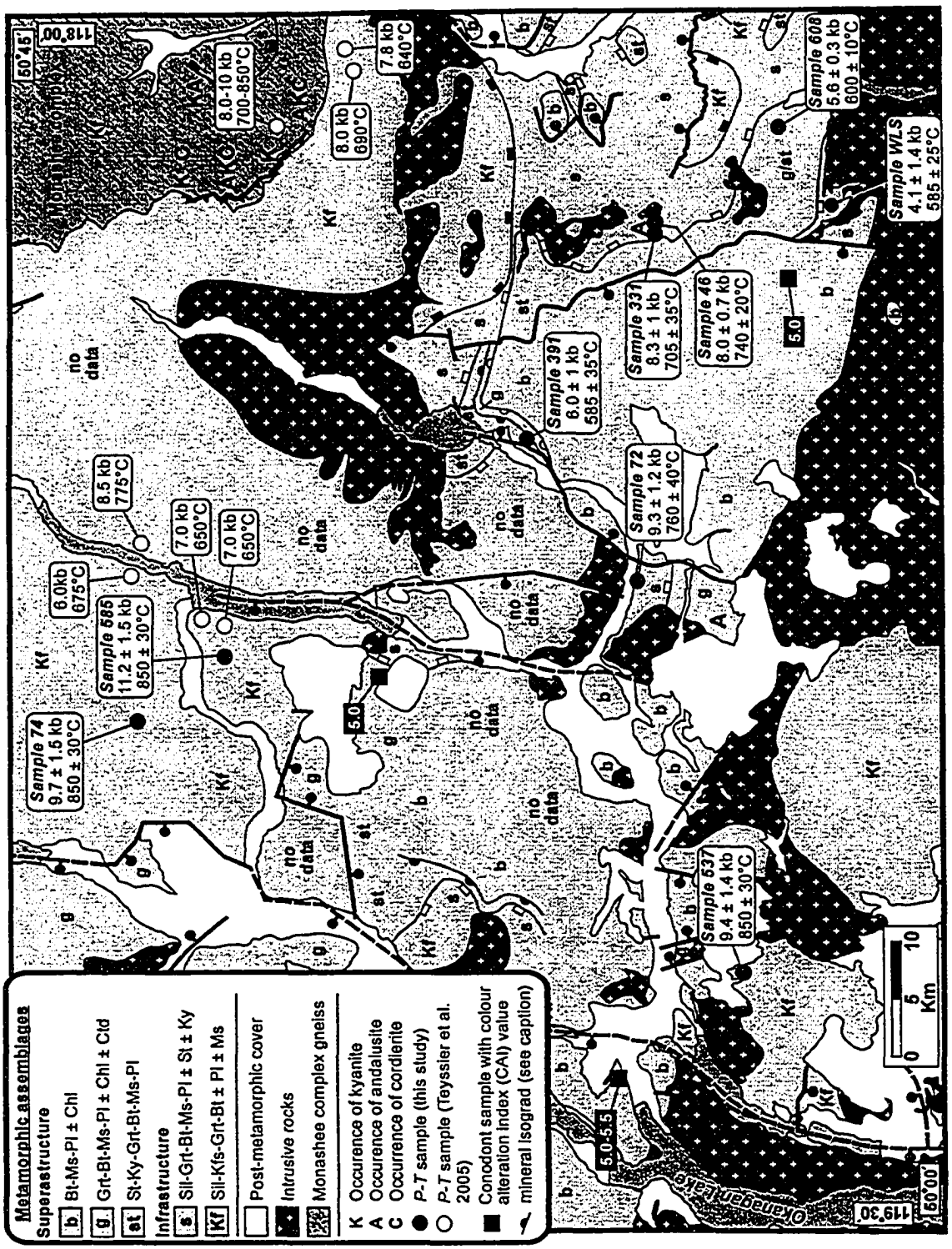

Fig. 4-5. Metamorphic map of the study area showing the location of thermobarometry samples and *P-T* estimates. The location of metamorphic isograds is modified from Reesor and Moore (1971), Carr (1990), Unterschutz (2002), and this study. Isograds: open half-circle - garnet-in; filled half-circle - staurolite-in; open rectangle sillimanite-in; filled rectangle - second sillimanite isograd.

dome, early Tertiary granitic rocks comprise 50-100% of exposed rock. Staurolite-kyanite zone rocks occur near the contact with the superstructure (Fig. 4-5).

Superstructure rocks are characterized by greenschist-facies mineral assemblages, with the exception of amphibolite-facies gneiss screens in the Middle Jurassic Wood Lake pluton south of Vernon (Chapter 3). Garnet-zone conditions are recorded near the base of the superstructure. Upper Triassic (Norian) conodonts recovered from carbonate rocks near the base of the superstructure yield conodont alteration index (CAI) values of 5.0-5.5, consistent with sub-garnet grade peak metamorphic conditions and maximum temperatures of 300-440°C (Fig. 4-2; cf. Rejebian et al. 1987).

The contact between the greenschist-facies superstructure and underlying upper amphibolite-facies infrastructure is commonly covered by drift or cut by steep, normal faults of Middle Eocene or younger age. There are several places along the base of the superstructure belt, however, where the transition between infrastructure and superstructure is exposed. Geological relationships are summarized from two of these areas, the Silver Star Mountain area (Fig. 4-6) and the Vidler Ridge-Pinnacles region (Fig. 4-7), in order to illustrate how the nature of the contact between superstructure and infrastructure varies across strike.

Silver Star Mountain area

On the western flank of Silver Star Mountain, 15 km northeast of Vernon, the transition between upper amphibolite-facies pelitic schist and quartzofeldspathic gneiss of the Devonian to Mississippian Silver Creek Formation, and greenschist-facies carbonaceous phyllite and argillite of the Upper Triassic to Lower Jurassic Slocan Group, is exposed several kilometres west of the summit (Fig. 4-6).

The transition between the Silver Creek Formation and the Slocan Group lies within a 1-2 km thick, east-dipping shear zone, characterized by a progressive increase in metamorphic grade from east to west (Fig. 4-6). The garnet, staurolite-kyanite, and sillimanite-in isograds occur within a structural thickness of approximately 1 km. The increase in metamorphic grade appears to be gradual, without any apparent structural breaks or jumps in grade. Isograd surfaces are inferred to be oriented subparallel to the metamorphic schistosity and compositional layering (S_T) at the map scale. Shear (C') bands cut the mylonitic foliation and metamorphic porphyroblasts. Compositional layering, the metamorphic foliation, and the mylonitic foliation are subparallel and dip moderately to the east (20-40°) within the shear zone. Abundant syn- to postkinematic granitic rocks, of inferred Late Paleocene to Early Eocene age, occur near the sillimanite-in isograd.

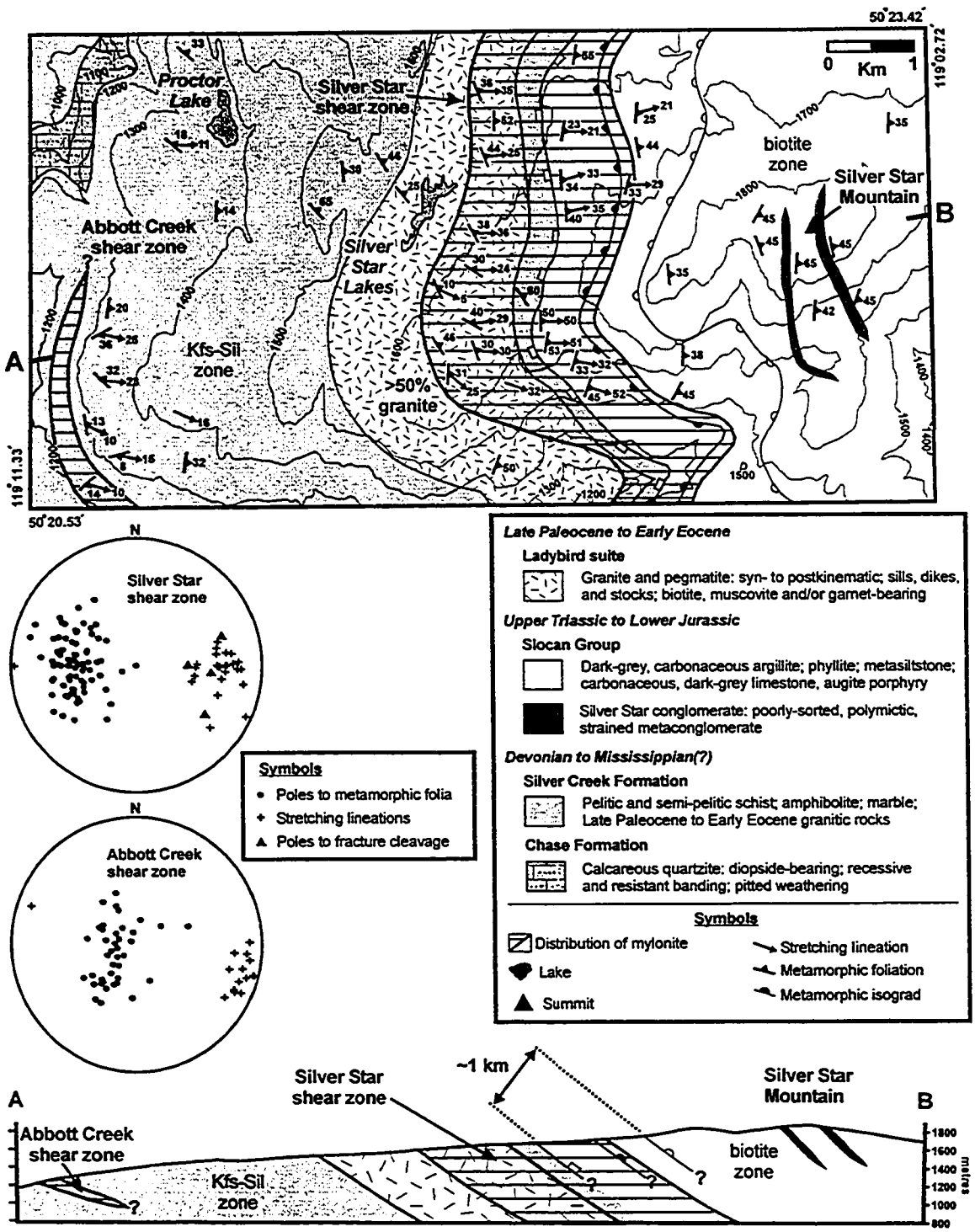

Fig. 4-6. Simplified geological map and cross section of the Silver Star Mountain area showing the distribution of metamorphic isograds, metamorphic zones, and mylonitic fabric. Elevation contours are drawn as thin solid black lines. Elevations are in metres above sea level. Fabric data from the Silver Star and Abbott Creek shear zones are plotted on lower hemisphere, equal-area projections (lower left). Mineral isograds as per Fig. 4-6.

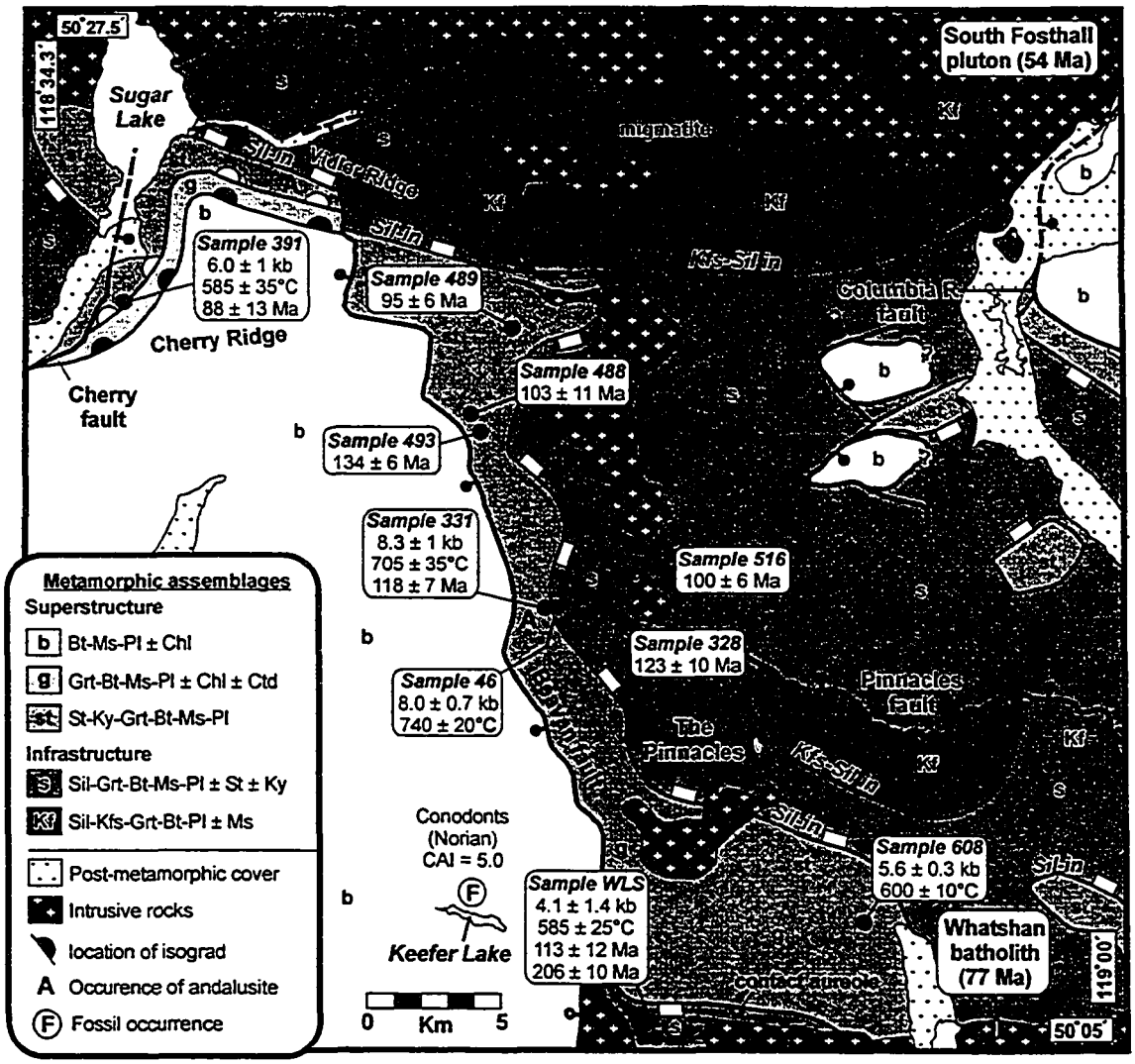

Fig. 4-7. Metamorphic map of the Vidler Ridge and Pinnacles region, showing the map trace of mineral isograd surfaces in pelitic rocks. *Mineral isograd symbols*: open half-circles - garnet-in; filled half-circles - staurolite-in; open rectangles - sillimanite-in; filled rectangles - second sillimanite isograd. Note the distance of 12 km between the trace of the Beaven fault and the Slocan Group outliers (centre) and the closely spaced isograds south of Vidler Ridge (upper left). The location of metamorphic isograds is modified from Reesor and Moore (1971), Carr (1990), and this study.

Within the metamorphic sequence, rocks are variably strained according to their structural level and metamorphic grade. Immediately above the shear zone superstructure rocks are folded and cleaved. Within the biotite and garnet zones, an east-trending mineral lineation, defined by elongate biotite clots, occurs on the foliation surface. Spaced fractures oriented perpendicular to the mineral lineation, filled with quartz and (or) calcite and, are developed locally within the garnet zone (Fig. 4-6, see stereoplots). Within the staurolite and sillimanite zones, evidence of plastic strain is present, including: (1) elongate quartz ribbons with lattice preferred orientation (LPO); (2) quartz grains with undulose extinction, serrated grain boundaries, and sub-grain development; and (3) fine-grained, micaceous shear bands (Fig. 4-8*a*). Delta and sigma porphyroclasts, muscovite fish, quarter structures, extensional (C') shear bands, and C-S fabric are visible in thin-sections oriented parallel to the stretching lineation and perpendicular to the foliation; they consistently record a top to the west shear-sense.

Vidler Ridge/Pinnacles area

In the southeast quadrant of the map area, a salient of greenschist-facies superstructure is bounded on the west by the steeply-dipping Cherry fault, and on the east by the moderately to steeply west-dipping Beaven fault. Where exposed, the Beaven fault is marked by a zone several metres wide of highly fractured rock and gouge. The Cherry fault is not exposed, but its presence is inferred based on map patterns.

Along the northern margin of the salient, in the valley between Cherry and Vidler Ridge, exposure is poor, but a rapid change in metamorphic grade, from biotite-grade to sillimanite-grade occurs over a horizontal distance of approximately 3 km, compatible with either closely spaced isograds (Fig. 4-7; Reesor and Moore 171; this study) or one or several faults (Carr 1990). Compositional layering and the metamorphic foliation dip steeply in this area, striking to the southeast, with variable dip directions.

A similar northward increase in metamorphic grade occurs to the east, within the footwall of the Beaven fault on the south flank Vidler Ridge (Fig. 4-7). The footwall does not preserve the biotite and garnet zones, but a change from the staurolite-kyanite zone to the potassium-feldspar-sillimanite zone occurs across a horizontal distance of less than two kilometres in the footwall (Fig. 4-7). Compositional layering and metamorphic folia have steep and variable dips, striking to the southeast. The sillimanite isograd strikes southward, flanking the Pinnacles Peaks parallel to the trace of the Beaven fault, before striking east south of the Pinnacles, towards Whatshan Lake (Fig. 4-7). Although the absence of suitable rock types prevented metamorphic isograds from being mapped in detail between the Pinnacles and the northern margin of the Whatshan batholith,

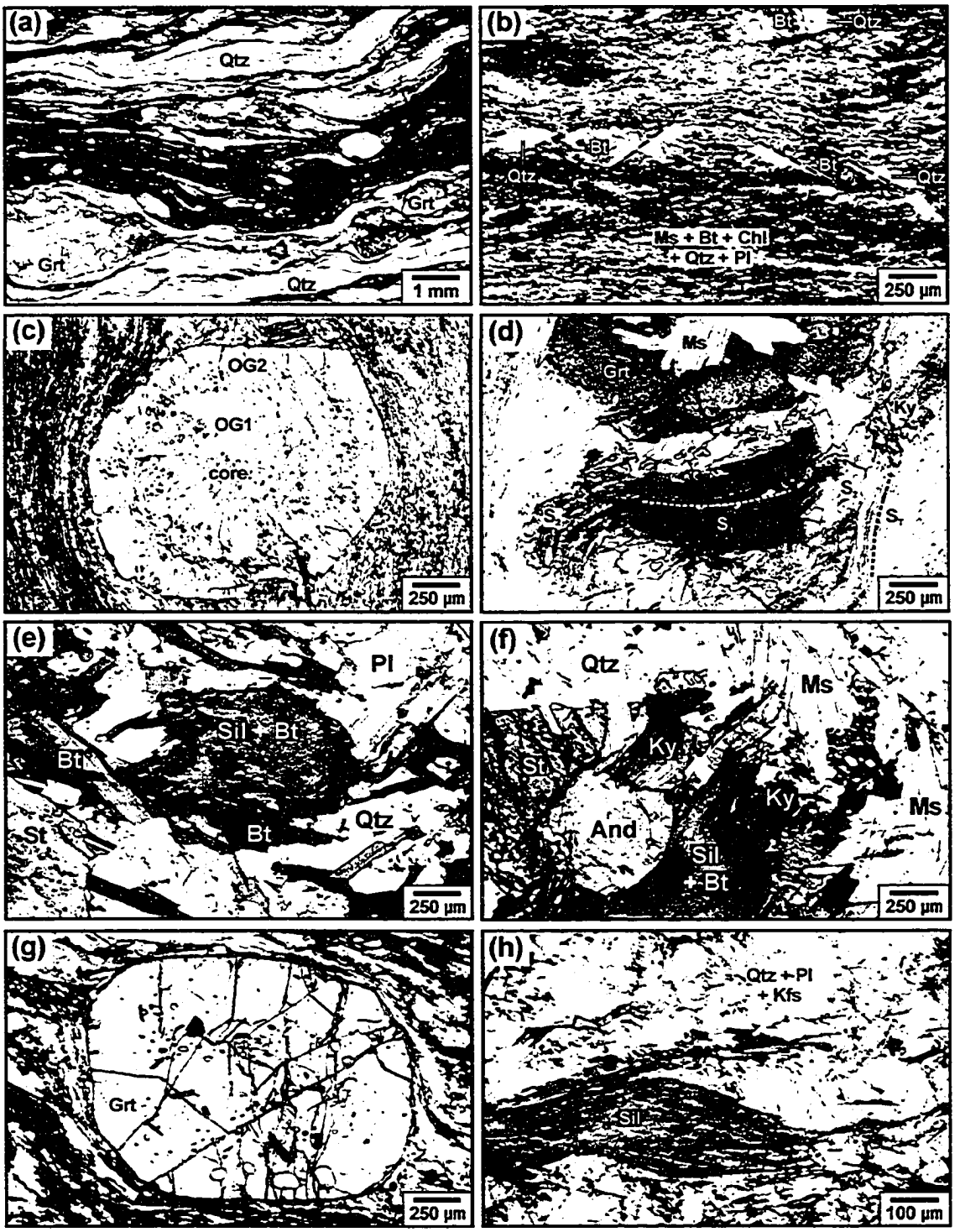

Fig. 4-8 (page 1 of 2). See next page for caption.

Fig. 4-8 (page 2 of 2). Thin-section photographs of metapelitic rocks from the Vernon area. All photos were taken in plane polarized light. (a) Mylonitic metapelitic schist from the sillimanite zone within the Silver Star shear zone. (b) Knotty phyllitic schist from the garnet zone in the vicinity of Cherry Ridge (sample 391). Note the large biotite books with quartz pressure shadows. Small normal faults adjacent to biotite grains have opposite shear-sense. (c) Large, idiomorphic, concentrically triple-zoned garnet from same outcrop as (b). See Figs. 4-10 and 4-11 for zoning patterns within this sample. OG: overgrowth. (d) Coarse-grained metapelitic staurolite schist from the south flank of Vidler Ridge (sample 493) showing typical textural relationships in the staurolite-kyanite zone. Note the zoned staurolite grain (bottom centre) and garnet with muscovite core (top centre). (e) Coarse-grained metapelitic schist from the sillimanite zone in the Pinnacles area. Note the inter-grown, fine-grained biotite and sillimanite mat, pseudomorphing an earlier staurolite or kyanite grain. (f) Coarse-grained pelitic schist (sample 330) located several hundred metres east of sample 331. Note the occurrence of all three Al_2SiO_5 polymorphs adjacent to one another. Sillimanite (fibrolite) is very fine-grained and intimately intergrown with fine-grained biotite in mats, pseudomorphing earlier (kyanite?) grains. (g) Large, ovoid garnet grain within migmatitic metapelitic schist located northwest of Mabel Lake showing the typical ovoid morphology of garnets within the potassium-feldspar-sillimanite zone. (h) Coarse-grained prismatic sillimanite from metapelitic schist within the K-feldspar-sillimanite zone. All mineral abbreviations after Kretz (1983).

metamorphic grade decreases southwards, from sillimanite to garnet grade. A sillimanite-grade contact aureole, approximately 1 km wide, is locally developed near the margin of the Whatshan batholith.

Thin section petrography

More than 200 thin sections were examined to study mineral assemblages, metamorphic textures, microstructures, and to select samples appropriate for thermobarometry and monazite EMP chemical dating.

Biotite zone

A typical mineral assemblage in low-Al metapelitic rocks within the superstructure is quartz, plagioclase, biotite, and muscovite, with or without primary chlorite. Graphite, ilmenite, and zircon occur as accessories. Biotite porphyroblasts commonly exhibit quartz-filled pressure shadows (Fig. 4-8*b*), indicating that deformation outlasted metamorphism.

Garnet zone

Garnet zone metapelitic rocks commonly contain quartz, plagioclase, muscovite, biotite, and garnet. Accessory phases include ilmenite, graphite, monazite, zircon and apatite.

Staurolite occurs in the garnet zone in high-Al metapelitic rocks, forming xenoblastic grains of variable size. These grains are interpreted to have formed from the breakdown of chloritoid (e.g., sample 391):

$$\text{chloritoid} = \text{garnet} + \text{staurolite} + H_2O \qquad (1)$$

Garnet commonly occurs as large (1-5 mm), idiomorphic porphyroblasts with sharp crystal faces. Concentric zoning is common, outlined by variations in the abundance and orientation of inclusions (Fig. 4-8*c*). Garnets commonly contain an internal fabric defined by elongate quartz inclusions (S_I), oriented at high angles to the matrix foliation (S_T) (e.g., Fig. 4-9; Sample 608). The matrix foliation wraps around garnet porphyroblasts, which commonly have quartz-filled pressure shadows, indicating that garnet growth was pre- to synkinematic (Fig. 4-8*c*).

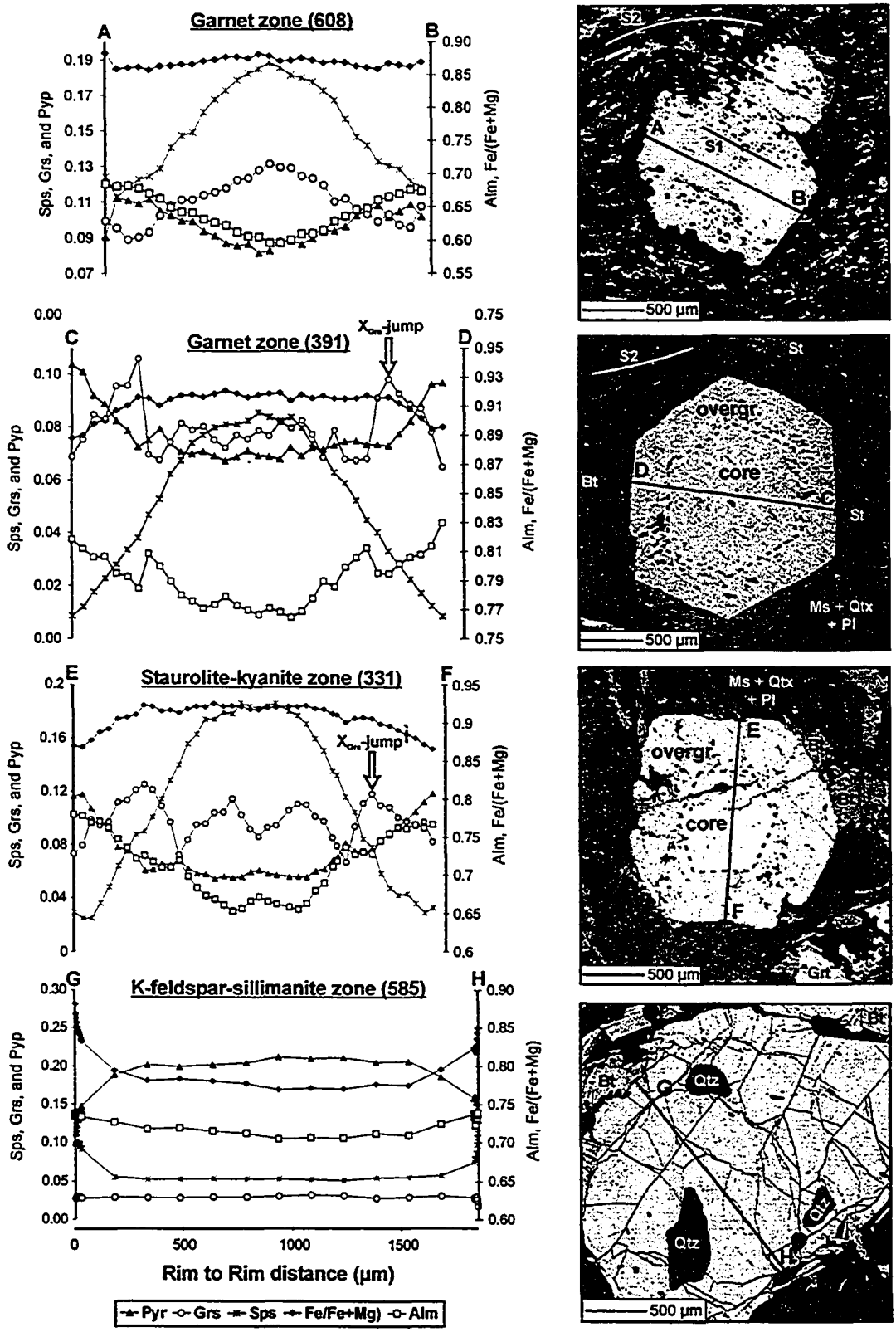

Fig. 4-9. Representative garnet rim-to-rim line analyses and zoning profiles. Spessartine (Sps), grossular (Grs), and pyrope (Pyr) components in garnet are scaled using the left Y-axis. Almandine (Alm) and Fe/(Fe+Mg) components are scaled using the right Y-axis. All graphs are plotted at the same scale. The positions of the line analyses are indicated in the backscattered electron (BSE) images on the right.

Staurolite-kyanite zone

A typical mineral assemblage in low-Al metapelitic rocks is quartz, plagioclase, muscovite, biotite, garnet, and staurolite, with or without chlorite, kyanite and fibrolite. Common accessory minerals include ilmenite, tourmaline, graphite, zircon, monazite, and apatite.

Staurolite typically occurs as large (0.5-5 cm), poikiloblastic, irregular xenoblasts, or as well-formed elongate porphyroblasts with six-sided basal sections and characteristic cruciform twins. Kyanite occurs as rare, ragged porphyroblasts with embayed margins. Near the sillimanite-in isograd, fine-grained fibrolite is common, intimately inter-grown with biotite in fine-grained fibrous mats that pseudomorph earlier kyanite or staurolite grains. Fibrolite within the mats is randomly oriented and post-kinematic (Fig. 4-8*e*). Fibrolite, kyanite, and andalusite have all been observed within the same sample within the staurolite-kyanite zone near Vidler Ridge and the Pinnacles (Figs. 4-7, 4-8*f*; see also Reesor and Moore 1971). In thin section, the textural relationships between the three polymorphs are ambiguous.

Garnet porphyroblasts within the staurolite-kyanite zone are characterized by embayed margins and irregular shapes. Garnet is consumed during the production of staurolite by the reaction:

$$\text{garnet} + \text{chlorite} + \text{muscovite} + \text{quartz} = \text{staurolite} + \text{biotite} + H_2O \qquad (2)$$

Sillimanite zone

A typical mineral assemblage in the sillimanite zone is quartz, plagioclase, muscovite, biotite, garnet, and fibrolite. Accessory minerals include ilmenite, zircon, monazite, tourmaline, and apatite.

The first appearance of sillimanite (randomly oriented fibrolite), which is intimately associated with fine-grained biotite in fibrous, radiating mats (Figs. 4-8*e*, 4-8*f*), is inferred to form during the breakdown of staurolite:

$$\text{staurolite} + \text{muscovite} + \text{quartz} = \text{garnet} + \text{biotite} + \text{fibrolite} + H_2O \qquad (3)$$

Biotite and sillimanite mats overgrow the matrix foliation (S_T), which is interpreted as indicating that fibrolite growth is post-kinematic. Rare, ragged kyanite grains, interpreted to be relict, occur locally.

Potassium-feldspar-sillimanite zone

A typical mineral assemblage is quartz, potassium-feldspar, plagioclase, biotite, and garnet, with or without muscovite and (or) kyanite. Common accessory phases include ilmenite, zircon, apatite and monazite. Potassium-feldspar (plus melt) is produced during the breakdown of muscovite:

$$\text{muscovite} + \text{plagioclase} + \text{quartz} = \text{K-feldspar} + \text{sillimanite} + \text{melt} \quad (4)$$

Garnet occurs as variably sized (100 μm to 1 cm), irregular, ovoid, inclusion-rich porphyroblasts or poikiloblasts (Fig. 4-8*g*), commonly with embayed and ragged margins and large quartz inclusions (Fig. 4-9, right). Prismatic sillimanite is common, forming elongate bundles within biotite-rich layers (Fig. 4-8*h*). Quartz, potassium-feldspar, and plagioclase form discontinuous, leucocratic layers millimetres to centimetres thick, oriented parallel to the metamorphic foliation, interpreted as crystallized *in situ* melt layers (stromatic migmatite). Muscovite is generally rare to absent in the potassium-feldspar-sillimanite zone, except along late fractures or within localized zones of retrogression, where it occurs inter-grown with very fine-grained quartz, plagioclase and ilmenite.

Within the study area, migmatitic rocks commonly contain up to 20-30% leucosome, suggesting that additional melt was injected or produced *in situ* by dehydration melting, as muscovite dehydration melting alone typically produces only modest (2-15%) amounts of melt (e.g., Clemens and Vielzeuf 1987; Le Breton and Thompson 1988; Patiño Douce et al. 1990; Gardien et al. 1995). Biotite dehydration melting may have occurred by the following reaction (cf. Spear and Parrish 1996):

$$\text{biotite} + \text{plagioclase} + \text{quartz} + \text{aluminosilicate} = \text{garnet} + \text{K-feldspar} + \text{melt} \quad (5)$$

Mineral compositions and thermobarometry results

Nine samples of garnet-bearing metapelitic schist and one calcschist were selected for thermobarometry (representative data listed in Table 4-1). Sampling strategy and analytical methods are summarized in Appendix A.

The following guidelines were used to evaluate equilibrium mineral assemblages: (1) major-element compositional maps (Fe, Mg, Ca, Mn) of garnets were made prior to quantitative line analyses; (2) samples with evidence of retrogression were avoided; (3) multiple, linearly-independent reaction equilibria were compared (when possible); (4) biotite composition was

Table 4-1 (page 1 of 1). Representative electron microprobe analyses from selected metapeliticrocks from the study area.

	Grt zone		St-Ky zone		Sil-Ms zone	Kfs-Sil zone			
Sample	391-g1	608-g1	331-g1	46-g2	WLS-g1	72-g1	585-g1	74-g1	537-g1
Garnet									
Position	rim	near rim	near rim	near rim	near rim	near rim	core	core	core
SiO_2	36.95	37.06	37.41	37.43	37.10	37.06	37.51	38.00	37.50
TiO_2	0.06	0.06	0.00	0.03	0.00	0.04	0.02	0.00	0.01
Al_2O_3	21.20	21.62	21.26	21.45	21.53	21.65	21.85	21.94	21.74
Cr_2O_3	0.03	0.05	0.03	na	0.02	0.02	0.02	0.03	0.03
FeO	37.13	30.50	35.90	33.50	32.55	32.71	32.63	32.78	33.69
MnO	0.38	5.42	1.17	2.04	4.45	2.61	2.39	1.38	1.64
MgO	2.64	2.79	3.24	3.64	2.53	3.28	5.28	5.75	4.76
CaO	2.43	3.19	2.63	1.79	2.36	2.93	1.07	1.61	1.56
Na_2O	0.00	0.00	0.00	na*	0.01	0.00	0.01	0.02	0.01
Total	100.81	100.68	101.66	99.88	100.57	100.30	100.78	101.52	100.94
n	1	3	1	6	2	2	8	6	5
Plagioclase (matrix average)									
SiO_2	59.07	45.52	60.41	60.64	56.64	58.06	61.88	60.13	59.45
Al_2O_3	25.85	35.47	24.79	24.23	27.77	26.69	23.13	24.99	
FeO	0.05	0.13	0.07	na	0.11	0.05	0.19	0.23	0.20
MgO	0.00	0.00	0.01	0.01	0.00	0.00	0.01	0.00	0.00
CaO	7.47	19.15	6.12	5.33	9.82	8.63	3.86	6.33	6.30
Na_2O	7.83	1.08	8.35	8.22	6.51	7.11	9.15	8.23	8.02
K_2O	0.11	0.04	0.14	0.16	0.12	0.24	0.30	0.26	0.32
Total	100.38	101.39	99.88	98.58	100.98	100.78	98.51	100.16	99.40
An	25	91	42	26	45	40	19	29	30
n	10	17	13	5	15	9	8	24	10
Biotite (matrix average)									
SiO_2	35.87	35.55	35.57	36.21	35.41	34.67	34.82	35.08	34.58
TiO_2	1.50	2.57	1.83	2.09	3.01	3.09	4.96	2.67	5.53
Al_2O_3	18.96	18.26	19.05	20.35	19.03	18.21	17.81	18.27	17.33
FeO	18.51	17.51	19.35	19.62	18.74	20.86	19.15	19.15	19.55
MnO	0.01	0.14	0.05	0.09	0.12	0.30	0.13	0.07	0.05
MgO	10.87	11.14	9.57	9.20	9.75	8.60	9.03	10.48	8.90
Na_2O	0.28	0.13	0.27	0.29	0.19	0.13	0.23	0.23	0.22
K_2O	8.40	8.91	8.72	8.72	9.22	9.25	9.61	9.69	9.46
Cl	0.03	0.01	0.02	0.01	0.02	0.07	0.14	0.14	0.02
Total	94.42	94.23	94.43	96.58	95.49	95.17	95.86	95.76	95.63
n	6	15	12	7	12	14	10	5	8
Muscovite (matrix average)									
SiO_2	46.30		45.86	47.17	46.16				
TiO_2	0.16		0.55	0.53	1.01				
Al_2O_3	36.29		35.71	35.93	35.63				
FeO	1.03		1.62	1.05	1.39				
MnO	0.01		0.00	0.01	0.02				
MgO	0.43		0.58	0.65	0.59				
Na_2O	1.45		1.03	0.90	0.64				
K_2O	9.40		9.48	10.25	10.03				
Cl	0.00		0.01	0.00	0.01				
Total	95.07		94.86	96.55	95.49				
n	14		15	9	15				

Table 4-1 (page 2 of 2).

	Grt zone		St-Ky zone		Sil-Ms zone	Kfs-Sil zone			
Sample	391-g1	608-g1	331-g1	46-g2	WLS-g1	72-g1	585-g1	74-g1	537-g1
Chlorite (matrix average)									
Na_2O	0.01								
SiO_2	24.33								
TiO_2	0.02								
Al_2O_3	22.76								
FeO	23.49								
MnO	0.02								
MgO	15.84								
K_2O	0.07								
Cl	0.01								
Total	86.54								
n	5								
Staurolite (matrix average)									
SiO_2	27.35		27.56						
TiO_2	0.39		0.52						
Al_2O_3	54.98		55.02						
FeO	13.83		13.60						
ZnO	0.30		0.31						
MnO	0.01		0.13						
MgO	1.67		1.71						
CaO	0.01		0.01						
Total	98.54		98.84						
n	15		15						

* na - not analyzed.

Standards: **Garnet**: MgO, SiO_2, CaO, Al_2O_3 - Roberts Victor garnet; FeO - Rockport fayalite; Na_2O, TiO_2 - Kakanui hornblende; MnO - willimite; Cr_2O_3 - Stillwater chromite. **Plagioclase**: Na_2O, K_2O - Kakanui anorthoclase; SiO_2, CaO, Al_2O_3 - Lake City, Oregon, plagioclase; FeO - U. of Alberta obsidian. **Biotite**: Na_2O, FeO, MgO, TiO_2 - Kakanui hornblende; SiO_2, Al_2O_3, K_2O - Calgary biotite; Cl - Brazil scapolite; MnO - willemite. **Muscovite**: Na_2O, FeO, MgO, TiO_2 - Kakanui hornblende; SiO_2, Al_2O_3, K_2O - Calgary muscovite; Cl - Brazil scapolite; MnO - willemite. **Staurolite**: SiO_2, MgO - Kakanui pyrope; TiO_2 - Kakanui hornblende; Al_2O_3 - University of Alberta kyanite; FeO - Rockport fayalite; ZnO Brazil gahnite; MnO - willemite; CaO - Roberts Victor garnet. **Chlorite**: same standards as biotite.

monitored with respect to distance from garnet; (5) thermobarometry results were compared with petrogenetic grid constraints; (6) where the equilibrium composition of mineral phases could not be determined with reasonable confidence, the petrogenetic grid was used to constrain *P-T* conditions; and (7) error parallelograms were constructed to examine the effect of intra-sample compositional heterogeneity on thermobarometry estimates.

Garnet zone

Garnets from within the garnet zone are typically concentrically zoned (Figs. 4-9, 4-10). Samples 391 and 608 contain typical bell-shaped profiles in X_{Sps} and Fe/(Fe+Mg) and bowl-shaped profiles in X_{Alm} and X_{Pyr} (Fig. 4-9). Some garnets contain a local increase in X_{Sps} and Fe/(Fe+Mg) at the rim. Zoning in X_{Grs} is highly variable between samples, but generally consistent within samples. For example, in sample 608, X_{Grs} decreases smoothly from core to rim, with a slight increase at the rim. In contrast, garnets from sample 391 contain abrupt changes in X_{Grs}. Garnets with three zones contain a high X_{Grs} core, a low X_{Grs} intermediate zone, and an overgrowth characterized by a sharp increase in X_{Grs}, followed by a gradual decrease towards the rim. Garnets with two concentric zones lack the high X_{Grs} core and may not have been cut through the centre of grains.

Possible explanations for the sharp drop in X_{Grs} from core to the low X_{Grs} intermediate zone include consumption of a calcic phase (epidote-clinozoisite, margarite, or calcite) during prograde metamorphism (e.g., Menard and Spear 1993) or Ca fractionation during garnet and (or) plagioclase growth (e.g., Frost and Tracy 1991). Apatite is common in both samples 391 and 608, but no other calcic matrix phases are evident.

In both samples 608 and 391, matrix biotite shows a modest variation in Fe/(Fe+Mg) (0.460-0.517) and in TiO_2 (1.39-3.23 wt.%). In sample 391, matrix plagioclase is characterized by patchy zoning within grains with X_{An} varying from 0.27 to 0.37. Sample 608, a quartz-rich calcsilicate rock, has anorthitic plagioclase (X_{An} = 0.86-0.93); no other calcium-bearing phases are present other than apatite.

Garnet zoning patterns in samples 391 and 608 are characteristic of prograde growth zoning (e.g., Tracy et al. 1976). Diffusional modification effects are inferred to be negligible at this grade (e.g., Spear 1993, and references therein). Near-rim garnet compositions (corresponding to the Fe/(Fe+Mg and Mn trough) were used in thermobarometry calculations. The pressure estimate of sample 608 is a maximum estimate, as the sample does not contain an aluminosilicate phase or muscovite. Pressure and temperature (*P-T*) estimates from both samples are listed in Table 4-2 and shown in Fig. 4-11*a*. The results are consistent with constraints from

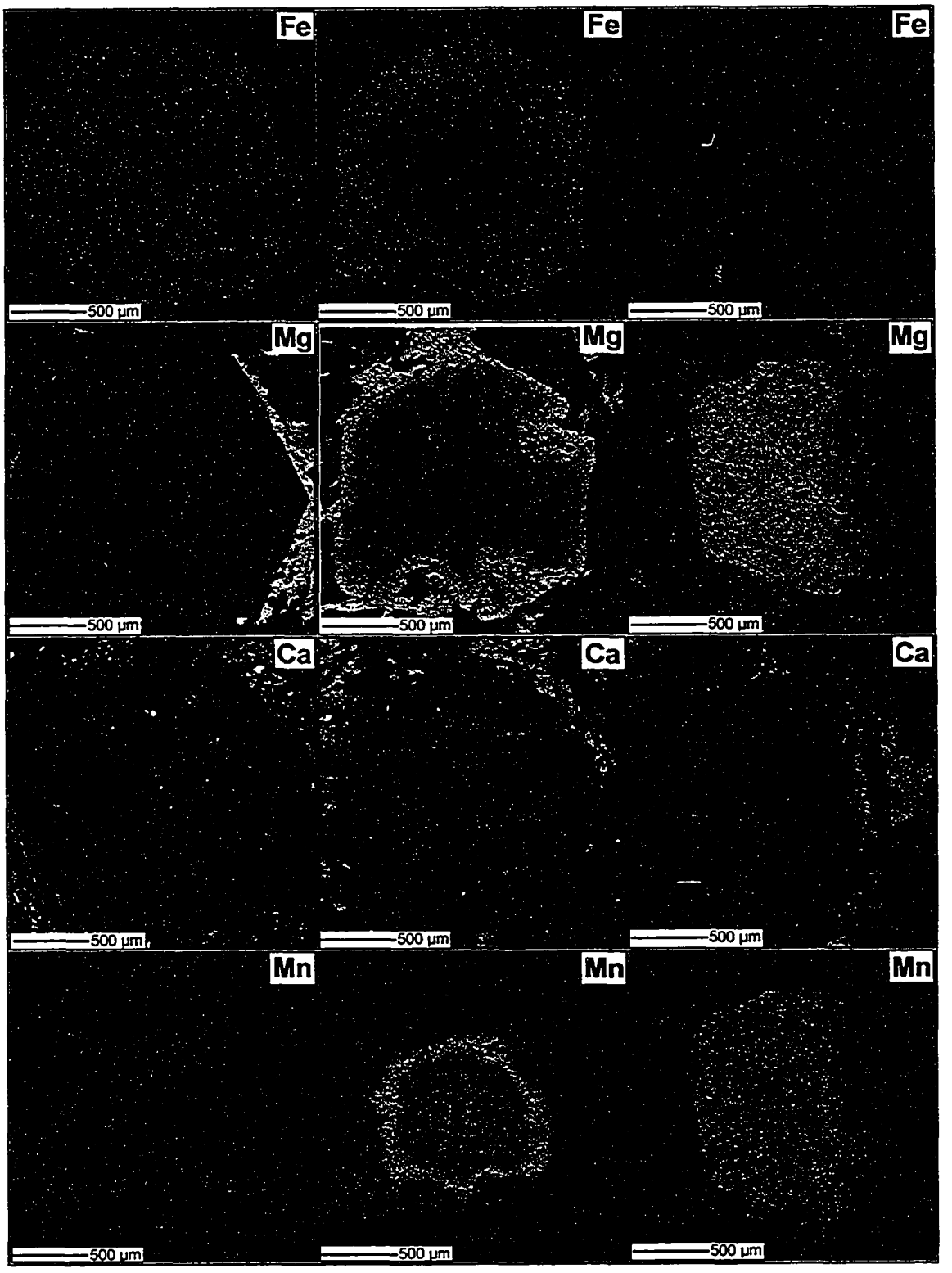

Fig. 4-10. Major element (Fe, Mg, Ca, and Mn) compositional maps for garnets from samples 391 (left; garnet zone), 331 (centre; staurolite-kyanite zone), and 585 (right; migmatite zone). See text for a discussion of garnet zoning. Sample location and *P-T* estimates are indicated in Table 4-2.

Table 4-2. Summary of thermobarometry results from metapelitic rocks from the study area.

Sample	Location (UTM[a])	Mineral Assemblage[b]	Grt d (um)[c]	Geobarometer[d]	Garnet	Thermobarometry P (kbar)[e]	Thermobarometry T (°C)[e]	Petrogenetic grid P (kbar), T (°C)	Garnet zoning
Garnet zone									
391	390827E 5576126N	Chl-Pl-Grt-Ms-St-Bt-Qtz	1600-1900	GPMB	rim	6.0 ± 1	585 ± 35	>4, , 450-575	growth zoning
608	418918E 5553336N	Grt-Pl-Bt-Qtz (no Al2SiO5)	1200-1500	GASP	near-rim	5.6 ± 0.3	600 ± 10	>4, , 450-600	growth zoning
Staurolite-kyanite zone									
331	407130E 5565038N	St-Gt-Pl-Ms-Bt-Qtz	1400-1800	GPMB	near-rim	8.3 ± 1	705 ± 35	7-8, 650-675	growth zoning
46	407374E 5565120N	Ky-Sil-Pl-Grt-Ms-Bio-St-Qtz	600-800	GPMB	near-rim	8.0 ± 0.7	740 ± 20	7-8, 650-675	X_{Sps}, Fe/(Fe+Mg) near-rim increase
Sillimanite zone									
WLS	411511E 5547671N	Sil-Grt-Pl-Bt-Ms-Qtz	100-200	GASP, SGAM	core	4.1 ± 1.4	585 ± 25	>3, 600-650	near-rim increase in X_{Grs}
Potassium-feldspar-sillimanite zone									
72	378960E 5567540N	Sil-Grt-Pl-Bt-Kfs-Qtz	300-1500	GASP	near-rim	9.3 ± 1.2	760 ± 40	7-9, 700-800	X_{Grs} minima near rim
585	372647E 5604833N	Sil-Pl-Kfs-Grt-Bio-Qtz	1200-2000	GASP	core	11.2 ± 1.5	850 ± 30	8-10, 825-850	X_{Sps}, Fe/(Fe+Mg) near-rim increase
74	370618E 5614894N	Sil-Grt-Pl-Bt-Kfs-Qtz	1800	GASP	core	9.7 ± 1.5	850 ± 30	8-10, 825-850	X_{Sps}, Fe/(Fe+Mg) near-rim increase
537	343725E 5559400N	Pl-Kfs-Qtz-Sil-Bt-Grt	400-500	GASP	core	9.4 ± 1.4	850 ± 30	8-10, 825-850	X_{Sps}, Fe/(Fe+Mg) near-rim increase

[a] All UTM coordinates using datum NAD83, Zone 11.

[b] Abbreviations after Kretz (1983); Mineral phases listed least to most abundant.

[c] Diameter of garnet used in thermobarometry calculations.

[d] GPMB: garnet-plagioclase-muscovite-biotite (e.g., Ghent and Stout 1981); GASP: garnet-aluminosilicate-silica-plagioclase (e.g., Ghent 1976); SGAM: silica-garnet-aluminosilicate-muscovite (e.g., Hodges and Crowley 1985).

[e] The values listed are the calculated mid-points of the upper and lower estimates. Any spot within the error parallelograms shown in Figure 4-12 is considered equally likely.

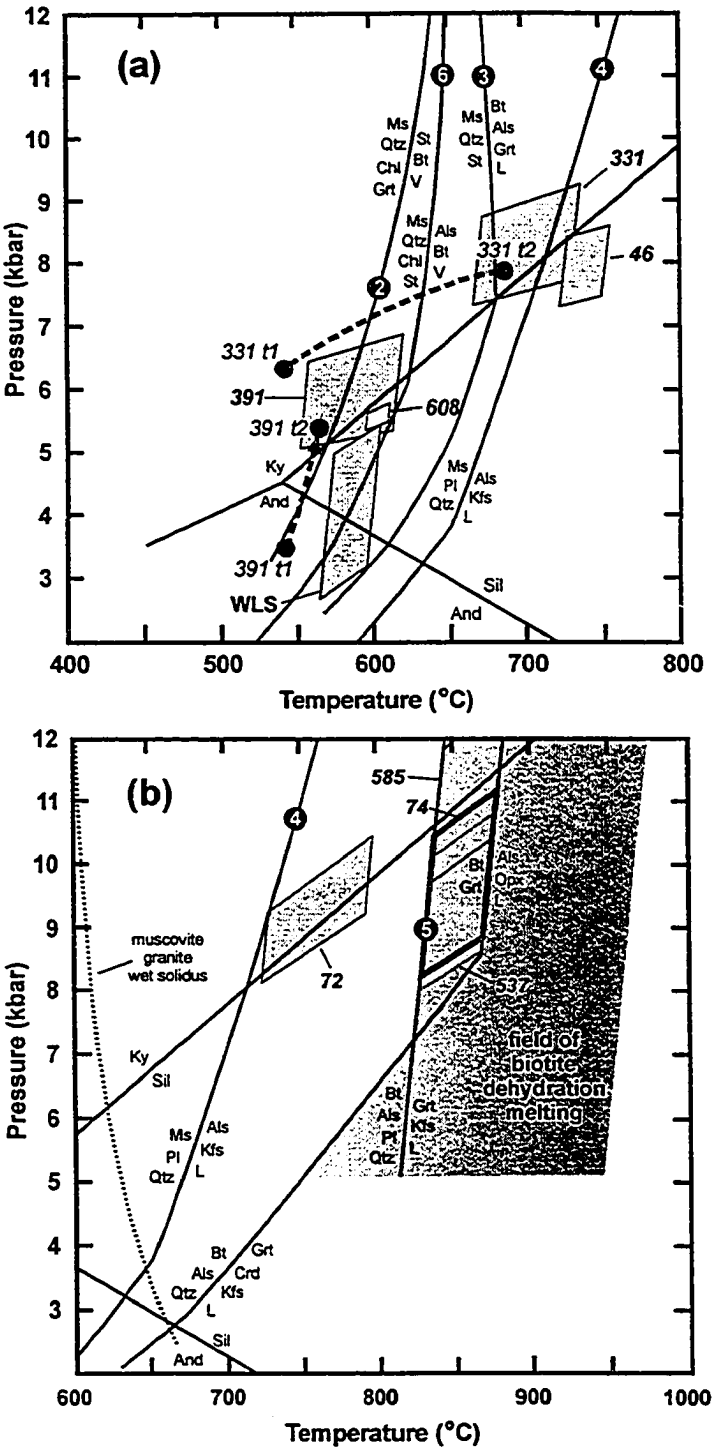

Fig. 4-11. Petrogenetic grid in the NaKFMASH system comparing thermobarometry results with the location of selected reaction equilibria. Grid modified from Spear et al. (1999). Muscovite granite wet solidus modified from Huang and Wyllie (1973). Field of biotite dehydration melting based on the modeling results of Patiño Douce and Johnston (1991). The Al_2SiO_5 triple point shown is that of Pattison (1992). The numbers on reaction curves correspond to reactions in the text. (a) Thermobarometry results from garnet, staurolite-kyanite, and sillimanite zone samples. See text for discussion of partial *P-T* paths. (b) Thermobarometry results from potassium-feldspar-sillimanite zone samples. Error boxes were generated using intra-sample compositional heterogeneity. Mineral abbreviations after Kretz (1982).

the petrogenetic grid. Sample 391, which is a high-Al pelite, contains garnet, staurolite, and primary chlorite, constraining the temperature to be above the garnet-in isograd (~ 450-500°C; Spear 1993). Sample 391 does not contain an aluminosilicate phase, indicating that reaction 6 (position indicated in Fig. 4-11*a*) was not reached.

Staurolite-kyanite zone

Garnet zoning profiles within sample 331 are bell-shaped with respect to X_{Sps} and Fe/(Fe+Mg), and bowl-shaped with respect to X_{Alm} and X_{Pyr} (Fig. 4-12). Like sample 391, zoning in X_{Grs} is variable, with peaks and troughs. The core is characterized by an increase in X_{Grs} from the centre outwards; there is a sharp decrease across an intermediate zone, and then a sharp increase into the mantling overgrowth, where X_{Grs} decreases gradually towards the rim. The jump in X_{Grs} is associated with a slight decrease in Fe/(Fe+Mg) and a slight flattening of the bell-shaped Mn profile. In addition, the overgrowth is more inclusion-rich than the core, suggesting there may have been a growth hiatus from core to overgrowth. Plagioclase inclusions within the high X_{Grs} overgrowth are more anorthitic (X_{An} = 0.48-0.53) than average matrix plagioclase (X_{An} = 0.42).

Matrix biotite is relatively homogeneous, with the exception of biotite grains adjacent to garnet, where both the highest and lowest Fe/(Fe+Mg) were measured (0.524-0.550). The biotite with the highest Fe/(Fe+Mg) is interpreted as having formed during retrograde net-transfer reactions (ReNTR's; e.g., Kohn and Spear 2000). The remainder of biotite grains within 100 μm of garnet exhibit decreasing Fe/(Fe+Mg) and increasing Ti content with increasing distance from garnet, suggesting that retrograde Mg-Fe diffusion occurred between garnet and biotite. Matrix plagioclase has a limited range in X_{An} (0.40-0.43).

Garnet in sample 46 (profile not shown) exhibits a different zoning pattern. The cores have flat compositional profiles, except for bell-shaped X_{Grs} zoning. A sharp increase in X_{Sps} and Fe/(Fe+Mg) occurs within the outer 50 microns of grains. Staurolite is twice as abundant as garnet, suggesting a portion of prograde garnet was consumed during staurolite production (e.g., Spear et al. 1991). The difference in garnet zoning patterns between samples 331 and 46, given the samples proximity to one another (~200 m), is inferred to result from differences in grain diameters (1600 vs. 800 μm, respectively). For instance, using Mg diffusivity data from Cygan and Lasaga (1985), at a temperature of 675°C (the inferred peak temperature) a garnet with a diameter of 800 μm will completely homogenize in X_{Pyr} in 8 m.y., while a garnet with a diameter of 1600 μm takes 30 m.y. The preservation of X_{Grs} zoning in sample 74 agrees with previous empirical studies which suggest that the diffusivity of Ca is slower in garnet relative to Fe, Mg,

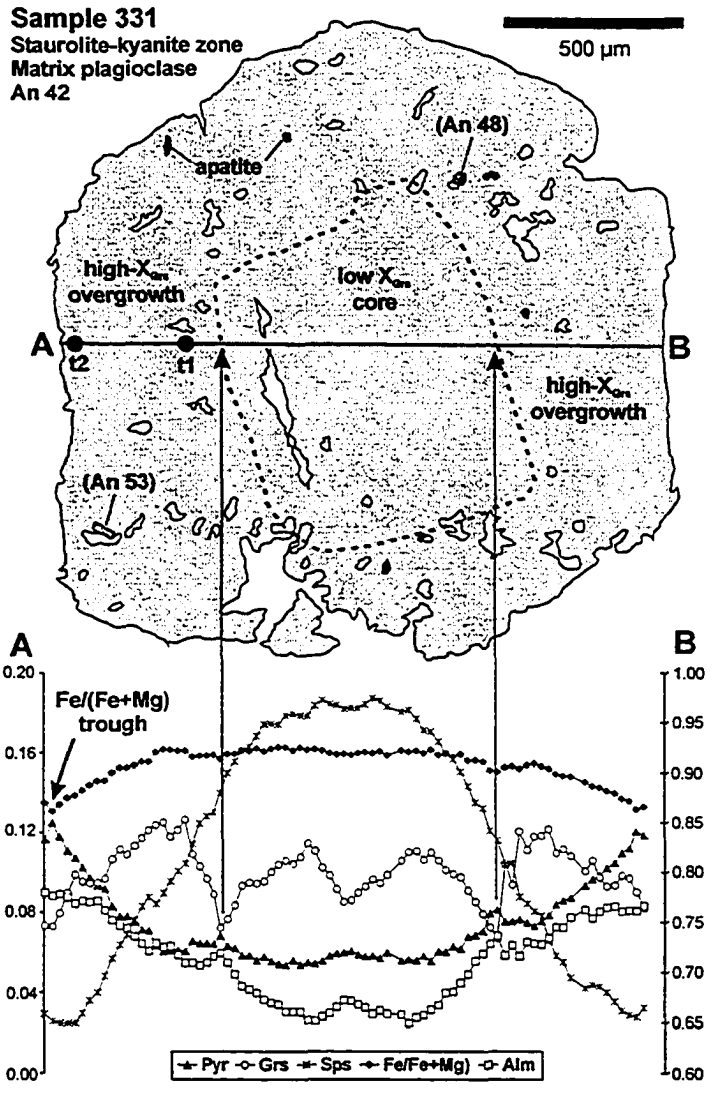

Fig. 4-12. Garnet line drawing and rim-to-rim compositional profile from sample 331. The black dashed line indicates the location of the sharp increase in X_{Grs} from core to overgrowth. The location and composition of plagioclase inclusions are indicated (dark grey shading). As garnet zoning is concentric (see Fig. 4-11), the position of the plagioclase inclusions was projected into the profile line and paired with the corresponding garnet composition in the Gibbs modelling. Quartz (white) and apatite (black) inclusions are also shown. An initial *P-T* estimate of 7.9 kbar and 685°C was calculated using the near rim garnet composition (part (a), point t2) and average matrix plagioclase, biotite, and muscovite compositions.

and Mn (e.g., Yardley 1977). Matrix biotite within sample 46 has a relatively uniform Fe/(Fe+Mg) (0.537-0.553) and TiO_2 content (2.438-2.639 wt.%). Plagioclase composition varies somewhat within the sample (X_{An} 0.24-0.30), although no systematic zoning pattern was detected.

Near-rim garnet compositions were combined with matrix phase compositions to derive (peak) *P-T* estimates. Comparison with the petrogenetic grid indicates that *P-T* estimates calculated for sample 331 are approximately ~50°C too high, as no aluminosilicate is present (Fig. 4-11*a*). Sample 46 yields a temperature estimate 75-100°C too high, as staurolite and muscovite are stable. This may result from the effect of ReNTR's, which can yield temperature estimates 100°C or more above peak temperatures (e.g., Duebendorfer and Frost 1988; Kohn and Spear 2000).

Sillimanite zone

Sample WLS occurs within the contact aureole of the Whatshan Lake pluton (Fig. 4-7; 77 ± 0.5 Ma; U-Pb zircon, Carr 1990).

Garnets are generally homogeneous in composition, except near the rim, where complex compositional fluctuations in X_{Grs}, X_{Alm}, X_{Pyr}, X_{Sps}, and Fe/(Fe+Mg) occur. Profiles at the rim on one side of a garnet may be opposite to those observed at the other rim. The homogeneity of the garnet cores suggests that peak temperatures were sufficient to homogenize the core by diffusion. Matrix biotite is relatively homogeneous, with the exception of grains adjacent to garnet, which are characterized by higher Fe/(Fe+Mg). Matrix plagioclase is variable in composition (X_{An} = 0.43-0.47).

The garnet core composition was used in conjunction with matrix phases to estimate peak *P-T* conditions of 585 ± 25°C and 4.1 ± 1.4 kbar (Table 4-2). Intersection of the GASP (e.g., Ghent 1976) and SGAM (e.g., Hodges and Crowley 1985) equilibria with the garnet-biotite thermometer yield differences in pressure of ~ 0.8 kbar. As garnets within sample WLS are quite small (100-200 μm), they would homogenize relatively quickly. Using the data of Cygan and Lasaga, homogenization of Mg at 585°C is expected within 2.9 and 11.4 m.y. for diameters of 100 μm and 200 μm, respectively. Retrograde Fe-Mg diffusion can also yield anomalously low peak temperatures using garnet cores, particularly in small garnets (e.g., Spear 1991). As such, the thermobarometry results from sample WLS are viewed with caution. Temperatures are considered to be 50-75°C too low, as fibrolite is interpreted to form from the breakdown of staurolite in this sample. The lower pressure constraints are too low, as fibrolite, not andalusite is present (Fig. 4-11*a*).

Potassium-feldspar-sillimanite zone

Four samples were analyzed from the potassium-feldspar-sillimanite zone. Sample 72 contains a relatively small volume of leucosome (<5%), whereas the remaining samples contain 15-30%.

Garnet zoning patterns are variable from sample 72. Larger garnets (1400 μm diameter) typically contain a high X_{Grs} core (0.121), decreases gradually in X_{Grs} towards the rim (0.081), with a slight increase at the rim. The increase in X_{Grs} at the garnet rim may be due equilibrium with a melt phase (e.g., Spear and Kohn 1996). Other major elements (Fe, Mg, Mn) have relatively homogeneous compositional profiles, with the exception of X_{Sps}, which increases slightly at the rim. In smaller garnets (300 μm diameter), this increase in X_{Sps} from core to rim (reverse zoning) is more pronounced (0.049-0.202). This pattern is interpreted to result from the effect of ReNTR's (e.g., Kohn and Spear 2000). Plagioclase inclusions in garnet (X_{An} = 0.39-0.46) are generally more anorthitic than the average matrix plagioclase. Matrix biotite is variable in composition, with Fe/(Fe+Mg) varying from 0.551-0.615 and TiO_2 from 2.57-5.11 wt.%. No relationship between Fe/(Fe+Mg) and Ti content of biotite and distance from garnet is apparent. Matrix plagioclase composition is variable (X_{An} = 0.36-0.44), with patchy, rather than concentric zoning.

The near-rim garnet composition was used in conjunction with matrix phases to obtain a peak P-T estimate (Table 4-2). The estimate is in reasonable agreement with the petrogenetic grid (Fig. 4-11*b*), as the parallelogram plots above the muscovite dehydration melting reaction. Pressure estimates are considered to be too high, as sillimanite, rather than kyanite, is present. The underlying cause of the pressure overestimate is not clear, but matrix plagioclase may not be in equilibrium with the chosen garnet composition.

The remaining three samples (74, 537, and 585) are similar in terms of modal mineralogy and volume of leucosome. Garnets from samples 74 and 585 are large (2 cm in diameter), irreguiar to lozenge-shaped, with abundant irregular-shaped quartz and elongate biotite inclusions. In contrast, garnets in sample 537 are more abundant, smaller (average 100-200 μm in diameter) and have few inclusions. Garnet zoning patterns and compositional profiles, however, are similar from all three samples. Cores are homogeneous, with X_{Grs} decreasing slightly at the rim. Both X_{Sps} and Fe/(Fe+Mg) increase sharply within the first 50 μm inward of the rims (Figs. 4-9, 4-10, right column). Where biotite inclusions are present, a local increase in Fe/(Fe+Mg) occurs within the 50 μm surrounding the inclusion, with no corresponding increase in X_{Sps}.

A considerable degree of intra-sample biotite compositional variation occurs in samples 74, 537, and 585, which appears to be controlled by the proximity of the biotite grain to the

nearest garnet. For instance, in sample 74, biotite grains proximal to garnet are lowest in Fe/(Fe+Mg), while those furthest away are highest in Fe/(Fe+Mg) (Fig. 4-13*a*). This pattern is interpreted to reflect Fe-Mg diffusional exchange between garnet and biotite during cooling. In samples 537 and 585, the opposite trend is observed. Biotite highest in Fe/(Fe+Mg) is proximal to garnet (Fig. 4-13*b*). Biotite inclusions in garnet within sample 585 have a lower Fe/(Fe+Mg) (0.417-0.473) and higher TiO_2 (5.03-5.29 wt.%) than matrix biotite. This is interpreted to result from the enrichment of matrix biotite in Fe during ReNTR's (e.g., Duebendorfer and Frost 1988; Kohn and Spear 2000).

It is apparent from garnet zoning profiles and biotite compositional variations, that both Fe-Mg diffusion during cooling and ReNTR's occurred after peak conditions (cf. Spear and Parrish 1996). Estimating peak temperatures using the garnet core compositions with the average matrix biotite compositions yields temperatures of 797-885°C. The lowest and highest temperatures were obtained from sample 537. Peak temperatures can be loosely constrained using the petrogenetic grid (Fig. 4-11*b*). As no primary muscovite is present, peak temperatures must be above reaction 4. No orthopyroxene or cordierite was observed anywhere within the potassium-feldspar-sillimanite zone, constraining peak temperatures to below ~875°C.

Peak pressures were estimated using the GASP equilibria (e.g., Ghent 1976) with garnet core compositions and matrix plagioclase. Intersection of the GASP equilibria with the grid temperature constraints yields pressures of 7 to 12 kbar (Fig. 4-11*b*). Results over 10 kbar are considered to be anomalously high, as sillimanite, rather than kyanite, is present in all samples. Berman (1991) reported anomalously high pressure estimates from within the staurolite and sillimanite zones of the northern Monashee complex, and a difference in pressure estimates between the GASP and SGAM geobarometers of up to 10 kbar, suggesting that anomalously high pressure estimates using the GASP geobarometer may be a common problem in this region.

Summary of thermobarometry estimates

Estimates of peak *P-T* conditions agree reasonably well with constraints from the petrogenetic grid, particularly in garnet zone samples (391, 608; 585-600°C, 5.6-6.0 kbar), where the effects of diffusion and ReNTR's are considered to be negligible (Fig. 4-11*a*; Table 4-2). Staurolite-kyanite zone samples (74, 331) yield temperature estimates (705-740°C at 8.0-8.3 kbar) that are considered 50-75°C too high, as staurolite is present. The *P-T* estimate from sample WLS (4.1 ± 1.4, 585 ± 25°C), situated within the sillimanite zone contact aureole around the Whatshan Lake pluton, is considered to be unreliable due to the small diameter of the garnets (100-200 μm) and the inconsistent near-rim zoning patterns. Hence, the peak temperature

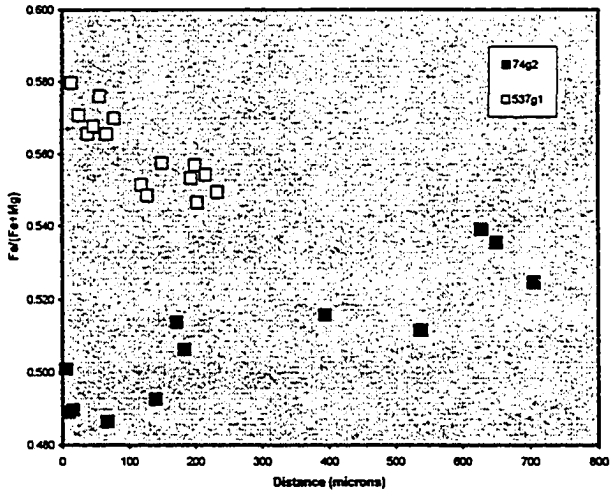

Fig. 4-13. Comparison of Fe/(Fe+Mg) content of biotite compared with distance from garnet rim in migmatite-grade metapelitic rocks in sample 74g2 and 537g1. See text for interpretation of the data.

estimate is considered ~ 75° too low, probably due to Fe-Mg diffusional modification of garnet during cooling (e.g., Spear 1991). Potassium-feldspar-sillimanite zone temperatures (760-850°C), constrained using the grid (Fig. 4-11*b*), are compatible with indirect evidence of biotite dehydration melting. Pressure estimates (9.3-11.2 kbar) obtained using the GASP equilibria are systematically high, as sillimanite is present, although the underlying reason is not clear. Disequilibrium between garnet core compositions and matrix plagioclase is suspected.

Rocks within the superstructure belt are within the biotite zone of the greenschist facies, below the garnet-in isograd (~450°C, Spear 1993). Maximum temperatures of 330-440°C are consistent with CAI values from Upper Triassic conodonts recovered from the superstructure belt (Fig. 4-2). Underlying infrastructure rocks yield peak *P-T* estimates of approximately 10 kbar and 850°C, consistent with uppermost amphibolite- to granulite-facies conditions. Differences in peak *P-T* conditions between infrastructure and superstructure rocks of 5-7 kbar and 400-500°C are implied by the results of this study.

Gibbs modeling

In addition to geothermobarometry, partial *P-T* paths were modelled for samples 391 and 331 using the Gibbs method (e.g., Spear and Selverstone 1983; Spear et al. 1984). The Gibbs method involves formulating the phase equilibrium of a given mineral assemblage through a system of linear differential equations, so that variations in *P* and *T* can be calculated from changes in phase composition. Program GIBBS (Spear and Menard 1989) was used to perform the calculations.

Sample 331, located near the contact between the staurolite-kyanite and the sillimanite zones (Fig. 4-7), contains the mineral assemblage: quartz, biotite, muscovite, plagioclase, garnet, and staurolite (the presence of an H_2O fluid is assumed), for a total of 7 phases (Table 4-3). This assemblage can be modelled using the nine-component system MnNCKFMASH (MnO-Na_2O-CaO-K_2O-FeO-MgO-Al_2O_3-H_2O). According to the phase rule, the thermodynamic variance of the system is four, indicating that changes in four phase compositions must be specified to calculate the corresponding change in *P-T* conditions.

Garnet within sample 331 is concentrically zoned and contains plagioclase inclusions (Figs. 4-10, 4-12). Assuming that: (1) the chosen mineral compositions are in equilibrium; (2) the outer portion (high X_{Grs} overgrowth) of the garnet grew continuously in equilibrium with the matrix mineral assemblage; and (3) the composition of the garnet has not been modified significantly by diffusion subsequent to growth, the *P-T* path of the sample during the time of

Table 4-3. Parameters used for Gibbs modeling.

Mineral	Component	Mole fraction (matix/Grt rim)	Mole fraction (Grt inner rim)	ΔX
Sample 331, Garnet 1 (MnNCKFMASH)				
Quartz	qtz	1.0000		
Plagioclase	ab	0.5716		
	an	0.2861	0.3831	0.0971
Garnet	prp	0.1250	0.0603	-0.0647
	alm	0.7763	0.7090	-0.0673
	sps	0.0257		
	grs	0.0729	0.1265	0.0536
Muscovite	ms	0.8578		
	pg	0.1421		
	mrg	0.0001		
Biotite	phl	0.4678		
	ann	0.5307		
	mnbt	0.0015		
Staurolite	mgst	0.1819		
	fest	0.8103		
	mnst	0.0078		
Water	H_2O	1.0000		
Sample 391, Garnet 1 (MnNCKFMASH)				
Quartz	qtz	1.0000		
Plagioclase	ab	0.6370		
	an	0.3568		
Garnet	prp	0.1036	0.0722	-0.0314
	alm	0.8181	0.7842	-0.0339
	sps	0.0085		
	grs	0.0687	0.1058	0.0371
Muscovite	ms	0.8096		
	pg	0.1903		
	mrg	0.0001		
Biotite	phl	0.5112		
	ann	0.4886		
	mnbt	0.0002		
Staurolite	mgst	0.1770		
	fest	0.8222		
	mnst	0.0008		
Chlorite	mgchl	0.3632		
	fechl	0.6366		
	mnchl	0.0002		
Water	H_2O	1.0000		

overgrowth formation can in principle be calculated if changes in four compositional variables are specified.

The first assumption is difficult to evaluate, but the starting conditions are consistent with constraints from the petrogenetic grid (Fig. 4-11*a*). The effects of ReNTR's (e.g., Kohn and Spear 2000) appear to be relatively minor in the garnet, as increase in Mn and Fe/(Fe+Mg) at the rim is minor. The second assumption is also difficult to evaluate, as no inclusions other than quartz and plagioclase, are present within the overgrowth. In the absence of anomalous inclusions within the garnet overgrowth such as chlorite or chloritoid, the overgrowth of the garnet is assumed to have grown in equilibrium with the matrix minerals. The third assumption is presumed valid, given the delicate compositional zoning preserved throughout the garnet and the diameter of the garnet (1700 μm), although some minor diffusional modification of Fe, Mg, and Mn may have occurred.

Using program TWEEQU (v. 2.02; Berman 1991), peak *P-T* conditions were estimated at 685°C and 7.9 kbar using the near-rim, Fe/(Fe+Mg)-trough garnet composition (Fig. 4-11*a*, point labelled "331 t2"; Fig. 4-12) in conjunction with average matrix minerals. Three of the compositional variables (X_{Fe}, X_{Ca}, and X_{Mg}) can be obtained from the garnet zoning. The change in *P-T* conditions between the near-rim garnet composition (Fig. 4-12, point t2) and the highest X_{Grs} point near the inner portion of the overgrowth (Fig. 4-12, point t1) were calculated (Table 4-3). The fourth variable was chosen to be the plagioclase composition. The average matrix plagioclase has an X_{An} of 0.29, and the overgrowth contains two plagioclase inclusions, one with an X_{An} of 0.34 and another with an X_{An} of 0.38. Both of these inclusions are more anorthitic than the average matrix plagioclase, indicating that plagioclase became more albitic during garnet growth (i.e., normal zoning; e.g., Spear et al. 1991). To calculate a partial *P-T* path, it was assumed that the most anorthitic plagioclase (X_{An} = 0.38) formed in equilibrium with the maximum X_{Grs} composition of garnet near the inner section of the high X_{Grs} overgrowth. Although this assumption cannot be proven, it seems reasonable given that both plagioclase inclusions within the overgrowth are more anorthitic than the matrix plagioclase. Using the composition of the other plagioclase inclusion (X_{An}= 0.34) in the calculation does not significantly affect the *P-T* trajectory. The calculation indicates a prograde *P-T* path characterized by heating and loading (Fig. 4-11*a*, point 331 t1). The core of the garnet cannot be used to model the *P-T* path, as the mineral assemblage in which the core crystallized is not known.

Sample 391 contains the assemblage quartz, biotite, staurolite, muscovite, garnet, plagioclase, and primary chlorite (+H_2O fluid; Table 4-3). This assemblage can be modelled using the nine-component system MnNCKFMASH, which results in a thermodynamic variance of three. Garnets within sample 391 are concentrically zoned, and have either two or three zones

defined by abrupt variations in X_{Grs} (Figs. 4-9, 4-10). Garnets with three zones contain an overgrowth with relatively high X_{Grs}, an intermediate zone low in X_{Grs}, and a high X_{Grs} core. Garnet maps with only two zones, lacking the high X_{Grs} core, may not represent a section cut through the centre of the garnet. The garnet rim composition with the average matrix phase composition yielded a *P-T* estimate of 565°C and 5.4 kbar (Fig. 4-11, point t2).

Equilibrium is difficult to demonstrate, but a comparison of the rim *P-T* conditions with a petrogenetic grid (Spear et al. 1999) suggests that the thermobarometry results are reasonable. Garnets from sample 391 have sharp crystal faces, suggesting that garnet was not consumed during the production of staurolite. Sample 391 is relatively low-grade (garnet zone), and there is no evidence of diffusional Fe-Mg exchange near the rims or the effects of ReNTR's. As the only inclusions within the garnet are either quartz or apatite, it is difficult to evaluate whether the high X_{Grs} overgrowth grew in equilibrium with the matrix mineral assemblage. Staurolite is interpreted to have formed earlier from the breakdown of chloritoid (reaction 1), rather than from the consumption of garnet. The Mn and Fe/(Fe+Mg) zoning profiles are both consistent with continuous growth zoning (Fig. 4-9). The sharp zoning in X_{Grs} suggests that diffusion has not significantly modified prograde growth zoning in Ca.

As the thermodynamic variance of the assemblage in sample 391 is three in the MnNCaKFMASH system, compositional changes in the garnet overgrowth alone can be used to model a partial *P-T* path (Table 4-3). The modelling suggests that the overgrowth grew during near-isothermal loading of approximately 2 kbar (Fig. 4-11*a*, point 391 t1). This result is consistent with the occurrence of relict andalusite occurring in nearby metapelitic rocks near Cherry Ridge (Fig. 4-8; Reesor and Moore 1971).

Origin of the increase in X_{Grs} in samples 391 and 331

Both samples 391 and 331 contain abrupt increases in X_{Grs} from core to overgrowth, with X_{Grs} gradually decreasing towards the rim (Figs. 4-9, 4-10). There is little change in Fe/(Fe+Mg) and X_{Sps} across this transition, other than a slight dip in the Fe/(Fe+Mg) profile and a slight flattening in the bell-shaped X_{Sps} profile (Fig. 4-12). Whereas Gibbs modelling can be used to model the change in *P-T* conditions during the growth of the high X_{Grs} overgrowth, the method cannot be used to recover *P-T* conditions in which the core grew, as the mineral assemblage in equilibrium with the garnet core compositions cannot be recovered without mineral inclusions.

Whitney and Ghent (1993) reported similar X_{Grs} zoning from staurolite-bearing metapelitic rocks from the Mica Creek area, situated along the northeast margin of the SMC (Fig. 4-1, top left). They suggested, based on the presence of chloritoid inclusions within the core, but

none in the overgrowth, that the abrupt increase in X_{Grs} from core to overgrowth resulted from the consumption of chloritoid during staurolite and garnet growth. A younger metamorphic event was ruled out based on available geochronological data that suggested that the area experienced a single metamorphic event. A subsequent detailed geochronological study in the nearby Mica Creek area, however, has documented evidence for five discrete thermotectonic events, occurring at 175-160, 140-120, 110, 100-90, and 75-50 Ma, within an apparently continuous stratigraphic and metamorphic sequence (Crowley et al. 2000). In addition, as the reactants in the chloritoid-consuming reaction do not contain significant amounts of calcium, it is difficult to explain the increase in X_{Grs} by the consumption of chloritoid.

Chernoff and Carlson (1997) have reported a similar pattern of X_{Grs} spikes in garnet from amphibolite-facies metaquartzite located in the Picuris Range, north-central New Mexico. They noted a strong positive correlation between X_{Sps} content in garnet cores and garnet size. Based on this observation, the X_{Sps} content of the core was assumed to be a proxy for the timing of garnet nucleation. Abrupt increases in X_{Grs} near the midpoint of garnets were present in all garnets, regardless of core X_{Sps} content, leading them to conclude that the garnets grew at different times during a protracted metamorphic episode. They interpreted this to imply that the spike in X_{Grs} did not represent a specific *P-T* event, but a process. They interpreted the zoning to result from local matrix disequilibrium surrounding the garnet, resulting from slower inter-granular matrix diffusion of Ca relative to Fe, Mg, and Mn.

The interpretation of Chernoff and Carlson (1997) is not considered likely for the X_{Grs} zoning patterns observed in garnets from the study area, as the abundance and orientation of elongate quartz inclusions differs from core to overgrowth in both samples 391 and 331, suggesting a hiatus between core and overgrowth crystallization (Fig. 4-9). In the absence of an additional calcic phase, such as clinozoisite-epidote, calcite, or margarite, in a closed system, X_{Grs} is dependent on the pressure-sensitive GASP equilibria (e.g., Ghent 1976). Alternatively, Ca may have been added to the system, possibly during regional flux of Ca-rich fluids (e.g., Stowell et al. 1996). As there is no evidence of a regional Ca-rich metasomatic event, the abrupt increase in X_{Grs} from core to overgrowth in both samples 391 and 331 is interpreted to reflect an increase in pressure resulting from tectonic loading. This conclusion is supported by the occurrence of relict andalusite within the staurolite-kyanite zone several hundred metres from sample 331, indicating that an earlier portion of the *P-T* path was within the andalusite field (Fig. 4-11*a*). This suggests a *P-T* path characterized by early, nearly isothermal loading, followed by continued loading and heating, followed by exhumation for sample 331 (Fig. 4-11*a*).

Geochronology

Thirteen samples of metapelitic schist were selected for monazite EMP chemical dating (Suzucki and Adachi 1991; Montel et al. 1996; Cocherie et al. 1998; Williams et al. 1999). Of concern to this particular study is the fact that the EMP chemical dating method is generally less precise (and possibly less accurate) than conventional isotopic dating methods, and typically cannot be applied to populations younger than 100-50 Ma (e.g., Montel et al. 1996). Monazites as young as 50-30 Ma can be dated, however, if they are high in Th and U (Montel et al. 1996; Suzucki and Adachi 1998). For instance, Suzuki and Adachi (1998) have reported Late Cretaceous to Paleocene chemical dates (60-90 Ma) from high-Th monazites with errors as small as ±1.4 Ma from the Ryoke metamorphic belt in Japan. The limiting factor for young samples is the detection limit of Pb during EMP analyses compared with the amount of radiogenic Pb present. Another concern in poly-metamorphosed rocks is whether the precision is sufficient to discriminate between closely spaced crystallization events. This last issue is of particular concern in the southeast Canadian Cordillera, where geochronological studies have documented evidence of five distinct thermotectonic events occurring between 175 and 50 Ma (Crowley et al. 2000; Gibson et al. 2004; Chapter 3).

Analytical methods, statistical treatment of error, and methods used to calculate ages are summarized in Appendix B. Representative microprobe monazite data are shown Figure 4-14 and listed in Table 4-4. The detection limit of PbO during analyses was calculated to be 0.0055 wt.%. A more conservative estimate of the limit of quantifiable analysis, the so-called limit of determination, corresponds to the concentration associated with counts at the peak position that are six standard deviations above the mean background counts (Potts 1987). The limit of determination for PbO is 0.0109 wt.% PbO, or approximately 100 ppm Pb. Accordingly, analyses with less than 100 ppm Pb were not used in age calculations. This cut-off resulted in 8 out of 413 spot analyses from five different samples to be discarded.

Monazite was dated in metapelitic rocks ranging from the garnet zone to the potassium-feldspar-sillimanite zone. At all grades, monazite occurs along grain boundaries or as inclusions in quartz, plagioclase, biotite, and rarely garnet. Within the garnet zone (e.g., sample 391), monazite grains are small (5-20 μm along the long axis), with morphologies ranging from long, thin needles, to groups of irregular globular masses, or sponge-like, xenoblastic textures with abundant inclusions (images of grains and spot locations provided in Appendix F). At higher metamorphic grades, monazite is generally idioblastic, relatively larger (up to 100 μm), ovoid or lozenge-shaped, and has fewer inclusions. Needle-like and delicate sponge-like varieties rarely occur in migmatite-grade rocks. The transition from xenoblastic to generally idioblastic

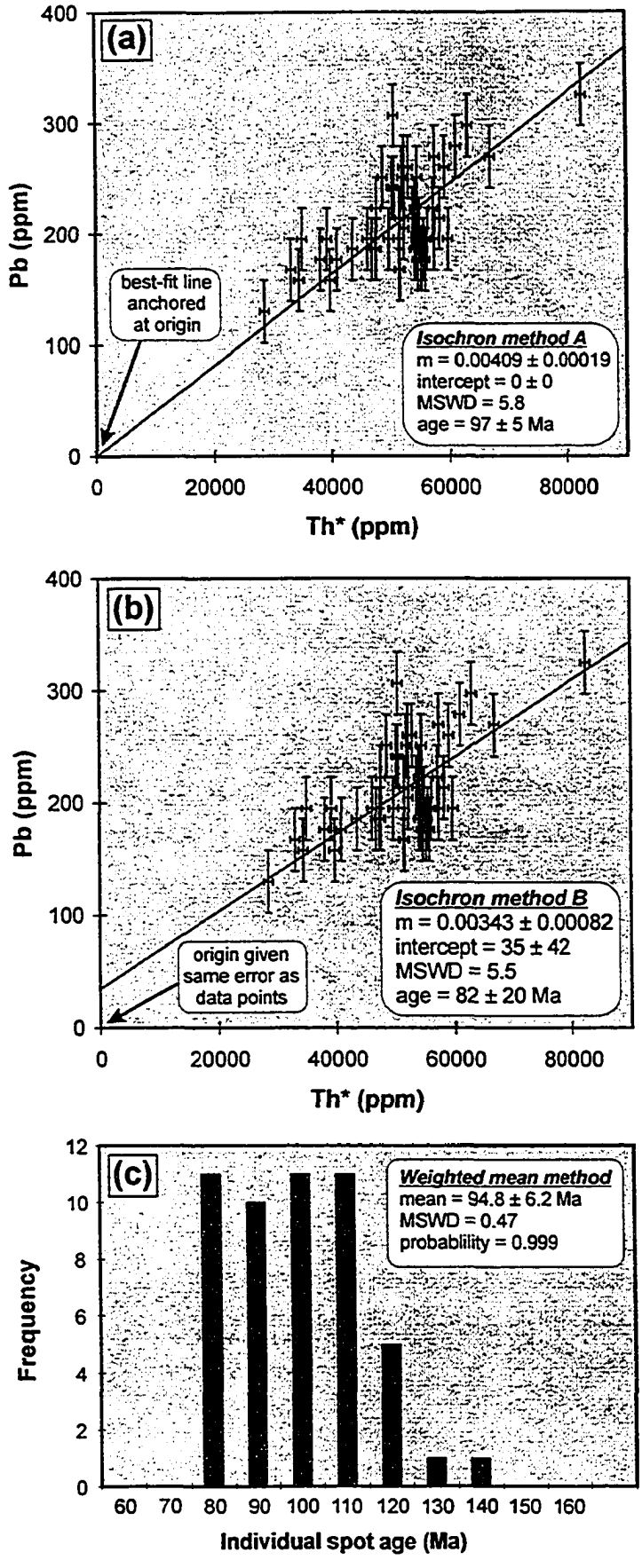

Fig. 4-14. Comparison of different methods used to calculate chemical monazite ages for sample 489.

(a) Isochron method A (best-fit line anchored at the origin).

(b) Isochron method B (origin point assigned the same error as individual spot ages).

(c) Weighted mean method with histogram showing the distribution of individual spot ages.

Table 4-4 (page 1 of 1). Representative electron microprobe spot analyses from monazite grains from sample 00TWG489.

Spot	CaO	Ce_2O_3	P_2O_5	PbO	SiO_2	Nd_2O_3	La_2O_3	ThO_2	Pr_2O_3	Y_2O_3	Sm_2O_3	UO_2	Gd_2O_3	Total	Age (Ma)
489-m1-1	0.997	28.542	30.094	0.029	0.295	12.749	13.440	4.673	3.145	0.893	2.606	0.568	1.848	99.879	**106**
489-m1-2	1.000	28.281	30.534	0.028	0.281	12.593	13.631	4.114	3.158	1.359	2.500	0.580	1.832	99.891	**112**
489-m1-3	1.068	28.097	30.106	0.030	0.351	12.770	13.410	4.992	3.241	0.942	2.556	0.593	1.847	100.003	**104**
489-m1-4	0.716	29.246	30.445	0.017	0.266	12.848	14.079	3.026	3.179	1.333	2.543	0.455	1.790	99.943	**90**
489-m1-5	0.778	29.157	30.122	0.019	0.185	12.906	14.308	3.270	3.165	1.006	2.559	0.420	1.803	99.698	**98**
489-m1-6	1.039	28.548	30.093	0.028	0.360	12.558	13.693	4.936	3.113	0.887	2.599	0.544	1.747	100.145	**100**
489-m1-7	0.919	28.782	30.038	0.024	0.225	12.630	13.971	3.991	3.097	1.013	2.444	0.431	1.703	99.268	**106**
489-m1-8	1.043	28.388	30.612	0.019	0.209	11.798	13.929	4.070	3.016	1.993	2.181	0.675	1.555	99.488	**73**
489-m2-1	0.955	28.530	30.445	0.028	0.191	12.796	13.591	4.305	3.113	1.436	2.468	0.496	1.654	100.008	**113**
489-m2-2	0.436	22.116	27.072	0.025	0.151	9.803	10.952	2.307	2.008	1.278	1.853	0.536	1.371	79.908	**ba***
489-m2-3	0.872	28.768	30.375	0.027	0.187	12.884	13.617	3.736	3.077	1.437	2.586	0.544	1.973	100.083	**117**
489-m2-4	1.083	27.991	30.225	0.029	0.262	12.169	13.364	4.681	3.174	1.504	2.431	0.890	1.760	99.563	**92**
489-m2-5	0.979	28.523	30.201	0.023	0.111	11.871	14.004	3.748	2.985	1.953	2.199	0.643	1.513	98.753	**94**
489-m2-6	1.022	28.622	30.509	0.020	0.116	12.086	13.670	3.999	3.039	2.061	2.296	0.705	1.661	99.806	**76**
489-m2-7	0.937	29.075	30.514	0.018	0.149	12.221	13.896	3.855	3.115	1.723	2.342	0.612	1.541	99.998	**74**
489-m2-8	1.047	28.616	30.613	0.027	0.112	12.335	13.864	4.113	3.020	1.582	2.291	0.635	1.726	99.981	**105**
489-m3-1	0.888	28.853	30.694	0.020	0.170	12.747	13.943	3.499	3.027	1.586	2.396	0.555	1.711	100.089	**90**
489-m3-2	0.965	28.445	30.651	0.027	0.200	12.826	13.479	4.049	3.162	1.608	2.454	0.566	1.874	100.306	**110**
489-m3-3	1.011	28.395	30.796	0.022	0.161	12.190	13.751	3.943	3.132	1.927	2.367	0.699	1.673	100.067	**86**
489-m3-4	0.517	30.292	30.532	0.014	0.160	13.046	14.676	2.079	3.450	1.376	2.301	0.355	1.407	100.205	**104**
489-m3-5	0.984	28.295	30.622	0.024	0.193	12.224	13.643	3.972	3.108	2.037	2.303	0.664	1.659	99.728	**94**
489-m4-1	0.601	30.696	30.717	0.010	0.076	13.113	14.722	1.811	3.536	1.592	2.199	0.247	1.148	100.468	**92**
489-m4-2	0.891	28.129	30.419	0.021	0.154	12.876	13.187	3.606	3.176	1.841	2.672	0.624	1.784	99.380	**89**
489-m4-3	0.997	28.325	30.318	0.019	0.135	12.408	13.550	3.974	2.978	1.903	2.302	0.724	1.685	99.318	**72**
489-m4-4	0.871	28.591	30.453	0.021	0.129	12.730	13.679	3.183	2.986	2.452	2.447	0.389	1.535	99.466	**113**
489-m4-5	0.864	29.384	30.570	0.020	0.156	12.483	13.939	3.655	3.103	1.514	2.386	0.536	1.627	100.237	**89**
489-m5-1	0.993	28.303	30.221	0.022	0.198	12.704	13.533	4.067	3.097	1.664	2.451	0.571	1.756	99.580	**89**
489-m5-2	0.925	29.751	30.181	0.026	0.132	12.265	14.280	3.682	3.252	1.250	2.330	0.616	1.680	100.370	**110**
489-m5-3	0.880	30.282	30.564	0.021	0.165	12.630	14.278	2.986	3.453	1.440	2.195	0.300	1.148	100.342	**127**
489-m5-4	0.688	30.283	30.594	0.018	0.152	12.785	14.177	2.920	3.338	1.489	2.202	0.256	1.288	100.190	**115**
489-m5-5	0.764	28.819	30.128	0.020	0.169	12.927	13.907	3.211	3.264	1.644	2.652	0.528	1.764	99.797	**97**
489-m5-6	0.868	29.563	30.357	0.021	0.150	12.188	14.341	3.737	3.152	1.472	2.202	0.457	1.281	99.789	**96**
489-m5-7	0.988	28.703	30.462	0.020	0.120	12.179	13.772	3.981	3.045	2.046	2.167	0.667	1.459	99.609	**78**
489-m5-8	0.643	31.086	30.404	0.017	0.128	12.979	14.599	2.794	3.378	1.144	2.281	0.342	1.368	101.163	**104**

Table 4-4 (page 2 of 2).

Spot	CaO	Ce_2O_3	P_2O_5	PbO	SiO_2	Nd_2O_3	La_2O_3	ThO_2	Pr_2O_3	Y_2O_3	Sm_2O_3	UO_2	Gd_2O_3	Total	Age (Ma)
489-m6-1	1.023	27.947	30.893	0.033	0.112	12.026	13.395	3.268	3.063	2.985	2.341	0.752	1.683	99.521	**138**
489-m6-2	0.967	28.568	30.707	0.022	0.137	12.499	13.785	3.902	3.023	1.879	2.514	0.703	1.824	100.530	**85**
489-m6-3	0.990	28.623	30.498	0.021	0.137	12.371	13.669	3.864	3.000	1.886	2.372	0.716	1.806	99.953	**81**
489-m6-4	1.002	28.679	30.564	0.021	0.141	12.299	13.747	4.000	3.099	1.928	2.338	0.728	1.753	100.299	**79**
489-m6-5	1.120	28.139	30.758	0.021	0.101	12.070	13.607	4.396	3.103	2.189	2.198	0.731	1.592	100.025	**74**
489-m7-1	1.023	28.764	30.991	0.024	0.126	12.119	13.865	3.996	3.033	2.058	2.243	0.765	1.545	100.552	**89**
489-m7-2	1.045	28.376	30.854	0.021	0.138	12.277	13.696	4.075	3.206	1.985	2.374	0.749	1.747	100.543	**77**
489-m7-3	0.925	29.258	30.485	0.018	0.146	12.100	14.272	3.720	3.204	1.733	2.376	0.650	1.627	100.514	**74**
489-m8-1	1.312	27.835	30.216	0.035	0.291	12.289	13.534	5.841	3.049	0.617	2.507	1.081	1.821	100.428	**90**
489-m8-2	0.835	29.735	30.601	0.020	0.252	12.843	14.210	3.489	3.294	0.931	2.486	0.579	1.717	100.992	**89**
489-m8-3	1.041	28.541	30.627	0.020	0.121	12.310	13.820	3.869	3.105	2.002	2.212	0.697	1.620	99.985	**78**
489-m9-1	0.961	29.112	30.278	0.023	0.205	12.562	13.916	4.217	3.265	1.280	2.430	0.576	1.711	100.536	**90**
489-m9-2	0.888	29.804	30.324	0.026	0.250	13.069	13.957	4.004	3.377	0.692	2.508	0.529	1.720	101.148	**109**
489-m9-3	1.036	29.159	30.346	0.019	0.182	12.020	14.207	4.295	3.174	1.647	2.146	0.586	1.391	100.208	**73**
489-m10-1	0.626	29.904	30.473	0.019	0.174	13.081	14.073	2.987	3.227	1.140	2.628	0.409	1.997	100.738	**105**
489-m10-2	1.105	28.519	31.082	0.023	0.084	12.119	13.647	4.297	2.885	2.144	2.146	0.712	1.508	100.271	**83**
489-m10-3	1.039	28.076	30.277	0.032	0.266	12.414	13.549	5.018	3.125	1.264	2.534	0.655	1.965	100.214	**107**

* ba: bad analysis; data excluded from age calculations.

Standards: Ca - apatite; P - apatite; Pb - synthetic Pb silicate glass; Th - synthetic ThO2; U - natural UO2; Y and REEs - Smithsonian distributed synthetic REE phosphate.

metamorphic monazite with increasing metamorphic grade has been reported in other prograde metapelitic sequences (e.g., Franz et al. 1996; Rubatto et al. 2001; Wing et al. 1993).

In garnet and staurolite-kyanite zone samples, zoning was rarely observed in BSE images. At higher grades (potassium-feldspar-sillimanite zone), compositional zoning is common, varying from patchy and irregular in shape to concentric (Figs. 4-15, 4-16). Within a single grain, spot analyses from different zones visible in BSE images may yield approximately the same age, or have different ages. Zoning in monazite has been suggested to result from variations in Y, Th and possibly U and LREE's, particularly Ce (e.g., Pyle et al. 2001; Gibson et al. 2004).

The composition of monazites from metapelitic rocks in the Vernon area is variable (Table 4-5). In monazites analysed, ThO_2 varies from 1.1-7.9 wt.% (average = 4.2 wt.%), UO_2 varies from 0.10-1.50 wt.% (average = 0.52 wt.%), and PbO varies from 0.007-0.074 wt.% (average = 0.029 wt.%) (Table 4-5). The most abundant LREE's, Ce and La, vary from 25-31 wt.% Ce_2O_3 (average = 29 wt.%) and 13-18 wt.% La_2O_3 (average = 14 wt.%), respectively. Yttrium content is variable between samples (0.02-6.18 wt.%; average = 1.521 wt.%), and within single grains (e.g., sample 391; 1.087-6.184 wt.%). There is no clear relationship between metamorphic grade and monazite composition. Yttrium content varies with age in several samples. For example, sample 585, which contains three age domains, shows a clear relationship between Y content and age (Fig. 4-16*c*). The two older populations are characterized by variable but relatively high Y content, whereas the younger population is characterized by very low Y content and high Th content (Fig. 4-16*d*).

Monazite chemical age data

Calculated monazite chemical dates for each sample are listed in Table 4-5. Statistical methods used to calculate ages are described in Appendix B. Monazites ages vary from 210 to 60 Ma, with errors ranging from 50 to 5 Ma (Fig. 4-17; Table 4-5). Even though the absolute error estimates are small, the relative errors are large (e.g., 100 ± 10 Ma corresponds to a 10% relative error).

The chemical ages fall within four broad groups (210-190, 180-150, 140-80, and 70-50 Ma). As monazite ages are relatively young and all fall within a period of 160 m.y., it is reasonable to test whether the EMP chemical dating technique has the sensitivity to discriminate between age populations separated by less than 50-30 m.y. There are two lines of evidence that suggest that the ages are geologically significant. First, there is a correlation between BSE zoning and age. For example, in samples 584 and 585, there is a strong correlation between age groups and BSE domains (Figs. 4-15, 4-16). Three age components may be present within a single

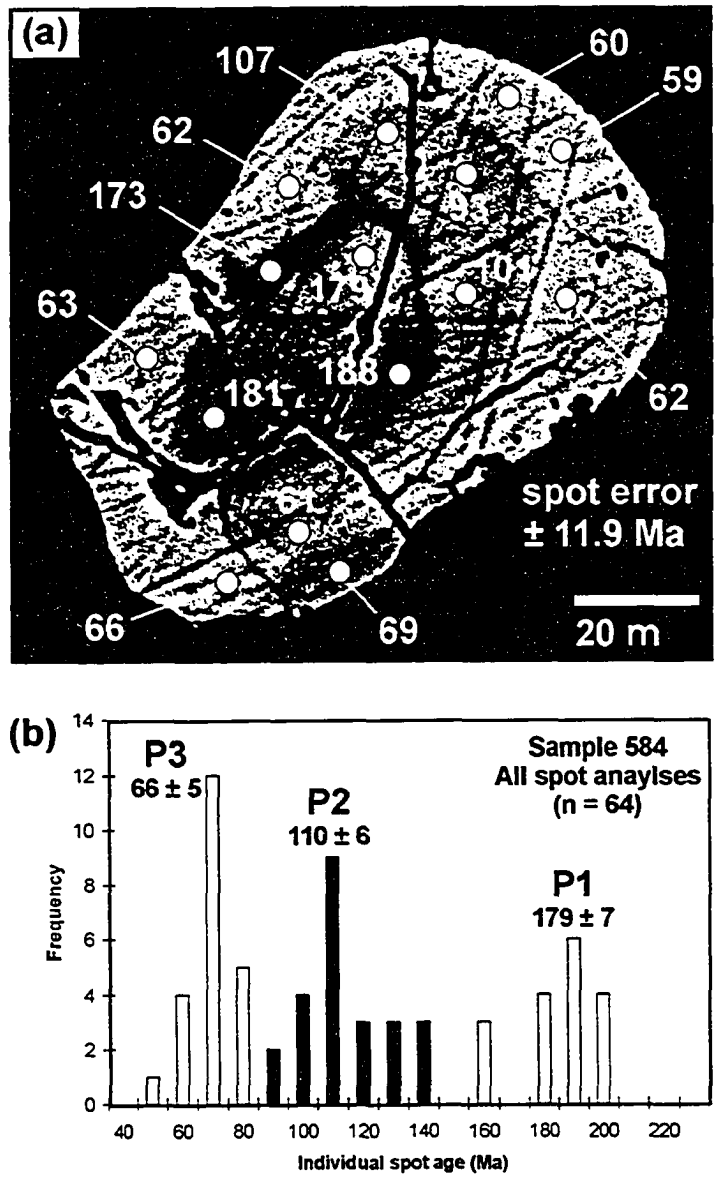

Fig. 4-15. Monazite EMP chemical dating results from sample 584. (a) BSE image of zoned monazite grain displaying three individual domains with distinct ages. The location and age (in Ma) of individual spot analyses are indicated. Linear grooves are the result of polishing during grain-mount preparation. (b) Summary histogram of all individual spot analyses from sample 584 (n = 64), showing the mean and two sigma standard deviation of the three age groups that correlate with the domains shown in part (a).

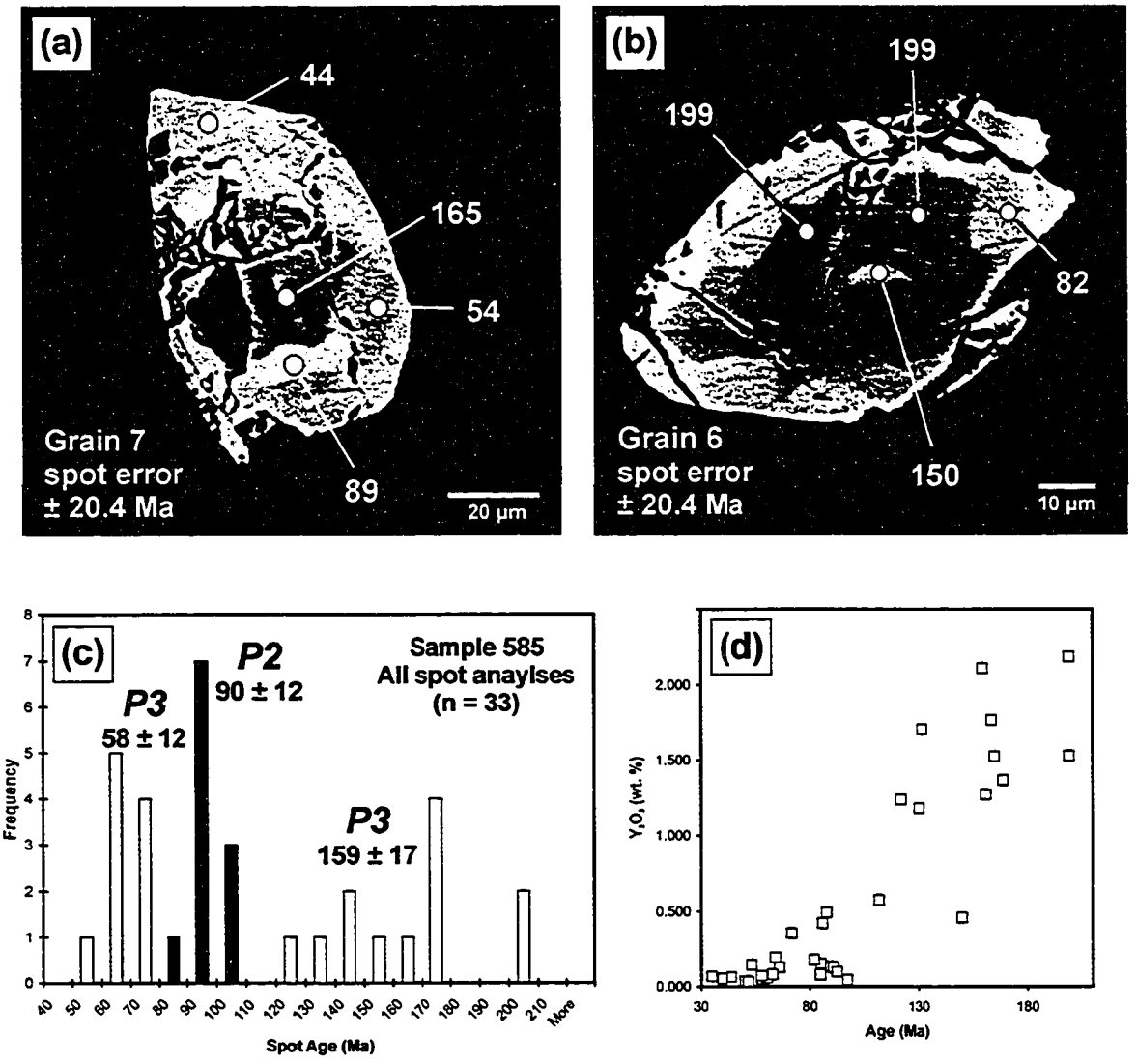

Fig. 4-16. Back-scattered electron (BSE) microprobe images, spot age histogram, and Y_2O_3 versus age plot for sample 585. (a) BSE image of grain 7 showing the correlation between BSW domains and age. (b) BSE image of grain 6 showing the correlation between BSE domains and age. Young age (150 Ma) in center of grain may be due to alteration or the orientation of the grain mount. (c) Summary histogram of all individual spot analyses from sample 585 (n = 33), showing the mean and two sigma standard deviation of the three age groups that correlate with the domains shown in parts (a) and (b). (d) Plot of age (Ma) versus Y_2O_3 (wt. %) for all individual spot analyses from sample 585. Note low Y content of spot ages younger than 70 Ma.

Table 4-5. Results of monazite chemical EMP age dating from metapelitic rocks within the Vernon area.

Sample	Location[a] (UTM)	Meta. zone	Mineral Assemblage[b]	Age pop.	n[c]	ThO_2 conc. (wt.%)	UO_2 conc. (wt.%)	PbO conc.[d] (wt.%)	Spot error (Ma)(2σ)	Isochron age Method A (Ma) (± 2σ)	Isochron age Method B (Ma) (± 2σ)	Weighted mean age (Ma) (± 2σ)
Vernon area												
431	345013E 5553979N	Kfs-Sil	Sil-Grt-Bt-Kfs-Pl-Qtz	1	15	4.664 - 7.855	0.210 - 0.974	0.039 - 0.072	10.1	178 ± 6	176 ± 22	171 ± 6
537	343725E 5559400N	Kfs-Sil	Pl-Kfs-Qtz-Sil-Bt-Grt	1	22	2.710 - 4.374	0.142 - 0.694	0.015 - 0.045	15.5	162 ± 10	187 ± 38	152 ± 9
Trinity Hills area												
584	372900E 5603785N	Kfs-Sil	Sil-Grt-Bt-Kfs-Pl-Qtz	1	23	4.355 - 5.557	0.508 - 0.714	0.014 - 0.023	11.9	69 ± 3	69 ± 16	66 ± 5
				2	23	3.919 - 5.613	0.399 - 0.972	0.024 - 0.042	11.9	115 ± 7	124 ± 31	110 ± 6
				3	18	2.678 - 7.032	0.359 - 1.460	0.039 - 0.074	11.9	188 ± 7	199 ± 24	179 ± 7
585	372647E 5604833N	Kfs-Sil	Sil-Pl-Kfs-Grt-Bt-Qtz	1	11	4.195 - 6.268	0.143 - 0.213	0.011 - 0.017	20.4	61± 6	58 ± 18	58 ± 12
				2	11	4.192 - 6.193	0.104 - 0.290	0.018 - 0.026	20.4	95 ± 6	93 ± 18	90 ± 12
				3	11	3.043 - 4.469	0.133 - 0.544	0.020 - 0.049	20.4	173 ± 18	199 ± 50	159 ± 17
Vidler Ridge - Pinnacles area												
391	390827E 5576126N	Grt (+St)	Chl-Pl-Grt-Ms-St-Bt-Qtz	1	15	1.960 - 4.244	0.124 - 0.545	0.011 - 0.025	15.8	88 ± 14	71 ± 43	88 ± 13
331	407130E 5565038N	St-Ky	St-Grt-Pl-Ms-Bt-Qtz	1	34	2.516 - 7.039	0.354 - 0.697	0.018 - 0.042	19.7	122 ± 4	112 ± 13	118 ± 7
488	404011E 5572467N	St-Ky	Ms-Bt-Pl-Qtz	1	19	2.927 - 5.939	0.469 - 1.036	0.019 - 0.047	10.9	108 ± 12	112 ± 43	103 ± 11
489	405774E 5574020N	St-Ky	Ky-Grt-Pl-Ms-Sil-Qtz-St	1	49	2.079 - 5.841	0.247 - 1.081	0.014 - 0.035	22.3	97 ± 5	82 ± 20	95 ± 6
493	404043E 5572050N	St-Ky	Ms-Pl-Bt-Qtz-St-Grt	1	24	3.123 - 5.399	0.495 - 0.631	0.026 - 0.042	16.0	140 ± 3	139 ± 13	134 ± 6
516	409877E 5567121N	Sil	Sil-Grt-Ms-Bt-Pl-Qtz	1	28	3.074 - 4.523	0.418 - 0.819	0.018 - 0.033	13.2	104 ± 6	102 ± 31	100 ± 6
328	408087E 5564744N	Sil	Grt-Sil-Pl-Bt-Ms-Qtz	1	29	1.125 - 5.480	0.385 - 0.792	0.015 - 0.045	28.7	129 ± 4	130 ± 15	123 ± 10
WLS	411511E 5547671N	Sil	Sil-Grt-Pl-Bt-Ms-Qtz	1	14	2.325 - 6.897	0.297 - 0.475	0.014 - 0.036	23.1	119 ± 7	120 ± 20	113 ± 12
				2	22	2.869 - 5.894	0.356 - 0.741	0.033 - 0.069	23.1	214 ± 5	203 ± 18	206 ± 10
72	378960E 5567540N	Kfs-Sil	Sil-Grt-Pl-Bt-Kfs-Qtz	1	32	2.603 - 6.172	0.366 - 0.697	0.012 - 0.035	13.1	109 ± 9	90 ± 38	106 ± 8
				2	3	4.207 - 4.714	0.486 - 0.557	0.039 - 0.052	13.1	204 ± 6	204 ± 12	195 ± 15

[a] All coordinates using datum NAD83, UTM Zone 11.

[b] Mineral phases listed least to most abundant.

[c] The number of individual spot analyses used to calculate the age.

[d] All spot analyses below the limit of determination (0.0109 wt. % PbO) were discarded.

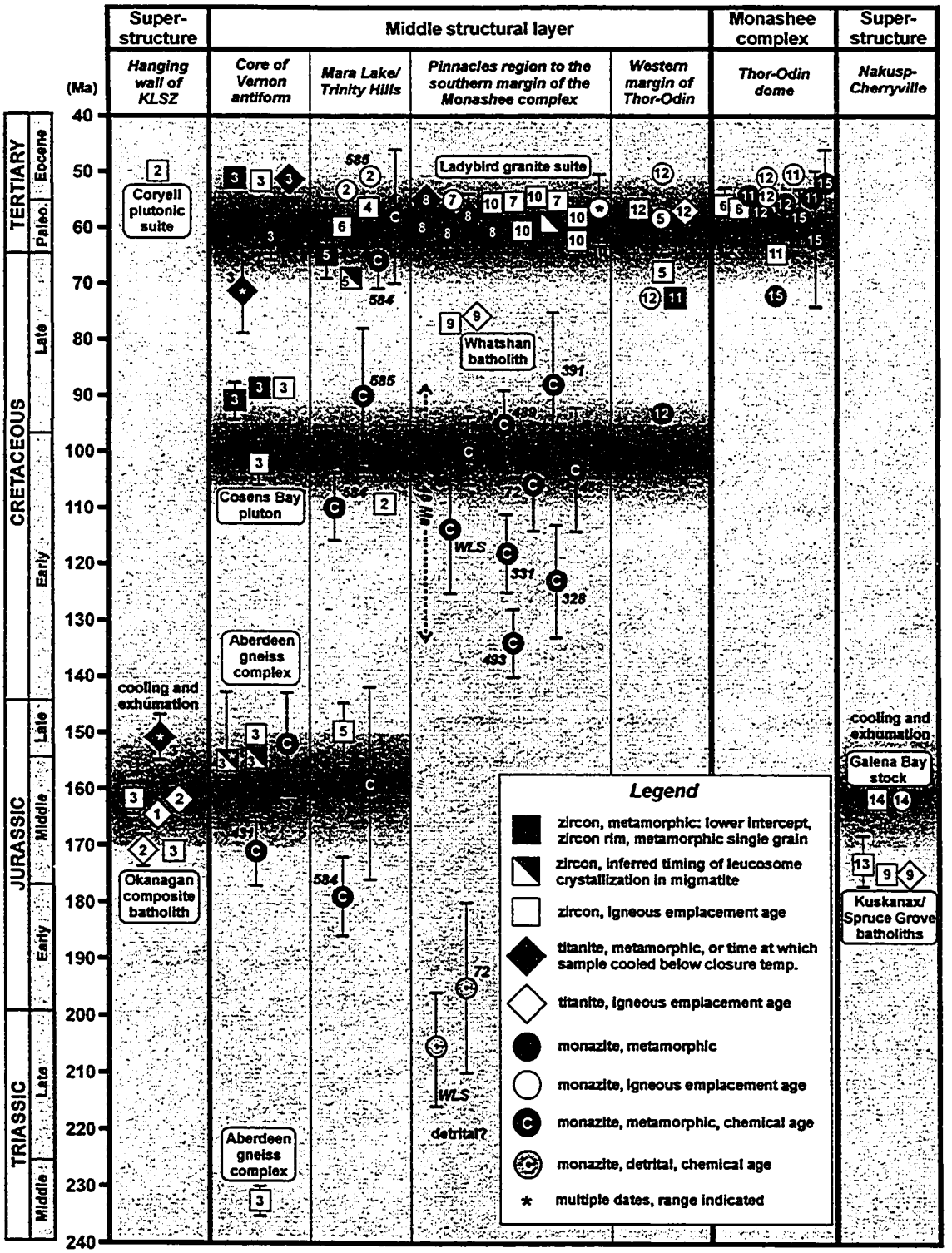

Fig. 4-17. Compilation of U-Pb geochronology data from the SMC between latitudes 50° and 51° N. *Data sources*: 1 - Thompson and Daughtry (1996); 2 - R.I. Thompson, unpublished data; 3 - Glombick et al. (in press); 4 - Bardoux (1993); 5 - Johnson (1994); 6 -Vanderhaeghe et al. (1999); 7 - Parrish et al. (1988); 8 - Carr (1990); 9 - Carr (1991); 10 - Carr (1992); 11 - Parkinson (1992); 12 - Johnston et al. (2000); 13 - Parrish and Wheeler (1983); 14 - Parrish and Armstrong (1987); 15 - Kuiper (2003).

concentrically-zoned grain, with the oldest ages in the core, intermediate ages in the inner rim and the youngest ages near the outer rim (Fig. 4-15). Other monazites may contain two or only one age component. Second, there is a good correspondence between the three monazite age populations inferred from the EMP data and three high-grade metamorphic events recorded in the core of the Vernon antiform (~160-150, 100-90, and 70-50 Ma) and elsewhere within the SMC (Parrish 1995, and references therein; Crowley et al. 2000), deduced using U-Pb isotopic dating methods (Fig. 4-17).

The distribution of EMP ages varies with location across the study area. For instance, the data from two infrastructure samples (431, 537) situated within the core of the Vernon antiform (Fig. 4-5) contain Jurassic-aged monazite (Fig. 4-17; Table 4-5). Sample 431, a migmatitic metapelite that has yielded igneous zircon dated precisely at 154.5 ± 0.4 Ma (Chapter 3), yielded an older monazite chemical date of 171 Ma. A single monazite grain included within garnet from this sample yielded the same date as matrix monazite, suggesting that monazite growth overlapped or predated the timing of garnet growth. Sample 537, a migmatitic metapelite from the core of the Vernon antiform, yielded a single metamorphic monazite population dated at 152 ± 9 Ma (Fig. 4-17; Table 4-5).

Two samples of migmatitic metapelite from the Trinity Hills area (584, 585) both yielded evidence of three generations of monazite growth (Fig. 4-17; Table 4-5). As discussed above, the distribution of dates correlates with compositional zoning visible in BSE images (Figs. 4-15, 4-16). The three populations from both samples overlap within error and are in good agreement with thermotectonic events recorded in the core of the Vernon antiform (Fig. 4-17).

Farther east, in the Vidler Ridge and Pinnacles Peaks areas, monazite chemical dates from nine samples define two, loosely-grouped age populations (210-190 Ma and 140-80 Ma; Fig. 4-17). The older population, of Late Triassic to Early Jurassic age, is present in two samples (72, WLS), which both contain bimodal distributions (Table 4-5). Lower-grade rocks, situated in the hanging wall of early Tertiary extension faults, have yielded Late Triassic (Norian) conodonts (Fig. 4-7). In the absence of a known metamorphic event of this age within the SMC (e.g., Parrish 1995) the older population from these samples is interpreted as detrital in origin.

All nine samples from the Vidler Ridge and Pinnacles areas contain Cretaceous monazite (Fig. 4-17). The dates vary from 88 ± 13 to 134 ± 6 Ma. There is no apparent correlation between date and: (1) metamorphic grade; (2) bulk rock mineralogy; (3) monazite composition; (4) monazite size; (5) structural level; or (6) area. It is unclear whether the range in dates results from poor accuracy of the chemical dating method, numerous, closely-spaced episodes of monazite growth, or protracted metamorphism. Monazite has been shown to be resistant to lead-loss during

upper amphibolite to granulite-facies metamorphism (e.g., Smith and Giletti 1997; Zhu and O'Nions 1999; Cherniak et al. 2004), so lead loss is considered unlikely. Nor is there visible textural evidence of overgrowths, recrystallization, or alteration.

Without additional information, such as trace-element contents and distribution in garnet and monazite, it is difficult to assign definite geological significance to the monazite dates. In the light of recent studies that link monazite-growth events to specific metamorphic reactions (e.g., Smith and Barreiro 1990; Kingsbury et al. 1993; Pyle and Spear 2003; Wing et al. 2003; Gibson et al. 2004; Kohn and Malloy 2004), making an *a priori* assumption that monazites ages reflect the timing of peak metamorphic conditions is unjustified.

Based on petrographic observations, a number of workers have suggested that during greenschist-facies metamorphism, detrital and low-grade metamorphic monazite may break down to form allanite, which in turn, breaks down between 500°C and 600°C (at approximately the staurolite-in isograd) to form metamorphic monazite (Smith and Barreiro 1990; Wing et al. 2003). Kohn and Malloy (2004) have suggested that monazite growth may result from the breakdown of major silicate phases at the staurolite-in isograd and does not necessarily involve accessory phases such as allanite. Based on thermodynamic modelling using Gibbs method, Pyle and Spear (2003) have proposed a possible monazite-producing reaction at the staurolite-in isograd:

$$Grt + Chl + Ms + Ap = St + Pl + Bt + Qtz + Mnz + H_2O \quad (6)$$

As four samples from the Vidler Ridge and Pinnacles area are within the staurolite-kyanite zone and contain staurolite, this reaction may have been responsible for monazite production in these samples. Sample 488, however, is within the staurolite-kyanite zone, but contains the mineral assemblage: muscovite, biotite, plagioclase, and quartz, suggesting that metamorphic monazite may form from other reactions.

It has been suggested that monazite may form during crystallization of melt, by the reactions (Pyle and Spear 2003):

$$Grt + Kfs + melt = Qtz + Pl + Ms + Mnz \quad (7)$$

and (or)

$$Sil + melt = Qtz + Pl + Ms + Mnz \quad (8)$$

Hence, metamorphic monazite in migmatite-grade samples may have formed from these reactions or an earlier reaction at lower grades. Monazite has also been shown to be susceptible to re-crystallization during low-temperature circulation of fluids (e.g., Townsend et al. 2000).

Discussion

Geological mapping of metamorphic assemblages, petrographic observations, peak *P-T* estimates calculated using thermobarometry, Gibbs modelling, and monazite chemical dating from the study area indicate a complex and episodic metamorphic evolution that varies with region and structural level.

Metamorphic evolution of the superstructure

The superstructure contains thermochronological evidence of a major Middle Jurassic metamorphic event, followed by relatively rapid cooling and exhumation (Figs. 4-18; 4-19). Peak metamorphic conditions within most areas of the superstructure are within the biotite zone, below the garnet-in isograd (>450-500°C, Spear 1993). This is in agreement with peak temperatures of 330-440°C, indicated by Upper Triassic conodont CAI values of 5.0-5.5 (Fig. 4-2). Locally, lower amphibolite conditions were attained adjacent to the Wood Lake pluton (Fig 4-4). Geochronological data (U-Pb zircon) from the Wood Lake gneiss records U-Pb zircon evidence of a single metamorphic event at ca. 170, synchronous with the emplacement of large, regionally extensive, syn- to post-kinematic, calcalkaline batholiths of the Okanagan composite batholith and the Nelson plutonic suite (175-155 Ma; Parrish and Wheeler 1983; Parrish and Armstrong 1987; Carr 1990; Woodworth et al. 1991; Parrish 1995). A post-kinematic pegmatite dyke of the Wood Lake pluton (164.4 ± 2.0 Ma; Thompson and Daughtry 1996), dated at 161.6 ± 2.8 (U-Pb, zircon), cuts the fabric within the Wood Lake gneiss, indicating that ductile deformation within the superstructure predated ~162 Ma (Fig. 4-4).

Cooling of the superstructure within 10-15 m.y. following peak regional metamorphic conditions is indicated by Middle to Late Jurassic U-Pb titanite closure ages and K-Ar hornblende and biotite cooling ages (Figs. 4-18, 4-19; Mathews 1981; Carr 1990; Vanderhaeghe et al. 2003). The inferred temperature-time path suggests the superstructure cooled from above 500°C to below 250°C between 155 and 145 Ma. If an average geothermal gradient of 25°C/km is assumed during the Middle Jurassic, then 10 km of exhumation is implied between approximately 145 and 155 Ma. The superstructure has not been heated above 250°C since Late Jurassic time, except locally near its base (W.H. Mathews, unpublished data).

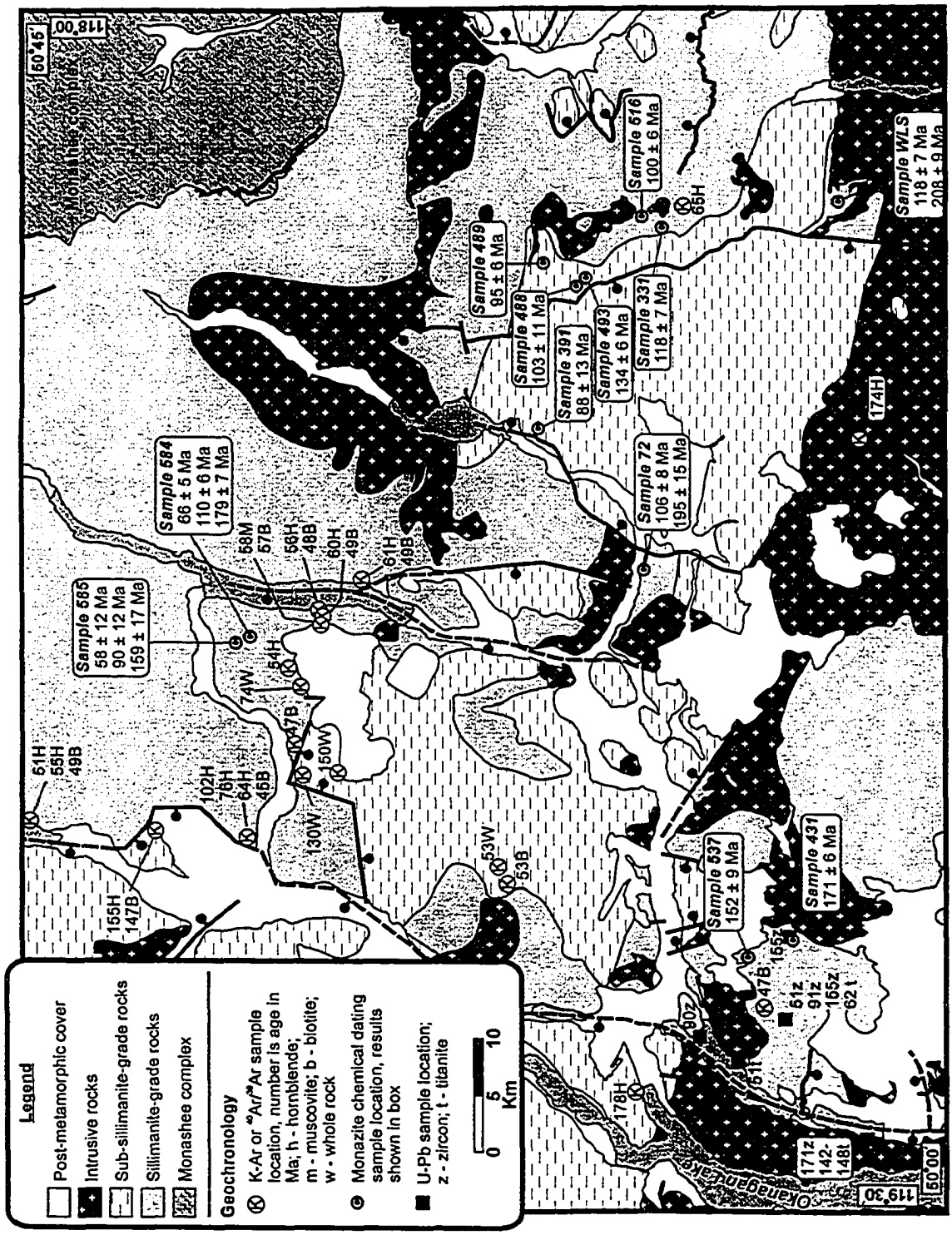

Fig. 4-18. Simplified metamorphic map of the study area showing the location of monazite chemical dating samples (dates indicated in boxes). The location and results of previously published and unpublished K-Ar and U-Pb geochronology samples are also shown (data from W.H. Mathews, unpublished data; Mathews 1981; Carr 1990; Johnson 1994; Vanderhaeghe et al. 2003; R.I. Thompson, unpublished data).

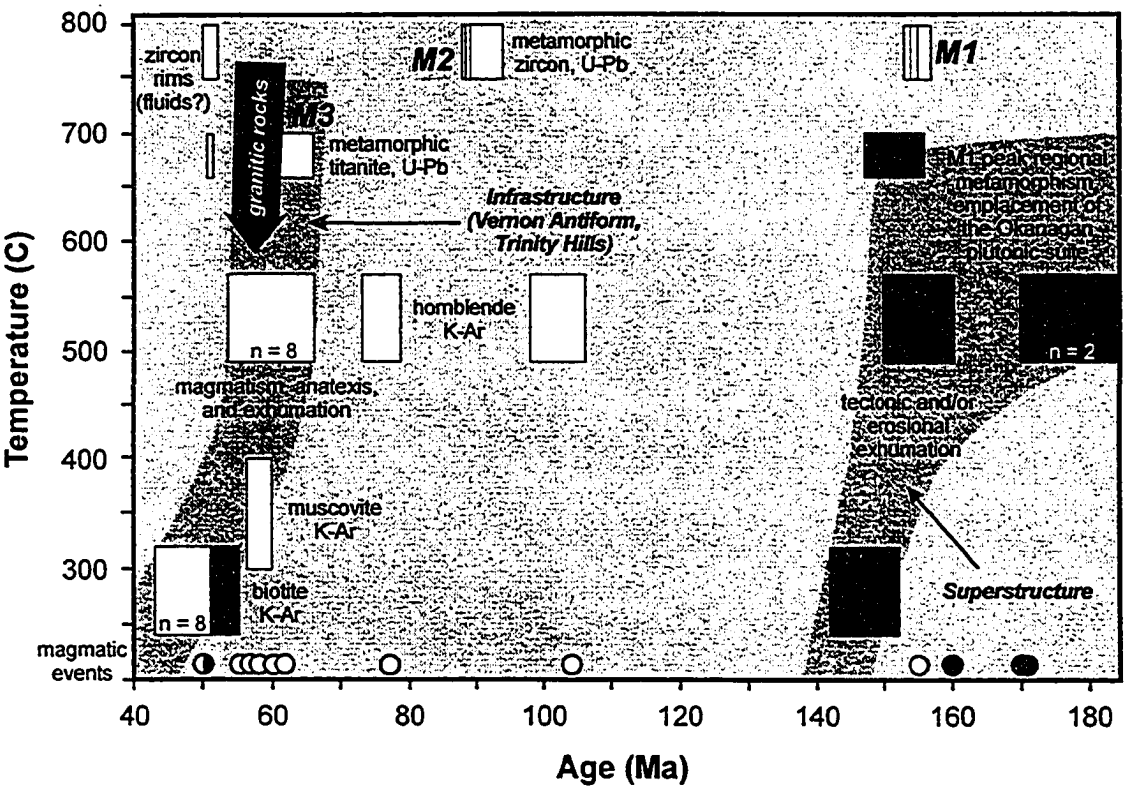

Fig. 4-19. Temperature-time plot showing K-Ar and $^{40}Ar/^{39}$ Ar (hornblende, muscovite, and biotite) and U-Pb (titanite and zircon) data from suprastructure (grey) and infrastructure (white) rocks from the study area. Inferred temperature-time (*T-t*) paths are shaded light grey. Circles near the bottom axis indicate the timing of known magmatic events in the suprastructure (grey) and infrastructure (white). Closure temperatures after Heaman and Parrish (1991) and Scott and St-Onge (1995). Unless otherwise indicated, individual boxes indicate data from a single sample. *Data sources*: W.H. Mathews, unpublished data; Mathews (1981); Carr (1990); Johnson (1994); Vanderhaghe et al. (2003); this study, Chapter 3, and R.I. Thompson, unpublished data.

Metamorphic evolution of the infrastructure

Geochronological data from middle structural layer of the infrastructure reveal a complex and episodic evolution with three primary events: (1) Middle to Late Jurassic metamorphism; (2) Late Cretaceous metamorphism; and (3) Late Cretaceous to Middle Eocene metamorphism (Fig. 4-18; Table 4-5).

Middle to Late Jurassic (155-150 Ma)

An upper amphibolite-facies Middle Jurassic metamorphic event is recorded within the core of the Vernon antiform, southeast of Vernon (Fig. 4-5) and within the Trinity Hills area (Fig. 4-2).

In the core of the Vernon antiform, Middle to Late Jurassic metamorphism resulted in dehydration melting of pelitic rocks, extensive migmatization of Early Triassic tonalite, and the emplacement of tonalite within the Aberdeen gneiss complex (Chapter 3). Leucosome from migmatitic metapelite within Aberdeen gneiss complex (sample 431) has been dated precisely (U-Pb zircon) at 154.5 ± 0.4 Ma (Chapter 3). A thin-section of the same sample contains abundant metamorphic monazite dated at 171 ± 6 Ma using the chemical dating method (Fig. 4-18; Table 4-5). The difference between the precise U-Pb zircon date and the monazite chemical date is inferred to reflect the limitations associated with the chemical dating method. Monazite included within garnet yielded the identical age as matrix monazite, indicating that metamorphic monazite growth within the matrix overlapped with, or predated garnet growth. A sample of migmatitic metapelite (537) from the flank of the Aberdeen gneiss complex yielded metamorphic monazite dated at 152 ± 9 Ma, and a peak *P-T* estimate of 9.4 ± 1.4 kbar and 850 ± 30°C (Tables 4-2, 4-5), consistent with upper amphibolite-facies to lower granulite conditions. The chemical date from sample 537 is in good agreement with U-Pb zircon data from the Aberdeen gneiss complex (Fig. 4-17).

Evidence of Middle to Late Jurassic metamorphism from the Trinity Hills area includes chemical monazite dates from two samples of migmatitic pelitic schist (Table 4-5). Each sample (584, 585) contains Early to Middle Jurassic-aged homogeneous grains, as well as Jurassic cores within concentrically zoned grains, mantled by Late Cretaceous and Paleocene to Eocene rims (Figs. 4-16, 4-17). A migmatitic metapelite from the southern flank of the Hunters Range (Fig. 4-5, sample 74), yielded a peak *P-T* estimate of 9.7 ± 1.5 kbar and 850 ± 30°C (Table 4-2), consistent with peak *P-T* conditions attained in the Vernon antiform, although the time at which peak conditions were reached in this area is not clear. Johnson (1994) reported an upper intercept of 150.0 +5.6/-5.0 Ma from a pegmatite in the Hunters Range (Fig. 4-17, plotted in the Mara

Lake column), interpreted as the igneous crystallization age of the pegmatite, which suggests that *P-T* conditions may have been of sufficient grade to have caused dehydration melting within pelitic lithologies.

Late Cretaceous (100(?)-90 Ma)

Geochronological evidence of a widespread Early to Late Cretaceous metamorphic event (~130-90 Ma) is found within the middle structural layer of the infrastructure across the study area (Fig. 4-17).

Geochronological data within the core of the Vernon antiform supporting a metamorphic event during the Late Cretaceous (ca.100-90 Ma) include: growth of metamorphic zircon rims in diorite gneiss (91.0 ± 3.3 Ma), metamorphic zircon growth in diorite gneiss (88.7 ± 0.2 Ma), emplacement of granodiorite (Cosens Bay pluton; 102.2 ± 3.8 Ma), and local migmatization of metapelitic rocks (88.7 ± 0.2 Ma; Fig. 4-17; Chapter 3). In the Trinity Hills area, evidence of a Cretaceous metamorphism includes crystallization of metamorphic monazite in migmatitic gneiss dated at 90 ± 12 Ma and 110 ± 6 Ma (Fig. 4-17).

Evidence of metamorphism in the Vidler Ridge and Pinnacles Peaks region includes widespread Early to Late Cretaceous metamorphic monazite in metapelitic rocks (Fig. 4-17; Table 4-5). Peak *P-T* conditions in kyanite-staurolite zone rocks within the footwall of the Beaven fault west of the Pinnacles Peaks are estimated at 8.0 kbar and 650-675°C (Fig. 4-7). Sillimanite zone metapelitic rocks situated within the footwall of the Cherry fault yielded *P-T* estimates of 9.3 kbar and 760°C and metamorphic monazite dated at 106 ± 8 Ma (Fig. 11*a*; Table 4-2).

Gibbs modelling from sample 391, a garnet zone, staurolite-bearing high-aluminium metapelitic rock sampled from near the base of the superstructure near Cherry Ridge (Fig. 4-7), suggests that the garnet overgrowth and staurolite grew synchronously during a period of nearly isothermal loading from 3.3 to 5.3 kbar. Metamorphic monazite from sample 391 yielded a chemical date of 88 ± 13 Ma (Table 4-5). Although the age of monazite growth cannot be linked to a specific metamorphic reaction, it is possible that monazite was produced during the production of staurolite on the prograde path (e.g., Smith and Barreiro 1990; Pyle and Spear 2003; Kohn and Malloy 2004).

Gibbs modelling from sample 331, a metapelitic rock from the staurolite-kyanite zone situated in the footwall of the Beaven fault indicates a *P-T* path characterized by heating from 530 to 680°C and loading from 6.3 to 7.8 kbar (Fig. 4-20). In addition, the jump in X_{Grs} from core to overgrowth observed in garnets from samples 391 and 331 is interpreted to reflect an earlier

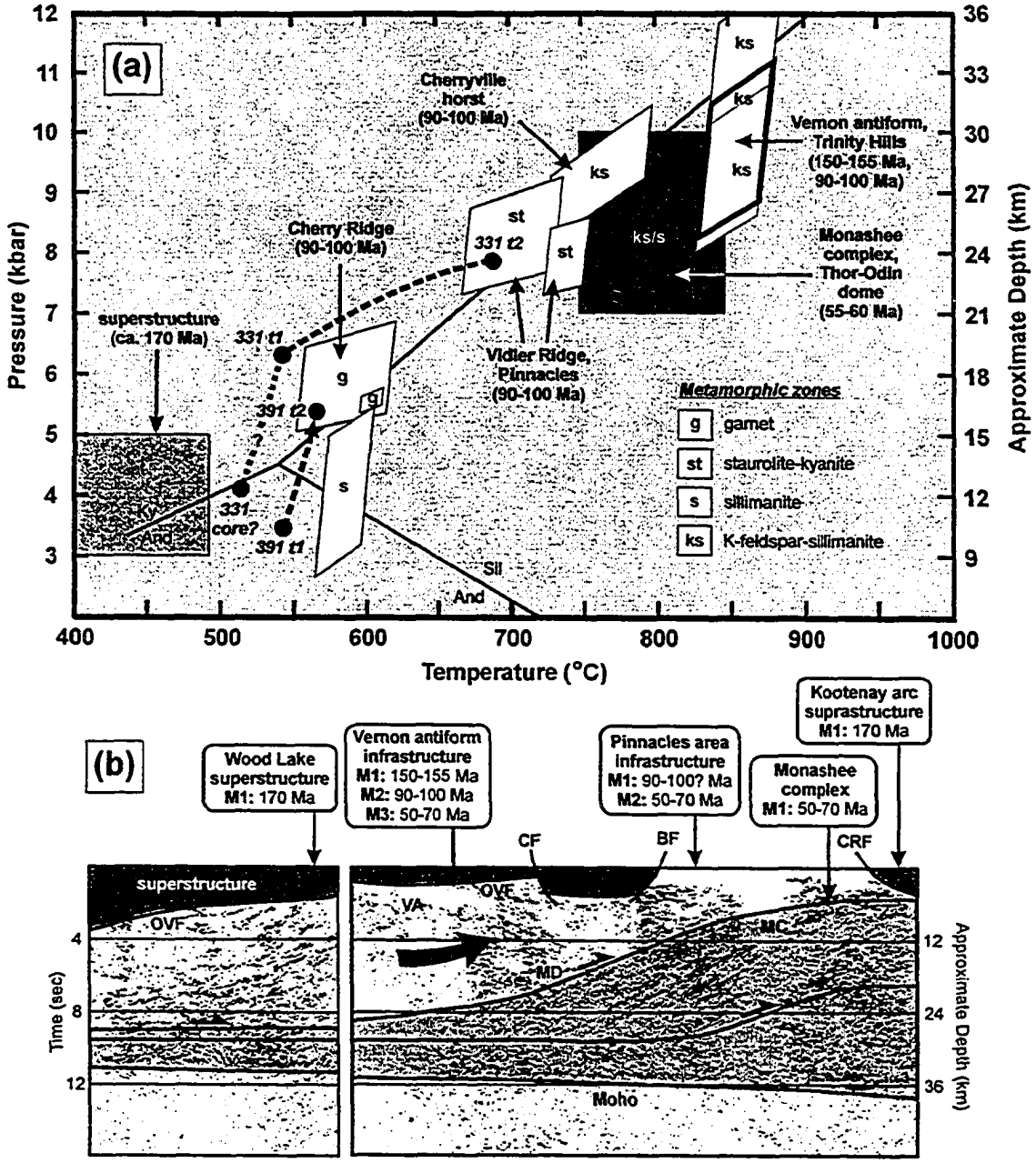

Fig. 4-20. (a) Pressure-temperatre diagram summarizing maximum *P-T* estimates from metapelitic rocks from various areas and structural levels within the study area, inferred timing of peak metamorphism, and inferred partial *P-T* paths for samples 391 and 331. Dashed line indicates partial *P-T* paths calculated using Program Gibbs. Inferred portions of the *P-T* path, consistent with petrological data, shown as dotted lines. The location of the Al_2SiO_5 triple point from Pattison (1992). Monashee complex *P-T* constraints from Norlander et al. (2002). (b) Interpreted Lithoprobe seismic reflection lines 7 to 9 through the Vernon area (after Cook et al. 1992). *Abbreviations*: CF - Cherry fault; CRF - Columbia River fault; BF - Beaven fault; MC - Monashee complex; MD - Monashee décollement; OVF - Okanagan Valley fault; VA - core of Vernon antiform. *Fill patterns*: (1) superstructure (dark grey); (2) infrastructure: middle structural layer (white), and allochthonous and autochthonous Paleoproterozoic North American rocks (light grey); and (3) upper mantle (bottom white). The timing of major metamorphic events, deduced from new and published geochronological data (Fig. 4-17), are shown on section.

loading event of unknown, but possibly Middle Jurassic age. A loading event is supported by occurrence of relict andalusite in both areas.

In summary, although a definite link between the peak *P-T* estimates from the Vidler Ridge and Pinnacles Peaks region and Cretaceous chemical (metamorphic) monazite ages cannot be made, the ages are interpreted as the time at which monazite crystallized in metapelitic rocks during prograde metamorphic reactions, particularly staurolite-producing reactions (cf. Smith and Barreiro 1990; Kingsbury et al. 1993; Pyle and Spear 2003; Wing et al. 2003; Gibson et al. 2004; Kohn and Malloy 2004). As the only evidence of metamorphic monazite growth in the Vidler Ridge and Pinnacles Peaks region is during the Cretaceous, it is interpreted that the chemical monazite dates reflect the timing of prograde, but not necessarily peak metamorphism in this region.

Late Cretaceous to Middle Eocene (70-50 Ma)

The Late Cretaceous to Middle Eocene metamorphic event is of particular importance within the SMC, as it: (1) coincides with peak metamorphism of rocks at lower structural levels of the middle structural layer and within the Monashee complex (e.g., Carr 1990; Parrish 1995; Vanderhaeghe et al. 1999; Crowley et al. 2001); (2) overlaps the timing of orogenic collapse and the initiation of sub-parallel, north-striking extension faults (e.g., Parrish et al. 1988); (3) coincides with the emplacement of the Ladybird granite suite (e.g., Carr 1992); and (4) overlaps the cooling and exhumation of the infrastructure from above 500°C to below 250°C (e.g., Mathews 1981; Vanderhaeghe et al. 2003). The cause and effect relationships between these events remain incompletely understood.

Examination of U-Pb and chemical data from infrastructure rocks in the Vernon area reveal that Late Cretaceous to Early Middle Eocene metamorphism was accompanied by the metamorphic crystallization of zircon, monazite, and titanite in a variety of rock types (Fig. 4-17). Syn-kinematic Late Paleocene to Early Eocene granitic rocks of the Ladybird suite (~62-55 Ma) were emplaced at all levels of the middle structural layer in the study area during this period (Fig. 4-17). If middle structural layer rocks were at elevated temperatures (700-800°C) prior to the onset of exhumation, then decompression and (or) the infiltration of extension-related fluids may have triggered partial melting (e.g., Kuiper 2003). Holk and Taylor (1997), based on homogeneous $\delta^{18}O$ values within quartz and feldspar from a 6 km thick section of the middle structural layer located south of the Thor-Odin dome, proposed that widespread melting was initiated by dehydration melting of pelitic rocks. In that model, as melt rises in the crustal column due to buoyancy forces, heating of higher structural levels is facilitated by advection of heat and

the latent heat of crystallization. Water, released during the uplift and the crystallization of melt, initiates additional melting of fertile rock types (quarto-feldspathic gneiss and pelitic schist) at higher structural levels, ultimately resulting in widespread melting and $^{18}O/^{16}O$ isotopic homogenization of the infrastructure. Fluids, released from crystallizing melts, may have precipitated metamorphic zircon and monazite as late at 50 Ma (Fig. 4-17).

Although it is clear from the crystallization of metamorphic minerals and the emplacement of granitic rocks that temperatures were elevated within the infrastructure, K-Ar dates of <70 Ma from the middle structural layer directly underlying the superstructure indicate that the period between 65 and 50 Ma was characterized by significant cooling and exhumation, at least locally (Figs. 4-18, 4-19). It is possible that lower structural levels of the middle structural layer and the Monashee complex were experiencing their thermal peak between 70 and 50 Ma while upper structural levels of the infrastructure were cooling (e.g., Gibson et al. 1999; Crowley et al. 2001). This is consistent with thermal modelling of orogens, which suggests that the thermal peak should be younger with increasing structural depth (e.g., Thompson and England 1984; Patiño Douce et al. 1990). As a result, it may be misleading to correlate metamorphic events between different areas and levels of the infrastructure, because the thermal maximum was likely a transient thermal front that was diachronous with respect to region and structural level.

As the infrastructure cooled and was exhumed, post-tectonic plutons, including quartz-poor syenitic rocks of the Coryell plutonic suite and local granitic stocks and pegmatite dykes, were emplaced at all structural levels between 55 and 50 Ma, including the superstructure and Monashee complex (Parrish et al. 1988; Parkinson 1992; Parrish 1995; Johnston et al. 2000; Chapter 3). Middle Eocene volcanoes (~48-42 Ma; Mathews 1981) formed locally above brittle normal faults systems (Fig. 4-2).

The infrastructure-superstructure contact

Pressure and temperature estimates from thermobarometry indicate differences of peak *P-T* conditions between superstructure and the middle structural layer of the infrastructure of 5-7 kbar and 400-500°C (Fig. 4-20*a*). Peak metamorphism of the superstructure occurred in the Middle Jurassic (ca. 170 Ma), while peak *P-T* conditions in the underlying middle structural layer were attained in the Middle to Late Jurassic (155-150 Ma) in the Vernon antiform and Trinity Hills areas and the Late Cretaceous (100-90 Ma) in the Vidler Ridge and Pinnacles Peaks region.

The superstructure and middle structural layer are locally separated by discontinuous kilometre-thick ductile shear zones of Late Paleocene to Early Eocene age, such as in the Silver Star Mountain and Trinity Hills areas (Fig. 4-6), or a transitional zone characterized by steep

metamorphic gradients, but no evidence of ductile non-coaxial shear, such as in the Vidler Ridge and Pinnacles Peaks region (Fig. 4-7). Similar steep metamorphic gradients have been reported from the margins of a sillimanite-grade gneiss dome flanked by blueschist facies rocks within the Seward Peninsula, Alaska (Miller et al. 1992). Miller et al. (1992) proposed that the metamorphic gradient was attenuated by coaxial ductile strain during Cretaceous exhumation of the gneiss dome. In the Silver Star Mountain and Trinity Hills areas, an attenuated metamorphic sequence occurs within 1-2 km thick, ductile shear zones with top to the west shear-sense indicators. Synkinematic granitic rocks that occur within this zone have been dated at ~60-56 Ma (Bardoux 1993; Vanderhaeghe et al. 1999), indicating that a component of strain post-dates this time, although some displacement on the zone may be older. Petrological data also indicate that shearing outlasted metamorphism. Farther west, in the Vidler Ridge and Pinnacles Peaks region, evidence of an attenuated metamorphic section occurs, but non-coaxial ductile shear zones are not evident (Fig. 4-7). The reason for the lack of shear zones is not clear, but one possibility is that the Beaven fault has cut the shear zone, and exposures of the shear zone in the footwall have been removed by erosion. Another possibility, supported by a kinematic and AMS study of Late Paleocene to Early Paleocene granitic rocks within the middle structural layer across the Vernon area (Teyssier et al. 2005), is that deformation was dominantly coaxial in this area. Regardless, the metamorphic data require a significant amount of *relative* motion between the infrastructure and superstructure during the Late Cretaceous to Early Eocene (Fig. 4-20*a*).

A number of authors have suggested that the shear zones exposed in the Silver Star Mountain and Trinity Hills areas represent the eastward extension of the Okanagan Valley fault, a proposed Late Paleocene to Middle Eocene extensional detachment fault with 30 to 90 km of top to the west displacement (e.g., Tempelman-Kluit and Parkinson 1986; Parrish et al. 1988; Bardoux 1993; Johnson and Brown 1996). Such an interpretation implies the superstructure lies within the upper plate of a crustal-scale detachment fault that roots in the middle to lower crust. Infrastructure rocks are proposed to have been progressively exhumed during fault motion, as they were "dragged out" from the overlying upper plate.

Detachment fault models are, however, inconsistent with the continuity of the superstructure in the Vernon area. Even without taking post-Middle Eocene erosion into account, the limited gaps make large-displacement geometrically impossible (see discussion in Chapter 2). In short, the underlying infrastructure rocks cannot have been exhumed from depths of 15-21 km since Late Cretaceous time by tectonic removal of the superstructure belt on low-angle detachment faults, because, for the most part, the superstructure belt is largely still intact, directly

overlying upper amphibolite-facies infrastructure rocks above sub-horizontal shear zones or structurally above an attenuated metamorphic gradient.

Tectonic model

Metamorphic and geochronological data from the hinterland of the North American Sevier orogen have been interpreted as evidence that during the Late Cretaceous the crust was 50-60 km thick (e.g., Coney and Harms 1984). Mulch et al. (2004) have proposed, based on K-Ar dates and hydrogen isotope data from sheared granitic rocks exposed in the Vernon area, that Early Eocene paleoelevations were ~4000-4300 m, consistent with an elevated region underlain by thick crust. Thick crust is independently indicated by the abundance of Late Paleocene to Early Eocene granitic rocks within the middle crust of the southeast Canadian Cordillera (e.g., Carr 1992), which requires crustal thickness of greater than 50 km to produce abundant mid-crustal melts under geologically reasonable geothermal gradients (e.g., Patiño Douce et al. 1990).

Thermal modelling of thickened continental crust suggests that anatexis is a predictable outcome of radiogenic heating, thermal relaxation and incubation (England and Thompson 1984, 1986; Zen 1988). In orogens where melting occurs in the middle to lower crust, such as beneath the present-day Tibetan plateau (e.g., Nelson et al. 1996), it has been suggested that flow of partially molten crust from regions of thick crust (plateaus) to regions of thinner crust occurs in response to gravitational potential energy gradients (Bird 1991; Royden 1996; Clark and Royden 2000; Beaumont et al. 2004). Late Cretaceous to Early Tertiary mid-crustal flow during gravitational collapse of hinterland of the Sevier orogen is one of the competing hypotheses to account for the uplift of the 2 km-high Colorado plateau, which was at sea level prior to the Late Cretaceous (e.g., McQuarrie and Chase 2000).

Recent coupled thermal-mechanical models of convergent orogens have refined understanding of how channel flow may operate in orogens, and how changing variables, such as rheology, temperature, erosion rate, convergence rate, etc., can affect the development of zones of channel flow (e.g., Jamieson et al. 2002; Beaumont et al. 2004). In the most basic scenario, a zone of channel flow develops, flowing towards the foreland side of the orogen. The upper and lower boundaries of the channel are characterized by zones of non-coaxial (simple) shear with opposite sense. One test of channel flow, therefore, is whether granitic rocks of coeval age with opposite shear-sense indicators are present at the upper and lower boundaries of the proposed channel. Whereas strain along the boundaries of the channel is dominantly non-coaxial, deformation in the centre of the channel may be dominated by coaxial or general shear strain (e.g., Vanney and Grassmann 2001). If focused erosion occurs within the foreland, or the zone of channel flow is

forced up an underlying ramp, channel flow can be an efficient mechanism for exhuming partially molten mid-crustal rocks (e.g., Jamieson et al. 2002; Beaumont et al. 2004).

Within the SMC, syn- to post-kinematic granitic rocks coeval with exhumation (i.e. the Ladybird suite) intruded within the middle, rather than the lower, crust. Thermal modelling of the North American Cordillera suggests that this is a predictable function of the configuration of the pre-orogenic passive margin, where a thick sequence of "fertile" metasedimentary rocks, high in radiogenic heat-producing elements and hydrous minerals, were deposited on a previously metamorphosed, and relatively "infertile" cratonic basement. Melting occurred during orogenesis when the tectonically thickened "fertile" metasedimentary sequence entered the temperature interval sufficient to induce dehydration melting of hydrous minerals, including muscovite (730-750°C) and, at higher temperatures, biotite (800-875°C). The crustal column used by Patiño Douce et al. (1990) in their model is consistent with cross sections of the hinterland of the North American Cordillera, including the southern Canadian Cordillera, where a thickened metasedimentary sequence overlies previously metamorphosed upper amphibolite to granulite-facies Paleoproterozoic rocks (e.g., Cook et al. 1992). Geological and isotopic data from Late Paleocene to Early Eocene granitic rocks, combined with the paucity of granitic rocks of this age within the superstructure and basement, suggests that the middle structural layer was the source region for the melt (Carr 1992; Holk and Taylor 1997).

Paleorheological modeling of the southern Canadian Cordillera hinterland crust in the Late Cretaceous to the Early Paleocene suggests that strength was limited to the upper 10 km (e.g., Lowe and Ranalli 1993; Lui and Furlong 1993). An additional strength boundary may have existed deeper in the crust (~25-30km), at the contact between the partially molten middle structural layer and underlying previously metamorphosed, melt-poor Paleoproterozoic basement of the Monashee complex. Limited penetrative deformation of Paleoproterozoic basement during Cordilleran orogenesis is suggested by the existence of a strain gradient within the upper structural levels of the Frenchman Cap dome of the northern Monashee complex, where the intensity of Cordilleran deformation decreases with increasing structural depth (Crowley et al. 2001). The Late Cretaceous paleorheological profile for the hinterland suggests that ductile deformation, including channel flow, would be restricted to a melt-weakened, middle structural layer situated between the Monashee complex and the superstructure (Glombick et al. 2002). Flow of lower crustal rocks near the base of the crust may have also occurred, maintaining a flat Moho boundary beneath the southeast Canadian Cordillera (Cook et al. 1992).

Geochronological data from the present study area (Fig. 4-17), the Mica Dam area (Crowley et al. 2000), and the northern Monashee complex (Sevigny et al. 1991; Scammell 1993;

Parrish 1995; Digel et al. 1998), suggest that the period from the Early to Late Cretaceous (~130-90 Ma) was characterized by crustal thickening, prograde metamorphism, and minor plutonism. Continued crustal thickening and radiogenic heating during the Late Cretaceous to Middle Eocene (70-50 Ma) resulted in peak metamorphism of lower structural levels of the middle structural layer (Carr 1990; Parkinson 1992; Parrish 1995; Gibson et al. 1999; Crowley et al. 2001), the Valhalla complex (Parrish 1995; Ducea et al. 2004), and the basement culminations of the Monashee complex (Carr 1990; Parrish 1995; Gibson et al. 1999; Crowley et al. 2001). Peak metamorphic conditions at the deepest levels of the middle structural layer were sufficient to induce biotite dehydration melting of pelitic rocks (e.g., Nyman et al. 1995), resulting in widespread partial melting and generation of the earliest phases of the Ladybird granite suite (Carr 1992).

We propose that the rising crustal temperatures and the generation of melt within the middle to lower crust in the Late Cretaceous may have initiated foreland-directed channel flow within the hinterland of the southeast Canadian Cordillera. One test of channel flow is to compare the shear-sense from coeval syn-kinematic granitic rocks at the top and bottom of proposed channel. Mylonitic granitic rocks dated at 60-56 Ma (U-Pb, zircon) with well-developed C-S fabric from the superstructure-infrastructure transition zone in the Silver Star Mountain and Trinity Hills areas, the proposed upper boundary of Late Cretaceous to Early Eocene channel flow, record a top to the west shear-sense (Bardoux 1993; Vanderhaeghe et al. 1999; Chapter 2). In contrast, synkinematic granitic rocks near the contact between the Thor-Odin dome and the overlying paragneiss sequence of the middle structural layer, the lower boundary of proposed channel flow, have been dated at 59 ± 0.3 Ma (U-Pb, zircon) and record a top to the east shear-sense (Carr 1990). Teyssier et al. (2005) conducted a petrological and AMS study of Late Paleocene to Early Eocene granitic rocks from the Trinity Hills area to south of Thor-Odin dome, effectively traversing from the top to the bottom of the proposed zone of east-directed channel flow. They reported a change in shear-sense from top-to-the-west in the Trinity Hills area, near the top of the channel, to top-to-the-east south of Thor-Odin dome, near the bottom. At the approximate midpoint of the channel, located north of Vidler Ridge in the vicinity of Sugar Mountain (Fig. 4-2), they reported conflicting shear-sense indicators and evidence of coaxial deformation.

Examination of the Lithoprobe seismic refection lines 7-9 from the southern Canadian Cordillera, which transect the study area from east to west (Fig. 4-2), reveals a prominent series of west-dipping sub-parallel reflectors than can be traced from the upper crust to a depth of nearly 30 km (Fig. 4-20*b*). This series of reflectors, which have an amplitude of nearly 20 km, has been

interpreted as a crustal-scale shear zone with top to the east shear-sense, the Monashee décollement (Cook et al. 1992). Within north-trending Lithoprobe line 6, this surface has an apparent dip to the south (Cook et al. 1992). The contact between Paleoproterozoic basement and the cover sequence is exposed to the north, where this feature is projected to surface (Fig. 4-2). Deeper in the section, beneath the Monashee complex block, at a depth of 20 to 30 km another west-facing series of reflectors with a relief of approximately 10 km is visible, which has been interpreted as a southwest-facing ramp in autochthonous cratonic basement (Fig. 4-20*b*; Cook et al. 1992).

If existing interpretations of the Lithoprobe data are correct, and the west-facing ramp with nearly 20 km of amplitude parallels the boundary between partially molten middle structural layer rocks and underlying Paleoproterozoic basement, then flow of the middle structural layer up the ramp would have resulted in decompression melting, exhumation, cooling, and doming of the channel (the middle crustal level) above it ("channel underthrusting" of Beaumont et al. 2004). Similarly, the block of Paleoproterozoic crust underlying the middle structural layer would be exhumed as it was thrust up the ramp in the underlying cratonic basement.

As the zone of channel flow is tilted to the west against the ramp, the surface section examined by Teyssier et al. (2005), would represent a top to the bottom section of the channel moving from west to east. Such a large-magnitude subsurface feature should be reflected by changes in structural level at the surface across the ramp. This is not, however, what is observed. The superstructure overlies the entire length of the section without a perceptible change in metamorphic grade or structural level. This implies one of two things: (1) that the reflectors visible in the Lithoprobe data are not of Cordilleran age; or (2) that the middle structural layer absorbed the change in the thickness of the underlying cratonic basement, essentially flowing as a "fluid" up the ramp through a constriction between the top of the ramp and the overlying superstructure.

The exposure of Paleoproterozoic basement of the Monashee complex near the top of the proposed ramp is consistent with the latter model. Other exposures of amphibolite-facies rocks flanked by greenschist-facies rocks within the southern Canadian Cordillera occur above ramp-like features, including the Nicola Horst (Cook et al. 1992) and the Valhalla complex (Spear 2004). This suggests that the reflectors visible in the middle crust are, in fact, of Cordilleran age. In addition, extreme attenuation of the middle structural layer should be observed above the ramp. Strong east or west trending stretching lineations and the parallel alignment of fold axes of the metasedimentary and metavolcanic succession overlying the Thor-Odin dome of the Monashee complex indicate intense east-west stretching and attenuation (e.g., Reesor and Moore 1971;

Spark 2002), although some of this attenuation may have occurred during shortening (e.g., Williams and Jiang 2005). The lineation is well-developed in Paleocene to Early Eocene granitic rocks that were emplaced during crustal extension (e.g., Carr 1992). This implies that the zone of channel flow accommodates lateral thickness variations caused by variations in the thickness of underlying Paleoproterozoic basement and(or) temperature gradients (cf. Wernicke 1995).

The Vernon antiform, a domal feature visible in the upper to middle crust beneath the Aberdeen gneiss complex, may represent a "lump" or block of Paleoproterozoic basement incorporated into the zone of channel flow. Although no Proterozoic basement has been found at surface within the core of the antiform (see Chapter 3), its domal pattern may indicate a stack of pericratonic thrust slices, or a basement high. This may explain why the Vernon antiform records a Middle to Late Jurassic metamorphic event that is not recorded by rocks in the Vidler Ridge-Pinnacles region. If there were a block of Paleoproterozoic crust beneath the Vernon antiform, this would limit the thickness of the mid-crustal channel to the thickness of middle crustal level present between continental crust and the overlying superstructure.

Conclusions

1. Superstructure and infrastructure rocks exposed in the study area, presently juxtaposed by 1-2 km thick ductile shear zones or attenuated metamorphic gradients, experienced very different metamorphic histories prior to the Middle Eocene.
2. The superstructure, which overlies metamorphic infrastructure rocks from one margin of the complex to the other, experienced a single metamorphic event at ~170 Ma, coeval with regional deformation and emplacement of calcalkaline Middle Jurassic batholiths.
3. The middle structural layer of the infrastructure experienced a complex and episodic metamorphic evolution, recording three major metamorphic events in the Middle to Late Jurassic (155-150 Ma), Late Cretaceous (100-90 Ma), and Cretaceous to Eocene (70-50 Ma). Evidence of all three metamorphic events is recorded in the core of the Vernon antiform and Trinity Hills areas, while the Vidler Ridges and Pinnacles Peaks region only record evidence of the Late Cretaceous and Cretaceous to Eocene events. The lowest structural level in the area, the Thor-Odin dome of the Monashee complex, only records geochronological evidence of the youngest event.
4. Exhumation of the middle structural layer of the infrastructure cannot be explained by removal of the superstructure, as suggested by large-displacement, detachment models, as the superstructure is still largely intact across the study area.

5. The occurrence of a zone of foreland-directed, mid-crustal channel of partially molten rocks in response to gradient in gravitational potential energy is supported by opposite shear-sense indicators from coeval granitic rocks along the top and bottom of the middle crustal layer, the proposed zone of channel flow.
6. Exhumation of the middle crustal layer is proposed to have occurred through a combination of thinning of the channel and flow of the channel up a crustal-scale ramp in underlying Paleoproterozoic basement rocks.
7. The Paleoproterozoic basement of the Thor-Odin complex in the Monashee complex may have been exhumed as it was thrust up an underlying ramp in the cratonic margin.
8. An area of Proterozoic-aged continental crust, similar to the Monashee complex, may underlie the Vernon antiform.

References

Anderson, G.M. 1976. Error propagation by the Monte Carlo method in geochemical calculations. Geochimica et Cosmochimica Acta, **40**: 1533-1538.

Archibald, D.A., Glover, J.K., Price, R.A., Farrar, E., and Carmichael, D.M. 1983. Geochronology and tectonic implications of magmatism and metamorphism, southern Kootenay arc and neighbouring regions, southeastern British Columbia. Part I. Jurassic to mid-Cretaceous: Canadian Journal of Earth Sciences, **20**: 1891-1913.

Armstrong, R.L., Parrish, R.R., Van der Heyden, P., Scott, K., Runkle, D., and Brown, R.L. 1991. Early Proterozoic basement exposures in the southern Canadian Cordillera: core gneiss of Frenchman Cap, Unit L of the Grand Forks Gneiss, and the Vaseaux Formation. Canadian Journal of Earth Sciences, **28**: 1169-1201.

Bardoux, M. 1993. The Okanagan Valley fault from Penticton to Enderby, south-central British Columbia. Ph.D. thesis, Carleton University, Ottawa.

Bardoux, M., and Mareschal, J.C. 1994. Extension in south-central British Columbia: mechanical and thermal controls. Tectonophysics, **238**: 451-470.

Beaumont, C., Jamieson, R.A., Nguyen, M.H., and Medvedev, S. 2004. Crustal channel flows: 1. Numerical models with applications to the tectonics of the Himalayan-Tibetan orogen. Journal of Geophysical Research, **109**: B06406, doi:10.1029/2003JB002809.

Berman, R.G. 1988. Internally consistent thermodynamic data for minerals in the system Na_2O-K_2O-CaO-MgO-FeO-Fe_2O_3-Al_2O_3-SiO_2-TiO_2-H_2O-CO_2. Journal of Petrology, **29**: 445-522.

Berman, R.G. 1990. Mixing properties of Ca-Mg-Fe-Mn garnets. American Mineralogist, **75**: 328-344.

Berman RG. 1991. Thermobarometry using multiequilibrium calculations: a new technique with petrologic applications. Canadian Mineralogist, **29**: 833-855.

Berman, R.G., and Aranowich, L.Y. 1996. Optimized standard state and mixing properties of minerals: I. Model calibration for olivine, orthopyroxene, cordierite, garnet, and ilmenite in the system FeO-MgO-CaO-Al_2O_3-TiO_2-SiO_2. Contributions to Mineralogy and Petrology, **126**: 1-24.

Bird, P. 1991. Lateral extrusion of the lower crust from under high topography, in the isostatic limit. Journal of Geophysical Research, **83**: 4975-4987.

Brown, R.L., Journeay, J.M., Lane, L.S., Murphy, D.C., and Rees, C. 1986. Obduction, backfolding and piggyback thrusting in the metamorphic hinterland of the southeast Canadian Cordillera. Journal of Structural Geology, **8**: 255-268.

Carr, S.D. 1990. Late Cretaceous-early Tertiary tectonic evolution of the southern Omineca Belt, Canadian Cordillera. Ph.D. thesis, Carleton University, Ottawa.

Carr, S.D. 1991. U-Pb zircon and titanite ages of three Mesozoic igneous rocks south of the Thor-Odin-Pinnacles area, southern Omineca Belt, British Columbia. Canadian Journal of Earth Sciences, **28**: 1877-1882.

Carr, S.D. 1992. Tectonic setting and U-Pb geochronology of the early Tertiary Ladybird leucogranite suite, Thor-Odin-Pinnacles area, southern Omineca Belt, British Columbia. Tectonics, **11**: 258-278.

Chackraborty, S., and Ganguly, G. 1990. Compositional zoning and cation diffusion in garnets. *In* Diffusion, atomic ordering, and mass transport: selected problems in geochemistry. *Edited by* J. Ganguly. Springer-Verlag, New York.

Chatterjee, N.D., and Froese, E. 1975. A thermodynamic study of the pseudobinary join muscovite-paragonite in the system $KAlSi_3O_8$-$NaAlSi_3O_8$-Al_2O_3-SiO_2-H_2O. American Mineralogist, **60**: 985-993.

Cherniak, D.J., Watson, E.B., Grove, M., and Harrison, T.M. 2004. Pb diffusion in monazite: a combined RBS/SIMS study. Geochimica et Cosmochimica Acta, **68**: 829-840.

Chernoff, C.B., and Carlson, W.D. 1997. Disequilibrium for Ca during growth of pelitic garnet. Journal of Metamorphic Geology, **15**: 421-438.

Clark, M.K., and Royden, L.H. 2000. Topographic ooze: building the eastern margin of Tibet by lower crustal flow. Geology, **28**: 703-706.

Clemens, J.D., Vielzeuf, D. 1987. Constraints on melting and magma production in the crust. Earth and Planetary Science Letters, **86**: 287-306.

Cocherie, A., Legendre, O. Peucat, J.J. , and Kouamelan, A. 1998. Geochronology of polymetamorphic monazites constrained by in situ electron microprobe Th-U-total-Pb determination: Implications for Pb behaviour in monazite. Geochimica et Cosmochimica Acta, **62**: 2475-2497.

Coney, P.B. 1980. Cordilleran metamorphic core complexes: an overview. *In* Cordilleran metamorphic core complexes. *Edited by* M.D. Crittenden, Jr., P.J. Coney, and G.H. Davis. Geological Society of America Memoir 153, pp. 7-31.

Coney, P.B., and Harms, T.A. 1984. Cordilleran metamorphic core complexes: Cenozoic extensional relics of Mesozoic compression. Geology, **12**: 550-554.

Cook, F.A., Varsek, J.L., Clowes, R.M., Kanasewich, E.R., Spencer, C.S., Parrish, R.R., Brown, R.L., Carr, S.D., Johnson, B.J., and Price, R.A. 1992. Lithoprobe crustal reflection cross

section on the southern Canadian Cordillera, 1, Foreland Thrust and Fold Belt to Fraser River fault. Tectonics, **11**: 12-35.

Crowley, J.L. 1997. U-Pb geochronological constraints on the cover sequence of the Monashee complex, Canadian Cordillera: Paleoproterozoic deposition on basement. Canadian Journal of Earth Sciences, **34**: 1008-1022.

Crowley, J.L., Ghent, E.D., Carr, S.D., Simony, P.S., and Hamilton, M.A. 2000. Multiple thermotectonic events in a continuous metamorphic sequence, Mica Creek area, southeastern Canadian Cordillera: Geological Materials Research, **2**: 1-45.

Crowley, J.L., Brown, R.L., and Parrish, R.R. 2001. Diachronous deformation and a strain gradient beneath the Selkirk allochthon, northern Monashee complex, southeastern Canadian Cordillera. Journal of Structural Geology, **23**: 1103-1121.

Cygan, R.T., and Lasaga, A.C. 1985. Self-diffusion of magnesium in garnet at 750°C to 900°C. American Journal of Science, **285**: 328-350.

Davis, E.E., and Lewis, T.J. 1984. Heat flow in a back-arc environment: Intermontane and Omineca Crystalline belts, southern Canadian Cordillera. Canadian Journal of Earth Sciences, **21**: 715-726.

Digel, S.G., Ghent, E.D., Carr, S.D., and Simony, P.S. 1998. Early Cretaceous kyanite-sillimanite metamorphism and Paleocene sillimanite overprint near Mount Cheadle, southeastern British Columbia: geometry, geochronology, and metamorphic implications. Canadian Journal of Earth Sciences, **35**: 1070-1087.

Ducea, M.N., Ganguly, J., Rosenberg, E.J., Patchett, P.J., Cheng, W., and Isachsen, C. 2003. Sm-Nd dating of spatially controlled domains of garnet single crystals: a new method of high-temperature thermochronology. Earth and Planetary Science Letters, **213**: 31-42.

Duebendorfer, E.M., and Frost, B.R. 1988. Retrogressive dissolution of garnet: effect on garnet-biotite geothermometry. Geology, **16**: 875-877.

England, P.C., and Thompson, A.B. 1984. Pressure-temperature-time paths during regional metamorphism I. Heat transfer during the evolution of regions of thickened continental crust. Journal of Petrology, **25**: 894-928.

England, P.C., and Thompson, A.B. 1986. Some thermal and tectonic models for crustal melting in continental collision zones. *In* Collisional Tectonics. *Edited by* M.P. Coward, and A.C. Ries. Geological Society Special Publication 19, pp. 83-94.

Erdmer, P., Thompson, R.I., and Daughtry, K.L. 1999. Pericratonic Paleozoic succession in Vernon and Ashcroft map areas, British Columbia. *In* Current Research 1999-A. Geological Survey of Canada, pp. 205-215.

Erdmer, P., Heaman, L., Creaser, R.A., Thompson, R.I., and Daughtry, K.L. 2001. Eocambrian granite clasts in southern British Columbia shed light on Cordilleran hinterland crust. Canadian Journal of Earth Sciences, **38**: 1007-1016.

Finger, F., Broska, I., Roberts, M.P., and Schermaier, A. 1998. Replacement of primary monazite by apatite-allanite-epidote coronas in an amphibolite facies granite gneiss from the eastern Alps. American Mineralogist, **83**: 248-258.

Franz, G., Andrehs, D., and Rhede, G. 1996. Crystal chemistry of monazite and xenotime from Saxothuringian-Moldanubian metapelites, NE Bavaria, Germany. European Journal of Mineralogy, **8**: 1097-1108.

Frost, B.R., and Tracy, R.J. 1991. P-T paths from zoned garnets: some minimum criteria. American Journal of Science, **291**: 917-939.

Fuhrman, M.L. and Lindsley, D.H. 1988. Ternary-feldspar modeling and thermometry: The American Mineralogist, **73**: 201-216.

Gardien, V., Thompson, A.B., Grujic, D., and Ulmer, P. 1995. Experimental melting of biotite + plagioclase + quartz + or - muscovite assemblages and implications for crustal melting. Journal of Geophysical Research, B, Solid Earth and Planets, **100**: 15581-15591.

Ghent, E.D. 1976. Plagioclase-garnet-Al_2SiO_5-quartz: a potential geobarometer-geothermometer. American Mineralogist, **61**: 710-714.

Ghent, E.D., and Stout, M.Z. 1981. Geobarometry and geothermometry of plagioclase-biotite-garnet-muscovite-assemblages. Contributions to Mineralogy and Petrology, **76**: 92-97.

Ghent, E. D., Nicholls, J., Stout, M. Z. & Rottenfusser, B. 1977. Clinopyroxene amphibolite boudins from Three Valley Gap, British Columbia. Canadian Mineralogist, **15**: 269-282.

Gibson, H.D., Brown, R.L., and Parrish, R.R. 1999. Deformation-induced metamorphic field gradients: an example from the southeastern Canadian Cordillera. Journal of Structural Geology, **21**: 751-767.

Gibson, H.D., Carr, S.D., Brown, R.L., and Hamilton, M.A. 2004. Correlations between chemical and age domains in monazite, and metamorphic reactions involving major pelitic phases: an integration of ID-TIMS and SHRIMP geochronology with Y-Th-U X-ray mapping. Chemical Geology, **211**: 237-260.

Gough, I.D. 1986. Mantle upflow tectonics in the Canadian Cordillera. Journal of Geophysical Research, **91**(B2): 1909-1919.

Glombick, P., and Thompson, R.I. 2004. Geology of the Creighton Creek map area, British Columbia (NTS 82L/02). Geological Survey of Canada Open File 4371, scale 1:50 000.

Glombick, P., Thompson, R.I., and Erdmer, P. 2002. The role of a melt-rich middle crust layer in core complex formation: evidence from the Shuswap metamorphic complex, south-central British Columbia. *In* Abstracts with Programs, Geological Society of America, 2002 annual meeting, p. 109.

Glombick, P., Thompson, R.I., and Daughtry, K.L. 2004. Geology of the Oyama map area, British Columbia (NTS 82L/03). Geological Survey of Canada Open File 4372, scale 1:50 000.

Heaman, L.M., and Parrish, R.R. 1991. U-Pb geochronology of accessory minerals. *In* Applications of Radiogenic isotopic systems to problems in geology. *Edited by* L. Heaman and J.N. Ludden. Mineralogical Association of Canada, pp. 59-102.

Holk, G.J., and Taylor, H.P. Jr. 1997. $^{18}O/^{16}O$ homogenization of the middle crust during anatexis: the Thor-Odin metamorphic core complex, British Columbia. Geology, **25**: 31-34.

Hodges, K.V., and Crowley, P.D. 1985. Error estimates and empirical geothermobarometry for pelitic systems. American Mineralogist, **70**: 702-709.

Huang, W.L., and Wyllie, P.J. (1973). Melting relations of muscovite-granite to 35 kbar as a model for fusion on metamorphosed subducted oceanic sediments. Contributions to Mineralogy and Petrology, **42**: 1-14.

Jamieson, R.A., Beaumont, C., Nguyen, M.H., and Lee, B. 2002. Interaction of metamorphism, deformation, and exhumation in large convergent orogens. Journal of Metamorphic Geology, **20**: 1-16

Johnson, B.J. 1994. Structure and tectonic setting of the Okanagan Valley fault system in the Shuswap Lake area, southern British Columbia. Unpublished Ph.D. thesis, Carleton University, Ottawa.

Johnson, B.J., and Brown, R.L. 1996. Crustal structure and early Tertiary extensional tectonics of the Omineca belt at 51°N latitude, southern Canadian Cordillera. Canadian Journal of Earth Sciences, **33**: 1596-1611.

Johnston, D.H. 1998. Structural and thermal evolution of northwest Thor-Odin dome, Monashee complex, British Columbia. Ph.D. thesis, University of New Brunswick, Fredericton.

Johnston, D.H., Williams, P.F., Brown, R.L., Crowley, J.L., and Carr, S.D. 2000. Northeastward extrusion and extensional exhumation of crystalline rocks of the Monashee complex, southeastern Canadian Cordillera. Journal of Structural Geology, **22**: 603-625.

Kingsbury, J.A., Miller, C.F., Wooden, J.L., and Harrison, T.M. 1993. Monazite paragenesis and U-Pb systematics in rocks of the eastern Mohave Desert, California, U.S.A.: implications for thermochronometry. Chemical Geology, **110**: 147-167.

Klepacki, D.W. 1985. Stratigraphy and structural geology of the Goat Ranges area, southeastern British Columbia. PhD thesis, Massachusetts Institute of Technology, Massachusetts.

Kohn, M.J., and Malloy, M., A. 2004. Formation of monazite via prograde metamorphic reactions among common silicates: implications for age determinations. Geochimica et Cosmochimica Acta, **68**: 101-113.

Kohn, M.J. and Spear, F.S. 2000. Retrograde net-transfer reaction insurance for pressure-temperature estimates. Geology, **28**: 1127-1130.

Kretz, R. 1983. Symbols for rock-forming minerals. American Mineralogist, **68**: 277-279.

Kuiper, Y. 2003. Geochronological, petrological and microstructural studies on the Thor-Odin dome, Monashee complex, southern Canadian Cordillera. Ph.D. thesis, University of New Brunswick, Fredericton.

Lane, L.S.1984. Brittle deformation in the Columbia River fault zone near Revelstoke, southeastern British Columbia. Canadian Journal of Earth Sciences, **21**: 584-598.

Le Breton, N., and Thompson, A.B. 1988. Fluid-absent (dehydration) melting of biotite in metapelites in the early stages of crustal anatexis. Contributions to Mineralogy and Petrology, **99**: 226-237.

Lemieux, Y., Thompson, R.I., and Erdmer, P. 2003. Stratigraphy and structure of the Upper Arrow Lake area, southeastern British Columbia: new perspectives for the Columbia River fault zone. *In* Current Research 2003, Geological Survey of Canada, 2003-A7.

Lister, G.S., and Davis, G.A. 1989. The origin of metamorphic core complexes and detachment faults formed during Tertiary continental extension in the northern Colorado River region, U.S.A. Journal of Structural Geology, **11**: 65-94.

Lowe, C., and Ranalli, G. 1993. Density, temperature, and rheological models for the southeastern Canadian Cordillera: implications for its geodynamic evolution. Canadian Journal of Earth Science, **30**: 77-93.

Lui, M., and Furlong, K. 1993. Crustal shortening and Eocene extension in the southeastern Canadian Cordillera: some thermal and rheological considerations. Tectonics, **12**: 776-786.

MacCready, T., Snoke, A.W., Wright, J.E., and Howard, K.A. 1997. Mid-crustal flow during Tertiary extension in the Ruby Mountains core complex, Nevada. Geological Society of America Bulletin, **109**: 1576-1594.

Marr, R.A., Pattison, D.R.M., Heaman, L.M., Chacko, T., and Mariano, A.N. 2002. Chemical analysis and age dating by electron microprobe of six monazites dated by thermal ionisation

mass spectrometry (TIMS). *In* Abstracts with Programs, Geological Society of America, p. 171.

Mathews, W.H. 1981. Early Cenozoic resetting of potassium-argon dates and geothermal history of north Okanagan area, British Columbia. Canadian Journal of Earth Sciences, **18**: 1310-1319.

McDonough, M.R., and Parrish, R.R. 1991. Proterozoic gneisses of the Malton Complex, near Valemount, British Columbia: U-Pb ages and Nd isotopic signatures. Canadian Journal of Earth Sciences, **28**: 1202-1216.

McQuarrie, N., and Chase, C.G. 2000. Raising the Colorado Plateau. Geology, **28**: 91-94.

Menard, T., and Spear, F.S. 1993. Metamorphism of calcic pelitic schists, Strafford dome, Vermont: compositional zoning and reaction history. Journal of Petrology, **34**: 977-1005.

Miller, E.L. Calvert, A.T., Little, T.A. 1992. Strain-collapsed metamorphic isograds in a sillimanite gneiss dome, Seward Peninsula, Alaska. Geology, **20**: 487-490.

Monger, J.W.H., Price, R.A., and Tempelman-Kluit, D.J. 1982. Tectonic accretion and the origin of the two major metamorphic and plutonic welts in the Canadian Cordillera. Geology, **10**: 70-75.

Monger, J.W.H., Wheeler, J.O., Tipper, H.W., Gabrielse, H., Harms, T., Struick, L.C., Campbell, R.B., Dodds, C.J., Gehrels, G.E., and O'Brien, J. 1991. Upper Devonian to Middle Jurassic assemblages. Part B. Cordilleran terranes, Chapter 8. *In* Geology of the Cordilleran orogen in Canada. *Edited by* H. Gabrielse and C.J. Yorath. Geological Survey of Canada, Geology of Canada no. 4, pp. 281-327.

Montel, J.M., Veschambre, M., Nicollet, C., and Provost, A. 1996. Electron microprobe dating of monazite. Chemical Geology, **131**: 37-53.

Mulch, A., Teyssier, C., Cosca, M.A., Vanderhaeghe, O., Vennemann, T.W. 2004. Reconstructing paleoelvation in eroded orogens. Geology, **32**: 525-528.

Nelson, K.D., Zhao, W., Brown, L.D., Kuo, J., Che, J., Liu, X., Klemperer, S.L., Makovsky, Y., Meissner, R., Mechie, J., Kind, R., Wenzel, F., Ni, J., Nabelek, J., Leshou, C., Ten, H., Wei, W., Jones, A.G., Booker, J., Unsworth, M., Kidd, W.S.F., Hauck, M., Alsdorf, D., Ross, A., Cogan, M., Wu, C., Sandoval, E., and Edwards, M. 1996. Partially molten middle crust beneath southern Tibet: synthesis of Project INDEPTH results. Science, **274**: 1684-1688.

Norlander, B.H., Whitney, D.L., Teyssier, C., and Vanderhaeghe, O. 2002. Partial melting and decompression of the Thor-Odin dome, Shuswap metamorphic core complex, Canadian Cordillera. Lithos, **61**: 103-125.

Nyman, M. W., Pattison, D. R. M. & Ghent, E. D. 1995. Melt extraction during formation of K-feldspar + sillimanite migmatites, west of Revelstoke, British Columbia. Journal of Petrology, **36**: 351-372.

Okulitch, A.V. 1984. The role of the Shuswap Metamorphic Complex in Cordillera tectonism: a review. Canadian Journal of Earth Sciences, **21**: 1171-1193.

Okulitch, A.V. 1987. Comment and Reply on "Extension across the Eocene Okanagan crustal shear in southern British Columbia". Geology, **15**: 187-188.

Parkinson, D.L. 1991. Age and isotopic character of Early Proterozoic basement gneisses in the southern Monashee Complex, southeastern British Columbia. Canadian Journal of Earth Sciences, **28**: 1159-1168.

Parkinson, D.L. 1992. Age and tectonic evolution of the southern Monashee Complex, southeastern British Columbia: a window into the deep crust. Ph.D. thesis, University of California, Santa Barbara.

Parrish, R.R. 1995. Thermal evolution of the southeastern Canadian Cordillera. Canadian Journal of Earth Sciences, **32**: 1618-1642.

Parrish, R.R., and Armstrong, R.L. 1987. The ca. 162 Ma Galena Bay stock and its relationship to the Columbia River fault zone, southeast British Columbia. *In* Radiogenic Age and Isotopic Studies: Report 1. Geological Survey of Canada, Paper 87-2, pp. 25-32.

Parrish, R.R., and Wheeler, J.O. 1983. U-Pb zircon age of the Kuskanax batholith, southeastern British Columbia. Canadian Journal of Earth Sciences, **20**: 1751-1756.

Parrish, R.R., Carr, S.D., and Parkinson, D.L. 1988. Eocene extensional tectonics and geochronology of the southern Omineca Belt, British Columbia and Washington. Tectonics, **7**: 181-212.

Patiño Douce, A.E., and Johnston, A.D. 1991. Phase equilibria and melt productivity in the pelitic system: implication for the origin of peraluminous granitoids and aluminous granulites. Contributions to Mineralogy and Petrology, **107**: 202-218.

Patiño Douce, A.E., Humphreys, E.D., and Johnston, A.D. 1990. Anatexis and metamorphism in tectonically thickened continental crust exemplified by the Sevier hinterland, western North America. Earth and Planetary Science Letters, **97**: 290-315.

Pattison, D.R.M. 1992. Stability of andalusite and sillimanite and the Al_2SiO_5 triple point: constraints from the Ballachulish aureole, Scotland. Journal of Geology, **100**: 423-446.

Potts, P.J. 1987. A handbook of silicate rock analyses. Chapman and Hall, Great Britain.

Price, R.A., and Carmichael, D. 1986. Geometric test for Late Cretaceous-Paleogene intracontinental transform faulting in the Canadian Cordillera. Geology, **14**: 468-471.

Pyle, J.M., and Spear, F.S. 2003. Four generations of accessory-phase growth in low-pressure migmatites from SW New Hamphsire. American Mineralogist, **88**: 338-351.

Pyle, J.M., Spear, F.S., Rudnick, R.L., and McDonough, W.F. 2001. Monazite-xenotime-garnet equilibrium in metapelites and a new monazite-garnet thermometer. Journal of Petrology, **42**: 2083-2107.

Ranalli, G., Brown, R.L., and Bosdachin, R. 1989. A geodynamic model for extension in the Shuswap core complex, southeastern Canadian Cordillera. Canadian Journal of Earth Sciences, **26**: 1647-1653.

Read, P.B., and Okulitch, A.V. 1977. The Triassic unconformity of south-central British Columbia. Canadian Journal of Earth Sciences, **14**: 606-638.

Read, P.B., Woodsworth, G.J., Greenwood, H.J., Ghent, E.D., and Evenchick, C.A. 1991. Metamorphic map of the Canadian Cordillera. Geological Survey of Canada, Map 1714A, scale 1:2 000 000.

Reesor, J.E., and Moore, J.M. 1971. Petrology and structure of the Thor-Odin gneiss dome, Shuswap metamorphic complex, British Columbia. Geological Survey of Canada, Bulletin 195.

Rejebian, V.A., Harris, A.J., and Huebner, J.S. 1987. Conodont colour and textural alteration: an index to regional metamorphism, contact metamorphism, and hydrothermal alteration. Geological Society of America Bulletin, **99**: 471-479.

Royden, L.H. 1996. Coupling and decoupling of crust and mantle in convergent orogens: implications for strain partitioning in the crust. Journal of Geophysical Research, **101**: 17679-17705.

Rubatto, D., Williams, I.S., and Buick, I.S. 2001. Zircon and monazite response to metamorphism in the Reynolds Range, central Australia. Contributions to Mineralogy and Petrology, **140**: 458-468.

Scammell, R.J. 1993. Mid-Cretaceous to Tertiary thermotectonic history of former mid-crustal rocks, southern Omineca Belt, Canadian Cordillera. Ph.D. thesis, Queen's University, Kingston, Ontario.

Scammell, R.J., and Brown, R.L. 1990. Cover gneisses of the Monashee Terrane: a record of synsedimentary rifting in the North American Cordillera. Canadian Journal of Earth Sciences, **27**: 712-726.

Scott, D.J., and St-Onge, M.R. 1995. Constraints on Pb closure temperature in titanite based on rocks from the Ungava orogen, Canada: implications for U-Pb geochronology and P-T-t path determinations. Geology, **23**: 1123-1126.

Sevigny, J.H., Parrish, R.R., Donelick, R.R., and Ghent, E.D. 1991. Northern Monashee Mountains, Omineca Crystalline Belt, British Columbia: timing of metamorphism, anatexis and tectonic denudation. Geology, **18**: 103-106.

Smith, H.A., and Barreiro, B. 1990. Monazite U-Pb dating of staurolite grade metamorphism in pelitic schists. Contributions to Mineralogy and Petrology, **105**: 602-615.

Smith, H.A., and Gilleti, B.J. 1997. Lead diffusion in monazite. Geochimica et Cosmochimica Acta, **61**: 1047-1055.

Spark, R.N. 2002. Crustal thickening and tectonic denudation within the Thor-Odin culmination, Monashee complex, southern Canadian Cordillera. Ph.D. thesis, University of New Brunswick, Fredericton.

Spear, F.S. 1991. On the interpretation of peak metamorphic temperatures in light of garnet diffusion during cooling. Journal of Metamorphic Geology, **9**: 379-388.

Spear, F.S. 1993. Metamorphic phase equilibria and pressure-temperature-time paths. Mineralogical Society of America Monograph, Washington, D.C.

Spear, F.S. 2004. Fast cooling and exhumation of the Valhalla metamorphic core complex, southeastern British Columbia. International Geology Review, **46**: 193-209.

Spear, F.S. and Kohn, M.J. 1996. Trace element zoning in garnet as a monitor of crustal melting. Geology, **24**: 1099-1102.

Spear, F.S., and Menard, M. 1989. Program GIBBS; a generalized Gibbs method algorithm. American Mineralogist, **74**: 942-943.

Spear, F.S. and Parrish, R.R. 1996. Petrology and petrologic cooling rates of the Valhalla Complex, British Columbia, Canada. Journal of Petrology, **37**: 733-765.

Spear, F.S., and Selverstone, J. 1983. Quantitative P-T paths from zoned minerals: theory and tectonic applications. Contributions to Mineralogy and Petrology, **83**: 348-357.

Spear, F.S., Selverstone, J., Hickmott, D., Crowley, P., and Hodges, K.V. 1984. P-T paths from garnet zoning: a new technique for deciphering tectonic processes in crystalline terranes. Geology, **12**: 87-90.

Spear, F.S., Kohn, M.J., and Cheney, J.T. 1999. P-T paths from anatectic pelites. Contributions to Mineralogy and Petrology, **134**: 17-32.

Spear, F.S., Kohn, M.J., Florence, F.P., and Menard, T. 1991. A model for plagioclase growth in pelitic schists: implications for thermobarometry and P-T path determinations. Journal of Metamorphic Geology, **8**: 683-696.

Stowell, H.H., Menard, T., and Ridgeway, C.K. 1996. Ca-metasomatism and chemical zonation of garnet in contact-metamorphic aureoles, Juneau gold belt, southeastern Alaska. Canadian Mineralogist, **34**: 1195-1209.

Suzucki, K., and Adachi, M. 1991. Precambrian provenance and Silurian metamorphism of the Tsubonosawa paragneiss in the South Kitakami terrane, Northeast Japan, revealed by the chemical Th-U-total lead isochron ages of monazite, zircon, and xenotime. Geochemical Journal, **25**: 357-376.

Suzucki, K., and Adachi, M. 1998. Denudation history of the high T/P Ryoke metamorphic belt, southwest Japan: constraints from CHIME monazite ages of gneisses and granitoids. Journal of Metamorphic Geology, **16**: 23-37.

Tempelman-Kluit, D., and Parkinson, D. 1986. Extension across the Eocene Okanagan crustal shear in southern British Columbia. Geology, **14**: 318-321.

Teyssier, C., Ferré, E., Whitney, D.L., Norlander, B., Vanderhaeghe, O., and Parkinson, D. (2005). Flow of partially molten crust and origin of detachments during collapse of the Cordilleran orogen. Geological Society of London, Special Publication on high strain zones.

Thompson, A.B., and England, P.C. 1984. Pressure-temperature-time paths of regional metamorphism II: their influence and interpretation using mineral assemblages in metamorphic rocks. Journal of Petrology, **25**: 929-955.

Thompson, R.I. 2004*a*. Geology of the Salmon Arm map area, British Columbia (NTS 82L/11). Geological Survey of Canada Open File 4380, scale 1:50 000.

Thompson, R.I. 2004*b*. Geology of the Gates Creek map area, British Columbia (NTS 82L/09). Geological Survey of Canada Open File 4378, scale 1:50 000.

Thompson, R.I. (in press). Geology of the Monte Creek map area, British Columbia (NTS 82L/12). Geological Survey of Canada Open File 4381, scale 1:50 000.

Thompson, R.I. (in press). Geology of the Chase map area, British Columbia (NTS 82L/13). Geological Survey of Canada Open File 4382, scale 1:50 000.

Thompson, R.I. (in press). Geology of the Sorrento map area, British Columbia (NTS 82L/14). Geological Survey of Canada Open File 4383, scale 1:50 000.

Thompson, R.I. (in press). Geology of the Malakwa map area, British Columbia (NTS 82L/15). Geological Survey of Canada Open File 4384, scale 1:50 000.

Thompson, R.I. (in press). Geology of the Revelstoke map area, British Columbia (NTS 82L/16). Geological Survey of Canada Open File 4385, scale 1:50 000.

Thompson, R.I., and Daughtry, K.L. 1996. New stratigraphic and tectonic interpretations, north Okanagan Valley, British Columbia. *In* Current Research 1996-A. Geological Survey of

Canada, pp. 135-141. Thompson, R.I. 2004*a*. Geology of the Salmon Arm map area, British Columbia (NTS 82L/11). Geological Survey of Canada Open File 4380, scale 1:50 000.

Thompson, R.I. and Glombick, P. 2004*a*. Geology of the Shuswap Falls map area, British Columbia (NTS 82L/07). Geological Survey of Canada Open File 4376, scale 1:50 000.

Thompson, R.I., and Glombick, P. 2004*b*. Geology of the Mabel Lake map area, British Columbia (NTS 82L/10). Geological Survey of Canada Open File 4379, scale 1:50 000.

Thompson, R.I., and Unterschutz, J.L.E. 2004. Geology of the Vernon map area, British Columbia (NTS 82L/06). Geological Survey of Canada Open File 4375, scale 1:50 000.

Thompson, R.I. and Glombick, P., and Lemieux, Y. (compilers). 2004*a*. Geology of the Eureka Mountain map area, British Columbia (NTS 82L/01). Geological Survey of Canada Open File 4370, scale 1:50 000.

Thompson, R.I. and Glombick, P., and Lemieux, Y. (compilers). 2004*b*. Geology of the Mount Fosthall map area, British Columbia (NTS 82L/08). Geological Survey of Canada Open File 4377, scale 1:50 000.

Townsend, K.J., Miller, C.F., D'Andrea, J.L., Ayers, J.C., Harrison, T.M., and Coath, C.D. 2000. Low temperature replacement of monazite in the Ireteba granite, southern Nevada: geochronological implications. Chemical Geology, **172**: 95-112.

Tracy, R.J., Robinson, P., and Thompson, A.B. 1976. Garnet composition and zoning in the determination of temperature and pressure of metamorphism, central Massachusetts. American Mineralogist, **61**: 762-775.

Unterschutz, J.L.E., Creaser, R.A., Erdmer, P., Thompson, R.I., and Daughtry, K.L. 2002. North American margin origin of Quesnel Terrane strata in the southern Canadian Cordillera: inferences from geochemical and Nd isotopic characteristics of Triassic metasedimentary rocks. Geological Society of America Bulletin, **114**: 462-475.

Vanderhaeghe, O., Teyssier, C., and Wysoczanski, R. 1999. Structural and geochronological constraints on the role of partial meting during the formation of the Shuswap metamorphic complex at the latitude of Thor-Odin dome, British Columbia. Canadian Journal of Earth Sciences, **36**: 917-943.

Vanderhaeghe, O., Teyssier, C., McDougall, I., and Dunlap, W.J. 2003. Cooling and exhumation of the Shuswap Metamorphic Core Complex constrained by 40Ar/39Ar thermochronology. Geological Society of America Bulletin, **115**: 200-216.

Vannay, J.C and Grasemann, B. 2001. Himalayan inverted metamorphism and syn-convergence extension as a consequence of a general shear extrusion. Geological Magazine, **138**: 253-276.

Wernicke, B. 1995. The fluid crustal layer and its implications for continental dynamics. *In* Exposed Cross-sections of the Continental Crust. *Edited by* M.H. Salisbury and D.M. Fountain. NATO ASI Series. Series C. Mathematical and Physical Sciences, 317. D. Reidel Publishing Company, Dordrecht-Boston, pp. 509-544.

Wheeler, J.O., Brookfield, A.J., Gabrielse, H., Monger, J.W.H., Tipper, H.W., and Woodsworth, G.J. (compilers). 1991. Terrane map of the Canadian Cordillera. Geological Survey of Canada, Map 1713A, scale 1:2 000 000.

Whitney, D.L., and Ghent, E.D. 1993. Prograde and garnet zoning reversals in staurolite schist, British Columbia: significance for thermobarometric interpretations. Journal of Metamorphic Geology, **11**: 779-788.

Williams, M.L., Jercinovic, M.J., and Terry, M.P. 1999. Age mapping and dating of monazite on the electron microprobe: deconvoluting multistage tectonic histories. Geology, **27**: 1023-1026.

Williams, P.F., and Jiang, D. 2005. An investigation of lower crustal deformation: evidence for channel flow and its implications for tectonics and structural studies. Journal of Structural Geology, **27**: 1486-1504.

Wing, B., A., Ferry, J.M., and Harrison, T.M. 2003. prograde destruction and formation of monazite and allanite during contact and regional metamorphism of pelites. Contributions to Mineralogy and Petrology, 145: 228-250.

Woodsworth, G.J., Anderson, R.G., and Armstrong, R.L. 1991. Plutonic regimes, Chapter 15. *In* Geology of the Cordilleran orogen in Canada. *Edited by* H. Gabrielse and C.J. Yorath. Geological Survey of Canada, Geology of Canada no. 4, pp. 491-531.

Yardley, B.W.D. 1977. An empirical study of diffusion in garnet. American Mineralogist, **62**: 793-800.

Zen, E.A. 1988. Thermal modelling of step-wise anatexis in a thrust-thickened sialic crust. Transactions of the Royal Society of Edinburgh, Earth Science, **79**: 223-235.

Zhu, X.K., and O'Nions, R.K. 1999. Zonation of monazite in metamorphic rocks and its implications for high temperature thermochronology: a case study from the Lewisian terrain. Earth and Planetary Science Letters, **171**: 209-220.

APPENDIX 4*a*: GEOTHERMOBAROMETRY - ANALYTICAL TECHNIQUE, SAMPLING STRATEGY, AND STATISTICAL TREATMENT

All samples were analyzed using a JEOL 8900 electron microprobe located at the University of Alberta. Analytical conditions of 15kV and 15nA were used for all mineral analyses. Standards used for calibration are listed in Table 4-1.

Three garnets of varying size were selected from each sample for major element (Fe, Mg, Ca, Mn) compositional mapping (Fig. 4-10). Rim to rim line analyses of the garnets were made based on zoning patterns visible in the X-ray composition maps. In the line analyses, the distance between spot analyses varied from 20 μm to 50 μm, depending on the size of the garnet (larger spacing for larger garnets). Where significant compositional gradients were visible near the garnet rim, spot spacing was increased to 2 μm for the first 20 μm in from the rim, and then increased to standard spacing within the core. Spot locations and spacing was automatically calculated using in-house microprobe software, then visually checked to avoid inclusions or fractures. For plagioclase, muscovite, staurolite and chlorite, an average of 15 to 20 spots were selected from several matrix grains in the vicinity of, but not in contact with the garnet grains, yielding approximately 45 to 60 analyses of each mineral phase per sample. For biotite, several grains were chosen with variable proximity to the garnet, ranging from grains directly in contact with garnet, to those up to 500 μm distant. The composition of biotite and plagioclase inclusions in garnet, where present, and the adjacent garnet composition was also measured.

Compositional data from mineral phases was used to calculate the position of reaction equilibria using the TWEEQU (version 2.02) program of Berman (1991), which utilizes an internally consistent thermodynamic database (Berman 1988; 1990). Activity models were used to model non-ideal behaviour in garnet (Berman and Aranovich 1996), biotite (Berman and Aranovich, unpublished data), plagioclase (Fuhrman and Lindsley 1988), and muscovite (Chatterjee and Froese 1975).

Rather than calculate intersection of reaction equilibria pressure using a particular garnet composition and average matrix plagioclase, biotite, muscovite, and chlorite compositions, error parallelograms were generated using a chosen garnet composition with a range of matrix mineral compositions. For the biotite-garnet Fe-Mg exchange geothermometer, biotite analyses with the highest and lowest (Fe/[Fe+Mg]) values were used to calculate upper and lower temperatures. In samples where the GASP net transfer geobarometer was used, the garnet composition was paired with the highest and lowest X_{An} values of the matrix plagioclase to constrain the upper and lower limits of the parallelogram. The average of muscovite, chlorite, and staurolite compositions were

used in the calculations. When plagioclase or biotite inclusions were analyzed, the average composition was used.

APPENDIX 4*b*: MONAZITE EMP CHEMICAL AGE DATING - ANALYTICAL TECHNIQUE FOR AND STATISTICAL TREATMENT

Standard, carbon-coated polished thin sections were analyzed using the JEOL 8900 electron microprobe located at the University of Alberta. A previous study comparing TIMS and EMP chemical ages for a numbers of monazite samples dated at the University of Alberta have shown reasonably good agreement (Marr et al. 2002). Prior to analysis, a systematic assessment of peak overlaps was performed. Monazite grains were identified by their extreme contrast in backscattered electron (BSE) images. An accelerating voltage of 20 kV, a beam current of 150 nA, and a beam diameter of 3 μm were used during spot analyses. Standards are listed in Table 4-4. Count times of 300, 30, and 120 s were used for Pb, Th, and U respectively. Count times of 15, 20, 15, 20, 20, 10, 20, 20, 20, 20, 20, and 20 s were used for Ca, Ce, P, Si, Nd, La, Pr, Y, Sm, and Gd. Background count times were half of the count time for that element. The duration of a single spot analysis was approximately 11 minutes, permitting 5 spot analyses per hour.

The errors associated with individual spot analyses were calculated using a Monte Carlo approach (Anderson 1976). First, the relative precision of a representative spot analyses (the spot with the lowest PbO above the minimum cut-off was selected) is calculated using the formula:

$$\sqrt{\frac{n_p}{t_p^2}+\frac{n_b}{t_b^2}}\Bigg/\left(\frac{n_p}{t_p}+\frac{n_p}{t_b}\right)$$

where n_p and n_b are the total counts on the peak and background, respectively, and t_p and t_b are total counting times on the peak and background, respectively. The relative precision is then converted into the oxide standard deviation. Using the measured oxide value and the calculated oxide standard deviation, a series of 1000 random numbers with a normal distribution is generated separately for ThO, UO_2, and PbO. These values are used to calculate 1000 ages, from which the standard deviation is calculated. As this error estimate only considers counting statistics, it is an absolute minimum error.

If all the Pb within a monazite grain is radiogenic (i.e., no initial common Pb) and the original ratios of Pb, Th of U have not changed, except by radioactive decay, then a chemical age of a monazite grain can be calculated provided that the concentrations of Pb, Th, and U can be measured with reasonable accuracy using an electron microprobe (e.g., Suzucki and Adachi

1991). Various studies have demonstrated that, in many cases, these assumptions appear to be valid, even in high-grade, polymetamorphic monazite grains (Montel et al. 1996; Cocherie et al. 1998; Williams et al. 1999).

There are several different methods commonly used to calculate chemical ages from monazite data. In the isochron method, the U content of each individual spot analyses is converted to the equivalent amount of Th that would have decayed to produce an equal amount of Pb. This amount is added to the measured Th to yield a corrected (Th*) value. The age of a sample can be calculated from the slope on a Th* vs. Pb plot of all the data points from a single age population (e.g., Suzuki and Adachi 1991). Ages can also be calculated using bell-shaped probability curves (Montel et al. 1996) or by the weighted mean (e.g., Finger et al. 1998).

Two variations of the isochron method were used (Table 4-5). In method A, the error associated with the origin is set to zero, forcing the isochron through the origin (e.g., Suzuki and Adachi 1991). In method B, the error associated with the origin is equal to the error of the data points, resulting in a non-zero intercept (e.g., Cocherie et al. 1998). Method A yields ages that are similar to the weighted mean ages, but the calculated error is considerably less than the error calculated using method B. This is, in effect, the result of the anchoring of the isochron at the origin. Method B yields larger, and perhaps a more meaningful errors, but in samples with a limited range in Th* and Pb values, the slope may not cross the Y-axis near the origin, yielding an age dissimilar to the mean age of a sample. The weighted mean age for each sample was also calculated (Table 4-5).

CHAPTER 5

Deflation of the middle crust: evidence from the central Shuswap metamorphic complex, southeast Canadian Cordillera

Introduction

Orogenic collapse of the southeast Canadian Cordillera occurred during the Late Paleocene to Middle Eocene, resulting in the exhumation of high-grade metamorphic rocks and the formation of structural culminations collectively known as the Shuswap metamorphic complex (SMC). Northerly-striking, low-angle, brittle-ductile shear zones and brittle normal faults bounding the culminations have been interpreted as crustal-scale, large displacement detachments (e.g., Parrish et al. 1988). In those models, the middle crust is exhumed or "dragged out" from beneath a brittle upper plate during fault motion (cf. Lister and Davis 1989).

This chapter summarizes new geological mapping from the central Shuswap metamorphic complex, where a belt of greenschist-facies superstructure is preserved, overlying upper amphibolite-facies metamorphic infrastructure. The continuity of the superstructure, which extends from the western to eastern margin of the complex with limited gaps, is inconsistent with large-displacement detachment models. The discrepancy between the geological data and existing models suggests that the Late Cretaceous to Early Eocene tectonic evolution of the SMC needs to be re-examined. Based on this new mapping and existing metamorphic, structural, geochronological, and geophysical data, a new model for the exhumation of the middle crust is proposed whereby exhumation occurs through channel flow.

New geological mapping data from the Vernon area of the Shuswap metamorphic complex

The study area is located within the central SMC, between latitudes 50° and 51°N and longitudes 118°00' and 119°30' (Fig. 5-1). In this region, a nearly intact belt of greenschist-facies superstructure extends across the complex, from the Okanagan Valley on the west, to the Columbia River on the east.

The superstructure is separated from upper amphibolite-facies metamorphic infrastructure by low-angle Late Paleocene to Middle Eocene ductile shear zones and attenuated metamorphic sections (Chapter 2). The superstructure, which attained peak metamorphic conditions during the Middle Jurassic, has yielded Middle Jurassic to Late Cretaceous (K-Ar; hornblende and micas) cooling dates, whereas the underlying infrastructure, metamorphosed at amphibolite-facies during the Middle Jurassic to Late Cretaceous (Mathews 1981; Parrish 1995, and references therein; Chapter 4), has yielded Paleocene to Middle Eocene K-Ar and $^{40}Ar/^{39}Ar$ cooling dates (Mathews 1981; Vanderhaeghe et al. 2003). The infrastructure can be separated into Paleoproterozoic

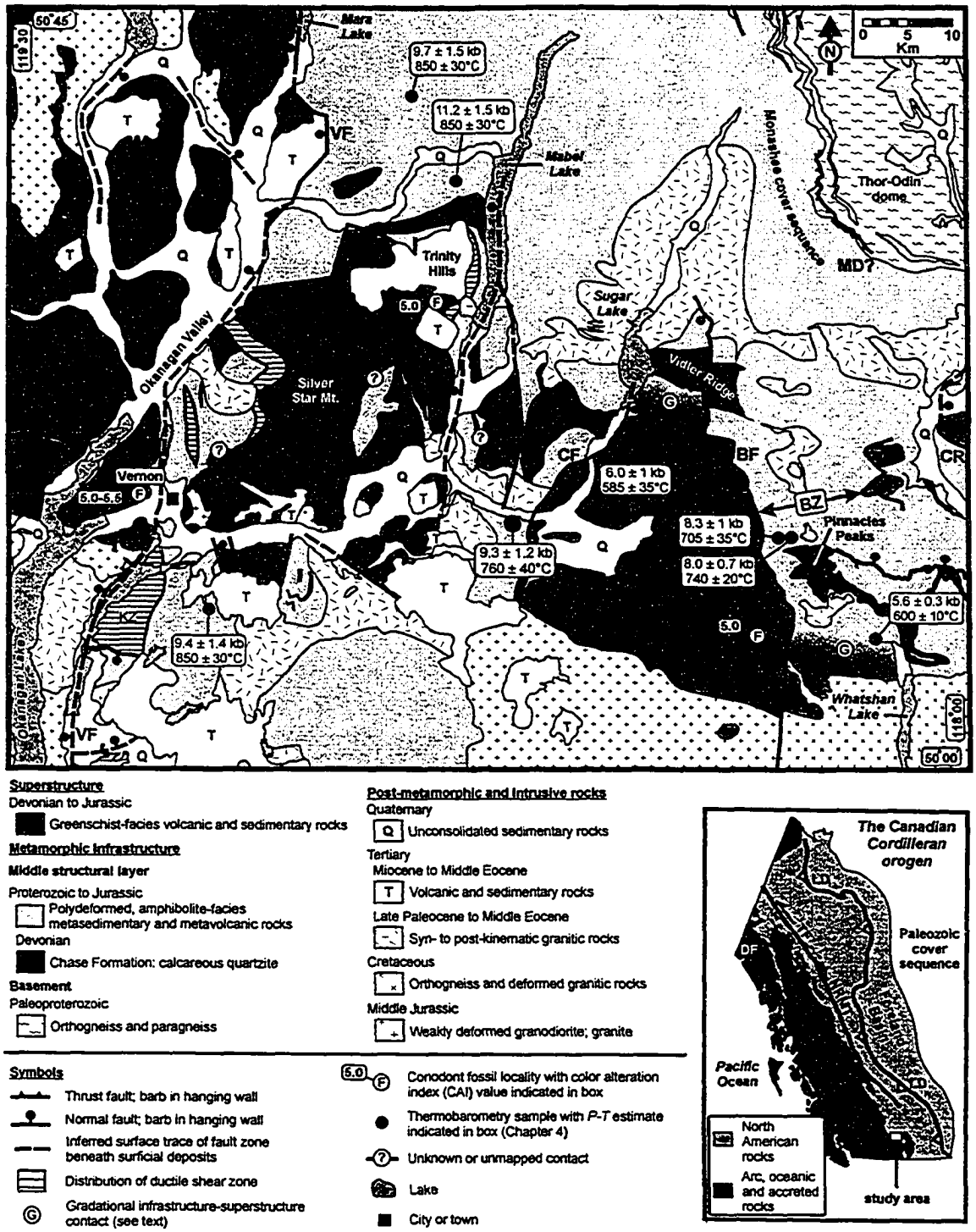

Fig. 5-1. Generalized tectonic map of the central Shuswap metamorphic complex showing the distribution of superstructure and metamorphic infrastructure and the location of major early Tertiary extension faults (modified from Fig. 4-2). *Abbreviations*: BF - Beaven fault; BZ -break-away zone (discussed in text); CF - Cherry fault; CR - Columbia River fault; KZ - Kalamalka Lake shear zone; MD - Monashee décollement; VF - Vernon fault. **Lower right:** Tectonic elements of the Canadian Cordillera (modified from Wheeler et al. 1991). Metamorphic data is from Chapter 4.

basement, such as the Thor-Odin dome of the southern Monashee complex, and the overlying 10-15 km thick middle structural layer, composed of upper amphibolite-facies Paleoproterozoic to Jurassic(?) metasedimentary and metavolcanic rocks. The middle structural layer is suffused with syn- to postkinematic Late Paleocene to Early Eocene granitic rocks, which are rare to absent within the superstructure and Paleoproterozoic basement (Carr 1992).

The superstructure belt that transects the Vernon area has been interpreted to lie within the upper plate of a crustal-scale, top to the west detachment, the northeastward extension of the Okanagan Valley fault (OVF; Carr 1990; Bardoux 1993). Estimates of top to the west displacement on the OVF vary from 30 km (Parrish et al. 1988; Johnson and Brown 1996) to 90 km (Tempelman-Kluit and Parkinson 1986). The moderately southwest-dipping Beaven fault, which crops out in the Pinnacles area (Fig. 5-1), has been inferred to be the easternmost surface trace, or near-surface breakaway of the OVF (Carr 1990). Estimates of dip-slip displacement on the east-dipping CRF, which bounds the eastern margin of the SMC, vary from 1-10 km (Lane 1984) to 20-40 km (Parrish et al. 1988; Parkinson 1992).

Three lines of evidence indicate that the infrastructure in the Vernon area was not exhumed by tectonic removal or thinning of the superstructure: (1) the superstructure is, to a large degree, still intact and lacks evidence of internal thinning by faulting; (2) despite the occurrence of diffuse ductile shear zones near the infrastructure-superstructure contact, a regionally continuous detachment fault is not evident; and (3) the base of the superstructure belt is subparallel to the orientation of lithostratigraphic units within the infrastructure across the complex.

The first point is evident from the continuity of superstructure across the Vernon area. Even without taking into account the effects of post-Middle Eocene erosion and (steep) normal faulting, the superstructure forms a nearly intact cover, directly overlying infrastructure rocks (Fig. 5-1). The widest horizontal gap in the superstructure, 12 km across, occurs between the traces of the Beaven and the Columbia River faults (Fig. 5-1). This 12 km gap has been interpreted as the locus of a "breakaway zone" between the oppositely-dipping Okanagan Valley and Columbia River extension faults (Fig. 5-1, labelled "BZ"; Carr 1990; Bardoux 1993). Palinspastic restoration of the proposed 30-90 km of displacement on the OVF (e.g., Tempelman-Kluit and Parkinson 1986) and 20-40 km of displacement on the CRF (e.g., Parkinson 1992), however, results in a combined 40-120 km of overlap between the fault traces. This inconsistency cannot be explained by internal thinning of the superstructure through faulting or multiple detachments, as such structures are lacking. Nor can different timing on the two faults explain the

map relationships, as this would strand the breakaway of the older fault in the upper plate of the younger fault.

The second line of evidence stems from the observation that the contact between superstructure and infrastructure is not a sharp detachment fault, but a gradational zone ~2 km thick, characterized by a complete, but attenuated metamorphic sequence with no sharp structural or metamorphic breaks. In some areas (Fig. 5-1, Silver Star Mountain, Trinity Hills) the transition is overprinted by a top to the west-directed ductile shear zone. In the Silver Star Mountain area, the ductile shear zone is approximately ~2 km thick and has gradational upper and lower boundaries (Chapters 2, 4). The upper boundary coincides with the uppermost occurrence of early Tertiary Ladybird granitic rocks. Conversely, in the Vidler Ridge and Pinnacles areas, no low-angle shear zones or detachment faults are evident. In these areas, the transition from superstructure to infrastructure is marked by a gradational zone with closely-spaced metamorphic isograds, but no evidence of non-coaxial shear (see Chapter 2). While in itself, these characteristics do not rule out a large-displacement, detachment model, a regionally extensive, detachment fault is lacking in the Vernon area. Where present, ductile shear zones differ from "classical" detachment faults described from other core complexes within western North America, such as the regionally extensive detachment faults present in core complexes of the southwest United States, such as in the Whipple Mountains (e.g., Lister and Davis 1989).

Lastly, at the regional scale, the superstructure-infrastructure contact is sub-parallel to lithostratigraphic units within the underlying infrastructure (Fig. 5-1). For instance, a distinctive map unit, the Devonian Chase Formation, is shown in Figure 5-1 (black shading). The Chase Formation is not repeated by folding or thrusting at the regional scale and is exposed from the eastern to western margin of the complex within the study area, directly underlying the superstructure (Fig. 5-1; Thompson et al. 2002). Examination of the map patterns reveal that the superstructure-infrastructure contact is subparallel to the Chase Formation from east to west, across the complex, parallel to the extension direction. In other words, the infrastructure-superstructure contact does not cut down-section across a distance of over 80 km measured parallel to the dominant extension direction, an observation that is inconsistent with the contact being a crustal-scale shear zone that cuts down through the crust.

It is possible that the contact was rotated to the horizontal during or after displacement, such as in a rolling hinge-type detachment model (e.g., Axen and Bartley 1997). Such a model, however, predicts attenuation and rotation of the superstructure through faulting, which is not supported by mapping of the superstructure. Another possibility is that the shear zone developed parallel to the Chase Formation, with an initial dip of ~30° to the west, and was later rotated to

the horizontal (e.g., see Parrish et al. 1988; Johnson and Brown 1996). If this occurred, western exposures of the superstructure would have been buried 35 to 40 km deeper than the easternmost exposures. This is not supported by similar metamorphic grades and identical conodont CAI values of 5.0-5.5 across the base of the superstructure (Fig. 5-1). The implication is that infrastructure-superstructure contact was initiated in a sub-horizontal orientation.

Deflation of the Canadian Cordillera

Map patterns from the study area indicate that infrastructure, metamorphosed at upper amphibolite conditions during the Late Cretaceous (e.g., Parrish 1995; Chapters 3, 4), was not exhumed by removal of the overlying superstructure, in that the superstructure is still largely intact. Clearly, an alternative mechanism is required to explain the juxtaposition of upper amphibolite-facies infrastructure and greenschist-facies superstructure across the study area.

Paleorheological modelling studies of the southern Canadian Cordillera during the Late Cretaceous to Paleocene (e.g., Lowe and Ranalli 1993) have calculated that the strength of the crust was limited to the upper 10 km during the Late Cretaceous to Early Eocene (Fig. 5-2*a*). This temperature-dependent relationship would be amplified by the large amount of Late Paleocene to Early Eocene granitic rocks within the infrastructure (e.g., Carr 1992; Vanderhaeghe et al. 1999). Another rheological interface is proposed to have been present at the contact between the melt-rich middle structural layer and the relatively competent Paleoproterozoic basement of the Monashee complex, which was only weakly overprinted by Cordilleran tectonism at its deepest exposed structural level (Fig. 5-2*b*; Crowley et al. 2001). The implication of the paleorheological strength profile is that the bulk of Late Cretaceous to Early Eocene strain would have been accommodated by the 10-15 km weak middle structural layer sandwiched between the strong upper crust (superstructure) and melt-deficient Paleoproterozoic basement (Glombick et al. 2002).

Comparisons with coupled thermal-mechanical modeling experiments of large convergent orogens

Recent investigations into the complex interaction between crustal thickening, metamorphism, partial melting, and orogenic evolution using wedge-type, coupled thermal-mechanical models have provided insight into the role of the ductile middle crust during orogenesis (e.g., Jamieson et al. 2002; Beaumont et al. 2004). The models suggest that in large, convergent orogens, a channel of low-viscosity (partially molten) rock may develop and flow towards the foreland side of the model in response to a gradient in gravitational potential energy.

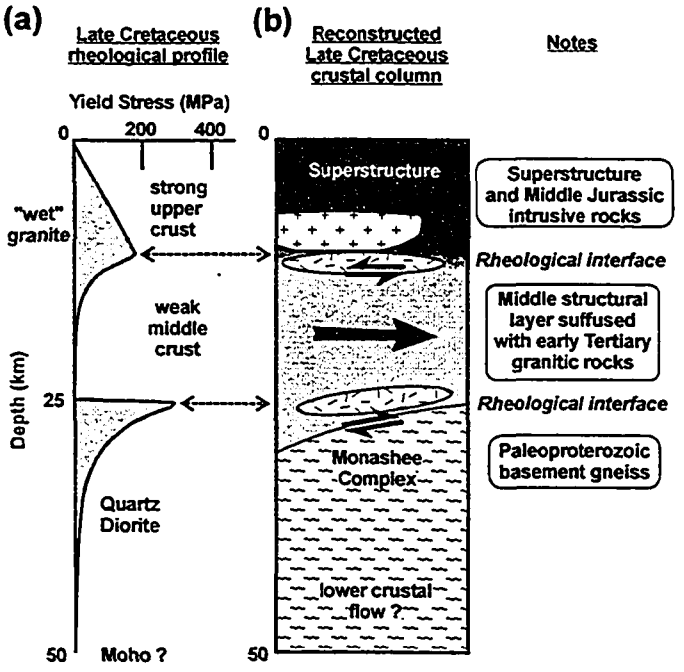

Fig. 5-2. (a) Schematic paleorheological strength profile of the southeast Canadian Cordillera in the Late Cretaceous to Early Paleocene (modified from Dunbar and Sawyer 1989). Upper 25 km of the crust is approximated using a wet granite model, while the lower 25 km uses quartz diorite. (b) Reconstructed Late Cretaceous to Early Paleocene crustal column of the southeast Canadian Cordillera.

Lateral spreading of the orogen occurs by "tunnelling" of weak, partially molten rocks within a zone of channel flow.

Metamorphic and geochronological data from the southeast Canadian Cordillera suggest that the crust was 50-60 km thick in the late Cretaceous to Paleocene (Coney and Harms 1984; Parrish 1995). Based on hydrogen isotopes from muscovite from high strain zones, Mulch et al. (2004) have suggested that Early Eocene paleoelevations in the Vernon area were ~4000-4300 m, consistent with high elevations and thick crust. The abundance of granitic rocks of Late Paleocene to Early Eocene age within the infrastructure indicates that the middle structural layer contained a melt fraction of ~30% during this time (e.g., Reesor and Moore 1971; Carr 1992), consistent with crustal thickness of 50-60 km (Patiño Douce et al. 1990). A plateau 50-60 km thick underlain by a partially molten middle crust may have extended from near the Fraser River fault (e.g., see Erdmer et al. 2002) to the Kootenay arc, a distance of over 300 km.

Mapping data from the Vernon area indicates that the superstructure is largely still intact. Yet underlying infrastructure rocks with Late Cretaceous (peak) metamorphic ages record maximum *P-T* estimates compatible with burial depths of 25-30 km (Fig. 5-1). Insight into this apparent paradox can be gained from examining Lithoprobe seismic reflection profiles through the study area (Fig. 5-3; Cook et al. 1992). A composite profile of lines 7-9 reveals a series of west-dipping reflectors that persist into the lower crust (e.g., Cook et al. 1992). This series of reflectors forms a (south?)west-facing ramp with nearly 20 km of amplitude (Fig. 5-3). The Monashee complex does not contain any evidence of Cordilleran-related metamorphism prior to the Paleocene to Eocene time (e.g., Parrish 1995) which precludes the Monashee complex from being buried beneath infrastructure rocks while they were metamorphosed during the Early to Late Cretaceous (see also Gibson 1999; Crowley et al. 2001).

A possible solution is that infrastructure rocks of the middle structural level were tectonically emplaced above the lower structural level rocks of the Monashee complex during the Late Paleocene to Middle Eocene, resulting in a brief period of metamorphism coeval with exhumation and cooling of overlying infrastructure rocks. This is possible by either thrusting on a Monashee décollement (Gibson et al. 1999; Crowley et al. 2001), or east-directed channel flow of the middle crust (Glombick et al. 2002). The primary difference between these models is whether the upper crust (superstructure) is carried in a passive manner in the upper plate of the décollement, or the middle crust flows east relative to both the overlying upper crust and underlying basement. In either case, rocks within the zone of channel flow would be forced up the basement (Monashee) ramp, where they would be "squeezed" between the overlying crust and the Monashee complex. The paleorheological modelling predicts that the middle crust, as the weakest

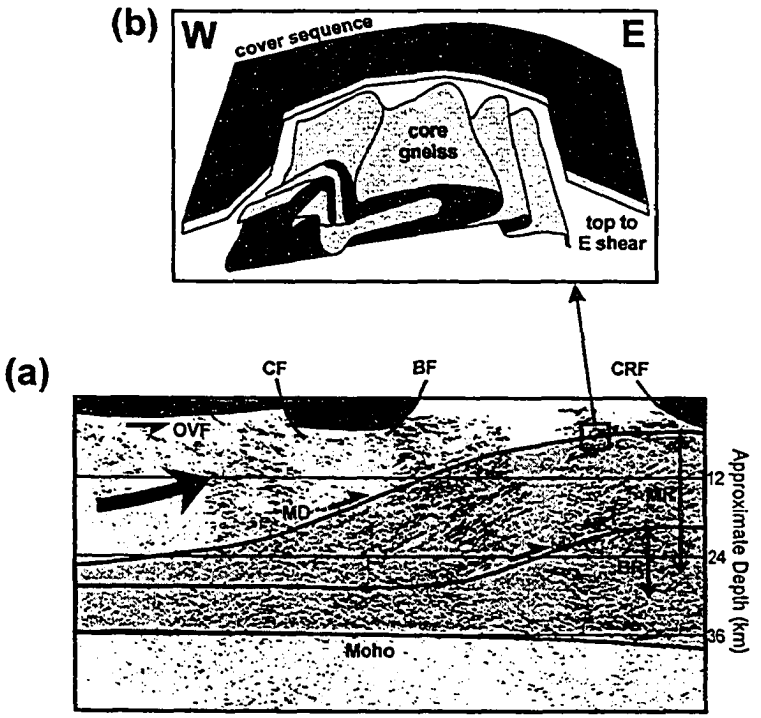

Fig. 5-3. (a) Interpreted Lithoprobe seismic reflection profiles 7 to 9 from the southern Canadian Cordillera showing extent of proposed channel flow. Light grey shading indicates autochthonous and allochthonous North American basement rocks. The middle structural layer, the proposed zone of channel flow, is shaded white. Superstructure is shaded dark grey. *Abbreviations*: BF - Beaven fault; BR - basement ramp; CF - Cherry fault; CRF - Columbia River fault; MD - Monashee décollement; MR: Monashee ramp; OVF - Okanagan Valley fault. Large black arrow indicates direction of inferred channel flow. (b) Schematic diagram showing the difference in structural style between the Thor-Odin dome of the Monashee complex and the overlying middle structural layer (modified from Spark [2002]).

layer, would accommodate the strain during attenuation and thinning. Such thinning of the middle crust is clearly evident in the Thor-Odin dome, where an upwards structural transition from complex structure preserved within the Paleoproterozoic basement to the pervasive east-west stretching of the overlying dominantly metasedimentary cover succession of the middle structural layer is clearly evident (Fig. 5-3; Reesor and Moore 1971; Spark 2002). The relief on the Monashee ramp is mirrored by a change thickness of middle structural layer, the inferred zone of channel flow (Fig. 5-3).

If mid-crustal rocks were exhumed during Late Cretaceous to Early Eocene channel flow up a ramp, coeval non-coaxial strain fabrics with opposite shear-sense would characterize the upper and lower boundaries of that channel. Carr (1992) bracketed the timing of top to the east shearing at interface between the Thor-Odin dome and the middle structural layer at 59-58 Ma, although Crowley et al. (2001) demonstrated that ductile boudinage of deeper levels of the northern Monashee complex, associated with D_2 east-west stretching, continued until 51-49 Ma. Geochronology from synkinematic granitic rocks within ductile shear zones at the infrastructure-superstructure contact in the Vernon area, the proposed upper boundary of the channel, indicate that a component of top to the west, non-coaxial strain occurred between 60 and 48 Ma (Mathews 1981; Vanderhaeghe et al. 1999). Latest motion on the top to the west-directed Kalamalka Lake shear zone, part of the Okanagan Valley fault system, is constrained between 50 and 48 Ma (Fig. 5-1; Heaman et al. 1999). Consequently, geochronological data from synkinematic coeval granitic rocks with opposite shear-sense situated along the upper and lower boundaries of the proposed zone of channel flow support a channel flow model for the central SMC during Late Paleocene to Eocene time. The duration of channel flow and mid-crustal thinning in the southern Canadian Cordillera is unknown, but it may have been occurring during the Cretaceous (see Scammell 1993) and accelerated during Paleocene to Early Eocene melting of the middle structural layer.

Conclusions

Geological data from the Vernon area of the central SMC are consistent with ductile shear zones between superstructure and infrastructure developing along a rheological interface between partially molten mid-crustal rocks and cool superstructure at the upper boundary of a zone of channelized flow in the Late Paleocene to Early Eocene, rather than as crustal-scale detachments. This is supported by paleorheological modelling of the hinterland, which suggests that the crust was rheologically stratified during the Late Cretaceous to Early Eocene with a strong upper crust, a weak middle structural layer, and relatively competent Paleoproterozoic basement. Comparisons of geological data with coupled thermal-mechanical models of large, hot

convergent orogens indicates that geological, structural, and metamorphic data in the Vernon area are best explained by a channel flow model. Upward flow of the middle structural layer up a ramp in underlying Paleoproterozoic basement caused exhumation, decompression melting, thinning of the channel above the ramp, and brief (1-2 m.y.) metamorphism of the underlying basement.

References

Axen, G.J., and Bartley, J.M. 1997. Field tests of rolling hinges; existence, mechanical types, and implications for extensional tectonics. Journal of Geophysical Research, B, Solid Earth and Planets, **102**: 20515-20537.

Bardoux, M. 1993. The Okanagan Valley fault from Penticton to Enderby, south-central British Columbia. Ph.D. thesis, Carleton University, Ottawa.

Beaumont, C., Jamieson, R.A., Nguyen, M.H., and Medvedev, S. 2004. Crustal channel flows: 1. Numerical models with applications to the tectonics of the Himalayan-Tibetan orogen. Journal of Geophysical Research, **109**: B06406, dio:10.1029/2003JB002809.

Carr, S.D. 1990. Late Cretaceous-early Tertiary tectonic evolution of the southern Omineca Belt, Canadian Cordillera. Ph.D. thesis, Carleton University, Ottawa.

Carr, S.D. 1992. Tectonic setting and U-Pb geochronology of the early Tertiary Ladybird leucogranite suite, Thor-Odin-Pinnacles area, southern Omineca Belt, British Columbia. Tectonics, **11**: 258-278.

Coney, P.J., and Harms, T.A. 1984. Cordilleran metamorphic core complexes: Cenozoic extensional relics of Mesozoic compression. Geology, **12**: 550-554.

Cook, F.A., Varsek, J.L., Clowes, R.M., Kanasewich, E.R., Spencer, C.S., Parrish, R.R., Brown, R.L., Carr, S.D., Johnson, B.J., and Price, R.A. 1992. Lithoprobe crustal reflection cross section on the southern Canadian Cordillera, 1, Foreland Thrust and Fold Belt to Fraser River fault. Tectonics, **11**: 12-35.

Crowley, J.L., Brown, R.L., and Parrish, R.R. 2001. Diachronous deformation and a strain gradient beneath the Selkirk allochthon, northern Monashee complex, southeastern Canadian Cordillera: Journal of Structural Geology, **23**: 1103-1121.

Dunbar, J.A., and Sawyer, D.S. 1989. How preexisting weaknesses control the style of continental breakup. Journal of Geophysical Research, B, Solid Earth and Planets, **94**: 7278-7292.

Erdmer, P., Moore, J.M., Heaman, L.M., Thompson, R.I., Daughtry, K.L., and Creaser, R.A. 2002. Extending the ancient margin outboard in the Canadian Cordillera; record of Proterozoic crust and Paleocene regional metamorphism in the Nicola horst, southern British Columbia. Canadian Journal of Earth Sciences, **39**: 1605-1623.

Gibson, H.D., Brown, R.L., and Parrish, R.R. 1999. Deformation-induced inverted metamorphic field gradients: an example from the southeastern Canadian Cordillera. Journal of Structural Geology, **21**: 751-767.

Glombick, P., Thompson, R.I., and Erdmer, P. 2002. The role of a melt-rich middle crust layer in core complex formation; evidence from the Shuswap metamorphic complex, south-central British Columbia. *In* Abstracts with Programs, Geological Society of America, 2002 annual meeting, p. 109.

Heaman, L.M., Erdmer, P., Thompson, R.I., and Daughtry, K.L. 1999. Preliminary U-Pb geochronology results from the Vernon area, British Columbia. *In* Proceedings, Lithoprobe Report No. 69: Cordilleran Tectonics Workshop, Calgary, Alberta, pp. 196-201.

Jamieson, R.A., Beaumont, C., Nguyen, M.H., and Lee, B. 2002. Interaction of metamorphism, deformation, and exhumation in large convergent orogens. Journal of Metamorphic Geology, **20**: 1-16.

Johnson, B.J., and Brown, R.L. 1996. Crustal structure and early Tertiary extensional tectonics of the Omineca belt at 51°N latitude, southern Canadian Cordillera. Canadian Journal of Earth Sciences, **33**: 1596-1611.

Lane, L.S. 1984. Brittle deformation in the Columbia River fault zone near Revelstoke, southeastern British Columbia. Canadian Journal of Earth Sciences, **21**: 584-598.

Lister, G.S., and Davis, G.A. 1989. The origin of metamorphic core complexes and detachment faults formed during Tertiary continental extension in the northern Colorado River region, U.S.A. Journal of Structural Geology, **11**: 65-94.

Lowe, C., and Ranalli, G. 1993. Density, temperature, and rheological models for the southeastern Canadian Cordillera: implications for its geodynamic evolution. Canadian Journal of Earth Sciences, **30**: 77-93.

Mathews, W.H. 1981. Early Cenozoic resetting of potassium-argon dates and geothermal history of north Okanagan area, British Columbia. Canadian Journal of Earth Sciences, **18**: 1310-1319.

Mulch, A., Teyssier, C., Cosca, M.A., Vanderhaeghe, O., and Vennemann, T.W. 2004. Reconstructing paleoelevation in eroded orogens. Geology, **32**: 525-528.

Parkinson, D.L. 1992. Age and tectonic evolution of the southern Monashee Complex, southeastern British Columbia: a window into the deep crust. Ph.D. thesis, University of California, Santa Barbara.

Parrish, R.R. 1995. Thermal evolution of the southeastern Canadian Cordillera. Canadian Journal of Earth Sciences, **32**: 1618-1642.

Parrish, R.R., Carr, S.D., and Parkinson, D.L. 1988. Eocene extensional tectonics and geochronology of the southern Omineca Belt, British Columbia and Washington. Tectonics, **7**: 181-212.

Patiño Douce, A.E., Humphreys, E.D., and Johnston, A.D. 1990. Anatexis and metamorphism in tectonically thickened continental crust exemplified by the Sevier hinterland, western North America. Earth and Planetary Science Letters, **97**: 290-315.

Reesor, J.E., and Moore, J.M. 1971. Petrology and structure of the Thor-Odin gneiss dome, Shuswap metamorphic complex, British Columbia. Geological Survey of Canada Bulletin 195.

Scammell, R.J. 1993. Mid-Cretaceous to Tertiary thermotectonic history of former mid-crustal rocks, southern Omineca Belt, Canadian Cordillera. Ph.D. thesis, Queen's University, Kingston, Ontario.

Spark, R.N. 2002. Crustal thickening and tectonic denudation within the Thor-Odin culmination, Monashee complex, southern Canadian Cordillera. Ph.D. thesis, University of New Brunswick, Fredericton.

Tempelman-Kluit, D., and Parkinson, D. 1986. Extension across the Eocene Okanagan crustal shear in southern British Columbia. Geology, **14**: 318-321.

Thompson, R.I., Glombick, P., Acton, S., Heaman, L., Friedman, R., Daughtry, K.L., Erdmer, P., and Paradis, S. 2002. New constraints on the age and distribution of the Chase Quartzite, Vernon (82L) and Lardeau (82K) map areas: regional implications. *In* Proceedings, Cordilleran Tectonics Workshop, Lithoprobe Report no. 82, pp. 92-94.

Vanderhaeghe, O., Teyssier, C., and Wysoczanski, R. 1999. Structural and geochronological constraints on the role of partial melting during the formation of the Shuswap metamorphic core complex at the latitude of the Thor-Odin dome, British Columbia. Canadian Journal of Earth Sciences, **36**: 917-943.

Vanderhaeghe, O., Teyssier, C., McDougall, I., and Dunlap, W.J. 2003. Cooling and exhumation of the Shuswap Metamorphic Core Complex constrained by 40Ar/39Ar thermochronology. Geological Society of America Bulletin, **115**: 200-216.

Wheeler, J.O., Brookfield, A.J., Gabrielse, H., Monger, J.W.H., Tipper, H.W., and Woodsworth, G.J. (compilers). 1991. Terrane map of the Canadian Cordillera. Geological Survey of Canada, Map 1713A, scale 1:2 000 000.

CHAPTER 6

Conclusions

This chapter summarizes the implications of this thesis for the Mesozoic to Cenozoic tectonic evolution of the central Shuswap metamorphic complex (SMC) and the southeastern Canadian Cordillera. Due to the paper format used in this thesis, data is compartmentalized into separate subjects (e.g., structural geology, geochronology, metamorphic petrology) to facilitate publication. This chapter is intended to review the salient points from each chapter and discuss their significance for various aspects of Cordilleran evolution. Readers are encouraged to seek out additional geological mapping, structural, geochronological, and metamorphic data from the relevant chapter, appendix, or geological map.

The significance of early Tertiary low-angle shear zones within the study area

Perhaps the most fundamental conclusion of this study is that early Tertiary low-angle shear zones exposed along the western margin of the SMC between latitudes 50°00' and 50°45'N are not crustal-scale detachments, as previously proposed (Fig. 6-1; see Parrish et al. 1988 for a discussion of this model). This conclusion stems from four main observations, based on detailed (1:20 000 to 1:50 000 scale) bedrock mapping (Glombick et al. 2004; Glombick and Thompson 2004; Thompson 2004*a*; 2004*b*; Thompson and Glombick 2004*a*, 2004*b*; Thompson et al. 2004*a*; 2004*b*; Thompson and Unterschutz 2004) and geometrical arguments (presented in Chapter 2, see discussion): (1) the continuity of a belt of greenschist-facies superstructure across the complex, trending approximately perpendicular to the dominant extension direction; (2) the lack of internal thinning of superstructure by internal faulting; (3) the transitional zone between infrastructure and superstructure and the lack of detachment faults (*sensu stricto*) within that zone; and (4) the parallel orientation between the transitional contact between infrastructure and superstructure and lithostratigraphic units within underlying middle structural layer across the complex, a distance of approximately 80 km, measured parallel to the syn-extensional early Tertiary stretching lineation, essentially ruling it out as a significant crustal-scale normal fault that cuts through the crustal column (Fig. 6-2).

The first observation is demonstrated by the extent and continuity of superstructure between latitudes 50°00' and 50°45'N and the Okanagan and Columbia River valleys (Fig. 6-2). Although there are gaps within the superstructure, the sum of the gaps equals the total displacement possible on any proposed extension fault or shear zone near the base of the superstructure. This is a maximum estimate, as it does not account for post-Early Eocene normal

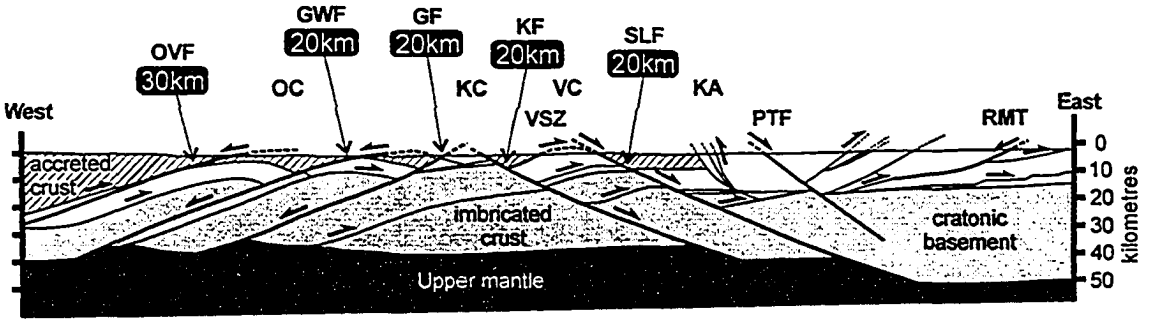

Fig. 6-1. Simplified interpreted geological cross section through the southern Shuswap metamorphic complex (after Parrish et al. 1988) depicting early Tertiary extension faults as large-displacement, crustal-scale shear zones that penetrate into the upper mantle. The amount of fault displacement (in kilometers) for individual faults (from Parrish et al. 1988) is indicated in the black boxes. Some estimates of displacement on the OVF are as high as 90 km (e.g., Tempelman-Kluit and Parkinson 1986). *Abbreviations*: GF - Granby fault; GWF - Greenwood fault; KA - Kootenay Arc; KC - Kettle complex; KF - Kettle fault; OC - Okanagan complex; OVF - Okanagan Valley fault; PTF - Purcell Trench fault; RMT - Rocky Mountain Trench; SLF - Slocan Lake fault; VC - Valhalla complex; VSZ - Valhalla shear zone. Early Tertiary extension faults are shown as heavy black lines. Early Proterozoic crust is shaded light grey. Middle Proterozoic to Jurassic pericratonic rocks are shaded white. Accreted rocks are shaded with horizontal striped pattern. Plutonic rocks have been omitted for clarity.

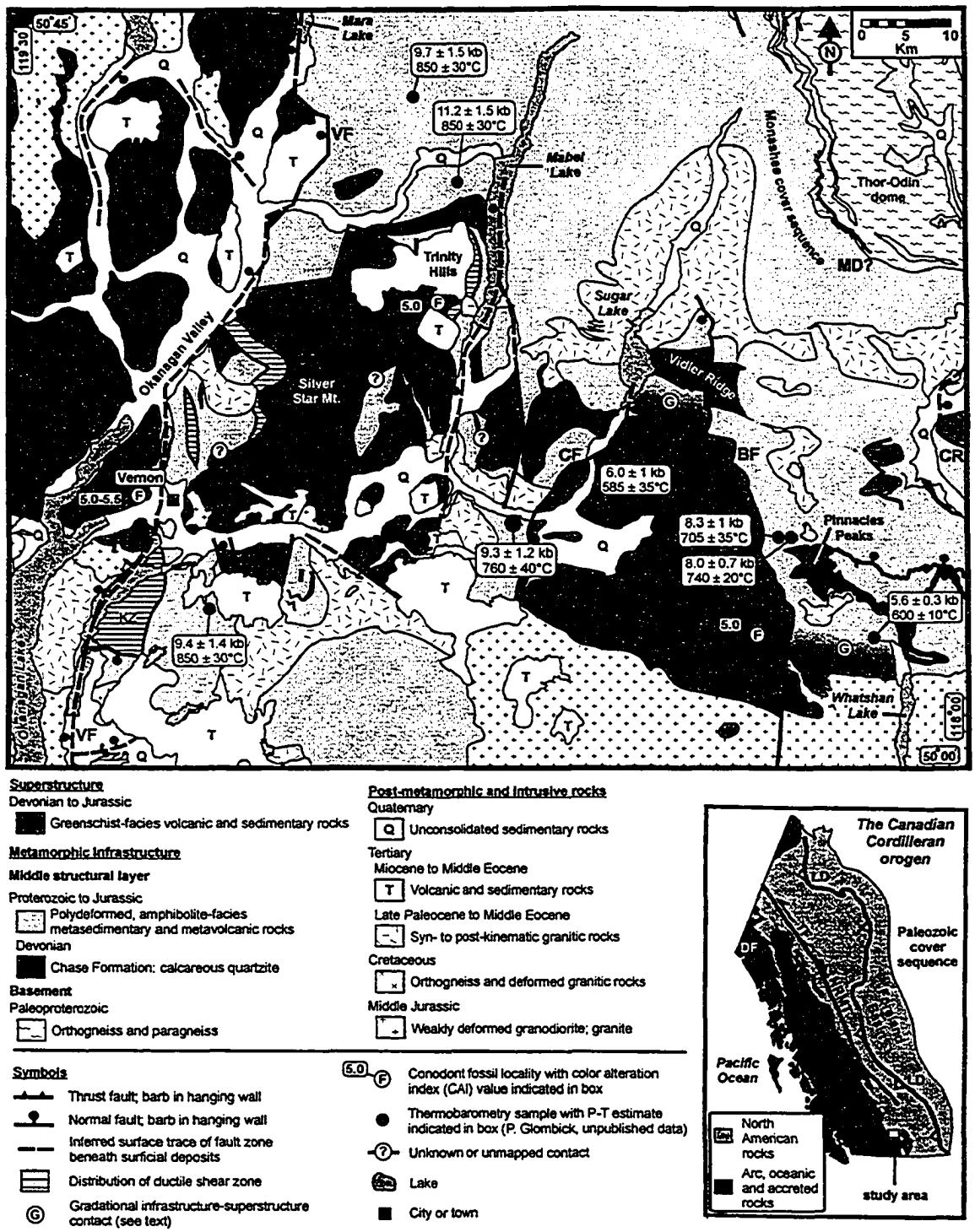

Fig. 6-2. Generalized tectonic map of the central Shuswap metamorphic complex showing the distribution of suprastructure and metamorphic infrastructure and the location of major early Tertiary extension faults (modified from Fig. 4-2). *Abbreviations*: BF - Beaven fault; CF - Cherry fault; CR - Columbia River fault; KZ - Kalamalka Lake shear zone; MD - Monashee décollement; VF - Vernon fault. **Lower right:** Tectonic elements of the Canadian Cordillera (modified from Wheeler et al. 1991). Metamorphic data is from Chapter 4.

faulting and erosion of the superstructure. In addition to normal erosion between the Middle Eocene and the present, the study area was incised by Pleistocene ice sheets that covered the Thompson plateau (e.g., Fulton and Halstead 1972), sculpting parallel ridges and grooves into the underlying bedrock. These ice sheets presumably preferably eroded less resistant bedrock, such as non-crystalline, greenschist-facies superstructure rocks such as phyllite, argillite, and limestone. Glacially-carved, southwest-trending ridges and intervening troughs are clearly visible in the present-day topography of the Thompson Plateau southeast of Vernon, where Pleistocene and post-Pleistocene erosion has partially eroded Miocene flood basalts, Middle Eocene to Oligocene volcanic and sedimentary rocks, and underlying bedrock (Glombick et al. 2004). If the effects of post-Middle Eocene faulting and erosion are considered, it is inferred that the gaps within the superstructure were minor between the Okanagan Valley and the Columbia River during the Early to Middle Eocene, implying that superstructure was essentially continuous across the complex. Some infrastructure rocks were exposed at surface by Middle Eocene time, as they are locally unconformably overlain by Middle Eocene (~42-49 Ma) volcanic and sedimentary rocks (e.g., Mathews 1981). Map patterns in the Trinity Hills area and elsewhere indicate that steep faults of Middle Eocene age were instrumental in controlling the localized uplift and exhumation of infrastructure. As many Middle Eocene faults are estimated to have minor (1-5 km) heaves (Fig. 6-3; e.g., Thompson and Daughtry 1996), the superstructure was likely relatively thin (5-10 km) in the Middle Eocene, consistent with Middle Jurassic to Late Cretaceous biotite K-Ar dates from the superstructure, indicating temperatures less than 250°C (e.g., Mathews 1981).

Between the Okanagan Valley and Columbia River fault, the largest gap in the superstructure occurs in the Pinnacles area, between the surface trace of the Beaven fault and two greenschist-facies outliers of the Slocan Group, a distance of 12 km (Fig. 6-2; Chapter 2). The Beaven fault has been proposed by a number of authors (e.g., Carr 1990, Bardoux 1993) to be the westernmost surface trace of the Okanagan Valley detachment system, while the Slocan Group outliers have been interpreted as klippe of the Columbia River fault (Read and Brown 1981; Carr 1990). The gap of 12 km is an inadequate distance to accommodate displacement on two oppositely dipping extension faults with proposed estimates of combined displacement between 40-130 km (Chapter 2, see discussion).

One method of accommodating a large magnitude of displacement on two oppositely-dipping extension faults with surfaces traces separated by a short distance is by internal thinning and extension of the upper plate by a series of domino-style faults that root into a master detachment (e.g., Gross and Hillemeyer 1982; Lister and Davis 1989). This style of faulting was not observed within the superstructure within the study area. Although structural markers are

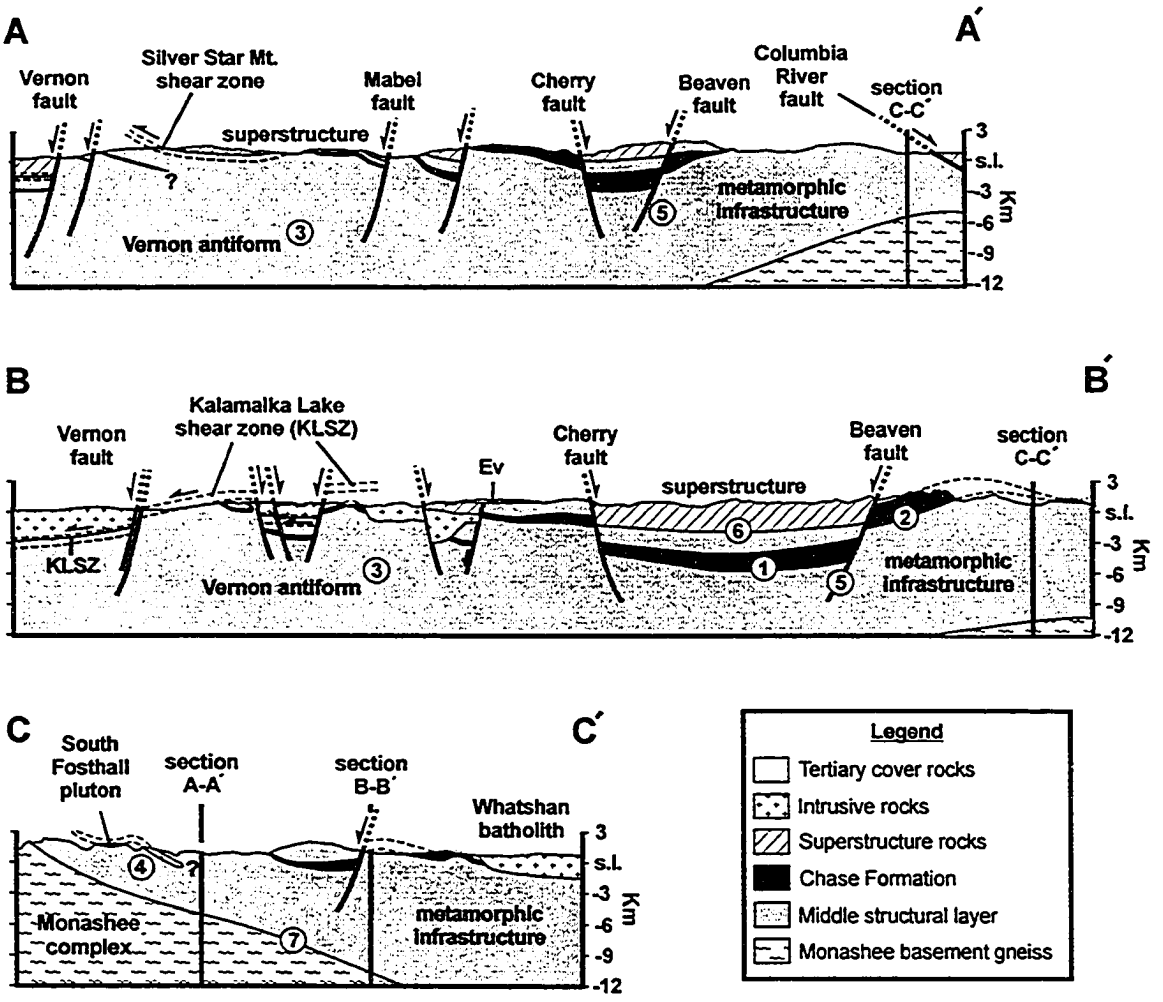

Fig. 6-3. Generalized geological cross sections through the Vernon area. The large, capital bold letters in Fig. 6-2 indicates the location of the section lines. No vertical exaggeration. *Abbreviations*: s.l. - sea level. *Notes:* (1) The Chase Formation is shown as a gently-dipping sheet in the sub-surface on the basis of surface map patterns (Fig. 6-2). (2) This structure is interpreted as a broad, west-trending antiform, with the northern limb down-dropped by a steep normal fault, rather than a map-scale recumbent isoclinal fold (e.g., Carr 1990), on the basis of detailed geological mapping in this area (see Lemieux et al. 2003; Thompson et al. 2004*a*). (3) The Vernon antiform is a domal series of reflectors visible at upper to mid-crustal depths near Vernon (Fig. 4-20*b*; Cook et al. 1992). (4) The geometry of the South Fosthall pluton in the subsurface is not well constrained. (5) The Beaven fault cuts the contact between infrastructure and superstructure, and therefore cannot be the "breakaway" of an Okanagan Valley-Eagle River detachment fault system. Middle Eocene steeply-dipping normal faults are inferred to root into the Middle Eocene brittle-ductile transition. (6) While this line is shown as a sharp contact in the sections, it is transitional in the field, occurring over a structural thickness of 1-2 km (see text). (7) Basement-cover contact is drawn parallel to south-dipping reflectors are visible in Lithoprobe line 6.

admittedly rare within the superstructure and exposure is poor locally, normal faults cut both superstructure and infrastructure, and therefore cannot root into a basal detachment at the base of the superstructure (Figs. 6-2, 6-3). In addition, pervasive extension should be apparent at all scales, from the regional map to the thin section. Evidence of thinning within the superstructure is lacking and structures are indicative of shortening, likely of Middle Jurassic age (e.g., Chapter 3). Lister and Davis (1989) state, "In all of the core complexes, the upper plate (above the detachment fault) is intensely fractured. It has clearly been subjected to significant horizontal extension, utilizing multiple generations of high-angle normal faults, some of which now have shallow-dipping orientations." This style of deformation is not developed within the superstructure in the study area. Multiple generations of high-angle normal faults within the superstructure are absent. In summary, the pervasive faulting and significant amount of extension developed within the upper plate of metamorphic core complexes within the western United States is absent from the superstructure within the study area.

Detailed geological mapping near the base of the superstructure failed to locate detachment faults similar to regionally extensive detachment faults exposed in the Whipple Mountains and other core complexes located within the western United States (e.g., Crittenden et al. 1980, and references therein; Davis et al. 1986; Lister and Davis 1989). Tempelman-Kluit and Parkinson (1986) reported fractured and faulted zeolite-facies volcanic rocks overlying retrogressed mylonitic gneiss above a discrete (detachment) fault in the southern Okanagan Valley. Bardoux (1993) inferred detachment faults to bound the base of several Middle Eocene volcanic outliers of the Marron Formation (~52 Ma) in the Kelowna area, although an exposed contact or detachment fault was never described. Conglomerate units located at the base of several outliers of the Marron Formation east of Kelowna contain gneissic cobbles, similar in character to the underlying basement, which suggests, but does not prove the existence of an unconformable contact (Bardoux 1985, 1986; Okulitch 1987, and references therein; P. Erdmer and R.I. Thompson, unpublished data).

Within the study area, the contact between superstructure and infrastructure was found to be transitional in nature. This transition is best exposed along a system of cross-country ski trails approximately 15 km northeast of Vernon, several kilometres west of the summit of Silver Star Mountain within the Sovereign Lakes ski area, where the transition between upper amphibolite-facies rocks of the Silver Creek Formation and greenschist-facies rocks of the Slocan Group occurs (Fig. 6-4). The transition from the Silver Creek Formation to the Slocan Group coincides with a ductile shear zone characterized by diffuse boundaries and heterogeneously distributed strain (for a full description of the shear zone and metamorphic transition, see Chapters 2 and 4,

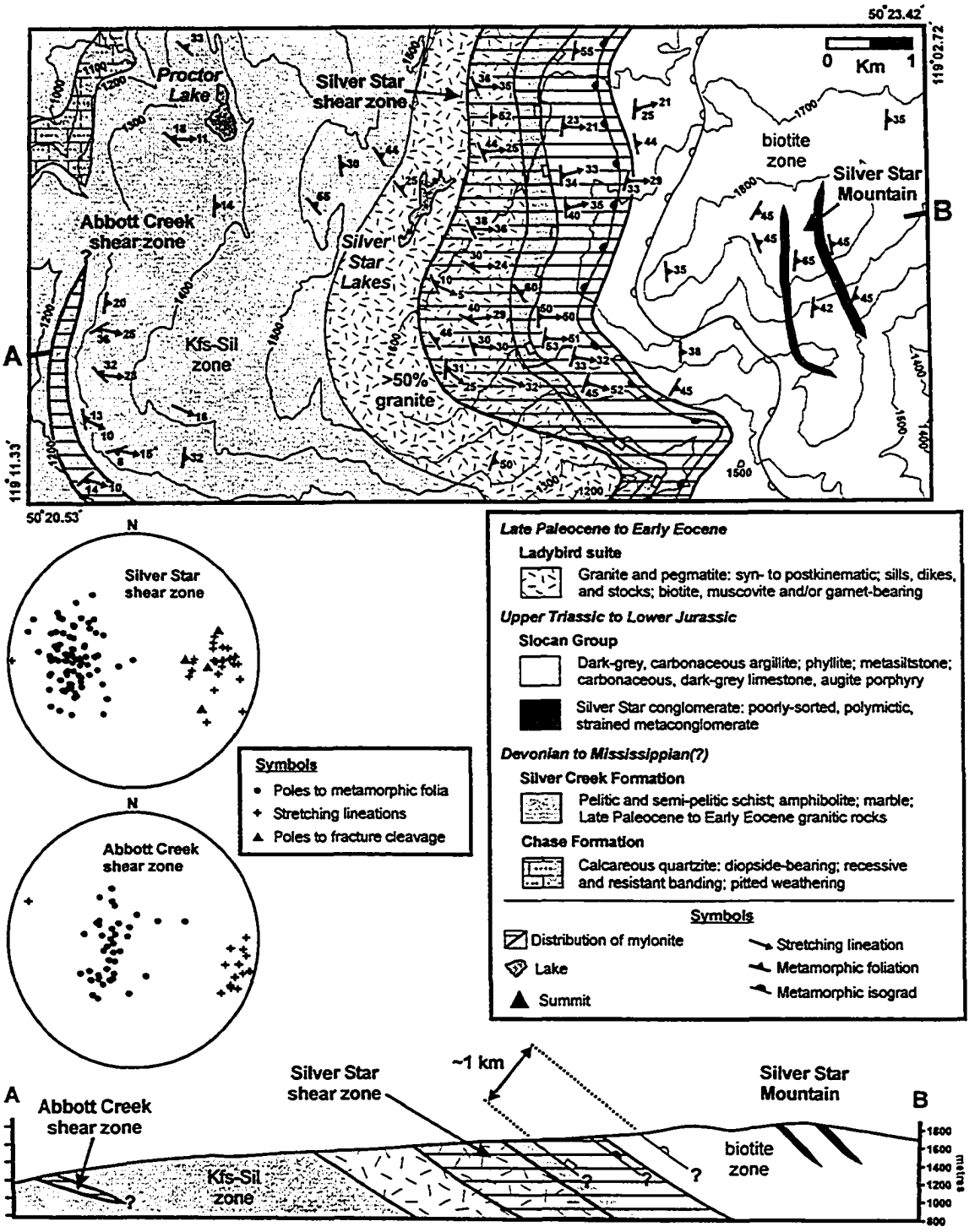

Fig. 6-4. Simplified geological map and cross section of the Silver Star Mountain area showing the distribution of metamorphic isograds, metamorphic zones, and mylonitic fabric. Elevation contours drawn as thin solid black lines. Elevations in metres above sea level. Fabric data from is plotted on lower hemisphere, equal-area projections (lower left). Mineral isograds as per Fig. 4-6. Mineral abbreviations after Kretz (1983).

respectively). Synkinematic granitic rocks of inferred early Tertiary age (55-62 Ma) that occur within the shear zone consistently yield top-to-the-west shear-sense. The transition from amphibolite-facies (sillimanite zone) metamorphic infrastructure to greenschist-facies (biotite zone) superstructure appears to be gradual, occurring across a zone ~2 km thick (measured perpendicular to the metamorphic foliation), without an abrupt increase in metamorphic grade (Fig. 6-4). The increase in metamorphic grade appears to be gradual, with the garnet, staurolite-kyanite, and sillimanite-in isograds present. A sharp break between upper amphibolite and greenschist-facies rocks, or a detachment fault (*sensu stricto*), was not found anywhere within the Silver Star Mountain area or the entire study area. A brittle overprint of ductile shear fabrics, common in most detachment fault systems (e.g., Lister and Davis 1989) is lacking within the Silver Star shear zone, although brittle fractures are developed at upper levels of the zone, at lower (garnet and biotite zone) metamorphic grades.

At the regional scale, the transition between metamorphic infrastructure and superstructure is oriented approximately sub-parallel to lithostratigraphic units within the underlying middle structural layer, a relationship that is inconsistent with the contact between infrastructure and superstructure being a crustal-scale detachment. For instance, in Figure 6-2, in which only the Devonian Chase Formation is shown within the infrastructure for clarity, the contact between infrastructure and superstructure does not cut up or down structural section for more than several kilometres across the study area and is located in relatively close proximity to the upper contact of the Chase Formation across the study area, which comprises the entire width of the SMC at this latitude. This finding is inconsistent with observations from other detachment faults. For instance, Wernicke (1995, p.557) states "the field observation most significant to the new conceptual framework [of Cenozoic extensional tectonism in the Cordillera] is the widespread occurrence of large subhorizontal faults...across which stratigraphic or structural succession is omitted..." The sub-parallel alignment between the infrastructure-superstructure transition and underlying lithostratigraphic units in the study area is inconsistent with the transitional contact being a crustal-scale detachment fault that cuts down through the entire crust (e.g., Parrish et al. 1988) or cuts down into the middle crust, where it becomes sub-horizontal (e.g., Cook et al. 1992; Johnson and Brown 1996).

The consistent metamorphic grade at the base of the superstructure across the study area, as indicated by similar CAI values of 5.0-5.5 from Upper Triassic conodonts (Fig. 6-2) and from mineral assemblages indicates that the superstructure-infrastructure transition initiated at a gently-dipping or sub-horizontal orientation and has not been tilted significantly since formation, except locally by Middle Eocene or younger faults. This indicates that the contact did not initiate at a

higher angle and later rotate to a gently dipping orientation, due to isostatic rebound of the lower plate, for example.

The conclusions presented above lead to an obvious question: why did detachment faults not form between infrastructure and superstructure within the study area, when they have been reported from the southern SMC (Tempelman-Kluit and Parkinson 1986)? Detachment faults are one of the three essential components that comprise the so-called "Cordilleran metamorphic core complexes" (e.g., Crittenden et al. 1980, and references therein) located within the western United States.

One possible reason is that the ductile shear zones exposed along the base of the superstructure in the Silver Star Mountain and Trinity Hills areas formed below the brittle-ductile transition and were never exhumed to shallow crustal levels. If displacement on the shear zone halted prior to the shear zone being exhumed above the brittle-ductile transition, only the ductile portion of the strain path would be preserved. In this scenario, the ductile shear zone would provide a "snapshot" of the ductile deformation path of a detachment fault that was never overprinted by brittle deformation during subsequent exhumation and uplift. Such a model can account for the lack of a pervasive brittle overprint in the Kalamalka Lake, the Silver Star Mountain, and the Trinity Hills shear zones.

Certain characteristics of the shear zone exposed in the Silver Star Mountain area, however, are inconsistent with this scenario. Detailed petrographic study of strained rocks from the shear zone indicates that quartz deformed in a plastic manner. Evidence of recovery and recrystallization in quartz grains includes: undulose extinction, subgrain development, undulating and bulging grain boundaries, and composite elongate grains with length to width ratios greater than 10:1, indicating temperatures of deformation of 400-700°C (Passchier and Trouw 2000). Feldspars at upper levels of the Silver Star shear zone deformed primarily by fracturing, indicative of temperatures in the range of 300-400°C. Structurally lower within the Silver Star shear zone, core and mantle structures are commonly observed on feldspar grains, indicating that recrystallization occurred, indicative of deformation at temperatures of 400-500°C, or higher (Passchier and Trouw 2000).

But structures and metamorphic mineral assemblages preserved within the upper half of the Silver Star shear zone are consistent with lower-grade conditions. Mineral assemblages are consistent with peak metamorphic conditions of the garnet to biotite zones of the greenschist facies (Fig. 6-4). Quartz displays evidence of limited recovery and recrystallization, such as undulose extinction, subgrain development, and slightly elongated grains, but elongate recrystallized quartz ribbons with extreme length to width ratios, indicative of recrystallization at

temperatures above 400-500°C, are not present. Feldspars behaved in a purely brittle manner during deformation at this level of the zone. A weak mineral lineation, defined by elongate clots of biotite visible on the foliation surface, is present within the garnet and biotite zones. At the same structural level, a spaced fracture cleavage is locally developed, oriented perpendicular to the mineral lineation (Fig. 6-4, see equal-area projections). Quartz and (or) calcite-filled fractures parallel to the spaced fracture cleavage are locally developed within granitic rocks.

Superstructure rocks within the study area yield dominantly Middle Jurassic cooling dates (K-Ar; hornblende and micas), but younger dates are present locally (e.g., Mathews 1981). The pattern of cooling dates, combined with the structures and metamorphic assemblages of the superstructure, are inconsistent with the Silver Star shear zone having formed completely below the brittle-ductile transition. If it had formed entirely within the ductile regime, below the brittle-ductile transition, both the upper and lower plate would record peak amphibolite-facies metamorphic conditions, and ductile structures would have been progressively overprinted as the shear zone was exhumed through the brittle-ductile transition, into the brittle regime (e.g., Lister and Davis 1989). This is not what is observed, leading to the conclusion that, as the lower plate is composed of rocks that deformed at ductile conditions during the Late Cretaceous to Early Eocene, and the upper plate comprises rocks that were deforming within the brittle regime during the same time, *the shear zone must have formed within or along the fossil Late Paleocene to Early Eocene brittle-ductile transition.* The ductile strain may have attenuated a pre-existing metamorphic field gradient. These observations also imply that the shear zone cannot represent a crustal-scale detachment system that originated within the middle or lower crust within the ductile regime, to be progressively exhumed into the brittle regime during extension and exhumation (cf. Lister and Davis 1989). Instead, the mapping, metamorphic, and petrographic data imply that the Silver Star shear zone initiated at a sub-horizontal orientation between rocks that were deforming by dominantly ductile flow and overlying rocks that were situated within the brittle regime (<250°C) during the Late Cretaceous to Early Eocene. This is consistent with the shear zone representing an exhumed "fossilized" brittle-ductile transition zone. This interpretation is not proposed for all low-angle shear zones exposed within the SMC, but is consistent with the mapping, structural, geochronological, and metamorphic data from the Vernon area.

Controls on the initiation of Late Paleocene to Early Eocene low-angle shear zones within the study area

The structural level of Late Paleocene to Early Eocene low-angle shear zones within the crust corresponds closely with the structurally highest-level occurrence of early Tertiary granitic

rocks within the middle structural layer of the infrastructure. Accordingly, this structural level is inferred to represent a significant paleorheological boundary that facilitated the initiation of ductile shear zones that accommodated differential motion between infrastructure and superstructure rocks during the Late Cretaceous to the early Tertiary (Fig. 6-5; e.g., Vanderhaeghe et al. 1999). The superstructure was situated within the upper 5-10 km of the crust during the Late Cretaceous to Early Paleocene, as indicated by Jurassic to Cretaceous cooling dates from hornblende and biotite, combined with conservative estimates of geothermal gradients between 25°C and 35°C (Fig. 6-6; Mathews 1981; Carr 1990). Paleorheological studies suggest that significant crustal strength was restricted to the upper ~10 km of the crust during the Late Cretaceous to the Paleocene within the southeast Canadian Cordillera as a result of high heat flow and elevated geothermal gradients (Fig. 6-5; e.g., Lowe and Ranalli 1993, Lui and Furlong 1993). Geological observations on the occurrence of Late Paleocene to Early Eocene granitic rocks and their spatial association with low-angle shear zones within the infrastructure-superstructure transition suggest that their emplacement affected the rheology of the crust, ultimately controlling the structural level at which low-angle ductile shear zones formed (Fig. 6-4; cf. Simony and Carr 1997).

South of approximately latitude 50°20' N, early Tertiary granitic rocks are inferred to have risen within the crust up to the base of large Middle Jurassic batholiths of the Okanagan composite batholith, where they may have ponded (Figs. 6-2, 6-3, 6-5; cf. Simony and Carr 1997). The Okanagan composite batholith (Woodsworth et al. 1991) is the time-equivalent of the Middle to Late Jurassic (170-150 Ma) Nelson plutonic suite to the east (Fig. 6-1; Parrish 1992; Sevigny and Parrish 1993; Ghosh 1995). This structural relationship between early Tertiary and Middle Jurassic intrusive rocks has been observed in the Valhalla complex, where the low-angle, early Tertiary Valkyr shear zone developed along the contact (a significant rheological interface) between early Tertiary granitic rocks and overlying relatively cool and competent Middle Jurassic batholiths (e.g., Simony and Carr 1997). In the Vernon area, Middle Jurassic intrusive rocks, such as the Wood Lake pluton, are common in the upper plate of the Kalamalka Lake shear zone, but rare to absent within the lower plate. Mylonitic granitic rocks of inferred Middle Jurassic age with potassium feldspar augen occur locally in the Kelowna area, several kilometres east of the airport on Farmers Road; but for the most part, Middle Jurassic granitic rocks are restricted to the superstructure south of 50°20' N, where they are weakly deformed and post-date the development of the metamorphic foliation (Chapter 3). The opposite relationship is observed with Late Paleocene to Early Eocene granitic rocks, which are ubiquitous within the middle structural layer of the infrastructure, but rare to absent within the superstructure.

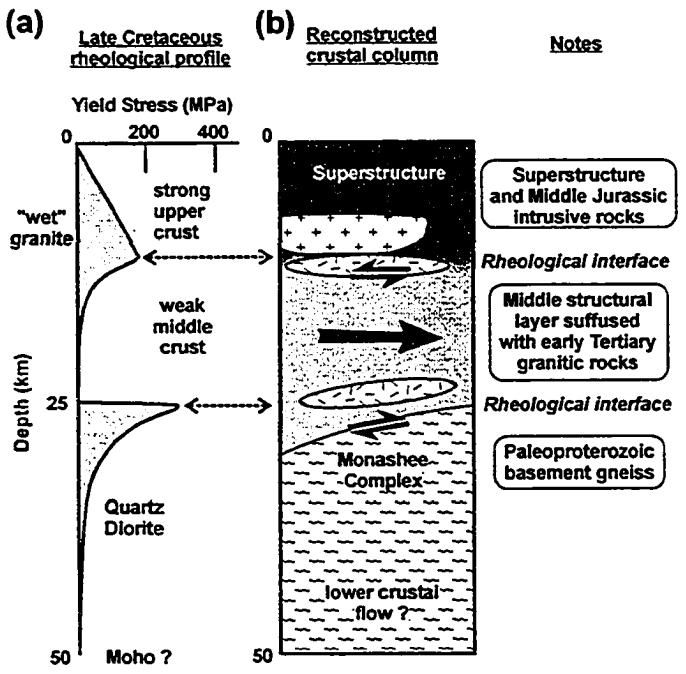

Fig. 6-5. (a) Schematic paleorheological strength profile of the southeast Canadian Cordillera in the Late Cretaceous to Early Paleocene (modified from Dunbar and Sawyer 1989). Upper 25 km of the crust is approximated using a wet granite model, while the lower 25 km uses quartz diorite. (b) Reconstructed Late Cretaceous to Early Paleocene crustal column of the southeast Canadian Cordillera.

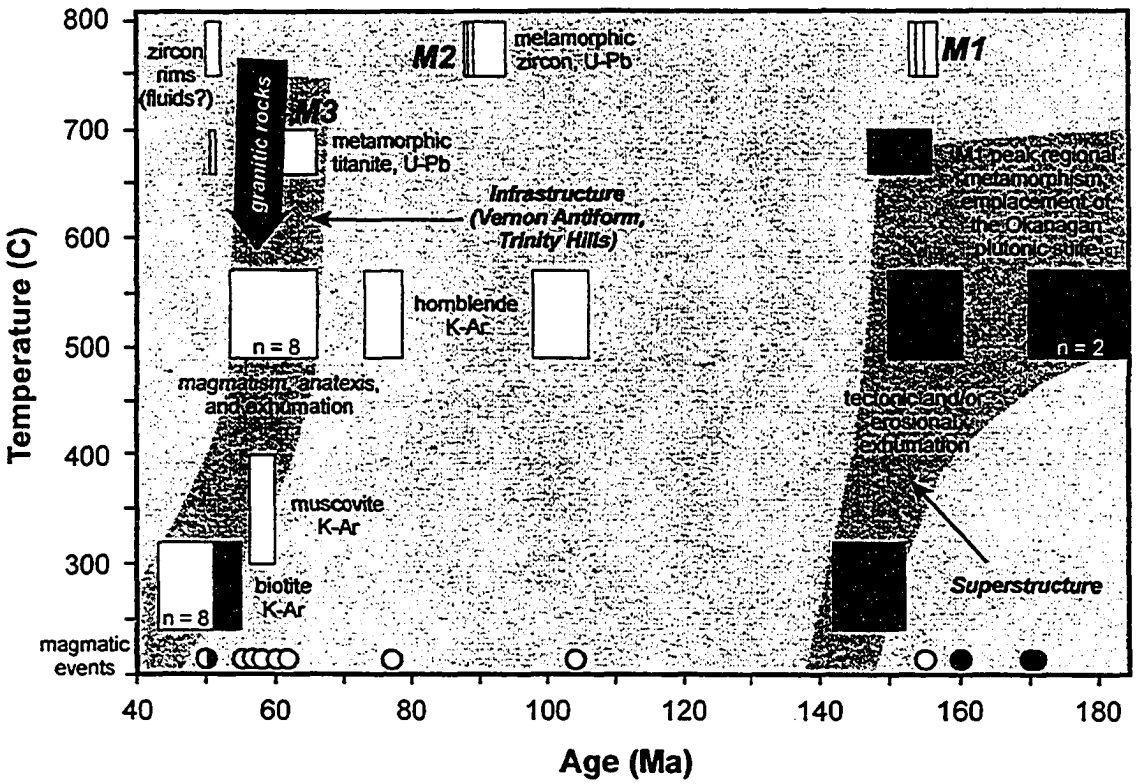

Fig. 6-6. Temperature-time plot showing K-Ar and $^{40}Ar/^{39}$ Ar (hornblende, muscovite, and biotite) and U-Pb (titanite and zircon) data from suprastructure (grey) and infrastructure (white) rocks from the study area. Inferred temperature-time (*T-t*) paths are shaded light grey. Circles near the bottom axis indicate the timing of known magmatic events in the suprastructure (grey) and infrastructure (white). Closure temperatures after Heaman and Parrish (1991) and Scott and St-Onge (1995). Unless otherwise indicated, individual boxes indicate data from a single sample. *Data sources*: W.H. Mathews, unpublished data; Mathews (1981); Carr (1990); Johnson (1994); Vanderhaghe et al. (2003); this study, Chapter 3, and R.I. Thompson, unpublished data.

North of approximately 50°20' N latitude, large Middle Jurassic batholiths are absent within the superstructure, comprised of the Slocan Group, between the Okanagan Valley and the Columbia River. The transitional contact between infrastructure and superstructure coincides with the uppermost structural occurrence of abundant Late Paleocene to Early Eocene granitic rocks (Fig. 6-2; e.g., Vanderhaeghe et al. 1999; Chapter 2). This is evident in the Silver Star Mountain area, where the Silver Star shear zone coincides with the first down-section occurrence of abundant early Tertiary granitic rocks (Fig. 6-4). A similar relationship has been documented in the Trinity Hills area (e.g., Vanderhaeghe et al. 1999; Thomson and Glombick 2004*a*, 2004*b*).

Metamorphic infrastructure rocks underlying the superstructure belt yield Late Paleocene to Middle Eocene K-Ar dates from hornblende, muscovite and biotite (Fig. 6-6; Mathews 1981; Parrish et al. 1988; Carr 1990; Vanderhaeghe et al. 2003). These cooling dates have been interpreted to indicate quenching of the metamorphic infrastructure as a result of rapid tectonic exhumation on low-angle, crustal-scale detachment faults (e.g., Parrish et al. 1988; Carr 1990; Bardoux 1993; Vanderhaeghe et al. 1999, 2003). The actual amount of exhumation that occurred between the Late Paleocene to Middle Eocene is difficult to quantify, and is dependent on assumptions of the pre-extension Paleocene geothermal gradient. As the entire middle structural layer is permeated with Late Paleocene to Middle Eocene granitic rocks (Reesor and Moore 1971; Carr 1992; Bardoux 1993; Holk and Taylor 1997; Vanderhaeghe et al. 1999), this implies that most (if not all) of the K-Ar and $^{40}Ar/^{39}Ar$ samples were located in close proximity (10's to 100's of m) to early Tertiary granitic rocks. It is possible, then, that the metamorphic country rocks had cooled earlier and were located at a relatively shallow level of the crust prior to being reheated during the intrusion of early Tertiary granitic rocks. As such, the amount of exhumation indicated by the K-Ar dates and inferred cooling paths (e.g., Fig. 6-6) are uncertain and open to interpretation. Cretaceous $^{40}Ar/^{39}Ar$ dates have been reported from the Thor-Odin dome of the southern Monashee complex (Kuiper 2003). She noted an empirical correlation between $^{40}Ar/^{39}Ar$ dates and oxygen and hydrogen isotope ratios, with amphibolite younger than 70-75 Ma showing the most ^{18}O- and D-depletion.

Perhaps a more reliable constraint on the pre-extension depth of the infrastructure is the timing of metamorphism in the Vidler Ridge and Pinnacles region combined with estimates of near-peak *P-T* conditions of approximately 8 kbar and 675-700°C (Fig. 6-7*a*; Chapter 4). Although there is a spread in the metamorphic monazite chemical dates from the Vidler Ridge-Pinnacles area, there is a cluster near 100-90 Ma (Fig. 6-8), which coincides with a major period of metamorphism within the southeast Canadian Cordillera (e.g., Parrish 1995; Crowley et al.

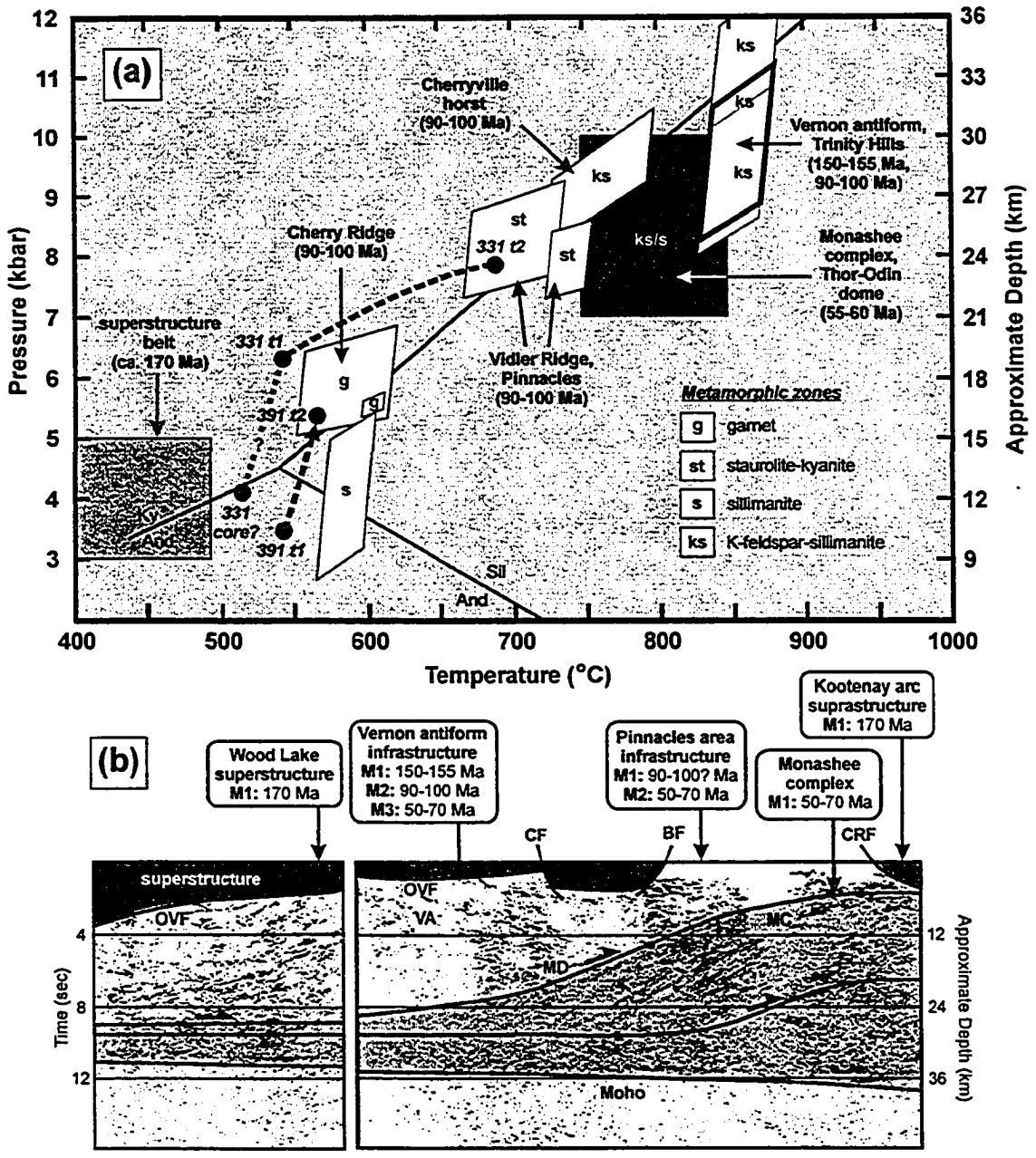

Fig. 6-7. (a) Pressure-temperature diagram summarizing maximum *P-T* estimates from metapelitic rocks from various areas and structural levels within the study area, inferred timing of peak metamorphism, and inferred partial *P-T* paths for samples 391 and 331. Dashed line indicates partial *P-T* paths calculated using Program Gibbs. Inferred portions of the *P-T* path, consistent with petrological data, shown as dotted lines. The location of the Al_2SiO_5 triple point from Pattison (1992). Monashee complex *P-T* constraints from Norlander et al. (2002). (b) Interpreted Lithoprobe seismic reflection lines 7 to 9 through the Vernon area (after Cook et al. 1992). *Abbreviations*: CF - Cherry fault; CRF - Columbia River fault; BF - Beaven fault; MC - Monashee complex; MD - Monashee décollement; OVF - Okanagan Valley fault; VA - core of Vernon antiform. *Fill patterns*: (1) superstructure (dark grey); (2) infrastructure: middle structural layer (white), and allochthonous and autochthonous Paleoproterozoic North American rocks (light grey); and (3) upper mantle (bottom white). The timing of major metamorphic events, deduced from new and published geochronological data (Fig. 4-17), are shown on section.

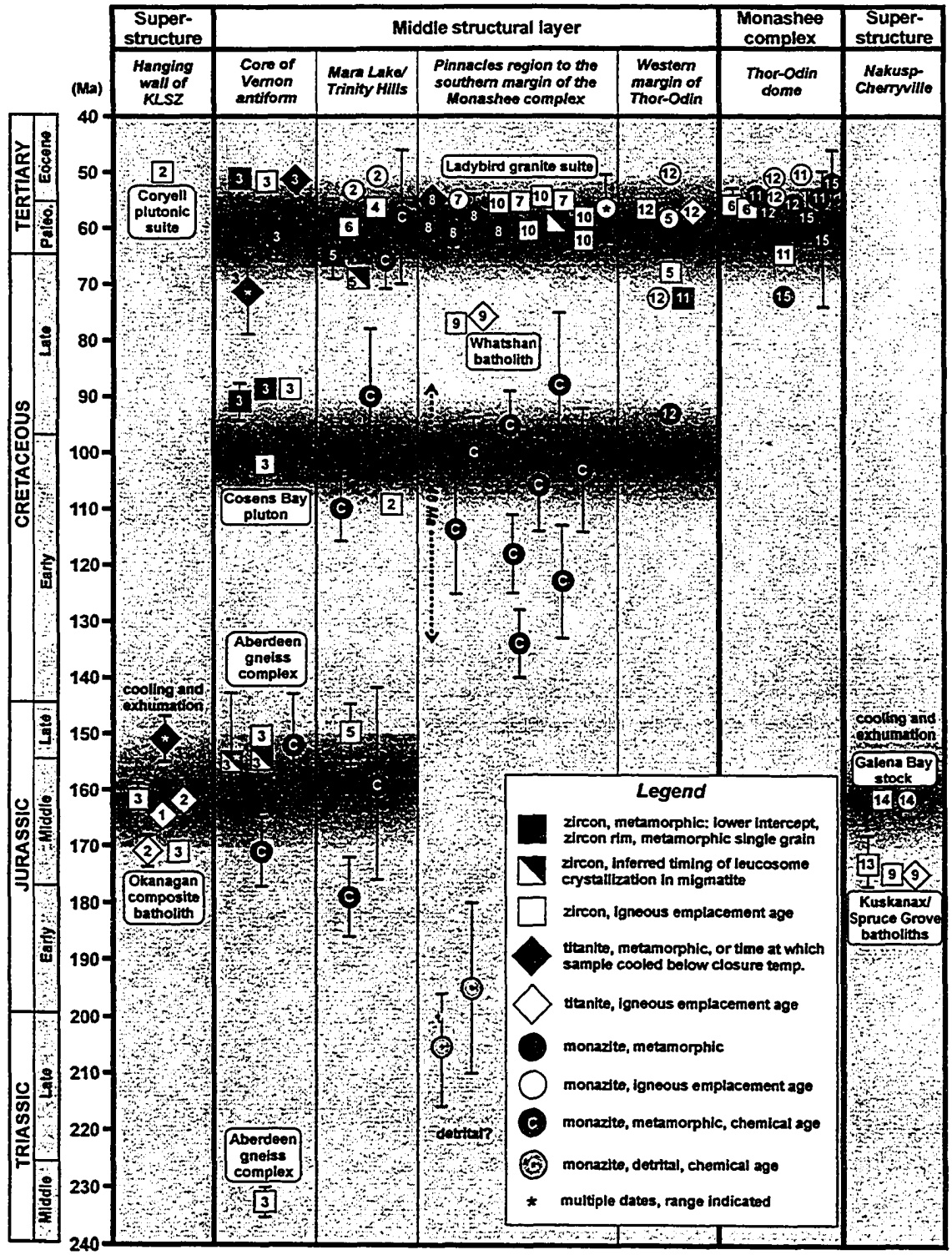

Fig. 6-8. Compilation of U-Pb geochronology data from the SMC between latitudes 50° and 51° N. *Data sources*: 1 - Thompson and Daughtry (1996); 2 - R.I. Thompson, unpublished data; 3 - Glombick et al. (in press); 4 - Bardoux (1993); 5 - Johnson (1994); 6 -Vanderhaeghe et al. (1999); 7 - Parrish et al. (1988); 8 - Carr (1990); 9 - Carr (1991); 10 - Carr (1992); 11 - Parkinson (1992); 12 - Johnston et al. (2000); 13 - Parrish and Wheeler (1983); 14 - Parrish and Armstrong (1987); 15 - Kuiper (2003).

2000). The data suggest that, during the Late Cretaceous, middle layer rocks exposed in the Vidler Ridge-Pinnacles region were buried at depths of ~25 km.

In summary, the metamorphic data indicate that the infrastructure and superstructure, which are presently juxtaposed by low-angle ductile shear zones (Chapter 2) or steep metamorphic field gradients (Chapter 4), were formerly separated by a thickness of 15 km of crust during the Late Cretaceous. In the absence of detachment faults that cut down structural section, the juxtaposition of the rocks separated by a thickness of 15 km of crust in the Late Cretaceous requires some other means of exhumation.

The continuity of the superstructure across the Vernon area highlights an apparent paradox: the metamorphic and geochronological data indicate a significant amount of cooling and exhumation of the infrastructure between the Late Cretaceous and the Middle Eocene, but the superstructure, or cover of the complex, is largely still preserved over the "top" of the complex at the latitude of the study area. As a result, the exhumation of the infrastructure cannot have occurred by tectonic removal of the superstructure (cover), dragging out the infrastructure from beneath an extending and fracturing upper plate (e.g., Lister and Davis 1989). In areas where the superstructure has been removed by erosion, such as to the south, in the Penticton area, large-displacement detachment models appear to be viable, as few geological constraints on fault displacement or upper crustal faulting are available (e.g., Tempelman-Kluit and Parkinson 1986). Previous studies of low-angle extensional shear zones have not, however, presented unequivocal piercing points, relying instead on indirect arguments, such as: (1) proposed matches between plutons within the lower plate and volcanic successions of similar age and composition overlying rocks of the upper plate (Tempelman-Kluit and Parkinson 1986); and (or) (2) apparent metamorphic omission across the proposed fault zone, combined with estimates of pre-faulting *P-T* conditions, geothermal gradients, and fault dips (Parrish et al. 1988; Bardoux 1993; Johnson and Brown 1996). Within the study area, the continuity, the structural style, and the gaps of the superstructure place strict constraints on the maximum allowable displacement on proposed low-angle shear zones, which is much less than published estimates of displacement on proposed detachment fault systems (e.g., Tempelman-Kluit and Parkinson 1986; Parrish et al. 1988; Carr 1990; Bardoux 1993; Johnson and Brown 1996).

The nature of the sub-Middle Eocene unconformity in the study area

Published interpretations of Vernon area geology, based on regional-scale mapping, infer zeolite-facies Middle Eocene (~42-49 Ma; Mathews 1981; Breitsprecher 1998) outliers, exposed in the Vernon and Kelowna areas, to comprise the upper plate of low-angle detachment faults

(Carr 1990; Bardoux 1993; Vanderhaeghe et al. 1999). During this study, the sub-Eocene contact was observed, or narrowed down to within tens of metres, in several locations.

Approximately 3 km due east of the southern end of Kalamalka Lake, an outlier of fine-grained, plagioclase-phyric, intermediate-composition volcanic flows is exposed, directly overlying migmatitic schist within the Kalamalka Lake shear zone (Fig. 6-9, centre; Glombick et al. 1999). The composition of the volcanic rocks is similar to other Middle Eocene volcanic successions in the Trinity Hills (e.g., Mathews 1981; Breitsprecher 1998) and Kelowna area (e.g., Bardoux 1993). The basal contact is well exposed in roadcut, where a sharp, undulating surface is present between the basal volcanic flow and underlying mylonitic sillimanite schist (Fig. 6-10*a*). The underlying schist contains a 10-30 cm thick zone of reddish brown and friable schist, interpreted as a Middle Eocene regolith. There is no evidence of cataclasis at the contact. Several hundred of metres away, the contact between volcanic flows and schist is not directly exposed, but was narrowed down to within metres. The flows contain angular to sub-rounded clasts of schist and gneiss, ranging in size from several cm to 10's of cm across (Fig. 6-10*b*).

Mathews (1981) observed a similar contact at the base of the Trinity Hills outlier. Although the contact along the base of the Trinity Hills outlier was not directly observed during this study, along the northern margin of the outlier, the contact was narrowed down to within tens of metres. The basal unit within the outlier is a poorly sorted, polymictic conglomerate with variable-sized angular to sub-rounded clasts. Mathews (1981) reported clasts 10's of metres across from the basal conglomerate of the Trinity Hills outlier. The lithological characteristics of clasts in the basal conglomerate reflect the rock type and metamorphic grade of the underlying bedrock. Where contacts in the bedrock are crossed, the clast rock types in the basal conglomerate reflect the change, indicating that the clasts are of local derivation. The size and angularity of the clasts in the basal conglomerate of the Trinity Hills outlier is interpreted to reflect rapid catastrophic deposition into a local fault-bounded basin. Rock types higher in the Middle Eocene succession include water-lain sandstones, siltstones, and mudstones, suggestive of a lower energy depositional setting in a submarine environment. Fine-grained clastic sedimentary rocks are overlain by volcanic flows of varying composition (e.g., Mathews 1981; Breitsprecher 1998).

Similar unconformable relationships have been observed from the base of Middle Eocene (~52 Ma) Marron Formation outliers in the Kelowna area (Okulitch 1987). Bardoux (1993) suggested that older volcanic rocks of the Marron formation were detached, situated within the upper plate of the OVF, but younger phases of the Marron formation were deposited directly onto exhumed mylonitic footwall rocks. At the base of the Black Knight Mountain outlier, however, at

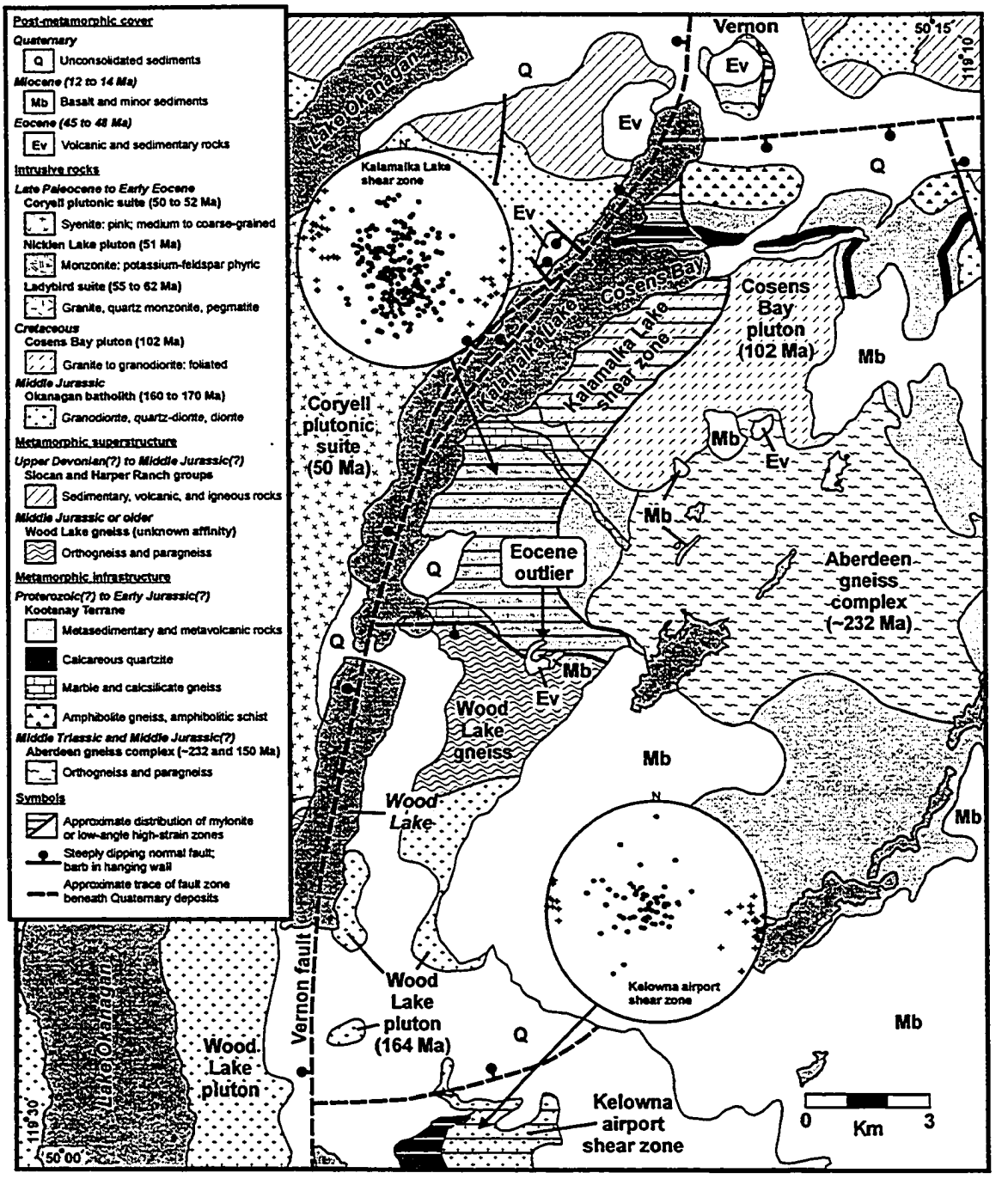

Fig. 6-9. Simplified geological map of the Kalamalka Lake area, showing the distribution of mylonite zones (striped pattern) and fabric data from the Kalamalka Lake and Kelowna airport shear zones. Fabric data are plotted on lower hemisphere, equal-area projections. *Symbols*: solid circles - poles to mylonitic foliation; crosses - stretching lineations. Geological contacts modified from Glombick et al. (2004).

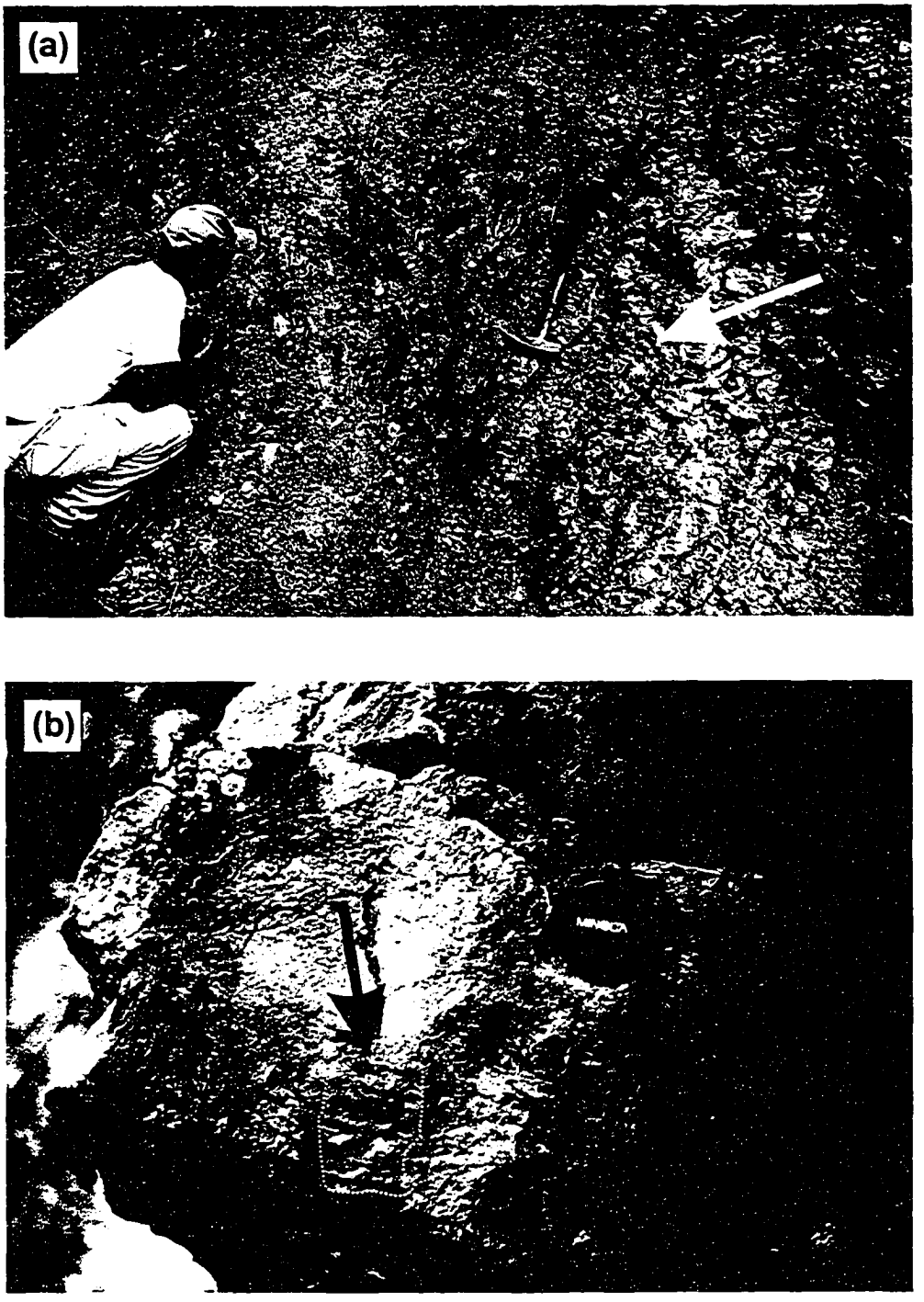

Fig. 6-10. Outcrop photographs of the Middle Eocene basal unconformity east of Kalamalka Lake. (a) basal volcanic flow of intermediate composition (right) overlying friable regolith surface developed within the underlying mylonitic pelitic schist. White arrow points to the contact. Geological hammer for scale. (b) Gneissic clast within the basal volcanic flow at a different location several hundred metres away. The basal contact is not exposed at this locality. Large black arrow points at clast (outlined by dotted white line). Lens cap for scale (centre, right). See Glombick et al. (1999) for a detailed description and the location of the outcrops.

the type area for the OVF in the Kelowna area (R. Brown, personal communication to P. Glombick, 1998), the basal contact is not exposed. The lowest units exposed within the Black Knight outlier are finely-bedded siliciclastic rocks with no signs of cataclasis or fracturing.

In summary, north of the Penticton area, there is no documented evidence of Middle Eocene volcanic rocks in low-angle fault contact with underlying upper amphibolite-facies mylonitic gneiss. Basal contacts, where exposed within the study area, are unequivocally depositional, requiring existing maps and models to be revised.

Metamorphic evolution of the SMC within the study area

Geological mapping near the base of the superstructure in the study area determined that the contact between superstructure and infrastructure is transitional, characterized by a gradational, but rapid increase in metamorphic grade (steep metamorphic field gradients). Detachment faults were not found within this zone.

This transition is best exposed in the Silver Star Mountain area, located approximately 15 km northeast of Vernon (Fig. 6-4; see detailed description in Chapters 2 and 4). In this area, the transition corresponds with a zone of ductile shear ~2 km thick with diffuse boundaries and heterogeneously distributed strain. Shear-sense indicators from granitic rocks of inferred early Tertiary age consistently yield a top-to-the-west shear sense. Synkinematic, lineated granitic rocks with C-S fabric and a gently plunging west-trending lineation (yielding a top-to-the-west shear-sense) within the transition zone in the Trinity Hills area yielded a U-Pb zircon age of 56-60 Ma (Bardoux 1993; Vanderhaeghe et al. 1999).

Farther east, near the geographical axis of the complex, in the Vidler Ridge-Pinnacles area, the transition from superstructure to infrastructure is marked by closely-spaced metamorphic isograds across a structural thickness of several kilometres, but evidence of non-coaxial strain is lacking (Fig. 6-11). Ductile strain in this area, possibly resulting in the attenuation of the metamorphic field gradient, may have been dominantly coaxial. A recent AMS and kinematic study of high-temperature fabric from early Tertiary granitic rocks suggests that strain was predominantly coaxial in this area (Fig. 6-2; Teyssier et al. 2005). Late Cretaceous(?) to Early Eocene, low-angle, non-coaxial shear zones developed near the margins of the SMC, but near the geographic axis of the complex ductile deformation was dominated by coaxial strain (Teyssier et al. 2005).

Estimates of peak *P-T* conditions from garnet-bearing migmatitic pelitic rocks within the middle structural layer, within 1-2 km of the superstructure-infrastructure transition, indicate pressures of 8-10 kbar and temperatures above 800°C, which corresponds to burial depths of 25-

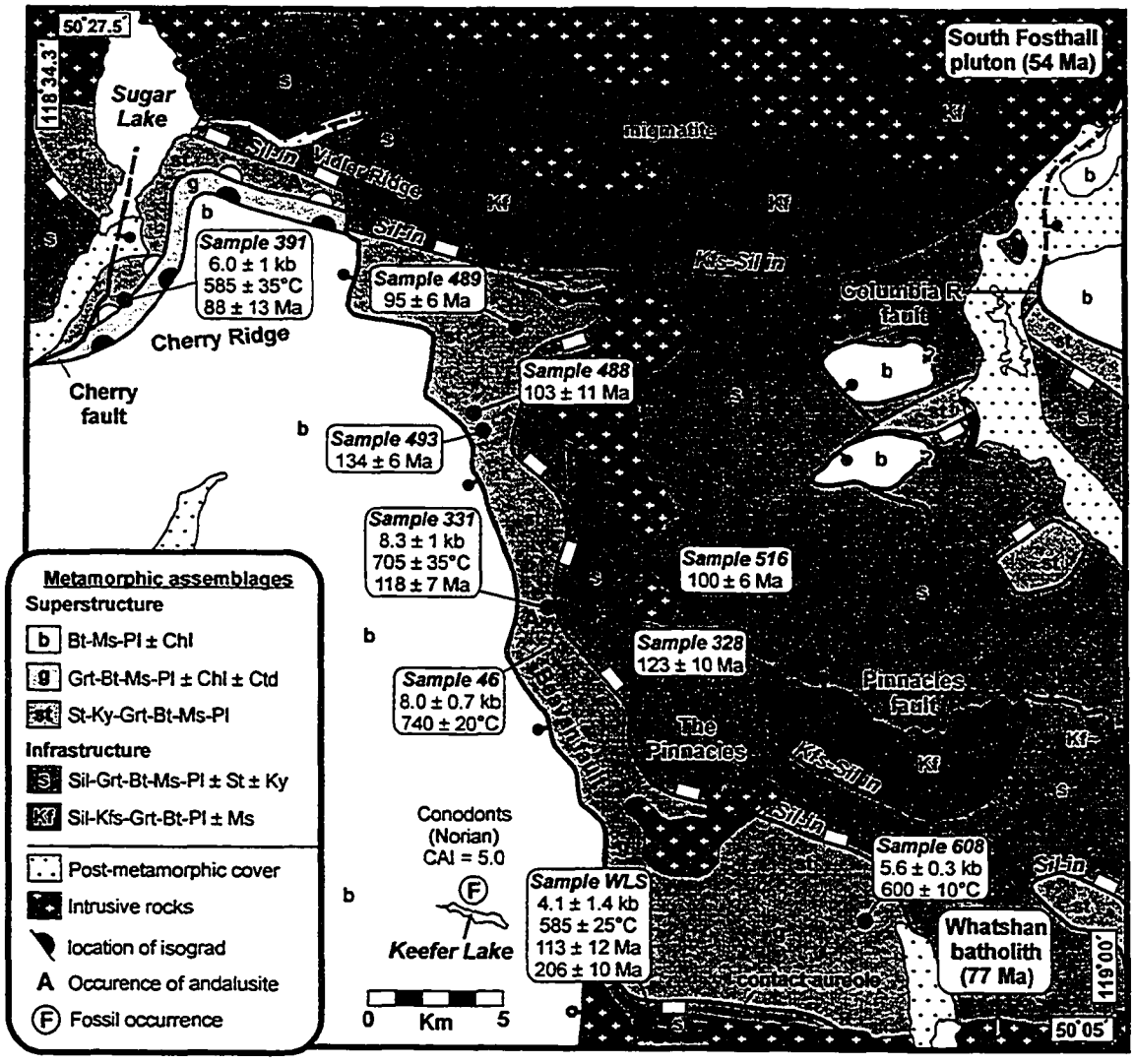

Fig. 6-11. Metamorphic map of the Vidler Ridge-Pinnacles area showing the location of isograds and thermobarometry and monazite EMP chemical dating samples. Isograds as per Fig. 4-6. The location of metamorphic isograds is based on Reesor and Moore (1971), Carr (1990), and this study (Chapter 4).

30 km (Figs. 6-2, 6-7*a*; Chapter 4). A transect across the ~10 km thick middle structural layer yielded similar *P-T* estimates (Teyssier et al. 2005).

Geochronological data from the study area suggest a complex and episodic metamorphic evolution (Fig. 6-8). The superstructure records a single metamorphic event at 171 Ma, whereas the underlying middle structural level records multiple events at 155-150 Ma, 100-90 Ma, and 70-50 Ma, depending on the area (Figs. 6-7, 6-8). The deepest exposed structural level, the Paleoproterozoic basement exposed within the Thor-Odin culmination of the southern Monashee complex, only records evidence of the youngest of the infrastructure metamorphic events.

The current juxtaposition of the superstructure with middle structural layer rocks of the infrastructure that were buried at depths of approximately 25 km in the Early to Late Cretaceous requires differential exhumation of these tectonostratigraphic units since Late Cretaceous time. The mapping data require exhumation of the infrastructure without removal of the overlying superstructure on low-angle detachments or by erosion.

One method of achieving this exhumation would be ductile thinning of the entire middle structural layer beneath the superstructure during orogenic collapse. As discussed above, the superstructure was situated within the strong upper crust and would not likely be affected by ductile deformation during Late Cretaceous to Early Eocene orogenic collapse and extension. If the entire middle structural layer was thinned, essentially by coaxial strain, then one would predict attenuation of the metamorphic field gradient throughout the entire middle structural layer. This is not, however, what is observed. The attenuated metamorphic section is located at the top of the middle structural layer and there is evidence of non-coaxial deformation near the western margin of the complex, in the Silver Star Mountain and Trinity Hills areas. As documented by Teyssier et al. (2005), metamorphic grade appears to be quite consistent throughout the ~10 km thick exposed structural section of the mid-crustal layer.

A possible explanation, which is supported by the geochronological data from the study area, is that the metamorphism was diachronous throughout the infrastructure (Figs. 6-7, 6-8; see also Parrish 1995; Gibson et al. 1999; Crowley et al. 2001). If the orogen achieved a steady-state wedge configuration, rocks would be incorporated into the advancing wedge, either through frontal or basal accretion (e.g., Platt 1986), and metamorphosed at depths of approximately 30 km (Parrish 1995; Brown 2004). Rocks metamorphosed near the base would be progressively exhumed by a combination of erosion along the upper surface of the wedge and intra-wedge extension to maintain critical taper (e.g., Brown 2004). Once the wedge has maintained a steady-state configuration, rocks at all structural levels should yield similar peak *P-T* estimates

(assuming that no retrogression occurred), but the age of metamorphism should become progressively younger at structurally deeper levels (Parrish 1995; Brown 2004).

An orogenic wedge model can account for the consistent metamorphic grade throughout the middle structural layer. The geochronological data from the study area do not, however, show a progressive increase in metamorphic age, but a complex and episodic metamorphic evolution, with three metamorphic events: (1) Middle to Late Jurassic (155-150 Ma); (2) Early to Late Cretaceous (100-90 Ma); and (3) Late Cretaceous to Eocene (70-50 Ma; Figs. 6-7, 6-8). The Middle to Late Jurassic event recorded in the Vernon antiform and Trinity Hills area is not recorded within the middle structural layer in the Vidler Ridge or Pinnacles area or within the Thor-Odin dome of the southern Monashee complex. Similarly, the Late to Early Cretaceous event recorded within all of the middle structural layer throughout the study area is not recorded with the Thor-Odin dome of the southern Monashee complex, which only records evidence of the latest Late Cretaceous to Eocene event (Figs. 6-7, 6-8; Carr 1990; Parkinson 1992; Vanderhaeghe et al. 1999; Johnston et al. 2000). The Late Cretaceous to Eocene event (70-50 Ma) overlaps the timing of orogenic collapse and extension. This pattern of ages, though consistent with a broad younging pattern of metamorphic ages with structural level, indicates that metamorphic (and perhaps crustal thickening?) events were episodic, rather than continuous, and that upper structural levels of the middle structural layer were affected by all metamorphic events, rather than just the oldest event. The episodic nature of metamorphic events may reflect accretion events at the plate margin.

A similar pattern of metamorphic ages to those recorded within the middle structural level of the study area was documented by Crowley et al. (2000), who documented evidence for five distinct thermotectonic events (175-160, 140-120, 110, 100-90, 75-50 Ma) in an apparently continuous metamorphic and stratigraphic section near Mica Creek, along the northeast margin of the SMC (Fig. 4-1). Parrish (1995) identified three major periods of metamorphism within the SMC at 175-160, 100-90, and 75-60 Ma, and suggested that the age of metamorphism should become younger with increasing structural depth. While at the orogen scale, the age of metamorphism does appear to become younger at deeper structural levels (in that older events are not recorded at deeper structural levels), the data from this study and the Mica Creek area (Crowley et al. 2000) suggest that the thermotectonic and metamorphic evolution of the complex may be considerably more complex than proposed by current models (e.g., Parrish 1995; Brown 2004).

Channel flow within the middle crust of the southeast Canadian Cordillera?

Recent coupled thermal-mechanical models have predicted that a zone of channel flow will develop in large convergent orogens if the middle to lower crust is sufficiently hot (Jamieson et al. 2002; Beaumont et al. 2001*a*; 2004). In these models, a melt fraction in the middle to lower crust is simulated by a temperature-dependent reduction in viscosity, which produces a zone of channel flow that tunnels towards the foreland side of the orogen at mid-crustal depths. The exhumation and rate of flow within the zone of channel flow is coupled to erosion rates at the foreland of the orogen (e.g., Jamieson et al. 2002). If erosion rates are low, the channel may remain unexposed, unless it is exhumed by subsequent extension faulting.

Extrusion, or channel flow models, have been proposed to account for the exhumation of the Greater Himalayan Crystalline Sequence within the Himalayan orogen (e.g., Grujic et al. 1996; Nelson et al. 1996; Beaumont et al. 2001*b*; Hodges et al. 2001; Vannay and Grasemann 2001) and the eastward propagation of the Tibetan plateau (Royden 1996; Clark and Royden 2000; Shen et al. 2001). Recent geophysical investigations of the southern Tibetan plateau have identified a zone within the middle crust interpreted as partially molten (e.g., Nelson et al. 1996). It has been proposed that a channel of partially molten rocks was extruded southwards from beneath the Tibetan plateau in response to lateral potential energy gradients towards the foreland of the orogen, where focussed erosion along the southern flank of the Himalayan range resulted in rapid exhumation of the Greater Himalayan Zone (e.g., Beaumont et al. 2001*b*). The Greater Himalayan Zone is bounded at the bottom by the top-to-the-south-directed Main Central Thrust, while the top of the zone is bounded by the top-to-the-north-directed South Tibetan detachment system (e.g., Hodges 2000, and references therein). Some workers have suggested, based on physiographic river profiles, that the southward extrusion of the Greater Himalayan Crystalline Sequence continues to occur today (e.g., Hodges et al. 2001). An obvious question, therefore, is whether channel flow occurred within the southeast Canadian Cordillera.

During the 1980's and 1990's, workers within the SMC focussed on low-angle shear zones and moderate to steeply dipping normal faults exposed near the margins of structural and metamorphic culminations (e.g., Tempelman-Kluit and Parkinson 1986; Carr et al. 1987; Parrish et al. 1988; Bardoux 1993; Johnson and Brown 1996). With few exceptions (e.g., Scammell 1993; Johnston 1998; Williams 1999), the possible role of orogen-scale ductile mid-crustal flow was not discussed. In most extension models, early Tertiary ductile deformation was generally considered to be confined to the upper 1-2 km of the footwall, where ductile fabrics were progressively overprinted by brittle structures during exhumation, as the footwall was "dragged out" from beneath the extending brittle upper plate (e.g., Bardoux 1993).

During the 1990's, however, the possible role of ductile exhumation slowly became apparent, as an increasing number of studies within the hinterland of the Sevier orogen in the western United States (e.g., Hodges and Walker 1992, and references therein; Applegate and Hodges 1995; Camilleri and Chamberlain 1997; Wells 1997; Camilleri 1998) and southeast British Columbia (e.g., Scammell 1993) documented evidence of cooling and exhumation of mid-crustal rocks during the Cretaceous, often without identifying discrete extensional shear zones of that age. Alternating pulses of crustal thickening and exhumation were generally interpreted as gravitational spreading of thrust sheets following heating and relaxation of geotherms (e.g., Scammell 1993; Wells 1997; Hoisch et al. 2002). Similarly, geological and seismic studies of metamorphic core complexes exposed within the hinterland of the Sevier orogen and within the Basin and Range province concluded that ductile flow of a "fluid" mid-crustal layer occurred during extension, flowing in response to discrepancies in the amount of upper crustal extension to maintain a constant crustal thickness and a flat Moho (e.g., Kruger and Johnson 1994; McCarthy and Parsons 1994; Wernicke 1995; MacCready et al. 1997). All of these studies contributed to the emerging awareness of the role of mid-crustal flow during orogenesis.

More recently, several studies within the southeastern Canadian Cordillera have suggested that orogen-scale extrusion (Johnston 1998; Johnston et al. 2000) or channel flow (Glombick et al. 2002; Chapter 5) may have contributed to the exhumation of mid-crustal rocks during the Late Cretaceous to early Tertiary. The model proposed by Johnston et al. (2000) draws analogies to the extrusion of a Himalayan-style wedge, but it is difficult to reconcile with the existing map relationships and Lithoprobe seismic reflection data from the area. Comparisons between the thickness of Paleoproterozoic basement in the present-day cross section across the SMC at the latitude of the Monashee complex and a schematic cross section showing the basic elements of the extrusion model reveal drastic differences in the expected thickness of North American basement underlying the Monashee complex. In addition, the thickness of accreted crust shown in the model of Johnston et al. (2000) is inconsistent with recent work west of the SMC which suggests that rocks presently assigned to the Quesnel Terrane (Quesnellia) may be a thin veneer originally deposited on North American basement and pericratonic sedimentary and volcanic successions (Erdmer et al. 1999, 2002).

The channel flow model presented in Chapter 5 is attractive in that it can successfully account for many of the apparently enigmatic and contradictory geological observations within the study area and elsewhere within the SMC. For instance, superstructure and infrastructure rocks, separated by ductile top-to-the-west shear zones and zones of attenuated metamorphic field gradients, experienced markedly different metamorphic evolutions and exhumation histories. The

metamorphic and geochronological data indicate that during the Late Cretaceous, the infrastructure was buried at depths of approximately 25 km. Yet, these upper amphibolite-facies rocks are juxtaposed with a cover of greenschist-facies superstructure rocks. As discussed above, the continuity and structural style of the superstructure preclude tectonic exhumation of the infrastructure by removal of the superstructure on detachments or shear zones within the study area. If the cover was not removed, then an alternate way of juxtaposing these tectonostratigraphic packages is to "move the middle in", or in other words, to inject low viscosity, melt-rich upper amphibolite-facies rocks into the crustal column through channel flow or orogenic "tunnelling" (cf. Jamieson et al. 2002).

The model also provides explanations for a number of other observations. Coeval shear zones with an opposite shear-sense would bound the top and bottom of the channel. Shear-sense indicators from Late Paleocene to Early Eocene granitic rocks that occur within the shear zone between superstructure and the middle crustal layer of the infrastructure in the Trinity Hills area, the proposed top of the zone of channel flow (Fig. 7*b*), have been dated at 56-60 Ma (Bardoux 1993; Vanderhaeghe et al. 1999). Mylonitic (top-to-the-east) deformation near the contact between Paleoproterozoic basement of the Thor-Odin culmination of the southern Monashee complex and the overlying middle crustal layer of the infrastructure, the proposed bottom of the zone of channel flow (Fig. 7*b*) , have been constrained between 58 and 59 Ma (Carr 1990). At deeper structural levels, ductile east-west boudinage or stretching is known to have continued until 54 Ma (Johnston et al. 2000; Spark 2002). Therefore, coeval granitic rocks with opposite shear-sense at the top and bottom of the proposed channel support a channel flow during the Late Paleocene to Early Eocene. Unfortunately, there is little information that constrains how long-lived this pattern of crustal flow was. Geochronological data from the northern SMC supports cooling of middle structural layer during the Early to Late Cretaceous (e.g., Scammell 1993), suggesting that channel flow may have been operative for 20-30 m.y. within the southeast Canadian Cordillera.

Channel flow can also explain the inverted metamorphic field gradient reported from the base of the middle structural level where it overlies the Frenchman Cap culmination of the northern Monashee complex (e.g., Journeay 1986; Gibson et al. 1999). Subsequent metamorphic, structural, and geochronological studies have suggested that the younging pattern of ages and inverted metamorphic field gradient in that area could not have been produced by thrusting of hotter over cooler rocks along a shear zone (the Monashee décollement; e.g., Parrish 1995), but that deformation and top-to-the-east shearing of the metamorphic sequence is required to explain the observed geochronological and metamorphic data (e.g., Gibson et al. 1999; Crowley et al.

2001). This shearing and top-to-the-east flow of rocks is easily incorporated in the context of a channel flow model (Glombick et al. 2002). A similar model has been proposed to explain the inverted metamorphic gradient near the base of Greater Himalayan Crystalline Sequence (e.g., Grujic et al. 1996; Beaumont et al. 2001; Hodges et al. 2001; Vannay and Grasemann 2001).

A channel flow model is further supported by the occurrence of mylonitic Paleocene granitic rocks (~ 64 Ma) with a shallowly plunging, east or west-trending stretching lineation within a fault-bounded metamorphic culmination located approximately 80 km west of the study area, known as the Nicola horst. Greenschist-facies volcanic and sedimentary rocks of the Upper Triassic Nicola Group intruded by Late Triassic to Early Jurassic batholiths and plutons surround the Nicola horst (Erdmer et al. 2002, and references therein). There is little evidence of extension within the Nicola Group, other than the bounding faults of the Nicola horst, suggesting that flow of partially molten rocks within a regional zone of channel flow may have been occurring beneath a thin (5-10 km) strong upper crust across a significant width of the southern Canadian Cordillera, possibly from the Fraser River fault, to east of the Valhalla complex, or even the Purcell thrust, a distance of several hundred kilometres.

A regional channel flow model is more difficult to reconcile with geological relationships exposed in the Valhalla complex, where the early Tertiary shear zone between superstructure and metamorphic infrastructure has a top-to-the-east shear sense (e.g., Carr 1987; Simony and Carr 1997). In addition, a top-to-the-east directed ductile shear zone, the Gwillim Creek shear zone, is exposed at lower structural levels of the complex, leading several authors to propose that exhumation occurred as mid-crustal rocks were thrust up a ramp in the Gwillim Creek shear zone or an underlying shear zone (Spear and Parrish 1996; Schaubs et al. 2002; Spear 2004). Thrusting on the Gwillim Creek shear zone has been linked with coeval shortening with the foreland Rocky Mountain fold and thrust belt (Varsek and Cook 1994; Cook and Van der Velden 1995). It is unclear at this stage how these relationships fit in with a channel flow model, but shear zones, accommodating zones of differing velocity within the channel, are expected as a result of differences in rock type, rheology, and (or) temperature.

If channel flow was a regional-scale process within the southern Canadian Cordillera in the Late Cretaceous to Early Eocene, a certain amount of displacement of mid-crustal rocks, relative to overlying and underlying rocks outside the channel, is expected. If the primary direction of channel flow was to the east, consistent with shear-sense from early Tertiary granitic rocks exposed within the study area and modelling experiments (e.g., Jamieson et al. 2002; Beaumont et al. 2004), injection of the channel at mid-crustal levels is expected east of the SMC. The leading edge of the zone of channel flow at the cessation of flow is unclear, but the brief

metamorphic event recorded within the northern Monashee complex is consistent with the proposed metamorphic event having a duration of a few million years (Crowley and Ghent 1999). This may indicate that the channel flowed up the basement ramp and over the Monashee complex just prior to the end of channel flow. Later exhumation was accommodated by displacement on moderately to steeply dipping brittle faults, such as the Columbia River fault (e.g., Lane 1984).

Another possible indication of the extent of early Tertiary channel flow may be apparent in the Kootenay Lake area, where an elongate, north-trending metamorphic belt is exposed (e.g., Read et al. 1991). The core of the metamorphic belt records sillimanite (after kyanite) zone metamorphic conditions. There have been no major bounding faults identified along the margins of the metamorphic belt, such as in the Valhalla complex. K-Ar cooling dates from surrounding metamorphic rocks in this area are dominantly Middle Jurassic to Late Cretaceous (Mathews 1983; Archibald et al. 1983, 1984). Centred on the metamorphic belt, however, is a belt defined by Paleocene to Eocene cooling dates (Mathews 1983; Archibald et al. 1984). To date, no direct cause for the localized resetting of K-Ar ages, such as plutonism or uplift, has been found. We hypothesize that this zone may reflect the extent of channel flow in the Late Paleocene to Middle Eocene, where rocks within the zone of channel flow approached the surface, locally resetting the K-Ar ages of overlying rocks, but the channel itself remained blind due to limited erosion.

It is hypothesized that channel flow contributed to orogenic collapse of the southern Canadian Cordillera through the spreading of a thickened crustal welt centred on the SMC. Channel flow develops in hot orogens where there is a topographic gradient, which provides the gravitational potential energy gradient that drives the spreading of the crust through a low-viscosity zone (e.g., Jamieson et al. 2002; Beaumont et al. 2004). If such a hypothesis is correct, then the timing of known channel flow, from the Late Paleocene to Early Eocene, must overlap the timing of thrusting within the foreland fold and thrust belt. A new method of dating motion on shallow thrust faults using X-ray modelling combined with sample encapsulation suggests that motion on the Lewis thrust, one of the major thrusts in the foreland fold and thrust belt of the southeastern Canadian Cordillera, was active at ~52 Ma (van der Pluijm et al. 2001). This lower age estimate of thrusting in the foreland indicates that the timing of thrusting overlapped the timing of proposed channel flow within the hinterland of the southern Canadian Cordillera.

Although certain aspects of the mapping, geochronological, structural, and metamorphic data are consistent with channel flow occurring within the southern Canadian Cordillera during the early Tertiary, the model requires additional testing through additional studies from other regions of the SMC, where the ductile strain history and metamorphic evolution still remain unstudied or obscure. Much more kinematic data from exhumed mid-crustal rocks exposed within

the SMC is needed to rigorously test the channel flow model and to improve our understanding of how ductile flow of the middle to lower crust contributes to the crustal evolution of orogenic belts.

References

Applegate, J.D.R., and Hodges, K.V. 1995. Mesozoic and Cenozoic extension recorded by metamorphic rocks in the Funeral Mountains, California. Geological Society of America Bulletin, **107**: 1063-1076.

Archibald, D.A., Glover, J.K., Price, R.A., Farrar, E., and Carmichael, D.M. 1983. Geochronology and tectonic implications of magmatism and metamorphism, southern Kootenay Arc and neighbouring regions, southeastern British Columbia. Part I. Jurassic to mid-Cretaceous. Canadian Journal of Earth Sciences, **20**: 1891-1913.

Archibald, D.A., Krogh, T.E., Armstrong, R.L., and Farrar, E. 1984. Chronology and tectonic implications of magmatism and metamorphism, southern Kootenay Arc and neighbouring regions, southeastern British Columbia: Part II, Mid-Cretaceous to Eocene. Canadian Journal of Earth Sciences, **21**: 567-583.

Bardoux, M. 1985. The Kelowna detachment zone, Okanagan Valley, south-central British Columbia. *In* Current Research, Part A. Geological Survey of Canada, Paper 85-1A, pp. 333-339.

Bardoux, M. 1986. Characteristics of the Okanagan Valley shear zone around Kelowna, south-central British Columbia. *In* Program with Abstracts, v. 11. Geological Association of Canada, p. 43.

Bardoux, M. 1993. The Okanagan Valley fault from Penticton to Enderby, south-central British Columbia. Ph.D. thesis, Carleton University, Ottawa.

Beaumont, C., Jamieson, R.A., Nguyen, M.H., and Lee, B. 2001*a*. Mid-crustal channel flow in large hot orogens: results from coupled thermal-mechanical models. *In* Slave-Northern Cordillera Lithospheric Evolution (SNORLCE) and Cordilleran Tectonics Workshop: Report of 2001 Combined Meeting. *Compiled by* F. Cook and P. Erdmer. Lithoprobe Report 79, pp. 112-170.

Beaumont, C., Jamieson, R.A., Nguyen, M.H., and Lee, B. 2001*b*. Himalayan tectonics explained by extrusion of a low-viscosity channel coupled to focused surface denudation. Nature, **414**: 738-742.

Beaumont, C., Jamieson, R.A., Nguyen, M.H., and Medvedev, S. 2004. Crustal channel flows: 1. Numerical models with applications to the tectonics of the Himalayan-Tibetan orogen. Journal of Geophysical Research, **109**: B06406, dio:10.1029/2003JB002809.

Breitsprecher, K. 1998. Volcanic stratigraphy, petrology and tectonic setting of the eastern margin of the Eocene Kamloops Group, south-central British Columbia. M.Sc. Thesis, Simon Fraser University, Vancouver.

Brown, R.L. 2004. Thrust belt accretion and hinterland underplating of orogenic wedges: an example from the Canadian Cordillera. *In* Thrust Tectonics and Petroleum Systems. *Edited by* K. McClay American Association of Petroleum Geologists, Memoir 82, pp. 1-14.

Camilleri, P.A. 1998. Prograde metamorphism, strain evolution, and collapse of footwalls of thick thrust sheets: a case study from the Mesozoic Sevier hinterland. Journal of Structural Geology, **20**: 1023-1042.

Camilleri, P.A., and Chamberlain, K.R. 1997. Mesozoic tectonics and metamorphism in the Pequop Mountains and Wood Hills region, northeast Nevada; implications for the architecture and evolution of the Sevier orogen. Geological Society of American Bulletin, **109**: 74-94.

Carr, S.D. 1990. Late Cretaceous-early Tertiary tectonic evolution of the southern Omineca Belt, Canadian Cordillera. Ph.D. thesis, Carleton University, Ottawa.

Carr, S.D. 1991. U-Pb zircon and titanite ages of three Mesozoic igneous rocks south of the Thor-Odin-Pinnacles area, southern Omineca Belt, British Columbia. Canadian Journal of Earth Sciences, **28**: 1877-1882.

Carr, S.D. 1992. Tectonic setting and U-Pb geochronology of the early Tertiary Ladybird leucogranite suite, Thor-Odin-Pinnacles area, southern Omineca Belt, British Columbia. Tectonics **11**: 258-278.

Carr, S.D., Parrish, R.R., and Brown, R.L. 1987. Eocene structural development of the Valhalla complex, southeastern British Columbia. Tectonics, **6**: 175-196.

Clark, M.K., and Royden, L.H. 2000. Topographic ooze: building the eastern margin of Tibet by lower crustal flow. Geology, **28**: 703-706.

Cook, F., and Van der Velden, A. 1995. Three-dimensional crustal structure of the Purcell Anticlinorium in the Cordillera of southwestern Canada. Geological Society of America Bulletin, **107**: 642-664.

Cook, F.A., Varsek, J.L., Clowes, R.M., Kanasewich, E.R., Spencer, C.S., Parrish, R.R., Brown, R.L., Carr, S.D., Johnson, B.J., and Price, R.A. 1992. Lithoprobe crustal reflection cross section on the southern Canadian Cordillera, 1, Foreland Thrust and Fold Belt to Fraser River fault. Tectonics, **11**: 12-35.

Crittenden, M.D., Jr., Coney, P.J., and Davis, G.H. (editors). 1980. Cordillera Metamorphic Core Complexes. Geological Society of America Memoir 153.

Crowley, J.L., and Ghent, E.D. 1999. An electron microprobe study of the U-Th-Pb systematics of metamorphosed monazite: the role of Pb diffusion versus overgrowth and recrystallization. Chemical Geology, **157**: 285-302.

Crowley, J.L., Ghent, E.D., Carr, S.D., Simony, P.S., and Hamilton, M.A. 2000. Multiple thermotectonic events in a continuous metamorphic sequence, Mica Creek area, southeastern Canadian Cordillera: Geological Materials Research, **2**: 1-45.

Crowley, J.L., Brown, R.L., and Parrish, R.R. 2001. Diachronous deformation and a strain gradient beneath the Selkirk allochthon, northern Monashee complex, southeastern Canadian Cordillera. Journal of Structural Geology **23**: 1103-1121.

Davis, G.A., Lister, G.S., and Reynolds, S.J. 1986. Structural evolution of the Whipple and South Mountains shear zones, south-western United States. Geology, **14**: 7-10.

Dunbar, J.A., and Sawyer, D.S. 1989. How pre-existing weaknesses control the style of continental break-up. Journal of Geophysical Research, B, Solid Earth and Planets, **94**: 7278-7292.

Erdmer, P., Thompson, R.I., and Daughtry, K.L. 1999. Pericratonic Paleozoic succession in Vernon and Ashcroft map areas, British Columbia. *In* Current Research 1999-A. Geological Survey of Canada, pp. 205-215.

Erdmer, P., Moore, J.M., Heaman, L., Thompson, R.I., Daughtry, K.L., and Creaser, R.A. 2002. Extending the ancient margin outboard in the Canadian Cordillera: record of Proterozoic crust and Paleocene regional metamorphism in the Nicola horst, southern British Columbia. Canadian Journal of Earth Sciences, **39**: 1605-1623.

Fulton, R.J., and Halstead, E.C. 1972. Quaternary geology of the southern Canadian Cordillera. Guidebook, International Geological Congress. 24, Part AO2.

Ghosh, D.K. 1995. U-Pb geochronology of Jurassic to early Tertiary granitic intrusives from the Nelson-Castlegar area, southeastern British Columbia, Canada. Canadian Journal of Earth Sciences, **32**: 1668-1680.

Gibson, H.D., Brown, R.L., and Parrish, R.R. 1999. Deformation-induced metamorphic field gradients: an example from the southeastern Canadian Cordillera. Journal of Structural Geology, **21**: 751-767.

Glombick, P., and Thompson, R.I. 2004. Geology of the Creighton Creek map area, British Columbia (NTS 82L/02). Geological Survey of Canada Open File 4371, scale 1:50 000.

Glombick, P., Erdmer, P., Thompson, R.I., and Daughtry, K.L. 1999. Ductile shear zones and an Eocene unconformity between Kalamalka Lake and Oyama Lake, Vernon map area, British Columbia. *In* Current Research 1999-A. Geological Survey of Canada, pp. 193-198.

Glombick, P., Thompson, R.I., and Erdmer, P. 2002. The role of a melt-rich middle crust layer in core complex formation; evidence from the Shuswap metamorphic complex, south-central

British Columbia. *In* Abstracts with Programs, Geological Society of America, 2002 annual meeting, p. 109.

Glombick, P., Thompson, R.I., and Daughtry, K.L. 2004. Geology of the Oyama map area, British Columbia (NTS 82L/03). Geological Survey of Canada Open File 4372, scale 1:50 000.

Gross, W.W., and Hillemeyer, F.L.B. 1982. Geometric analysis of upper-plate fault patterns in the Whipple-Buckskin detachment terrane, California and Arizona. *In* Mesozoic-Cenozoic tectonic evolution of the Colorado River region, California, Arizona, and Nevada. *Edited by* E.G. Frost and D.L. Martin. Cordilleran Publications, San Diego, California, U.S., pp. 256-266.

Grujic, D., Casey, M., Davidson, C, Hollister, L.S., Kundig, R., Pavlis, T., and Schmid, S. 1996. Ductile extrusion of the Higher Himalayan crystalline in Bhutan: evidence from quartz microfabrics. Tectonophysics, **260**: 21-43.

Heaman, L.M., and Parrish, R.R. 1991. U-Pb geochronology of accessory minerals. *In* Applications of Radiogenic isotopic systems to problems in geology. *Edited by* L. Heaman and J.N. Ludden. Mineralogical Association of Canada, pp. 59-102.

Hodges, K.V. 2000. Tectonics of the Himalaya and southern Tibet from two perspectives. Geological Society of America Bulletin, **112**: 324-350.

Hodges, K.V., and Walker, J.D. 1992. Extension in the Cretaceous Sevier orogen, North American Cordillera. Geological Society of America Bulletin, **104**: 560-569.

Hodges, K.V., Hurtado, J.M., and Whipple, K.X. 2001. Southward extrusion of Tibetan crust and its effect on Himalayan tectonics. Tectonics, **20**: 799-809.

Hoisch, T.D., Wells, M.L., and Hanson, L.M. 2002. Pressure-temperature paths from garnet zoning; evidence for multiple episodes of thrust burial in the hinterland of the Sevier orogenic belt. American Mineralogist, **87**: 115-131.

Holk, G.J., and Taylor, H.P. Jr. 1997. $^{18}O/^{16}O$ homogenization of the middle crust during anatexis: the Thor-Odin metamorphic core complex, British Columbia. Geology, **25**: 31-34.

Jamieson, R.A., Beaumont, C., Nguyen, M.H., and Lee, B. 2002. Interaction of metamorphism, deformation, and exhumation in large convergent orogens. Journal of Metamorphic Geology, **20**: 1-16.

Johnson, B.J. 1994. Structure and tectonic setting of the Okanagan Valley fault system in the Shuswap Lake area, southern British Columbia. Unpublished Ph.D. thesis, Carleton University, Ottawa.

Johnson, B.J., and Brown, R.L. 1996. Crustal structure and early Tertiary extensional tectonics of the Omineca belt at 51°N latitude, southern Canadian Cordillera. Canadian Journal of Earth Sciences, **33**: 1596-1611.

Johnston, D.H. 1998. Structural and thermal evolution of northwest Thor-Odin dome, Monashee complex, British Columbia. Ph.D. thesis, University of New Brunswick, Fredericton.

Johnston, D.H., Williams, P.F., Brown, R.L., Crowley, J.L., and Carr, S.D. 2000. Northeastward extrusion and extensional exhumation of crystalline rocks of the Monashee complex, southeastern Canadian Cordillera. Journal of Structural Geology, **22**: 603-625.

Journeay, J.M. 1986. Stratigraphy, internal strain and thermotectonic evolution of northern Frenchman Cap dome: an exhumed duplex structure, Omineca hinterland, SE Canadian Cordillera. Ph.D. thesis, Queen's University, Kingston.

Kretz, R. 1983. Symbols for rock-forming minerals. American Mineralogist, **68**: 277-279.

Kruger, J.M., and Johnson, R.A. 1994. Raft model of crustal extension: evidence from reflection data in southeast Arizona. Geology, **22**: 351-354.

Kuiper, Y. 2003. Geochronological, petrological and microstructural studies on the Thor-Odin dome, Monashee complex, southern Canadian Cordillera. Ph.D. thesis, University of New Brunswick, Fredericton.

Lane, L.S.1984. Brittle deformation in the Columbia River fault zone near Revelstoke, southeastern British Columbia. Canadian Journal of Earth Sciences, **21**: 584-598.

Lemieux, Y., Thompson, R.I., and Erdmer, P. 2003. Stratigraphy and structure of the Upper Arrow Lake area, southeastern British Columbia: new perspectives for the Columbia River fault zone. *In* Current Research 2003, Geological Survey of Canada, 2003-A7.

Lister, G.S., and Davis, G.A. 1989. The origin of metamorphic core complexes and detachment faults during Tertiary continental extension in the northern Colorado River Region, U.S.A. Journal of Structural Geology, **11**: 65-94.

Lowe, C., and Ranalli, G. 1993. Density, temperature, and rheological models for the southeastern Canadian Cordillera: implications for its geodynamic evolution. Canadian Journal of Earth Science, **30**: 77-93.

Lui, M., and Furlong, K. 1993. Crustal shortening and Eocene extension in the southeastern Canadian Cordillera: some thermal and rheological considerations. Tectonics, **12**: 776-786.

MacCready, T., Snoke, A.W., Wright, J.E., and Keith, K.A. 1997. Mid-crustal flow during Tertiary extension in the Ruby Mountains core complex, Nevada. Geological Society of America Bulletin, **109**: 1576-1594.

Mathews, W.H. 1981. Early Cenozoic resetting of potassium-argon dates and geothermal history of north Okanagan area, British Columbia. Canadian Journal of Earth Sciences, **18**: 1310-1319.

Mathews, W.H. 1983. Early Tertiary resetting of potassium-argon dates in the Kootenay Arc, southeastern British Columbia. Canadian Journal of Earth Sciences, **20**: 867-872

McCarthy, J., and Parsons, T. 1994. Insights into the kinematic Cenozoic evolution of the Basin and Range-Colorado Plateau transition from coincident seismic refraction and reflection data. Geological Society of America Bulletin, **106**: 747-759.

Nelson, K.D., Zhao, W., Brown, L.D., Kuo, J., Che, J., Liu, X., Klemperer, S.L., Makovsky, Y., Meissner, R., Mechie, J., Kind, R., Wenzel, F., Ni, J., Nabelek, J., Leshou, C., Ten, H., Wei, W., Jones, A.G., Booker, J., Unsworth, M., Kidd, W.S.F., Hauck, M., Alsdorf, D., Ross, A., Cogan, M., Wu, C., Sandoval, E., and Edwards, M. 1996. Partially molten middle crust beneath southern Tibet: synthesis of Project INDEPTH results. Science, **274**: 1684-1688.

Norlander, B.H., Whitney, D.L., Teyssier, C., and Vanderhaeghe, O. 2002. Partial melting and decompression of the Thor-Odin dome, Shuswap metamorphic core complex, Canadian Cordillera. Lithos, **61**: 103-125.

Okulitch, A.V. 1987. Comment and reply on "Extension across the Eocene Okanagan crustal shear in southern British Columbia." Geology, **15**: 187-188.

Parkinson, D.L. 1992. Age and tectonic evolution of the southern Monashee Complex, southeastern British Columbia: a window into the deep crust. Ph.D. thesis, University of California, Santa Barbara.

Parrish, R.R. 1992. U-Pb ages of Jurassic-Eocene plutonic rocks in the vicinity of the Valhalla complex, southeast British Columbia. *In* Radiogenic age and isotopic studies, Report 5. Geological Survey of Canada, Paper, pp. 115-134.

Parrish, R.R. 1995. Thermal evolution of the southeastern Canadian Cordillera. Canadian Journal of Earth Sciences, **32**: 1618-1642.

Parrish, R.R., and Armstrong, R.L. 1987. The ca. 162 Ma Galena Bay stock and its relationship to the Columbia River fault zone, southeast British Columbia. *In* Radiogenic Age and Isotopic Studies: Report 1. Geological Survey of Canada, Paper 87-2, pp. 25-32.

Parrish, R.R., and Wheeler, J.O. 1983. U-Pb zircon age of the Kuskanax batholith, southeastern British Columbia. Canadian Journal of Earth Sciences, **20**: 1751-1756.

Parrish, R.R., Carr, S.D., and Parkinson, D.L. 1988. Eocene extensional tectonics and geochronology of the southern Omineca Belt, British Columbia and Washington. Tectonics, 7: 181-212.

Passchier, C.W., and Trouw, R.A.J. 2000. Microtectonics. Springer-Verlag, Berlin-Heidelberg-New York.

Pattison, D.R.M. 1992. Stability of andalusite and sillimanite and the Al_2SiO_5 triple point: constraints from the Ballachulish aureole, Scotland. Journal of Geology, **100**: 423-446.

Platt, J. P. 1986. Dynamics of orogenic wedges and the uplift of high-pressure metamorphic rocks. Geological Society of America Bulletin, **97**: 1037-1053.

Read, P.B., Woodsworth, G.J., Greenwood, H.J., Ghent, E.D., and Evenchick, C.A. 1991. Metamorphic map of the Canadian Cordillera. Geological Survey of Canada, Map 1714A, scale 1:2 000 000.

Reesor, J.E., and Moore, J.M. 1971. Petrology and structure of the Thor-Odin gneiss dome, Shuswap metamorphic complex, British Columbia. Geological Survey of Canada Bulletin 195.

Royden, L.H. 1996. Coupling and decoupling of crust and mantle in convergent orogens: implications for strain partitioning in the crust. Journal of Geophysical Research, **101**: 17679-17705.

Scammell, R.J. 1993. Mid-Cretaceous to Tertiary thermotectonic history of former mid-crustal rocks, southern Omineca Belt, Canadian Cordillera. Ph.D. thesis, Queen's University, Kingston, Ontario.

Schaubs, P.M., Carr, S.D., and Berman, R.G. 2002. Structural and metamorphic constraints on ca. 70 Ma deformation of the northern Valhalla complex, British Columbia: implications for the tectonic evolution of the southern Omineca belt. Journal of Structural Geology, **24**: 1195-1214.

Scott, D.J., and St-Onge, M.R. 1995. Constraints on Pb closure temperature in titanite based on rocks from the Ungava orogen, Canada: implications for U-Pb geochronology and P-T-t path determinations. Geology, **23**: 1123-1126.

Sevigny, J.H., and Parrish, R.R. 1993. Age and origin of Late Jurassic and Paleocene granitoids, Nelson batholith, southern British Columbia. Canadian Journal of Earth Sciences, **30**: 2305-2314.

Shen, F., Royden, L.H., and Burchfiel, B.C. 2001. Large-scale crustal deformation of the Tibetan Plateau. Journal of Geophysical Research, **106**: 6793-6816.

Simony, P.S., and Carr, S.D. 1997. Large lateral ramps in the Eocene Valkyr shear zone: extensional ductile faulting controlled by plutonism in southern British Columbia. Journal of Structural Geology, **19**: 769-784.

Spark, R.N. 2002. Crustal thickening and tectonic denudation within the Thor-Odin culmination, Monashee complex, southern Canadian Cordillera. Ph.D. thesis, University of New Brunswick, Fredericton.

Spear, F.S. 2004. Fast cooling and exhumation of the Valhalla metamorphic core complex, southeastern British Columbia. International Geology Review, **46**: 193-209.

Spear, F.S. and Parrish, R.R. 1996. Petrology and petrologic cooling rates of the Valhalla Complex, British Columbia, Canada. Journal of Petrology **37**: 733-765.

Tempelman-Kluit, D., and Parkinson, D. 1986. Extension across the Eocene Okanagan crustal shear in southern British Columbia. Geology, **14**: 318-321.

Teyssier, C., Ferré, E., Whitney, D.L., Norlander, B., Vanderhaeghe, O., and Parkinson, D. (2005). Flow of partially molten crust and origin of detachments during collapse of the Cordilleran orogen. Geological Society of London, Special Publication on high strain zones.

Thompson, R.I. 2004*a*. Geology of the Salmon Arm map area, British Columbia (NTS 82L/11). Geological Survey of Canada Open File 4380, scale 1:50 000.

Thompson, R.I. 2004*b*. Geology of the Gates Creek map area, British Columbia (NTS 82L/09). Geological Survey of Canada Open File 4378, scale 1:50 000.

Thompson, R.I., and Daughtry, K.L. 1996. New stratigraphic and tectonic interpretations, north Okanagan Valley, British Columbia. *In* Current Research 1996-A. Geological Survey of Canada, pp. 135-141.

Thompson, R.I. and Glombick, P. 2004*a*. Geology of the Shuswap Falls map area, British Columbia (NTS 82L/07). Geological Survey of Canada Open File 4376, scale 1:50 000.

Thompson, R.I., and Glombick, P. 2004*b*. Geology of the Mabel Lake map area, British Columbia (NTS 82L/10). Geological Survey of Canada Open File 4379, scale 1:50 000.

Thompson, R.I., and Unterschutz, J.L.E. 2004. Geology of the Vernon map area, British Columbia (NTS 82L/06). Geological Survey of Canada Open File 4375, scale 1:50 000.

Thompson, R.I. and Glombick, P., and Lemieux, Y. (compilers). 2004*a*. Geology of the Eureka Mountain map area, British Columbia (NTS 82L/01). Geological Survey of Canada Open File 4370, scale 1:50 000.

Thompson, R.I. and Glombick, P., and Lemieux, Y. (compilers). 2004*b*. Geology of the Mount Fosthall map area, British Columbia (NTS 82L/08). Geological Survey of Canada Open File 4377, scale 1:50 000.

Vanderhaeghe, O., Teyssier, C., and Wysoczanski, R. 1999. Structural and geochronological constraints on the role of partial meting during the formation of the Shuswap metamorphic

complex at the latitude of Thor-Odin dome, British Columbia. Canadian Journal of Earth Sciences, **36**: 917-943.

Vanderhaeghe, O., Teyssier, C., McDougall, I., and Dunlap, W.J. 2003. Cooling and exhumation of the Shuswap Metamorphic Core Complex constrained by 40Ar/39Ar thermochronology. Geological Society of America Bulletin, **115**: 200-216.

van der Pluijm, B.A., Hall, C.M., Vrolijk, P.J., Pevear, D.R., and Covey, M.C. 2001. The dating of shallow faults in the Earth's crust. Nature, **412**: 172-175.

Vannay, J.C., and Grasemann, B. 2001. Himalayan inverted metamorphism and syn-convergence extension as a consequence of a general shear extrusion. Geological Magazine, **138**: 253-276.

Varsek, J., and Cook, F. 1994. Three-dimensional crustal structure of the eastern Cordillera, southwestern Canada and northwestern United States. Geological Society of America Bulletin, **106**: 803-823.

Wells, M.L. 1997. Alternating contraction and extension in the hinterlands of orogenic belts; an example from the Raft River mountains, Utah. Geological Society of America Bulletin, **109**: 107-126.

Wernicke, B. 1995. The fluid crustal layer and its implications for continental dynamics. *In* Exposed Cross-sections of the Continental Crust. *Edited by* M.H. Salisbury and D.M. Fountain. NATO ASI Series. Series C. Mathematical and Physical Sciences, 317. D. Reidel Publishing Company, Dordrecht-Boston, pp. 509-544.

Wheeler, J.O., Brookfield, A.J., Gabrielse, H., Monger, J.W.H., Tipper, H.W., and Woodsworth, G.J. (compilers). 1991. Terrane map of the Canadian Cordillera. Geological Survey of Canada, Map 1713A, scale 1:2 000 000.

Williams, P.F. 1999. Interpretation of thrust-like structures in middle and lower crustal rocks. *In* Tectonic and Magmatic Processes in Crustal Growth: a Pan-Lithoprobe Perspective. Lithoprobe Report 75, pp. 67-68.

Woodsworth, G.J., Anderson, R.G., and Armstrong, R.L. 1991. Plutonic regimes, Chapter 15. *In* Geology of the Cordilleran orogen in Canada. *Edited by* H. Gabrielse and C.J. Yorath. Geological Survey of Canada, Geology of Canada no. 4, pp. 491-531.

APPENDIX A

Description of map units

Description of map units

Introduction

This appendix is intended to accompany and supplement the following National Topographic System (NTS) 1:50 000 map sheets: (1) Eureka Mountain (82L/01; Thompson et al. 2004*a*); (2) Creighton Creek (82L/02; Glombick and Thompson 2004); (3) Oyama (82L/03; Glombick et al. 2004); (4) Vernon (82L/06; Thompson and Unterschutz 2004); (5) Shuswap Falls (82L/07; Thompson and Glombick 2000*a*); (6) Mount Fosthall (82L/08; Thompson et al. 2004*b*); and (7) Mabel Lake (82L/10; Thompson and Glombick 2004*b*).

The author was primarily responsible for mapping and compiling the majority of 82L/03, 82L/02, and 82L/01. These three map sheets, which represent one of the primary products of this thesis, are included in the map pocket at the back of the thesis. Other areas, located between the Okanagan Valley and Upper Arrow Lake in which critical geological relationships between superstructure and infrastructure were exposed, such as the Silver Star Mountain and Trinity Hills areas, were also mapped by the author (Fig. A-1). Descriptions of map units are limited to geological units mapped by the author in these areas.

Division of the rocks within the study area

In the following section, map units within the study area are grouped into the following four divisions: (1) infrastructure rocks; (2) superstructure rocks; (3) intrusive rocks; and (4) Tertiary volcanic and sedimentary rocks.

For the purpose of this appendix, infrastructure rocks are sillimanite-grade metamorphic rocks that are included within the Shuswap metamorphic complex (SMC) as defined by Okulitch (1984). Superstructure rocks are sub-sillimanite grade rocks that flank the margins of the complex or form a semi-continuous, southeast-striking belt that transects the study area between the Okanagan Valley and Upper Arrow Lake. The division between the two, as used here, is purely based on metamorphic grade and therefore has no tectonic implications.

Infrastructure rocks (middle structural level)

The Hunters Range assemblage

In the northern region of the study area, locally known the Trinity Hills and Hunters Range, upper amphibolite-facies pelitic to semi-pelitic schist and psammitic gneiss (Pqfh), and calcsilicate gneiss, marble, and amphibolite gneiss (Pcgma) of the Hunters Range assemblage is exposed (see also, Johnson 1994). The most common rock type within the Hunters Range

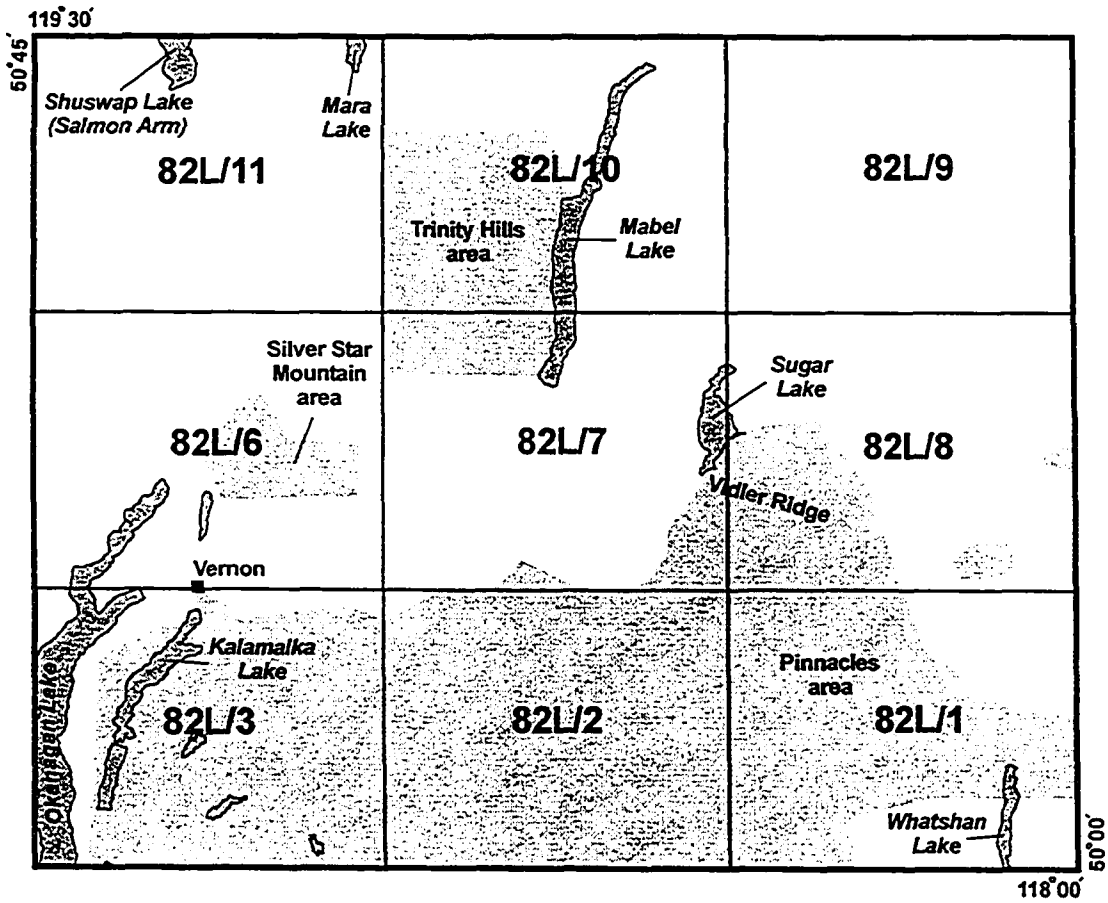

Fig. A-1. Portions of NTS 1:50 000 topographic map sheets mapped by the author during the period of 1998 to 2001.

succession is a grey to purplish-weathering, migmatitic pelitic schist. Leucosome layers millimetres to centimetres thick, comprised of quartz and feldspar, are oriented parallel to the metamorphic foliation, which is folded by open to isoclinal folds. The most abundant constituents of the pelitic schist are quartz, potassium-feldspar, and biotite, with lesser amounts of garnet, sillimanite, plagioclase-feldspar, ilmenite, zircon, and monazite. Leucosome, interpreted as having formed in-situ, comprises up to 30% (by volume) of outcrops locally, indicating that a significant amount of partial melting occurred.

The mountainous region south of the Trans-Canada Highway between Sicamous and Three Valley Gap is underlain by a monotonous succession of dominantly migmatitic pelitic rocks, with lesser amounts of calcsilicate gneiss, marble, and amphibolite gneiss, and Devonian granodioritic orthogneiss. Near Sicamous, Johnson (1994) mapped these rocks and grouped them into the Hunters Range assemblage. Further east, near Three Valley Gap, Johnston (1998) mapped a similar succession in terms of rock types, metamorphic grade, structure, and appearance, but named it the Three Valley Gap/Grizzly Flats assemblage. A division between the Hunters Range assemblage and the Three Valley Gap/Grizzly Flats assemblage cannot be recognized in the field, leading to the suggestion that they are both the same age (Thompson et al., in review[1]). Thompson and Daughtry (2000) have mapped a distinctive marble-calcsilicate-amphibolite-quartzite succession exposed in the vicinity of Joss Mountain, westward to Mabel Lake, where it is informally known as the Kingfisher succession, suggesting that the Hunters Range and Three Valley Gap/Grizzly Flats assemblages may be correlative.

At present, the only published isotopic age control on the age of the Hunters Range and Three Valley Gap/Grizzly Flats assemblages is from an amphibolite boudin exposed within a dominantly pelitic schist succession exposed along the Trans-Canada Highway that has yielded a U-Pb (zircon) upper intercept age of 1572 ± 76 Ma (Parkinson 1992). Regardless of whether the boudin is a metamorphosed and deformed dyke or flow, it provides a minimum age constraint. This age is older than current geochronological constraints on the initiation of the Purcell Supergroup at *ca.* 1490 Ma (Anderson and Parrish 2000), making a correlation between the two

---

[1] Thompson, R.I., Glombick, P., Erdmer, P., Daughtry, K.L., Heaman, L., and Friedman, R.L. (in review). Evolution of the ancestral Pacific margin, southern Canadian Cordillera: Insights from new geologic maps. *Submitted to* Colpron, M., Nelson, J. L. and Thompson, R. I. (editors.), Paleozoic evolution and metallogeny of pericratonic terranes at the ancient Pacific margin of North America, Canadian and Alaskan Cordillera. Geological Association of Canada, Special Paper.

unlikely. If the Hunters Range assemblage and Three Valley Gap/Grizzly Flats assemblages are correlative, as Thompson et al. (in review) suggest, then pelitic schist, calcsilicate gneiss, and amphibolite mapped by the author west of Mabel Lake may be 1570 Ma or older in age.

The Kalamalka Lake metamorphic assemblage

Southeast of the town of Vernon, the region southeast of Kalamalka Lake is underlain by a heterolithic paragneiss succession, informally known as the Kalamalka Lake metamorphic assemblage (82L/03; Erdmer et al. 1998; Glombick et al. 1999). Rock types within the assemblage include: pelitic and semi-pelitic schist (Pqfh), psammitic gneiss (also included in Pqfh), calcsilicate gneiss (Pcga), and amphibolite (DPas).

The principle rock type is a medium to coarse-grained biotite schist (Pqfh), locally with garnet and(or) sillimanite. Pelitic schist is commonly migmatitic, with delicate leucosomes, several millimetres thick, oriented parallel to the metamorphic foliation. Near the southern end of Kalamalka Lake, plagioclase feldspar-biotite-hornblende gneiss dominates. The weathering of biotite and other iron-rich minerals impart a characteristic red staining to the rock. The irregular distribution of biotite and hornblende grains within the dominantly quartzofeldspathic matrix results in a characteristic "salt and pepper" appearance.

Near the southeastern end of Kalamalka Lake, calcsilicate rocks occur within two layers several hundred metres in thickness (Pcga). Rock types within the calcsilicate unit include: calcsilicate gneiss, impure quartzite, marble, and minor amphibolite gneiss. Calcsilicate gneiss is composed of quartz, plagioclase feldspar, calcite, grossular garnet, diopside, and hornblende. Weathered exposures of this unit are yellowish-brown to orange in colour, giving the rock a distinctive weathered appearance.

Along the eastern shore of Kalamalka Lake, the Kalamalka Lake metamorphic assemblage is overprinted by the Kalamalka Lake shear zone, a gently west-dipping mylonite zone over five hundred metres thick (Erdmer et al. 1998; Glombick et al. 1999; Chapter 2). Rodded quartz grains, aligned bundles of sillimanite needles, and aggregates of biotite and feldspar visible on the foliation surface define a well-developed, gently plunging, east or west-trending stretching lineation. Shear-sense indicators, including C-S fabric, delta and sigma porphyroclasts, back-rotated boudins, and (C') extensional shear bands, consistently yield a top to the west shear-sense (Erdmer et al. 1998; Glombick et al. 1999). While rodded quartz layers indicate plastic deformation of quartz during strain, feldspar grains deformed in a brittle fashion, resulting in broken and milled potassium feldspar porphyroclasts which are visible on the foliation surface.

The Kalamalka Lake metamorphic assemblage is host to abundant syn- to post-kinematic granitic sills, dykes, and stocks of probable early Tertiary age. A stock of fine-grained, moderately foliated, biotite-bearing granite exposed along the eastern shore of Kalamalka Lake has been dated at 50 Ma (Heaman et al. 1999), indicating that a component of ductile deformation post-dates this time.

East of Kalamalka Lake, the Kalamalka Lake metamorphic assemblage is intruded by the Middle Triassic Aberdeen gneiss complex (TAG). The densely wooded region in the Buck Hills is underlain by a succession of pelitic and semi-pelitic schist (Pqfh) with lesser amounts of calcsilicate gneiss (Pcga) and amphibolite, similar in character to the Kalamalka Lake metamorphic assemblage (82L/02; 82L/03; Glombick et al. 2000).

The age of the Kalamalka Lake metamorphic assemblage is not clear. The Aberdeen gneiss complex (TAG), which has yielded a Middle Triassic U-Pb zircon date (~232 Ma), provides a minimum age constraint. Near Cosens Bay, the Kalamalka Lake metamorphic assemblage contains a distinctive, pitted-weathering calcareous quartzite unit (Dcqm), which has been correlated with the Chase Formation, of known Devonian age (Thompson et al. 2001). At present, this is the most reliable information regarding the age of the Kalamalka Lake metamorphic succession.

The Cherryville horst metamorphic assemblage

Along Highway 6, between Shuswap Falls and Cherryville, a complexly deformed suite of amphibolite-facies rocks is preserved in a normal fault bounded horst. The horst is bounded on the west by the Mabel fault and on the east by the Cherry fault (82L/02). Rocks types within the succession include sillimanite-bearing pelitic schist, calcsilicate gneiss, marble, amphibolite gneiss, and lesser amounts of grey micaceous quartzite. Large amounts of syn- to postkinematic granitic sills and dykes of the Paleocene to Early Eocene Ladybird suite (ELBg) occur.

The age of the rocks within the Cherryville fault block is uncertain. They may be correlative with the pelitic and calcsilicate gneiss succession exposed to the north, along the eastern shore of Mabel Lake, as they contain similar rock types. If this correlation is correct, the rocks may be Proterozoic in age, which is the best age estimate for the Grizzly Flats/Three Valley Gap succession. Chemical electron microprobe (EMP) dates from monazite within a metapelitic sample from within the Cherryville horst, however, has yielded Upper Triassic dates, which, in the absence of a known metamorphic event of that age in this area, are interpreted as detrital (Chapter 4). If this is the case, then the rocks exposed within the core of the Cherryville horst may

be high-grade equivalents of lower-grade Upper Triassic (Norian) rocks that flank the horst to the west.

The Chase Formation

The Chase Formation (Thompson et al. 2001; Thompson et al., in review) provides a useful stratigraphic and structural marker unit within the Vernon area, as it is distinguished from other calcsilicate or carbonate units exposed within the Vernon map area by its unique composition, distinctive weathering pattern, and predictable position within a regionally extensive lithostratigraphic succession.

The unit is composed almost entirely of calcite and quartz, in approximately equal amounts. Minor amounts (less than 5% by volume) of diopside, feldspar, and mica also occur locally, with diopside being the most common. Other (aluminous) minerals commonly found in calcsilicate rocks, such as tremolite, actinolite, wollastonite, and grossular garnet are generally absent, indicating that the calcareous quartzite unit is deficient in aluminium. This suggests the unit was deposited in a high-energy depositional environment, lacking in fine-grained clastic input.

Weathered surfaces of the Chase Formation exhibit a characteristic light brown to buff-coloured pitted appearance, caused by the preferential weathering of the calcite grains relative to the quartz grains. This results in a pitted appearance, which is granular and crumbly upon close inspection. Alternating resistant and recessive centimetre-scale banding is typical, resulting from minor variations in the proportion of calcite and quartz. The resistant and recessive layers commonly outline outcrop-scale isoclinal fold hinges. Fresh exposures are white in colour.

The association between unit Dcqm and other rock types make it a useful marker unit at the regional scale. Unit Dcqm is invariably underlain by rusty-weathering biotite and(or) hornblende schist of unit Pqfh. Unit Dcqm is overlain by yellow to orange-weathering pelitic schist of the Silver Creek Formation (Dqfb) and locally by amphibolite and amphibolitic schist (DPas), informally known as the Tsalkom South Formation (Ken Daughtry, personal communication, 1999).

Earlier workers in the Vernon (82L) and adjacent Lardeau (82K) map areas recognized the potential of the distinctive calcareous quartzite unit as a potential marker horizon, but did not follow it outside their respective map areas (Hyndman 1968; Reesor and Moore 1971). This prediction has proven true, as, despite the apparent structural complexity of high-grade metamorphic rocks in the Vernon map area, particularly within the Thor-Odin dome (e.g.,

Williams and Jiang 2005), the calcareous quartzite unit has been mapped as a semi-continuous layer of variable thickness from the western margin of the Lardeau (82K) map area, across the entire width of the Vernon (82L) map area (Thompson et al. 2002). This continuity, although surprising considering the abundant outcrop-scale evidence for isoclinal folding and intense transposition, may reflect in part the original stratigraphic extent of the Chase Formation.

The Chase Formation has been constrained to be Devonian in age. Near the town of Chase, a sample of the Chase Formation has yielded three nearly concordant single grain zircon grains, interpreted as detrital in origin, with $^{207}Pb/^{206}Pb$ dates of 405 +/- 13 Ma, 424 +/- 13 Ma, and 1008 +/- 2 Ma. In this same area, a foliated granodiorite has been dated as Late Devonian. The granodiorite intrudes the Silver Creek Formation, which overlies the Chase Formation, constraining the Chase Formation to be Devonian in age (Thompson et al., in review).

The Silver Creek Formation

The Chase Formation is overlain by a highly deformed, heterolithic succession of amphibolite-facies metamorphic rocks grouped within the Silver Creek Formation. Determining age and stratigraphic position within this succession is complicated by the complex structure and high metamorphic grade, which excludes the use of paleontological methods and the principle of superposition.

The definition of the Silver Creek Formation has changed over time. Jones (1959), who originally defined the formation, used it to refer to garnet-grade micaceous schist exposed west of the Okanagan Valley. On his map, the Chase Formation was designated as a sub-member that occurred within the Silver Creek Formation. High-grade rocks exposed east of the Okanagan Valley, although of similar lithology, were included within the Monashee Group, of inferred Archean age (Jones 1959).

More recently, however, it has been shown that the Chase Formation occurs east of the Okanagan Valley, within the Monashee Group of Jones (1959) (82L/11; Thompson et al. 2002). East of the Okanagan Valley, the Chase Formation overlies rocks of the Hunters Range assemblage of Johnson (1994).

The dominant rock type within the Silver Creek Formation is garnet-muscovite-biotite schist (Dqfb), with or without kyanite, sillimanite, andalusite, staurolite, and primary chlorite. The Silver Creek Formation also includes lesser amounts of dark-grey carbonaceous schist, impure, dark to light-grey micaceous quartzite, grey to white impure marble (Dm), amphibolitic schist, amphibolite, and rarely metaconglomerate (Dcg).

A distinctive layer of staurolite schist, 10's to greater than 100 m in thickness, occurs as a sub-unit within the Silver Creek Formation (Dqfbs). The distinctiveness of this layer is due to its structural position – it always occurs structurally above the Chase Formation – and because of its large, well-developed staurolite crystals (5 cm or larger), many of which show characteristic bow-tie twinning. Staurolite porphyroblasts are randomly oriented within the metamorphic foliation, but are locally cut by extensional shear bands. The consistent current structural position of this layer within the lithostratigraphic succession, occurring several hundreds of metres above the Chase Formation, makes this layer, much like the Chase Formation, a useful regional marker horizon. The unusual mineralogy of this layer, which is a result its high aluminium content, may reflect a clay-rich sedimentary protolith. The remarkable continuity of this staurolite-bearing layer and its consistent position several hundreds of metres above the Chase Formation may result from an original depositional sequence.

Another distinctive layer that occurs within the Silver Creek Formation is a dark-grey to black-weathering amphibolitic schist or amphibolite gneiss (DPas), comprised primarily of hornblende, biotite, and plagioclase, although actinolite and chlorite are present locally. In places, the layer is a true amphibolite. The thickness and occurrence of this layer are more variable than other metasedimentary layers within the Silver Creek Formation, which is interpreted to reflect original depositional heterogeneity. Based on the rock type and layered nature of the unit, a metavolcanic origin is likely. In light of this interpretation, it is reasonable that the irregular distribution of this unit within the Silver Creek Formation is the result of scattered volcanic centres. Near the Trinity Hills and Grindrod, exposures of this unit are known locally as the "Tsalkom South Formation" (K.L. Daughtry, personal communication, 1999).

The age of the Silver Creek Formation is uncertain. The Chase Formation, which it overlies, is constrained to be Devonian in age. It seems reasonable, therefore, that unless the entire succession is overturned, or there is a significant unconformity between the two formations, the lowest section of the Silver Creek Formation is Devonian or younger in age. The Silver Creek Formation is also overlain, in places, by the Spa Creek succession (see below), which, in turn, is overlain unconformably by the Upper Triassic Slocan Group (Read and Okulitch 1977). The age of the Silver Creek Formation, therefore, is most likely between Latest Devonian and Upper Triassic.

In some locations, however, the Silver Creek Formation has yielded Upper Triassic chemical monazite ages (Chapter 4). These results are open to interpretation, but in many areas of the SMC the boundary between rocks of the Silver Creek Formation and compositionally similar but lower-grade rocks of the Slocan Group is delineated based on solely on metamorphic grade or

composition. In many areas, such as near Silver Star Mountain, the apparent metamorphic grade is controlled by variations in protolith composition. Pelitic rocks, when metamorphosed, transform into coarse-grained pelitic schist with coarse garnet and staurolite porphyroblasts, which intuitively appear to be higher grade than adjacent fine-grained, carbonaceous siliceous dark clastic rocks.

As isotopic evidence suggests that peak regional metamorphism in the Vernon area occurred in the Middle Jurassic and Late Cretaceous (Chapter 4), inferring ages based on metamorphic grade and structural position can lead to erroneous conclusions regarding the age of a map unit. This is particularly true given the preservation of abundant isoclinal folds within the succession (e.g., Williams and Jiang 2005). It is possible, therefore, that in some areas, amphibolite-facies rocks presently included within the Silver Creek Formation are actually high-grade equivalents of the Upper Triassic Slocan Group (see Chapter 4).

The Spa Creek succession

At several localities on both sides of the Okanagan Valley near Enderby, the Silver Creek Formation is structurally overlain by a heterolithic succession of ductilely deformed, amphibolite-facies rocks known as the Spa Creek succession (Thompson and Daughtry 1996; Erdmer et al. 1999, 2001; Unterschutz 2002). Lithologies within the Spa Creek succession include biotite-amphibole schist, heterolithic metavolcanic rocks (DCSC), marble (DCSCm), quartzite, pelitic schist, and a distinctive polymictic metaconglomerate (DCSCcg). Interested readers are referred to the above sources for more information about the occurrence, internal structure, and characteristics of the Spa Creek succession. Only a few important relationships are discussed here.

Near Hendry Creek, 7 km east of Armstrong (82L/06), the Spa Creek succession includes pelitic schist, marble, chlorite-amphibole schist, intermediate to felsic metavolcanic rocks, and stretched quartzite-pebble metaconglomerate (Thompson and Daughtry 1996; Erdmer et al. 1999; Unterschutz 2002). Structural relationships within the Kendry Creek area are complex, but the Spa Creek succession overlies the Silver Creek Formation and, in turn, is overlain by greenschist-facies clastic rocks of the Triassic Slocan Group to the east, which appear to truncate map patterns in the underlying Spa Creek succession. This relationship has been interpreted as evidence of a sub-Triassic unconformity in this area (Erdmer et al. 1999).

Near Spa Creek, on the west side of the Okanagan Valley approximately 10 km northwest of Glenemma, a metaconglomerate dominated by granitic clasts occurs within the Spa Creek succession (Erdmer et al. 2001). A massive, medium-grained biotite-bearing granitic clast

from the metaconglomerate yielded a date of 555.6 +/- 2.5 Ma (Erdmer et al. 2001). At this locality, ductilely deformed, amphibolite-facies rocks of the Spa Creek succession are overlain by greenschist-facies carbonaceous siliciclastic rocks of the Upper Triassic Slocan Group. The contact is not exposed, but was narrowed down to within tens of metres (Erdmer at al. 2001). No evidence of a structural contact was found, and the orientation of the contact and the lithological layering in the overlying Triassic strata appears to truncate steeply dipping fabric in the underlying Spa Creek succession (see Read and Okulitch 1977, for a discussion of evidence for a regional sub-Triassic unconformity).

The Wood Lake gneiss

Southwest of Vernon, west of Wood Lake, a succession of upper amphibolite-facies gneiss and Middle Jurassic intrusive rocks occur within a fault-bounded block (82L/03; Glombick et al. 2000).

The northern half of the fault block is dominated by a highly altered, heterogeneous gneiss succession. Rock types include: quartz-feldspar-hornblende gneiss, quartz-feldspar-biotite gneiss, amphibolite gneiss, and grey-weathering marble. Pink-weathering, potassium feldspar-quartz granitic veining is common, both parallel to, and cutting gneissic layering. Exposures of the gneiss are typically highly altered, with a bleached appearance and a greenish hue. Primary mafic minerals are rare; hornblende and biotite have been altered to chlorite and epidote. Feldspars have sericitized. The extensive hydrothermal alteration of the gneiss succession may have occurred during the emplacement of the Middle Jurassic Wood Lake pluton, or from fluids related to early Tertiary extension faulting and volcanism.

The southern half of the fault block is underlain by weakly deformed to massive, medium to course-grained granodiorite of the Middle Jurassic Wood Lake pluton (JWLm). Potassium-feldspar megacrystic varieties are common. Exposure in this area is limited, due to extensive glacial deposits. A sample of the Wood Lake pluton sampled near the southern end of Wood Lake has yielded a date of U-Pb titanite date of 164.4 ± 2.0 Ma (Chapter 3). Near the contact with the gneiss succession, there is a zone of mixing, where veins and dykes of granodiorite are roughly in equal proportion to highly altered gneiss.

On the west side of Wood Lake, within the hanging wall of the Vernon fault and the upper plate of the Kalamalka Lake shear zone, numerous gneiss enclaves are exposed within the Middle Jurassic Wood Lake pluton. Several enclaves, hundreds of metres across, are exposed in road cut adjacent to Highway 97A along the western shore of Wood Lake (Thompson and Daughtry 1996). The gneiss within the enclaves is similar in composition and appearance to the

gneiss succession exposed on the east side of the lake. A sample of hornblende gneiss from one of the enclaves yielded a concordant zircon fraction, interpreted as reflecting the igneous emplacement age of a dyke, with a date of 171.0 ± 0.8 Ma. This date agrees well with a lower intercept age from eight discordant multigrain fractions from the same sample of 171.1 +3/-4.7 Ma, which is interpreted at the timing of zircon growth during igneous emplacement (Chapter 3).

The age of the Wood Lake gneiss is unknown, but it must be older than 171 Ma, the age of the oldest phases of the Wood Lake pluton. The Middle Jurassic Okanagan plutonic suite intrudes rocks of the Harper Ranch Group to the north, near Vernon. It is possible, therefore, that the Wood Lake gneiss represents high-grade equivalents of the Harper Ranch Group. Alternatively, the Wood Lake pluton may have intruded along a structure that faults rocks of the Wood Lake gneiss against the lower-grade Harper Ranch Group. The second interpretation is considered unlikely, however, as a phase of the Okanagan plutonic suite sample near Adventure Bay (82L/03) yielded a date of 173 Ma, which is older than the metamorphic age from the Wood Lake gneiss. This requires that the Wood Lake gneiss and the Harper Ranch Group to be at similar structural levels at ~ 173 Ma, because they were both intruded by rocks of the Okanagan plutonic suite at that time. A regional metamorphic event at 171 Ma could not have produced the Wood Lake gneiss without affecting the rest of the Harper Ranch Group.

Superstructure rocks (upper structural level)

A belt of greenschist-facies superstructure rocks of the Slocan and Harper Ranch groups strikes southeast across the width of the SMC in the Vernon area. This belt is part of a regionally extensive belt of low-grade rocks of Devonian to Jurassic age extending from north of Kamloops to the Kootenay Arc (Monger et al. 1991). This belt makes a prominent bend to the east at the latitude of Vernon.

The Harper Ranch Group

East of the Okanagan Valley, rocks of the Harper Ranch Group are confined to the south of the Coldstream Valley, where they host Middle Jurassic laccoliths of the Okanagan plutonic suite and mafic to ultramafic plutonic rocks (82L/03; 82L/02; 82L/01).

Jones (1959) included rocks of the Harper Ranch Group occurring in the Vernon area within the Cache Creek Group. Monger (1975) later recognized them as a distinct group on the basis of the lack of abundant bedded cherts that are characteristic of the Cache Creek Group. Although the type area for the Harper Ranch Group is in the Kamloops area, Monger (1975)

decided to include the rocks of the Vernon area within the Harper Ranch Group on the basis of similar age and rock types.

Near Vernon, the Harper Ranch Group includes abundant metamorphosed intermediate volcanic rocks and volcanic breccia (PHRv), clastic sedimentary rocks (PHRu), and variably recrystallized limestone (PHRls). Metamorphic grade is typically low, within the chlorite zone of the greenschist facies, but biotite, and even garnet are present locally.

Clastic rocks of the Harper Ranch Group are dominated by dark, carbonaceous argillite and phyllite. Argillite is typically dark grey, dark greenish-grey, or dark green and may be siliceous (cherty). Clastic rocks are typically fissile, but siliceous varieties may lack cleavage. Fine-grained biotite, chlorite, and muscovite are visible with a hand lens on the cleavage surface. Primary sedimentary structures are rare, but millimetre to centimetre-scale compositional layering defined by alternating light and dark bands is present locally.

The dominant rock type within the Harper Ranch Group is meta-andesite (greenstone). Meta-andesite flows are typically fine grained, dark green to dark grey, and massive. Augite, hornblende, and plagioclase-phyric varieties occur locally. Flow breccia and agglomerate are common, and typically are stained brown by weathering and extensive alteration. Primary minerals are rare. Heterolithic volcanic breccia is locally present, with angular to rounded clasts of volcanic rocks and diorite with varying composition, and texture. Calcite veining is common is common within metavolcanic rocks.

Limestone commonly occurs as subhorizontal or gently dipping slabs or blocks 10's to 100's of metres thick and several 100's of metres across enclosed within a matrix of metavolcanic flows and breccia (82L/03; 82L/02; 82L/01). Limestone varies in colour from pure white to dark or brown-grey. Light and dark grey banded varieties are present, but not common. The texture of the limestone is typically microcrystalline. Macroscopic fossil fragments, including corals and crinoid ossicles are rarely preserved. These limestone sheets and blocks are interpreted to have formed as shallow water carbonate mounds or reefs on submarine volcanic edifices.

The age of the Harper Ranch Group in the Vernon area is not well constrained. The age of the Harper Ranch Group near Kamloops ranges from the Latest Devonian to Late Permian (e.g., Orchard 1987; Beatty 2002). In the Vernon area, paleontological control is sparse, but, thus far, only Permian and Lower Mississippian fossils have been recovered (82L/03; 82L/02; 82L/01), suggesting that the base of the Harper Ranch Group is not exposed in the Vernon area.

The depositional setting of the Harper Ranch Group is uncertain, but the association of submarine volcanic rocks, agglomerates, shallow water limestone, and fine-grained clastic rocks suggest that the Harper Ranch Group may have formed within an oceanic volcanic arc, possibly

within a back-arc setting (T. Beatty, personal communication, 2002). There are several areas west of Vernon, where the Nicola Group unconformably overlies the Harper Ranch Group, implying that the middle to upper Paleozoic Harper Ranch Group is basement to the Upper Triassic Nicola arc (Monger et al. 1991).

In the study area, the relationship between the Harper Ranch and Nicola groups has been obscured by intense deformation, although an unconformable relationship is preserved west of the Okanagan Valley (82L/05). An important observation, however, is that while carbonaceous clastic rocks of the Slocan Group are abundant north of the approximate latitude of the Coldstream Valley, east of the Okanagan Valley (82L/01, 82L/02, and 82L/03), rocks of the Harper Ranch Group and Okanagan plutonic suite are conspicuously absent. This hypothetical line has been interpreted to reflect the position of a south-dipping basement ramp, the Vernon monocline, which has been interpreted as the margin of a Paleozoic basin (Price and Monger 2003). They speculate that during the closure of an (Slide Mountain?) ocean basin of uncertain width (including Middle to Upper Paleozoic oceanic-type rocks), rocks of the Harper Ranch and Okanagan plutonic suite were thrust over the Vernon monocline.

The Slocan Group

Rocks of the Upper Triassic Slocan Group form a thin veneer of complexly deformed, low-grade, dominantly carbonaceous, fine-grained clastic rocks overlying higher-grade rocks within the Vernon area. The fine-grained clastic rocks of the Slocan Group are thought to represent the eastern clastic basin to the coeval Nicola volcanic arc located approximately 100 km to the west (Monger et al. 1991).

In the Vernon area, the Slocan Group is dominated by dark grey, carbonaceous argillite and phyllite (uTsu), with lesser amounts of dark grey pyritic quartzite (PTpq), argillite, carbonaceous limestone (uTsc), dark grey calcareous mudstone, metasiltstone, metasandstone, metaconglomerate, and rare layers of augite porphyry (uTNmcp). Primary sedimentary structures are rare, but rare coarse-grained siltstone and sandstone beds rarely preserve planar laminations, cross-bedding, loading structures, and trace fossils (Unterschutz 2002).

Augite porphyry occurs within the Slocan Group as layers up to several metres wide. The matrix is dark green and aphanitic. Primary augite has often been pseudomorphed by amphibole. Primary minerals are rare. Due to the lack of recognizable bedding within the homogeneous phyllitic rocks of the Slocan Group, it is unclear whether these augite porphyry layers represent flows, dikes, or both. Exposures of augite porphyry occur within the Slocan Group near

Sovereign Lakes and Silver Star Mountain (82L/06; Unterschutz 2002) and on Cherry Ridge, northeast of Cherryville (82L/07; 82L/08).

On the west flank of Silver Star Mountain, on the road to the Silver Star ski resort, several layers of ductilely strained, polymictic conglomerate (lJSSC) up to several metres thick occur near the base of the Slocan Group (82L/06). The intense deformation and metamorphism experienced by rocks in this area make the identification of the base of the Slocan Group difficult. Metamorphic grade within the Slocan Group is typically low, within the chlorite zone of the greenschist facies, although biotite and even garnet grade is reached locally. The nature of the contact between greenschist-facies clastic rocks of the Slocan Group and amphibolite-facies rocks of the underlying Silver Creek Formation appears to be transitional in this area (Chapters 2 and 4).

The age of the Slocan Group in the Vernon area is constrained to be Upper Triassic to Lower Jurassic in age. Norian fossils have been recovered from several carbonate layers. Okulitch and Cameron (1976) documented Late Triassic conodonts obtained from an outcrop of argillaceous limestone exposed approximately 6.5 km east of Lumby adjacent to Highway 6 (82L/07). Additional sample sites that have yielded Triassic fossils include one north of Keefer Lake (82L/01), and various localities along the northern slope of the Coldstream Valley east of Vernon (82L/03).

In many areas of the SMC, including in the Vernon area, rocks of the Slocan Group directly overlie higher-grade metamorphic rocks of the SMC (e.g., Read and Okulitch 1977). Several workers have examined this relationship in the Vernon area and have interpreted the original contact either as an unconformity, possibly reactivated during early Tertiary extension faulting (Read and Okulitch 1977; Erdmer et al. 2001; Unterschutz 2002; Lemieux et al. 2003), or as the bounding thrust of the Quesnel terrane, later reactivated as low-angle, early Tertiary extension faults (Carr 1990; Bardoux 1993; Vanderhaeghe et al. 1999). Post-Middle Jurassic deformation, metamorphism, and early Tertiary extension faulting have obscured original relationships within the study area. The present nature of this contact is described in detail in Chapters 2 and 4.

Intrusive rocks

The Aberdeen gneiss complex

The Aberdeen gneiss complex (AGC; unit TAG) consists of migmatitic gneiss exposed southeast Vernon (82L/03; 82L/02; Chapter 4). The AGC is situated within the core of the Vernon antiform, a domal series of reflector visible at middle to upper crustal depths in seismic

reflection profiles through the Vernon area (e.g., Cook et al. 1992). The AGC intrudes rocks of the Kalamalka Lake metamorphic assemblage and was deformed and metamorphosed together with its host rock succession during Mesozoic intense ductile deformation and upper amphibolite-facies regional metamorphism (Chapter 4).

Exposures of the Aberdeen gneiss complex are heterogeneous in terms of composition at all scales, with several orthogneiss phases commonly present within a single exposure. The most common rock type within the AGC is a strongly foliated, medium-grained, biotite-bearing metatonalite; but medium to coarse-grained, hornblende-biotite diorite gneiss, fine to medium-grained granite, and pegmatite also are present.

Based on crosscutting relationships, the diorite gneiss phase appears to be the oldest. This phase commonly occurs as rounded to angular blocks (resembling agmatic migmatite), boudins, or isoclinally folded layers within a metatonalite matrix. The blocks of diorite gneiss commonly contain a metamorphic foliation or gneissic layering that is discordant to the fabric of the enclosing tonalite. Multiple phases of tonalitic and granitic veining cut the dioritic gneiss blocks. In places, the contact between phases is wispy and appears to be a zone of magmatic mixing.

The diorite gneiss and the metatonalite were sampled for dating (Chapter 3). Isotopic systematics in both samples are complex, with multiple episodes of zircon growth preserved. The emplacement age of the diorite gneiss is inferred to be ~232 Ma, while the best estimate for the age of the metatonalite is ~150 Ma. The implications of these results and the thermotectonic evolution of the Vernon antiform are discussed in Chapter 3.

Ultramafic and mafic rocks

Ultramafic and mafic rocks occur as isolated and scattered bodies within the Vernon area. Most occurrences of ultramafic and mafic rocks are confined to the Chapperon and Harper Ranch groups, but highly deformed and metamorphosed bodies occur within infrastructure rocks as well.

Within the Chapperon Group, altered ultramafic rocks, known as the Old Dave intrusions (Jones, 1959), occur predominantly as serpentinized, subvertical dykes, some of which exceed 100 m in width (82L/04; 82L/05; Pum; Daughtry 2000). The Old Dave intrusions are composed dominantly of serpentine, but lesser amounts of talc, carbonate, magnetite, chromite, olivine, and pyroxene are present.

Numerous mafic to ultramafic intrusive bodies and dykes occur within the Harper Ranch Group (82L/03; 82L/02; Coldstream ultramafic rocks; PJum) . The composition of the Coldstream ultramafic intrusive rocks ranges from diorite to pyroxenite, although the primary mineralogy is seldom preserved. In unaltered varieties, grain size is typically medium to coarse,

grading to fine near the margins of the intrusions. Altered varieties are composed primarily of serpentine, talc, chlorite, and carbonate.

A large body of coarse-grained pyroxenite occurs within argillite of the Harper Ranch Group on Okanagan Lake, immediately west of Vernon (82L/03). The pyroxenite, which is medium to coarse-grained near the centre of the intrusion, grades to fine-grained diorite near its margins.

Other occurrences of mafic to ultramafic bodies within the Harper Ranch Group include coarse-grained pyroxenite exposed on the south and west slopes of Mount Middleton near Vernon (82L/03), coarse-grained pyroxenite exposed along the south side of the Coldstream Valley immediately south of Lavington (82L/03), medium to fine-grained diorite exposed along the south slope of the Creighton Valley south of the Camel's Hump (82L/02), and a large layered dioritic intrusion exposed on the ridge to the east of Heckman Creek (82L/02).

Numerous, small (10's of metres) concordant lenses of ultramafic rocks, altered and metamorphosed to varying degrees, were reported by Reesor and Moore (1971; their unit A) within high-grade, ductilely deformed rocks of the middle structural level and the Monashee complex. In most places, these lenses are too small to indicate on maps, but larger bodies occur in several locations, including southeast of Vidler Ridge near the headwaters of Cherry Creek (82L/08), near Sitkum Lake (82L/08), and on Fosthall Ridge (82L/08). Where primary mineralogy is preserved, the rocks range in composition from dunite to harzburgite, with variable amounts of olivine, orthopyroxene, and amphibole.

Near Vidler Ridge, a body of metamorphosed and altered meta-ultramafic rock several hundreds of metres across is exposed (82L/08). Near the margins of the body, no primary mineralogy is preserved, and constituent minerals are dominated by tremolite, chlorite, and talc. Near the centre of the body, large, well-formed magnetite octahedrons up to 2 cm long occur within a green-coloured matrix composed of fine-grained chlorite.

Other occurrences of ultramafic rocks in the Vernon area include highly altered, bright green-coloured pods and layers in the Hunters Range several metres across (82L/011).

Weakly deformed to undeformed, fine-grained, augite-phyric layers several metres across occur within carbonaceous clastic rocks of the Slocan Group near Silver Star Mountain (82L/06) and on Cherry Ridge (82L/07; 82L/08). It is unclear whether these layers represent flows within the Slocan/Nicola Group, where augite-bearing flows are common in the volcanic-dominated Nicola Group to the west, or whether they are intrusive dykes.

The age of the Old Dave intrusions is unknown, but individual dykes cut the contact between the Chapperon and Harper Ranch groups (82L/04) but do not intrude the Slocan Group,

suggesting that the intrusions are Permian or Lower Triassic in age. Similarly, the Coldstream ultramafic rocks, which occur in the Harper Ranch Group, do not occur in the overlying Slocan Group, suggesting that they are correlative with the Old Dave intrusions. It is not known whether the metamorphosed ultramafic bodies that occur within the middle structural level are Permian in age or older.

The Okanagan plutonic suite

The region between the Okanagan fault and the Pasayten fault to the west is underlain by an Early to Middle Jurassic intrusive complex with at least seven distinct phases (Woodsworth et al. 1991). Although various plutons within the complex have been given individual names, such as Similkameen, Osprey Lakes, Pennask, and Okanagan, the name Okanagan composite batholith has been proposed (Woodsworth et al. 1991). Marginal phases of the complex, such as the Pennask batholith, have yielded Early Jurassic ages, suggesting an affinity with the Guichon batholith. Intrusive phases near the core tend to yield younger Middle Jurassic ages (Woodsworth et al. 1991).

In the Vernon area, the Okanagan composite batholith is dominated by medium to coarse-grained, biotite and(or) hornblende-bearing granite, quartz monzonite, granodiorite, and quartz diorite laccoliths of Middle Jurassic age locally known as the Okanagan plutonic suite (unit JOmd; Glombick et al. 2004). Potassium-feldspar megacrystic varieties are common, particularly near Wood Lake (82L/03). Exposures of the Okanagan plutonic suite are typically massive to weakly foliated, although the intensity of the fabric increases near the margins.

Near Vernon, rocks of the Okanagan plutonic suite intrude rocks of the Harper Ranch Group and the Wood Lake gneiss (82L/03). They have not been recognized within the middle structural level or within the Monashee complex.

The Okanagan plutonic suite is Middle Jurassic in age. A sample of potassium-feldspar megacrystic quartz monzonite sampled from the southeast side of Wood Lake (JWLm) yielded a U-Pb titanite date of 164.4 ± 2.0 Ma (82L/03; R.I. Thompson and R. Friedman, unpublished data). An undeformed pegmatite vein of the Wood Lake pluton within the Wood Lake gneiss has yielded a U-Pb zircon date of 161.6 ± 2.8 Ma (Chapter 3). A dioritic phase, sampled from Adventure Bay on Okanagan Lake southwest of Vernon, yielded an older date of ~ 171 Ma from several concordant titanite fractions (82L/03; R.I. Thompson and R. Friedman, unpublished data). East of Vernon, a sample of hornblende biotite granodiorite from the Middle Jurassic Spruce Grove batholith has yielded an U-Pb zircon date of 174.8 ± 0.8 Ma (82L/02; Carr 1990). These data suggest an emplacement age between 160 and 175 Ma.

The age, composition, and structural setting of the Okanagan plutonic suite is nearly identical to the well-studied Middle Jurassic Nelson pluton suite, located to the east within the Kootenay arc, suggesting that the two suites form part of a larger Middle Jurassic calcalkaline arc (Woodsworth et al. 1991).

The Cosens Bay pluton

The Cosens Bay pluton (KCBgd) is a sheet-like intrusive body that crops out along the eastern shore of Kalamalka Lake, south of Cosens Bay (82L/03).

The pluton is dominantly composed of strongly foliated to gneissic, medium-grained biotite and(or) hornblende-bearing granodiorite, although biotite-bearing, foliated granite occurs locally.

Near the margins of the pluton, rafts of metasedimentary gneiss are enclosed within the pluton, indicating that the emplacement of the pluton post-dates the development of an early metamorphic foliation and gneissic layering. The margins of the pluton are themselves overprinted by the mylonitic fabric of the Kalamalka Lake shear zone (Erdmer et al. 1998).

A previous attempt to date a sample of the Cosens Bay pluton by L. Heaman at the University of Alberta yielded an imprecise Cretaceous age. Additional zircon and titanite fractions were dated during the course of this study, constraining the age of the pluton to be 102.2 ± 3.8 Ma (Chapter 3).

The Whatshan Lake pluton

The Late Cretaceous Whatshan Lake pluton (KWLgd) occurs near the eastern margin of the SMC near Whatshan Lake (82L/01). The pluton is composed primarily of potassium-feldspar megacrystic, hornblende-bearing quartz monzonite, but hornblende diorite is locally present (Carr 1990). Although the pluton appears to be massive near its centre, it is moderately foliated near its margins.

The pluton is inferred to have a sheet-like geometry in the subsurface on the basis of sub-horizontal, near-surface reflectors visible in Lithoprobe seismic reflection line 9 (Carr 1990). Near Barnes Creek, west of Whatshan Lake, exposures of the pluton are bounded above and below by metasedimentary rocks, further suggesting a thin, sheet-like geometry.

At the northern margin of the pluton, on the east side of Whatshan Lake, veins and sills occur both parallel to and cutting the host rock foliation. The veins, which cut the metamorphic foliation at a low angle, are tightly folded and the axial surfaces are approximately parallel to the transposition foliation.

A sample of the Whatshan Lake pluton has yielded an age of 77 ± 0.5 Ma (U-Pb zircon; Carr 1990). This indicates that, while the dominant metamorphic foliation is older than 77 Ma, the tight folding (F3 folding of Carr 1990) postdates this time.

The Ladybird granite suite

The Ladybird suite is part of a regionally extensive intrusive suite of Late Paleocene to Early Eocene, S-type, peraluminous granitic rocks that are ubiquitous within high-grade metamorphic rocks of the middle structural level in the Vernon area and other exposures of high-grade metamorphic rocks within the SMC (Carr et al. 1987; Parrish et al. 1988; Sevigny et al. 1989; Carr 1992; Vanderhaeghe et al. 1999).

Granitic rocks of the Ladybird suite vary in composition from granite (ELBg) to quartz-monzonite (ELBqm), with muscovite and(or) biotite-bearing varieties being the most common. Garnet, sillimanite, and(or) tourmaline may be present. Pegmatitic postkinematic varieties are common (ELBpqm). In some areas of the middle structural level, particularly between the southern margin of the Thor-Odin dome and the Pinnacles area, pegmatitic rocks of the Ladybird suite are so voluminous that they cannot be separated from the enclosing metamorphic succession at the map scale (82L/08). In these areas, rocks are mapped as having greater than 50% pegmatite (Pqfh2) or less than 50% pegmatite (Pqfh1).

Intrusive rocks of the Ladybird suite are postkinematic with respect to the regional metamorphic foliation, but vary from syn- to postkinematic with respect to early Tertiary extensional fabrics (e.g., Carr 1992; Vanderhaeghe et al. 1999).

The age of the Ladybird intrusive suite is well constrained in the region between the southern margin of the Thor-Odin dome and the Pinnacles, where granitic rocks have yielded U-Pb zircon and monazite dates of 62 Ma to 54 Ma (Carr 1992).

Between the Pinnacles area and Vernon, age control of granitic rocks is lacking, with the exception of a mylonitic, lineated, medium-grained, biotite and muscovite-bearing granite that has been dated at ~ 60 Ma in the Trinity Hills area (82L/07; Vanderhaeghe et al. 1999). This strained granitic body occurs within a high-strain zone spatially associated with the transition from amphibolite-facies to greenschist-facies metamorphic rocks, and constrains the age of extension-related shearing to be younger, at least in part, than 60 Ma (Chapter 4).

West of Silver Star Mountain, near Sovereign Lakes, extensive outcrops of muscovite and garnet-bearing synkinematic granite and postkinematic pegmatite occur, comprising nearly 100% of exposed rock in some areas (82L/06; Chapter 2). Jones (1959) included these granitic bodies within the Silver Star intrusions, which he inferred were Jurassic in age. Although they

remain of uncertain age (see Unterschutz 2002), their composition, occurrence, state of strain, and association with extensional shear zones, all suggest that they are correlative with the Ladybird suite.

Of note is the complete lack of Ladybird suite granitic rocks within the upper structural level. Their uppermost structural occurrence is near the staurolite isograd within the metamorphic transition zone between superstructure and infrastructure rocks (Chapter 4).

The Nicklen Lake pluton

Southeast of Vernon, several intrusive bodies of weakly-foliated to massive, medium to coarse-grained monzonite and quartz monzonite (ENLmd) intrude upper amphibolite-facies metamorphic rocks of the Aberdeen gneiss complex and its enclosing gneiss succession (82L/03). Potassium-feldspar megacrystic varieties are common. Fresh varieties are light pink in colour. Contacts with the surrounding gneiss are sharp. Hornblende is the dominant primary mafic mineral, with lesser biotite.

Extensive hydrothermal alteration, particularly near brittle faults, has altered primary mafic minerals to chlorite and epidote. Where the rock is altered, it typically has a chalky appearance and greenish hue resulting from the alteration of the feldspars and mafic minerals.

A sample of potassium-feldspar megacrystic monzonite of the Nicklen Lake pluton sampled from near Grizzly Swamp has yielded a date of 51.7 ± 0.7 Ma (Chapter 3).

The Coryell intrusive suite

Within south-central British Columbia, a widespread suite of intrusive rocks of Middle Eocene age located between the Okanagan Valley and the Slocan Lake fault is known as the Coryell intrusive suite (Little 1960, 1982). Rocks of the Coryell intrusive suite occur as post-kinematic stocks and plutons. It has been suggested that rocks of the Coryell intrusive suite are the intrusive equivalents to alkaline volcanic flows of the Marron Formation (Church 1973; Little 1982). The composition of the Coryell plutonic suite is variable: syenitic, granitic, dioritic, and monzonitic varieties have all been observed (Little 1960, 1982). Biotite, hornblende, and less commonly, pyroxene form the dominant mafic phases.

Within the Vernon area, rocks of the Coryell intrusive suite are exposed on Ellison Ridge between Okanagan and Kalamalka Lakes (82L/03). At this location, rocks grade from medium to coarse-grained, pink, biotite and(or) pyroxene-bearing monzonite to syenite (ECsy) to fine-grained, pink subvolcanic porphyry (ECv). A sample of coarse-grained syenite from the Coryell

intrusive suite exposed in the Vernon area has yielded an age of ~50 Ma (R.I. Thompson, unpublished data).

A suite of granitic rocks of similar age and composition, named the Sheppard intrusive suite, occurs south of Trail, British Columbia. The Sheppard intrusive suite has been dated at ~47 Ma (Parrish et al. 1988). The similarity in age, composition, and occurrence between the Coryell intrusive suite, the Nicklen Lake pluton, and the Sheppard intrusive suite suggest that they belong to a cogenetic suite of extension-related, quartz-poor intrusive rocks of Middle Eocene age that are widespread within south-central British Columbia.

Tertiary volcanic and sedimentary rocks

Middle Eocene volcanic and sedimentary rocks

During the Eocene, the Canadian Cordillera was the locus of intense volcanic activity. Remnants of the Eocene Challis-Kamloops volcanic belt extend from the Yukon down to the Yellowstone region of the western United States (Souther 1991).

In south-central British Columbia, on the basis of geographical location and composition, Middle Eocene volcanic and sedimentary rocks have been grouped into the Kamloops Group (Ewing 1981*a*, 1981*b*) and the Penticton Group (Church 1973). Volcanic rocks of the Kamloops Group are dominantly calcalkaline in composition (Ewing 1981*b*), while volcanic rocks of the Penticton Group are more alkaline, although calcalkaline varieties occur within the Penticton Group in the Kelowna area (Church 1973; Bardoux 1993).

Several (Middle Eocene?) outliers of volcanic and sedimentary rocks occur near Vernon. It is unclear whether the outliers are erosional remnants of a regionally extensive volcanic sheet, or whether they reflect localized volcanic centres. The outliers are almost invariably spatially associated with steep normal faults of inferred Middle Eocene age. The faults may have provided conduits for magma to rise to the surface, and clastic detritus and volcanic flows may have filled fault-bounded basins. Bedding attitudes within Middle Eocene sedimentary successions, including coal beds and water-lain deposits, are commonly steep, with dips as great as 80°, indicating a significant amount of syn- to post-depositional tilting.

In the Vernon area, east of the Okanagan Valley, volcanic outliers of inferred and known Middle Eocene age are preserved near the Enderby Cliffs (82L/011; Mathews 1991; Breitsprecher 1998), the Trinity Hills (82L/07; 82L/010; Mathews 1981; Breitsprecher 1998), Bobbie Burns Mountain (82L/07), the Camels Hump (82L/02), Heckman Creek (82L/02), Mount Middleton (82L/03), on the north slope of the Coldstream Valley near Lavington (82L/03; 82L/06), and Bluenose Mountain (82L/03); numerous smaller outliers also occur. The basal units of outliers are

generally comprised of sedimentary and volcaniclastic rocks (Escg), including: coarse-grained, heterolithic conglomerate, sandstone, shale, tuffaceous rocks, and thin coal beds. Basal sedimentary units are overlain by volcanic flows of variable composition, with andesitic to dacitic aphanitic to plagioclase phyric varieties being the most common (Eiv). Potassium-argon dates (whole rock and biotite) reported from the Enderby cliffs and the Trinity Hills outliers range from 49 to 42 Ma (Mathews 1981; Breitsprecher 1998).

Several workers have suggested that Middle Eocene outliers exposed in the Vernon area are situated within the upper plate of gently dipping extensional detachment faults (Bardoux 1993; Carr 1990; Vanderhaeghe 1999). During this study, the basal contact of volcanic and sedimentary rocks of inferred Middle Eocene age was observed at several locations and the contact was found to be an unconformity at all locations.

For instance, several kilometres southeast of Kalamalka Lake, volcanic flows of inferred Middle Eocene age overlie mylonitic rocks of the Kalamalka Lake metamorphic assemblage (82L/03). The basal contact, which is clearly exposed in roadcut, is an angular unconformity, and a regolith surface is developed within the underlying schist succession (Glombick et al. 1999). Basal flows contain abundant angular clasts of mylonitic gneiss.

Similarly, in the Trinity Hills region, the contact between basal sedimentary units and underlying amphibolite-facies schist, gneiss, and granitic rocks was narrowed down to within a few metres. The lowermost sedimentary unit consists of a poorly sorted, polymictic conglomerate (Escg). Clast size ranges from millimetres to tens of metres across. The rounding of the clasts is variable, ranging from angular to well rounded. The matrix, which is composed of poorly sorted pebbly sand, is generally buff-coloured. The contact between the outlier and the basement overlaps a lithological boundary in the underlying basement gneiss. On the east, the basement is composed of upper amphibolite-facies pelitic schist and quartzofeldspathic gneiss of the Silver Creek Formation (Dqfb) with abundant Ladybird-type granite (ELBg); on the west, the basement is composed of chloritic greenstone and phyllite of the "Tsalkom South Formation" (Dpas). The contact between the two basement rock types is not exposed at this location. The clast compositions in the basal unit of the Trinity Hills outlier reflect the rock types of the underlying basement, changing as the contact in the underlying basement rocks is crossed. This indicates that the Trinity Hills outlier rests unconformably on basement gneiss, and is not in the upper plate of a low-angle detachment (Bardoux 1993; Vanderhaeghe et al. 1999).

Miocene basalt and underlying sedimentary rocks

Regionally extensive, subhorizontal erosional outliers of Miocene to Pliocene basalt (**Mb**) are common in the southern portion of the map area (82L/02, 82L/03; Mathews 1988). Locally, the cumulative thickness of the flows exceeds 200 m. The basalt is black on fresh surfaces, weathering to a reddish-brown colour. Small olivine and plagioclase phenocrysts, up to several millimetres across, are present locally. Flows are commonly columnar jointed and vesicular.

Locally, fluvial channels of poorly sorted, sandy conglomerate (**Mcg**) with rounded quartzite pebbles are preserved beneath the basalt flows. The channel deposits, which have yielded Oligocene fossils, have been explored and locally mined for uranium and placer gold deposits (K.L. Daughtry, personal communication, 1999).

References

Anderson, H.E., and Parrish, R.R. 2000. U-Pb geochronologal evidence for the geological history of the Belt-Purcell Supergroup, southeastern British Columbia. Chapter 7. *In* The Geological Environment of the Sullivan Deposit, British Columbia. *Editted by* J.W. Lydon, T. Hoy, J.F. Slack, and M.E. Knapp. Geological Association of Canada, Mineral Deposits Division, Special Publication No. 1, pp. 113-126.

Bardoux, M. 1993. The Okanagan Valley fault from Penticton to Enderby, south-central British Columbia. Ph.D. thesis, Carleton University, Ottawa.

Beatty, T. W. 2002. New geological and paleontological data from the Harper Ranch Group, Kamloops, British Columbia. *In* Current Research, Geological Survey of Canada, A14.

Breitsprecher, K. 1998. Volcanic stratigraphy, petrology and tectonic setting of the eastern margin of the Eocene Kamloops Group, south-central British Columbia. M.Sc. Thesis, Simon Fraser University, Vancouver.

Carr, S.D. 1990. Late Cretaceous-early Tertiary tectonic evolution of the southern Omineca Belt, Canadian Cordillera. Ph.D. thesis, Carleton University, Ottawa.

Carr, S.D. 1992. Tectonic setting and U-Pb geochronology of the early Tertiary Ladybird leucogranite suite, Thor-Odin-Pinnacles area, southern Omineca Belt, British Columbia. Tectonics **11**: 258-278.

Carr, S.D., Parrish, R.R., and Brown, R.L. 1987. Eocene structural development of the Valhalla complex, southeastern British Columbia. Tectonics, **6**: 175-196.

Church, B.N. 1973. Geology of the White Lake basin. British Columbia Department of Mines and Petroleum Resources, Bulletin 61.

Cook, F.A., Varsek, J.L., Clowes, R.M., Kanasewich, E.R., Spencer, C.S., Parrish, R.R., Brown, R.L., Carr, S.D., Johnson, B.J., and Price, R.A. 1992. Lithoprobe crustal reflection cross-section on the southern Canadian Cordillera, 1, Foreland Thrust and Fold Belt to Fraser River fault. Tectonics, **11**: 12-35.

Daughtry, K.L. 2000. New field studies of the Chapperon Group, Vernon southwest map area, British Columbia. Geological Survey of Canada Current Research 2000-A19.

Erdmer, P., Thompson R.I., and Daughtry, K.L. 1998. The Kalamalka Lake metamorphic assemblage, tectonic infrastructure in the Vernon map area, British Columbia. *In* Current Research 1998-A. Geological Survey of Canada, pp. 189-194.

Erdmer, P., Thompson, R.I., and Daughtry, K.L. 1999. Pericratonic Paleozoic succession in Vernon and Ashcroft map areas, British Columbia. *In* Current Research 1999-A. Geological Survey of Canada, pp. 205-215.

Erdmer, P., Heaman, L., Creaser, R.A., Thompson, R.I., and Daughtry, K.L. 2001. Eocambrian granite clasts in southern British Columbia shed light on Cordilleran hinterland crust. Canadian Journal of Earth Sciences, **38**: 1007-1016.

Ewing, T.E. 1981*a*. Regional stratigraphy and structural setting of the Kamloops Group, south-central British Columbia. Canadian Journal of Earth Sciences, **18**: 1464-1477.

Ewing, T.E. 1981*b*. Petrology and geochemistry of the Kamloops Group volcanics, British Columbia. Canadian Journal of Earth Sciences, **18**: 1478-1491.

Glombick, P., and Thompson, R.I. 2004. Geology of the Creighton Creek map area, British Columbia (NTS 82L/02). Geological Survey of Canada Open File 4371, scale 1:50 000.

Glombick, P., Erdmer, P., Thompson, R.I., and Daughtry, K.L. 1999. Ductile shear zones and an Eocene unconformity between Kalamalka Lake and Oyama Lake, Vernon map area, British Columbia. *In* Current Research 1999-A. Geological Survey of Canada, pp. 193-198.

Glombick, P., Erdmer, P., Thompson, R.I., and Daughtry, K.L. 2000. Geology of the Oyama map sheet, Vernon map area, British Columbia. Geological Survey of Canada Current Research 2000-A14.

Glombick, P., Thompson, R.I., and Daughtry, K.L. 2004. Geology of the Oyama map area, British Columbia (NTS 82L/03). Geological Survey of Canada Open File 4370, scale 1:50 000.

Heaman, L.M., Erdmer, P., Thompson, R.I., and Daughtry, K.L. 1999. Preliminary U-Pb geochronology results from the Vernon area, British Columbia. *In* Proceedings, Lithoprobe Report No. 69: Cordilleran Tectonics Workshop, Calgary, Alberta, pp. 196-201.

Hyndman, D.W. 1968. Petrology and structure of the Nakusp map-area, British Columbia. Geological Survey of Canada Bulletin 161.

Johnson, B.J. 1994. Structure and tectonic setting of the Okanagan Valley fault system in the Shuswap Lake area, southern British Columbia. Unpublished Ph.D. thesis, Carleton University, Ottawa.

Johnston, D.H. 1998. Structural and thermal evolution of northwest Thor-Odin dome, Monashee complex, British Columbia. Ph.D. thesis, University of New Brunswick, Fredericton.

Jones, A.G. 1959. Vernon map area, British Columbia. Geological Survey of Canada, Memoir 296.

Lemieux, Y., Thompson, R.I., and Erdmer, P. 2003. Stratigraphy and structure of the Upper Arrow Lake area, southeastern British Columbia: new perspectives for the Columbia River fault zone. *In* Current Research 2003, Geological Survey of Canada, 2003-A7.

Little, H.W. 1960. Nelson map-area, west half, British Columbia (82F W ½). Geological Survey of Canada, Memoir 308.

Little, H.W. 1982. Geology of the Rossland-Trail map-area, British Columbia. Geological Survey of Canada, Paper 79-26.

Mathews, W.H. 1981. Early Cenozoic resetting of potassium-argon dates and geothermal history of north Okanagan area, British Columbia. Canadian Journal of Earth Sciences, **18**: 1310-1319.

Mathews, W.M. 1988. Neogene geology of the Okanagan Highland, British Columbia. Canadian Journal of Earth Sciences, **25**: 725-731.

Monger, J.W.H. 1975. Upper Paleozoic rocks of the western Canadian Cordillera and their bearing on Cordilleran evolution. Canadian Journal of Earth Sciences, **14**: 1832-1859.

Monger, J.W.H., Wheeler, J.O., Tipper, H.W., Gabrielse, H., Harms, T., Struick, L.C., Campbell, R.B., Dodds, C.J., Gehrels, G.E., and O'Brien, J. 1991. Upper Devonian to Middle Jurassic assemblages. Part B. Cordilleran terranes, Chapter 8. *In* Geology of the Cordilleran orogen in Canada. *Edited by* H. Gabrielse and C.J. Yorath. Geological Survey of Canada, Geology of Canada no. 4, pp. 281-327.

Okulitch, A.V. 1984. The role of the Shuswap Metamorphic Complex inn Cordillera tectonism: a review. Canadian Journal of Earth Sciences, **21**: 1171-1193.

Okulitch, A.V., and Cameron, B.E.B. 1976. Stratigraphic revisions of the Nicola, Cache Creek, and Mount Ida groups based on conodont collections from the western margin of the Shuswap metamorphic complex, south-central British Columbia. Canadian Journal of Earth Sciences, **13**: 44-53.

Orchard, M.J. 1987. Conodont biostratigraphy and correlation of the Harper Ranch Group (Devonian-Permian), Ashcroft map-area, southern British Columbia. *In* Current Research, Part A, Geological Survey of Canada, Paper 87-1A, pp. 743-749.

Parkinson, D.L. 1992. Age and tectonic evolution of the southern Monashee complex, southeastern British Columbia: a window into the deep crust. Ph.D. thesis, University of California, Santa Barbara..

Parrish, R.R., Carr, S.D., and Parkinson, D.L. 1988. Eocene extensional tectonics and geochronology of the southern Omineca Belt, British Columbia and Washington. Tectonics, 7: 181-212.

Price, R.A., and Monger, J.W.H. 2003. A transect of the southern Canadian Cordillera from Calgary to Vancouver. Geological Association of Canada, Cordilleran Section, Vancouver, fieldtrip guidebook.

Read, P.B., and Okulitch, A.V. 1977. The Triassic unconformity of south-central British Columbia. Canadian Journal of Earth Sciences, **14**: 606-638.

Reesor, J.E., and Moore, J.M. 1971. Petrology and structure of the Thor-Odin gneiss dome, Shuswap metamorphic complex, British Columbia. Geological Survey of Canada Bulletin 195.

Sevigny, J.H., Parrish, R.R., and Ghent, E.D. 1989. Petrogenesis of peraluminous granites, Monashee Mountains, southeastern Canadian Cordillera. Journal of Petrology, **30**: 557-581.

Souther, J.G. 1991. Volcanic regimes, Chapter 14. *In* Geology of the Cordilleran orogen in Canada. *Edited by* H. Gabrielse and C.J. Yorath. Geological Survey of Canada, Geology of Canada no. 4, pp. 457-490.

Thompson, R.I., and Daughtry, K.L. 1996. New stratigraphic and tectonic interpretations, north Okanagan Valley, British Columbia. *In* Current Research 1996-A. Geological Survey of Canada, pp. 135-141.

Thompson, R.I., and Daughtry, K.L. 2000. Stratigraphic linkage of carbonate-rich units across east-central Vernon map area, British Columbia: are Kingfisher (Colby) and Big Ledge zinc-lead occurrences part of the same regional marker succession? Geological Survey of Canada, Current Research 2000-A18.

Thompson, R.I. and Glombick, P. 2004*a*. Geology of the Shuswap Falls map area, British Columbia (NTS 82L/07). Geological Survey of Canada Open File 4376, scale 1:50 000.

Thompson, R.I., and Glombick, P. 2004*b*. Geology of the Mabel Lake map area, British Columbia (NTS 8282L/010). Geological Survey of Canada Open File 4379, scale 1:50 000.

Thompson, R.I., and Unterschutz, J.L.E. 2004. Geology of the Vernon map area, British Columbia (NTS 82L/06). Geological Survey of Canada Open File 4375, scale 1:50 000.

Thompson, R.I. and Glombick, P., and Lemieux, Y. (compilers). 2004*a*. Geology of the Eureka Mountain map area, British Columbia (NTS 82L/01). Geological Survey of Canada Open File 4370, scale 1:50 000.

Thompson, R.I. and Glombick, P., and Lemieux, Y. (compilers). 2004*b*. Geology of the Mount Fosthall map area, British Columbia (NTS 82L/08). Geological Survey of Canada Open File 4377, scale 1:50 000.

Thompson, R.I., Glombick, P., Daughtry, K.L., and Erdmer, P. 2001. Upper Paleozoic stratigraphic linkage between Kootenay Arc and "Vernon Antiform": New constraints on southern Canadian Cordilleran evolution. *In* Lithoprobe Report No. 79, Cordilleran Tectonics Workshop, pp. 104-105.

Thompson, R.I., Glombick, P., Acton, S., Heaman, L., Friedman, R., Daughtry, K.L., Erdmer, P., and Paradis, S. 2002. New constraints on the age and distribution of the Chase Quartzite, Vernon (82L) and Lardeau (82K) map areas: regional implications. *In* Lithoprobe Report No. 82, Cordilleran Tectonics Workshop, pp. 92-94.

Unterschutz, J. 2002. Geological and geochemical links between Quesnel "terrane" strata and ancestral North America, southern Canadian Cordillera. M.Sc. thesis, University of Alberta, Edmonton, Alberta.

Vanderhaeghe, O., Teyssier, C., and Wysoczanski, R. 1999. Structural and geochronological constraints on the role of partial melting during the formation of the Shuswap metamorphic core complex at the latitude of the Thor-Odin dome, British Columbia. Canadian Journal of Earth Sciences, **36**: 917-943.

Williams, P.F., and Jiang, D. 2005. An investigation of lower crustal deformation: evidence for channel flow and its implications for tectonics and structural studies. Journal of Structural Geology, **27**: 1486-1504.

Woodsworth, G.J., Anderson, R.G., and Armstrong, R.L. 1991. Plutonic regimes, Chapter 15. *In* Geology of the Cordilleran orogen in Canada. *Edited by* H. Gabrielse and C.J. Yorath. Geological Survey of Canada, Geology of Canada no. 4, pp. 491-531.

APPENDIX A

Description of map units

Station location data

Notes:

1. First two digits refer to the year
2. Letters following year refer to outcrop type (outcrop noted - O) or operator (TWG - P. Glombick)
3. All UTM coordinates were measured in UTM Zone 11 using NAD 83 datum

Number	Station[1,2]	Easting[3]	Northing[3]	Number	Station[1,2]	Easting[3]	Northing[3]
1	00O0001	351387	5564256	51	00O0051	344228	5560524
2	00O0002	351458	5564098	52	00O0052	344900	5560590
3	00O0003	351506	5564000	53	00O0053	345015	5560571
4	00O0004	351379	5563464	54	00O0054	345178	5560634
5	00O0005	349622	5564408	55	00O0055	345266	5560687
6	00O0006	348838	5564078	56	00O0056	344810	5560507
7	00O0007	348125	5563510	57	00O0057	345107	5560358
8	00O0008	347910	5563298	58	00O0058	345437	5560261
9	00O0009	347837	5563206	59	00O0059	345573	5560417
10	00O0010	347804	5563086	60	00O0060	345531	5560519
11	00O0011	346603	5563107	61	00O0061	345653	5560554
12	00O0012	346611	5563208	62	00O0062	345791	5560511
13	00O0013	345981	5564273	63	00O0063	346136	5560545
14	00O0014	345855	5564353	64	00O0064	345648	5562062
15	00O0015	345651	5564156	65	00O0065	346242	5562145
16	00O0016	345614	5564069	66	00O0066	346869	5562315
17	00O0017	339754	5566619	67	00O0067	347282	5562251
18	00O0018	339823	5566820	68	00O0068	347789	5562936
19	00O0019	340146	5567485	69	00O0069	347570	5561765
20	00O0020	339869	5567341	70	00O0070	347124	5561107
21	00O0021	339793	5567407	71	00O0071	348045	5561375
22	00O0022	339686	5567447	72	00O0072	348080	5561322
23	00O0023	339598	5567362	73	00O0073	348031	5561076
24	00O0024	339313	5567232	74	00O0074	348003	5560949
25	00O0025	339177	5567367	75	00O0075	348138	5560936
26	00O0026	339017	5567396	76	00O0076	348090	5560728
27	00O0027	339189	5567518	77	00O0077	348098	5560257
28	00O0028	339258	5567681	78	00O0078	347317	5560127
29	00O0029	339440	5567849	79	00O0079	347054	5560089
30	00O0030	339562	5567963	80	00O0080	346916	5560024
31	00O0031	339752	5567860	81	00O0081	346833	5559878
32	00O0032	339734	5567730	82	00O0082	346790	5559808
33	00O0033	339894	5567923	83	00O0083	346075	5559522
34	00O0034	340019	5567817	84	00O0084	345569	5559481
35	00O0035	339973	5567628	85	00O0085	345658	5559784
36	00O0036	338691	5567850	86	00O0086	345093	5559634
37	00O0037	338631	5567847	87	00O0087	345158	5559399
38	00O0038	338597	5568008	88	00O0088	344879	5559157
39	00O0039	338606	5567863	89	00O0089	344320	5559348
40	00O0040	338598	5567960	90	00O0090	345309	5558718
41	00O0041	338544	5567837	91	00O0091	345654	5558963
42	00O0042	338585	5567772	92	00O0092	345816	5559036
43	00O0043	343177	5562548	93	00O0093	345266	5558448
44	00O0044	343399	5561834	94	00O0094	345719	5558481
45	00O0045	343740	5562292	95	00O0095	346070	5558566
46	00O0046	343627	5560443	96	00O0096	346717	5558391
47	00O0047	343495	5560359	97	00O0097	346699	5558314
48	00O0048	343146	5560227	98	00O0098	345323	5557787
49	00O0049	343059	5559774	99	00O0099	344537	5558087
50	00O0050	343339	5559473	100	00O0100	344857	5558122

Number	Station[1,2]	Easting[3]	Northing[3]	Number	Station[1,2]	Easting[3]	Northing[3]
101	00O0101	343889	5558240	157	00O0157	349673	5552104
102	00O0102	343051	5558477	158	00O0158	349525	5552080
103	00O0103	344046	5554088	159	00O0159	349085	5552222
104	00O0104	344115	5554090	160	00O0160	349229	5553350
105	00O0105	344345	5555023	161	00O0161	349117	5553178
106	00O0106	345076	5555412	162	00O0162	349197	5553929
107	00O0107	344395	5555868	163	00O0163	349532	5554439
108	00O0108	344605	5556026	164	00O0164	349589	5554618
109	00O0109	344716	5556023	165	00O0165	349258	5555467
110	00O0110	344814	5557071	166	00O0166	349006	5555647
111	00O0111	345460	5557148	167	00O0167	349280	5555967
112	00O0112	345615	5557228	168	00O0168	350486	5556303
113	00O0113	346026	5557097	169	00O0169	350590	5556369
114	00O0114	346076	5557377	170	00O0170	351620	5557112
115	00O0115	346277	5556960	171	00O0171	351048	5557056
116	00O0116	346444	5557985	172	00O0172	351337	5557371
117	00O0117	346522	5557832	173	00O0173	351475	5558129
118	00O0118	347440	5558273	174	00O0174	351497	5558327
119	00O0119	347547	5558072	175	00O0175	351495	5558525
120	00O0120	347398	5558032	176	00O0176	351468	5558932
121	00O0121	347473	5557894	177	00O0177	351292	5559032
122	00O0122	347685	5557954	178	00O0178	351018	5558834
123	00O0123	347828	5557789	179	00O0179	350650	5558552
124	00O0124	347636	5556490	180	00O0180	350560	5558663
125	00O0125	347151	5556819	181	00O0181	349851	5558675
126	00O0126	347073	5556863	182	00O0182	349662	5558614
127	00O0127	346863	5556813	183	00O0183	349541	5558508
128	00O0128	346846	5556958	184	00O0184	349459	5558672
129	00O0129	356885	5551754	185	00O0185	349185	5558681
130	00O0130	356768	5552278	186	00O0186	348553	5559055
131	00O0131	355824	5551959	187	00O0187	348412	5559013
132	00O0132	355890	5552146	188	00O0188	348243	5558990
133	00O0133	355902	5552379	189	00O0189	347927	5559055
134	00O0134	355263	5552262	190	00O0190	347674	5559304
135	00O0135	354423	5552320	191	00O0191	347606	5559528
136	00O0136	356510	5553436	192	00O0192	347623	5559627
137	00O0137	356464	5553492	193	00O0193	349075	5557487
138	00O0138	356360	5553490	194	00O0194	348917	5557553
139	00O0139	356135	5553486	195	00O0195	348828	5557484
140	00O0140	356003	5553540	196	00O0196	348825	5557359
141	00O0141	355923	5553433	197	00O0197	348685	5557410
142	00O0142	356899	5554742	198	00O0198	348770	5556798
143	00O0143	352132	5552107	199	00O0199	348547	5556739
144	00O0144	351611	5553111	200	00O0200	348766	5556606
145	00O0145	355416	5555463	201	00O0201	348222	5556505
146	00O0146	355308	5555618	202	00O0202	348218	5556419
147	00O0147	355333	5555983	203	00O0203	348514	5555993
148	00O0148	354830	5555430	204	00O0204	348707	5556217
149	00O0149	354465	5555615	205	00O0205	348802	5556275
150	00O0150	353944	5554948	206	00O0206	346953	5556109
151	00O0151	353992	5555779	207	00O0207	346808	5556011
152	00O0152	353214	5555376	208	00O0208	346684	5556055
153	00O0153	352805	5554824	209	00O0209	346607	5556143
154	00O0154	352437	5554944	210	00O0210	346539	5556277
155	00O0155	351610	5554594	211	00O0211	346666	5556332
156	00O0156	349827	5551943	212	00O0212	346279	5556315

Number	Station[1,2]	Easting[3]	Northing[3]	Number	Station[1,2]	Easting[3]	Northing[3]
213	00O0213	346170	5556263	269	00O0269	346950	5555283
214	00O0214	345414	5556000	270	00O0270	348083	5555841
215	00O0215	345505	5556018	271	00O0271	348153	5555577
216	00O0216	345581	5555722	272	00O0272	353028	5542070
217	00O0217	345664	5555426	273	00O0273	352031	5541348
218	00O0218	345676	5555316	274	00O0274	351552	5541163
219	00O0219	345490	5555120	275	00O0275	351722	5541038
220	00O0220	347309	5552203	276	00O0276	351252	5540722
221	00O0221	347488	5551972	277	00O0277	351189	5541018
222	00O0222	348088	5551982	278	00O0278	351198	5541187
223	00O0223	355253	5556746	279	00O0279	351781	5541419
224	00O0224	356110	5556292	280	00O0280	351630	5541697
225	00O0225	356197	5555900	281	00O0281	351703	5542092
226	00O0226	355858	5556418	282	00O0282	350437	5541603
227	00O0227	355544	5557293	283	00O0283	350364	5541658
228	00O0228	356126	5557753	284	00O0284	350261	5541575
229	00O0229	356325	5557847	285	00O0285	349959	5541811
230	00O0230	356281	5558077	286	00O0286	349752	5541920
231	00O0231	356336	5558623	287	00O0287	349632	5541919
232	00O0232	355693	5562337	288	00O0288	349531	5542009
233	00O0233	354094	5559606	289	00O0289	349408	5542118
234	00O0234	353029	5559693	290	00O0290	348957	5542446
235	00O0235	354756	5558695	291	00O0291	348810	5542401
236	00O0236	354879	5558145	292	00O0292	349045	5545178
237	00O0237	354919	5558028	293	00O0293	349248	5545875
238	00O0238	354938	5557909	294	00O0294	350228	5546795
239	00O0239	353529	5557487	295	00O0295	350393	5547246
240	00O0240	353232	5557600	296	00O0296	349157	5546445
241	00O0241	352949	5557613	297	00O0297	348716	5546751
242	00O0242	353051	5556966	298	00O0298	348538	5546970
243	00O0243	352124	5558126	299	00O0299	347318	5545500
244	00O0244	352288	5558323	300	00O0300	346936	5544350
245	00O0245	352317	5558422	301	00O0301	346157	5543686
246	00O0246	353299	5558571	302	00O0302	345997	5544083
247	00O0247	352017	5562777	303	00O0303	346070	5544686
248	00O0248	351984	5562432	304	00O0304	346094	5545022
249	00O0249	350062	5562100	305	00O0305	345029	5544094
250	00O0250	349800	5561968	306	00O0306	344559	5543495
251	00O0251	349391	5562274	307	00O0307	343117	5544157
252	00O0252	350266	5560763	308	00O0308	342671	5542302
253	00O0253	350011	5560932	309	00O0309	343779	5544246
254	00O0254	349649	5560237	310	00O0310	343738	5545309
255	00O0255	350365	5559630	311	00O0311	343800	5545660
256	00O0256	351709	5559416	312	00O0312	346722	5545923
257	00O0257	352209	5559622	313	00O0313	346945	5546321
258	00O0258	352223	5559705	314	00O0314	346879	5546352
259	00O0259	347741	5552824	315	00O0315	346833	5546641
260	00O0260	347360	5554305	316	00O0316	346842	5546921
261	00O0261	348154	5554452	317	00O0317	347009	5547308
262	00O0262	348201	5554493	318	00O0318	346305	5547250
263	00O0263	348059	5554613	319	00O0319	346084	5547172
264	00O0264	347880	5554657	320	00O0320	344672	5546755
265	00O0265	348155	5554935	321	00O0321	344631	5546820
266	00O0266	347724	5555418	322	00O0322	344379	5546848
267	00O0267	347627	5555492	323	00O0323	344266	5546751
268	00O0268	347107	5555671	324	00O0324	344914	5550864

Number	Station[1,2]	Easting[3]	Northing[3]	Number	Station[1,2]	Easting[3]	Northing[3]
325	00O0325	345306	5550784	381	00O0381	362680	5549739
326	00O0326	347766	5548436	382	00O0382	363225	5549616
327	00O0327	348283	5549025	383	00O0383	363331	5549656
328	00O0328	348711	5549180	384	00O0384	365894	5550691
329	00O0329	348498	5549513	385	00O0385	365346	5550642
330	00O0330	349435	5548846	386	00O0386	365114	5550601
331	00O0331	349317	5548749	387	00O0387	364769	5550578
332	00O0332	349775	5551793	388	00O0388	364453	5550379
333	00O0333	356396	5550796	389	00O0389	364352	5550286
334	00O0334	355312	5549433	390	00O0390	364248	5550155
335	00O0335	354759	5549156	391	00O0391	364170	5550009
336	00O0336	353261	5548722	392	00O0392	364141	5549768
337	00O0337	353235	5548642	393	00O0393	363868	5549717
338	00O0338	352838	5549901	394	00O0394	363778	5549808
339	00O0339	352759	5549846	395	00O0395	363631	5549865
340	00O0340	354506	5548569	396	00O0396	363090	5549886
341	00O0341	354227	5548410	397	00O0397	362952	5550020
342	00O0342	354192	5548228	398	00O0398	362776	5550064
343	00O0343	354251	5547681	399	00O0399	362661	5550056
344	00O0344	353327	5548059	400	00O0400	362617	5550238
345	00O0345	353231	5547951	401	00O0401	362637	5550410
346	00O0346	351817	5546697	402	00O0402	362425	5550226
347	00O0347	351202	5544600	403	00O0403	360877	5551529
348	00O0348	351273	5544377	404	00O0404	361034	5551430
349	00O0349	355521	5548474	405	00O0405	360860	5551316
350	00O0350	355395	5548438	406	00O0406	360955	5551222
351	00O0351	355040	5547458	407	00O0407	360976	5550454
352	00O0352	355872	5547802	408	00O0408	360639	5550357
353	00O0353	355920	5547793	409	00O0409	360203	5550236
354	00O0354	356099	5547742	410	00O0410	358451	5550061
355	00O0355	356265	5547772	411	00O0411	358127	5550136
356	00O0356	356505	5547803	412	00O0412	357495	5549580
357	00O0357	356703	5547854	413	00O0413	357643	5549586
358	00O0358	356761	5547761	414	00O0414	357762	5549527
359	00O0359	356662	5547471	415	00O0415	357248	5548734
360	00O0360	356832	5547388	416	00O0416	360743	5551615
361	00O0361	355224	5546243	417	00O0417	360601	5552323
362	00O0362	354868	5546263	418	00O0418	360489	5552671
363	00O0363	354747	5546224	419	00O0419	360418	5553023
364	00O0364	343637	5549436	420	00O0420	360370	5553046
365	00O0365	343552	5549318	421	00O0421	360852	5554961
366	00O0366	343251	5549048	422	00O0422	360211	5554704
367	00O0367	366105	5544479	423	00O0423	359005	5554835
368	00O0368	366023	5544606	424	00O0424	359825	5553914
369	00O0369	365821	5544429	425	00O0425	359520	5553989
370	00O0370	365015	5544663	426	00O0426	359188	5553513
371	00O0371	361689	5547443	427	00O0427	358430	5553489
372	00O0372	361774	5547841	428	00O0428	358589	5554092
373	00O0373	361768	5548219	429	00O0429	358598	5554210
374	00O0374	356974	5547384	430	00O0430	358387	5554436
375	00O0375	361777	5549133	431	00O0431	357616	5554143
376	00O0376	361944	5549142	432	00O0432	357203	5554735
377	00O0377	362056	5549229	433	00O0433	363185	5555478
378	00O0378	362299	5549406	434	00O0434	368990	5553947
379	00O0379	362844	5549254	435	00O0435	363390	5554697
380	00O0380	362687	5549602	436	00O0436	363272	5555086

Number	Station[1,2]	Easting[3]	Northing[3]	Number	Station[1,2]	Easting[3]	Northing[3]
437	00O0437	363719	5555267	493	00O0493	367954	5560666
438	00O0438	364149	5555209	494	00O0494	367820	5560645
439	00O0439	364431	5555132	495	00O0495	367445	5560644
440	00O0440	365607	5554686	496	00O0496	367377	5560739
441	00O0441	365881	5554385	497	00O0497	367102	5560182
442	00O0442	366090	5554205	498	00O0498	364260	5556740
443	00O0443	366597	5552388	499	00O0499	364003	5556677
444	00O0444	366512	5552091	500	00O0500	363942	5556812
445	00O0445	366981	5552630	501	00O0501	363718	5556850
446	00O0446	367053	5552258	502	00O0502	363424	5556771
447	00O0447	370036	5552069	503	00O0503	363370	5556533
448	00O0448	370875	5553576	504	00O0504	363472	5556509
449	00O0449	371163	5555122	505	00O0505	363626	5556433
450	00O0450	371267	5555311	506	00O0506	364590	5557657
451	00O0451	371152	5555350	507	00O0507	364040	5558672
452	00O0452	370898	5556283	508	00O0508	364010	5558833
453	00O0453	369629	5555575	509	00O0509	360855	5556226
454	00O0454	368970	5556045	510	00O0510	360486	5556258
455	00O0455	368968	5555965	511	00O0511	359513	5555911
456	00O0456	368892	5555911	512	00O0512	357519	5556417
457	00O0457	368559	5556085	513	00O0513	358071	5556753
458	00O0458	368364	5556134	514	00O0514	358389	5557052
459	00O0459	368197	5556184	515	00O0515	358429	5557271
460	00O0460	367091	5557600	516	00O0516	358306	5557375
461	00O0461	367937	5557899	517	00O0517	358994	5557286
462	00O0462	367880	5557731	518	00O0518	358397	5558985
463	00O0463	371097	5557677	519	00O0519	362493	5560365
464	00O0464	370799	5557441	520	00O0520	362450	5560445
465	00O0465	370487	5557345	521	00O0521	370502	5562605
466	00O0466	369779	5557416	522	00O0522	370492	5563965
467	00O0467	370403	5558090	523	00O0523	371544	5565882
468	00O0468	370705	5558319	524	00O0524	370760	5565723
469	00O0469	370484	5558351	525	00O0525	369908	5565926
470	00O0470	370561	5558500	526	00O0526	368686	5563916
471	00O0471	369289	5558805	527	00O0527	368594	5563273
472	00O0472	369007	5558793	528	00O0528	368527	5563090
473	00O0473	369273	5558512	529	00O0529	368434	5562854
474	00O0474	369044	5558338	530	00O0530	368481	5562759
475	00O0475	368802	5558478	531	00O0531	368206	5562812
476	00O0476	367235	5559030	532	00O0532	364513	5563438
477	00O0477	367288	5558979	533	00O0533	362558	5563632
478	00O0478	367374	5558916	534	00O0534	367187	5565377
479	00O0479	367532	5559316	535	00O0535	371551	5566994
480	00O0480	368709	5560165	536	00O0536	370958	5567459
481	00O0481	368924	5560149	537	00O0537	371056	5567755
482	00O0482	369116	5560200	538	00O0538	371544	5568673
483	00O0483	369343	5560080	539	00O0539	371491	5568838
484	00O0484	369182	5560300	540	00O0540	371463	5569030
485	00O0485	369590	5560317	541	00O0541	371438	5569329
486	00O0486	369635	5560638	542	00O0542	371449	5569504
487	00O0487	371377	5561011	543	00O0543	371594	5570049
488	00O0488	371421	5561439	544	00O0544	369747	5569507
489	00O0489	370740	5561273	545	00O0545	369754	5569573
490	00O0490	371003	5561689	546	00O0546	384208	5542073
491	00O0491	368346	5561036	547	00O0547	384100	5541884
492	00O0492	367999	5560634	548	00O0548	383988	5541741

Number	Station[1,2]	Easting[3]	Northing[3]	Number	Station[1,2]	Easting[3]	Northing[3]
549	00O0549	383900	5541600	605	00O0605	381453	5544369
550	00O0550	383828	5541564	606	00O0606	381570	5544710
551	00O0551	383696	5541314	607	00O0607	381238	5544872
552	00O0552	383292	5541271	608	00O0608	381061	5544608
553	00O0553	383292	5540870	609	00O0609	379438	5544317
554	00O0554	383100	5540866	610	00O0610	379471	5544118
555	00O0555	383096	5540983	611	00O0611	379466	5543851
556	00O0556	382961	5541142	612	00O0612	380916	5541369
557	00O0557	382734	5541555	613	00O0613	380946	5541205
558	00O0558	382734	5541657	614	00O0614	381005	5540826
559	00O0559	382782	5541710	615	00O0615	380728	5540487
560	00O0560	382948	5541567	616	00O0616	379748	5540918
561	00O0561	382990	5541706	617	00O0617	379836	5541236
562	00O0562	382998	5541835	618	00O0618	379828	5541143
563	00O0563	383060	5542027	619	00O0619	379677	5540999
564	00O0564	382985	5542471	620	00O0620	379618	5540892
565	00O0565	383035	5542497	621	00O0621	379480	5540809
566	00O0566	383385	5542378	622	00O0622	378032	5540402
567	00O0567	383077	5542964	623	00O0623	378241	5540477
568	00O0568	383535	5542817	624	00O0624	379328	5544938
569	00O0569	383770	5543342	625	00O0625	377958	5544904
570	00O0570	383426	5544085	626	00O0626	378135	5545071
571	00O0571	382734	5544453	627	00O0627	378094	5545360
572	00O0572	382866	5545327	628	00O0628	379145	5545440
573	00O0573	383639	5545600	629	00O0629	378820	5545566
574	00O0574	384578	5544730	630	00O0630	379228	5546171
575	00O0575	384605	5544599	631	00O0631	379209	5546342
576	00O0576	384942	5544382	632	00O0632	379410	5546439
577	00O0577	385178	5543652	633	00O0633	379639	5546775
578	00O0578	385186	5543567	634	00O0634	379779	5546962
579	00O0579	385179	5543492	635	00O0635	379836	5547088
580	00O0580	385227	5543296	636	00O0636	379842	5547248
581	00O0581	385170	5545426	637	00O0637	379875	5547481
582	00O0582	384653	5545959	638	00O0638	380078	5547472
583	00O0583	384474	5546289	639	00O0639	380207	5547648
584	00O0584	384392	5546420	640	00O0640	378699	5546320
585	00O0585	384497	5547669	641	00O0641	377398	5547225
586	00O0586	384002	5547373	642	00O0642	377632	5547758
587	00O0587	382428	5546213	643	00O0643	377829	5547934
588	00O0588	382331	5546067	644	00O0644	378325	5548250
589	00O0589	382235	5545809	645	00O0645	378519	5548332
590	00O0590	382189	5545567	646	00O0646	378773	5548667
591	00O0591	382228	5541786	647	00O0647	378909	5548606
592	00O0592	381995	5541838	648	00O0648	380263	5548566
593	00O0593	381875	5542020	649	00O0649	380447	5548986
594	00O0594	381706	5542193	650	00O0650	380279	5549139
595	00O0595	381552	5542371	651	00O0651	380511	5549275
596	00O0596	381418	5542927	652	00O0652	380587	5549439
597	00O0597	381385	5543102	653	00O0653	381936	5549756
598	00O0598	381338	5543273	654	00O0654	382346	5550110
599	00O0599	381441	5543420	655	00O0655	382764	5550250
600	00O0600	381471	5543840	656	00O0656	382443	5550522
601	00O0601	381468	5544016	657	00O0657	378603	5549701
602	00O0602	381491	5544103	658	00O0658	376864	5549168
603	00O0603	381534	5544190	659	00O0659	377276	5548298
604	00O0604	381377	5544031	660	00O0660	376814	5548119

Number	Station[1,2]	Easting[3]	Northing[3]	Number	Station[1,2]	Easting[3]	Northing[3]
661	00O0661	376780	5551120	717	00O0717	371585	5558136
662	00O0662	375920	5550215	718	00O0718	371594	5558240
663	00O0663	376224	5549564	719	00O0719	371573	5558464
664	00O0664	374611	5550831	720	00O0720	371628	5560323
665	00O0665	373421	5548496	721	00O0721	371624	5560504
666	00O0666	372891	5548125	722	00O0722	371828	5560639
667	00O0667	372701	5547848	723	00O0723	371815	5560915
668	00O0668	372587	5547839	724	00O0724	371532	5561389
669	00O0669	372568	5546996	725	00O0725	371536	5561670
670	00O0670	373625	5547592	726	00O0726	373217	5560631
671	00O0671	373806	5547036	727	00O0727	373224	5558702
672	00O0672	373862	5546916	728	00O0728	374268	5561991
673	00O0673	374039	5546529	729	00O0729	375057	5561380
674	00O0674	374325	5545713	730	00O0730	378626	5560155
675	00O0675	374047	5545546	731	00O0731	378551	5560830
676	00O0676	374302	5545515	732	00O0732	376311	5562150
677	00O0677	373758	5545344	733	00O0733	376112	5562114
678	00O0678	373032	5545351	734	00O0734	380716	5557906
679	00O0679	374070	5544355	735	00O0735	380410	5557502
680	00O0680	372904	5543718	736	00O0736	381647	5557030
681	00O0681	372381	5543831	737	00O0737	382854	5559629
682	00O0682	373911	5542584	738	00O0738	385406	5560614
683	00O0683	372506	5542561	739	00O0739	385287	5560686
684	00O0684	372512	5542396	740	00O0740	385225	5560725
685	00O0685	372356	5542379	741	00O0741	385003	5560794
686	00O0686	372622	5540179	742	00O0742	384021	5561023
687	00O0687	372558	5549612	743	00O0743	383942	5560988
688	00O0688	371469	5552490	744	00O0744	383769	5560965
689	00O0689	371619	5552595	745	00O0745	383500	5561002
690	00O0690	371921	5552858	746	00O0746	383794	5561269
691	00O0691	371830	5553022	747	00O0747	383753	5561324
692	00O0692	371777	5553132	748	00O0748	385346	5559363
693	00O0693	371728	5553248	749	00O0749	385174	5559791
694	00O0694	371811	5553528	750	00O0750	384890	5559580
695	00O0695	371758	5553554	751	00O0751	384828	5559392
696	00O0696	371841	5553670	752	00O0752	384286	5559548
697	00O0697	371851	5553828	753	00O0753	383905	5559536
698	00O0698	371766	5554120	754	00O0754	384613	5558986
699	00O0699	371743	5554529	755	00O0755	384776	5558813
700	00O0700	371535	5554991	756	00O0756	385269	5558384
701	00O0701	372754	5553602	757	00O0757	385253	5558286
702	00O0702	373169	5557844	758	00O0758	385321	5558007
703	00O0703	373251	5557968	759	00O0759	385400	5557896
704	00O0704	378462	5556008	760	00O0760	385245	5557617
705	00O0705	374676	5558029	761	00O0761	385108	5557943
706	00O0706	378215	5557294	762	00O0762	384668	5558015
707	00O0707	378336	5557824	763	00O0763	383844	5558069
708	00O0708	378176	5557896	764	00O0764	383736	5557882
709	00O0709	378299	5558006	765	00O0765	383641	5557538
710	00O0710	378212	5558124	766	00O0766	383721	5557278
711	00O0711	378192	5558335	767	00O0767	383585	5556767
712	00O0712	376932	5560662	768	00O0768	383450	5556775
713	00O0713	376615	5560312	769	00O0769	382974	5556799
714	00O0714	376908	5560087	770	00O0770	384464	5557028
715	00O0715	376960	5559999	771	00O0771	384577	5556743
716	00O0716	377512	5559268	772	00O0772	384454	5556525

Number	Station[1,2]	Easting[3]	Northing[3]	Number	Station[1,2]	Easting[3]	Northing[3]
773	00O0773	384776	5556097	829	00O0829	387502	5541081
774	00O0774	384786	5555948	830	00O0830	387454	5541188
775	00O0775	384617	5555839	831	00O0831	387742	5541480
776	00O0776	384494	5555684	832	00O0832	387925	5541617
777	00O0777	384389	5555531	833	00O0833	388067	5541647
778	00O0778	384044	5555998	834	00O0834	388350	5541167
779	00O0779	383986	5555939	835	00O0835	388237	5541301
780	00O0780	383920	5555911	836	00O0836	388180	5541741
781	00O0781	383847	5555904	837	00O0837	387882	5541812
782	00O0782	383788	5555859	838	00O0838	388036	5541933
783	00O0783	383720	5555887	839	00O0839	388207	5542049
784	00O0784	383702	5555766	840	00O0840	388371	5542116
785	00O0785	383628	5555612	841	00O0841	388041	5542122
786	00O0786	382840	5556030	842	00O0842	388469	5543232
787	00O0787	382719	5555901	843	00O0843	388607	5543521
788	00O0788	382596	5555860	844	00O0844	388630	5543745
789	00O0789	382462	5555717	845	00O0845	388669	5543664
790	00O0790	385472	5552862	846	00O0846	388564	5543849
791	00O0791	383288	5553455	847	00O0847	388605	5544034
792	00O0792	383167	5553303	848	00O0848	388594	5544276
793	00O0793	383117	5553693	849	00O0849	388575	5544623
794	00O0794	378093	5551212	850	00O0850	388396	5544799
795	00O0795	380771	5554697	851	00O0851	388521	5544369
796	00O0796	381112	5555073	852	00O0852	388497	5544017
797	00O0797	380231	5555442	853	00O0853	386220	5544151
798	00O0798	379963	5556512	854	00O0854	386256	5544406
799	00O0799	376792	5552069	855	00O0855	386287	5544539
800	00O0800	376622	5552981	856	00O0856	386094	5545012
801	00O0801	376672	5553152	857	00O0857	385874	5545367
802	00O0802	376685	5553261	858	00O0858	391548	5541111
803	00O0803	376446	5553484	859	00O0859	392095	5541868
804	00O0804	376549	5553699	860	00O0860	392285	5542360
805	00O0805	376566	5553978	861	00O0861	393448	5541080
806	00O0806	376115	5553858	862	00O0862	393425	5541305
807	00O0807	375469	5553611	863	00O0863	393431	5541402
808	00O0808	375091	5554175	864	00O0864	393360	5541831
809	00O0809	374878	5553502	865	00O0865	393317	5541924
810	00O0810	374406	5553300	866	00O0866	393337	5542079
811	00O0811	374219	5552933	867	00O0867	393201	5542229
812	00O0812	373439	5553997	868	00O0868	393322	5542324
813	00O0813	373204	5553927	869	00O0869	393366	5542359
814	00O0814	372570	5553769	870	00O0870	393687	5542273
815	00O0815	372558	5552981	871	00O0871	394107	5542160
816	00O0816	372766	5552019	872	00O0872	394223	5541958
817	00O0817	372691	5551928	873	00O0873	395180	5541899
818	00O0818	372976	5551553	874	00O0874	395258	5541659
819	00O0819	373243	5551468	875	00O0875	395053	5541605
820	00O0820	373380	5551370	876	00O0876	394179	5545907
821	00O0821	373496	5551515	877	00O0877	393890	5545995
822	00O0822	373465	5551356	878	00O0878	393802	5546012
823	00O0823	374565	5551460	879	00O0879	394230	5546043
824	00O0824	386940	5540088	880	00O0880	394826	5546205
825	00O0825	386736	5540256	881	00O0881	395068	5546317
826	00O0826	386714	5540396	882	00O0882	394655	5546589
827	00O0827	388242	5540677	883	00O0883	394033	5547033
828	00O0828	387442	5541095	884	00O0884	388555	5545126

Number	Station[1,2]	Easting[3]	Northing[3]	Number	Station[1,2]	Easting[3]	Northing[3]
885	00O0885	390094	5544671	941	00O0941	391562	5549247
886	00O0886	390216	5544716	942	00O0942	391599	5549480
887	00O0887	390944	5545792	943	00O0943	391680	5549270
888	00O0888	391225	5547751	944	00O0944	391369	5550111
889	00O0889	391249	5547989	945	00O0945	391270	5549840
890	00O0890	393652	5548206	946	00O0946	391136	5549503
891	00O0891	393194	5548237	947	00O0947	391125	5549079
892	00O0892	393050	5548378	948	00O0948	390854	5548626
893	00O0893	393019	5550489	949	00O0949	390705	5548366
894	00O0894	392925	5550318	950	00O0950	390405	5548141
895	00O0895	387406	5547072	951	00O0951	366103	5544482
896	00O0896	386620	5547715	952	00O0952	366025	5544626
897	00O0897	387339	5548169	953	00O0953	365817	5544441
898	00O0898	386713	5548283	954	00O0954	365017	5544677
899	00O0899	386931	5548457	955	00O0955	363752	5547007
900	00O0900	387391	5549155	956	00O0956	361686	5547445
901	00O0901	385854	5549806	957	00O0957	361777	5547844
902	00O0902	386589	5550566	958	00O0958	361765	5548219
903	00O0903	385678	5550899	959	00O0959	356975	5547392
904	00O0904	385595	5550916	960	00O0960	361774	5549143
905	00O0905	386653	5549218	961	00O0961	361945	5549146
906	00O0906	386558	5549344	962	00O0962	362066	5549243
907	00O0907	386211	5549306	963	00O0963	362303	5549421
908	00O0908	388594	5548494	964	00O0964	362418	5550221
909	00O0909	388947	5548413	965	00O0965	362503	5550491
910	00O0910	389051	5548474	966	00O0966	362054	5550396
911	00O0911	389172	5548640	967	00O0967	362636	5550404
912	00O0912	389349	5548793	968	00O0968	362623	5550229
913	00O0913	389508	5548852	969	00O0969	362662	5550062
914	00O0914	389631	5549016	970	00O0970	362782	5550069
915	00O0915	389694	5549191	971	00O0971	362947	5550026
916	00O0916	389610	5549129	972	00O0972	363090	5549889
917	00O0917	389896	5549371	973	00O0973	363639	5549865
918	00O0918	390097	5549575	974	00O0974	363779	5549813
919	00O0919	390032	5549809	975	00O0975	363860	5549733
920	00O0920	389961	5549983	976	00O0976	364148	5549776
921	00O0921	390028	5550033	977	00O0977	364162	5550006
922	00O0922	389793	5550281	978	00O0978	364240	5550153
923	00O0923	389558	5550434	979	00O0979	364351	5550289
924	00O0924	389386	5550474	980	00O0980	364455	5550377
925	00O0925	390295	5550066	981	00O0981	364766	5550581
926	00O0926	390568	5549906	982	00O0982	365113	5550606
927	00O0927	390456	5550220	983	00O0983	365339	5550647
928	00O0928	390319	5550318	984	00O0984	365901	5550702
929	00O0929	390163	5550425	985	00O0985	362680	5549756
930	00O0930	390128	5550647	986	00O0986	362686	5549618
931	00O0931	390205	5550859	987	00O0987	363250	5549621
932	00O0932	390876	5550251	988	00O0988	363328	5549663
933	00O0933	390963	5550406	989	00O0989	362851	5549268
934	00O0934	391071	5550542	990	00O0990	357250	5548732
935	00O0935	391149	5550701	991	00O0991	357515	5549586
936	00O0936	391660	5550618	992	00O0992	357655	5549599
937	00O0937	391604	5550532	993	00O0993	357769	5549533
938	00O0938	391544	5550352	994	00O0994	358137	5550135
939	00O0939	391554	5550151	995	00O0995	358449	5550073
940	00O0940	391392	5549641	996	00O0996	360213	5550231

Number	Station[1,2]	Easting[3]	Northing[3]	Number	Station[1,2]	Easting[3]	Northing[3]
997	00O0997	360639	5550365	1053	00O1053	387098	5560883
998	00O0998	360975	5550461	1054	00O1054	386913	5560723
999	00O0999	360959	5551235	1055	00O1055	386539	5560516
1000	00O1000	360859	5551327	1056	00O1056	386439	5560197
1001	00O1001	361034	5551426	1057	00O1057	386193	5560000
1002	00O1002	360882	5551534	1058	00O1058	386239	5559909
1003	00O1003	393549	5552356	1059	00O1059	390478	5559733
1004	00O1004	392169	5552467	1060	00O1060	392586	5559328
1005	00O1005	392109	5553691	1061	00O1061	393037	5559540
1006	00O1006	395203	5553770	1062	00O1062	394320	5560169
1007	00O1007	395460	5553836	1063	00O1063	393983	5560441
1008	00O1008	389343	5551107	1064	00O1064	398510	5560020
1009	00O1009	386963	5552048	1065	00O1065	389979	5561104
1010	00O1010	387096	5552335	1066	00O1066	390248	5561778
1011	00O1011	386837	5552230	1067	00O1067	390484	5560686
1012	00O1012	385761	5553892	1068	00O1068	391766	5560205
1013	00O1013	386456	5553925	1069	00O1069	391949	5560159
1014	00O1014	386434	5554071	1070	00O1070	391379	5560618
1015	00O1015	387885	5554762	1071	00O1071	391372	5561292
1016	00O1016	387879	5555054	1072	00O1072	397024	5556936
1017	00O1017	387817	5555242	1073	00O1073	396754	5558126
1018	00O1018	387762	5555366	1074	00O1074	388284	5572189
1019	00O1019	387378	5555972	1075	00O1075	388295	5572291
1020	00O1020	387819	5555529	1076	00O1076	389552	5572669
1021	00O1021	385746	5555368	1077	00O1077	399032	5569364
1022	00O1022	385977	5555477	1078	00O1078	376568	5563873
1023	00O1023	386105	5554962	1079	00O1079	376485	5563879
1024	00O1024	389267	5553103	1080	00O1080	376402	5563896
1025	00O1025	389165	5553214	1081	00O1081	376375	5564201
1026	00O1026	389247	5553290	1082	00O1082	376368	5564452
1027	00O1027	389132	5553566	1083	00O1083	375666	5564821
1028	00O1028	389120	5553655	1084	00O1084	375561	5564562
1029	00O1029	389905	5554663	1085	00O1085	375542	5564866
1030	00O1030	389960	5554763	1086	00O1086	375235	5565041
1031	00O1031	390008	5554868	1087	00O1087	375103	5565027
1032	00O1032	390270	5555335	1088	00O1088	374945	5565036
1033	00O1033	390061	5556093	1089	00O1089	374872	5565116
1034	00O1034	389779	5556262	1090	00O1090	374148	5565174
1035	00O1035	389353	5556780	1091	00O1091	373994	5564952
1036	00O1036	389276	5556856	1092	00O1092	373601	5564698
1037	00O1037	389289	5557030	1093	00O1093	373468	5564697
1038	00O1038	385752	5557902	1094	00O1094	373056	5564708
1039	00O1039	387679	5557619	1095	00O1095	372947	5564701
1040	00O1040	387721	5557744	1096	00O1096	372848	5564722
1041	00O1041	387782	5557875	1097	00O1097	372606	5564928
1042	00O1042	387872	5558007	1098	00O1098	373373	5565061
1043	00O1043	388076	5558238	1099	00O1099	373368	5565175
1044	00O1044	387822	5558684	1100	00O1100	373203	5565431
1045	00O1045	387881	5558764	1101	00O1101	373234	5565538
1046	00O1046	388003	5559000	1102	00O1102	373545	5565370
1047	00O1047	392245	5556564	1103	00O1103	373628	5565511
1048	00O1048	391965	5557951	1104	00O1104	373704	5565538
1049	00O1049	389612	5560314	1105	00O1105	373705	5565628
1050	00O1050	389546	5560436	1106	00O1106	373769	5565769
1051	00O1051	389132	5560827	1107	00O1107	371887	5565729
1052	00O1052	386916	5560364	1108	00O1108	371753	5565740

Number	Station[1,2]	Easting[3]	Northing[3]	Number	Station[1,2]	Easting[3]	Northing[3]
1109	00O1109	374533	5562509	1165	00TWG0018	357217	5554305
1110	00O1110	374144	5562377	1166	00TWG0019	357193	5553106
1111	00O1111	374184	5562518	1167	00TWG0020	356830	5552815
1112	00O1112	374218	5562654	1168	00TWG0021	356641	5551377
1113	00O1113	374317	5562835	1169	00TWG0022	357945	5552847
1114	00O1114	374244	5562981	1170	00TWG0023	358132	5552297
1115	00O1115	371725	5567009	1171	00TWG0024	357849	5551789
1116	00O1116	371991	5567042	1172	00TWG0025	357551	5551501
1117	00O1117	377948	5566187	1173	00TWG0026	357606	5551101
1118	00O1118	377895	5566251	1174	00TWG0027	358449	5551849
1119	00O1119	377412	5566522	1175	00TWG0028	358863	5551998
1120	00O1120	376390	5567010	1176	00TWG0029	358768	5553178
1121	00O1121	375648	5567423	1177	00TWG0030	358577	5553178
1122	00O1123	371989	5568107	1178	00TWG0031	359519	5554854
1123	00O1124	371751	5568077	1179	00TWG0032	359660	5555005
1124	00O1125	373154	5568862	1180	00TWG0033	360352	5555032
1125	00O1126	372868	5569083	1181	00TWG0034	360258	5555891
1126	00O1127	372679	5569238	1182	00TWG0035	359555	5555694
1127	00O1128	372539	5569314	1183	00TWG0036	359610	5554245
1128	00O1129	372393	5569421	1184	00TWG0037	359419	5553949
1129	00O1130	372258	5569556	1185	00TWG0038	360929	5553909
1130	00O1131	372328	5569772	1186	00TWG0039	360806	5553415
1131	00O1132	372319	5569935	1187	00TWG0040	360701	5552074
1132	00O1133	371903	5570060	1188	00TWG0041	356950	5610500
1133	00O1134	372038	5570631	1189	00TWG0042	356761	5559521
1134	00O1135	372100	5570632	1190	00TWG0043	356654	5559319
1135	00O1136	372500	5570340	1191	00TWG0044	356611	5558892
1136	00O1137	372712	5570417	1192	00TWG0045	356302	5557773
1137	00O1138	372785	5570230	1193	00TWG0046	356350	5558400
1138	00O1139	373458	5569958	1194	00TWG0047	356350	5559150
1139	00O1140	373864	5569672	1195	00TWG0048	353018	5543654
1140	00O1141	374080	5569320	1196	00TWG0049	353332	5544500
1141	00O1142	374294	5569038	1197	00TWG0050	352686	5544017
1142	00O1143	378509	5567676	1198	00TWG0051	352962	5544286
1143	00O1144	378758	5567676	1199	00TWG0052	352735	5544681
1144	00O1145	379628	5567228	1200	00TWG0053	351305	5543380
1145	00O1146	378055	5568587	1201	00TWG0054	351260	5544293
1146	00O1147	376367	5569237	1202	00TWG0055	350928	5545550
1147	00TWG0001	356634	5563193	1203	00TWG0056	352345	5546636
1148	00TWG0002	356527	5562771	1204	00TWG0057	354134	5546071
1149	00TWG0003	356248	5562642	1205	00TWG0058	354173	5547207
1150	00TWG0004	356068	5562601	1206	00TWG0059	354976	5547422
1151	00TWG0005A	355961	5562468	1207	00TWG0060	355193	5548198
1152	00TWG0005B	355159	5562047	1208	00TWG0061	357107	5548909
1153	00TWG0006	355386	5561756	1209	00TWG0062	357367	5548764
1154	00TWG0007	355371	5561339	1210	00TWG0063	357148	5549539
1155	00TWG0008	355135	5561118	1211	00TWG0064	359505	5550053
1156	00TWG0009	355134	5561021	1212	00TWG0065	354256	5547717
1157	00TWG0010	355057	5560491	1213	00TWG0066	354646	5548455
1158	00TWG0011	355186	5559776	1214	00TWG0067	354985	5548855
1159	00TWG0012	357379	5556413	1215	00TWG0068	355385	5550130
1160	00TWG0013	358065	5555815	1216	00TWG0069	356257	5550908
1161	00TWG0014	359212	5555461	1217	00TWG0070	379843	5567070
1162	00TWG0015	358666	5555014	1218	00TWG0071	379716	5567196
1163	00TWG0016	358453	5554494	1219	00TWG0072	378960	5567540
1164	00TWG0017	358199	5554509	1220	00TWG0073	378160	5567660

Number	Station[1,2]	Easting[3]	Northing[3]	Number	Station[1,2]	Easting[3]	Northing[3]
1221	00TWG0074	375100	5567580	1277	00TWG0130	364753	5563446
1222	00TWG0075	374800	5567710	1278	00TWG0131	364605	5563492
1223	00TWG0076	374220	5569260	1279	00TWG0132	364407	5563282
1224	00TWG0077	373740	5569860	1280	00TWG0133	368539	5563840
1225	00TWG0078	373060	5570110	1281	00TWG0134	370815	5564336
1226	00TWG0079	373700	5570290	1282	00TWG0135	379961	5557391
1227	00TWG0080	361440	5561573	1283	00TWG0136	380068	5557865
1228	00TWG0081	361584	5561490	1284	00TWG0137	380307	5558401
1229	00TWG0082	362219	5560766	1285	00TWG0138	380675	5559390
1230	00TWG0083	364379	5556755	1286	00TWG0139	381150	5558425
1231	00TWG0084	363351	5556728	1287	00TWG0140	380618	5558116
1232	00TWG0085	364794	5555366	1288	00TWG0141	380935	5558055
1233	00TWG0086	364619	5555153	1289	00TWG0142	380365	5557380
1234	00TWG0087	365116	5554693	1290	00TWG0143	379990	5556500
1235	00TWG0088	363358	5555501	1291	00TWG0144	377029	5554431
1236	00TWG0089	363291	5555509	1292	00TWG0145	376802	5555063
1237	00TWG0090	363120	5555465	1293	00TWG0146	376991	5555518
1238	00TWG0091	364047	5558976	1294	00TWG0147	379374	5562233
1239	00TWG0092	362119	5561589	1295	00TWG0148	380075	5562222
1240	00TWG0093	362327	5561326	1296	00TWG0149	381551	5562135
1241	00TWG0094	362438	5561274	1297	00TWG0150	381620	5561961
1242	00TWG0095	362903	5561031	1298	00TWG0151	381710	5561694
1243	00TWG0096	362774	5561579	1299	00TWG0152	382732	5560043
1244	00TWG0097	363225	5561827	1300	00TWG0153	382885	5559059
1245	00TWG0098	363525	5561971	1301	00TWG0154	382446	5558162
1246	00TWG0099	363938	5561479	1302	00TWG0155	382042	5557596
1247	00TWG0100	365666	5556938	1303	00TWG0156	381609	5556852
1248	00TWG0101	366613	5558197	1304	00TWG0157	381045	5555435
1249	00TWG0102	367043	5558843	1305	00TWG0158	359695	5562890
1250	00TWG0103	367895	5560693	1306	00TWG0159	358813	5562798
1251	00TWG0104	374503	5558634	1307	00TWG0160	358489	5562829
1252	00TWG0105	373797	5560319	1308	00TWG0161	358350	5562120
1253	00TWG0106	373971	5563038	1309	00TWG0162	358570	5562000
1254	00TWG0107	374912	5562526	1310	00TWG0163	358100	5562033
1255	00TWG0108	374864	5561407	1311	00TWG0164	360173	5561592
1256	00TWG0109	375218	5559936	1312	00TWG0165	358802	5559605
1257	00TWG0110	376236	5559722	1313	00TWG0166	368139	5559716
1258	00TWG0111	376920	5560504	1314	00TWG0167	368608	5559977
1259	00TWG0112	376339	5559309	1315	00TWG0168	369233	5559621
1260	00TWG0113	377426	5559285	1316	00TWG0169	369233	5559621
1261	00TWG0114	377874	5559717	1317	00TWG0170	370466	5558599
1262	00TWG0115	377570	5559754	1318	00TWG0171	366484	5557197
1263	00TWG0116	378566	5560798	1319	00TWG0172	369625	5557120
1264	00TWG0117	378040	5559725	1320	00TWG0173	370018	5557989
1265	00TWG0118	378573	5560261	1321	00TWG0174	368056	5556306
1266	00TWG0119	378877	5560883	1322	00TWG0175	369491	5555659
1267	00TWG0120	366429	5563685	1323	00TWG0176	372913	5553404
1268	00TWG0121	366521	5563591	1324	00TWG0177	375217	5553522
1269	00TWG0122	365927	5562865	1325	00TWG0178	375225	5554000
1270	00TWG0123	365704	5562743	1326	00TWG0179	376743	5554180
1271	00TWG0124	365455	5562893	1327	00TWG0180	376242	5551140
1272	00TWG0125	365386	5563032	1328	00TWG0181	362460	5562710
1273	00TWG0126	365569	5563222	1329	00TWG0182	362037	5563183
1274	00TWG0127	365489	5563452	1330	00TWG0183	362073	5563223
1275	00TWG0128	365137	5563491	1331	00TWG0184	362212	5563522
1276	00TWG0129	364826	5563380	1332	00TWG0185	362433	5564478

Number	Station[1,2]	Easting[3]	Northing[3]	Number	Station[1,2]	Easting[3]	Northing[3]
1333	00TWG0186	361622	5564627	1389	00TWG0242	386572	5557919
1334	00TWG0187	360845	5564471	1390	00TWG0243	385684	5555740
1335	00TWG0188	360176	5563622	1391	00TWG0244	386469	5557324
1336	00TWG0189	360062	5563524	1392	00TWG0245	387400	5555700
1337	00TWG0190	359843	5563528	1393	00TWG0246	387860	5560128
1338	00TWG0191	359357	5563270	1394	00TWG0247	388607	5560435
1339	00TWG0192	370392	5567954	1395	00TWG0248	388103	5556640
1340	00TWG0193	370979	5568078	1396	00TWG0249	388017	5557168
1341	00TWG0194	374320	5565030	1397	00TWG0250	387742	5557543
1342	00TWG0195	373524	5564989	1398	00TWG0251	388004	5558517
1343	00TWG0196	373263	5564744	1399	00TWG0252	387883	5558566
1344	00TWG0197	372265	5565126	1400	00TWG0253	388377	5557815
1345	00TWG0198	373283	5564814	1401	00TWG0254	388842	5557652
1346	00TWG0199	360686	5553118	1402	00TWG0255	390056	5555059
1347	00TWG0200	360806	5551728	1403	00TWG0256	389666	5554095
1348	00TWG0201	360911	5551417	1404	00TWG0257	389287	5553743
1349	00TWG0202	361055	5551025	1405	00TWG0258	389188	5553429
1350	00TWG0203	361121	5550570	1406	00TWG0259	389236	5553144
1351	00TWG0204	360351	5550250	1407	00TWG0260	386958	5555226
1352	00TWG0205	359468	5550046	1408	00TWG0261	387235	5555672
1353	00TWG0206	357638	5549871	1409	00TWG0262	369026	5563021
1354	00TWG0207	358276	5549319	1410	00TWG0263	369350	5562641
1355	00TWG0208	358753	5549337	1411	00TWG0264	371135	5566877
1356	00TWG0209	356515	5547967	1412	00TWG0265	371563	5566791
1357	00TWG0210	356466	5547645	1413	00TWG0266	371633	5566544
1358	00TWG0211	354952	5546375	1414	00TWG0267	371897	5565871
1359	00TWG0212	389026	5560887	1415	00TWG0268	372179	5565822
1360	00TWG0213	388055	5560657	1416	00TWG0269	372436	5566391
1361	00TWG0214	386903	5559659	1417	00TWG0270	362474	5565631
1362	00TWG0215	386944	5560224	1418	00TWG0271	363080	5565590
1363	00TWG0216	387105	5560514	1419	00TWG0272	363435	5565177
1364	00TWG0217	387171	5560682	1420	00TWG0273	361617	5550596
1365	00TWG0218	386822	5560669	1421	00TWG0274	361826	5550503
1366	00TWG0219	385495	5560316	1422	00TWG0275	362203	5550253
1367	00TWG0220	385449	5560556	1423	00TWG0276	362246	5549575
1368	00TWG0221	385143	5560870	1424	00TWG0277	361231	5548055
1369	00TWG0222	384891	5560644	1425	00TWG0278	363403	5549830
1370	00TWG0223	384323	5560846	1426	00TWG0279	364731	5550581
1371	00TWG0224	384004	5561109	1427	00TWG0280	365020	5550645
1372	00TWG0225	383924	5561264	1428	00TWG0281	362766	5549450
1373	00TWG0226	383583	5561250	1429	00TWG0282	363134	5549694
1374	00TWG0227	383144	5561363	1430	00TWG0283	362958	5549104
1375	00TWG0228	385492	5559326	1431	00TWG0284	364999	5554894
1376	00TWG0229	384828	5569491	1432	00TWG0285	364742	5554422
1377	00TWG0230	384271	5559399	1433	00TWG0286	364681	5554422
1378	00TWG0231	383856	5559245	1434	00TWG0287	364368	5554002
1379	00TWG0232	383750	5558211	1435	00TWG0288	364084	5553531
1380	00TWG0233	383860	5556975	1436	00TWG0289	363754	5553672
1381	00TWG0234	383129	5556651	1437	00TWG0290	363604	5553707
1382	00TWG0235	384591	5559122	1438	00TWG0291	363706	5553962
1383	00TWG0236	385280	5557719	1439	00TWG0292	363325	5554201
1384	00TWG0237	384060	5556217	1440	00TWG0293	363376	5554362
1385	00TWG0238	382964	5556127	1441	00TWG0294	391720	5550965
1386	00TWG0239	382457	5555657	1442	00TWG0295	365320	5568153
1387	00TWG0240	382485	5555290	1443	00TWG0296	366936	5568157
1388	00TWG0241	383438	5555042	1444	00TWG0297	372067	5570642

Number	Station[1,2]	Easting[3]	Northing[3]	Number	Station[1,2]	Easting[3]	Northing[3]
1445	00TWG0298	372456	5570394	1501	00TWG0355	372537	5542709
1446	00TWG0299	372600	5570300	1502	00TWG0356	372420	5541680
1447	00TWG0300	384077	5547273	1503	00TWG0357	374525	5541643
1448	00TWG0301	383446	5541086	1504	00TWG0358	374820	5541699
1449	00TWG0302	366259	5540345	1505	00TWG0359	372918	5540166
1450	00TWG0303	366150	5544365	1506	00TWG0360	379205	5562181
1451	00TWG0304	374493	5564747	1507	00TWG0361	378986	5562174
1452	00TWG0305	374747	5565051	1508	00TWG0362	379254	5561866
1453	00TWG0306	379464	5562847	1509	00TWG0363	379280	5561718
1454	00TWG0307	379329	5563379	1510	00TWG0364	379442	5561614
1455	00TWG0308	377296	5563387	1511	00TWG0365	405216	5580325
1456	00TWG0309	376922	5563683	1512	00TWG0366	405678	5580049
1457	00TWG0310	376920	5563810	1513	00TWG0367	406447	5580263
1458	00TWG0311	376783	5563852	1514	00TWG0368	403246	5577549
1459	00TWG0312	372693	5547522	1515	00TWG0369	403554	5577882
1460	00TWG0313	371564	5545852	1516	00TWG0370	403741	5578031
1461	00TWG0314	374168	5545561	1517	00TWG0371	403654	5578458
1462	00TWG0315	373948	5543457	1518	00TWG0372	403258	5578699
1463	00TWG0316	373628	5543816	1519	00TWG0373	403133	5578903
1464	00TWG0317	373438	5543843	1520	00TWG0374	403068	5579356
1465	00TWG0318	373112	5543820	1521	00TWG0375	402678	5579737
1466	00TWG0319	410231	5563029	1522	00TWG0376	402431	5579896
1467	00TWG0320	410350	5563500	1523	00TWG0377	402479	5580430
1468	00TWG0321	410375	5563601	1524	00TWG0378	387660	5572400
1469	00TWG0322	410496	5563687	1525	00TWG0379	387689	5571807
1470	00TWG0323	410150	5563626	1526	00TWG0380	387933	5572118
1471	00TWG0324	407236	5563562	1527	00TWG0381	388007	5571505
1472	00TWG0325	407794	5564159	1528	00TWG0382	388368	5572211
1473	00TWG0326	407833	5564349	1529	00TWG0383	389245	5572357
1474	00TWG0327	407858	5564491	1530	00TWG0384	389564	5572690
1475	00TWG0328	408087	5564744	1531	00TWG0385	390245	5573004
1476	00TWG0329	407611	5565038	1532	00TWG0386	390485	5573508
1477	00TWG0330	407374	5565120	1533	00TWG0387	390776	5574343
1478	00TWG0331	407130	5565038	1534	00TWG0388	390625	5574413
1479	00TWG0332	407130	5565038	1535	00TWG0389	391441	5576171
1480	00TWG0333	406128	5564980	1536	00TWG0390	391104	5576123
1481	00TWG0334	405500	5565051	1537	00TWG0391	390827	5576126
1482	00TWG0336	384643	5555422	1538	00TWG0392	391546	5575802
1483	00TWG0337	384708	5555608	1539	00TWG0393	392079	5576334
1484	00TWG0338	384500	5555700	1540	00TWG0394	392205	5575581
1485	00TWG0339	384041	5554646	1541	00TWG0395	403333	5578579
1486	00TWG0340	383644	5553436	1542	00TWG0396	401967	5579845
1487	00TWG0341	383108	5553779	1543	00TWG0397	401454	5579720
1488	00TWG0342	384352	5553144	1544	00TWG0398	400686	5579875
1489	00TWG0343	384434	5552942	1545	00TWG0399	400131	5579893
1490	00TWG0344	384277	5553171	1546	00TWG0400	399486	5579791
1491	00TWG0345	385367	5555696	1547	00TWG0401	399551	5579625
1492	00TWG0346	385560	5555434	1548	00TWG0402	392799	5575553
1493	00TWG0347	385923	5555575	1549	00TWG0403	391113	5573314
1494	00TWG0348	386119	5555555	1550	00TWG0404	391497	5573428
1495	00TWG0349	385804	5555142	1551	00TWG0405	392003	5573547
1496	00TWG0350	386157	5555210	1552	00TWG0406	392386	5573612
1497	00TWG0351	386043	5554805	1553	00TWG0407	395081	5574826
1498	00TWG0352	385286	5554973	1554	00TWG0408	395464	5575219
1499	00TWG0353	375390	5544643	1555	00TWG0409	395959	5575518
1500	00TWG0354	373916	5543011	1556	00TWG0410	395450	5574829

Number	Station[1,2]	Easting[3]	Northing[3]	Number	Station[1,2]	Easting[3]	Northing[3]
1557	00TWG0411	395785	5574982	1613	00TWG0467	392748	5561432
1558	00TWG0412	339917	5549934	1614	00TWG0468	392813	5559353
1559	00TWG0413	340004	5550165	1615	00TWG0469	393319	5559428
1560	00TWG0414	340325	5550241	1616	00TWG0470	392782	5559530
1561	00TWG0415	340887	5550181	1617	00TWG0471	392167	5559600
1562	00TWG0416	341952	5550297	1618	00TWG0472	394834	5559855
1563	00TWG0417	341872	5550400	1619	00TWG0473	394808	5560078
1564	00TWG0418	342586	5551183	1620	00TWG0474	394312	5560133
1565	00TWG0419	342238	5551222	1621	00TWG0475	394042	5560405
1566	00TWG0420	338977	5546023	1622	00TWG0476	394690	5560521
1567	00TWG0421	340604	5546593	1623	00TWG0477	394772	5560740
1568	00TWG0422	341157	5547344	1624	00TWG0478	395744	5560386
1569	00TWG0423	340883	5547514	1625	00TWG0479	396771	5560210
1570	00TWG0424	341947	5547415	1626	00TWG0480	397839	5560055
1571	00TWG0425	342198	5547575	1627	00TWG0481	397663	5561236
1572	00TWG0426	342710	5547766	1628	00TWG0482	398603	5559988
1573	00TWG0427	343371	5549125	1629	00TWG0483	399261	5560133
1574	00TWG0428	343480	5549285	1630	00TWG0484	399838	5560240
1575	00TWG0429	343997	5550241	1631	00TWG0485	400473	5560507
1576	00TWG0430	345013	5553979	1632	00TWG0486	402366	5572486
1577	00TWG0431	343742	5559532	1633	00TWG0487	402659	5572520
1578	00TWG0432	404115	5566915	1634	00TWG0488	404011	5572467
1579	00TWG0433	403158	5566661	1635	00TWG0489	405774	5574020
1580	00TWG0434	404205	5567128	1636	00TWG0490	405765	5574220
1581	00TWG0435	404535	5566870	1637	00TWG0491	405459	5574559
1582	00TWG0436	404115	5566915	1638	00TWG0492	406166	5574707
1583	00TWG0437	391236	5559294	1639	00TWG0493	404043	5572050
1584	00TWG0438	391841	5559164	1640	00TWG0494	403605	5571530
1585	00TWG0439	391263	5559415	1641	00TWG0495	410548	5563148
1586	00TWG0440	390976	5559775	1642	00TWG0496	411795	5562159
1587	00TWG0441	390683	5559935	1643	00TWG0497	411853	5561815
1588	00TWG0442	390175	5560400	1644	00TWG0498a	411985	5561304
1589	00TWG0443	389828	5560761	1645	00TWG0498b	412240	5561129
1590	00TWG0444	389672	5560895	1646	00TWG0499	412282	5561064
1591	00TWG0445	389659	5561059	1647	00TWG0500	412062	5562820
1592	00TWG0446	389733	5561955	1648	00TWG0501	412363	5562954
1593	00TWG0447	389777	5562338	1649	00TWG0502	412668	5563052
1594	00TWG0448	389953	5560677	1650	00TWG0503	412549	5563445
1595	00TWG0449	389797	5561045	1651	00TWG0504	412516	5563664
1596	00TWG0450	389993	5560977	1652	00TWG0505	412416	5563741
1597	00TWG0451	390062	5561311	1653	00TWG0506	412373	5563822
1598	00TWG0452	390122	5561491	1654	00TWG0507	412281	5563893
1599	00TWG0453	390194	5561608	1655	00TWG0508	411990	5564078
1600	00TWG0454	390259	5560740	1656	00TWG0509	411761	5564193
1601	00TWG0455	390456	5560607	1657	00TWG0510	411195	5564200
1602	00TWG0456	390733	5560383	1658	00TWG0511	411014	5565064
1603	00TWG0457	390966	5560429	1659	00TWG0512	410053	5565371
1604	00TWG0458	390735	5560821	1660	00TWG0513	410029	5565692
1605	00TWG0459	390815	5561181	1661	00TWG0514	409772	5565791
1606	00TWG0460	391302	5560247	1662	00TWG0515	409855	5566859
1607	00TWG0461	391385	5560075	1663	00TWG0516	409877	5567121
1608	00TWG0462	391923	5560385	1664	00TWG0517	409724	5567204
1609	00TWG0463	392090	5560187	1665	00TWG0518	409467	5567378
1610	00TWG0464	391694	5561167	1666	00TWG0519	409486	5567665
1611	00TWG0465	391776	5561219	1667	00TWG0520	409486	5567665
1612	00TWG0466	392186	5561551	1668	00TWG0521	406123	5565186

Number	Station[1,2]	Easting[3]	Northing[3]	Number	Station[1,2]	Easting[3]	Northing[3]
1669	00TWG0522	406789	5565296	1725	00TWG0578	396204	5551718
1670	00TWG0523	406636	5566182	1726	00TWG0579	395221	5549090
1671	00TWG0524	406470	5566302	1727	00TWG0580	395561	5548845
1672	00TWG0525	406584	5566674	1728	00TWG0581	395551	5548683
1673	00TWG0526	406592	5566797	1729	00TWG0582	395337	5548500
1674	00TWG0527	405127	5567518	1730	00TWG0583	394346	5547283
1675	00TWG0528	406901	5575075	1731	00TWG0584	395208	5549285
1676	00TWG0529	407220	5575078	1732	00TWG0585	395482	5549362
1677	00TWG0530	407434	5575025	1733	00TWG0586	396113	5549207
1678	00TWG0531	407850	5574868	1734	00TWG0587	397560	5550108
1679	00TWG0532	408039	5574827	1735	00TWG0588	428035	5552862
1680	00TWG0533	408419	5575095	1736	00TWG0589	426566	5551601
1681	00TWG0534	408514	5575134	1737	00TWG0590	425344	5550011
1682	00TWG0535	408605	5575195	1738	00TWG0591	425538	5549901
1683	00TWG0536	408816	5575549	1739	00TWG0592	425865	5549600
1684	00TWG0537	409623	5575815	1740	00TWG0593	425743	5549433
1685	00TWG0538	409676	5575753	1741	00TWG0594	425480	5549169
1686	00TWG0539	409170	5575515	1742	00TWG0595	425066	5548783
1687	00TWG0540	409037	5575402	1743	00TWG0596	424851	5548726
1688	00TWG0541	408890	5575281	1744	00TWG0597	426279	5546726
1689	00TWG0542	408891	5575281	1745	00TWG0598	426339	5545844
1690	00TWG0543	408640	5575134	1746	00TWG0599	425158	5544988
1691	00TWG0544	362951	5546072	1747	00TWG0600	423200	5549180
1692	00TWG0545	362309	5545567	1748	00TWG0601	422200	5549220
1693	00TWG0546	393661	5558913	1749	00TWG0602	421180	5549780
1694	00TWG0547	393452	5558736	1750	00TWG0603	422070	5550260
1695	00TWG0548	393422	5558511	1751	00TWG0604	420051	5548900
1696	00TWG0549	393780	5558263	1752	00TWG0605	419896	5548533
1697	00TWG0550	394399	5557669	1753	00TWG0606	420440	5553537
1698	00TWG0551	396342	5557074	1754	00TWG0607	418900	5553608
1699	00TWG0552	396872	5556937	1755	00TWG0608	418918	5553336
1700	00TWG0553	398472	5557014	1756	00TWG0609	418511	5553126
1701	00TWG0554	397336	5557724	1757	00TWG0610	419021	5552841
1702	00TWG0555	396950	5557790	1758	00TWG0611	418808	5552527
1703	00TWG0556	398924	5556800	1759	00TWG0612	418892	5552209
1704	00TWG0557	400633	5555255	1760	00TWG0613	418310	5552492
1705	00TWG0558	400773	5554936	1761	00TWG0614	417870	5552562
1706	00TWG0559	408291	5552625	1762	00TWG0615	418284	5551920
1707	00TWG0560	405301	5553577	1763	00TWG0616	417794	5552259
1708	00TWG0561	403803	5554101	1764	00TWG0617	417684	5553121
1709	00TWG0562	404199	5554076	1765	00TWG0618	417280	5552964
1710	00TWG0563	404640	5554084	1766	00TWG0619	416620	5552961
1711	00TWG0564	404905	5554159	1767	00TWG0620	415328	5552071
1712	00TWG0565	404966	5554170	1768	00TWG0621	418431	5554643
1713	00TWG0566	404696	5554148	1769	00TWG0622	418032	5554624
1714	00TWG0567	404536	5554151	1770	00TWG0623	417206	5554729
1715	00TWG0568	404341	5554222	1771	00TWG0624	414516	5555572
1716	00TWG0569	404206	5554179	1772	00TWG0625	414449	5555204
1717	00TWG0570	404213	5554626	1773	00TWG0626	414750	5554969
1718	00TWG0571	404069	5554719	1774	00TWG0627	416938	5554819
1719	00TWG0572	404233	5555013	1775	00TWG0628	417421	5555174
1720	00TWG0573	402526	5554505	1776	00TWG0629	418235	5556090
1721	00TWG0574	402652	5554595	1777	00TWG0630	417802	5555832
1722	00TWG0575	402717	5554725	1778	00TWG0631	417532	5556080
1723	00TWG0576	398110	5552805	1779	00TWG0632	416996	5555856
1724	00TWG0577	396820	5552621	1780	00TWG0633	416312	5555907

Number	Station[1,2]	Easting[3]	Northing[3]	Number	Station[1,2]	Easting[3]	Northing[3]
1781	00TWG0634	417575	5556635	1837	00TWG0690	431813	5588679
1782	00TWG0635	416351	5556426	1838	00TWG0691	431835	5592076
1783	00TWG0636	415729	5556405	1839	01TWG001	340965	5557289
1784	00TWG0637	415111	5556525	1840	01TWG002	340072	5555971
1785	00TWG0638	417637	5557266	1841	01TWG003	339552	5555265
1786	00TWG0639	422646	5570610	1842	01TWG004	339119	5555389
1787	00TWG0640	421358	5569822	1843	01TWG005	341687	5555426
1788	00TWG0641	421087	5569406	1844	01TWG006	363776	5600083
1789	00TWG0642	420803	5569165	1845	01TWG007	367746	5602346
1790	00TWG0643	420276	5568942	1846	01TWG008	374021	5604484
1791	00TWG0644	420684	5568554	1847	01TWG009	374859	5603460
1792	00TWG0645	420974	5568341	1848	01TWG010	375253	5604164
1793	00TWG0646	420733	5568437	1849	01TWG011	374049	5602766
1794	00TWG0647	420418	5568285	1850	01TWG012	374067	5602234
1795	00TWG0648	419871	5568064	1851	01TWG013	374931	5600091
1796	00TWG0649	419737	5567826	1852	01TWG014	374820	5599646
1797	00TWG0650	418932	5567734	1853	01TWG015	374337	5600866
1798	00TWG0651	418461	5567620	1854	01TWG016	374473	5599661
1799	00TWG0652	419029	5567595	1855	01TWG017	374612	5599074
1800	00TWG0653	419427	5567086	1856	01TWG018	371040	5600298
1801	00TWG0654	418502	5567359	1857	01TWG019	372321	5600514
1802	00TWG0655	418026	5566763	1858	01TWG020	372285	5598311
1803	00TWG0656	419180	5568390	1859	01TWG021	372359	5598958
1804	00TWG0657	418760	5568350	1860	01TWG022	372856	5599806
1805	00TWG0658	417523	5565167	1861	01TWG023	373431	5590156
1806	00TWG0659	474803	5587146	1862	01TWG024	373993	5589916
1807	00TWG0660	482472	5569795	1863	01TWG025	374777	5590946
1808	00TWG0661	422752	5572503	1864	01TWG026	372191	5578650
1809	00TWG0662	422200	5572211	1865	01TWG027	361562	5601212
1810	00TWG0663	421711	5571922	1866	01TWG028	364632	5601641
1811	00TWG0664	421584	5571710	1867	01TWG029	363572	5604215
1812	00TWG0665	422054	5570848	1868	01TWG030	360740	5604045
1813	00TWG0666	421975	5570972	1869	01TWG031	361382	5604469
1814	00TWG0667	421699	5570688	1870	01TWG032	362544	5605197
1815	00TWG0668	421634	5570870	1871	01TWG033	362472	5605783
1816	00TWG0669	419823	5571556	1872	01TWG034	364206	5607630
1817	00TWG0670	419233	5571288	1873	01TWG035	365105	5608195
1818	00TWG0671	417059	5570677	1874	01TWG036	365652	5608825
1819	00TWG0672	416983	5570439	1875	01TWG037	366949	5611005
1820	00TWG0673	415887	5568029	1876	01TWG038	361075	5605459
1821	00TWG0674	417572	5569875	1877	01TWG039	379221	5608328
1822	00TWG0675	417319	5569856	1878	01TWG040	380131	5609317
1823	00TWG0676	417201	5569883	1879	01TWG041	380096	5610065
1824	00TWG0677	428073	5580835	1880	01TWG042	380584	5611410
1825	00TWG0678	428588	5581791	1881	01TWG043	381341	5613636
1826	00TWG0679	428521	5581868	1882	01TWG044	378172	5607186
1827	00TWG0680	428488	5582246	1883	01TWG045	363447	5604237
1828	00TWG0681	428586	5582344	1884	01TWG046	361805	5603840
1829	00TWG0682	429432	5583084	1885	01TWG047	361398	5603742
1830	00TWG0683	428773	5581823	1886	01TWG048	360087	5603871
1831	00TWG0684	429021	5582094	1887	01TWG049	360971	5605253
1832	00TWG0685	430796	5582703	1888	01TWG050	361011	5605402
1833	00TWG0686	427815	5582532	1889	01TWG051	363497	5608215
1834	00TWG0687	428692	5583231	1890	01TWG052	363024	5608237
1835	00TWG0688	430255	5583871	1891	01TWG053	363246	5608512
1836	00TWG0689	431117	5587908	1892	01TWG054	363272	5608785

Number	Station[1,2]	Easting[3]	Northing[3]	Number	Station[1,2]	Easting[3]	Northing[3]
1893	01TWG055	362739	5608867	1949	01TWG111	376475	5622390
1894	01TWG056	362289	5609095	1950	01TWG112	376603	5624633
1895	01TWG057	361668	5609203	1951	01TWG113	350151	5580950
1896	01TWG058	360378	5609781	1952	01TWG114	350198	5580752
1897	01TWG059	359973	5611286	1953	01TWG115	350151	5580652
1898	01TWG060	363171	5609998	1954	01TWG116	350093	5580527
1899	01TWG061	362717	5610639	1955	01TWG117	349807	5580603
1900	01TWG062	362977	5611245	1956	01TWG118	349640	5580571
1901	01TWG063	363633	5612909	1957	01TWG119	349477	5580220
1902	01TWG064	363461	5608323	1958	01TWG120	349324	5580201
1903	01TWG065	365213	5610068	1959	01TWG121	349250	5580214
1904	01TWG066	356944	5601379	1960	01TWG122	349228	5580269
1905	01TWG067	357153	5598789	1961	01TWG123	349216	5580444
1906	01TWG068	357045	5598582	1962	01TWG124	349274	5580525
1907	01TWG069	355372	5603771	1963	01TWG125	349443	5580571
1908	01TWG070	355442	5604446	1964	01TWG126	349414	5580469
1909	01TWG071	355640	5604261	1965	01TWG127	349488	5580469
1910	01TWG072	369749	5614313	1966	01TWG128	349251	5580671
1911	01TWG073	369309	5614923	1967	01TWG129	349410	5580883
1912	01TWG074	370618	5614894	1968	01TWG130	349220	5580917
1913	01TWG075	370576	5615788	1969	01TWG131	349317	5581122
1914	01TWG076	369285	5616375	1970	01TWG132	349418	5581326
1915	01TWG077	367748	5618315	1971	01TWG133	349503	5581275
1916	01TWG078	367493	5618474	1972	01TWG134	349399	5581131
1917	01TWG079	367100	5619062	1973	01TWG135	349603	5580758
1918	01TWG080	370965	5610765	1974	01TWG136	376681	5604766
1919	01TWG081	370657	5609894	1975	01TWG137	376604	5604108
1920	01TWG082	371096	5609905	1976	01TWG138	375838	5601723
1921	01TWG083	370731	5610412	1977	01TWG139	375812	5601433
1922	01TWG084	367033	5605245	1978	01TWG140	375790	5601305
1923	01TWG085	366487	5604571	1979	01TWG141	375888	5600281
1924	01TWG086	436909	5649955	1980	01TWG142	375862	5599885
1925	01TWG087	374114	5608429	1981	01TWG143	375640	5598300
1926	01TWG088	375128	5609177	1982	01TWG144	375695	5597646
1927	01TWG089	374693	5609530	1983	01TWG145	375783	5596970
1928	01TWG090	375489	5611440	1984	01TWG146	375923	5596250
1929	01TWG091	375017	5611373	1985	01TWG147	376021	5595847
1930	01TWG092	375020	5611620	1986	01TWG148	375961	5595367
1931	01TWG093	375108	5612648	1987	01TWG149	375964	5594558
1932	01TWG094	375303	5613002	1988	01TWG150	375971	5593882
1933	01TWG095	375786	5612294	1989	01TWG151	375515	5591364
1934	01TWG096	375063	5614610	1990	01TWG152	340062	5555916
1935	01TWG097	374926	5614160	1991	01TWG153	339517	5555278
1936	01TWG098	373795	5614452	1992	01TWG154	338453	5556049
1937	01TWG099	373466	5614212	1993	01TWG155	336265	5556312
1938	01TWG100	374928	5614857	1994	01TWG156	332437	5551851
1939	01TWG101	375119	5615998	1995	01TWG157	351378	5581646
1940	01TWG102	373982	5620581	1996	01TWG158	350878	5582170
1941	01TWG103	372252	5620278	1997	01TWG159	350902	5582393
1942	01TWG104	372188	5620529	1998	01TWG160	351072	5582500
1943	01TWG105	372147	5620872	1999	01TWG161	351096	5582373
1944	01TWG106	371955	5621018	2000	01TWG162	351197	5582700
1945	01TWG107	370048	5625372	2001	01TWG163	351083	5583135
1946	01TWG108	370295	5624033	2002	01TWG164	350734	5583572
1947	01TWG109	375468	5621848	2003	01TWG165	350574	5583677
1948	01TWG110	376367	5622285	2004	01TWG166	349994	5583371

Number	Station[1,2]	Easting[3]	Northing[3]	Number	Station[1,2]	Easting[3]	Northing[3]
2005	01TWG167	349997	5583316	2061	98TWG0046a	334836	5559319
2006	01TWG168	349902	5583235	2062	98TWG0046b	334505	5558980
2007	01TWG169	349828	5582711	2063	98TWG0047	334249	5558862
2008	01TWG170	349645	5581458	2064	98TWG0048	334072	5558878
2009	01TWG171	350233	5580532	2065	98TWG0049	333826	5558305
2010	01TWG172	347948	5588761	2066	98TWG0050	333667	5558111
2011	01TWG173	348252	5588311	2067	98TWG0051	333264	5557762
2012	01TWG175	348560	5587529	2068	98TWG0052	332937	5557384
2013	01TWG178	349260	5587241	2069	98TWG0053	332626	5557444
2014	01TWG179	349258	5587929	2070	98TWG0054	332341	5556759
2015	01TWG180	349258	5587929	2071	98TWG0055	331579	5554532
2016	01TWG181	350724	5583564	2072	98TWG0056	342350	5563340
2017	98TWG0001	339657	5563689	2073	98TWG0057	342580	5563763
2018	98TWG0002	339292	5563456	2074	98TWG0058	342250	5563360
2019	98TWG0003	343362	5564229	2075	98TWG0059	342157	5563345
2020	98TWG0005	342349	5563844	2076	98TWG0060	342230	5563197
2021	98TWG0006	341940	5563570	2077	98TWG0061	342499	5562981
2022	98TWG0008	341433	5563897	2078	98TWG0062	342526	5562949
2023	98TWG0009	341535	5563478	2079	98TWG0063	342259	5562915
2024	98TWG0010	341427	5563337	2080	98TWG0064	342539	5562825
2025	98TWG0011	341232	5563407	2081	98TWG0065	342783	5562799
2026	98TWG0012	336622	5563479	2082	98TWG0066	342768	5562287
2027	98TWG0013	336617	5563515	2083	98TWG0067	342315	5562139
2028	98TWG0014	336362	5563465	2084	98TWG0068	342067	5562435
2029	98TWG0015	336319	5563421	2085	98TWG0069	341923	5563081
2030	98TWG0016	336423	5563465	2086	98TWG0070	340441	5579815
2031	98TWG0017	337454	5564199	2087	98TWG0071a	340564	5580067
2032	98TWG0018	337617	5564249	2088	98TWG0071b	340698	5580081
2033	98TWG0019	337906	5564644	2089	98TWG0072	341072	5580273
2034	98TWG0020	338731	5564830	2090	98TWG0073	341292	5580222
2035	98TWG0021	338697	5564840	2091	98TWG0074	341317	5580422
2036	98TWG0022	339007	5564806	2092	98TWG0075	341485	5580882
2037	98TWG0023	340005	5564834	2093	98TWG0076	341565	5580890
2038	98TWG0024	339612	5564409	2094	98TWG0077	341768	5581215
2039	98TWG0025	339601	5563894	2095	98TWG0078	341881	5581623
2040	98TWG0026	338287	5562273	2096	98TWG0079	341900	5581623
2041	98TWG0027	337224	5563351	2097	98TWG0080	331621	5538728
2042	98TWG0028	335888	5561380	2098	98TWG0082	333277	5535388
2043	98TWG0029	340089	5561983	2099	98TWG0083	328451	5550948
2044	98TWG0030	340766	5561490	2100	98TWG0084	334244	5558102
2045	98TWG0031	340616	5561035	2101	98TWG0085	334373	5558168
2046	98TWG0032	336347	5561172	2102	98TWG0086	334613	5557985
2047	98TWG0033	335951	5560679	2103	98TWG0087	334841	5557916
2048	98TWG0034	337716	5561749	2104	98TWG0088	334916	5557730
2049	98TWG0035	337711	5561501	2105	98TWG0089	334962	5557775
2050	98TWG0036	337614	5561283	2106	98TWG0090	335030	5557583
2051	98TWG0037	337426	5561288	2107	98TWG0091	340072	5562544
2052	98TWG0038	337240	5561226	2108	98TWG0092	340020	5562009
2053	98TWG0039	336997	5560859	2109	98TWG0094	339133	5560960
2054	98TWG0040	336580	5560450	2110	98TWG0095	338614	5560685
2055	98TWG0041	336097	5560319	2111	98TWG0096	338379	5560337
2056	98TWG0042	335937	5560204	2112	98TWG0097	338816	5559685
2057	98TWG0043	335818	5560198	2113	98TWG0098	338519	5559604
2058	98TWG0044a	336062	5560519	2114	98TWG0099	338308	5559153
2059	98TWG0044b	335736	5560160	2115	98TWG0100	338961	5561912
2060	98TWG0045	335288	5559686	2116	98TWG0101	332512	5551868

Number	Station[1,2]	Easting[3]	Northing[3]	Number	Station[1,2]	Easting[3]	Northing[3]
2117	98TWG0102	334060	5553376	2173	98TWG0168	338605	5564817
2118	98TWG0103	334125	5553784	2174	98TWG0169	340818	5564780
2119	98TWG0104	336334	5556361	2175	98TWG0170	331171	5550157
2120	98TWG0105	336283	5556600	2176	98TWG0171	331873	5552550
2121	98TWG0106	336592	5556670	2177	98TWG0172	331873	5552500
2122	98TWG0107	337244	5557694	2178	98TWG0173	332056	5551785
2123	98TWG0108	337010	5557839	2179	98TWG0174	332132	5551650
2124	98TWG0109	336266	5556303	2180	98TWG0175	333002	5552942
2125	98TWG0110	336130	5556265	2181	98TWG0176	333528	5553315
2126	98TWG0111	335983	5555750	2182	98TWG0177	333561	5553464
2127	98TWG0112	336350	5555735	2183	98TWG0178	333642	5553002
2128	98TWG0113	337884	5557957	2184	98TWG0179	334438	5552617
2129	98TWG0114	336021	5556737	2185	98TWG0180	334725	5553402
2130	98TWG0115	335688	5556928	2186	98TWG0181	335265	5554222
2131	98TWG0116	335441	5557152	2187	98TWG0182	335265	5554175
2132	98TWG0117	335390	5557152	2188	98TWG0183	336317	5553819
2133	98TWG0118	335394	5557400	2189	98TWG0184	336691	5553796
2134	98TWG0119	335290	5557476	2190	98TWG0185	337012	5553852
2135	98TWG0120	335249	5557557	2191	98TWG0186	336117	5553956
2136	98TWG0121	335505	5557860	2192	98TWG0187	336265	5554297
2137	98TWG0122	335406	5557800	2193	98TWG0188	334080	5553353
2138	98TWG0123	335695	5557933	2194	98TWG0189	333996	5553452
2139	98TWG0124	335760	5557880	2195	98TWG0190	334064	5553236
2140	98TWG0125	335696	5557709	2196	98TWG0191	334205	5553281
2141	98TWG0126	335797	5557418	2197	98TWG0192	334528	5553503
2142	98TWG0127	335856	5557207	2198	98TWG0193	334776	5553397
2143	98TWG0128	335965	5557149	2199	98TWG0194	334781	5553431
2144	98TWG0129	336953	5557873	2200	98TWG0195	335118	5553513
2145	98TWG0130	336332	5557930	2201	98TWG0196	335342	5553413
2146	98TWG0131	336268	5558318	2202	98TWG0197	335484	5553481
2147	98TWG0132	336207	5558860	2203	98TWG0198	335963	5553425
2148	98TWG0133	336402	5558784	2204	98TWG0199	336015	5553635
2149	98TWG0134	336652	5558698	2205	98TWG0200	335084	5553945
2150	98TWG0135	336798	5558657	2206	98TWG0201	334913	5553906
2151	98TWG0136	336859	5558515	2207	98TWG0202	334860	5553837
2152	98TWG0137	337087	5558297	2208	98TWG0203	334863	5553787
2153	98TWG0138	337328	5558204	2209	98TWG0204	334364	5553580
2154	98TWG0139	339052	5558272	2210	98TWG0205	334383	5553446
2155	98TWG0140	338785	5559185	2211	98TWG0206	334353	5553422
2156	98TWG0150	339380	5558077	2212	98TWG0207	334425	5553237
2157	98TWG0151	339406	5558236	2213	98TWG0208	334325	5553569
2158	98TWG0152	339551	5557937	2214	98TWG0209	334197	5553504
2159	98TWG0154	340697	5564347	2215	98TWG0210	334180	5553450
2160	98TWG0155	340589	5564292	2216	98TWG0211	334158	5553308
2161	98TWG0156	340403	5564485	2217	98TWG0212	334282	5553400
2162	98TWG0157	340587	5564353	2218	98TWG0213	334034	5553217
2163	98TWG0158	340388	5564347	2219	98TWG0214	334045	5553159
2164	98TWG0159	340164	5564293	2220	98TWG0215	334125	5553784
2165	98TWG0160	339182	5564262	2221	98TWG0216	333947	5553605
2166	98TWG0161	338959	5564224	2222	98TWG0217	333869	5553411
2167	98TWG0162	338830	5564114	2223	98TWG0218	333789	5553263
2168	98TWG0163	338395	5563929	2224	98TWG0219	334025	5553730
2169	98TWG0164	338256	5563534	2225	98TWG0220	350172	5581087
2170	98TWG0165	337949	5563477	2226	98TWG0222	335696	5556098
2171	98TWG0166	337691	5563696	2227	98TWG0223	335525	5556247
2172	98TWG0167	337753	5564307	2228	98TWG0224	335162	5556271

Number	Station[1,2]	Easting[3]	Northing[3]	Number	Station[1,2]	Easting[3]	Northing[3]
2229	98TWG0225	334805	5557065	2285	98TWG0278	335420	5555610
2230	98TWG0226	334813	5556903	2286	98TWG0279	335216	5555808
2231	98TWG0227	334645	5556909	2287	98TWG0280	334999	5555724
2232	98TWG0228	334369	5556978	2288	98TWG0281	334886	5555670
2233	98TWG0229	334314	5556737	2289	98TWG0282	334760	5555873
2234	98TWG0230	334366	5556480	2290	98TWG0283	334560	5555923
2235	98TWG0231	334545	5556274	2291	98TWG0284	334193	5555733
2236	98TWG0232	334788	5556194	2292	98TWG0285	334195	5555943
2237	98TWG0233	334847	5556158	2293	98TWG0286	333922	5555809
2238	98TWG0234a	334900	5556158	2294	98TWG0287	333621	5555726
2239	98TWG0234b	335164	5556038	2295	98TWG0288	333351	5555731
2240	98TWG0234c	339306	5557272	2296	98TWG0289	333184	5555430
2241	98TWG0235	339157	5557089	2297	98TWG0290	333387	5555261
2242	98TWG0236	338868	5556900	2298	98TWG0291	333697	5555241
2243	98TWG0237	338432	5556169	2299	98TWG0292	333816	5555325
2244	98TWG0238	338943	5556162	2300	98TWG0293	334059	5555170
2245	98TWG0239	338841	5555763	2301	98TWG0294	334363	5555316
2246	98TWG0240	339096	5555434	2302	98TWG0295	334809	5555060
2247	98TWG0241	339117	5555463	2303	98TWG0296	332429	5552714
2248	98TWG0242	338036	5556269	2304	98TWG0297	332450	5552740
2249	98TWG0243	337938	5556230	2305	98TWG0298	332698	5553068
2250	98TWG0244	337559	5556065	2306	98TWG0299	333280	5554140
2251	98TWG0245	337571	5555061	2307	98TWG0300	333205	5554116
2252	98TWG0246	339037	5557131	2308	98TWG0301	333520	5554140
2253	98TWG0247	337498	5556741	2309	98TWG0302	333700	5554160
2254	98TWG0248	336657	5555947	2310	98TWG0303	333840	5554150
2255	98TWG0249	335776	5555039	2311	98TWG0304	333920	5554160
2256	98TWG0250	336791	5560625	2312	98TWG0305	334000	5554160
2257	98TWG0251	336895	5560407	2313	98TWG0306	334638	5554159
2258	98TWG0252	336925	5560430	2314	98TWG0307	333983	5553001
2259	98TWG0253	337276	5559982	2315	98TWG0308	333546	5552872
2260	98TWG0254	337466	5559922	2316	98TWG0309	333076	5552650
2261	98TWG0255	337380	5560420	2317	98TWG0310	333008	5552919
2262	98TWG0256	337423	5560631	2318	98TWG0311	332153	5551699
2263	98TWG0257	339120	5558182	2319	98TWG0312	334045	5553159
2264	98TWG0258	338558	5558722	2320	98TWG0313	334725	5553402
2265	98TWG0259	338519	5557911	2321	98TWG0314	334801	5553458
2266	98TWG0260	338363	5557915	2322	98TWG0315	334837	5553661
2267	98TWG0261	337628	5557982	2323	98TWG0316	335140	5553720
2268	98TWG0262	337628	5558200	2324	98TWG0317	335302	5553835
2269	98TWG0263	338317	5559111	2325	98TWG0318	335320	5553790
2270	98TWG0264	337933	5556248	2326	98TWG0319	335250	5553750
2271	98TWG0265	337802	5556042	2327	98TWG0320	335414	5553588
2272	98TWG0266	337741	5555940	2328	98TWG0321	335585	5553441
2273	98TWG0267	337619	5555824	2329	98TWG0322a	335802	5553178
2274	98TWG0268a	337772	5555797	2330	98TWG0322b	335675	5552851
2275	98TWG0268b	338082	5555689	2331	98TWG0323	335366	5552425
2276	98TWG0269	338254	5555813	2332	98TWG0324	335295	5552617
2277	98TWG0270	338407	5556073	2333	98TWG0325	335187	5552566
2278	98TWG0271	338146	5556480	2334	98TWG0326	335051	5552832
2279	98TWG0272	338040	5556164	2335	98TWG0327	334800	5552910
2280	98TWG0273	340106	5557456	2336	98TWG0328	334777	5552962
2281	98TWG0274	340659	5557474	2337	98TWG0329	333610	5553235
2282	98TWG0275	342091	5559227	2338	98TWG0330	333641	5553193
2283	98TWG0276	342198	5560651	2339	98TWG0331	329442	5555640
2284	98TWG0277	335576	5555441	2340	98TWG0332	330037	5557375

Number	Station[1,2]	Easting[3]	Northing[3]	Number	Station[1,2]	Easting[3]	Northing[3]
2341	98TWG0333	330404	5557908	2397	98TWG0411	337236	5557063
2342	98TWG0334	331186	5560301	2398	98TWG0412	336648	5557282
2343	98TWG0336	337020	5553829	2399	98TWG0413	337309	5557681
2344	98TWG0337	336787	5553879	2400	98TWG0414	339360	5559072
2345	98TWG0338	336627	5553792	2401	98TWG0415	339640	5559053
2346	98TWG0339	336497	5553673	2402	98TWG0416	339848	5559137
2347	98TWG0340	336517	5554287	2403	98TWG0417	339902	5559055
2348	98TWG0341	336488	5554405	2404	98TWG0418	339887	5558943
2349	98TWG0342	337122	5554873	2405	98TWG0419	340417	5559470
2350	98TWG0343	336449	5554895	2406	98TWG0420	340732	5559407
2351	98TWG0344	336316	5554907	2407	98TWG0421	340771	5559384
2352	98TWG0345	336131	5554969	2408	98TWG0422	340919	5559299
2353	98TWG0346	335969	5554605	2409	98TWG0423	341145	5559424
2354	98TWG0347	335794	5554532	2410	98TWG0424	341388	5559140
2355	98TWG0348	335587	5554240	2411	98TWG0425	341254	5558901
2356	98TWG0349	335864	5554211	2412	98TWG0426	341003	5558770
2357	98TWG0350	335449	5554189	2413	98TWG0427	340898	5558801
2358	98TWG0351	335071	5554300	2414	98TWG0428	340710	5558804
2359	98TWG0352	335094	5554453	2415	98TWG0429	340574	5558709
2360	98TWG0353	335165	5554690	2416	98TWG0430	340318	5558331
2361	98TWG0354	335075	5554864	2417	98TWG0431	340147	5558313
2362	98TWG0355	335405	5554899	2418	98TWG0432	339801	5558700
2363	98TWG0356	335339	5555129	2419	98TWG0433	339711	5558774
2364	98TWG0357	340878	5564572	2420	98TWG0434	339520	5558714
2365	98TWG0358	336088	5555680	2421	98TWG0435	340561	5557624
2366	98TWG0359	336265	5555753	2422	98TWG0436	340514	5557569
2367	98TWG0360	335959	5555973	2423	98TWG0437	340295	5557656
2368	98TWG0361	336140	5556248	2424	98TWG0438	338615	5555352
2369	98TWG0362	336220	5556330	2425	98TWG0439	338660	5554841
2370	98TWG0363	336353	5556262	2426	98TWG0440	341042	5557580
2371	98TWG0364	336471	5556097	2427	98TWG0441	340755	5556510
2372	98TWG0365	336742	5556205	2428	98TWG0442	340042	5555785
2373	98TWG0366	336821	5556048	2429	98TWG0443	339537	5555310
2374	98TWG0367	336864	5555933	2430	98TWG0444	340724	5555961
2375	98TWG0368	336806	5556176	2431	98TWG0445	339961	5554741
2376	98TWG0369	336882	5556287	2432	98TWG0446	339491	5554537
2377	98TWG0370	337036	5556586	2433	98TWG0447	337546	5552460
2378	98TWG0371	336939	5556566	2434	98TWG0448	341261	5558387
2379	98TWG0372	336820	5556982	2435	98TWG0449	341137	5558591
2380	98TWG0373	336772	5557076	2436	98TWG0450	341109	5558799
2381	98TWG0396a	336882	5553480	2437	98TWG0451	341209	5558678
2382	98TWG0396b	336762	5553058	2438	98TWG0452	341307	5558633
2383	98TWG0397	337290	5552807	2439	98TWG0453	341349	5558595
2384	98TWG0398	337925	5553074	2440	98TWG0455	341653	5558706
2385	98TWG0399	338189	5553681	2441	98TWG0456	341601	5558542
2386	98TWG0400	338040	5553722	2442	98TWG0457	341754	5558866
2387	98TWG0401	338654	5553801	2443	98TWG0458	341972	5558549
2388	98TWG0402	338616	5554038	2444	98TWG0459	341997	5558619
2389	98TWG0403	338612	5554135	2445	98TWG0460	342193	5558505
2390	98TWG0404	338138	5554045	2446	98TWG0461	342271	5558952
2391	98TWG0405	337596	5553850	2447	98TWG0462	342304	5559292
2392	98TWG0406	337073	5553962	2448	98TWG0463	342181	5559139
2393	98TWG0407	335964	5561473	2449	98TWG0464	342572	5559550
2394	98TWG0408	332238	5557881	2450	98TWG0465	342487	5559501
2395	98TWG0409	337561	5556973	2451	98TWG0466	342536	5559646
2396	98TWG0410	337284	5556998	2452	98TWG0467	342646	5560039

Number	Station[1,2]	Easting[3]	Northing[3]	Number	Station[1,2]	Easting[3]	Northing[3]
2453	98TWG0468	342991	5560108	2509	98TWG0524	342723	5553768
2454	98TWG0469	337741	5545044	2510	98TWG0525	342987	5554100
2455	98TWG0470	341689	5559680	2511	98TWG0526	343220	5552816
2456	98TWG0471	341071	5559931	2512	98TWG0527	333144	5553220
2457	98TWG0472	340825	5560304	2513	98TWG0528	333096	5553300
2458	98TWG0473	341073	5560416	2514	98TWG0529	333126	5553656
2459	98TWG0474	341342	5560481	2515	98TWG0530	332864	5554132
2460	98TWG0475	341560	5560544	2516	98TWG0531	332669	5554243
2461	98TWG0476	341752	5560707	2517	98TWG0532	332590	5554352
2462	98TWG0477	342024	5561047	2518	98TWG0533	332353	5554436
2463	98TWG0478	342356	5561407	2519	98TWG0534	332129	5554477
2464	98TWG0479	342433	5561647	2520	98TWG0535	332086	5554247
2465	98TWG0480	338684	5548556	2521	98TWG0536	332383	5553422
2466	98TWG0481	337895	5548402	2522	99TWG0001	328745	5545572
2467	98TWG0482	334116	5549969	2523	99TWG0002	328745	5545472
2468	98TWG0483	341069	5556003	2524	99TWG0003	328701	5544665
2469	98TWG0484	341473	5555975	2525	99TWG0004	328898	5544630
2470	98TWG0485	341582	5555560	2526	99TWG0005	329218	5544604
2471	98TWG0486	341589	5555254	2527	99TWG0006	329322	5544792
2472	98TWG0487	341554	5555095	2528	99TWG0007	329986	5544311
2473	98TWG0488	341386	5554851	2529	99TWG0008	330089	5545001
2474	98TWG0489	341723	5555420	2530	99TWG0009	331978	5551055
2475	98TWG0490	342072	5555479	2531	99TWG0010	331580	5550690
2476	98TWG0491	342092	5555125	2532	99TWG0011	331581	5550707
2477	98TWG0492	342042	5554556	2533	99TWG0012	331401	5549867
2478	98TWG0493	341643	5556093	2534	99TWG0013	331311	5549890
2479	98TWG0494	341962	5556264	2535	99TWG0014	331275	5549890
2480	98TWG0495	342194	5556356	2536	99TWG0015	330928	5549695
2481	98TWG0496	342680	5556363	2537	99TWG0016	331020	5549482
2482	98TWG0497	343037	5556497	2538	99TWG0017	331020	5549432
2483	98TWG0498	343365	5556460	2539	99TWG0018	330792	5549400
2484	98TWG0499	343949	5556820	2540	99TWG0019	330882	5549241
2485	98TWG0500	344106	5557054	2541	99TWG0020	330932	5549241
2486	98TWG0501	344088	5557350	2542	99TWG0021	331057	5548862
2487	98TWG0502	343969	5557467	2543	99TWG0022	331227	5549239
2488	98TWG0503	343817	5557689	2544	99TWG0023	331300	5549150
2489	98TWG0504	343439	5557541	2545	99TWG0024	331323	5548500
2490	98TWG0505	342984	5557398	2546	99TWG0025	331253	5548755
2491	98TWG0506	342726	5557332	2547	99TWG0026	331494	5549388
2492	98TWG0507	342392	5557334	2548	99TWG0027	331775	5549413
2493	98TWG0508	341732	5556951	2549	99TWG0028	331777	5549388
2494	98TWG0509	342569	5552391	2550	99TWG0029	333306	5549966
2495	98TWG0510	341970	5552176	2551	99TWG0030	331026	5550604
2496	98TWG0511	341145	5551745	2552	99TWG0031	329102	5547057
2497	98TWG0512	340912	5552369	2553	99TWG0032	329474	5546845
2498	98TWG0513	340898	5552576	2554	99TWG0033	329473	5546829
2499	98TWG0514	340898	5552565	2555	99TWG0034	330920	5546327
2500	98TWG0515	342982	5552297	2556	99TWG0035	331208	5546786
2501	98TWG0516	340203	5553582	2557	99TWG0036	331514	5546746
2502	98TWG0517	340715	5553465	2558	99TWG0037	331534	5546752
2503	98TWG0518	340921	5553397	2559	99TWG0038	332840	5546123
2504	98TWG0519	341161	5553377	2560	99TWG0039	333709	5546087
2505	98TWG0520	341351	5553369	2561	99TWG0040	334262	5543376
2506	98TWG0521	341608	5553444	2562	99TWG0041	333048	5542821
2507	98TWG0522	341809	5553413	2563	99TWG0042	332603	5542734
2508	98TWG0523	342535	5553396	2564	99TWG0043	332475	5542717

Number	Station[1,2]	Easting[3]	Northing[3]	Number	Station[1,2]	Easting[3]	Northing[3]
2565	99TWG0044	332200	5542745	2621	99TWG0099	325589	5549743
2566	99TWG0045	329171	5547758	2622	99TWG0100	325423	5550786
2567	99TWG0046	328888	5547686	2623	99TWG0101	325277	5551282
2568	99TWG0047	328952	5547796	2624	99TWG0102	324589	5551794
2569	99TWG0048	329145	5548470	2625	99TWG0103	324998	5552764
2570	99TWG0049	329141	5548865	2626	99TWG0104	330225	5541592
2571	99TWG0050	329424	5549355	2627	99TWG0105	330432	5541572
2572	99TWG0051	329531	5549768	2628	99TWG0106	330842	5541767
2573	99TWG0052	329632	5548390	2629	99TWG0107	331191	5541770
2574	99TWG0053	328829	5547031	2630	99TWG0108	331346	5541620
2575	99TWG0054	338752	5546838	2631	99TWG0109	331616	5541676
2576	99TWG0055	338441	5547220	2632	99TWG0110	332004	5541913
2577	99TWG0056	337459	5548061	2633	99TWG0111	332431	5541763
2578	99TWG0057	337461	5548048	2634	99TWG0112	332633	5541694
2579	99TWG0058	336697	5547049	2635	99TWG0113	333361	5541941
2580	99TWG0059	336531	5546437	2636	99TWG0114	333651	5542225
2581	99TWG0060	335545	5549080	2637	99TWG0115	334152	5542435
2582	99TWG0061	335857	5551225	2638	99TWG0116	332669	5542658
2583	99TWG0062	338686	5551310	2639	99TWG0117	332122	5542448
2584	99TWG0063	337080	5550873	2640	99TWG0118	331977	5542313
2585	99TWG0064	337027	5551120	2641	99TWG0119	331469	5542127
2586	99TWG0065	334253	5547600	2642	99TWG0120	331046	5542225
2587	99TWG0066	334925	5549603	2643	99TWG0121	330633	5538862
2588	99TWG0067	335960	5549975	2644	99TWG0122	330677	5539080
2589	99TWG0068a	336507	5550573	2645	99TWG0123	331329	5538182
2590	99TWG0068b	337203	5548612	2646	99TWG0124	331449	5538963
2591	99TWG0069	337309	5549507	2647	99TWG0125	331312	5539282
2592	99TWG0070	337822	5550138	2648	99TWG0126	331420	5539579
2593	99TWG0071	338930	5550452	2649	99TWG0127	331835	5539940
2594	99TWG0072	339045	5550146	2650	99TWG0128	332317	5540128
2595	99TWG0073	339250	5549359	2651	99TWG0129	332759	5541458
2596	99TWG0074	338723	5549351	2652	99TWG0130	333981	5542974
2597	99TWG0075	337783	5547626	2653	99TWG0131	334242	5541830
2598	99TWG0076	338242	5548351	2654	99TWG0132	333225	5540799
2599	99TWG0077	339113	5548473	2655	99TWG0133	333732	5540828
2600	99TWG0078	336115	5544892	2656	99TWG0134a	334584	5541168
2601	99TWG0079	337286	5545465	2657	99TWG0134b	334385	5541208
2602	99TWG0080	337943	5546925	2658	99TWG0135	336580	5541243
2603	99TWG0081	338758	5547216	2659	99TWG0136	338889	5544357
2604	99TWG0082	338838	5547286	2660	99TWG0137	332458	5537337
2605	99TWG0083	327377	5546933	2661	99TWG0138	332460	5537678
2606	99TWG0084	327341	5547048	2662	99TWG0139	332490	5538525
2607	99TWG0085	327641	5547805	2663	99TWG0140	332298	5538980
2608	99TWG0086	327662	5548363	2664	99TWG0141	332670	5538157
2609	99TWG0087	327659	5548492	2665	99TWG0142	332715	5538919
2610	99TWG0088	327651	5548619	2666	99TWG0143	332833	5537089
2611	99TWG0089	327847	5549359	2667	99TWG0144	333173	5536671
2612	99TWG0090	328083	5549722	2668	99TWG0145	333420	5535876
2613	99TWG0091	328199	5550011	2669	99TWG0146	333320	5535067
2614	99TWG0092	328318	5550241	2670	99TWG0147	332142	5537149
2615	99TWG0093	328427	5550723	2671	99TWG0148	333518	5525636
2616	99TWG0094	328677	5552072	2672	99TWG0149	339093	5527979
2617	99TWG0095	328536	5551706	2673	99TWG0150	338115	5530364
2618	99TWG0096	325277	5549352	2674	99TWG0151	338932	5533376
2619	99TWG0097	325128	5550207	2675	99TWG0152	338726	5534541
2620	99TWG0098	325429	5550251	2676	99TWG0153	338434	5534661

Number	Station[1,2]	Easting[3]	Northing[3]	Number	Station[1,2]	Easting[3]	Northing[3]
2677	99TWG0154	338613	5537706	2733	99TWG0210	345678	5553619
2678	99TWG0155	338600	5538314	2734	99TWG0211	345722	5553974
2679	99TWG0156	338998	5538772	2735	99TWG0212	345637	5554121
2680	99TWG0157	338966	5537520	2736	99TWG0213	345462	5554373
2681	99TWG0158	338946	5537520	2737	99TWG0214	345093	5554273
2682	99TWG0159	340008	5546970	2738	99TWG0215a	344929	5554204
2683	99TWG0160	340433	5548054	2739	99TWG0215b	345005	5554516
2684	99TWG0161	339864	5549523	2740	99TWG0216	346083	5552930
2685	99TWG0162	340050	5549735	2741	99TWG0217	346783	5551994
2686	99TWG0163	339917	5549934	2742	99TWG0218	347567	5552730
2687	99TWG0164	340167	5550126	2743	99TWG0219	348116	5552889
2688	99TWG0165	341102	5550220	2744	99TWG0220	348402	5552706
2689	99TWG0166	341160	5549964	2745	99TWG0221	349124	5553160
2690	99TWG0167	341753	5549333	2746	99TWG0222	349250	5553940
2691	99TWG0168	342149	5549780	2747	99TWG0223	349684	5554191
2692	99TWG0169	342628	5549128	2748	99TWG0224	349583	5554800
2693	99TWG0170	342678	5549128	2749	99TWG0225	349997	5555471
2694	99TWG0171	343109	5549232	2750	99TWG0226	350472	5555984
2695	99TWG0172	342574	5549625	2751	99TWG0227	351833	5556921
2696	99TWG0173	342671	5550188	2752	99TWG0228	351972	5557861
2697	99TWG0174	341915	5549840	2753	99TWG0229	352474	5558666
2698	99TWG0175	343181	5550643	2754	99TWG0230	352273	5558920
2699	99TWG0176	343191	5550796	2755	99TWG0231	352578	5560225
2700	99TWG0177	343135	5551041	2756	99TWG0232	352199	5562245
2701	99TWG0178	343100	5551071	2757	99TWG0233	354263	5561933
2702	99TWG0179	342666	5550960	2758	99TWG0234	354186	5561617
2703	99TWG0180	342336	5550734	2759	99TWG0235	331456	5543638
2704	99TWG0181	342289	5551005	2760	99TWG0236	331240	5543130
2705	99TWG0182	342410	5551141	2761	99TWG0237	331420	5543000
2706	99TWG0183	342769	5551350	2762	99TWG0242a	344864	5562190
2707	99TWG0184	342664	5551727	2763	99TWG0242b	344654	5562042
2708	99TWG0185	343093	5552124	2764	99TWG0243	344016	5561153
2709	99TWG0186	342624	5552173	2765	99TWG0244	344016	5560964
2710	99TWG0187	342088	5551995	2766	99TWG0245	343839	5560477
2711	99TWG0188	341631	5551624	2767	99TWG0246	342709	5559296
2712	99TWG0189	341535	5551364	2768	99TWG0247	344516	5560580
2713	99TWG0190	341558	5550834	2769	99TWG0248	346302	5560374
2714	99TWG0191	341392	5551062	2770	99TWG0249	345917	5559560
2715	99TWG0192	346725	5552265	2771	99TWG0250	347817	5559911
2716	99TWG0193	341300	5551520	2772	99TWG0251	347831	5561548
2717	99TWG0194	341123	5551725	2773	99TWG0252	345196	5562689
2718	99TWG0195	340987	5551958	2774	99TWG0253	343590	5558623
2719	99TWG0196	340988	5552124	2775	99TWG0254	342926	5558681
2720	99TWG0197	341935	5552091	2776	99TWG0255	343229	5558198
2721	99TWG0198	342729	5553238	2777	99TWG0256	343382	5557895
2722	99TWG0199	342871	5553512	2778	99TWG0257	343827	5557777
2723	99TWG0200	343092	5553882	2779	99TWG0258	343927	5557814
2724	99TWG0201	344316	5552042	2780	99TWG0259	344110	5558224
2725	99TWG0202	344341	5552298	2781	99TWG0260	344098	5558429
2726	99TWG0203	344100	5552331	2782	99TWG0261	344163	5558582
2727	99TWG0204	344543	5552196	2783	99TWG0262	344133	5558753
2728	99TWG0205	344473	5553359	2784	99TWG0263	344272	5559303
2729	99TWG0206	345194	5553585	2785	99TWG0264	344341	5559780
2730	99TWG0207	345026	5553646	2786	99TWG0265	344387	5560299
2731	99TWG0208	344833	5554168	2787	99TWG0266	344496	5560312
2732	99TWG0209	345603	5553474	2788	99TWG0267	344449	5560558

Number	Station[1,2]	Easting[3]	Northing[3]	Number	Station[1,2]	Easting[3]	Northing[3]
2789	99TWG0268	345470	5558493	2845	99TWG0324	348882	5556451
2790	99TWG0269	344320	5558173	2846	99TWG0325	349242	5556392
2791	99TWG0270	344832	5558422	2847	99TWG0326	349836	5556550
2792	99TWG0271	347242	5558183	2848	99TWG0327	349696	5556487
2793	99TWG0272	347132	5555931	2849	99TWG0328	350602	5557482
2794	99TWG0273	346817	5556224	2850	99TWG0329	351831	5557807
2795	99TWG0274	347037	5556611	2851	99TWG0330	351827	5558224
2796	99TWG0275	346920	5556942	2852	99TWG0331	351636	5558842
2797	99TWG0276	346760	5557300	2853	99TWG0332	352828	5560278
2798	99TWG0277	346509	5556925	2854	99TWG0333	352265	5559866
2799	99TWG0278	346226	5556697	2855	99TWG0334	352591	5560363
2800	99TWG0279	346573	5556090	2856	99TWG0335	352488	5560604
2801	99TWG0280	346045	5556546	2857	99TWG0336	351360	5562329
2802	99TWG0281	345777	5556492	2858	99TWG0337	351408	5562115
2803	99TWG0282	345475	5556570	2859	99TWG0338	349981	5564528
2804	99TWG0283	345306	5556382	2860	99TWG0339	349517	5563686
2805	99TWG0284	344888	5556414	2861	99TWG0340	349768	5563407
2806	99TWG0285	344887	5556883	2862	99TWG0341	349535	5562145
2807	99TWG0286	344594	5556747	2863	99TWG0342	349917	5561853
2808	99TWG0287	344939	5557082	2864	99TWG0343	350134	5562037
2809	99TWG0288	343474	5557333	2865	99TWG0344	350370	5562000
2810	99TWG0289	343542	5557137	2866	99TWG0345	350505	5562150
2811	99TWG0290	343651	5556826	2867	99TWG0346	350596	5562333
2812	99TWG0291	343392	5556163	2868	99TWG0347	350953	5562823
2813	99TWG0292	343275	5555747	2869	99TWG0348	351091	5563024
2814	99TWG0293	343280	5555439	2870	99TWG0349	351397	5563506
2815	99TWG0294	343455	5555573	2871	99TWG0350	351441	5563686
2816	99TWG0295	344163	5556696	2872	99TWG0351	346477	5552428
2817	99TWG0296	344943	5556301	2873	99TWG0352	346980	5553505
2818	99TWG0297	344863	5555983	2874	99TWG0353	346880	5553505
2819	99TWG0298	344864	5555727	2875	99TWG0354	346226	5553111
2820	99TWG0299	344958	5555009	2876	99TWG0355	346506	5553196
2821	99TWG0300	344512	5555777	2877	99TWG0356	345819	5551994
2822	99TWG0301	344288	5555605	2878	99TWG0357	347536	5552680
2823	99TWG0302	345468	5556202	2879	99TWG0358	347743	5552425
2824	99TWG0303	345653	5555651	2880	99TWG0359	347406	5551906
2825	99TWG0304	345869	5555202	2881	99TWG0360	347758	5552090
2826	99TWG0305	345790	5554661	2882	99TWG0361	348088	5551965
2827	99TWG0306	345581	5554307	2883	99TWG0362	345461	5551147
2828	99TWG0307	345008	5554469	2884	99TWG0363	345306	5550878
2829	99TWG0308	344550	5554640	2885	99TWG0364	345199	5549325
2830	99TWG0309	344300	5554709	2886	99TWG0365	343733	5545195
2831	99TWG0310	344144	5554332	2887	99TWG0366	342471	5543100
2832	99TWG0311	347418	5555619	2888	99TWG0367	342183	5542963
2833	99TWG0312	347014	5555230	2889	99TWG0368	342790	5542061
2834	99TWG0313	346885	5554785	2890	99TWG0369	344370	5544607
2835	99TWG0314	348329	5555985	2891	99TWG0370	344029	5543179
2836	99TWG0315	348501	5555634	2892	99TWG0371	344696	5543184
2837	99TWG0316	348749	5555959	2893	99TWG0372	345654	5546696
2838	99TWG0317	349257	5556026	2894	99TWG0373	346322	5542795
2839	99TWG0318	349722	5555201	2895	99TWG0374	348969	5542119
2840	99TWG0319	349324	5555027	2896	99TWG0375	348064	5541876
2841	99TWG0320	349328	5555426	2897	99TWG0376	347309	5541547
2842	99TWG0321	348323	5555577	2898	99TWG0377	348923	5541521
2843	99TWG0322	348221	5554999	2899	99TWG0378	349969	5541654
2844	99TWG0323	347557	5554601	2900	99TWG0379	350070	5541878

Number	Station[1,2]	Easting[3]	Northing[3]	Number	Station[1,2]	Easting[3]	Northing[3]
2901	99TWG0380	350933	5541106	2957	99TWG0435	353288	5556890
2902	99TWG0381	351376	5540587	2958	99TWG0436	353568	5557240
2903	99TWG0382	351799	5541638	2959	99TWG0437	353883	5557240
2904	99TWG0383	352960	5542150	2960	99TWG0438	354169	5557716
2905	99TWG0384	353707	5541497	2961	99TWG0439	354758	5558663
2906	99TWG0385	351841	5541985	2962	99TWG0440	354449	5558719
2907	99TWG0386	352652	5542996	2963	99TWG0441	354327	5558340
2908	99TWG0387	353278	5543071	2964	99TWG0442	353842	5557697
2909	99TWG0388	353470	5542916	2965	99TWG0443	353910	5558209
2910	99TWG0389	353615	5543179	2966	99TWG0444	353522	5557573
2911	99TWG0390	354057	5543353	2967	99TWG0445	352587	5556712
2912	99TWG0391	352060	5542753	2968	99TWG0446	355054	5559012
2913	99TWG0392	350112	5565781	2969	99TWG0447	355480	5559637
2914	99TWG0393	350826	5563417	2970	99TWG0448	355527	5560336
2915	99TWG0394	350394	5563176	2971	99TWG0449	355556	5561310
2916	99TWG0395	350187	5563132	2972	99TWG0450	355003	5564929
2917	99TWG0396	349610	5563672	2973	99TWG0451	351703	5562760
2918	99TWG0397	349090	5563950	2974	99TWG0452a	354006	5554778
2919	99TWG0398	349194	5563841	2975	99TWG0452b	357147	5562073
2920	99TWG0399	348612	5564159	2976	99TWG0453	351947	5555516
2921	99TWG0400	349057	5564585	2977	99TWG0454	352440	5554878
2922	99TWG0401	349202	5564470	2978	99TWG0455	354006	5554778
2923	99TWG0402	349509	5564672	2979	99TWG0456	353556	5555728
2924	99TWG0403	349563	5564986	2980	99TWG0457	354845	5556925
2925	99TWG0404	338537	5567751	2981	99TWG0458	355064	5557507
2926	99TWG0405	338661	5567588	2982	99TWG0459	355031	5558146
2927	99TWG0406	338989	5567422	2983	99TWG0460	355839	5556646
2928	99TWG0407	339031	5567237	2984	99TWG0461	356402	5556021
2929	99TWG0408	338919	5567330	2985	99TWG0462	356227	5556211
2930	99TWG0409	339015	5567100	2986	99TWG0463	357428	5555485
2931	99TWG0410	339404	5566837	2987	99TWG0464	356485	5556054
2932	99TWG0411	340127	5566917	2988	99TWG0465	356646	5556302
2933	99TWG0412	340082	5567152	2989	99TWG0466	355911	5556216
2934	99TWG0413	339975	5566986	2990	99TWG0467	353673	5554271
2935	99TWG0414	339922	5566543	2991	99TWG0468	354482	5555117
2936	99TWG0415	339133	5566559	2992	99TWG0469	355201	5554951
2937	99TWG0416	339874	5568125	2993	99TWG0470	355439	5553572
2938	99TWG0417	349103	5553178	2994	99TWG0471	356851	5554780
2939	99TWG0418	349338	5553249	2995	99TWG0472	351314	5561462
2940	99TWG0419	349123	5552131	2996	99TWG0473	350480	5561150
2941	99TWG0420	349355	5551816	2997	99TWG0474	350509	5561067
2942	99TWG0421	349542	5551749	2998	99TWG0475	350728	5560768
2943	99TWG0422	349138	5551061	2999	99TWG0476	351791	5560539
2944	99TWG0423	349234	5550937	3000	99TWG0477	345425	5564100
2945	99TWG0424	348939	5550748	3001	99TWG0478	345595	5564300
2946	99TWG0425	348157	5551802	3002	99TWG0479	345790	5564375
2947	99TWG0426	349982	5551222	3003	99TWG0480	346000	5564450
2948	99TWG0427a	350242	5550518	3004	99TWG0481	346180	5564190
2949	99TWG0427b	351939	5553138	3005	99TWG0482	345810	5563995
2950	99TWG0428	351193	5554042	3006	99TWG0483	345620	5564110
2951	99TWG0429	351114	5554288	3007	99TWG0484	346600	5563225
2952	99TWG0430	350879	5556094	3008	99TWG0485	345000	5562375
2953	99TWG0431	351501	5555294	3009	99TWG0486	355750	5553185
2954	99TWG0432	351884	5556903	3010	99TWG0487	355900	5553300
2955	99TWG0433	352820	5556144	3011	99TWG0488	355850	5553675
2956	99TWG0434	353164	5556568	3012	99TWG0489	356450	5553615

Number	Station[1,2]	Easting[3]	Northing[3]	Number	Station[1,2]	Easting[3]	Northing[3]
3013	99TWG0490	356180	5553150	3069	99TWG0546	344280	5562800
3014	99TWG0491	354800	5552595	3070	99TWG0547	347800	5578925
3015	99TWG0492	355600	5552600	3071	99TWG0548	346100	5579160
3016	99TWG0493	354610	5552500	3072	99TWG0549	345610	5580050
3017	99TWG0494	333240	5561400	3073	99TWG0550	346175	5579910
3018	99TWG0495	355000	5552140	3074	99TWG0551	345350	5579200
3019	99TWG0496	354500	5552400	3075	99TWG0552	344650	5579650
3020	99TWG0497	354642	5550661	3076	99TWG0553	344920	5580380
3021	99TWG0498	351550	5551600	3077	99TWG0554	344980	5580680
3022	99TWG0499	351700	5551750	3078	99TWG0555	345250	5581000
3023	99TWG0500	352100	5552100	3079	99TWG0556	346575	5582170
3024	99TWG0501	352675	5552550	3080	99TWG0557	346350	5582970
3025	99TWG0502	353550	5553300	3081	99TWG0558	345800	5582800
3026	99TWG0503	349375	5565380	3082	99TWG0559	352400	5557780
3027	99TWG0504	348801	5564647	3083	99TWG0560	352480	5558230
3028	99TWG0505	348800	5564405	3084	99TWG0561	352580	5558470
3029	99TWG0506	348390	5564350	3085	99TWG0562	352620	5558580
3030	99TWG0507	348300	5564200	3086	99TWG0563	352720	5558900
3031	99TWG0508	348175	5564150	3087	99TWG0564	352870	5559300
3032	99TWG0509	347900	5564000	3088	99TWG0565	352990	5559560
3033	99TWG0510	348003	5563673	3089	99TWG0566	353160	5560000
3034	99TWG0511	348075	5563575	3090	99TWG0567	353750	5560620
3035	99TWG0512	348120	5563450	3091	99TWG0568	353900	5561190
3036	99TWG0513	348402	5563124	3092	99TWG0569	354660	5562540
3037	99TWG0514	348505	5562997	3093	99TWG0570	373181	5570232
3038	99TWG0515	348131	5562766	3094	99TWG0571	389039	5560777
3039	99TWG0516	348128	5562421	3095	99TWG0572	390315	5547861
3040	99TWG0517	347850	5562350	3096	99TWG0573	398657	5559823
3041	99TWG0518	347725	5562600	3097	99TWG0574	403787	5562945
3042	99TWG0519	347673	5564165	3098	99TWG0575	346300	5583600
3043	99TWG0520	347800	5564330	3099	99TWG0576	346200	5584420
3044	99TWG0521	347850	5564425	3100	99TWG0577	346100	5584790
3045	99TWG0522	347125	5564500	3101	99TWG0578	346040	5585250
3046	99TWG0523	347125	5564300	3102	99TWG0579	346460	5586521
3047	99TWG0524	347125	5564200	3103	99TWG0580	346313	5586481
3048	99TWG0525	347100	5564000	3104	99TWG0581	371746	5605115
3049	99TWG0526	346600	5563100	3105	99TWG0582	372175	5604690
3050	99TWG0527	341300	5558000	3106	99TWG0583	371700	5603390
3051	99TWG0528	341300	5557775	3107	99TWG0584	372900	5603785
3052	99TWG0529	341080	5557300	3108	99TWG0585	372647	5604833
3053	99TWG0530	341370	5557050	3109	99TWG0586	374097	5604328
3054	99TWG0531	342075	5557640	3110	99TWG0587	374825	5603300
3055	99TWG0532	342650	5557990	3111	99TWG0588	375190	5603425
3056	99TWG0533	342750	5558475	3112	99TWG0589	375300	5603900
3057	99TWG0534	343133	5558710	3113	99TWG0590	375500	5603900
3058	99TWG0535	343170	5559150	3114	99TWG0591	374300	5602450
3059	99TWG0536	343225	5559500	3115	99TWG0592	374629	5601385
3060	99TWG0537	343725	5559400	3116	99TWG0593	374800	5601180
3061	99TWG0538	343950	5553870	3117	99TWG0594	374920	5600350
3062	99TWG0539	343793	5563761	3118	99TWG0595	374800	5599575
3063	99TWG0540	343474	5563448	3119	99TWG0596	374560	5601200
3064	99TWG0541	343498	5563285	3120	99TWG0597	374480	5600600
3065	99TWG0542	343229	5562771	3121	99TWG0598	374461	5599736
3066	99TWG0543	343875	5562450	3122	99TWG0599	374500	5598950
3067	99TWG0544	344030	5562400	3123	99TWG0600	370350	5603400
3068	99TWG0545	344175	5562570	3124	99TWG0601	370400	5603950

Number	Station[1,2]	Easting[3]	Northing[3]	Number	Station[1,2]	Easting[3]	Northing[3]
3125	99TWG0602	370400	5604350	3181	99TWG0658	362650	5590900
3126	99TWG0603	370300	5604800	3182	99TWG0659	362875	5590750
3127	99TWG0604	370375	5605915	3183	99TWG0660	362875	5590875
3128	99TWG0605	369430	5603475	3184	99TWG0661	362860	5591110
3129	99TWG0606	369610	5604200	3185	99TWG0662	361775	5592085
3130	99TWG0607	369380	5604500	3186	99TWG0663	361875	5592120
3131	99TWG0608	367800	5602315	3187	99TWG0664	362120	5592450
3132	99TWG0609	367500	5601990	3188	99TWG0665	362350	5593040
3133	99TWG0610	367300	5601575	3189	99TWG0666	361885	5593550
3134	99TWG0611	367175	5602250	3190	99TWG0667	362910	5591990
3135	99TWG0612	366750	5601500	3191	99TWG0668	363500	5592275
3136	99TWG0613	365700	5600700	3192	99TWG0669	363090	5592175
3137	99TWG0614	365220	5600470	3193	99TWG0670	363580	5592100
3138	99TWG0615	363610	5600050	3194	99TWG0671	363300	5593200
3139	99TWG0616	361550	5599170	3195	99TWG0672	364085	5589225
3140	99TWG0617	360585	5597910	3196	99TWG0673	363900	5589000
3141	99TWG0618	359700	5597500	3197	99TWG0674	364440	5587975
3142	99TWG0619	359170	5596100	3198	99TWG0675	365550	5588625
3143	99TWG0620	360850	5597900	3199	99TWG0676	366100	5590600
3144	99TWG0621	360420	5595625	3200	99TWG0677	366120	5591525
3145	99TWG0622	360710	5595600	3201	99TWG0678	366300	5592500
3146	99TWG0623	360710	5594970	3202	99TWG0679	366600	5592700
3147	99TWG0624	360700	5594650	3203	99TWG0680	373400	5590200
3148	99TWG0625	360700	5593390	3204	99TWG0681	373400	5591475
3149	99TWG0626	360720	5593200	3205	99TWG0682	372585	5591600
3150	99TWG0627	360700	5592770	3206	99TWG0683	372900	5589590
3151	99TWG0628	363939	5597507	3207	99TWG0684	373800	5589730
3152	99TWG0629	366160	5597700	3208	99TWG0685	374150	5590000
3153	99TWG0630	366000	5596650	3209	99TWG0686	373700	5589400
3154	99TWG0631	368570	5598350	3210	99TWG0687	369650	5590600
3155	99TWG0632	368650	5598225	3211	99TWG0688	370960	5590000
3156	99TWG0633	371320	5599120	3212	99TWG0689	371000	5589550
3157	99TWG0634	371475	5598920	3213	99TWG0690	373780	5588400
3158	99TWG0635	371175	5598700	3214	99TWG0691	357385	5590660
3159	99TWG0636	371050	5598800	3215	99TWG0692	357030	5591551
3160	99TWG0637	372050	5597265	3216	99TWG0693	357190	5591550
3161	99TWG0638	371400	5596700	3217	99TWG0694	417554	5569899
3162	99TWG0639	370750	5596300	3218	99TWG0695	416287	5570030
3163	99TWG0640	372720	5597100	3219	99TWG0696	334125	5537960
3164	99TWG0641	372750	5598475	3220	99TWG0697	334770	5538800
3165	99TWG0642	368790	5601380	3221	99TWG0698	334865	5539400
3166	99TWG0643	371100	5600385	3222	99TWG0699	335435	5539700
3167	99TWG0644	373800	5601800	3223	99TWG0700	335955	5540160
3168	99TWG0645	360800	5595600	3224	99TWG0701	336190	5540260
3169	99TWG0646	361200	5595700	3225	99TWG0702	336380	5540190
3170	99TWG0647	362020	5596275	3226	99TWG0703	335070	5539300
3171	99TWG0648	362875	5596000	3227	99TWG0704	335990	5539440
3172	99TWG0649	362675	5595900	3228	99TWG0705	336230	5539620
3173	99TWG0650	364090	5595700	3229	99TWG0706	336400	5539800
3174	99TWG0651	364980	5595775	3230	99TWG0707	336550	5540000
3175	99TWG0652	364060	5594950	3231	99TWG0708	337100	5540380
3176	99TWG0653	360875	5595900	3232	99TWG0709	336500	5539575
3177	99TWG0654	361160	5597625	3233	99TWG0710	337280	5539530
3178	99TWG0655	361765	5597385	3234	99TWG0711	337225	5539380
3179	99TWG0656	362250	5591550	3235	99TWG0712	335900	5538600
3180	99TWG0657	362450	5591350	3236	99TWG0713	335940	5538500

Number	Station[1,2]	Easting[3]	Northing[3]
3237	99TWG0714	336300	5538680
3238	99TWG0715	336450	5538670
3239	99TWG0716	333900	5537900
3240	99TWG0717	336308	5535239
3241	99TWG0718	336785	5536900
3242	99TWG0719	312167	5461995
3243	99TWG0720	351640	5580360
3244	99TWG0721	351350	5580200
3245	99TWG0722	350950	5580120
3246	99TWG0723	350545	5580095
3247	99TWG0724	350950	5580200
3248	99TWG0725	350775	5580210
3249	99TWG0726	350625	5580200
3250	99TWG0727	350370	5580550
3251	99TWG0728	350280	5580470
3252	99TWG0729	350200	5580500
3253	99TWG0730	350300	5580600
3254	99TWG0731	350430	5580765
3255	99TWG0732	350350	5581100
3256	99TWG0733	350140	5580800
3257	99TWG0734	349990	5580750
3258	99TWG0735	349600	5580850
3259	99TWG0736	349545	5580970
3260	99TWG0737	349430	5581150
3261	99TWG0738	349300	5581210
3262	99TWG0739	349190	5581300
3263	99TWG0740	349050	5581450
3264	99TWG0741	348700	5581825
3265	99TWG0742	348470	5582500
3266	99TWG0743	338250	5535360
3267	99TWG0744	348300	5535885
3268	99TWG0745	338000	5535885
3269	99TWG0746	336780	5534715
3270	99TWG0747	336900	5534265
3271	99TWG0748	337250	5536565
3272	99TWG0749	337515	5536700
3273	99TWG0750	336920	5537480
3274	99TWG0751	337140	5537735
3275	99TWG0752	338100	5536800
3276	99TWG0753	337680	5538000
3277	99TWG0754	339625	5536600
3278	99TWG0755	338500	5534225
3279	99TWG0756	338050	5533120
3280	99TWG0757	338450	5533110
3281	99TWG0759	340450	5579800
3282	99TWG0760	340340	5580110
3283	99TWG0761	340300	5580500
3284	99TWG0762	340585	5581500
3285	99TWG0763	340650	5581800
3286	99TWG0764	340100	5581500
3287	99TWG0765	341200	5582800
3288	99TWG0767	341250	5582950
3289	99TWG0768	341100	5582600
3290	99TWG0772	345500	5565125
3291	99TWG0773	342050	5566300

APPENDIX C

Fabric data

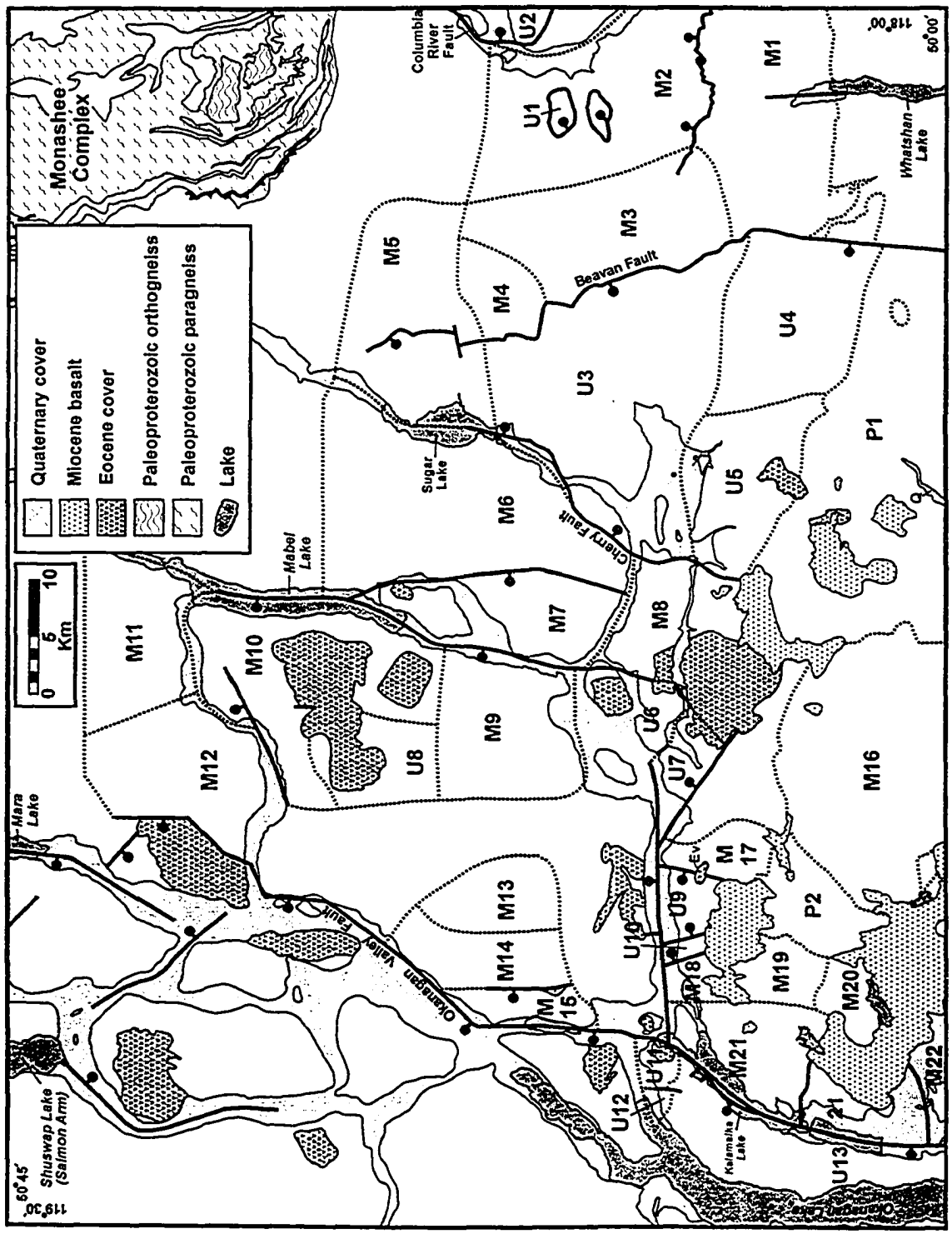

Fig. C-1. Domain map. Dashed lined indicate domain boundaires, solid black lines indicate exposed or inferred fault traces. Domains are bounded by both faults and dotted lines.

Fabric Data

Notes:

1. First two digits refer to the year
2. Letters following year refer to outcrop type (outcrop noted - O) or operator (TWB - T. Beattie, TWF - K. Franz, TWM - M. Mylod, TWG - P. Glombick, TW - R. Thompson, TWE - P. Erdmer, SG - S. Gareau)
3. All UTM coordinates were measured in UTM Zone 11 using NAD 83 datum
4. Abbreviations: sufol - transposition foliation, subed - bedding, lu - mineral lineation, l-fold1 - F2/F3 fold axis, buax - axial plane to l-fold1 folds, s-fol1 - crenulation cleavage axial plane
5. All measurments are given in strike/dip using right hand rule
6. B - Basement Zone; M - Middle Zone; U - Upper Zone; E - Eocene sediments; P - pluton

Number	Station[1,2]	Easting[3]	Northing[3]	Structure[4]	Azimuth[5]	Dip	Domain[6]
1	00TWB0002	339717	5546787	sufol	330	20	M19
2	00TWB0003	339650	5547049	sufol	300	55	M20
3	00TWB0003	339650	5547049	sufol	310	24	M20
4	00TWB0004	343465	5549230	sufol	60	41	M20
5	00TWF0002	354579	5549048	sufol	40	3	M16
6	00TWF0003	354138	5548137	sufol	135	12	M16
7	00TWF0005	353904	5549109	sufol	144	15	M16
8	00TWF0006	353921	5549394	sufol	45	18	M16
9	00TWF0006	353921	5549394	l-fold1	290	26	M16
10	00TWF0010	353184	5548561	sufol	140	9	M19
11	00TWF0012	352740	5549615	sufol	40	15	M19
12	00TWF0012	352740	5549615	sufol	40	15	M16
13	00TWF0014	349585	5549403	sufol	120	45	P2
14	00TWF0014	349585	5549403	sufol	120	45	M19
15	00TWF0016	349528	5548889	lu	94	14	M16
16	00TWF0017	366086	5564822	subed	125	50	U6
17	00TWF0018	366439	5564877	subed	120	68	U6
18	00TWF0020	366335	5565139	subed	158	66	U6
19	00TWF0028	367065	5565389	subed	138	63	U6
20	00TWF0033	367054	5564098	subed	320	48	U6
21	00TWF0048	349212	5548698	sufol	10	86	M16
22	00TWF0057	347242	5547797	sufol	352	65	P2
23	00TWF0059	347215	5547846	sufol	312	58	P2
24	00TWF0061	371152	5567452	sufol	50	36	M8
25	00TWF0068	371225	5566507	sufol	248	35	M8
26	00TWF0069	371250	5566600	sufol	333	11	M8
27	00TWF0079	371389	5570052	sufol	34	38	M8
28	00TWF0079	371389	5570052	lu	115	15	M8
29	00TWF0080	371450	5569890	l-fold1	28	12	M8
30	00TWF0080	371450	5569890	l-fold1	28	28	M8
31	00TWF0080	371450	5569890	sufol	60	12	M8
32	00TWF0083	372392	5569725	sufol	24	43	M8
33	00TWF0083	372392	5569725	lu	85	40	M8
34	00TWF0084	373229	5568803	sufol	65	38	M8
35	00TWF0085	376012	5569414	sufol	112	60	M8
36	00TWF0087	387522	5564012	sufol	305	45	U7
37	00TWF0088	389136	5561642	sufol	97	54	U7
38	00TWF0089	389372	5560590	sufol	105	90	U7
39	00TWF0091	391438	5558722	sufol	90	30	U7
40	00TWF0096	365459	5554512	sufol	349	65	M16
41	00TWF0098	365787	5552840	sufol	94	66	M16
42	00TWF0114	375081	5567697	sufol	62	35	M8
43	00TWF0117	383601	5549030	subed	12	74	E6
44	00TWF0119	383739	5549140	subed	190	20	E6
45	00TWF0121	408730	5562452	sufol	169	20	M3

Number	Station[1,2]	Easting[3]	Northing[3]	Structure[4]	Azimuth[5]	Dip	Domain[6]
46	00TWF0124	408639	5562047	sufol	205	30	M3
47	00TWF0125	408798	5561967	l-fold1	235	25	M1
48	00TWF0125	408798	5561967	l-fold1	234	30	M1
49	00TWF0125	408798	5561967	l-fold1	224	30	M3
50	00TWF0126	409276	5561908	sufol	190	25	M3
51	00TWF0128	409828	5562021	sufol	176	28	M3
52	00TWF0130	410035	5562245	sufol	150	35	M3
53	00TWF0131	407033	5562397	sufol	148	35	M3
54	00TWF0132	407202	5561891	sufol	166	25	M3
55	00TWF0133	407145	5561529	sufol	170	31	M3
56	00TWF0134	407058	5561492	sufol	154	25	M3
57	00TWF0135	406879	5561446	sufol	150	38	M3
58	00TWF0137	406486	5560976	subed	116	60	U3
59	00TWF0140	375615	5556294	sufol	106	34	M8
60	00TWF0141	375565	5556291	sufol	117	43	M8
61	00TWF0146	376537	5561931	sufol	90	30	M8
62	00TWF0148	376762	5562311	sufol	96	46	M8
63	00TWF0149	376778	5562404	sufol	121	37	M8
64	00TWF0150	391216	5581072	sufol	295	69	M3
65	00TWF0151	390893	5580517	sufol	276	68	M3
66	00TWF0152	390958	5580691	sufol	278	70	M3
67	00TWF0153	391313	5587467	sufol	144	43	M3
68	00TWF0156	393049	5589936	sufol	50	25	M6
69	00TWF0157	393713	5590486	sufol	68	30	M3
70	00TWF0160	403430	5582670	sufol	135	48	M4
71	00TWF0161	403295	5582621	sufol	136	52	M4
72	00TWF0162	403150	5582463	sufol	148	49	M4
73	00TWF0163	403070	5582475	sufol	185	48	M4
74	00TWF0164	403024	5582415	sufol	110	90	M4
75	00TWF0165	402806	5582300	sufol	114	90	M4
76	00TWF0166	402850	5582260	sufol	226	38	M4
77	00TWF0169	392336	5579071	sufol	346	60	U3
78	00TWF0170	392514	5579600	sufol	302	72	U3
79	00TWF0172	393915	5580841	sufol	290	75	M5
80	00TWF0176	393953	5578386	subed	287	74	U3
81	00TWF0177	394158	5578370	l-fold1	250	30	U3
82	00TWF0177	394158	5578370	subed	263	75	U3
83	00TWF0180	388039	5576145	sufol	96	27	M3
84	00TWF0182	403693	5563208	sufol	270	74	U3
85	00TWF0182	403693	5563208	subed	163	17	U3
86	00TWF0184	403625	5563855	subed	220	73	U3
87	00TWF0185	403472	5561122	subed	132	15	U3
88	00TWF0188	404545	5560254	subed	285	30	U3
89	00TWF0189	405225	5559690	subed	256	43	U3
90	00TWF0195	406801	5557626	subed	23	50	U3
91	00TWF0198	406771	5556699	subed	65	68	U4
92	00TWF0201	405850	5558120	subed	114	45	U3
93	00TWF0203	407516	5586535	sufol	200	0	M5
94	00TWF0205	407699	5586776	sufol	200	25	M5
95	00TWF0206	407982	5586788	sufol	234	29	M5
96	00TWF0207	408104	5586737	sufol	239	37	M5
97	00TWF0208	408173	5586792	sufol	186	36	M5
98	00TWF0209	408357	5586985	sufol	230	15	M5
99	00TWF0210	408631	5587238	sufol	215	40	M5
100	00TWF0211	408893	5587277	sufol	250	49	M5
101	00TWF0212	408975	5587411	sufol	246	35	M5

Number	Station[1,2]	Easting[3]	Northing[3]	Structure[4]	Azimuth[5]	Dip	Domain[6]
102	00TWF0213	409243	5587621	sufol	250	43	M5
103	00TWF0214	409342	5587973	sufol	229	45	M5
104	00TWF0215	409339	5588127	sufol	265	18	M5
105	00TWF0216	409371	5588318	sufol	198	33	M5
106	00TWF0217	409566	5588467	sufol	196	22	M5
107	00TWF0221	393298	5551449	sufol	279	47	U7
108	00TWF0234	393269	5550088	subed	318	69	P1
109	00TWF0238	393855	5541984	sufol	190	90	P1
110	00TWF0241	395062	5542018	sufol	350	76	P1
111	00TWF0244	393586	5540912	sufol	343	85	P1
112	00TWF0255	362727	5553036	sufol	326	78	M16
113	00TWF0258	362657	5553705	sufol	323	34	M16
114	00TWF0261	380719	5564998	subed	335	90	U3
115	00TWF0263	380103	5565383	subed	130	57	U3
116	00TWF0264	380570	5565230	subed	45	84	U3
117	00TWF0264	380570	5565230	subed	60	66	U3
118	00TWF0265	381736	5565248	subed	319	41	U3
119	00TWF0266	381331	5567136	subed	54	72	U3
120	00TWF0268	383861	5565279	subed	78	44	U3
121	00TWF0269	341796	5550389	sufol	5	36	M20
122	00TWF0270	341592	5550484	sufol	34	25	M20
123	00TWF0271	341495	5550500	sufol	10	42	M20
124	00TWF0275	340397	5550762	sufol	351	44	M20
125	00TWF0276	340403	5551123	sufol	265	23	M20
126	00TWF0277	340718	5551020	sufol	288	45	M20
127	00TWF0278	341038	5550919	sufol	287	36	M20
128	00TWF0279	341247	5551139	sufol	38	32	M20
129	00TWF0279	341247	5551139	l-fold1	148	39	M20
130	00TWF0280	341325	5551136	sufol	333	33	M20
131	00TWF0282	341838	5551140	sufol	353	20	M20
132	00TWF0284	342106	5551216	sufol	275	36	M20
133	00TWF0286	394105	5565317	sufol	265	84	U3
134	00TWF0289	393765	5565703	sufol	290	48	U3
135	00TWF0290	395534	5566056	subed	322	48	U3
136	00TWF0292	399885	5567126	subed	227	15	U3
137	00TWF0293	399754	5567322	subed	300	20	U3
138	00TWF0294	400501	5568945	subed	203	37	U3
139	00TWF0295	400400	5569994	subed	250	62	U3
140	00TWF0296	400701	5570234	subed	265	53	U3
141	00TWF0296	400701	5570234	subed	113	76	U3
142	00TWF0298	399872	5570043	subed	357	54	U3
143	00TWF0298	399872	5570043	sufol	10	53	U3
144	00TWF0299	399268	5568217	subed	270	30	U3
145	00TWF0300	398927	5567642	subed	247	25	U3
146	00TWF0301	398491	5567042	subed	283	25	U3
147	00TWF0303	396925	5567942	subed	325	25	U3
148	00TWF0304	397158	5568569	subed	272	45	U3
149	00TWF0306	399227	5569439	subed	333	25	U3
150	00TWF0307	392975	5577986	sufol	80	24	U3
151	00TWF0309	393571	5577623	subed	21	20	U3
152	00TWF0310	395008	5577059	sufol	321	24	U3
153	00TWF0312	394699	5576886	subed	5	5	U3
154	00TWF0313	395054	5576370	subed	274	28	U3
155	00TWF0315	397096	5576390	sufol	248	56	U3
156	00TWF0318	391027	5588957	sufol	316	55	M6
157	00TWF0322	397468	5593600	sufol	235	48	M5

Number	Station[1,2]	Easting[3]	Northing[3]	Structure[4]	Azimuth[5]	Dip	Domain[6]
158	00TWF0324	398240	5592575	sufol	105	47	M5
159	00TWF0324	398240	5592575	s-fol1	13	35	M5
160	00TWF0331	363950	5546355	sufol	50	70	M16
161	00TWF0332	364522	5545880	sufol	31	49	M16
162	00TWF0333	365026	5546025	sufol	52	70	M16
163	00TWF0334	364701	5546068	sufol	49	57	M16
164	00TWF0336	363624	5547015	sufol	33	74	M16
165	00TWG0001	356634	5563193	sufol	106	70	P2
166	00TWG0005B	355159	5562047	sufol	6	31	M17
167	00TWG0005B	355159	5562047	l-fold1	115	19	M17
168	00TWG0007	355371	5561339	sufol	10	48	M17
169	00TWG0008	355135	5561118	sufol	52	54	M17
170	00TWG0009	355134	5561021	sufol	14	62	M17
171	00TWG0010	355057	5560491	sufol	12	57	M17
172	00TWG0011	355186	5559776	sufol	350	52	M17
173	00TWG0030	358577	5553178	sufol	95	90	M16
174	00TWG0032	359660	5555005	sufol	296	75	M16
175	00TWG0033	360352	5555032	sufol	328	50	M16
176	00TWG0037	359419	5553949	l-fold1	147	33	M16
177	00TWG0046	356350	5558400	sufol	80	40	M17
178	00TWG0048	353018	5543654	sufol	49	26	M16
179	00TWG0050	352686	5544017	sufol	80	32	M16
180	00TWG0050	352686	5544017	lu	107	13	M16
181	00TWG0051	352962	5544286	sufol	40	37	M16
182	00TWG0053	351305	5543380	sufol	109	33	M16
183	00TWG0054	351260	5544293	sufol	60	48	M16
184	00TWG0055	350928	5545550	sufol	70	36	M16
185	00TWG0056	352345	5546636	sufol	10	12	M16
186	00TWG0064	359505	5550053	sufol	38	24	M16
187	00TWG0065	354256	5547717	sufol	70	15	M16
188	00TWG0067	354985	5548855	sufol	291	26	M16
189	00TWG0067	354985	5548855	l-fold1	59	24	M16
190	00TWG0069	356257	5550908	sufol	113	61	M16
191	00TWG0071	379716	5567196	sufol	62	57	M8
192	00TWG0072	378960	5567540	sufol	70	30	M8
193	00TWG0073	378160	5567660	sufol	16	15	M8
194	00TWG0073	378160	5567660	l-fold1	180	24	M8
195	00TWG0074	375100	5567580	sufol	68	38	M8
196	00TWG0075	374800	5567710	sufol	38	53	M8
197	00TWG0077	373740	5569860	sufol	54	47	M8
198	00TWG0079	373700	5570290	sufol	42	51	M8
199	00TWG0079	373700	5570290	l-fold1	135	44	M8
200	00TWG0080	361440	5561573	subed	341	49	U5
201	00TWG0092	362119	5561589	l-fold1	60	15	U5
202	00TWG0092	362119	5561589	sufol	75	57	U5
203	00TWG0093	362327	5561326	l-fold1	56	55	U5
204	00TWG0093	362327	5561326	subed	271	73	U5
205	00TWG0094	362438	5561274	subed	284	58	U5
206	00TWG0103	367895	5560693	subed	230	76	E3
207	00TWG0105	373797	5560319	s-fol2	63	25	M8
208	00TWG0105	373797	5560319	sufol	126	70	M8
209	00TWG0107	374912	5562526	sufol	123	57	M8
210	00TWG0108	374864	5561407	sufol	120	65	M8
211	00TWG0109	375218	5559936	sufol	294	70	M8
212	00TWG0111	376920	5560504	sufol	323	50	M8
213	00TWG0112	376339	5559309	sufol	312	72	M8

Number	Station[1,2]	Easting[3]	Northing[3]	Structure[4]	Azimuth[5]	Dip	Domain[6]
214	00TWG0114	377874	5559717	sufol	20	79	M8
215	00TWG0116	378566	5560798	sufol	98	49	M8
216	00TWG0118	378573	5560261	sufol	105	46	U7
217	00TWG0119	378877	5560883	sufol	113	54	U7
218	00TWG0148	380075	5562222	subed	106	64	U3
219	00TWG0152	382732	5560043	sufol	42	30	U7
220	00TWG0155	382042	5557596	subed	302	25	U7
221	00TWG0158	359695	5562890	sufol	254	47	U5
222	00TWG0159	358813	5562798	sufol	285	50	M19
223	00TWG0160	358489	5562829	sufol	283	55	M19
224	00TWG0161	358350	5562120	sufol	308	79	M19
225	00TWG0162	358570	5562000	sufol	314	44	M19
226	00TWG0163	358100	5562033	sufol	305	81	P2
227	00TWG0164	360173	5561592	sufol	232	41	M19
228	00TWG0165	358802	5559605	sufol	338	44	P2
229	00TWG0168	369233	5559621	subed	104	90	E3
230	00TWG0174	368056	5556306	subed	125	90	E3
231	00TWG0179	376743	5554180	lu	110	28	P1
232	00TWG0179	376743	5554180	sufol	349	35	P1
233	00TWG0188	360176	5563622	subed	66	71	U5
234	00TWG0189	360062	5563524	subed	50	70	U5
235	00TWG0192	370392	5567954	sufol	8	25	M8
236	00TWG0194	374320	5565030	sufol	60	28	M8
237	00TWG0195	373524	5564989	sufol	77	67	M8
238	00TWG0196	373263	5564744	sufol	73	70	M8
239	00TWG0197	372265	5565126	sufol	93	55	M8
240	00TWG0198	373283	5564814	sufol	247	58	M8
241	00TWG0201	360911	5551417	sufol	73	26	M16
242	00TWG0203	361121	5550570	sufol	60	40	M16
243	00TWG0204	360351	5550250	sufol	50	48	M16
244	00TWG0205	359468	5550046	sufol	40	24	M19
245	00TWG0206	357638	5549871	sufol	60	21	M16
246	00TWG0207	358276	5549319	sufol	10	15	M16
247	00TWG0208	358753	5549337	sufol	74	34	M16
248	00TWG0210	356466	5547645	sufol	76	8	M16
249	00TWG0211	354952	5546375	sufol	80	20	M16
250	00TWG0212	389026	5560887	subed	112	35	U7
251	00TWG0217	387171	5560682	subed	114	32	U7
252	00TWG0218	386822	5560669	sufol	118	68	U7
253	00TWG0221	385143	5560870	subed	85	79	U7
254	00TWG0238	382964	5556127	subed	297	86	U7
255	00TWG0246	387860	5560128	subed	80	58	U7
256	00TWG0246	387860	5560128	subed	115	73	U7
257	00TWG0261	387235	5555672	subed	55	35	E4
258	00TWG0265	371563	5566791	sufol	115	18	M8
259	00TWG0269	372436	5566391	sufol	359	0	M8
260	00TWG0273	361617	5550596	sufol	47	51	M16
261	00TWG0274	361826	5550503	sufol	71	54	M16
262	00TWG0275	362203	5550253	sufol	78	60	M16
263	00TWG0277	361231	5548055	l-fold1	183	38	M16
264	00TWG0277	361231	5548055	l-fold1	201	18	M16
265	00TWG0277	361231	5548055	sufol	56	50	M16
266	00TWG0278	363403	5549830	sufol	79	61	M16
267	00TWG0279	364731	5550581	sufol	53	59	M16
268	00TWG0282	363134	5549694	sufol	92	80	M16
269	00TWG0282	363134	5549694	l-fold1	265	36	M16

Number	Station[1,2]	Easting[3]	Northing[3]	Structure[4]	Azimuth[5]	Dip	Domain[6]
270	00TWG0282	363134	5549694	l-fold1	290	16	M16
271	00TWG0283	362958	5549104	sufol	61	74	M16
272	00TWG0307	379329	5563379	sufol	33	41	M8
273	00TWG0310	376920	5563810	lu	285	3	M8
274	00TWG0311	376783	5563852	sufol	89	27	M8
275	00TWG0313	371564	5545852	sufol	338	31	M16
276	00TWG0314	374168	5545561	sufol	291	38	P1
277	00TWG0314	374168	5545561	sufol	64	45	P1
278	00TWG0314	374168	5545561	sufol	338	30	P1
279	00TWG0314	374168	5545561	l-fold1	79	17	P1
280	00TWG0318	373112	5543820	sufol	334	27	M16
281	00TWG0318	373112	5543820	sufol	27	47	M16
282	00TWG0319	410231	5563029	sufol	165	18	M3
283	00TWG0319	410231	5563029	sufol	322	28	M3
284	00TWG0320	410350	5563500	sufol	261	19	M3
285	00TWG0321	410375	5563601	l-fold1	251	37	M3
286	00TWG0321	410375	5563601	l-fold1	255	9	M3
287	00TWG0323	410150	5563626	sufol	225	25	M3
288	00TWG0324	407236	5563562	sufol	204	43	M3
289	00TWG0326	407833	5564349	sufol	204	28	M3
290	00TWG0328	408087	5564744	sufol	204	25	M3
291	00TWG0329	407611	5565038	sufol	185	37	M3
292	00TWG0330	407374	5565120	sufol	221	61	M3
293	00TWG0330	407374	5565120	lu	232	11	M3
294	00TWG0331	407130	5565038	sufol	228	48	M3
295	00TWG0332	407130	5565038	sufol	220	40	M3
296	00TWG0336	384643	5555422	subed	105	70	U7
297	00TWG0338	384500	5555700	subed	125	86	U7
298	00TWG0338	384500	5555700	subed	170	71	U7
299	00TWG0338	384500	5555700	subed	105	76	U7
300	00TWG0338	384500	5555700	subed	85	65	U7
301	00TWG0338	384500	5555700	subed	291	63	U7
302	00TWG0339	384041	5554646	subed	129	69	U7
303	00TWG0343	384434	5552942	lu	310	17	P1
304	00TWG0344	384277	5553171	sufol	331	71	P1
305	00TWG0345	385367	5555696	subed	131	68	U7
306	00TWG0347	385923	5555575	subed	97	52	U7
307	00TWG0348	386119	5555555	subed	146	38	U7
308	00TWG0349	385804	5555142	subed	126	53	U7
309	00TWG0350	386157	5555210	subed	98	18	U7
310	00TWG0352	385286	5554973	subed	120	26	U7
311	00TWG0355	372537	5542709	lu	86	40	P1
312	00TWG0356	372420	5541680	lu	81	30	P1
313	00TWG0356	372420	5541680	sufol	349	30	P1
314	00TWG0360	379205	5562181	sufol	58	54	M8
315	00TWG0362	379254	5561866	sufol	85	57	M8
316	00TWG0363	379280	5561718	sufol	70	36	M8
317	00TWG0364	379442	5561614	subed	79	44	U7
318	00TWG0365	405216	5580325	sufol	114	36	M4
319	00TWG0366	405678	5580049	sufol	141	18	M4
320	00TWG0367	406447	5580263	sufol	216	43	M4
321	00TWG0368	403246	5577549	sufol	117	84	M4
322	00TWG0369	403554	5577882	sufol	110	52	M4
323	00TWG0370	403741	5578031	sufol	95	65	M4
324	00TWG0371	403654	5578458	sufol	92	60	M4
325	00TWG0372	403258	5578699	sufol	78	65	M4

Number	Station[1,2]	Easting[3]	Northing[3]	Structure[4]	Azimuth[5]	Dip	Domain[6]
326	00TWG0373	403133	5578903	sufol	96	43	M4
327	00TWG0374	403068	5579356	sufol	145	60	M4
328	00TWG0375	402678	5579737	sufol	68	34	M4
329	00TWG0375	402678	5579737	l-fold1	208	24	M4
330	00TWG0376	402431	5579896	l-fold1	224	23	M4
331	00TWG0376	402431	5579896	l-fold1	221	24	M4
332	00TWG0377	402479	5580430	sufol	115	30	M4
333	00TWG0378	387660	5572400	subed	30	25	U3
334	00TWG0382	388368	5572211	subed	320	72	U3
335	00TWG0382	388368	5572211	sufol	320	72	U3
336	00TWG0382	388368	5572211	sufol	73	62	U3
337	00TWG0382	388368	5572211	l-fold1	100	31	U3
338	00TWG0383	389245	5572357	sufol	88	9	U3
339	00TWG0383	389245	5572357	sufol	313	20	U3
340	00TWG0384	389564	5572690	sufol	330	31	U3
341	00TWG0385	390245	5573004	subed	299	39	U3
342	00TWG0388	390625	5574413	sufol	48	39	U3
343	00TWG0389	391441	5576171	subed	50	20	U3
344	00TWG0390	391104	5576123	subed	51	32	U3
345	00TWG0391	390827	5576126	sufol	0	37	U3
346	00TWG0396	401967	5579845	sufol	140	22	M4
347	00TWG0396	401967	5579845	l-fold1	210	24	M4
348	00TWG0396	401967	5579845	l-fold1	238	36	M4
349	00TWG0396	401967	5579845	l-fold1	219	42	M4
350	00TWG0397	401454	5579720	lu	245	42	M4
351	00TWG0397	401454	5579720	sufol	125	42	M4
352	00TWG0398	400686	5579875	sufol	125	55	M4
353	00TWG0399	400131	5579893	sufol	136	37	M4
354	00TWG0401	399551	5579625	sufol	280	36	U3
355	00TWG0403	391113	5573314	sufol	340	20	U3
356	00TWG0404	391497	5573428	sufol	335	26	U3
357	00TWG0405	392003	5573547	sufol	1	29	U3
358	00TWG0408	395464	5575219	sufol	357	37	U3
359	00TWG0408	395464	5575219	sufol	299	61	U3
360	00TWG0410	395450	5574829	l-fold1	112	25	U3
361	00TWG0410	395450	5574829	sufol	4	26	U3
362	00TWG0412	339917	5549934	sufol	104	76	M20
363	00TWG0413	340004	5550165	sufol	75	43	M20
364	00TWG0413	340004	5550165	sufol	260	20	M20
365	00TWG0415	340887	5550181	lu	92	1	M20
366	00TWG0416	341952	5550297	sufol	301	39	M20
367	00TWG0416	341952	5550297	sufol	344	31	M20
368	00TWG0416	341952	5550297	lu	104	31	M20
369	00TWG0418	342586	5551183	l-fold1	257	36	M20
370	00TWG0418	342586	5551183	sufol	87	45	M20
371	00TWG0419	342238	5551222	sufol	6	25	M20
372	00TWG0419	342238	5551222	lu	96	25	M20
373	00TWG0421	340604	5546593	sufol	25	17	M20
374	00TWG0421	340604	5546593	l-fold1	95	14	M20
375	00TWG0422	341157	5547344	sufol	123	90	M20
376	00TWG0425	342198	5547575	sufol	70	30	M20
377	00TWG0427	343371	5549125	sufol	76	46	M20
378	00TWG0428	343480	5549285	sufol	78	58	M20
379	00TWG0430	345013	5553979	sufol	29	48	M25
380	00TWG0430	345013	5553979	sufol	106	50	M25
381	00TWG0430	345013	5553979	sufol	7	59	M25

Number	Station[1,2]	Easting[3]	Northing[3]	Structure[4]	Azimuth[5]	Dip	Domain[6]
382	00TWG0430	345013	5553979	sufol	357	71	M25
383	00TWG0430	345013	5553979	lu	114	45	M25
384	00TWG0430	345013	5553979	sufol	83	72	M25
385	00TWG0430	345013	5553979	sufol	44	65	M25
386	00TWG0430	345013	5553979	sufol	21	57	M25
387	00TWG0430	345013	5553979	sufol	337	72	M25
388	00TWG0430	345013	5553979	sufol	42	42	M25
389	00TWG0430	345013	5553979	sufol	32	80	M25
390	00TWG0430	345013	5553979	l-fold1	190	50	M25
391	00TWG0430	345013	5553979	sufol	77	58	M25
392	00TWG0430	345013	5553979	sufol	106	46	M25
393	00TWG0430	345013	5553979	sufol	60	53	M25
394	00TWG0430	345013	5553979	sufol	50	37	M25
395	00TWG0430	345013	5553979	sufol	76	50	M25
396	00TWG0430	345013	5553979	sufol	44	77	M25
397	00TWG0430	345013	5553979	sufol	8	59	M25
398	00TWG0430	345013	5553979	sufol	339	89	M25
399	00TWG0430	345013	5553979	sufol	86	52	M25
400	00TWG0430	345013	5553979	sufol	88	40	M25
401	00TWG0430	345013	5553979	sufol	12	47	M25
402	00TWG0430	345013	5553979	sufol	25	44	M25
403	00TWG0430	345013	5553979	sufol	321	76	M25
404	00TWG0430	345013	5553979	sufol	350	88	M25
405	00TWG0430	345013	5553979	sufol	52	77	M25
406	00TWG0430	345013	5553979	sufol	44	59	M25
407	00TWG0430	345013	5553979	sufol	34	55	M25
408	00TWG0430	345013	5553979	sufol	330	75	M25
409	00TWG0430	345013	5553979	sufol	327	79	M25
410	00TWG0430	345013	5553979	sufol	45	71	M25
411	00TWG0430	345013	5553979	sufol	58	78	M25
412	00TWG0430	345013	5553979	sufol	252	76	M25
413	00TWG0430	345013	5553979	sufol	272	71	M25
414	00TWG0430	345013	5553979	sufol	22	53	M25
415	00TWG0430	345013	5553979	sufol	8	66	M25
416	00TWG0430	345013	5553979	sufol	44	55	M25
417	00TWG0430	345013	5553979	l-fold1	188	63	M25
418	00TWG0430	345013	5553979	l-fold1	204	69	M25
419	00TWG0430	345013	5553979	sufol	4	64	M25
420	00TWG0430	345013	5553979	sufol	39	52	M25
421	00TWG0430	345013	5553979	sufol	86	32	M25
422	00TWG0430	345013	5553979	sufol	59	58	M25
423	00TWG0430	345013	5553979	sufol	7	68	M25
424	00TWG0430	345013	5553979	sufol	82	50	M25
425	00TWG0430	345013	5553979	l-fold1	189	70	M25
426	00TWG0430	345013	5553979	l-fold1	180	58	M25
427	00TWG0430	345013	5553979	l-fold1	4	73	M25
428	00TWG0430	345013	5553979	l-fold1	175	63	M25
429	00TWG0430	345013	5553979	l-fold1	184	81	M25
430	00TWG0430	345013	5553979	l-fold1	191	65	M25
431	00TWG0430	345013	5553979	l-fold1	61	71	M25
432	00TWG0430	345013	5553979	l-fold1	195	65	M25
433	00TWG0430	345013	5553979	l-fold1	89	58	M25
434	00TWG0430	345013	5553979	l-fold1	159	65	M25
435	00TWG0430	345013	5553979	l-fold1	183	49	M25
436	00TWG0430	345013	5553979	l-fold1	200	40	M25
437	00TWG0431	343742	5559532	sufol	86	69	M25

Number	Station[1,2]	Easting[3]	Northing[3]	Structure[4]	Azimuth[5]	Dip	Domain[6]
438	00TWG0436	404115	5566915	sufol	104	74	U3
439	00TWG0437	391236	5559294	sufol	134	75	U7
440	00TWG0437	391236	5559294	sufol	129	54	U7
441	00TWG0439	391263	5559415	sufol	134	58	U7
442	00TWG0440	390976	5559775	sufol	110	64	U7
443	00TWG0440	390976	5559775	sufol	92	69	U7
444	00TWG0441	390683	5559935	sufol	93	45	U7
445	00TWG0441	390683	5559935	sufol	97	50	U7
446	00TWG0444	389672	5560895	sufol	110	55	U3
447	00TWG0444	389672	5560895	subed	110	55	U7
448	00TWG0445	389659	5561059	sufol	66	39	U7
449	00TWG0447	389777	5562338	sufol	118	86	U7
450	00TWG0449	389797	5561045	sufol	286	77	U7
451	00TWG0450	389993	5560977	sufol	104	77	U7
452	00TWG0451	390062	5561311	sufol	92	63	U7
453	00TWG0452	390122	5561491	sufol	299	84	U3
454	00TWG0460	391302	5560247	sufol	104	40	U7
455	00TWG0462	391923	5560385	sufol	118	71	U7
456	00TWG0463	392090	5560187	sufol	104	80	U7
457	00TWG0464	391694	5561167	sufol	283	53	U7
458	00TWG0468	392813	5559353	sufol	295	65	U7
459	00TWG0469	393319	5559428	subed	293	54	U4
460	00TWG0469	393319	5559428	sufol	293	54	U4
461	00TWG0470	392782	5559530	sufol	280	42	U7
462	00TWG0471	392167	5559600	sufol	298	77	U7
463	00TWG0473	394808	5560078	subed	127	87	U3
464	00TWG0473	394808	5560078	sufol	263	88	U3
465	00TWG0475	394042	5560405	sufol	290	44	U3
466	00TWG0475	394042	5560405	sufol	325	33	U3
467	00TWG0475	394042	5560405	subed	290	44	U3
468	00TWG0477	394772	5560740	sufol	80	68	U3
469	00TWG0478	395744	5560386	subed	332	70	U3
470	00TWG0478	395744	5560386	sufol	332	70	U3
471	00TWG0480	397839	5560055	sufol	121	84	U3
472	00TWG0482	398603	5559988	sufol	58	33	U3
473	00TWG0482	398603	5559988	sufol	106	44	U3
474	00TWG0483	399261	5560133	sufol	152	54	U3
475	00TWG0483	399261	5560133	subed	152	54	U3
476	00TWG0484	399838	5560240	subed	318	55	U3
477	00TWG0484	399838	5560240	sufol	318	55	U3
478	00TWG0485	400473	5560507	sufol	298	43	U3
479	00TWG0487	402659	5572520	sufol	76	9	U3
480	00TWG0488	404011	5572467	sufol	50	11	M3
481	00TWG0489	405774	5574020	sufol	112	79	M3
482	00TWG0490	405765	5574220	sufol	114	90	M3
483	00TWG0495	410548	5563148	sufol	230	15	M3
484	00TWG0496	411795	5562159	sufol	240	6	M3
485	00TWG0497	411853	5561815	l-fold1	310	3	M3
486	00TWG0497	411853	5561815	sufol	131	18	M3
487	00TWG0498a	411985	5561304	sufol	65	2	M3
488	00TWG0498b	412240	5561129	sufol	160	19	M3
489	00TWG0500	412062	5562820	sufol	0	0	M3
490	00TWG0500	412062	5562820	l-fold1	105	0	M3
491	00TWG0501	412363	5562954	l-fold1	278	14	M3
492	00TWG0501	412363	5562954	sufol	284	39	M3
493	00TWG0502	412668	5563052	sufol	96	36	M3

Number	Station[1,2]	Easting[3]	Northing[3]	Structure[4]	Azimuth[5]	Dip	Domain[6]
494	00TWG0502	412668	5563052	l-fold1	105	2	M3
495	00TWG0503	412549	5563445	sufol	307	43	M3
496	00TWG0503	412549	5563445	l-fold1	100	3	M3
497	00TWG0504	412516	5563664	sufol	285	76	M3
498	00TWG0504	412516	5563664	l-fold1	102	15	M3
499	00TWG0505	412416	5563741	l-fold1	278	2	M3
500	00TWG0506	412373	5563822	sufol	266	60	M3
501	00TWG0507	412281	5563893	sufol	277	50	M3
502	00TWG0507	412281	5563893	l-fold1	98	0	M3
503	00TWG0508	411990	5564078	sufol	265	53	M3
504	00TWG0510	411195	5564200	sufol	232	42	M3
505	00TWG0511	411014	5565064	sufol	247	60	M3
506	00TWG0512	410053	5565371	sufol	232	47	M3
507	00TWG0513	410029	5565692	sufol	215	41	M3
508	00TWG0515	409855	5566859	sufol	243	56	M3
509	00TWG0516	409877	5567121	sufol	232	81	M3
510	00TWG0516	409877	5567121	l-fold1	52	4	M3
511	00TWG0517	409724	5567204	sufol	228	81	M3
512	00TWG0519	409486	5567665	sufol	58	65	M3
513	00TWG0520	409486	5567665	sufol	290	58	M3
514	00TWG0521	406123	5565186	sufol	176	40	M3
515	00TWG0522	406789	5565296	sufol	232	45	M3
516	00TWG0523	406636	5566182	sufol	54	37	M3
517	00TWG0524	406470	5566302	sufol	105	24	M3
518	00TWG0526	406592	5566797	sufol	220	20	M3
519	00TWG0527	405127	5567518	sufol	202	27	U3
520	00TWG0529	407220	5575078	sufol	92	71	M3
521	00TWG0530	407434	5575025	sufol	97	74	M3
522	00TWG0531	407850	5574868	sufol	92	72	M3
523	00TWG0532	408039	5574827	sufol	87	71	M3
524	00TWG0535	408605	5575195	sufol	105	73	M3
525	00TWG0536	408816	5575549	sufol	99	55	M3
526	00TWG0539	409170	5575515	sufol	117	45	M3
527	00TWG0540	409037	5575402	sufol	110	66	M3
528	00TWG0542	408891	5575281	sufol	109	59	M3
529	00TWG0543	408640	5575134	sufol	58	72	M3
530	00TWG0546	393661	5558913	sufol	89	63	U4
531	00TWG0548	393422	5558511	l-fold1	133	81	U4
532	00TWG0548	393422	5558511	sufol	106	58	U4
533	00TWG0549	393780	5558263	sufol	293	76	U4
534	00TWG0550	394399	5557669	sufol	106	53	U4
535	00TWG0569	404206	5554179	subed	358	40	U4
536	00TWG0571	404069	5554719	subed	51	27	U4
537	00TWG0572	404233	5555013	subed	92	42	U4
538	00TWG0574	402652	5554595	sufol	101	72	U4
539	00TWG0575	402717	5554725	sufol	98	41	U4
540	00TWG0576	398110	5552805	sufol	105	57	U4
541	00TWG0580	395561	5548845	sufol	129	88	U4
542	00TWG0584	395208	5549285	subed	301	81	U4
543	00TWG0585	395482	5549362	subed	321	74	U4
544	00TWG0586	396113	5549207	subed	158	90	U4
545	00TWG0588	428035	5552862	sufol	315	48	M1
546	00TWG0589	426566	5551601	sufol	327	46	M1
547	00TWG0590	425344	5550011	sufol	280	85	M1
548	00TWG0591	425538	5549901	l-fold1	102	26	M1
549	00TWG0591	425538	5549901	sufol	95	83	M1

Number	Station[1,2]	Easting[3]	Northing[3]	Structure[4]	Azimuth[5]	Dip	Domain[6]
550	00TWG0592	425865	5549600	sufol	64	72	M1
551	00TWG0592	425865	5549600	l-fold1	72	36	M1
552	00TWG0593	425743	5549433	sufol	94	75	M1
553	00TWG0595	425066	5548783	sufol	286	87	M1
554	00TWG0596	424851	5548726	sufol	284	84	M1
555	00TWG0598	426339	5545844	sufol	83	90	M1
556	00TWG0600	423200	5549180	l-fold1	98	29	M1
557	00TWG0600	423200	5549180	sufol	98	90	M1
558	00TWG0601	422200	5549220	sufol	79	77	M1
559	00TWG0602	421180	5549780	sufol	280	74	M1
560	00TWG0603	422070	5550260	sufol	103	90	M1
561	00TWG0605	419896	5548533	sufol	302	63	M1
562	00TWG0606	420440	5553537	sufol	235	22	M1
563	00TWG0608	418918	5553336	l-fold1	82	24	M1
564	00TWG0608	418918	5553336	sufol	327	25	M1
565	00TWG0610	419021	5552841	sufol	299	24	M1
566	00TWG0612	418892	5552209	sufol	261	20	M1
567	00TWG0613	418310	5552492	sufol	307	56	M1
568	00TWG0614	417870	5552562	sufol	316	39	M1
569	00TWG0616	417794	5552259	sufol	290	64	M1
570	00TWG0618	417280	5552964	sufol	343	38	M1
571	00TWG0619	416620	5552961	sufol	350	46	M1
572	00TWG0621	418431	5554643	sufol	166	50	M1
573	00TWG0622	418032	5554624	sufol	99	43	M1
574	00TWG0623	417206	5554729	sufol	300	18	M1
575	00TWG0624	414516	5555572	sufol	38	20	M1
576	00TWG0625	414449	5555204	sufol	58	32	M1
577	00TWG0626	414750	5554969	sufol	52	28	M1
578	00TWG0627	416938	5554819	sufol	0	0	M1
579	00TWG0628	417421	5555174	sufol	118	45	M1
580	00TWG0628	417421	5555174	lu	289	4	M1
581	00TWG0629	418235	5556090	sufol	44	43	M1
582	00TWG0630	417802	5555832	sufol	46	36	M1
583	00TWG0631	417532	5556080	sufol	40	43	M1
584	00TWG0632	416996	5555856	sufol	84	36	M1
585	00TWG0633	416312	5555907	sufol	61	20	M1
586	00TWG0634	417575	5556635	sufol	66	51	M1
587	00TWG0635	416351	5556426	sufol	63	38	M1
588	00TWG0636	415729	5556405	sufol	38	45	M1
589	00TWG0637	415111	5556525	sufol	46	28	M1
590	00TWG0638	417637	5557266	sufol	58	35	M1
591	00TWG0638	417637	5557266	sufol	58	35	M1
592	00TWG0639	422646	5570610	sufol	237	17	M2
593	00TWG0640	421358	5569822	sufol	158	43	M2
594	00TWG0643	420276	5568942	l-fold1	285	32	M2
595	00TWG0643	420276	5568942	sufol	166	42	M2
596	00TWG0644	420684	5568554	sufol	117	41	M2
597	00TWG0644	420684	5568554	l-fold1	121	6	M2
598	00TWG0645	420974	5568341	sufol	145	28	M2
599	00TWG0646	420733	5568437	sufol	119	50	M2
600	00TWG0647	420418	5568285	sufol	146	36	M2
601	00TWG0648	419871	5568064	sufol	113	30	M2
602	00TWG0649	419737	5567826	sufol	170	65	M2
603	00TWG0650	418932	5567734	sufol	134	44	M2
604	00TWG0650	418932	5567734	l-fold1	277	25	M2
605	00TWG0651	418461	5567620	l-fold1	312	35	M2

Number	Station[1,2]	Easting[3]	Northing[3]	Structure[4]	Azimuth[5]	Dip	Domain[6]
606	00TWG0651	418461	5567620	l-fold1	314	28	M2
607	00TWG0652	419029	5567595	sufol	298	83	M2
608	00TWG0652	419029	5567595	l-fold1	101	1	M2
609	00TWG0653	419427	5567086	sufol	262	60	M2
610	00TWG0654	418502	5567359	sufol	272	35	M2
611	00TWG0655	418026	5566763	sufol	271	81	M2
612	00TWG0655	418026	5566763	l-fold1	276	30	M2
613	00TWG0656	419180	5568390	sufol	134	48	M2
614	00TWG0657	418760	5568350	sufol	109	37	M2
615	00TWG0658	417523	5565167	sufol	245	35	M2
616	00TWG0661	422752	5572503	sufol	262	24	M2
617	00TWG0661	422752	5572503	l-fold1	290	10	M2
618	00TWG0663	421711	5571922	sufol	230	20	M2
619	00TWG0664	421584	5571710	sufol	110	10	M2
620	00TWG0665	422054	5570848	sufol	112	28	M2
621	00TWG0666	421975	5570972	sufol	160	48	M2
622	00TWG0667	421699	5570688	sufol	129	25	M2
623	00TWG0669	419823	5571556	sufol	203	31	M2
624	00TWG0670	419233	5571288	sufol	155	42	M2
625	00TWG0671	417059	5570677	sufol	126	23	M2
626	00TWG0672	416983	5570439	sufol	159	23	M2
627	00TWG0673	415887	5568029	sufol	186	34	M2
628	00TWG0676	417201	5569883	sufol	171	55	M2
629	00TWM0004	386140	5555107	subed	129	39	U7
630	00TWM0014	377773	5563102	sufol	109	24	M8
631	00TWM0015	377569	5562216	sufol	67	37	M8
632	00TWM0016	377509	5562180	sufol	98	19	M8
633	00TWM0016	377509	5562180	sufol	96	24	M8
634	00TWM0016	377509	5562180	sufol	82	27	M8
635	00TWM0017	377509	5562160	sufol	114	45	M8
636	00TWM0024	406679	5574769	sufol	115	77	M3
637	00TWM0025	405770	5574213	sufol	20	84	M3
638	00TWM0026	405702	5574059	sufol	292	77	M3
639	00TWM0027	405817	5574126	sufol	118	88	M3
640	00TWM0028	405582	5574408	sufol	98	89	M3
641	00TWM0029	405474	5574552	sufol	98	89	M3
642	00TWM0030	402790	5572432	sufol	39	10	U3
643	00TWM0031	402190	5576073	sufol	282	59	M4
644	00TWM0032	405397	5576648	sufol	91	70	M3
645	00TWM0033	405357	5576683	sufol	101	70	M3
646	00TWM0034	405758	5577158	sufol	177	16	M3
647	00TWM0035	404240	5576723	sufol	282	66	M4
648	00TWM0036	402811	5575052	sufol	261	23	M3
649	00TWM0037	401927	5574952	sufol	24	22	U3
650	00TWM0038	400764	5575315	sufol	201	54	U3
651	00TWM0040	352480	5580479	sufol	5	42	M13
652	00TWM0042	351663	5580226	sufol	10	41	M13
653	00TWM0043	351207	5580225	sufol	351	56	M13
654	00TWM0044	350970	5580173	sufol	345	37	M13
655	00TWM0045	349510	5578981	sufol	21	50	M13
656	01TWG006	363776	5600083	sufol	48	33	M10
657	01TWG008	374021	5604484	sufol	58	40	M10
658	01TWG008	374021	5604484	lu	60	6	M10
659	01TWG009	374859	5603460	sufol	66	56	M10
660	01TWG010	375253	5604164	sufol	20	44	M10
661	01TWG011	374049	5602766	sufol	69	68	M10

Number	Station[1,2]	Easting[3]	Northing[3]	Structure[4]	Azimuth[5]	Dip	Domain[6]
662	01TWG012	374067	5602234	sufol	23	58	M10
663	01TWG013	374931	5600091	sufol	78	43	M10
664	01TWG014	374820	5599646	sufol	68	39	M10
665	01TWG015	374337	5600866	sufol	88	59	M10
666	01TWG018	371040	5600298	sufol	292	78	M10
667	01TWG019	372321	5600514	sufol	262	59	M10
668	01TWG023	373431	5590156	sufol	30	13	M10
669	01TWG023	373431	5590156	lu	94	11	M10
670	01TWG024	373993	5589916	sufol	74	21	M10
671	01TWG024	373993	5589916	lu	94	9	M10
672	01TWG025	374777	5590946	sufol	0	0	M10
673	01TWG027	361562	5601212	sufol	8	15	M12
674	01TWG027	361562	5601212	lu	84	14	M12
675	01TWG028	364632	5601641	sufol	70	75	M12
676	01TWG029	363572	5604215	sufol	42	31	M12
677	01TWG029	363572	5604215	lu	65	6	M12
678	01TWG030	360740	5604045	sufol	68	65	M12
679	01TWG032	362544	5605197	sufol	42	47	M12
680	01TWG033	362472	5605783	sufol	62	30	M12
681	01TWG034	364206	5607630	sufol	126	31	M12
682	01TWG034	364206	5607630	sufol	96	47	M12
683	01TWG034	364206	5607630	sufol	263	74	M12
684	01TWG034	364206	5607630	l-fold1	265	1	M12
685	01TWG035	365105	5608195	sufol	63	56	M12
686	01TWG036	365652	5608825	sufol	326	70	M12
687	01TWG039	379221	5608328	sufol	104	40	M11
688	01TWG040	380131	5609317	sufol	0	50	M11
689	01TWG040	380131	5609317	l-fold1	107	32	M11
690	01TWG041	380096	5610065	sufol	22	35	M11
691	01TWG042	380584	5611410	sufol	126	47	M11
692	01TWG043	381341	5613636	sufol	342	26	M11
693	01TWG043	381341	5613636	l-fold1	357	10	M11
694	01TWG045	363447	5604237	sufol	16	20	M12
695	01TWG046	361805	5603840	sufol	264	16	M12
696	01TWG047	361398	5603742	sufol	91	86	M12
697	01TWG047	361398	5603742	lu	269	12	M12
698	01TWG048	360087	5603871	sufol	75	59	M12
699	01TWG048	360087	5603871	sufol	308	48	M12
700	01TWG048	360087	5603871	sufol	320	33	M12
701	01TWG048	360087	5603871	l-fold1	91	26	M12
702	01TWG048	360087	5603871	l-fold1	81	20	M12
703	01TWG048	360087	5603871	buax	322	31	M11
704	01TWG049	360971	5605253	sufol	77	50	M12
705	01TWG053	363246	5608512	sufol	41	42	M12
706	01TWG053	363246	5608512	lu	96	34	M12
707	01TWG054	363272	5608785	sufol	59	24	M12
708	01TWG054	363272	5608785	lu	70	6	M12
709	01TWG055	362739	5608867	sufol	0	0	M12
710	01TWG055	362739	5608867	lu	75	1	M12
711	01TWG056	362289	5609095	sufol	102	10	M12
712	01TWG057	361668	5609203	sufol	121	23	M12
713	01TWG058	360378	5609781	sufol	147	22	M12
714	01TWG058	360378	5609781	lu	276	31	M12
715	01TWG059	359973	5611286	sufol	84	19	M12
716	01TWG060	363171	5609998	sufol	209	21	M12
717	01TWG061	362717	5610639	sufol	119	31	M12

Number	Station[1,2]	Easting[3]	Northing[3]	Structure[4]	Azimuth[5]	Dip	Domain[6]
718	01TWG063	363633	5612909	sufol	236	33	M12
719	01TWG064	363461	5608323	sufol	191	16	M12
720	01TWG065	365213	5610068	sufol	155	33	M12
721	01TWG065	365213	5610068	l-fold1	211	32	M12
722	01TWG069	355372	5603771	sufol	252	59	M12
723	01TWG070	355442	5604446	sufol	111	90	M12
724	01TWG071	355640	5604261	sufol	266	74	M12
725	01TWG072	369749	5614313	sufol	233	40	M11
726	01TWG073	369309	5614923	sufol	32	44	M11
727	01TWG074	370618	5614894	sufol	310	23	M11
728	01TWG074	370618	5614894	sufol	320	80	M11
729	01TWG074	370618	5614894	buax	313	64	M11
730	01TWG075	370576	5615788	sufol	225	41	M11
731	01TWG076	369285	5616375	sufol	264	47	M11
732	01TWG077	367748	5618315	sufol	186	15	M11
733	01TWG078	367493	5618474	sufol	322	50	M11
734	01TWG080	370965	5610765	sufol	177	32	M11
735	01TWG081	370657	5609894	sufol	226	33	M11
736	01TWG081	370657	5609894	sufol	283	54	M11
737	01TWG081	370657	5609894	buax	232	31	M11
738	01TWG083	370731	5610412	sufol	241	49	M11
739	01TWG084	367033	5605245	l-fold1	218	33	M12
740	01TWG084	367033	5605245	sufol	53	72	M12
741	01TWG085	366487	5604571	sufol	90	42	M12
742	01TWG085	366487	5604571	sufol	125	68	M12
743	01TWG085	366487	5604571	buax	330	30	M12
744	01TWG089	374693	5609530	sufol	35	14	M11
745	01TWG090	375489	5611440	sufol	150	16	M11
746	01TWG092	375020	5611620	sufol	37	66	M11
747	01TWG094	375303	5613002	sufol	232	47	M11
748	01TWG095	375786	5612294	sufol	237	38	M11
749	01TWG096	375063	5614610	sufol	270	53	M11
750	01TWG097	374926	5614160	sufol	358	38	M11
751	01TWG099	373466	5614212	sufol	20	44	M11
752	01TWG100	374928	5614857	sufol	256	44	M11
753	01TWG101	375119	5615998	sufol	188	28	M11
754	01TWG102	373982	5620581	sufol	306	47	M11
755	01TWG103	372252	5620278	sufol	147	54	M11
756	01TWG104	372188	5620529	sufol	198	26	M11
757	01TWG105	372147	5620872	sufol	199	25	M11
758	01TWG106	371955	5621018	l-fold1	340	12	M11
759	01TWG106	371955	5621018	sufol	135	5	M11
760	01TWG106	371955	5621018	sufol	156	66	M11
761	01TWG107	370048	5625372	sufol	163	41	M11
762	01TWG108	370295	5624033	sufol	181	60	M11
763	01TWG109	375468	5621848	sufol	116	20	M11
764	01TWG111	376475	5622390	sufol	148	25	M11
765	01TWG112	376603	5624633	sufol	117	31	M11
766	01TWG113	350151	5580950	sufol	58	51	M13
767	01TWG114	350198	5580752	sufol	45	54	M13
768	01TWG115	350151	5580652	sufol	30	57	M13
769	01TWG116	350093	5580527	sufol	46	37	M13
770	01TWG116	350093	5580527	lu	110	32	M13
771	01TWG117	349807	5580603	sufol	0	55	M13
772	01TWG118	349640	5580571	lu	94	30	M13
773	01TWG118	349640	5580571	sufol	342	30	M13

Number	Station[1,2]	Easting[3]	Northing[3]	Structure[4]	Azimuth[5]	Dip	Domain[6]
774	01TWG120	349324	5580201	lu	130	25	M13
775	01TWG120	349324	5580201	sufol	4	31	M13
776	01TWG124	349274	5580525	sufol	341	60	M13
777	01TWG125	349443	5580571	sufol	345	50	M13
778	01TWG127	349488	5580469	sufol	328	46	M13
779	01TWG128	349251	5580671	sufol	345	24	M13
780	01TWG129	349410	5580883	sufol	338	37	M13
781	01TWG131	349317	5581122	sufol	0	0	M13
782	01TWG131	349317	5581122	lu	270	3	M13
783	01TWG132	349418	5581326	sufol	348	45	M13
784	01TWG132	349418	5581326	lu	91	34	M13
785	01TWG133	349503	5581275	sufol	304	30	M13
786	01TWG133	349503	5581275	lu	89	24	M13
787	01TWG134	349399	5581131	sufol	331	44	M13
788	01TWG135	349603	5580758	sufol	342	30	M13
789	01TWG135	349603	5580758	lu	90	30	M13
790	01TWG136	376681	5604766	sufol	199	31	M10
791	01TWG137	376604	5604108	l-fold1	156	5	M10
792	01TWG137	376604	5604108	sufol	138	42	M10
793	01TWG137	376604	5604108	sufol	339	21	M10
794	01TWG138	375838	5601723	sufol	60	34	M10
795	01TWG140	375790	5601305	sufol	29	19	M10
796	01TWG141	375888	5600281	sufol	110	51	M10
797	01TWG142	375862	5599885	sufol	60	30	M10
798	01TWG143	375640	5598300	sufol	80	28	M10
799	01TWG144	375695	5597646	sufol	80	24	M10
800	01TWG145	375783	5596970	sufol	104	36	M10
801	01TWG146	375923	5596250	sufol	100	51	M10
802	01TWG147	376021	5595847	sufol	119	61	M10
803	01TWG148	375961	5595367	sufol	110	27	M10
804	01TWG150	375971	5593882	sufol	56	23	M10
805	01TWG151	375515	5591364	lu	88	23	M10
806	01TWG151	375515	5591364	sufol	357	28	M10
807	01TWG155	336265	5556312	sufol	66	6	MM24
808	01TWG155	336265	5556312	lu	105	3	MM24
809	01TWG157	351378	5581646	sufol	350	57	M13
810	01TWG158	350878	5582170	sufol	358	40	M13
811	01TWG158	350878	5582170	lu	78	35	M13
812	01TWG159	350902	5582393	sufol	351	44	M13
813	01TWG160	351072	5582500	lu	74	33	M13
814	01TWG160	351072	5582500	sufol	358	34	M13
815	01TWG161	351096	5582373	sufol	15	33	M13
816	01TWG161	351096	5582373	lu	90	29	M13
817	01TWG162	351197	5582700	s-fol1	68	18	M13
818	01TWG162	351197	5582700	lu	92	21	M13
819	01TWG162	351197	5582700	sufol	8	23	M13
820	01TWG163	351083	5583135	sufol	5	25	M13
821	01TWG165	350574	5583677	sufol	9	52	M13
822	01TWG167	349997	5583316	sufol	1	52	M13
823	01TWG168	349902	5583235	lu	91	35	M13
824	01TWG168	349902	5583235	sufol	342	36	M13
825	01TWG169	349828	5582711	sufol	339	44	M13
826	01TWG169	349828	5582711	lu	83	25	M13
827	01TWG170	349645	5581458	sufol	333	38	M13
828	01TWG170	349645	5581458	lu	90	36	M13
829	01TWG171	350233	5580532	sufol	0	50	M13

Number	Station[1,2]	Easting[3]	Northing[3]	Structure[4]	Azimuth[5]	Dip	Domain[6]
830	01TWG171	350233	5580532	lu	89	50	M13
831	01TWG172	347948	5588761	lu	110	15	M14
832	01TWG172	347948	5588761	sufol	24	24	M14
833	01TWG173	348252	5588311	lu	98	10	M14
834	01TWG178	349260	5587241	sufol	317	38	M14
835	01TWG179	349258	5587929	sufol	320	20	M14
836	01TWG180	349258	5587929	sufol	328	41	M14
837	93sg004	340825	5564488	sufol	286	34	MM24
838	93sg005	340762	5564519	sufol	275	39	MM24
839	93sg006	340617	5564555	sufol	284	42	MM24
840	93sg007	340876	5564601	sufol	276	61	MM24
841	93sg008	340886	5564823	sufol	296	41	MM24
842	93sg009	340604	5565051	sufol	325	40	M19
843	93sg010	340127	5564833	sufol	292	46	MM24
844	93sg021	332046	5552504	sufol	28	15	M24
845	93sg022	332247	5551990	sufol	61	46	M24
846	93sg023	332267	5551608	sufol	332	22	M24
847	93sg025	333038	5552966	l-fold1	143	51	M24
848	93sg025	333038	5552966	buax	325	81	M24
849	93sg025	333038	5552966	sufol	35	52	M24
850	93sg026	333880	5553358	ju	162	76	M24
851	93sg026	333880	5553358	sufol	140	48	M24
852	93sg027	334123	5553759	ju	265	56	MM24
853	93sg028	334722	5553825	sufol	210	33	MM24
854	93sg028	334722	5553825	sufol	145	32	MM24
855	93sg028	334722	5553825	sufol	36	35	MM24
856	93sg029	335197	5554162	sufol	74	19	MM24
857	93sg029	335197	5554162	ju	110	9	MM24
858	93sg029	335197	5554162	buax	253	72	MM24
859	93sg029	335197	5554162	l-fold1	260	48	MM24
860	93sg030	336311	5553819	sufol	105	44	MM24
861	93sg031	337012	5553840	sufol	358	32	MM24
862	93sg033	336175	5554772	buax	344	30	MM24
863	93sg033	336175	5554772	l-fold1	107	28	MM24
864	93sg034	335235	5554421	lu	92	10	MM24
865	93sg034	335235	5554421	sufol	80	45	MM24
866	93sg036	336011	5555334	buax	39	61	MM24
867	93sg036	336011	5555334	sufol	16	19	MM24
868	93sg036	336011	5555334	lu	107	16	MM24
869	93sg036	336011	5555334	l-fold1	60	58	MM24
870	93sg037	336153	5556337	sufol	22	36	MM24
871	93sg038	336297	5556374	lu	111	2	MM24
872	93sg038	336297	5556374	sufol	310	16	MM24
873	93sg040	337107	5556500	buax	280	34	MM24
874	93sg040	337107	5556500	l-fold1	34	37	MM24
875	93sg041	339013	5557277	sufol	66	46	MM24
876	93sg044	339109	5558472	ju	225	82	M19
877	93sg044	339109	5558472	sufol	32	31	MM24
878	93sg044	339109	5558472	lu	135	15	MM24
879	93sg045	340596	5557438	lu	296	17	MM24
880	93sg045	340596	5557438	sufol	315	12	MM24
881	93sg047	342698	5559694	l-fold1	64	19	M19
882	93sg047	342698	5559694	sufol	15	62	M19
883	93sg047	342698	5559694	buax	19	42	M19
884	93sg076	331664	5553774	sufol	110	31	M24
885	93sg077	331705	5554056	sufol	44	26	M24

Number	Station[1,2]	Easting[3]	Northing[3]	Structure[4]	Azimuth[5]	Dip	Domain[6]
886	93sg078	331706	5554208	sufol	64	19	M24
887	93sg079	331735	5554547	sufol	45	34	MM24
888	93sg080	331732	5554871	sufol	85	27	MM24
889	93sg081	331958	5556587	sufol	220	34	MM24
890	93sg082	332020	5557163	sufol	290	9	MM24
891	93sg083	332342	5557106	sufol	67	20	MM24
892	93sg084	332427	5556859	sufol	85	17	MM24
893	93sg085	332891	5557595	sufol	300	16	MM24
894	93sg086	333157	5557584	sufol	273	42	MM24
895	93sg087	333339	5557712	sufol	220	16	MM24
896	93sg088	334373	5558908	sufol	220	14	MM24
897	93sg089	334673	5559169	sufol	282	52	MM24
898	93sg090	335049	5559526	sufol	236	15	MM24
899	93sg091	335272	5559646	sufol	18	29	MM24
900	93sg092	335453	5559857	sufol	321	57	MM24
901	93sg093	335628	5560078	l-fold1	15	38	MM24
902	93sg093	335628	5560078	buax	330	64	MM24
903	93sg093	335628	5560078	sufol	240	19	MM24
904	93sg093	335628	5560078	buax	327	39	MM24
905	93sg093	335628	5560078	l-fold1	19	38	MM24
906	93sg094	336082	5560690	sufol	34	69	MM24
907	93sg096	336863	5566726	buax	320	90	E5
908	93sg096	336863	5566726	l-fold1	312	74	E5
909	93sg097	336678	5566226	subed	35	59	E5
910	93sg100	329609	5548268	ju	25	90	M24
911	93sg101	329220	5547337	d	40	60	M24
912	93sg101	329220	5547337	ju	43	43	M24
913	93sg103	337439	5545206	sufol	283	67	M20
914	93sg104	337235	5545612	sufol	152	56	M20
915	93sg105	328778	5545780	ju	14	42	M24
916	93sg105	328778	5545780	d	101	75	M24
917	93sg107	339303	5548436	sufol	130	29	M20
918	93sg108	339232	5548638	lu	276	12	M20
919	93sg108	339232	5548638	sufol	70	9	M20
920	93sg110	339018	5550300	sufol	50	19	M20
921	93sg110	339018	5550300	lu	87	10	M20
922	93sg112	333615	5562473	lu	96	51	U11
923	93sg113	332294	5562379	ju	16	68	U11
924	93sg113	332294	5562379	sufol	82	61	U11
925	93sg113	332294	5562379	lu	111	39	U11
926	93sg113	332294	5562379	d	90	60	U11
927	93sg114	340473	5548277	sufol	108	79	M20
928	93sg118	342661	5549479	sufol	261	82	M20
929	93sg120	341908	5550337	sufol	294	36	M20
930	93sg123	336095	5556102	sufol	0	32	MM24
931	93sg125	337044	5557909	sufol	292	30	MM24
932	93sg126	336912	5557241	sufol	310	20	MM24
933	93sg133	336538	5555745	sufol	331	17	MM24
934	93sg133	336538	5555745	sufol	13	11	MM24
935	93sg133	336538	5555745	lu	100	5	MM24
936	93sg134	336665	5556006	sufol	14	36	MM24
937	93sg135	336864	5556171	lu	85	9	MM24
938	93sg135	336864	5556171	sufol	45	12	MM24
939	93sg135	336864	5556171	sufol	15	15	MM24
940	93sg137	338754	5557539	sufol	36	14	MM24
941	93sg138	339682	5557879	sufol	317	22	MM24

Number	Station[1,2]	Easting[3]	Northing[3]	Structure[4]	Azimuth[5]	Dip	Domain[6]
942	93sg138	339682	5557879	lu	111	10	MM24
943	93sg142	341444	5558212	sufol	310	76	M19
944	93sg142	341444	5558212	sufol	289	51	M19
945	93sg144	341673	5558696	ju	7	15	M19
946	93sg145	342538	5559523	sufol	15	62	M19
947	93sg146	0	0	sufol	316	63	M19
948	93sg147	344098	5561346	sufol	338	62	M18
949	93sg148	344829	5562391	sufol	330	37	M18
950	93sg149	346064	5563182	sufol	358	50	U10
951	93sg151	343210	5552285	sufol	128	89	M19
952	93sg153	342804	5553566	sufol	84	40	M19
953	93sg154	341697	5553476	sufol	108	45	M19
954	93sg154	341697	5553476	lu	278	5	M19
955	93sg157	334012	5549604	sufol	123	12	M24
956	93sg158	334382	5550512	ju	240	56	M24
957	93sg161	344574	5552280	ju	14	90	M19
958	93sg161	344574	5552280	ju	73	85	M19
959	93sg175	327711	5548956	sufol	220	23	U13
960	93sg182	340687	5564353	sufol	240	48	MM24
961	93sg184	340605	5564466	sufol	319	32	MM24
962	93sg185	340518	5564425	sufol	303	59	MM24
963	93sg186	340418	5564478	sufol	301	31	MM24
964	93sg187	340167	5564381	sufol	173	28	MM24
965	93sg188	339881	5564065	sufol	228	33	MM24
966	93tw002	336732	5565792	subed	235	55	E5
967	93tw003	336632	5565609	subed	125	70	E5
968	93tw003	336632	5565609	subed	125	70	E5
969	93tw007	335612	5566542	subed	330	60	U11
970	93tw012	336404	5564636	sufol	265	30	U11
971	93tw013	336782	5565729	subed	280	38	E5
972	93tw013	336782	5565729	ju	180	65	E5
973	93tw014	336439	5565283	subed	280	35	U11
974	93tw014	336439	5565283	subed	300	45	U11
975	93tw025	334821	5565458	subed	90	65	U11
976	93tw027	334536	5565484	subed	105	80	U11
977	93tw030	334290	5565716	sufol	126	80	U11
978	93tw035	333967	5566180	sufol	110	55	U11
979	93tw036	333439	5565953	subed	184	65	U12
980	93tw041	332810	5566434	subed	130	90	U12
981	93tw055	331954	5566482	subed	160	50	U12
982	93tw056	332028	5566227	subed	170	53	U12
983	93tw057	331846	5566410	subed	160	90	U12
984	93tw071	337097	5567649	subed	90	60	U11
985	93tw078	335770	5566131	subed	320	40	U11
986	93tw079	336326	5567059	subed	40	10	U11
987	93tw080	335442	5566622	subed	50	35	U11
988	93tw117	328202	5569098	sufol	280	85	U11
989	93tw131	329845	5568173	subed	290	85	U11
990	93tw132	329524	5568321	subed	100	90	U11
991	93tw135	328633	5567982	subed	80	80	U11
992	93tw137	327923	5568884	subed	95	80	U11
993	93tw184	331235	5569033	sufol	118	85	U11
994	93tw216	331991	5552354	sufol	298	6	M24
995	93tw218	329520	5549714	sufol	90	30	M24
996	93tw221	326724	5543961	sufol	173	30	U13
997	93tw227	327717	5549394	sufol	270	70	U13

Number	Station[1,2]	Easting[3]	Northing[3]	Structure[4]	Azimuth[5]	Dip	Domain[6]
998	93tw332	345655	5565089	sufol	128	55	U10
999	93tw469	352398	5576706	sufol	4	40	M13
1000	93tw472	350469	5576530	lu	100	15	M13
1001	93tw473	350672	5577255	sufol	36	35	M13
1002	93tw477	353163	5561878	sufol	146	25	M17
1003	93tw479	353764	5560715	sufol	138	25	M17
1004	93tw495	350373	5562794	subed	2	3	U9
1005	93tw501	349891	5562433	subed	98	90	U9
1006	93tw506	348304	5562934	subed	272	10	U9
1007	93tw527	347977	5563828	sufol	110	90	U9
1008	93tw527	347977	5563828	sufol	100	75	U9
1009	93tw528	347787	5563585	ju	120	90	U9
1010	93tw535	347940	5564524	sufol	90	75	U9
1011	93tw536	347850	5564485	sufol	92	70	U9
1012	93tw539	347889	5564589	sufol	102	45	U9
1013	93tw540	345518	5564237	sufol	294	55	U10
1014	93tw542	345632	5563914	sufol	300	45	U10
1015	93tw544	346424	5563302	sufol	328	45	U10
1016	93tw550	344943	5562418	sufol	340	45	M18
1017	93tw552	343916	5562161	sufol	325	50	M18
1018	93tw552	343916	5562161	sufol	340	50	M18
1019	93tw553	343826	5562161	sufol	350	70	M18
1020	93tw554	343731	5562240	sufol	338	50	M18
1021	93tw554	343731	5562240	sufol	350	65	M18
1022	93tw556	344481	5564629	sufol	348	55	M18
1023	93tw557	344287	5564206	sufol	340	52	M18
1024	93tw559	343704	5563783	sufol	0	50	M18
1025	93tw560	343459	5563483	sufol	355	50	M18
1026	93tw561	343253	5563076	sufol	345	45	M18
1027	93tw563	343721	5562705	sufol	334	45	M18
1028	93tw564	343847	5562695	sufol	40	40	M18
1029	93tw565	343918	5562696	sufol	330	55	M18
1030	93tw566	344016	5562709	sufol	6	45	M18
1031	93tw567	340733	5562823	sufol	192	90	MM24
1032	93tw567	340733	5562823	sufol	42	55	MM24
1033	93tw569	340216	5562002	sufol	288	45	MM24
1034	93tw571	340178	5561413	sufol	45	30	MM24
1035	93tw572	341462	5561768	sufol	340	55	M18
1036	93tw573	341402	5561907	sufol	332	30	M18
1037	93tw574	341388	5562173	sufol	40	45	M18
1038	93tw575	341416	5562535	sufol	8	30	M18
1039	93tw576	341619	5562752	sufol	74	65	M18
1040	93tw576	341619	5562752	sufol	340	30	M18
1041	93tw577	341724	5562849	sufol	280	5	M18
1042	93tw578	341891	5562968	sufol	266	5	M18
1043	93tw579	342214	5563168	sufol	55	40	M18
1044	93tw580	342437	5563462	sufol	320	50	M18
1045	93tw581	340655	5564331	sufol	290	60	MM24
1046	93tw582	340491	5564449	sufol	256	45	MM24
1047	93tw583	339965	5564143	sufol	292	26	MM24
1048	93tw584	340052	5563985	sufol	266	35	MM24
1049	93tw585	339773	5563206	sufol	270	50	MM24
1050	93tw586	340632	5563261	sufol	230	45	MM24
1051	93tw586	340632	5563261	sufol	215	45	MM24
1052	93tw586	340632	5563261	sufol	276	35	MM24
1053	93tw588	341063	5563348	sufol	60	15	MM24

Number	Station[1,2]	Easting[3]	Northing[3]	Structure[4]	Azimuth[5]	Dip	Domain[6]
1054	93tw590	341620	5563499	sufol	264	40	M18
1055	93tw592	341852	5563653	sufol	290	55	M18
1056	93tw595	338435	5563365	sufol	272	30	MM24
1057	93tw596	338471	5563468	sufol	325	55	MM24
1058	93tw598	339563	5562898	sufol	240	55	MM24
1059	93tw599	338897	5562291	sufol	340	75	MM24
1060	93tw600	336937	5561514	sufol	220	5	MM24
1061	93tw608	349569	5579023	sufol	40	38	M13
1062	93tw608	349569	5579023	sufol	30	55	M13
1063	93tw609	350948	5580154	sufol	20	55	M13
1064	93tw610	351150	5580234	sufol	20	42	M13
1065	93tw611	350604	5580216	sufol	3	56	M13
1066	93tw612	350230	5580469	sufol	18	58	M13
1067	93tw614	350438	5580850	sufol	5	45	M13
1068	93tw615	350653	5580893	sufol	0	45	M13
1069	93tw616	350891	5580820	sufol	30	46	M13
1070	93tw617	351307	5581399	sufol	336	50	M13
1071	93tw617	351307	5581399	sufol	355	35	M13
1072	93tw622	352904	5580492	sufol	20	45	M13
1073	93tw626	354139	5582601	sufol	2	35	M13
1074	93tw634	343084	5578350	sufol	125	40	M15
1075	93tw636	350048	5578150	sufol	22	75	M13
1076	93tw637	350480	5578268	sufol	10	40	M13
1077	93tw639	353299	5581425	sufol	350	45	M13
1078	93tw640	352801	5581135	sufol	340	45	M13
1079	93tw640	352801	5581135	sufol	5	65	M13
1080	93tw641	352580	5581584	sufol	30	45	M13
1081	93tw642	349481	5578775	sufol	32	60	M13
1082	93tw643	350097	5581399	l-fold1	90	30	M13
1083	93tw643	350097	5581399	sufol	40	25	M13
1084	93tw645	350018	5581435	sufol	350	40	M13
1085	93tw647	341181	5576576	sufol	158	10	M15
1086	93tw648	341190	5576726	sufol	310	30	M15
1087	93tw650	341576	5577443	sufol	0	45	M15
1088	93tw651	342097	5578306	sufol	32	25	M15
1089	93tw653	342702	5579373	sufol	56	20	M15
1090	93tw654	341468	5576871	sufol	190	30	M15
1091	93tw655	340987	5576941	sufol	30	18	M15
1092	93tw656	340963	5577297	sufol	75	50	M15
1093	93tw658	340883	5578293	sufol	50	25	M15
1094	93tw661	339429	5573558	sufol	235	20	M15
1095	93tw664	341216	5580473	sufol	220	5	M15
1096	93tw665	341296	5580305	sufol	10	10	M15
1097	93tw666	341551	5580772	sufol	345	15	M15
1098	93tw667	341598	5581078	sufol	296	25	M15
1099	93tw668	341678	5581258	sufol	310	30	M15
1100	93tw669	342252	5581023	sufol	315	30	M15
1101	93tw670	343782	5580829	sufol	294	30	M15
1102	93tw671	343623	5581146	sufol	310	15	M15
1103	93tw672	343814	5581239	sufol	280	45	M15
1104	93tw673	344261	5585057	sufol	250	25	M14
1105	93tw674	344864	5585493	sufol	30	25	M14
1106	93tw675	346067	5584753	sufol	325	35	M14
1107	93tw677	345831	5586776	sufol	28	15	M14
1108	93tw678	346411	5586721	sufol	300	25	M14
1109	93tw678	346411	5586721	sufol	302	45	M14

Number	Station[1,2]	Easting[3]	Northing[3]	Structure[4]	Azimuth[5]	Dip	Domain[6]
1110	93tw680	345977	5585565	sufol	300	30	M14
1111	93tw680	345977	5585565	sufol	305	35	M14
1112	93tw681	345968	5584914	sufol	328	15	M14
1113	93tw682	346282	5583359	sufol	312	25	M14
1114	93tw683	347648	5581906	sufol	319	55	M13
1115	93tw684	347892	5582395	sufol	355	30	M13
1116	93tw685	348407	5582532	sufol	322	25	M13
1117	93tw686	348754	5582405	sufol	336	45	M13
1118	94tw001	336447	5560989	sufol	304	15	MM24
1119	94tw001	336447	5560989	sufol	10	25	MM24
1120	94tw002	336923	5560521	sufol	0	20	MM24
1121	94tw002	336923	5560521	sufol	0	20	MM24
1122	94tw002	336923	5560521	buax	326	10	MM24
1123	94tw002	336923	5560521	buax	320	30	MM24
1124	94tw003	337171	5560409	sufol	264	32	MM24
1125	94tw004	337560	5559915	sufol	340	8	MM24
1126	94tw005	336586	5559280	sufol	318	20	MM24
1127	94tw006	336434	5559500	sufol	298	30	MM24
1128	94tw007	336163	5559711	sufol	274	15	MM24
1129	94tw008	336073	5560044	sufol	300	30	MM24
1130	94tw024	334773	5559303	sufol	288	60	MM24
1131	94tw025	335156	5558990	sufol	294	72	MM24
1132	94tw026	335224	5558912	sufol	216	35	MM24
1133	94tw027	335292	5558687	sufol	260	30	MM24
1134	94tw028	335203	5558726	l-fold1	60	10	MM24
1135	94tw028	335203	5558726	sufol	295	10	MM24
1136	94tw029	335033	5558714	sufol	30	40	MM24
1137	94tw030	334572	5558726	sufol	298	35	MM24
1138	94tw031	334276	5558866	sufol	226	25	MM24
1139	94tw039	354680	5562485	sufol	0	45	M17
1140	94tw040	355184	5561745	sufol	15	15	M17
1141	94tw040	355184	5561745	sufol	10	45	M17
1142	94tw041	355022	5560629	sufol	0	30	M17
1143	94tw042	354833	5560407	sufol	10	50	M17
1144	94tw044	352111	5558114	sufol	320	55	M17
1145	94tw045	352881	5558033	sufol	4	45	M17
1146	94tw046	352959	5557924	sufol	330	45	M17
1147	94tw047	353066	5557909	sufol	24	45	M17
1148	94tw048	353182	5557936	sufol	0	45	M17
1149	94tw049	353501	5557711	sufol	10	50	M17
1150	94tw061	355155	5562694	sufol	340	45	M17
1151	94tw062	355607	5562636	sufol	14	55	P2
1152	94tw065	355503	5563206	sufol	350	65	P2
1153	94tw066	355663	5563100	sufol	338	65	P2
1154	94tw067	355528	5561426	sufol	20	65	M17
1155	94tw068	356366	5563358	sufol	145	60	P2
1156	94tw070	356422	5559258	sufol	106	22	M17
1157	94tw071	356531	5559231	sufol	120	55	M17
1158	94tw072	0	0	sufol	112	55	M17
1159	94tw073	355463	5561544	sufol	65	20	M17
1160	94tw074	355399	5560847	sufol	293	20	M17
1161	94tw076	355263	5560349	sufol	354	32	M17
1162	94tw077	355159	5560219	sufol	24	30	M17
1163	94tw080	355406	5557953	sufol	2	56	M17
1164	94tw082	355746	5556850	sufol	15	40	M17
1165	94tw084	356214	5556217	sufol	350	30	P2

Number	Station[1,2]	Easting[3]	Northing[3]	Structure[4]	Azimuth[5]	Dip	Domain[6]
1166	94tw085	356117	5559521	sufol	160	35	M17
1167	94tw088	357051	5560999	sufol	340	40	P2
1168	94tw089	356941	5560210	sufol	240	45	P2
1169	94tw090	357081	5559836	sufol	244	30	P2
1170	94tw096	358593	5562098	sufol	324	45	M19
1171	94tw105	359336	5562049	sufol	290	78	M19
1172	94tw111	359896	5561540	sufol	145	66	P2
1173	94tw114	358663	5559555	sufol	244	25	P2
1174	94tw116	358400	5558997	sufol	150	45	P2
1175	94tw117	359642	5558065	sufol	174	50	P2
1176	94tw125	359369	5561127	sufol	110	60	P2
1177	94tw127	360031	5560041	sufol	270	30	M19
1178	94tw129	360296	5560763	sufol	228	40	P2
1179	94tw138	361038	5561348	lu	220	65	P2
1180	94tw138	361038	5561348	sufol	190	60	P2
1181	94tw139	361763	5560730	sufol	230	80	P2
1182	94tw144	361976	5561762	sufol	50	60	U5
1183	94tw144	361976	5561762	sufol	82	60	U5
1184	94tw173	360219	5563687	sufol	256	30	U5
1185	94tw184	365176	5565328	sufol	90	70	U6
1186	94tw186	365343	5565540	sufol	90	90	U6
1187	94tw204	364748	5565903	sufol	300	70	U6
1188	94tw216	361972	5569588	sufol	120	75	M8
1189	94tw221	361717	5569851	sufol	118	80	M8
1190	94tw223	361860	5569981	sufol	110	80	M8
1191	94tw225	362189	5570444	sufol	300	80	M8
1192	94tw233	362132	5570010	sufol	284	65	M8
1193	94tw234	362452	5570246	sufol	280	68	M8
1194	94tw235	362604	5570345	sufol	310	62	M8
1195	94tw239	362130	5570719	sufol	120	90	M8
1196	94tw240	361929	5570548	sufol	292	60	M8
1197	94tw242	336060	5561543	sufol	280	25	MM24
1198	94tw243	335288	5560884	sufol	300	15	MM24
1199	94tw244	332665	5559117	sufol	0	22	MM24
1200	94tw245	332438	5558500	sufol	300	10	MM24
1201	95tw072	356785	5606153	sufol	280	12	M12
1202	95tw074	357498	5606600	sufol	30	10	M12
1203	95tw074	357498	5606600	sufol	80	18	M12
1204	95tw077	356051	5603911	sufol	280	44	M12
1205	95tw084	358865	5603885	sufol	318	23	M12
1206	95tw085	359914	5603247	sufol	230	20	M12
1207	95tw086	360124	5603854	sufol	335	45	M12
1208	95tw088	360120	5603854	l-fold1	110	20	M12
1209	95tw088	360120	5603854	sufol	44	30	M12
1210	95tw089	360026	5604225	sufol	70	15	M12
1211	95tw091	361016	5605248	sufol	64	32	M12
1212	95tw091	361016	5605248	l-fold1	180	8	M12
1213	95tw093	363856	5607725	sufol	54	18	M12
1214	95tw096	363500	5608324	sufol	172	26	M12
1215	95tw098	363000	5608220	sufol	202	45	M12
1216	95tw099	363274	5608940	sufol	70	15	M12
1217	95tw101	363147	5610094	sufol	110	15	M12
1218	95tw102	362962	5615789	sufol	72	30	M12
1219	97TWE0002	331479	5554524	sufol	90	25	MM24
1220	97TWE0003	331349	5554705	sufol	85	15	MM24
1221	97TWE0004	331425	5554863	lu	250	15	MM24

Number	Station[1,2]	Easting[3]	Northing[3]	Structure[4]	Azimuth[5]	Dip	Domain[6]
1222	97TWE0004	331425	5554863	sufol	110	20	MM24
1223	97TWE0005	331292	5556607	sufol	170	25	MM24
1224	97TWE0005	331292	5556607	lu	270	25	MM24
1225	97TWE0006	331379	5556797	sufol	245	20	MM24
1226	97TWE0006	331379	5556797	lu	285	18	MM24
1227	97TWE0007	331632	5557395	sufol	90	25	MM24
1228	97TWE0008	331718	5557486	lu	285	20	MM24
1229	97TWE0008	331718	5557486	sufol	245	30	MM24
1230	97TWE0009	332131	5557800	lu	275	0	MM24
1231	97TWE0009	332131	5557800	sufol	95	15	MM24
1232	97TWE0010	332360	5558180	sufol	245	10	MM24
1233	97TWE0012	332350	5558680	lu	290	10	MM24
1234	97TWE0012	332350	5558680	sufol	75	10	MM24
1235	97TWE0013	332511	5558957	lu	120	15	MM24
1236	97TWE0013	332511	5558957	sufol	20	20	MM24
1237	97TWE0014	333108	5559329	sufol	105	20	MM24
1238	97TWE0016	333932	5559282	lu	100	5	MM24
1239	97TWE0016	333932	5559282	sufol	100	18	MM24
1240	97TWE0017	334262	5559677	sufol	320	15	MM24
1241	97TWE0018	334553	5569992	lu	310	5	MM24
1242	97TWE0018	334553	5569992	sufol	350	10	MM24
1243	97TWE0019	335252	5560736	sufol	350	25	MM24
1244	97TWE0020	335759	5561286	sufol	330	15	MM24
1245	97TWE0021	336017	5561519	sufol	245	20	MM24
1246	97TWE0022	338206	5562388	sufol	245	25	MM24
1247	97TWE0023	338378	5562471	sufol	255	28	MM24
1248	97TWE0024	338375	5563178	sufol	255	40	MM24
1249	97TWE0025	337911	5563108	lu	290	14	MM24
1250	97TWE0025	337911	5563108	sufol	245	20	MM24
1251	97TWE0027	336307	5563358	sufol	245	32	MM24
1252	97TWE0027	336307	5563358	lu	290	20	MM24
1253	97TWE0028	336858	5563378	sufol	240	28	MM24
1254	97TWE0028	336858	5563378	lu	275	15	MM24
1255	97TWE0029	336851	5563858	lu	290	10	MM24
1256	97TWE0029	336851	5563858	sufol	270	35	MM24
1257	97TWE0030	337036	5564159	sufol	290	35	MM24
1258	97TWE0030	337036	5564159	lu	100	5	MM24
1259	97TWE0031	337754	5564810	sufol	245	40	MM24
1260	97TWE0032	337926	5565139	sufol	135	30	MM24
1261	97TWE0033	340797	5564439	sufol	240	45	MM24
1262	97TWE0034	339994	5563228	sufol	65	47	MM24
1263	97TWE0034	339994	5563228	lu	270	38	MM24
1264	97TWE0035	339599	5563197	lu	105	25	MM24
1265	97TWE0035	339599	5563197	sufol	75	47	MM24
1266	97TWE0036	339476	5562899	sufol	240	35	MM24
1267	97TWE0037	340072	5562546	sufol	250	43	MM24
1268	97TWE0038	340568	5562135	sufol	265	35	MM24
1269	97TWE0038	340568	5562135	lu	285	20	MM24
1270	97TWE0040	338939	5562292	sufol	250	30	MM24
1271	97TWE0041	336314	5560802	sufol	295	42	MM24
1272	98TWG0001	339657	5563689	sufol	265	51	MM24
1273	98TWG0002	339292	5563456	sufol	286	38	MM24
1274	98TWG0003	343362	5564229	sufol	322	35	MM24
1275	98TWG0006	341940	5563570	sufol	267	56	MM24
1276	98TWG0009	341535	5563478	sufol	217	55	MM24
1277	98TWG0012	336622	5563479	sufol	264	26	MM24

Number	Station[1,2]	Easting[3]	Northing[3]	Structure[4]	Azimuth[5]	Dip	Domain[6]
1278	98TWG0013	336617	5563515	sufol	280	13	MM24
1279	98TWG0013	336617	5563515	lu	303	5	MM24
1280	98TWG0014	336362	5563465	sufol	240	39	MM24
1281	98TWG0015	336319	5563421	sufol	280	33	MM24
1282	98TWG0015	336319	5563421	l-fold1	95	70	MM24
1283	98TWG0016	336423	5563465	sufol	273	25	MM24
1284	98TWG0017	337454	5564199	sufol	260	33	MM24
1285	98TWG0018	337617	5564249	sufol	260	30	MM24
1286	98TWG0020	338731	5564830	sufol	280	45	MM24
1287	98TWG0021	338697	5564840	sufol	300	47	MM24
1288	98TWG0023	340005	5564834	sufol	290	30	MM24
1289	98TWG0033	335951	5560679	sufol	350	10	MM24
1290	98TWG0035	337711	5561501	sufol	278	9	MM24
1291	98TWG0037	337426	5561288	sufol	310	40	MM24
1292	98TWG0038	337240	5561226	lu	290	25	MM24
1293	98TWG0038	337240	5561226	sufol	150	30	MM24
1294	98TWG0040	336580	5560450	sufol	130	15	MM24
1295	98TWG0044a	336062	5560519	sufol	270	35	MM24
1296	98TWG0044b	335736	5560160	sufol	104	15	MM24
1297	98TWG0045	335288	5559686	sufol	260	25	MM24
1298	98TWG0046a	334836	5559319	sufol	320	32	MM24
1299	98TWG0046b	334505	5558980	sufol	277	60	MM24
1300	98TWG0051	333264	5557762	sufol	300	15	MM24
1301	98TWG0052	332937	5557384	sufol	210	12	MM24
1302	98TWG0052	332937	5557384	lu	290	11	MM24
1303	98TWG0053	332626	5557444	sufol	200	35	MM24
1304	98TWG0053	332626	5557444	lu	270	30	MM24
1305	98TWG0054	332341	5556759	sufol	240	26	MM24
1306	98TWG0060	342230	5563197	sufol	330	45	M18
1307	98TWG0061	342499	5562981	sufol	333	50	M18
1308	98TWG0062	342526	5562949	sufol	344	18	M18
1309	98TWG0063	342259	5562915	sufol	350	34	M18
1310	98TWG0065	342783	5562799	sufol	340	46	M18
1311	98TWG0070	340441	5579815	sufol	104	24	M15
1312	98TWG0070	340441	5579815	lu	295	1	M15
1313	98TWG0071b	340698	5580081	sufol	130	20	M15
1314	98TWG0077	341768	5581215	sufol	300	26	M15
1315	98TWG0080	331621	5538728	sufol	315	16	M22
1316	98TWG0080	331621	5538728	l-fold2	126	15	M22
1317	98TWG0080	331621	5538728	l-fold1	38	24	M22
1318	98TWG0085	334373	5558168	sufol	220	11	MM24
1319	98TWG0086	334613	5557985	sufol	270	29	MM24
1320	98TWG0087	334841	5557916	sufol	340	28	MM24
1321	98TWG0087	334841	5557916	sufol	310	21	MM24
1322	98TWG0092	340020	5562009	sufol	210	13	MM24
1323	98TWG0094	339133	5560960	sufol	156	40	MM24
1324	98TWG0101	332512	5551868	sufol	60	45	M24
1325	98TWG0105	336283	5556600	sufol	320	23	MM24
1326	98TWG0109	336266	5556303	lu	286	11	MM24
1327	98TWG0109	336266	5556303	sufol	170	14	MM24
1328	98TWG0114	336021	5556737	sufol	242	25	MM24
1329	98TWG0122	335406	5557800	sufol	284	20	MM24
1330	98TWG0132	336207	5558860	sufol	299	46	MM24
1331	98TWG0134	336652	5558698	sufol	298	22	MM24
1332	98TWG0135	336798	5558657	sufol	252	22	MM24
1333	98TWG0152	339551	5557937	sufol	345	25	MM24

Number	Station[1,2]	Easting[3]	Northing[3]	Structure[4]	Azimuth[5]	Dip	Domain[6]
1334	98TWG0154	340697	5564347	sufol	270	27	MM24
1335	98TWG0158	340388	5564347	sufol	335	55	MM24
1336	98TWG0159	340164	5564293	sufol	270	27	MM24
1337	98TWG0164	338256	5563534	sufol	288	47	MM24
1338	98TWG0170	331171	5550157	sufol	30	40	M24
1339	98TWG0171	331873	5552550	sufol	184	20	M24
1340	98TWG0172	331873	5552500	sufol	112	30	M24
1341	98TWG0175	333002	5552942	sufol	50	29	M24
1342	98TWG0177	333561	5553464	sufol	10	71	M24
1343	98TWG0181	335265	5554222	sufol	68	15	MM24
1344	98TWG0181	335265	5554222	l-ss	114	14	MM24
1345	98TWG0183	336317	5553819	sufol	99	31	MM24
1346	98TWG0184	336691	5553796	sufol	14	40	MM24
1347	98TWG0185	337012	5553852	lu	120	23	MM24
1348	98TWG0185	337012	5553852	sufol	60	24	MM24
1349	98TWG0186	336117	5553956	sufol	136	24	MM24
1350	98TWG0193	334776	5553397	sufol	62	53	M24
1351	98TWG0194	334781	5553431	sufol	39	32	M24
1352	98TWG0195	335118	5553513	sufol	60	37	M24
1353	98TWG0225	334805	5557065	sufol	355	34	MM24
1354	98TWG0229	334314	5556737	sufol	242	22	MM24
1355	98TWG0229	334314	5556737	lu	256	17	MM24
1356	98TWG0231	334545	5556274	sufol	200	17	MM24
1357	98TWG0233	334847	5556158	lu	260	0	MM24
1358	98TWG0233	334847	5556158	sufol	0	0	MM24
1359	98TWG0235	339157	5557089	sufol	302	20	MM24
1360	98TWG0237	338432	5556169	sufol	340	4	MM24
1361	98TWG0247	337498	5556741	sufol	323	24	MM24
1362	98TWG0251	336895	5560407	sufol	328	21	MM24
1363	98TWG0255	337380	5560420	sufol	242	26	MM24
1364	98TWG0273	340106	5557456	sufol	30	10	MM24
1365	98TWG0277	335576	5555441	sufol	101	33	MM24
1366	98TWG0279	335216	5555808	sufol	353	35	MM24
1367	98TWG0281	334886	5555670	sufol	356	32	MM24
1368	98TWG0282	334760	5555873	sufol	352	27	MM24
1369	98TWG0284	334193	5555733	sufol	21	18	MM24
1370	98TWG0285	334195	5555943	sufol	0	0	MM24
1371	98TWG0288	333351	5555731	sufol	0	0	MM24
1372	98TWG0288	333351	5555731	lu	290	1	MM24
1373	98TWG0289	333184	5555430	sufol	40	34	MM24
1374	98TWG0290	333387	5555261	sufol	0	0	MM24
1375	98TWG0291	333697	5555241	lu	282	14	MM24
1376	98TWG0291	333697	5555241	sufol	0	0	MM24
1377	98TWG0293	334059	5555170	sufol	134	6	MM24
1378	98TWG0293	334059	5555170	lu	281	5	MM24
1379	98TWG0298	332698	5553068	sufol	64	48	M24
1380	98TWG0299	333280	5554140	sufol	102	22	MM24
1381	98TWG0300	333205	5554116	sufol	180	18	MM24
1382	98TWG0301	333520	5554140	sufol	142	18	MM24
1383	98TWG0302	333700	5554160	sufol	185	15	MM24
1384	98TWG0302	333700	5554160	lu	282	14	MM24
1385	98TWG0303	333840	5554150	sufol	204	5	MM24
1386	98TWG0307	333983	5553001	sufol	54	30	M24
1387	98TWG0309	333076	5552650	sufol	19	59	M24
1388	98TWG0310	333008	5552919	sufol	29	54	M24
1389	98TWG0311	332153	5551699	sufol	74	17	M24

Number	Station[1,2]	Easting[3]	Northing[3]	Structure[4]	Azimuth[5]	Dip	Domain[6]
1390	98TWG0314	334801	5553458	sufol	38	52	M24
1391	98TWG0315	334837	5553661	sufol	17	22	MM24
1392	98TWG0318	335320	5553790	sufol	70	45	MM24
1393	98TWG0319	335250	5553750	sufol	71	42	MM24
1394	98TWG0321	335585	5553441	sufol	12	33	MM24
1395	98TWG0327	334800	5552910	sufol	33	30	M24
1396	98TWG0328	334777	5552962	sufol	73	53	M24
1397	98TWG0329	333610	5553235	sufol	20	47	M24
1398	98TWG0330	333641	5553193	sufol	12	46	M24
1399	98TWG0336	337020	5553829	sufol	337	33	MM24
1400	98TWG0336	337020	5553829	lu	271	35	MM24
1401	98TWG0339	336497	5553673	sufol	76	28	MM24
1402	98TWG0340	336517	5554287	sufol	6	36	MM24
1403	98TWG0343	336449	5554895	lu	104	19	MM24
1404	98TWG0350	335449	5554189	sufol	284	32	MM24
1405	98TWG0357	340878	5564572	sufol	280	27	MM24
1406	98TWG0358	336088	5555680	sufol	90	23	MM24
1407	98TWG0361	336140	5556248	sufol	16	28	MM24
1408	98TWG0362	336220	5556330	sufol	268	23	MM24
1409	98TWG0372	336820	5556982	sufol	320	23	MM24
1410	98TWG0404	338138	5554045	sufol	85	48	MM24
1411	98TWG0411	337236	5557063	sufol	325	18	MM24
1412	98TWG0452	341307	5558633	sufol	7	21	MM24
1413	98TWG0461	342271	5558952	sufol	322	23	M19
1414	98TWG0464	342572	5559550	sufol	28	21	M19
1415	98TWG0499	343949	5556820	sufol	0	26	M19
1416	98TWG0500	344106	5557054	sufol	251	16	M19
1417	98TWG0501	344088	5557350	sufol	325	26	M19
1418	98TWG0502	343969	5557467	sufol	350	42	M19
1419	98TWG0510	341970	5552176	lu	89	34	M20
1420	98TWG0510	341970	5552176	sufol	356	36	M20
1421	98TWG0527	333144	5553220	sufol	31	39	M24
1422	98TWG0529	333126	5553656	sufol	45	23	M24
1423	98TWG0533	332353	5554436	sufol	292	34	MM24
1424	99TWF1702	331702	5542745	lu	90	35	M22
1425	99TWF1702	331702	5542745	sufol	8	38	M22
1426	99TWG0009	331978	5551055	sufol	242	6	M24
1427	99TWG0009	331978	5551055	lu	250	17	M24
1428	99TWG0015	330928	5549695	lu	265	0	M24
1429	99TWG0018	330792	5549400	sufol	270	10	M24
1430	99TWG0042	332603	5542734	sufol	150	30	M22
1431	99TWG0044	332200	5542745	sufol	332	7	M22
1432	99TWG0044	332200	5542745	l-fold1	110	35	M22
1433	99TWG0044	332200	5542745	l-fold1	295	19	M22
1434	99TWG0044	332200	5542745	l-fold1	300	10	M22
1435	99TWG0044	332200	5542745	l-fold1	325	2	M22
1436	99TWG0044	332200	5542745	l-fold1	120	4	M22
1437	99TWG0044	332200	5542745	l-fold1	135	7	M22
1438	99TWG0047	328952	5547796	sufol	90	25	M24
1439	99TWG0049	329141	5548865	sufol	90	41	M24
1440	99TWG0049	329141	5548865	sufol	50	50	M24
1441	99TWG0050	329424	5549355	sufol	335	13	M24
1442	99TWG0051	329531	5549768	sufol	285	34	M24
1443	99TWG0055	338441	5547220	sufol	74	27	M20
1444	99TWG0055	338441	5547220	l-fold1	92	47	M20
1445	99TWG0056	337459	5548061	sufol	105	54	M20

Number	Station[1,2]	Easting[3]	Northing[3]	Structure[4]	Azimuth[5]	Dip	Domain[6]
1446	99TWG0077	339113	5548473	sufol	15	13	M20
1447	99TWG0081	338758	5547216	sufol	125	14	M20
1448	99TWG0087	327659	5548492	sufol	227	17	U13
1449	99TWG0087	327659	5548492	sufol	215	16	U13
1450	99TWG0090	328083	5549722	sufol	285	35	U13
1451	99TWG0104	330225	5541592	sufol	71	37	M22
1452	99TWG0106	330842	5541767	sufol	348	17	M22
1453	99TWG0109	331616	5541676	sufol	43	14	M22
1454	99TWG0112	332633	5541694	lu	81	11	M22
1455	99TWG0113	333361	5541941	sufol	47	25	M22
1456	99TWG0116	332669	5542658	lu	277	3	M22
1457	99TWG0116	332669	5542658	sufol	143	9	M22
1458	99TWG0121	330633	5538862	sufol	321	7	M22
1459	99TWG0122	330677	5539080	sufol	58	21	M22
1460	99TWG0124	331449	5538963	sufol	330	11	M22
1461	99TWG0126	331420	5539579	sufol	203	7	M22
1462	99TWG0127	331835	5539940	sufol	8	12	M22
1463	99TWG0128	332317	5540128	sufol	90	75	M22
1464	99TWG0129	332759	5541458	lu	90	15	M22
1465	99TWG0130	333981	5542974	sufol	22	32	M22
1466	99TWG0131	334242	5541830	sufol	90	10	M22
1467	99TWG0134a	334584	5541168	lu	95	10	M22
1468	99TWG0134a	334584	5541168	sufol	58	14	M22
1469	99TWG0134b	334385	5541208	lu	94	11	M22
1470	99TWG0134b	334385	5541208	sufol	47	28	M22
1471	99TWG0135	336580	5541243	sufol	160	17	M22
1472	99TWG0135	336580	5541243	lu	265	12	M22
1473	99TWG0138	332460	5537678	sufol	354	27	M22
1474	99TWG0139	332490	5538525	sufol	14	1	M22
1475	99TWG0140	332298	5538980	sufol	350	25	M22
1476	99TWG0140	332298	5538980	lu	86	15	M22
1477	99TWG0141	332670	5538157	sufol	340	33	M22
1478	99TWG0142	332715	5538919	sufol	30	47	M22
1479	99TWG0144	333173	5536671	sufol	326	26	M22
1480	99TWG0145	333420	5535876	sufol	43	8	M22
1481	99TWG0146	333320	5535067	sufol	55	21	M22
1482	99TWG0147	332142	5537149	sufol	45	21	M22
1483	99TWG0147	332142	5537149	lu	103	7	M22
1484	99TWG0148	333518	5525636	sufol	26	53	M22
1485	99TWG0149	339093	5527979	sufol	156	17	M22
1486	99TWG0151	338932	5533376	sufol	14	8	M22
1487	99TWG0151	338932	5533376	lu	100	8	M22
1488	99TWG0152	338726	5534541	lu	92	3	M22
1489	99TWG0152	338726	5534541	sufol	290	9	M22
1490	99TWG0153	338434	5534661	lu	105	4	M22
1491	99TWG0153	338434	5534661	sufol	18	4	M22
1492	99TWG0154	338613	5537706	sufol	40	20	M22
1493	99TWG0154	338613	5537706	lu	96	20	M22
1494	99TWG0155	338600	5538314	sufol	62	58	M22
1495	99TWG0155	338600	5538314	lu	86	25	M22
1496	99TWG0156	338998	5538772	sufol	92	7	M22
1497	99TWG0157	338966	5537520	lu	100	6	M22
1498	99TWG0157	338966	5537520	sufol	320	10	M22
1499	99TWG0158	338946	5537520	lu	0	0	M22
1500	99TWG0158	338946	5537520	sufol	280	9	M22
1501	99TWG0161	339864	5549523	sufol	118	48	M20

Number	Station[1,2]	Easting[3]	Northing[3]	Structure[4]	Azimuth[5]	Dip	Domain[6]
1502	99TWG0162	340050	5549735	lu	278	11	M20
1503	99TWG0167	341753	5549333	sufol	141	38	M20
1504	99TWG0170	342678	5549128	sufol	265	85	M20
1505	99TWG0172	342574	5549625	sufol	72	21	M20
1506	99TWG0173	342671	5550188	sufol	140	20	M20
1507	99TWG0178	343100	5551071	sufol	319	20	M20
1508	99TWG0179	342666	5550960	lu	86	5	M20
1509	99TWG0181	342289	5551005	lu	104	26	M20
1510	99TWG0181	342289	5551005	sufol	339	26	M20
1511	99TWG0187	342088	5551995	sufol	38	35	M20
1512	99TWG0189	341535	5551364	lu	105	14	M20
1513	99TWG0191	341392	5551062	sufol	336	15	M20
1514	99TWG0195	340987	5551958	sufol	50	25	M20
1515	99TWG0195	340987	5551958	lu	86	9	M20
1516	99TWG0196	340988	5552124	sufol	306	56	M20
1517	99TWG0206	345194	5553585	sufol	33	55	M19
1518	99TWG0207	345026	5553646	l-fold1	145	70	M19
1519	99TWG0207	345026	5553646	l-fold1	115	65	M19
1520	99TWG0207	345026	5553646	l-fold1	103	68	M19
1521	99TWG0207	345026	5553646	l-fold1	118	55	M19
1522	99TWG0207	345026	5553646	l-fold1	104	64	M19
1523	99TWG0207	345026	5553646	l-fold1	166	38	M19
1524	99TWG0207	345026	5553646	l-fold1	183	48	M19
1525	99TWG0207	345026	5553646	l-fold1	204	62	M19
1526	99TWG0207	345026	5553646	l-fold1	193	60	M19
1527	99TWG0207	345026	5553646	l-fold1	211	43	M19
1528	99TWG0207	345026	5553646	l-fold1	190	50	M19
1529	99TWG0207	345026	5553646	l-fold1	113	73	M19
1530	99TWG0228	351972	5557861	sufol	300	45	M17
1531	99TWG0228	351972	5557861	sufol	304	40	M17
1532	99TWG0230	352273	5558920	sufol	340	43	M17
1533	99TWG0233	354263	5561933	sufol	348	39	M17
1534	99TWG0243	344016	5561153	sufol	332	60	M18
1535	99TWG0244	344016	5560964	sufol	325	75	M18
1536	99TWG0246	342709	5559296	sufol	0	23	M19
1537	99TWG0253	343590	5558623	sufol	343	30	M19
1538	99TWG0253	343590	5558623	l-fold1	34	30	M19
1539	99TWG0254	342926	5558681	sufol	335	30	M19
1540	99TWG0255	343229	5558198	sufol	290	44	M19
1541	99TWG0256	343382	5557895	sufol	305	36	M19
1542	99TWG0259	344110	5558224	sufol	312	35	M19
1543	99TWG0260	344098	5558429	sufol	350	30	M19
1544	99TWG0261	344163	5558582	sufol	299	70	M19
1545	99TWG0261	344163	5558582	sufol	80	53	M19
1546	99TWG0262	344133	5558753	sufol	313	59	M19
1547	99TWG0263	344272	5559303	sufol	311	50	M19
1548	99TWG0264	344341	5559780	sufol	323	85	M19
1549	99TWG0266	344496	5560312	sufol	10	70	M19
1550	99TWG0267	344449	5560558	sufol	350	39	M19
1551	99TWG0279	346573	5556090	sufol	38	45	M19
1552	99TWG0280	346045	5556546	sufol	9	45	M19
1553	99TWG0282	345475	5556570	sufol	26	45	M19
1554	99TWG0283	345306	5556382	sufol	304	40	M19
1555	99TWG0284	344888	5556414	sufol	338	26	M19
1556	99TWG0285	344887	5556883	sufol	153	86	M19
1557	99TWG0286	344594	5556747	sufol	340	45	M19

Number	Station[1,2]	Easting[3]	Northing[3]	Structure[4]	Azimuth[5]	Dip	Domain[6]
1558	99TWG0287	344939	5557082	l-fold1	130	15	M19
1559	99TWG0287	344939	5557082	sufol	322	49	M19
1560	99TWG0289	343542	5557137	sufol	343	40	M19
1561	99TWG0297	344863	5555983	sufol	356	39	M19
1562	99TWG0299	344958	5555009	sufol	110	74	M19
1563	99TWG0303	345653	5555651	sufol	352	45	M19
1564	99TWG0306	345581	5554307	sufol	94	47	M19
1565	99TWG0313	346885	5554785	sufol	45	90	P2
1566	99TWG0329	351831	5557807	sufol	310	50	M17
1567	99TWG0330	351827	5558224	sufol	350	45	M17
1568	99TWG0332	352828	5560278	sufol	353	64	M17
1569	99TWG0333	352265	5559866	sufol	317	43	M17
1570	99TWG0334	352591	5560363	sufol	295	67	M17
1571	99TWG0346	350596	5562333	subed	80	64	U9
1572	99TWG0353	346880	5553505	sufol	190	47	P2
1573	99TWG0376	347309	5541547	sufol	25	39	M22
1574	99TWG0379	350070	5541878	sufol	75	25	M19
1575	99TWG0380	350933	5541106	sufol	55	8	M22
1576	99TWG0380	350933	5541106	sufol	347	20	M22
1577	99TWG0380	350933	5541106	lu	105	4	M22
1578	99TWG0381	351376	5540587	sufol	145	10	M22
1579	99TWG0383	352960	5542150	sufol	108	27	P2
1580	99TWG0385	351841	5541985	sufol	78	20	P2
1581	99TWG0386	352652	5542996	sufol	86	19	P2
1582	99TWG0387	353278	5543071	sufol	79	20	M16
1583	99TWG0387	353278	5543071	lu	94	3	M16
1584	99TWG0388	353470	5542916	sufol	102	26	M16
1585	99TWG0389	353615	5543179	sufol	63	10	M16
1586	99TWG0390	354057	5543353	sufol	100	36	M16
1587	99TWG0390	354057	5543353	l-fold1	82	9	M16
1588	99TWG0391	352060	5542753	sufol	105	20	P2
1589	99TWG0406	338989	5567422	subed	345	56	E2
1590	99TWG0407	339031	5567237	subed	314	75	E2
1591	99TWG0412	340082	5567152	sufol	345	60	M23
1592	99TWG0414	339922	5566543	sufol	340	39	M23
1593	99TWG0423	349234	5550937	sufol	272	88	P2
1594	99TWG0424	348939	5550748	sufol	55	85	P2
1595	99TWG0434	353164	5556568	sufol	314	74	M17
1596	99TWG0435	353288	5556890	sufol	317	35	M17
1597	99TWG0436	353568	5557240	sufol	313	73	M17
1598	99TWG0439	354758	5558663	sufol	354	29	M17
1599	99TWG0441	354327	5558340	sufol	349	65	M17
1600	99TWG0442	353842	5557697	sufol	336	64	M17
1601	99TWG0443	353910	5558209	lu	135	45	M17
1602	99TWG0443	353910	5558209	sufol	315	80	M17
1603	99TWG0445	352587	5556712	sufol	336	47	M17
1604	99TWG0457	354845	5556925	sufol	88	75	M17
1605	99TWG0458	355064	5557507	sufol	5	64	M17
1606	99TWG0462	356227	5556211	sufol	318	29	P2
1607	99TWG0473	350480	5561150	subed	300	90	U9
1608	99TWG0477	345425	5564100	sulay	315	82	U10
1609	99TWG0478	345595	5564300	sufol	268	60	U10
1610	99TWG0478	345595	5564300	sulay	355	59	U10
1611	99TWG0478	345595	5564300	sufol	293	55	U10
1612	99TWG0478	345595	5564300	sulay	19	65	U10
1613	99TWG0479	345790	5564375	sufol	279	69	U10

Number	Station[1,2]	Easting[3]	Northing[3]	Structure[4]	Azimuth[5]	Dip	Domain[6]
1614	99TWG0480	346000	5564450	sufol	311	61	U10
1615	99TWG0481	346180	5564190	sufol	313	61	U10
1616	99TWG0481	346180	5564190	sulay	25	76	U10
1617	99TWG0482	345810	5563995	sufol	287	44	U10
1618	99TWG0483	345620	5564110	sufol	318	72	U10
1619	99TWG0483	345620	5564110	sufol	302	76	U10
1620	99TWG0484	346600	5563225	sufol	320	30	U10
1621	99TWG0485	345000	5562375	sufol	322	48	M18
1622	99TWG0487	355900	5553300	sufol	115	84	M16
1623	99TWG0488	355850	5553675	sufol	327	22	M16
1624	99TWG0489	356450	5553615	sufol	322	29	M16
1625	99TWG0491	354800	5552595	sufol	11	20	M16
1626	99TWG0494	333240	5561400	sufol	314	58	U13
1627	99TWG0497	354642	5550661	sufol	79	25	M16
1628	99TWG0503	349375	5565380	subed	297	78	U9
1629	99TWG0515	348131	5562766	subed	170	29	U9
1630	99TWG0518	347725	5562600	l-ss	190	24	U9
1631	99TWG0519	347673	5564165	sufol	93	73	U9
1632	99TWG0525	347100	5564000	subed	281	88	U9
1633	99TWG0526	346600	5563100	lu	125	5	U10
1634	99TWG0531	342075	5557640	l-fold1	181	50	M19
1635	99TWG0531	342075	5557640	l-fold1	335	56	M19
1636	99TWG0531	342075	5557640	l-fold1	10	39	M19
1637	99TWG0531	342075	5557640	l-fold1	352	40	M19
1638	99TWG0531	342075	5557640	l-fold1	17	47	M19
1639	99TWG0531	342075	5557640	l-fold1	17	25	M19
1640	99TWG0535	343170	5559150	sufol	338	57	M19
1641	99TWG0537	343725	5559400	sufol	99	78	M19
1642	99TWG0537	343725	5559400	sufol	29	43	M19
1643	99TWG0537	343725	5559400	sufol	309	87	M19
1644	99TWG0537	343725	5559400	sufol	105	73	M19
1645	99TWG0537	343725	5559400	l-fold1	95	45	M19
1646	99TWG0537	343725	5559400	l-fold1	136	36	M19
1647	99TWG0537	343725	5559400	l-fold1	103	45	M19
1648	99TWG0538	343950	5553870	sufol	250	37	M19
1649	99TWG0539	343793	5563761	sufol	333	69	M18
1650	99TWG0541	343498	5563285	sufol	335	45	M18
1651	99TWG0542	343229	5562771	sufol	0	45	M18
1652	99TWG0544	344030	5562400	sufol	348	58	M18
1653	99TWG0546	344280	5562800	sufol	350	58	M18
1654	99TWG0548	346100	5579160	sufol	7	32	M14
1655	99TWG0549	345610	5580050	sufol	25	26	M14
1656	99TWG0549	345610	5580050	sufol	52	35	M14
1657	99TWG0549	345610	5580050	sufol	315	32	M14
1658	99TWG0549	345610	5580050	lu	95	23	M14
1659	99TWG0550	346175	5579910	lu	115	16	M14
1660	99TWG0551	345350	5579200	sufol	75	8	M14
1661	99TWG0551	345350	5579200	lu	115	10	M14
1662	99TWG0551	345350	5579200	sufol	62	25	M14
1663	99TWG0551	345350	5579200	sufol	320	11	M14
1664	99TWG0551	345350	5579200	lu	103	15	M14
1665	99TWG0552	344650	5579650	lu	115	10	M14
1666	99TWG0552	344650	5579650	sufol	49	14	M14
1667	99TWG0552	344650	5579650	lu	107	10	M14
1668	99TWG0552	344650	5579650	lu	116	15	M14
1669	99TWG0552	344650	5579650	lu	105	5	M14

Number	Station[1,2]	Easting[3]	Northing[3]	Structure[4]	Azimuth[5]	Dip	Domain[6]
1670	99TWG0552	344650	5579650	sufol	275	35	M14
1671	99TWG0552	344650	5579650	sufol	100	16	M14
1672	99TWG0552	344650	5579650	l-fold1	132	12	M14
1673	99TWG0552	344650	5579650	sufol	62	28	M14
1674	99TWG0552	344650	5579650	lu	121	20	M14
1675	99TWG0552	344650	5579650	l-fold1	79	20	M14
1676	99TWG0552	344650	5579650	sufol	350	13	M14
1677	99TWG0553	344920	5580380	sufol	161	36	M14
1678	99TWG0553	344920	5580380	l-fold1	95	49	M14
1679	99TWG0554	344980	5580680	sufol	68	36	M14
1680	99TWG0554	344980	5580680	sufol	17	12	M14
1681	99TWG0554	344980	5580680	l-fold1	281	7	M14
1682	99TWG0554	344980	5580680	sufol	340	20	M14
1683	99TWG0554	344980	5580680	sufol	144	20	M14
1684	99TWG0554	344980	5580680	lu	290	12	M14
1685	99TWG0554	344980	5580680	sufol	346	17	M14
1686	99TWG0554	344980	5580680	lu	105	25	M14
1687	99TWG0555	345250	5581000	sufol	8	20	M14
1688	99TWG0556	346575	5582170	sufol	2	14	M14
1689	99TWG0557	346350	5582970	lu	89	11	M14
1690	99TWG0557	346350	5582970	sufol	311	18	M14
1691	99TWG0558	345800	5582800	sufol	30	4	M14
1692	99TWG0558	345800	5582800	lu	105	4	M14
1693	99TWG0560	352480	5558230	sufol	289	43	M17
1694	99TWG0562	352620	5558580	sufol	338	31	M17
1695	99TWG0562	352620	5558580	sufol	320	39	M17
1696	99TWG0563	352720	5558900	sufol	321	40	M17
1697	99TWG0564	352870	5559300	sufol	319	41	M17
1698	99TWG0565	352990	5559560	sufol	322	45	M17
1699	99TWG0566	353160	5560000	sufol	336	37	M17
1700	99TWG0567	353750	5560620	sufol	290	40	M17
1701	99TWG0569	354660	5562540	sufol	10	42	M17
1702	99TWG0574	403787	5562945	subed	270	77	U4
1703	99TWG0574	403787	5562945	subed	152	25	U4
1704	99TWG0576	346200	5584420	sufol	312	33	M14
1705	99TWG0577	346100	5584790	sufol	312	25	M14
1706	99TWG0578	346040	5585250	sufol	298	28	M14
1707	99TWG0579	346460	5586521	sufol	312	34	M14
1708	99TWG0579	346460	5586521	lu	95	13	M14
1709	99TWG0580	346313	5586481	sufol	307	45	M14
1710	99TWG0581	371746	5605115	sufol	65	68	M10
1711	99TWG0582	372175	5604690	lu	70	11	M10
1712	99TWG0582	372175	5604690	sufol	40	24	M10
1713	99TWG0583	371700	5603390	sufol	68	49	M10
1714	99TWG0584	372900	5603785	lu	65	22	M10
1715	99TWG0585	372647	5604833	sufol	55	44	M10
1716	99TWG0586	374097	5604328	lu	68	4	M10
1717	99TWG0586	374097	5604328	sufol	57	36	M10
1718	99TWG0587	374825	5603300	sufol	43	54	M10
1719	99TWG0588	375190	5603425	sufol	90	50	M10
1720	99TWG0590	375500	5603900	sufol	60	78	M10
1721	99TWG0591	374300	5602450	sufol	47	54	M10
1722	99TWG0593	374800	5601180	sufol	39	41	M10
1723	99TWG0595	374800	5599575	sufol	68	46	M10
1724	99TWG0596	374560	5601200	sufol	64	58	M10
1725	99TWG0597	374480	5600600	sufol	68	35	M10

Number	Station[1,2]	Easting[3]	Northing[3]	Structure[4]	Azimuth[5]	Dip	Domain[6]
1726	99TWG0598	374461	5599736	sufol	35	28	M10
1727	99TWG0598	374461	5599736	lu	90	19	M10
1728	99TWG0599	374500	5598950	sufol	77	35	M10
1729	99TWG0599	374500	5598950	lu	110	20	M10
1730	99TWG0600	370350	5603400	sufol	74	61	M10
1731	99TWG0601	370400	5603950	sufol	67	70	M10
1732	99TWG0602	370400	5604350	sufol	58	62	M10
1733	99TWG0603	370300	5604800	sufol	58	67	M10
1734	99TWG0604	370375	5605915	sufol	44	51	M10
1735	99TWG0607	369380	5604500	sufol	77	60	M10
1736	99TWG0608	367800	5602315	l-fold1	123	31	M10
1737	99TWG0608	367800	5602315	sufol	306	76	M10
1738	99TWG0608	367800	5602315	sufol	294	68	M10
1739	99TWG0610	367300	5601575	sufol	50	68	M10
1740	99TWG0611	367175	5602250	sufol	55	69	M10
1741	99TWG0612	366750	5601500	sufol	55	50	M10
1742	99TWG0613	365700	5600700	sufol	32	28	M10
1743	99TWG0615	363610	5600050	sufol	75	43	M10
1744	99TWG0616	361550	5599170	sufol	50	31	U8
1745	99TWG0617	360585	5597910	sufol	54	40	U8
1746	99TWG0618	359700	5597500	sufol	60	65	U8
1747	99TWG0619	359170	5596100	sufol	254	85	U8
1748	99TWG0620	360850	5597900	sufol	79	38	U8
1749	99TWG0621	360420	5595625	sufol	85	58	U8
1750	99TWG0622	360710	5595600	sufol	67	62	U8
1751	99TWG0623	360710	5594970	sufol	100	40	U8
1752	99TWG0625	360700	5593390	subed	130	35	E1
1753	99TWG0627	360700	5592770	subed	273	78	E1
1754	99TWG0635	371175	5598700	subed	90	81	E1
1755	99TWG0636	371050	5598800	subed	54	63	E1
1756	99TWG0644	373800	5601800	sufol	39	56	M10
1757	99TWG0646	361200	5595700	sufol	70	47	U8
1758	99TWG0647	362020	5596275	sufol	95	35	U8
1759	99TWG0648	362875	5596000	sufol	170	51	U8
1760	99TWG0649	362675	5595900	sufol	105	35	U8
1761	99TWG0650	364090	5595700	sufol	139	17	U8
1762	99TWG0651	364980	5595775	sufol	49	39	U8
1763	99TWG0654	361160	5597625	sufol	38	20	U8
1764	99TWG0656	362250	5591550	subed	259	21	E1
1765	99TWG0657	362450	5591350	subed	275	31	E1
1766	99TWG0658	362650	5590900	subed	99	33	E1
1767	99TWG0661	362860	5591110	subed	270	35	E1
1768	99TWG0662	361775	5592085	subed	305	12	E1
1769	99TWG0663	361875	5592120	subed	322	22	E1
1770	99TWG0667	362910	5591990	subed	278	21	E1
1771	99TWG0668	363500	5592275	subed	268	21	E1
1772	99TWG0669	363090	5592175	subed	210	28	E1
1773	99TWG0670	363580	5592100	subed	190	19	E1
1774	99TWG0671	363300	5593200	subed	165	28	E1
1775	99TWG0672	364085	5589225	sufol	51	8	U8
1776	99TWG0673	363900	5589000	sufol	352	18	U8
1777	99TWG0674	364440	5587975	sufol	261	80	U8
1778	99TWG0674	364440	5587975	s-fol1	182	76	U8
1779	99TWG0676	366100	5590600	sufol	170	48	U8
1780	99TWG0677	366120	5591525	sufol	257	24	U8
1781	99TWG0678	366300	5592500	sufol	252	61	U8

Number	Station[1,2]	Easting[3]	Northing[3]	Structure[4]	Azimuth[5]	Dip	Domain[6]
1782	99TWG0680	373400	5590200	sufol	21	18	M10
1783	99TWG0680	373400	5590200	lu	83	18	M10
1784	99TWG0681	373400	5591475	sufol	45	32	M10
1785	99TWG0681	373400	5591475	lu	75	20	M10
1786	99TWG0683	372900	5589590	sufol	340	20	M10
1787	99TWG0684	373800	5589730	sufol	45	33	M10
1788	99TWG0690	373780	5588400	sufol	295	47	M10
1789	99TWG0691	357385	5590660	sufol	5	59	U8
1790	99TWG0693	357190	5591550	s-fol1	171	62	U8
1791	99TWG0693	357190	5591550	s-fol1	143	74	U8
1792	99TWG0693	357190	5591550	sufol	19	59	U8
1793	99TWG0693	357190	5591550	sufol	58	72	U8
1794	99TWG0697	334770	5538800	sufol	108	19	M22
1795	99TWG0699	335435	5539700	sufol	110	12	M22
1796	99TWG0699	335435	5539700	lu	287	3	M22
1797	99TWG0702	336380	5540190	sufol	200	11	M22
1798	99TWG0702	336380	5540190	lu	276	10	M22
1799	99TWG0704	335990	5539440	sufol	305	58	M22
1800	99TWG0705	336230	5539620	sufol	53	16	M22
1801	99TWG0706	336400	5539800	sufol	110	41	M22
1802	99TWG0707	336550	5540000	sufol	230	14	M22
1803	99TWG0707	336550	5540000	lu	272	12	M22
1804	99TWG0708	337100	5540380	sufol	332	10	M22
1805	99TWG0708	337100	5540380	lu	95	9	M22
1806	99TWG0709	336500	5539575	sufol	326	7	M22
1807	99TWG0710	337280	5539530	lu	273	1	M22
1808	99TWG0711	337225	5539380	sufol	0	0	M22
1809	99TWG0711	337225	5539380	lu	98	1	M22
1810	99TWG0713	335940	5538500	sufol	245	9	M22
1811	99TWG0713	335940	5538500	lu	276	6	M22
1812	99TWG0714	336300	5538680	lu	273	6	M22
1813	99TWG0714	336300	5538680	sufol	145	7	M22
1814	99TWG0715	336450	5538670	sufol	135	8	M22
1815	99TWG0716	333900	5537900	sufol	23	26	M22
1816	99TWG0717	336308	5535239	lu	285	3	M22
1817	99TWG0717	336308	5535239	sufol	0	0	M22
1818	99TWG0718	336785	5536900	sufol	15	55	M22
1819	99TWG0720	351640	5580360	sufol	1	38	M13
1820	99TWG0720	351640	5580360	s-fol1	132	63	M13
1821	99TWG0721	351350	5580200	s-fol1	95	64	M13
1822	99TWG0721	351350	5580200	sufol	29	45	M13
1823	99TWG0722	350950	5580120	sufol	12	50	M13
1824	99TWG0724	350950	5580200	sufol	0	44	M13
1825	99TWG0724	350950	5580200	s-fol1	76	69	M13
1826	99TWG0725	350775	5580210	lu	99	32	M13
1827	99TWG0725	350775	5580210	sufol	17	33	M13
1828	99TWG0726	350625	5580200	sufol	20	45	M13
1829	99TWG0726	350625	5580200	lu	106	52	M13
1830	99TWG0727	350370	5580550	sufol	10	53	M13
1831	99TWG0727	350370	5580550	lu	92	51	M13
1832	99TWG0728	350280	5580470	l-fold1	35	65	M13
1833	99TWG0728	350280	5580470	sufol	15	76	M13
1834	99TWG0729	350200	5580500	l-fold1	150	18	M13
1835	99TWG0729	350200	5580500	sufol	337	51	M13
1836	99TWG0730	350300	5580600	lu	100	51	M13
1837	99TWG0730	350300	5580600	sufol	8	51	M13

Number	Station[1,2]	Easting[3]	Northing[3]	Structure[4]	Azimuth[5]	Dip	Domain[6]
1838	99TWG0731	350430	5580765	sufol	39	44	M13
1839	99TWG0732	350350	5581100	sufol	36	30	M13
1840	99TWG0732	350350	5581100	lu	92	18	M13
1841	99TWG0733	350140	5580800	lu	82	36	M13
1842	99TWG0734	349990	5580750	sufol	331	64	M13
1843	99TWG0735	349600	5580850	lu	82	29	M13
1844	99TWG0735	349600	5580850	sufol	299	40	M13
1845	99TWG0736	349545	5580970	sufol	326	60	M13
1846	99TWG0737	349430	5581150	sufol	337	47	M13
1847	99TWG0738	349300	5581210	lu	115	5	M13
1848	99TWG0738	349300	5581210	sufol	338	10	M13
1849	99TWG0739	349190	5581300	lu	88	20	M13
1850	99TWG0742	348470	5582500	sufol	328	44	M13
1851	99TWG0743	338250	5535360	lu	105	5	M22
1852	99TWG0743	338250	5535360	sufol	84	10	M22
1853	99TWG0744	348300	5535885	lu	100	2	M22
1854	99TWG0745	338000	5535885	lu	110	5	M22
1855	99TWG0746	336780	5534715	lu	100	2	M22
1856	99TWG0748	337250	5536565	lu	100	4	M22
1857	99TWG0750	336920	5537480	lu	95	11	M22
1858	99TWG0751	337140	5537735	sufol	308	15	M22
1859	99TWG0751	337140	5537735	lu	104	8	M22
1860	99TWG0752	338100	5536800	sufol	302	47	M22
1861	99TWG0753	337680	5538000	sufol	339	45	M22
1862	99TWG0753	337680	5538000	lu	119	34	M22
1863	99TWG0755	338500	5534225	lu	286	2	M22
1864	99TWG0755	338500	5534225	sufol	0	0	M22
1865	99TWG0757	338450	5533110	lu	125	7	M22
1866	99TWG0757	338450	5533110	sufol	35	7	M22
1867	99TWG0759	340450	5579800	lu	107	5	M15
1868	99TWG0759	340450	5579800	sufol	85	9	M15
1869	99TWG0761	340300	5580500	lu	284	2	M15
1870	99TWG0761	340300	5580500	sufol	260	10	M15
1871	99TWG0762	340585	5581500	sufol	328	31	M15
1872	99TWG0762	340585	5581500	lu	95	24	M15
1873	99TWG0764	340100	5581500	sufol	346	29	M15
1874	99TWG0765	341200	5582800	sufol	135	9	M15
1875	99TWG0767	341250	5582950	sufol	334	31	M15
1876	99TWG0773	342050	5566300	sufol	203	45	M23
1877	00TWF0403	406191	5548172	subed	156	71	U4
1878	00TWF0404	405955	5548165	subed	116	45	U4
1879	00TWF0405	405438	5548663	subed	144	34	U4
1880	00TWF0411	405912	5549481	subed	186	43	U4
1881	00TWF0415	404490	5547946	subed	290	56	U4
1882	00TWF0417	403969	5547880	subed	305	90	U4
1883	00TWF0418	403729	5547655	subed	195	70	U4
1884	00TWF0421	403204	5547759	subed	32	82	U4
1885	00TWF0422	404332	5548497	subed	135	39	U4
1886	00TWF0427	405116	5547948	subed	121	83	U4
1887	00TWF0429	404583	5547675	subed	58	46	U4
1888	00TWG0388	390625	5574413	sufol	48	39	U3
1889	00TWG0389	391441	5576171	subed	50	20	U3
1890	00TWG0390	391104	5576123	subed	51	32	U3
1891	00TWG0391	390287	5576126	subed	0	37	U3
1892	00TWG0396	401967	5579845	sufol	140	22	M4
1893	00TWG0396	401967	5579845	I-fold1	238	36	M4

Number	Station[1,2]	Easting[3]	Northing[3]	Structure[4]	Azimuth[5]	Dip	Domain[6]
1894	00TWG0396	401967	5579845	l-fold1	210	24	M4
1895	00TWG0397	401454	5579720	sufol	125	42	M4
1896	00TWG0397	401454	5579720	lu	245	42	M4
1897	00TWG0398	400686	5579875	sufol	125	55	M4
1898	00TWG0399	400131	5579893	sufol	136	37	M4
1899	00TWG0401	399551	5579625	sufol	280	36	U3
1900	00TWG0403	391113	5573314	sufol	340	20	U3
1901	00TWG0404	391497	5573428	sufol	335	26	U3
1902	00TWG0408	395464	5575219	sufol	357	37	U3
1903	00TWG0410	395450	5574829	sufol	4	26	U3
1904	00TWG0410	395450	5574829	l-fold1	112	25	U3
1905	00tw010	397958	5570597	subed	280	44	U3
1906	00tw012	404025	5572035	sufol	105	12	M3
1907	00tw013	404113	5571520	lu	70	5	M3
1908	00tw015	404569	5570997	sufol	160	35	M3
1909	00tw016	404720	5570982	sufol	74	38	M3
1910	00tw017	405317	5570847	sufol	136	39	M3
1911	00tw019	405982	5571097	sufol	90	35	M3
1912	00tw021	406180	5571048	sufol	160	10	M3
1913	00tw023	406361	5571054	sufol	90	48	M3
1914	00tw025	406801	5570991	sufol	52	22	M3
1915	00tw028	392900	5581082	sufol	114	55	M5
1916	00tw028	392900	5581082	lu	300	12	M5
1917	00tw029	394649	5582746	sufol	160	35	M5
1918	00tw030	395452	5583087	sufol	76	40	M5
1919	00tw030	395452	5583087	l-fold1	50	5	M5
1920	00tw032	397546	5582956	sufol	35	10	M5
1921	00tw033	397533	5583044	sufol	80	20	M5
1922	00tw036	394620	5583496	sufol	168	35	M5
1923	00tw039	395259	5583411	sufol	140	22	M5
1924	00tw040	394623	5584535	sufol	304	7	M5
1925	00tw041	395644	5586159	sufol	90	40	M5
1926	00tw046	399054	5588772	sufol	110	50	M5
1927	00tw047	399173	5588640	sufol	124	80	M5
1928	00tw048	399152	5588450	sufol	166	60	M5
1929	00tw049	394432	5583691	sufol	150	32	M5
1930	00tw050	395394	5584658	sufol	238	16	M5
1931	00tw051	395607	5584543	sufol	258	33	M5
1932	00tw052	396909	5585600	sufol	200	30	M5
1933	00tw053	396521	5584454	sufol	200	30	M5
1934	00tw054	396847	5584123	sufol	200	36	M5
1935	00tw055	397088	5584388	sufol	234	25	M5
1936	00tw056	397389	5584657	sufol	156	10	M5
1937	00tw057	398482	5584920	sufol	242	20	M5
1938	00tw058	398828	5584986	sufol	218	30	M5
1939	00tw059	398592	5585623	sufol	282	42	M5
1940	00tw060	398319	5585887	sufol	302	50	M5
1941	00tw061	398895	5585742	sufol	300	65	M5
1942	00tw063	395733	5582335	sufol	112	32	M5
1943	00tw064	395938	5582237	sufol	120	22	M5
1944	00tw065	396192	5582214	sufol	130	28	M5
1945	00tw066	396669	5581676	sufol	130	28	M5
1946	00tw067	395823	5581134	sufol	130	5	M5
1947	00tw068	395292	5581248	sufol	114	15	M5
1948	00tw069	393947	5580846	lu	298	14	M5
1949	00tw069	393947	5580846	sufol	111	80	M5

Number	Station[1,2]	Easting[3]	Northing[3]	Structure[4]	Azimuth[5]	Dip	Domain[6]
1950	00tw070	393329	5580578	sufol	270	50	M5
1951	00tw072	403026	5577244	sufol	125	90	M4
1952	00tw073	403903	5577123	sufol	78	86	M4
1953	00tw074	404157	5576766	sufol	94	78	M4
1954	00tw075	405422	5576258	sufol	82	76	M3
1955	00tw077	401628	5577542	sufol	96	83	M4
1956	00tw078	402619	5576030	sufol	270	75	M4
1957	00tw079	401972	5575980	sufol	270	60	M4
1958	00tw080	402554	5575103	subed	264	15	U3
1959	00tw081	401990	5574955	subed	10	25	U3
1960	00tw082	387450	5573611	subed	14	15	U3
1961	00tw083	387698	5573266	subed	18	35	U3
1962	00tw084	388423	5574085	subed	85	36	U3
1963	00tw085	388933	5574699	subed	78	32	U3
1964	00tw086	389025	5574921	sufol	0	30	U3
1965	00tw087	404402	5577363	sufol	110	75	M4
1966	00tw088	404175	5577790	sufol	92	67	M4
1967	00tw089	403984	5578285	sufol	100	50	M4
1968	00tw090	405486	5577816	sufol	120	40	M4
1969	00tw092	405833	5577047	sufol	148	28	M3
1970	00tw094	404648	5582892	sufol	142	85	M4
1971	00tw096	408540	5569952	sufol	320	60	M3
1972	00tw097	408836	5569909	sufol	310	68	M3
1973	00tw098	409187	5569844	sufol	300	30	M3
1974	00tw099	409201	5569541	sufol	314	70	M3
1975	00tw100	409388	5568929	sufol	344	35	M3
1976	00tw101	409383	5568441	sufol	274	65	M3
1977	00tw103	409016	5568871	sufol	20	85	M3
1978	00tw104	408742	5569298	sufol	282	70	M3
1979	00tw105	406759	5570738	sufol	72	25	M3
1980	00tw106	405024	5569781	sufol	346	30	M3
1981	00tw107	405372	5568780	sufol	148	21	M3
1982	00tw107	405372	5568780	lu	270	10	M3
1983	00tw108	405398	5568429	sufol	162	33	M3
1984	00tw109	405395	5568401	sufol	146	35	M3
1985	00tw110	405822	5567619	sufol	90	25	M3
1986	00tw112	404638	5570516	sufol	144	32	M3
1987	00tw113	404417	5570588	sufol	136	38	M3
1988	00tw115	405071	5572587	sufol	158	20	M3
1989	00tw116	405699	5574052	sufol	292	78	M3
1990	00tw117	405790	5574148	sufol	100	85	M3
1991	00tw118	405416	5574646	sufol	106	87	M3
1992	00tw121	405926	5575330	sufol	122	80	M3
1993	00tw122	406042	5575410	sufol	118	70	M3
1994	00tw123	406651	5574861	sufol	122	77	M3
1995	00tw124	404751	5572197	sufol	175	35	M3
1996	00tw125	405071	5572197	sufol	180	40	M3
1997	00tw126	405640	5572275	sufol	146	52	M3
1998	00tw127	406021	5572429	sufol	145	47	M3
1999	00tw129	405803	5571412	sufol	154	20	M3
2000	00tw130	396541	5571986	sufol	300	12	U3
2001	00tw131	396483	5573131	sufol	164	10	U3
2002	00tw132	394146	5568237	sufol	318	18	U3
2003	00tw134	394729	5569680	subed	300	12	U3
2004	00tw135	394729	5569680	subed	330	48	U3
2005	00tw138	393588	5565705	subed	62	15	U3

Number	Station[1,2]	Easting[3]	Northing[3]	Structure[4]	Azimuth[5]	Dip	Domain[6]
2006	00tw139	393698	5565946	subed	138	10	U3
2007	00tw142	394713	5566670	subed	155	21	U3
2008	00tw146	395500	5567276	sufol	219	20	U3
2009	00tw148	396269	5567851	sufol	290	30	U3
2010	00tw149	396321	5566988	sufol	270	35	U3
2011	00tw151	396229	5568285	subed	300	55	U3
2012	00tw153	394855	5587733	sufol	276	85	M5
2013	00tw158	396740	5589768	sufol	78	50	M5
2014	00tw159	397674	5590499	sufol	88	28	M5
2015	00tw160	397898	5590689	sufol	62	35	M5
2016	00tw162	397129	5590301	sufol	80	75	M5
2017	00tw170	403728	5583395	sufol	142	33	M5
2018	00tw171	403912	5583798	sufol	140	43	M5
2019	00tw172	403985	5583968	sufol	159	41	M5
2020	00tw173	403916	5584823	sufol	132	70	M5
2021	00tw177	403401	5585813	sufol	150	50	M5
2022	00tw179	402890	5586280	sufol	110	46	M5
2023	00tw180	402490	5586143	sufol	136	70	M5
2024	00tw181	402137	5586209	sufol	125	90	M5
2025	00tw183	400611	5585953	sufol	106	65	M5
2026	00tw184	400396	5585558	sufol	270	24	M5
2027	00tw186	400180	5585100	sufol	340	40	M5
2028	00tw187	405161	5586526	sufol	246	20	M5
2029	00tw188	400282	5583395	sufol	320	28	M5
2030	00tw190	425775	5570100	sufol	170	22	M2
2031	00tw192	428563	5582345	sufol	222	80	U2
2032	00tw192	428563	5582345	lu	250	15	U2
2033	00tw196	427253	5581363	sufol	76	50	U2
2034	00tw197	427285	5581290	sufol	110	30	U2
2035	00tw198	427222	5581163	sufol	106	65	U2
2036	00tw202	423594	5580624	sufol	122	28	M2
2037	00tw203	423211	5580167	sufol	69	26	M2
2038	00tw204	421863	5579891	sufol	140	10	M2
2039	00tw207	420315	5580239	sufol	36	50	M2
2040	00tw209	418869	5580932	sufol	80	34	M2
2041	00tw211	418548	5580917	sufol	130	40	M2
2042	00tw211	418548	5580917	l-fold1	170	10	M2
2043	00tw211	418548	5580917	s-fol1	168	70	M2
2044	00tw212	417731	5581163	sufol	103	47	M2
2045	00tw213	418491	5581241	sufol	270	27	M2
2046	00tw215	423572	5581267	sufol	117	5	M2
2047	00tw218	422537	5580895	sufol	50	12	M2
2048	00tw219	423422	5581720	sufol	120	20	M2
2049	00tw229	427502	5556544	sufol	52	37	M1
2050	00tw231	427208	5557807	sufol	112	25	M1
2051	00tw232	427244	5558574	sufol	117	30	M1
2052	00tw233	427167	5560112	sufol	222	20	M1
2053	00tw234	425691	5551045	sufol	60	30	M1
2054	00tw236	424277	5549900	sufol	280	85	M1
2055	00tw237	423532	5549604	sufol	90	85	M1
2056	00tw239	404941	5567545	subed	242	15	U3
2057	00tw243	405313	5567889	sufol	213	28	M3
2058	00tw245	406071	5576409	sufol	94	68	M3
2059	00tw246	406207	5576432	sufol	90	62	M3
2060	00tw247	406353	5576624	sufol	90	67	M3
2061	00tw248	406496	5577008	sufol	288	30	M3

Number	Station[1,2]	Easting[3]	Northing[3]	Structure[4]	Azimuth[5]	Dip	Domain[6]
2062	00tw250	406672	5577176	sufol	284	30	M3
2063	00tw250	406672	5577176	lu	276	5	M3
2064	00tw251	407018	5577109	sufol	78	35	M3
2065	00tw252	407209	5577195	sufol	78	20	M3
2066	00tw253	407662	5577201	sufol	90	20	M3
2067	00tw254	408137	5577202	sufol	90	22	M3
2068	00tw255	408226	5576849	sufol	94	36	M3
2069	00tw257	407957	5576271	sufol	110	45	M3
2070	00tw258	407625	5576222	sufol	85	53	M3
2071	00tw259	406933	5576268	sufol	90	60	M3
2072	00tw260	406690	5576187	sufol	100	58	M3
2073	00tw263	406259	5576264	sufol	90	80	M3
2074	00tw264	395805	5550702	sufol	82	65	U4
2075	00tw266	405908	5552870	subed	318	5	U4
2076	00tw268	408299	5552644	sufol	85	35	M1
2077	00tw269	408636	5553215	sufol	265	45	M1
2078	00tw270	409994	5553815	sufol	90	25	M1
2079	00tw271	410302	5553448	l-fold1	280	10	M1
2080	00tw271	410302	5553448	sufol	140	70	M1
2081	00tw271	410302	5553448	b-ax1	180	20	M1
2082	00tw273	408686	5554107	sufol	166	90	M1
2083	00tw275	406190	5551202	subed	290	20	U4
2084	00tw276	403689	5552397	subed	127	18	U4
2085	00tw280	414721	5544170	sufol	300	80	M1
2086	00tw281	414796	5544418	sufol	297	86	M1
2087	00tw286	411511	5547671	sufol	68	88	M1
2088	00tw289	410279	5549540	sufol	76	38	M1
2089	00tw290	409372	5551160	sufol	290	65	M1
2090	00tw291	409132	5552008	sufol	255	20	M1
2091	00tw292	409029	5552302	sufol	142	50	M1
2092	00tw293	409013	5552819	sufol	230	40	M1
2093	00tw294	409286	5553035	sufol	188	30	M1
2094	00tw301	411891	5545517	sufol	318	82	M1
2095	00tw303	411494	5546102	sufol	284	50	M1
2096	00tw305	409862	5546728	sufol	128	45	M1
2097	00tw306	409799	5546845	sufol	145	40	M1
2098	00tw308	409326	5547263	sufol	138	38	M1
2099	00tw310	408667	5547555	sufol	116	10	M1
2100	00tw311	408464	5547684	sufol	120	30	M1
2101	00tw313	408012	5548000	sufol	100	35	M1
2102	00tw318	408823	5548152	sufol	133	50	M1
2103	00tw319	408869	5548510	sufol	180	12	M1
2104	00tw320	408771	5548730	sufol	90	40	M1
2105	00tw329	407492	5547838	sufol	45	18	U4
2106	00tw330	406186	5548175	sufol	158	53	U4
2107	00tw332	378524	5593249	sufol	127	25	M6
2108	00tw333	379339	5594453	sufol	350	12	M6
2109	00tw334	379282	5594020	sufol	42	21	M6
2110	00tw335	379301	5593784	sufol	100	30	M6
2111	00tw337	381287	5594288	sufol	62	25	M6
2112	00tw342	411195	5552158	l-fold1	85	8	M1
2113	00tw342	411195	5552158	sufol	58	20	M1
2114	00tw343	411518	5551925	l-fold1	90	25	M1
2115	00tw344	412579	5551724	sufol	18	22	M1
2116	00tw345	413058	5551295	sufol	78	24	M1
2117	00tw346	413047	5551086	sufol	80	50	M1

Number	Station[1,2]	Easting[3]	Northing[3]	Structure[4]	Azimuth[5]	Dip	Domain[6]
2118	00tw347	412674	5550448	sufol	80	60	M1
2119	00tw350	412419	5548836	sufol	86	55	M1
2120	00tw352	426247	5572055	sufol	172	30	U2
2121	00tw353	426329	5572404	sufol	260	20	U2
2122	00tw354	426498	5572687	sufol	222	20	U2
2123	00tw355	426987	5572929	sufol	180	25	U2
2124	00tw356	428738	5573779	sufol	274	25	U2
2125	00tw368	424960	5576156	sufol	105	47	U2
2126	00tw369	425022	5576186	sufol	120	33	U2
2127	00tw374	426065	5575174	sufol	200	35	U2
2128	00tw375	426171	5575100	sufol	240	30	U2
2129	00tw376	426248	5574815	sufol	178	40	U2
2130	00tw377	426020	5574513	sufol	180	28	U2
2131	00tw380	425490	5574504	sufol	207	10	U2
2132	00tw408	427078	5570111	sufol	174	8	U2
2133	00tw410	427390	5570309	sufol	330	30	U2
2134	00tw411	427441	5570351	sufol	328	45	U2
2135	00tw413	428186	5570457	sufol	330	70	U2
2136	00tw414	428354	5570300	sufol	280	28	U2
2137	00tw415	428653	5570102	sufol	210	26	U2
2138	00tw416	428400	5569587	sufol	282	45	U2
2139	00tw417	428218	5569532	sufol	290	55	U2
2140	00tw418	428108	5569487	sufol	280	54	U2
2141	00tw420	425596	5567343	sufol	280	45	M2
2142	00tw421	425814	5566907	sufol	270	80	M2
2143	00tw422	425605	5566831	sufol	232	28	M2
2144	00tw423	424991	5566780	sufol	294	70	M2
2145	00tw424	424584	5566511	sufol	165	32	M2
2146	00tw425	424584	5566511	sufol	106	36	M2
2147	00tw425	424150	5566460	sufol	106	36	M2
2148	00tw426	423696	5567245	sufol	230	15	M2
2149	00tw427	423539	5567568	sufol	282	65	M2
2150	00tw448	423248	5567931	sufol	240	55	M2
2151	00tw449	423238	5567392	sufol	342	75	M2
2152	00tw450	423319	5567022	sufol	210	10	M2
2153	00tw451	423460	5566313	sufol	107	46	M2
2154	00tw453	423175	5565366	sufol	220	28	M2
2155	00tw454	423153	5565623	sufol	256	10	M2
2156	00tw455	422875	5565594	sufol	118	22	M2
2157	00tw456	422554	5565978	sufol	253	56	M2
2158	00tw457	422463	5566033	sufol	232	33	M2
2159	00tw458	422869	5565694	sufol	197	35	M2
2160	00tw469	422666	5575412	sufol	87	20	M2
2161	00tw470	422406	5575705	sufol	168	5	M2
2162	00tw471	420747	5575948	sufol	142	32	M2
2163	00tw472	419726	5575843	sufol	165	25	M2
2164	00tw473	418922	5575677	sufol	160	28	M2
2165	00tw475	417148	5574967	sufol	100	40	M2
2166	00tw476	416548	5574873	sufol	135	25	M2
2167	00tw478	415156	5575174	sufol	42	46	M2
2168	00tw479	418778	5575014	sufol	230	15	M2
2169	00tw481	419869	5574468	sufol	280	35	M2
2170	00tw483	421048	5573726	subed	158	52	U1
2171	00tw485	417260	5573438	sufol	160	22	M2
2172	00tw486	417059	5573516	sufol	20	40	M2
2173	00tw489	416043	5573639	sufol	140	15	M2

Number	Station[1,2]	Easting[3]	Northing[3]	Structure[4]	Azimuth[5]	Dip	Domain[6]
2174	00tw490	414222	5573775	sufol	270	22	M2
2175	00tw491	417654	5573367	sufol	258	10	M2
2176	00tw494	415416	5573072	sufol	270	40	M2
2177	00tw496	415027	5573119	sufol	145	18	M2
2178	00tw499	418796	5573224	subed	148	40	U1
2179	00tw500	419144	5573164	subed	205	25	U1
2180	00tw501	419543	5573336	subed	282	38	U1
2181	00tw502	419952	5573227	subed	96	35	U1
2182	00tw504	421169	5572442	sufol	305	41	M2
2183	00tw505	421056	5572746	sufol	226	35	M2
2184	00tw506	421082	5572732	sufol	203	31	M2
2185	00tw509	420854	5572813	sufol	222	35	M2
2186	00tw512	420468	5572562	sufol	255	12	M2
2187	00tw513	420034	5572558	sufol	222	30	M2
2188	00tw515	419891	5572454	sufol	176	65	M2
2189	00tw516	419980	5572306	sufol	268	40	M2
2190	00tw517	414684	5572618	sufol	284	20	M2
2191	00tw518	415795	5572639	sufol	162	10	M2
2192	00tw519	416429	5572710	sufol	258	25	M2
2193	00tw520	341357	5577345	sufol	53	32	M15
2194	99tw002	375648	5578775	sufol	288	25	M7
2195	99tw004	377487	5578293	sufol	305	16	M7
2196	99tw005	377617	5578272	subed	275	45	M7
2197	99tw006	376889	5577955	sufol	244	51	M7
2198	99tw007	376398	5578012	subed	350	75	M7
2199	99tw008	376209	5577857	subed	260	45	M7
2200	99tw009	374650	5579032	sufol	12	20	M7
2201	99tw012	376583	5579233	subed	268	65	M7
2202	99tw013	376313	5576449	subed	82	10	M7
2203	99tw014	375169	5576386	subed	344	45	M7
2204	99tw015	374971	5578082	subed	122	90	M7
2205	99tw019	376182	5576860	subed	125	45	M7
2206	99tw020	377483	5576629	subed	18	22	M7
2207	99tw021	378045	5576143	subed	93	50	M7
2208	99tw022	373205	5576702	sufol	330	50	M7
2209	99tw023	373381	5576473	sufol	320	62	M7
2210	99tw025	374720	5575606	sufol	26	50	M7
2211	99tw026	375187	5580230	sufol	302	24	M7
2212	99tw027	373844	5582768	sufol	346	55	M7
2213	99tw030	374894	5586035	lu	92	5	M7
2214	99tw030	374894	5586035	sufol	125	8	M7
2215	99tw031	374846	5585709	sufol	279	72	M7
2216	99tw033	376648	5584511	sufol	330	60	M7
2217	99tw035	376617	5584603	sufol	320	60	M7
2218	99tw036	377871	5590308	sufol	352	52	M7
2219	99tw037	376950	5589790	sufol	142	80	M7
2220	99tw040	379322	5588615	sufol	345	20	M6
2221	99tw041	379894	5589068	sufol	0	35	M6
2222	99tw042	380689	5589215	sufol	350	42	M6
2223	99tw043	381018	5589388	sufol	0	80	M6
2224	99tw044	381642	5588868	sufol	55	54	M6
2225	99tw045	380590	5589020	sufol	310	20	M6
2226	99tw045	380590	5589020	sufol	80	65	M6
2227	99tw047	379550	5589920	sufol	280	55	M6
2228	99tw048	379665	5590129	sufol	214	52	M6
2229	99tw049	380179	5589700	sufol	60	45	M6

Number	Station[1,2]	Easting[3]	Northing[3]	Structure[4]	Azimuth[5]	Dip	Domain[6]
2230	99tw049	380179	5589700	l-fold1	124	16	M6
2231	99tw051	380760	5591141	sufol	0	45	M6
2232	99tw053	378958	5591356	sufol	345	10	M6
2233	99tw054	379040	5591690	sufol	72	32	M6
2234	99tw055	379154	5591558	sufol	66	40	M6
2235	99tw057	379161	5592067	sufol	105	40	M6
2236	99tw058	379344	5591979	l-fold1	128	15	M6
2237	99tw059	378635	5592975	sufol	110	20	M6
2238	99tw060	378591	5594504	sufol	294	60	M6
2239	99tw061	378587	5594253	sufol	82	30	M6
2240	99tw062	378823	5594502	sufol	62	8	M6
2241	99tw063	379143	5595379	sufol	70	44	M6
2242	99tw064	379401	5595298	sufol	79	35	M6
2243	99tw067	379277	5594059	sufol	40	20	M6
2244	99tw068	379394	5593462	sufol	110	18	M6
2245	99tw069	379448	5593670	sufol	86	35	M6
2246	99tw070	379818	5594525	sufol	80	20	M6
2247	99tw071	380062	5594856	sufol	150	25	M6
2248	99tw072	380073	5594348	sufol	77	25	M6
2249	99tw073	380811	5594531	sufol	55	26	M6
2250	99tw074	378952	5593781	sufol	50	15	M6
2251	99tw075	371837	5572994	sufol	325	45	M7
2252	99tw077	372230	5572974	sufol	356	42	M7
2253	99tw078	372413	5573130	sufol	268	45	M7
2254	99tw086	372857	5572416	sufol	314	44	M7
2255	99tw090	373620	5585230	sufol	340	40	M7
2256	99tw091	373773	5584354	sufol	350	40	M7
2257	99tw092	374115	5584243	sufol	0	32	M7
2258	99tw093	374456	5584272	sufol	350	28	M7
2259	99tw095	374909	5584308	sufol	282	25	M7
2260	99tw096	375193	5584278	sufol	10	40	M7
2261	99tw097	375608	5585090	sufol	30	25	M7
2262	99tw099	375277	5585423	sufol	278	40	M7
2263	99tw101	374974	5586773	sufol	126	90	M7
2264	99tw103	373566	5576773	sufol	320	35	M7
2265	99tw104	373694	5576644	sufol	345	55	M7
2266	99tw105	373834	5576594	sufol	350	38	M7
2267	99tw106	373400	5576579	sufol	332	60	M7
2268	99tw107	374123	5576470	sufol	330	30	M7
2269	99tw108	374112	5576322	l-fold1	112	10	M7
2270	99tw108	374112	5576322	lu	115	0	M7
2271	99tw109	374214	5576005	lu	110	0	M7
2272	99tw112	374728	5576710	sufol	340	22	M7
2273	99tw113	374392	5577156	sufol	20	15	M7
2274	99tw114	374375	5577396	sufol	330	12	M7
2275	99tw116	374187	5577503	sufol	335	15	M7
2276	99tw117	374092	5577559	sufol	310	30	M7
2277	99tw118	374022	5577450	sufol	346	35	M7
2278	99tw119	373809	5577257	sufol	324	35	M7
2279	99tw120	372192	5575479	sufol	335	25	M7
2280	99tw122	372353	5575281	sufol	10	25	M7
2281	99tw124	372594	5575308	sufol	295	22	M7
2282	99tw125	373022	5575220	sufol	314	45	M7
2283	99tw127	372827	5574396	sufol	0	52	M7
2284	99tw131	372226	5574630	sufol	55	20	M7
2285	99tw137	368657	5575229	lu	113	35	M9

Number	Station[1,2]	Easting[3]	Northing[3]	Structure[4]	Azimuth[5]	Dip	Domain[6]
2286	99tw137	368657	5575229	sufol	340	40	U5
2287	99tw140	367742	5577839	sufol	73	82	M9
2288	99tw142	367484	5577721	sufol	302	65	M9
2289	99tw143	367209	5579043	subed	330	35	M9
2290	99tw144	366815	5582286	sufol	60	30	M9
2291	99tw145	366994	5582107	sufol	40	5	M9
2292	99tw146	367141	5581993	sufol	20	20	M9
2293	99tw147	367338	5582427	sufol	0	22	M9
2294	99tw149	367700	5580077	sufol	46	15	M9
2295	99tw156	363316	5575691	subed	300	65	M9
2296	99tw156	363316	5575691	sufol	32	65	M9
2297	99tw157	364737	5575126	sufol	2	58	M9
2298	99tw158	364941	5575218	sufol	30	48	M9
2299	99tw159	364551	5575608	sufol	320	65	M9
2300	99tw160	363936	5576963	sufol	80	40	M9
2301	99tw161	363721	5577796	subed	36	26	M9
2302	99tw161	363721	5577796	sufol	62	55	M9
2303	99tw162	363815	5578323	sufol	356	42	M9
2304	99tw163	364167	5578657	sufol	45	35	M9
2305	99tw164	365151	5576678	sufol	40	45	M9
2306	99tw165	365303	5578507	sufol	348	75	M9
2307	99tw166	362959	5577223	sufol	34	38	M9
2308	99tw167	362070	5576563	sufol	58	53	M9
2309	99tw169	362935	5577705	sufol	10	24	M9
2310	99tw173	363693	5578456	sufol	355	28	M9
2311	99tw175	363267	5578928	sufol	0	25	M9
2312	99tw178	362701	5579920	sufol	36	25	M9
2313	99tw179	364623	5579857	sufol	0	33	M9
2314	99tw182	362000	5574660	sufol	38	38	M9
2315	99tw183	364874	5579812	sufol	332	40	M9
2316	99tw185	366305	5582723	sufol	286	28	M9
2317	99tw186	365882	5583075	sufol	330	38	M9
2318	99tw189	364002	5586858	sufol	40	70	U8
2319	99tw191	368716	5577326	sufol	320	26	M9
2320	99tw193	369081	5576634	sufol	314	35	M9
2321	99tw194	368768	5577613	sufol	314	46	M9
2322	99tw194	368768	5577613	sufol	20	35	M9
2323	99tw195	369626	5577995	sufol	20	35	M9
2324	99tw196	369855	5578494	sufol	5	45	M9
2325	99tw197	370102	5578809	sufol	40	45	M9
2326	99tw198	370351	5577931	sufol	320	62	M9
2327	99tw200	362703	5581174	sufol	0	42	M9
2328	99tw201	362806	5582168	sufol	324	45	M9
2329	99tw201	362806	5582168	lu	88	32	M9
2330	99tw203	365106	5583020	sufol	322	25	M9
2331	99tw205	365570	5583585	sufol	0	36	M9
2332	99tw206	362421	5583099	sufol	335	40	M9
2333	99tw207	366581	5584905	subed	50	65	M9
2334	99tw210	367623	5584446	sufol	330	45	M9
2335	99tw211	367627	5584279	sufol	320	45	M9
2336	99tw212	367622	5583333	sufol	342	48	M9
2337	99tw213	367868	5583948	sufol	345	65	M9
2338	99tw215	369397	5585664	sufol	270	85	M9
2339	99tw216	369078	5585755	subed	90	65	M9
2340	99tw217	368925	5578719	subed	22	72	M9
2341	99tw218	369322	5579002	subed	10	50	M9

Number	Station[1,2]	Easting[3]	Northing[3]	Structure[4]	Azimuth[5]	Dip	Domain[6]
2342	99tw219	369504	5580070	sufol	30	85	M9
2343	99tw220	369640	5581710	subed	5	55	M9
2344	99tw221	369891	5582247	subed	318	45	M9
2345	99tw222	370377	5582736	subed	0	40	M9
2346	99tw223	369609	5582536	sufol	10	82	M9
2347	99tw224	369305	5582310	sufol	10	42	M9
2348	99tw225	369454	5581615	subed	350	50	M9
2349	99tw226	368592	5578817	subed	50	45	M9
2350	99tw227	369104	5578337	sufol	40	38	M9
2351	99tw227	369104	5578337	l-fold1	75	32	M9
2352	99tw228	368515	5579347	sufol	34	25	M9
2353	99tw229	368251	5579726	sufol	34	25	M9
2354	99tw230	368447	5579901	sufol	45	22	M9
2355	99tw231	368675	5579960	sufol	0	42	M9
2356	99tw233	368981	5579505	sufol	45	54	M9
2357	99tw235	370118	5578705	subed	60	46	M9
2358	99tw236	370077	5577148	subed	74	40	M9
2359	99tw237	373820	5589835	sufol	10	30	M10
2360	99tw240	374560	5590774	sufol	75	35	M10
2361	99tw241	374805	5591012	sufol	8	10	M10
2362	99tw242	375522	5591435	sufol	323	65	M10
2363	99tw244	372944	5589565	sufol	345	35	M10
2364	99tw245	373123	5589922	sufol	345	20	M10
2365	99tw245	373123	5589922	lu	98	20	M10
2366	99tw254	373635	5587794	sufol	304	64	M10
2367	99tw261	365460	5588705	sufol	310	20	U8
2368	99tw262	365997	5590745	sufol	20	68	U8
2369	99tw263	366425	5591822	sufol	270	50	U8
2370	99tw265	380191	5576878	sufol	355	55	M6
2371	99tw266	380272	5577102	sufol	310	45	M6
2372	99tw267	380922	5577107	sufol	30	30	M6
2373	99tw268	381189	5577767	sufol	22	30	M6
2374	99tw269	380919	5578217	sufol	50	15	M6
2375	99tw270	382003	5577945	sufol	322	35	M6
2376	99tw271	382313	5578797	sufol	30	42	M6
2377	99tw272	382320	5579276	sufol	40	30	M6
2378	99tw273	382408	5576340	sufol	32	25	M6
2379	99tw274	383344	5576646	sufol	40	26	M6
2380	99tw276	384816	5580069	sufol	14	36	M6
2381	99tw277	384001	5581684	sufol	8	44	M6
2382	99tw279	382929	5581465	sufol	20	30	M6
2383	99tw280	379199	5586511	sufol	302	42	M6
2384	99tw281	379020	5586105	sufol	290	40	M6
2385	99tw281	379020	5586105	sufol	90	55	M6
2386	99tw282	379201	5585752	sufol	140	52	M6
2387	99tw283	379353	5585476	sufol	10	27	M6
2388	99tw285	379222	5586188	sufol	306	60	M6
2389	99tw286	379433	5585948	sufol	260	72	M6
2390	99tw287	379489	5585600	sufol	296	75	M6
2391	99tw291	383841	5584506	sufol	324	57	M6
2392	99tw292	383674	5584328	sufol	322	62	M6
2393	99tw293	383908	5583742	sufol	310	55	M6
2394	99tw294	383679	5583671	sufol	320	60	M6
2395	99tw296	383173	5583515	sufol	90	75	M6
2396	99tw297	384167	5583255	sufol	335	82	M6
2397	99tw298	384224	5582606	sufol	304	65	M6

Number	Station[1,2]	Easting[3]	Northing[3]	Structure[4]	Azimuth[5]	Dip	Domain[6]
2398	99tw300	381797	5581917	sufol	355	24	M6
2399	99tw306	386283	5585771	sufol	105	40	M6
2400	99tw307	386271	5584579	sufol	10	40	M6
2401	99tw310	382191	5587305	sufol	320	14	M6
2402	99tw312	382849	5588217	sufol	340	36	M6
2403	99tw313	382836	5588349	sufol	2	46	M6
2404	99tw315	387490	5586867	sufol	330	12	M6
2405	99tw317	387207	5587790	sufol	330	16	M6
2406	99tw319	387364	5589021	sufol	110	40	M6
2407	99tw320	384894	5589807	sufol	250	30	M6
2408	99tw321	384833	5590051	sufol	120	40	M6
2409	99tw323	381864	5591377	sufol	116	20	M6
2410	99tw325	383107	5590360	sufol	100	45	M6
2411	99tw327	383111	5590608	sufol	93	75	M6
2412	99tw328	383130	5590055	sufol	78	39	M6
2413	99tw329	382128	5591826	sufol	65	60	M6
2414	99tw330	383232	5592252	sufol	90	65	M6
2415	99tw331	383755	5592037	sufol	86	35	M6
2416	99tw333	384331	5592050	sufol	108	50	M6
2417	99tw334	384379	5592070	sufol	86	38	M6
2418	99tw335	384732	5591237	sufol	110	80	M6
2419	99tw338	385281	5591678	sufol	62	50	M6
2420	99tw339	385442	5591892	sufol	100	67	M6
2421	99tw342	387564	5592166	sufol	60	22	M6
2422	99tw343	385359	5591484	sufol	335	45	M6
2423	99tw344	382017	5592218	sufol	60	75	M6
2424	99tw346	383040	5592733	sufol	55	40	M6
2425	99tw347	383490	5592777	sufol	86	40	M6
2426	99tw348	383879	5592917	sufol	10	70	M6
2427	99tw349	384584	5593177	sufol	50	48	M6
2428	99tw350	384937	5593348	sufol	90	35	M6
2429	99tw351	384137	5593386	sufol	76	36	M6
2430	99tw353	381819	5591810	sufol	40	30	M6
2431	99tw354	387820	5594010	sufol	104	40	M6
2432	99tw355	388240	5593690	sufol	102	22	M6
2433	99tw357	388960	5593150	sufol	94	42	M6
2434	99tw360	386728	5592887	sufol	76	25	M6
2435	99tw361	387397	5593919	sufol	106	20	M6
2436	99tw362	387279	5593450	sufol	125	30	M6
2437	99tw363	387217	5593251	l-fold1	260	20	M6
2438	99tw363	387217	5593251	sufol	110	20	M6
2439	99tw365	389665	5595140	sufol	90	50	M6
2440	99tw366	390851	5580474	sufol	292	80	M6
2441	99tw367	390910	5581275	sufol	284	70	M6
2442	99tw369	377776	5573938	sufol	40	70	M7
2443	99tw370	377763	5573620	subed	294	24	M7
2444	99tw372	377214	5573128	sufol	14	12	M7
2445	99tw376	375888	5572952	sufol	12	15	M7
2446	99tw378	375664	5573344	sufol	15	50	M7
2447	99tw380	379300	5573324	sufol	350	10	M6
2448	99tw381	379719	5573047	sufol	330	30	M6
2449	99tw382	380067	5573507	sufol	5	30	M6
2450	99tw383	380307	5573737	sufol	330	40	M6
2451	99tw385	379620	5575226	sufol	340	32	M6
2452	99tw386	380220	5575334	sufol	10	45	M6
2453	99tw387	382731	5574060	sufol	35	20	M6

Number	Station[1,2]	Easting[3]	Northing[3]	Structure[4]	Azimuth[5]	Dip	Domain[6]
2454	99tw388	382812	5573693	sufol	42	32	M6
2455	99tw389	383374	5573624	sufol	16	32	M6
2456	99tw391	380324	5568660	sufol	18	40	M6
2457	99tw394	380370	5569636	sufol	18	40	M6
2458	99tw396	383048	5571077	sufol	33	40	M6
2459	99tw397	382614	5571285	sufol	30	45	M6
2460	99tw398	382435	5571284	sufol	40	45	M6
2461	99tw399	383549	5571392	sufol	36	55	M6
2462	99tw400	383772	5572916	sufol	0	45	M6
2463	99tw401	383049	5570367	sufol	40	30	M6
2464	99tw402	382412	5569723	sufol	70	65	M6
2465	99tw403	383233	5570049	sufol	102	72	M6
2466	99tw405	377976	5572977	sufol	106	21	M7
2467	99tw407	389316	5578205	sufol	350	45	M6
2468	99tw409	388664	5576193	sufol	340	44	M6
2469	99tw410	388070	5576098	sufol	74	36	M6
2470	99tw412	387196	5580091	sufol	300	44	M6
2471	99tw415	390433	5579777	sufol	300	70	M6
2472	99tw416	390014	5579610	sufol	304	60	M6
2473	99tw417	390095	5579519	sufol	285	60	M6
2474	99tw418	389898	5579342	sufol	288	55	M6
2475	99tw419	389865	5579376	sufol	286	55	M6
2476	99tw420	389640	5578831	sufol	330	40	M6
2477	99tw421	389692	5578927	sufol	330	50	M6
2478	99tw424	389652	5575922	sufol	22	24	U3

APPENDIX D

Representative electron microprobe data used for thermobarometric calculations

Representative electron microprobe data used for thermobarometric calculations

Sample 00TWG331-garnet 1
Garnet (normalized to 12 O atoms)

Spot	d (μm)	Mg	Si	Ca	Fe	Na	Al	Ti	Mn	Cr	Total
1	2	0.350	3.002	0.220	2.342	0.000	1.992	0.004	0.088	0.001	8.00
2	22	0.384	2.971	0.224	2.384	0.000	1.989	0.000	0.079	0.002	8.03
3	42	0.361	2.977	0.243	2.378	0.000	1.993	0.000	0.075	0.001	8.03
4	62	0.338	2.981	0.274	2.368	0.003	1.986	0.000	0.075	0.002	8.03
5	82	0.332	2.986	0.306	2.380	0.000	1.953	0.000	0.077	0.002	8.04
6	102	0.312	2.954	0.290	2.344	0.000	2.034	0.002	0.090	0.000	8.03
7	122	0.299	2.942	0.290	2.362	0.003	2.028	0.006	0.110	0.000	8.04
8	142	0.285	2.954	0.290	2.355	0.004	2.023	0.002	0.122	0.000	8.03
9	162	0.281	2.952	0.296	2.327	0.004	2.026	0.002	0.147	0.000	8.03
10	182	0.253	2.955	0.325	2.294	0.009	2.024	0.003	0.174	0.000	8.04
11	202	0.238	2.955	0.340	2.276	0.003	2.025	0.000	0.194	0.002	8.03
12	222	0.239	2.957	0.334	2.276	0.000	2.016	0.000	0.211	0.002	8.03
13	242	0.230	2.962	0.346	2.249	0.005	2.007	0.000	0.233	0.003	8.04
14	262	0.217	2.964	0.357	2.220	0.002	2.014	0.001	0.253	0.001	8.03
15	282	0.217	2.965	0.371	2.210	0.006	1.999	0.000	0.268	0.002	8.04
16	302	0.189	2.986	0.370	2.183	0.002	2.022	0.000	0.252	0.000	8.00
17	322	0.182	2.974	0.376	2.180	0.000	2.030	0.000	0.269	0.000	8.01
18	342	0.183	2.973	0.355	2.188	0.000	2.027	0.000	0.288	0.000	8.01
19	362	0.184	2.977	0.365	2.163	0.000	2.018	0.001	0.303	0.000	8.01
20	382	0.181	2.988	0.379	2.127	0.000	2.016	0.000	0.313	0.000	8.00
21	402	0.198	2.961	0.330	2.149	0.000	2.028	0.006	0.346	0.000	8.02
22	422	0.195	2.943	0.312	2.139	0.000	2.052	0.005	0.377	0.002	8.02
23	442	0.196	2.943	0.294	2.155	0.000	2.047	0.004	0.390	0.001	8.03
24	462	0.194	2.957	0.269	2.163	0.000	2.040	0.003	0.393	0.001	8.02
25	482	0.208	2.952	0.220	2.193	0.001	2.028	0.003	0.427	0.001	8.03
26	502	0.191	2.978	0.232	2.148	0.000	2.007	0.003	0.454	0.002	8.01
27	522	0.187	2.969	0.252	2.104	0.000	2.028	0.003	0.469	0.001	8.01
28	542	0.176	2.975	0.282	2.076	0.002	2.009	0.006	0.487	0.002	8.01
29	562	0.176	2.962	0.287	2.069	0.000	2.026	0.005	0.493	0.001	8.02
30	582	0.168	2.969	0.284	2.043	0.004	2.027	0.008	0.506	0.002	8.01
31	602	0.175	2.964	0.289	2.037	0.000	2.028	0.000	0.528	0.002	8.02
32	622	0.168	2.962	0.303	2.028	0.000	2.028	0.003	0.528	0.000	8.02
33	642	0.164	2.962	0.316	2.028	0.000	2.024	0.001	0.529	0.001	8.02
34	662	0.163	2.971	0.322	2.012	0.000	2.003	0.005	0.544	0.001	8.02
35	682	0.172	2.935	0.320	2.025	0.000	2.041	0.000	0.550	0.002	8.04
36	702	0.162	2.974	0.325	1.995	0.008	2.017	0.000	0.540	0.000	8.02
37	722	0.166	2.971	0.347	1.973	0.005	2.019	0.000	0.540	0.000	8.02
38	742	0.163	2.981	0.333	1.958	0.006	2.020	0.000	0.552	0.000	8.01
39	762	0.168	2.973	0.309	1.979	0.009	2.021	0.000	0.563	0.000	8.02
40	782	0.175	2.985	0.296	1.986	0.011	2.009	0.000	0.556	0.000	8.02
41	802	0.179	2.987	0.275	2.001	0.008	2.009	0.000	0.553	0.000	8.01
42	822	0.179	2.989	0.255	2.017	0.012	2.006	0.005	0.546	0.000	8.01
43	842	0.183	2.998	0.259	2.021	0.005	1.993	0.000	0.550	0.000	8.01
44	862	0.176	2.991	0.269	2.001	0.014	2.007	0.005	0.546	0.000	8.01
45	882	0.174	2.974	0.279	2.000	0.007	2.026	0.002	0.554	0.000	8.02
46	902	0.176	2.963	0.293	2.002	0.005	2.019	0.000	0.569	0.001	8.03
47	922	0.173	2.974	0.286	2.007	0.000	2.010	0.004	0.564	0.000	8.02
48	942	0.180	2.972	0.298	1.988	0.006	2.021	0.001	0.552	0.001	8.02
50	982	0.170	2.969	0.322	2.002	0.000	2.010	0.001	0.549	0.002	8.02

Spot	d (µm)	Mg	Si	Ca	Fe	Na	Al	Ti	Mn	Cr	Total
51	1002	0.171	2.963	0.334	1.969	0.003	2.020	0.010	0.550	0.001	8.02
52	1022	0.169	2.957	0.335	1.985	0.000	2.030	0.006	0.536	0.002	8.02
53	1042	0.174	2.954	0.318	1.971	0.004	2.042	0.023	0.513	0.003	8.00
54	1062	0.169	2.944	0.334	2.016	0.002	2.041	0.004	0.519	0.002	8.03
55	1082	0.185	2.936	0.324	2.042	0.000	2.040	0.005	0.506	0.001	8.04
56	1102	0.180	2.993	0.303	2.036	0.009	2.007	0.001	0.478	0.000	8.01
57	1122	0.189	2.984	0.299	2.053	0.009	2.003	0.004	0.473	0.000	8.01
58	1142	0.187	2.958	0.296	2.094	0.016	2.023	0.004	0.457	0.000	8.03
59	1162	0.204	2.962	0.274	2.109	0.006	2.033	0.002	0.433	0.001	8.02
60	1182	0.207	2.976	0.257	2.151	0.007	2.013	0.001	0.408	0.000	8.02
61	1202	0.213	2.964	0.240	2.176	0.000	2.027	0.000	0.400	0.001	8.02
62	1222	0.241	2.962	0.219	2.215	0.006	2.020	0.000	0.367	0.001	8.03
63	1242	0.246	2.967	0.202	2.228	0.001	2.026	0.000	0.351	0.001	8.02
64	1262	0.228	2.959	0.317	2.178	0.006	2.024	0.001	0.315	0.001	8.03
65	1282	0.229	2.961	0.284	2.207	0.001	2.026	0.000	0.317	0.002	8.03
66	1302	0.233	2.945	0.368	2.186	0.000	2.037	0.000	0.267	0.000	8.04
67	1322	0.222	2.976	0.331	2.172	0.000	2.049	0.000	0.251	0.000	8.00
68	1342	0.221	2.982	0.356	2.204	0.000	2.006	0.001	0.243	0.000	8.01
69	1362	0.229	2.943	0.358	2.203	0.004	2.056	0.002	0.236	0.000	8.03
70	1382	0.237	2.957	0.368	2.221	0.000	2.038	0.002	0.199	0.000	8.02
71	1402	0.256	2.945	0.335	2.274	0.000	2.031	0.010	0.177	0.001	8.03
72	1422	0.261	2.959	0.339	2.263	0.001	2.020	0.010	0.168	0.001	8.02
73	1442	0.267	2.946	0.331	2.310	0.000	2.023	0.008	0.145	0.003	8.03
75	1482	0.285	2.947	0.307	2.326	0.006	2.030	0.005	0.128	0.002	8.04
76	1502	0.292	2.975	0.321	2.285	0.004	2.009	0.000	0.133	0.002	8.02
77	1522	0.298	2.978	0.295	2.300	0.001	2.013	0.000	0.130	0.001	8.01
78	1542	0.310	2.970	0.282	2.316	0.004	2.018	0.000	0.121	0.002	8.02
79	1562	0.321	2.964	0.287	2.345	0.000	2.005	0.000	0.109	0.002	8.03
80	1582	0.337	2.961	0.302	2.337	0.000	2.003	0.000	0.095	0.002	8.04
81	1602	0.341	2.986	0.295	2.313	0.004	1.993	0.000	0.088	0.000	8.02
82	1622	0.369	2.985	0.276	2.329	0.000	1.980	0.000	0.085	0.000	8.02
83	1642	0.365	2.978	0.252	2.355	0.000	1.981	0.000	0.100	0.000	8.03
Data not used:											
49	962	0.113	4.018	0.206	1.280	0.011	1.295	0.025	0.359	0.005	7.31
74	1462	0.265	2.961	0.301	2.311	0.000	2.043	0.000	0.136	0.001	8.02

Garnet (weight percent oxide)

Spot	d (µm)	MgO	SiO_2	CaO	FeO	Na_2O	Al_2O_3	TiO_2	MnO	Cr_2O_3	Total
1	2	2.96	37.86	2.59	35.31	0.00	21.31	0.06	1.31	0.01	101.41
2	22	3.24	37.41	2.63	35.90	0.00	21.26	0.00	1.17	0.03	101.66
3	42	3.02	37.20	2.83	35.53	0.00	21.13	0.00	1.11	0.02	100.83
4	62	2.86	37.57	3.22	35.70	0.02	21.24	0.00	1.12	0.03	101.76
5	82	2.76	36.98	3.54	35.25	0.00	20.52	0.00	1.12	0.03	100.21
6	102	2.64	37.33	3.42	35.42	0.00	21.81	0.04	1.34	0.00	102.01
7	122	2.52	36.96	3.40	35.48	0.02	21.61	0.10	1.64	0.00	101.71
8	142	2.40	37.07	3.39	35.34	0.03	21.54	0.03	1.80	0.00	101.59
9	162	2.36	37.00	3.46	34.88	0.02	21.54	0.03	2.18	0.00	101.48
10	182	2.14	37.19	3.82	34.53	0.06	21.61	0.04	2.58	0.00	101.97
11	202	1.99	36.98	3.97	34.05	0.02	21.49	0.00	2.87	0.03	101.40
12	222	2.01	37.07	3.90	34.12	0.00	21.44	0.00	3.12	0.03	101.68
13	242	1.94	37.21	4.06	33.78	0.03	21.39	0.00	3.45	0.05	101.90
14	262	1.82	37.12	4.17	33.25	0.01	21.39	0.01	3.74	0.02	101.54
15	282	1.82	37.05	4.32	33.02	0.04	21.20	0.00	3.95	0.03	101.44

Spot	d (μm)	MgO	SiO_2	CaO	FeO	Na_2O	Al_2O_3	TiO_2	MnO	Cr_2O_3	Total
16	302	1.59	37.37	4.33	32.68	0.01	21.47	0.00	3.72	0.00	101.17
17	322	1.52	37.06	4.37	32.48	0.00	21.46	0.00	3.96	0.00	100.86
18	342	1.53	37.05	4.13	32.61	0.00	21.44	0.00	4.23	0.00	100.99
19	362	1.54	37.18	4.26	32.30	0.00	21.38	0.02	4.47	0.00	101.16
20	382	1.51	37.22	4.41	31.68	0.00	21.31	0.00	4.60	0.00	100.73
21	402	1.65	36.80	3.83	31.94	0.00	21.38	0.10	5.08	0.00	100.78
22	422	1.62	36.53	3.61	31.75	0.00	21.61	0.09	5.52	0.03	100.76
23	442	1.64	36.70	3.42	32.13	0.00	21.65	0.06	5.73	0.02	101.34
24	462	1.62	36.91	3.13	32.28	0.00	21.60	0.06	5.80	0.01	101.40
25	482	1.74	36.87	2.56	32.75	0.01	21.49	0.05	6.29	0.01	101.77
26	502	1.59	37.12	2.70	32.01	0.00	21.22	0.06	6.68	0.02	101.40
27	522	1.56	37.01	2.93	31.37	0.00	21.44	0.06	6.90	0.02	101.29
28	542	1.47	36.93	3.27	30.81	0.01	21.16	0.09	7.13	0.02	100.89
29	562	1.47	36.77	3.33	30.71	0.00	21.34	0.08	7.23	0.02	100.94
30	582	1.41	37.18	3.31	30.58	0.03	21.53	0.13	7.48	0.03	101.68
31	602	1.46	36.97	3.37	30.38	0.00	21.45	0.00	7.77	0.03	101.42
32	622	1.40	36.83	3.52	30.15	0.00	21.39	0.04	7.76	0.00	101.10
33	642	1.37	36.90	3.67	30.21	0.00	21.39	0.02	7.78	0.01	101.35
34	662	1.36	36.87	3.73	29.85	0.00	21.09	0.08	7.97	0.02	100.97
35	682	1.41	36.02	3.66	29.72	0.00	21.25	0.00	7.97	0.03	100.07
36	702	1.36	37.06	3.78	29.73	0.05	21.32	0.00	7.94	0.00	101.24
37	722	1.38	36.95	4.02	29.34	0.03	21.30	0.00	7.92	0.00	100.95
38	742	1.36	37.22	3.88	29.23	0.04	21.40	0.00	8.13	0.00	101.26
39	762	1.40	36.89	3.58	29.36	0.06	21.27	0.00	8.24	0.00	100.79
40	782	1.46	37.13	3.44	29.53	0.07	21.20	0.00	8.16	0.00	100.97
41	802	1.48	36.79	3.16	29.47	0.05	20.99	0.00	8.04	0.00	99.97
42	822	1.48	36.85	2.94	29.72	0.07	20.98	0.08	7.94	0.00	100.05
43	842	1.52	37.10	2.98	29.91	0.03	20.92	0.00	8.03	0.00	100.48
44	862	1.46	36.88	3.09	29.50	0.09	21.00	0.08	7.95	0.00	100.04
45	882	1.44	36.60	3.21	29.44	0.04	21.15	0.03	8.05	0.00	99.96
46	902	1.47	36.78	3.40	29.72	0.03	21.27	0.00	8.35	0.02	101.03
47	922	1.43	36.71	3.30	29.63	0.00	21.05	0.06	8.22	0.00	100.40
48	942	1.50	36.92	3.45	29.52	0.04	21.29	0.02	8.10	0.02	100.86
50	982	1.42	36.94	3.74	29.78	0.00	21.22	0.02	8.07	0.02	101.21
51	1002	1.43	37.06	3.90	29.45	0.02	21.43	0.17	8.12	0.01	101.58
52	1022	1.42	36.85	3.90	29.58	0.00	21.45	0.10	7.89	0.03	101.22
53	1042	1.47	37.18	3.74	29.67	0.03	21.81	0.38	7.63	0.05	101.94
54	1062	1.40	36.51	3.87	29.90	0.01	21.48	0.07	7.60	0.04	100.87
55	1082	1.53	36.18	3.72	30.08	0.00	21.32	0.08	7.37	0.02	100.30
56	1102	1.50	37.23	3.52	30.28	0.06	21.18	0.02	7.02	0.00	100.82
57	1122	1.59	37.39	3.50	30.76	0.06	21.29	0.07	6.99	0.00	101.64
58	1142	1.56	36.87	3.44	31.22	0.10	21.39	0.07	6.73	0.00	101.39
59	1162	1.72	37.08	3.21	31.57	0.04	21.59	0.03	6.39	0.01	101.64
60	1182	1.73	37.07	2.99	32.03	0.04	21.27	0.02	6.00	0.00	101.15
61	1202	1.79	37.11	2.80	32.57	0.00	21.53	0.00	5.92	0.02	101.74
62	1222	2.02	36.99	2.56	33.07	0.04	21.40	0.00	5.41	0.01	101.49
63	1242	2.07	37.25	2.37	33.45	0.00	21.58	0.00	5.21	0.01	101.93
64	1262	1.92	36.99	3.70	32.55	0.04	21.47	0.02	4.65	0.01	101.34
65	1282	1.92	37.05	3.32	33.02	0.00	21.51	0.00	4.69	0.03	101.53
66	1302	1.93	36.43	4.25	32.33	0.00	21.37	0.00	3.91	0.00	100.22
67	1322	1.86	37.17	3.85	32.44	0.00	21.71	0.00	3.70	0.00	100.73
68	1342	1.84	36.94	4.12	32.64	0.00	21.09	0.02	3.55	0.00	100.20
69	1362	1.91	36.58	4.15	32.74	0.02	21.68	0.04	3.47	0.00	100.58
70	1382	1.97	36.64	4.25	32.91	0.00	21.43	0.04	2.91	0.01	100.15
71	1402	2.16	36.97	3.92	34.14	0.00	21.63	0.17	2.63	0.02	101.65
72	1422	2.20	37.24	3.98	34.05	0.01	21.57	0.16	2.49	0.01	101.71

Spot	d (μm)	MgO	SiO_2	CaO	FeO	Na_2O	Al_2O_3	TiO_2	MnO	Cr_2O_3	Total
73	1442	2.25	37.03	3.89	34.72	0.00	21.57	0.13	2.14	0.05	101.78
75	1482	2.40	37.00	3.60	34.92	0.04	21.63	0.08	1.90	0.03	101.59
76	1502	2.46	37.34	3.76	34.30	0.02	21.39	0.00	1.96	0.03	101.27
77	1522	2.51	37.43	3.46	34.56	0.00	21.47	0.00	1.93	0.02	101.38
78	1542	2.61	37.31	3.30	34.79	0.03	21.50	0.00	1.80	0.03	101.36
79	1562	2.70	37.21	3.36	35.20	0.00	21.36	0.00	1.61	0.04	101.48
80	1582	2.83	37.08	3.53	34.99	0.00	21.28	0.00	1.40	0.03	101.14
81	1602	2.85	37.29	3.43	34.54	0.02	21.11	0.00	1.29	0.00	100.53
82	1622	3.06	36.98	3.19	34.50	0.00	20.81	0.00	1.25	0.00	99.79
83	1642	3.01	36.69	2.90	34.69	0.00	20.71	0.00	1.45	0.00	99.46
Data not used:											
49	962	0.669	35.503	1.7	13.519	0.049	9.704	0.298	3.743	0.058	65.24
74	1462	1.873	31.196	2.955	29.108	0	18.259	0	1.686	0.018	85.10

Plagioclase (normalized to 8 O atoms)

Spot	Na	Si	Ca	Fe	Mg	Al	K	Total	Notes
1	0.682	2.621	0.350	0.025	0.001	1.360	0.006	5.043	Inclusion #1
2	0.690	2.626	0.348	0.024	0.000	1.353	0.004	5.045	Inclusion #1
3	0.675	2.627	0.353	0.024	0.000	1.351	0.009	5.040	Inclusion #1
4	0.682	2.628	0.351	0.023	0.000	1.351	0.007	5.041	Inclusion #1
5	0.637	2.591	0.394	0.027	0.000	1.384	0.007	5.039	Inclusion #2
6	0.639	2.601	0.389	0.024	0.000	1.375	0.007	5.034	Inclusion #2
7	0.634	2.588	0.400	0.023	0.000	1.386	0.007	5.039	Inclusion #2
8	0.626	2.579	0.404	0.023	0.000	1.400	0.005	5.037	Inclusion #2
9	0.632	2.582	0.393	0.023	0.001	1.400	0.006	5.037	Inclusion #2
10	0.630	2.588	0.400	0.021	0.000	1.390	0.006	5.035	Inclusion #2
11	0.737	2.699	0.287	0.004	0.001	1.292	0.008	5.028	
12	0.714	2.685	0.296	0.002	0.001	1.313	0.008	5.019	
13	0.735	2.715	0.275	0.001	0.000	1.282	0.009	5.016	
14	0.693	2.682	0.312	0.001	0.000	1.315	0.010	5.013	
15	0.707	2.694	0.295	0.001	0.000	1.307	0.007	5.010	
16	0.719	2.706	0.286	0.003	0.000	1.291	0.008	5.013	
17	0.720	2.704	0.286	0.002	0.000	1.294	0.008	5.014	
18	0.720	2.684	0.299	0.003	0.001	1.311	0.007	5.024	
19	0.722	2.671	0.292	0.006	0.000	1.331	0.009	5.030	
20	0.730	2.693	0.292	0.004	0.000	1.299	0.007	5.026	
21	0.737	2.693	0.294	0.002	0.001	1.297	0.008	5.031	
22	0.730	2.702	0.284	0.004	0.000	1.293	0.009	5.022	
23	0.717	2.682	0.303	0.001	0.001	1.314	0.006	5.023	

Plagioclase (weight percent oxide)

Spot	Na_2O	SiO_2	CaO	FeO	MgO	Al_2O_3	K_2O	Total	Notes
1	7.89	58.82	7.33	0.66	0.01	25.90	0.11	100.72	Inclusion #1
2	7.88	58.21	7.21	0.64	0.00	25.45	0.07	99.46	Inclusion #1
3	7.88	59.47	7.46	0.65	0.00	25.94	0.16	101.57	Inclusion #1
4	7.95	59.41	7.40	0.61	0.00	25.90	0.13	101.40	Inclusion #1
5	7.43	58.56	8.31	0.73	0.00	26.54	0.12	101.69	Inclusion #2
6	7.43	58.69	8.20	0.64	0.00	26.33	0.12	101.41	Inclusion #2
7	7.36	58.27	8.41	0.62	0.00	26.48	0.12	101.27	Inclusion #2
8	7.26	58.01	8.49	0.62	0.00	26.71	0.09	101.17	Inclusion #2
9	7.35	58.28	8.29	0.62	0.01	26.80	0.11	101.44	Inclusion #2
10	7.33	58.39	8.42	0.57	0.01	26.60	0.11	101.42	Inclusion #2
Spot	Na_2O	SiO_2	CaO	FeO	MgO	Al_2O_3	K_2O	Total	Notes

11	8.52	60.54	6.01	0.10	0.02	24.58	0.14	99.91
12	8.30	60.49	6.23	0.05	0.01	25.10	0.14	100.32
13	8.54	61.20	5.78	0.03	0.00	24.51	0.16	100.21
14	8.00	59.99	6.51	0.02	0.00	24.94	0.18	99.64
15	8.17	60.36	6.16	0.03	0.00	24.84	0.13	99.68
16	8.30	60.55	5.97	0.07	0.00	24.50	0.15	99.53
17	8.34	60.72	6.00	0.06	0.00	24.66	0.14	99.91
18	8.36	60.41	6.27	0.07	0.01	25.04	0.12	100.28
19	8.27	59.28	6.05	0.15	0.00	25.06	0.15	98.95
20	8.46	60.54	6.13	0.10	0.00	24.78	0.12	100.13
21	8.47	60.03	6.11	0.05	0.01	24.52	0.15	99.34
22	8.45	60.61	5.94	0.12	0.00	24.61	0.15	99.87
23	8.35	60.60	6.39	0.03	0.01	25.18	0.10	100.65

Biotite (normalized to 11 O atoms)

Spot	Na	Si	Cl	Fe	Mg	Al	K	Mn	Ti	Total
1	0.047	2.698	0.000	1.225	1.142	1.807	0.836	0.004	0.041	7.80
2	0.049	2.687	0.004	1.232	1.127	1.775	0.895	0.006	0.061	7.84
3	0.047	2.695	0.004	1.227	1.105	1.774	0.893	0.004	0.069	7.82
4	0.042	2.696	0.004	1.253	1.106	1.771	0.828	0.005	0.075	7.78
5	0.052	2.721	0.004	1.255	1.090	1.750	0.807	0.004	0.076	7.76
6	0.038	2.716	0.005	1.282	1.051	1.770	0.756	0.003	0.088	7.71
7	0.039	2.715	0.004	1.228	1.090	1.745	0.811	0.006	0.101	7.74
8	0.038	2.725	0.003	1.239	1.096	1.729	0.800	0.004	0.099	7.73
9	0.039	2.705	0.001	1.239	1.101	1.704	0.887	0.002	0.114	7.79
10	0.037	2.732	0.004	1.221	1.087	1.697	0.883	0.003	0.108	7.77
11	0.037	2.720	0.001	1.244	1.102	1.678	0.897	0.004	0.113	7.80
12	0.042	2.733	0.000	1.223	1.111	1.684	0.885	0.003	0.104	7.78
13	0.041	2.730	0.003	1.230	1.098	1.669	0.895	0.003	0.117	7.79
14	0.039	2.707	0.001	1.218	1.079	1.702	0.868	0.004	0.140	7.76
15	0.041	2.728	0.000	1.209	1.071	1.696	0.880	0.003	0.129	7.76

Biotite (weight percent oxide)

Spot	Na_2O	SiO_2	Cl	FeO	MgO	Al_2O_3	K_2O	MnO	TiO_2	Total
1	0.32	35.45	0.00	19.25	10.06	20.15	8.62	0.06	0.71	94.61
2	0.33	34.93	0.03	19.15	9.83	19.58	9.13	0.09	1.05	94.11
3	0.32	35.02	0.03	19.07	9.63	19.56	9.09	0.07	1.20	93.97
4	0.28	35.24	0.03	19.58	9.70	19.65	8.48	0.07	1.30	94.33
5	0.35	35.35	0.03	19.50	9.50	19.28	8.22	0.06	1.32	93.59
6	0.25	35.39	0.04	19.98	9.19	19.57	7.72	0.04	1.53	93.70
7	0.26	35.48	0.03	19.19	9.56	19.34	8.30	0.09	1.75	93.99
8	0.26	35.42	0.02	19.25	9.56	19.06	8.15	0.06	1.71	93.48
9	0.26	35.33	0.01	19.35	9.65	18.89	9.08	0.03	1.98	94.58
10	0.25	35.58	0.03	19.01	9.50	18.75	9.02	0.04	1.86	94.04
11	0.25	35.63	0.01	19.49	9.68	18.65	9.21	0.05	1.97	94.93
12	0.28	35.71	0.00	19.11	9.74	18.67	9.07	0.04	1.81	94.43
13	0.28	35.75	0.03	19.25	9.64	18.54	9.19	0.04	2.04	94.74
14	0.27	36.12	0.00	19.43	9.66	19.26	9.08	0.06	2.48	96.36
15	0.28	35.90	0.00	19.03	9.46	18.94	9.08	0.05	2.25	94.97

Muscovite (normalized to 11 O atoms)

Spot	Na	Si	Cl	Fe	Mg	Al	K	Mn	Ti	Total
1	0.142	3.040	0.001	0.068	0.059	2.868	0.725	0.001	0.028	6.93
2	0.141	3.044	0.000	0.154	0.063	2.800	0.779	0.000	0.018	7.00
3	0.149	3.082	0.002	0.069	0.062	2.795	0.839	0.000	0.009	7.01
4	0.118	3.045	0.002	0.196	0.057	2.773	0.780	0.001	0.023	6.99
5	0.126	3.074	0.000	0.065	0.057	2.822	0.819	0.000	0.012	6.98
6	0.119	3.031	0.000	0.099	0.054	2.852	0.733	0.000	0.041	6.93
7	0.142	3.059	0.000	0.069	0.061	2.792	0.843	0.000	0.036	7.00
8	0.133	3.058	0.000	0.080	0.054	2.792	0.835	0.000	0.039	6.99
9	0.139	3.055	0.000	0.073	0.062	2.788	0.857	0.000	0.037	7.01
10	0.155	3.064	0.000	0.068	0.061	2.791	0.841	0.000	0.029	7.01
11	0.132	3.062	0.002	0.067	0.061	2.842	0.727	0.000	0.027	6.92
12	0.119	3.070	0.005	0.082	0.051	2.801	0.815	0.000	0.026	6.97
13	0.135	3.063	0.005	0.088	0.057	2.791	0.826	0.000	0.028	6.99
14	0.138	3.069	0.003	0.058	0.052	2.804	0.835	0.000	0.028	6.99
15	0.118	3.051	0.002	0.126	0.055	2.777	0.854	0.000	0.031	7.02

Muscovite (weight percent oxide)

Spot	Na_2O	SiO_2	Cl	FeO	MgO	Al_2O_3	K_2O	MnO	TiO_2	Total
1	1.13	46.84	0.01	1.26	0.60	37.50	8.76	0.02	0.58	96.69
2	1.08	44.97	0.00	2.71	0.62	35.09	9.02	0.01	0.35	93.84
3	1.15	45.93	0.02	1.22	0.62	35.34	9.80	0.00	0.19	94.25
4	0.90	45.30	0.02	3.48	0.57	35.00	9.09	0.01	0.45	94.82
5	0.97	46.06	0.00	1.17	0.57	35.87	9.62	0.00	0.23	94.49
6	0.94	46.57	0.00	1.82	0.55	37.17	8.82	0.00	0.83	96.72
7	1.10	45.83	0.00	1.24	0.61	35.49	9.89	0.00	0.71	94.87
8	1.03	45.89	0.00	1.43	0.54	35.55	9.82	0.00	0.77	95.04
9	1.07	45.90	0.00	1.30	0.62	35.54	10.09	0.00	0.75	95.26
10	1.20	46.08	0.00	1.23	0.62	35.60	9.91	0.01	0.58	95.23
11	1.04	46.85	0.01	1.22	0.63	36.89	8.72	0.01	0.54	95.90
12	0.91	45.47	0.04	1.45	0.51	35.19	9.46	0.00	0.52	93.54
13	1.04	45.45	0.05	1.57	0.57	35.14	9.61	0.00	0.56	93.96
14	1.06	45.70	0.03	1.03	0.52	35.42	9.74	0.00	0.56	94.05
15	0.90	45.13	0.02	2.23	0.55	34.85	9.90	0.00	0.61	94.19

APPENDIX E

Monazite electron microprobe data from metapelitic rocks of the Vernon area

Appendix E. Monazite electron microprobe data from metapelitic rocks of the Vernon area

Analysis	CaO	Ce_2O_3	P_2O_5	PbO	SiO_2	Nd_2O_3	$La2O_3$	ThO_2	Pr_2O_3	Y_2O_3	Sm_2O_3	UO_2	Gd_2O_3	Total
Sample 99TWG584														
584-m1-1	0.980	28.460	30.093	0.062	0.349	12.052	14.051	4.244	3.098	1.411	2.301	1.052	1.613	99.77
584-m1-2	0.868	28.878	30.705	0.053	0.306	11.977	14.540	3.876	3.031	1.263	2.187	0.921	1.468	100.07
584-m1-3	1.104	28.473	30.892	0.037	0.164	11.291	14.110	4.543	2.942	2.648	1.854	0.623	1.387	100.07
584-m1-4	1.115	29.282	30.689	0.033	0.186	11.596	14.415	4.627	2.957	1.184	2.060	0.594	1.331	100.07
584-m1-5	1.014	28.509	30.220	0.066	0.410	11.851	13.901	4.717	3.127	1.245	2.319	1.089	1.397	99.87
584-m1-6	1.106	29.571	30.474	0.015	0.236	12.201	14.410	4.490	3.166	0.489	2.120	0.628	1.291	100.20
584-m1-7	1.189	28.909	30.688	0.029	0.179	11.891	14.170	4.691	3.145	0.933	2.129	0.633	1.526	100.11
584-m1-8	1.104	30.029	30.706	0.020	0.173	11.740	14.641	4.538	3.065	0.590	2.046	0.610	1.339	100.60
584-m1-9	1.161	30.002	30.954	0.017	0.144	11.696	14.731	4.665	2.984	0.596	2.121	0.695	1.209	100.98
584-m1-10	1.170	28.326	30.967	0.058	0.135	11.149	14.207	4.200	2.900	1.883	2.095	0.965	1.879	99.93
584-m2-1	1.192	29.689	31.515	0.017	0.185	11.604	14.514	4.821	2.951	1.119	2.035	0.637	1.349	101.63
584-m2-2	1.240	29.465	31.376	0.031	0.160	11.996	14.330	5.136	3.056	0.753	2.122	0.476	1.491	101.63
584-m2-3	1.185	29.229	31.276	0.027	0.183	11.822	14.155	4.792	2.954	1.075	2.102	0.677	1.469	100.95
584-m2-4	1.364	28.631	30.493	0.031	0.210	11.731	14.093	5.613	3.082	0.848	2.148	0.496	1.467	100.21
584-m2-5	1.253	28.989	30.858	0.036	0.187	11.578	14.272	5.157	3.043	1.179	2.042	0.542	1.490	100.63
584-m2-6	1.263	29.601	31.126	0.029	0.166	11.812	14.334	5.211	2.980	0.774	2.135	0.502	1.390	101.32
584-m3-1	1.184	28.224	30.773	0.030	0.135	11.378	13.551	4.838	2.885	2.333	2.094	0.634	1.513	99.57
584-m3-2	1.227	28.422	30.972	0.035	0.131	11.421	13.492	4.896	2.881	2.352	2.146	0.741	1.450	100.17
584-m3-3	1.186	28.245	30.632	0.027	0.146	11.314	13.727	4.895	2.808	2.217	2.123	0.637	1.646	99.60
584-m3-4	1.203	28.234	30.807	0.032	0.138	11.471	13.505	4.784	2.874	2.340	2.111	0.706	1.572	99.78
584-m3-5	1.183	28.591	30.792	0.031	0.136	11.337	13.570	4.637	3.059	2.256	2.141	0.650	1.481	99.86
584-m3-6	1.414	28.133	30.497	0.074	0.237	11.063	13.434	5.746	2.976	1.648	2.125	1.066	1.315	99.73
584-m3-7	1.483	27.724	30.608	0.074	0.214	11.039	13.172	5.890	2.931	1.801	2.141	1.034	1.572	99.68
584-m3-8	1.219	28.366	30.719	0.028	0.143	11.481	13.659	4.825	2.970	1.858	2.189	0.711	1.593	99.76
584-m3-9	1.086	28.879	30.224	0.060	0.307	11.612	14.161	4.672	3.019	1.498	2.111	0.981	1.251	99.86
584-m3-10	1.243	29.379	30.403	0.021	0.181	11.656	14.300	5.331	2.986	1.021	2.058	0.572	1.376	100.53
584-m4-1	1.144	28.626	30.917	0.024	0.101	11.505	13.597	4.534	2.924	2.519	2.097	0.576	1.464	100.03
584-m4-2	1.212	29.670	30.589	0.020	0.154	12.039	14.391	4.948	3.091	0.513	2.061	0.710	1.410	100.81
584-m4-3	1.230	29.458	30.490	0.019	0.152	11.746	14.569	5.204	3.029	0.787	2.087	0.590	1.411	100.77
584-m4-4	1.107	29.185	30.816	0.021	0.092	11.519	13.813	4.355	3.033	2.204	2.049	0.610	1.510	100.31
584-m4-5	1.243	29.606	30.490	0.020	0.132	11.516	14.281	4.910	3.094	0.861	2.037	0.652	1.461	100.30
584-m4-6	1.240	29.417	30.678	0.021	0.133	11.621	14.531	4.897	3.034	0.851	2.123	0.703	1.417	100.67
584-m4-7	1.220	29.783	30.607	0.022	0.140	11.574	14.445	4.807	3.065	0.801	2.019	0.628	1.517	100.63

Analysis	CaO	Ce_2O_3	P_2O_5	PbO	SiO_2	Nd_2O_3	$La2O_3$	ThO_2	Pr_2O_3	Y_2O_3	Sm_2O_3	UO_2	Gd_2O_3	Total
584-m4-8	1.224	29.299	30.403	0.021	0.154	11.840	14.140	5.149	3.131	0.815	2.057	0.632	1.468	100.33
584-m4-9	1.065	29.787	30.231	0.017	0.134	11.902	14.506	4.360	3.185	0.684	2.091	0.508	1.357	99.83
584-m4-10	1.292	29.127	30.390	0.023	0.157	11.779	14.265	5.357	3.024	0.897	2.042	0.699	1.400	100.45
584-m5-2	1.134	28.296	30.361	0.043	0.156	11.642	13.611	4.521	3.094	2.192	2.198	0.705	1.390	99.34
584-m5-3	1.176	29.984	30.324	0.014	0.137	11.953	14.591	4.631	3.102	0.450	2.116	0.646	1.341	100.47
584-m5-4	1.248	29.707	30.269	0.018	0.196	11.864	14.386	5.257	3.156	0.479	2.052	0.606	1.114	100.35
584-m5-5	0.923	29.864	30.098	0.049	0.239	12.191	14.334	3.813	3.193	1.259	2.091	0.867	1.075	100.00
584-m5-6	0.887	29.952	29.922	0.041	0.258	12.119	14.611	3.971	3.147	1.086	2.013	0.703	1.097	99.81
584-m5-7	1.205	28.588	30.632	0.049	0.120	11.223	13.824	4.632	3.072	2.224	1.914	0.667	1.422	99.57
584-m6-1	1.255	28.584	30.260	0.070	0.277	11.852	13.711	4.629	3.008	1.330	2.080	1.460	1.262	99.78
584-m6-2	0.953	30.057	30.346	0.049	0.200	11.936	14.520	3.878	3.070	1.103	1.998	0.720	1.189	100.02
584-m6-3	1.094	28.282	30.723	0.047	0.133	11.623	13.699	4.585	3.151	2.527	2.047	0.501	1.480	99.89
584-m6-4	0.843	31.105	30.546	0.039	0.153	11.748	15.245	2.768	3.168	1.117	2.052	0.810	1.086	100.68
584-m6-5	1.161	28.800	30.744	0.052	0.111	11.385	13.843	4.495	3.068	2.199	1.918	0.730	1.226	99.73
584-m6-6	1.224	29.726	30.398	0.032	0.105	11.943	14.054	4.939	3.217	0.874	2.161	0.677	1.496	100.85
584-m6-7	1.184	29.107	30.330	0.027	0.124	12.016	13.986	4.796	3.038	0.988	2.196	0.658	1.573	100.02
584-m6-8	1.168	29.674	30.572	0.029	0.134	11.903	14.044	4.737	3.003	1.096	2.127	0.656	1.452	100.60
584-m6-9	1.220	29.554	30.207	0.018	0.176	11.991	14.204	5.117	3.105	0.616	2.066	0.610	1.296	100.18
584-m6-10	1.158	28.997	30.257	0.020	0.168	11.749	13.752	4.807	2.987	1.628	2.136	0.657	1.492	99.81
584-m6-11	1.181	29.900	30.433	0.018	0.153	11.806	14.285	4.757	3.201	0.523	2.083	0.629	1.338	100.31
584-m6-12	1.187	29.903	30.414	0.018	0.181	11.962	14.309	5.136	3.174	0.516	2.053	0.543	1.349	100.75
584-m6-13	1.216	29.853	30.270	0.018	0.149	11.832	14.256	4.990	3.044	0.506	2.040	0.660	1.398	100.23
584-m6-14	1.318	29.284	30.263	0.019	0.199	11.733	14.087	5.557	3.255	0.532	2.150	0.645	1.369	100.43
584-m6-15	1.204	29.966	30.520	0.018	0.144	11.845	14.472	4.954	3.284	0.512	2.081	0.620	1.396	101.02
584-m6-16	1.198	29.906	30.124	0.020	0.176	11.833	14.447	5.112	3.021	0.410	2.062	0.657	1.414	100.38
584-m8-1	1.117	29.906	30.054	0.023	0.141	10.876	15.488	4.412	2.962	1.173	1.794	0.714	1.301	99.96
584-m8-2	1.099	30.213	30.276	0.029	0.151	10.944	15.282	4.322	2.961	1.222	1.869	0.738	1.301	100.41
584-m8-3	0.969	30.201	30.320	0.027	0.252	11.182	15.579	4.428	3.067	0.972	1.782	0.399	1.491	100.67
584-m9-1	0.461	30.079	28.075	0.054	1.408	11.248	16.054	7.032	3.046	0.263	1.365	0.359	0.608	100.05
584-m9-2	1.264	29.056	30.467	0.038	0.188	11.131	14.585	5.373	2.975	1.418	1.887	0.550	1.318	100.25
584-m9-3	1.159	29.635	30.359	0.039	0.256	10.890	15.110	5.366	2.934	1.316	1.750	0.492	1.315	100.62
584-m10-1	1.098	29.072	30.580	0.042	0.171	11.541	14.331	4.080	3.051	1.722	2.180	0.972	1.866	100.71
584-m10-2	1.045	28.967	30.218	0.039	0.197	11.419	14.373	3.919	2.935	1.623	2.107	0.929	1.656	99.63
Sample 00TWG489														
489-m1-1	0.997	28.542	30.094	0.029	0.295	12.749	13.440	4.673	3.145	0.893	2.606	0.568	1.848	99.88
489-m1-2	1.000	28.281	30.534	0.028	0.281	12.593	13.631	4.114	3.158	1.359	2.500	0.580	1.832	99.89

Analysis	CaO	Ce_2O_3	P_2O_5	PbO	SiO_2	Nd_2O_3	$La2O_3$	ThO_2	Pr_2O_3	Y_2O_3	Sm_2O_3	UO_2	Gd_2O_3	Total
489-m1-3	1.068	28.097	30.106	0.030	0.351	12.770	13.410	4.992	3.241	0.942	2.556	0.593	1.847	100.00
489-m1-4	0.716	29.246	30.445	0.017	0.266	12.848	14.079	3.026	3.179	1.333	2.543	0.455	1.790	99.94
489-m1-5	0.778	29.157	30.122	0.019	0.185	12.906	14.308	3.270	3.165	1.006	2.559	0.420	1.803	99.70
489-m1-6	1.039	28.548	30.093	0.028	0.360	12.558	13.693	4.936	3.113	0.887	2.599	0.544	1.747	100.15
489-m1-7	0.919	28.782	30.038	0.024	0.225	12.630	13.971	3.991	3.097	1.013	2.444	0.431	1.703	99.27
489-m1-8	1.043	28.388	30.612	0.019	0.209	11.798	13.929	4.070	3.016	1.993	2.181	0.675	1.555	99.49
489-m2-1	0.955	28.530	30.445	0.028	0.191	12.796	13.591	4.305	3.113	1.436	2.468	0.496	1.654	100.01
489-m2-2	0.436	22.116	27.072	0.025	0.151	9.803	10.952	2.307	2.008	1.278	1.853	0.536	1.371	79.91
489-m2-3	0.872	28.768	30.375	0.027	0.187	12.884	13.617	3.736	3.077	1.437	2.586	0.544	1.973	100.08
489-m2-4	1.083	27.991	30.225	0.029	0.262	12.169	13.364	4.681	3.174	1.504	2.431	0.890	1.760	99.56
489-m2-5	0.979	28.523	30.201	0.023	0.111	11.871	14.004	3.748	2.985	1.953	2.199	0.643	1.513	98.75
489-m2-6	1.022	28.622	30.509	0.020	0.116	12.086	13.670	3.999	3.039	2.061	2.296	0.705	1.661	99.81
489-m2-7	0.937	29.075	30.514	0.018	0.149	12.221	13.896	3.855	3.115	1.723	2.342	0.612	1.541	100.00
489-m2-8	1.047	28.616	30.613	0.027	0.112	12.335	13.864	4.113	3.020	1.582	2.291	0.635	1.726	99.98
489-m3-1	0.888	28.853	30.694	0.020	0.170	12.747	13.943	3.499	3.027	1.586	2.396	0.555	1.711	100.09
489-m3-2	0.965	28.445	30.651	0.027	0.200	12.826	13.479	4.049	3.162	1.608	2.454	0.566	1.874	100.31
489-m3-3	1.011	28.395	30.796	0.022	0.161	12.190	13.751	3.943	3.132	1.927	2.367	0.699	1.673	100.07
489-m3-4	0.517	30.292	30.532	0.014	0.160	13.046	14.676	2.079	3.450	1.376	2.301	0.355	1.407	100.21
489-m3-5	0.984	28.295	30.622	0.024	0.193	12.224	13.643	3.972	3.108	2.037	2.303	0.664	1.659	99.73
489-m4-1	0.601	30.696	30.717	0.010	0.076	13.113	14.722	1.811	3.536	1.592	2.199	0.247	1.148	100.47
489-m4-2	0.891	28.129	30.419	0.021	0.154	12.876	13.187	3.606	3.176	1.841	2.672	0.624	1.784	99.38
489-m4-3	0.997	28.325	30.318	0.019	0.135	12.408	13.550	3.974	2.978	1.903	2.302	0.724	1.685	99.32
489-m4-4	0.871	28.591	30.453	0.021	0.129	12.730	13.679	3.183	2.986	2.452	2.447	0.389	1.535	99.47
489-m4-5	0.864	29.384	30.570	0.020	0.156	12.483	13.939	3.655	3.103	1.514	2.386	0.536	1.627	100.24
489-m5-1	0.993	28.303	30.221	0.022	0.198	12.704	13.533	4.067	3.097	1.664	2.451	0.571	1.756	99.58
489-m5-2	0.925	29.751	30.181	0.026	0.132	12.265	14.280	3.682	3.252	1.250	2.330	0.616	1.680	100.37
489-m5-3	0.880	30.282	30.564	0.021	0.165	12.630	14.278	2.986	3.453	1.440	2.195	0.300	1.148	100.34
489-m5-4	0.688	30.283	30.594	0.018	0.152	12.785	14.177	2.920	3.338	1.489	2.202	0.256	1.288	100.19
489-m5-5	0.764	28.819	30.128	0.020	0.169	12.927	13.907	3.211	3.264	1.644	2.652	0.528	1.764	99.80
489-m5-6	0.868	29.563	30.357	0.021	0.150	12.188	14.341	3.737	3.152	1.472	2.202	0.457	1.281	99.79
489-m5-7	0.988	28.703	30.462	0.020	0.120	12.179	13.772	3.981	3.045	2.046	2.167	0.667	1.459	99.61
489-m5-8	0.643	31.086	30.404	0.017	0.128	12.979	14.599	2.794	3.378	1.144	2.281	0.342	1.368	101.16
489-m6-1	1.023	27.947	30.893	0.033	0.112	12.026	13.395	3.268	3.063	2.985	2.341	0.752	1.683	99.52
489-m6-2	0.967	28.568	30.707	0.022	0.137	12.499	13.785	3.902	3.023	1.879	2.514	0.703	1.824	100.53
489-m6-3	0.990	28.623	30.498	0.021	0.137	12.371	13.669	3.864	3.000	1.886	2.372	0.716	1.806	99.95
489-m6-4	1.002	28.679	30.564	0.021	0.141	12.299	13.747	4.000	3.099	1.928	2.338	0.728	1.753	100.30
489-m6-5	1.120	28.139	30.758	0.021	0.101	12.070	13.607	4.396	3.103	2.189	2.198	0.731	1.592	100.03

Analysis	CaO	Ce_2O_3	P_2O_5	PbO	SiO_2	Nd_2O_3	$La2O_3$	ThO_2	Pr_2O_3	Y_2O_3	Sm_2O_3	UO_2	Gd_2O_3	Total
489-m7-1	1.023	28.764	30.991	0.024	0.126	12.119	13.865	3.996	3.033	2.058	2.243	0.765	1.545	100.55
489-m7-2	1.045	28.376	30.854	0.021	0.138	12.277	13.696	4.075	3.206	1.985	2.374	0.749	1.747	100.54
489-m7-3	0.925	29.258	30.485	0.018	0.146	12.100	14.272	3.720	3.204	1.733	2.376	0.650	1.627	100.51
489-m8-1	1.312	27.835	30.216	0.035	0.291	12.289	13.534	5.841	3.049	0.617	2.507	1.081	1.821	100.43
489-m8-2	0.835	29.735	30.601	0.020	0.252	12.843	14.210	3.489	3.294	0.931	2.486	0.579	1.717	100.99
489-m8-3	1.041	28.541	30.627	0.020	0.121	12.310	13.820	3.869	3.105	2.002	2.212	0.697	1.620	99.99
489-m9-1	0.961	29.112	30.278	0.023	0.205	12.562	13.916	4.217	3.265	1.280	2.430	0.576	1.711	100.54
489-m9-2	0.888	29.804	30.324	0.026	0.250	13.069	13.957	4.004	3.377	0.692	2.508	0.529	1.720	101.15
489-m9-3	1.036	29.159	30.346	0.019	0.182	12.020	14.207	4.295	3.174	1.647	2.146	0.586	1.391	100.21
489-m10-1	0.626	29.904	30.473	0.019	0.174	13.081	14.073	2.987	3.227	1.140	2.628	0.409	1.997	100.74
489-m10-2	1.105	28.519	31.082	0.023	0.084	12.119	13.647	4.297	2.885	2.144	2.146	0.712	1.508	100.27
489-m10-3	1.039	28.076	30.277	0.032	0.266	12.414	13.549	5.018	3.125	1.264	2.534	0.655	1.965	100.21
Sample 00TWG328														
328-m1-1	0.711	28.551	30.669	0.027	0.168	12.639	13.735	2.926	3.172	2.053	2.556	0.582	1.800	99.59
328-m1-2	0.374	30.289	31.037	0.027	0.107	12.763	14.723	1.125	3.131	1.871	2.522	0.480	1.690	100.14
328-m1-3	0.468	29.462	31.031	0.020	0.129	12.812	14.450	1.648	3.080	1.964	2.559	0.565	1.751	99.94
328-m1-4	0.701	28.863	30.737	0.025	0.151	12.664	13.817	2.872	3.142	2.217	2.512	0.586	1.956	100.24
328-m2-1	0.920	27.651	30.447	0.032	0.230	12.289	13.205	4.166	3.008	2.164	2.406	0.620	1.960	99.10
328-m2-2	0.704	28.663	30.523	0.025	0.237	12.600	13.946	2.943	3.107	1.932	2.385	0.518	1.699	99.28
328-m2-3	1.025	27.611	31.332	0.034	0.335	12.008	13.590	4.462	3.037	2.192	2.345	0.736	1.636	100.34
328-m2-4	0.890	28.283	30.709	0.029	0.329	12.443	13.743	3.993	2.945	2.115	2.460	0.588	1.755	100.28
328-m3-1	0.822	28.486	31.064	0.028	0.199	12.536	13.694	3.619	3.006	2.052	2.379	0.514	1.745	100.14
328-m3-2	0.860	28.245	31.405	0.032	0.259	12.383	13.859	4.004	2.948	2.039	2.284	0.575	1.835	100.73
328-m3-3	1.207	27.484	30.576	0.045	0.318	11.407	13.455	5.480	2.854	2.300	2.064	0.792	1.497	99.48
328-m3-4	0.764	29.127	30.962	0.024	0.203	12.412	13.990	3.344	3.005	2.065	2.221	0.565	1.633	100.32
328-m4-1	0.911	28.231	30.871	0.032	0.279	11.972	13.390	4.132	3.110	2.169	2.375	0.544	1.884	99.90
328-m4-2	0.920	28.526	30.740	0.034	0.263	12.408	13.505	4.240	3.069	2.006	2.444	0.583	1.732	100.47
328-m4-3	0.705	28.990	30.732	0.028	0.171	12.696	13.888	3.034	3.155	2.013	2.370	0.477	1.913	100.17
328-m4-4	0.732	28.932	30.770	0.021	0.195	12.612	14.096	3.226	3.085	1.969	2.436	0.494	1.661	100.23
328-m5-1	1.005	27.765	30.921	0.030	0.274	12.180	13.303	4.461	3.043	2.140	2.393	0.599	1.869	99.98
328-m5-2	0.695	28.749	30.991	0.024	0.179	12.835	14.006	2.991	3.094	1.936	2.507	0.461	1.806	100.27
328-m5-3	0.723	28.945	31.218	0.022	0.197	12.727	13.834	3.218	3.183	2.031	2.564	0.439	1.843	100.94
328-m5-4	0.954	27.491	30.676	0.032	0.272	12.323	13.346	4.195	3.103	2.120	2.504	0.643	1.925	99.58
328-m6-1	0.838	28.242	30.912	0.021	0.251	12.380	13.345	3.688	3.158	2.071	2.496	0.592	2.047	100.04
328-m6-2	0.454	30.838	31.098	0.015	0.102	12.538	14.757	1.619	3.105	1.980	2.356	0.385	1.647	100.89
328-m6-3	0.828	28.501	30.854	0.028	0.203	12.474	13.711	3.623	3.133	2.151	2.402	0.519	1.719	100.15

Analysis	CaO	Ce_2O_3	P_2O_5	PbO	SiO_2	Nd_2O_3	$La2O_3$	ThO_2	Pr_2O_3	Y_2O_3	Sm_2O_3	UO_2	Gd_2O_3	Total
328-m6-4	0.852	28.277	30.702	0.029	0.281	12.080	13.587	3.806	2.973	2.196	2.412	0.569	1.757	99.52
328-m7-1	0.711	28.865	30.814	0.022	0.223	12.586	13.521	3.328	3.117	1.967	2.532	0.464	1.793	99.94
328-m7-2	0.901	28.528	30.514	0.033	0.286	12.253	13.748	4.106	3.033	1.927	2.281	0.543	1.664	99.82
328-m7-3	0.820	28.002	30.780	0.017	0.304	12.637	13.356	3.707	3.182	2.150	2.531	0.589	2.056	100.13
328-m7-4	0.702	28.922	30.865	0.024	0.220	12.605	13.846	3.168	3.393	1.920	2.456	0.462	1.819	100.40
328-m8-1	0.869	28.170	30.668	0.029	0.326	12.455	13.548	3.908	3.098	2.028	2.450	0.545	1.833	99.93
328-m8-2	0.847	28.197	30.628	0.026	0.325	12.393	13.485	3.777	3.189	2.269	2.424	0.534	1.892	99.99
328-m8-3	0.780	28.348	30.673	0.023	0.377	12.686	13.777	3.447	3.141	2.065	2.517	0.524	1.701	100.06
328-m8-4	0.898	28.415	30.637	0.027	0.399	12.213	13.370	3.983	3.191	2.239	2.424	0.542	1.849	100.19
Sample 00TWG391														
391-m1-1	0.568	25.322	26.115	0.009	0.516	11.309	13.068	2.271	2.783	1.438	2.170	0.514	1.531	87.61
391-m2-1	0.714	28.746	29.408	0.012	1.492	12.013	14.162	3.142	3.123	1.539	2.198	0.317	1.379	98.25
391-m2-2	0.528	28.791	28.129	0.017	1.245	12.150	13.975	2.478	3.021	1.217	2.046	0.190	1.235	95.02
391-m2-3	0.551	22.149	22.029	0.008	14.758	9.573	10.844	2.357	2.389	1.245	1.838	0.476	1.131	89.35
391-m3-1	0.670	25.455	30.077	0.025	0.756	11.532	12.875	3.049	2.887	6.184	2.222	0.492	1.826	98.05
391-m3-2	0.830	28.486	29.619	0.012	0.598	12.440	14.458	3.986	3.180	1.087	2.205	0.214	1.533	98.65
391-m4-1	0.038	2.516	0.028	0.027	2.951	0.000	0.000	0.027	0.000	0.036	0.000	0.098	0.000	5.72
391-m4-2	0.077	2.370	0.286	0.009	2.592	0.000	0.000	0.030	0.000	0.000	0.017	0.013	0.035	5.43
391-m4-3	0.098	2.426	0.191	0.000	2.902	0.000	0.000	0.021	0.000	0.012	0.000	0.042	0.084	5.78
391-m5-1	0.768	28.415	30.712	0.012	0.420	12.270	14.067	2.758	2.921	1.644	2.441	0.433	1.739	98.60
391-m5-2	0.720	28.381	30.220	0.012	2.301	12.199	14.117	2.588	3.039	1.735	2.312	0.545	1.718	99.89
391-m6-1	0.574	28.921	30.296	0.009	0.633	12.336	14.860	2.106	3.067	1.476	2.241	0.362	1.225	98.11
391-m6-2	0.869	28.273	30.132	0.018	0.262	12.359	13.908	3.718	3.141	1.636	2.315	0.454	1.568	98.65
391-m7-1	0.673	29.172	30.326	0.021	0.194	12.223	14.368	2.615	3.142	1.924	2.166	0.347	1.490	98.66
391-m7-2	0.730	30.653	30.753	0.013	0.206	11.798	14.966	2.798	3.027	1.513	2.013	0.268	1.216	99.95
391-m7-3	0.570	29.710	30.981	0.015	0.179	12.610	14.407	2.415	3.176	1.983	2.170	0.310	1.327	99.85
391-m7-4	0.445	30.434	32.235	0.011	0.164	12.896	14.886	1.960	3.364	1.765	2.246	0.163	1.199	101.77
391-m7-5	0.757	29.674	31.491	0.013	0.150	12.322	14.223	2.513	3.288	2.382	2.192	0.364	1.360	100.73
391-m7-6	0.825	29.484	30.567	0.013	0.276	12.409	13.794	4.197	3.234	1.485	2.296	0.377	1.510	100.47
391-m7-7	0.741	29.197	30.621	0.018	0.300	12.615	14.079	4.107	3.159	1.466	2.295	0.241	1.544	100.38
391-m7-8	0.406	30.796	30.504	0.010	0.312	12.502	14.848	1.677	3.325	1.598	2.135	0.206	1.442	99.76
391-m8-1	0.946	28.789	30.140	0.017	0.408	11.793	14.690	4.244	2.961	1.396	2.085	0.278	1.220	98.97
391-m8-2	0.518	30.100	30.771	0.013	0.161	12.487	15.257	2.368	3.097	1.475	2.192	0.124	1.291	99.85
391-m8-3	1.054	26.518	23.294	0.024	0.629	11.533	11.966	5.147	2.938	1.697	2.252	0.198	1.713	88.96
585-m1-1	1.011	30.724	29.826	0.017	0.555	11.728	15.235	6.268	3.113	0.053	1.839	0.213	0.904	101.49
585-m1-2	0.974	30.393	30.166	0.017	0.547	12.129	15.041	6.059	3.188	0.057	1.989	0.191	0.894	101.65

Analysis	CaO	Ce_2O_3	P_2O_5	PbO	SiO_2	Nd_2O_3	$La2O_3$	ThO_2	Pr_2O_3	Y_2O_3	Sm_2O_3	UO_2	Gd_2O_3	Total
585-m1-3	0.970	30.661	30.145	0.014	0.553	12.100	14.982	6.009	3.167	0.037	1.996	0.173	0.950	101.66
585-m1-4	0.947	30.586	29.912	0.016	0.545	11.659	15.340	6.006	3.143	0.072	1.834	0.175	0.891	101.13
585-m2-1	0.746	29.884	30.708	0.022	0.158	11.216	15.954	3.403	3.056	1.705	1.907	0.177	1.257	100.19
585-m2-2	0.761	31.413	30.189	0.015	0.437	11.735	15.566	4.808	3.190	0.127	2.010	0.185	0.908	101.34
585-m2-3	0.744	30.184	30.129	0.015	0.412	12.395	15.323	4.500	3.253	0.356	2.140	0.151	1.199	100.80
585-m2-4	0.767	30.986	30.146	0.025	0.675	12.621	14.846	5.695	3.239	0.046	1.867	0.131	0.645	101.69
585-m3-1	0.945	28.834	30.989	0.031	0.153	11.283	14.945	3.862	3.165	2.111	1.930	0.238	1.386	99.87
585-m3-2	0.988	29.446	30.997	0.035	0.091	11.678	15.385	3.654	3.068	1.368	2.044	0.398	1.404	100.56
585-m3-3	0.925	29.595	30.780	0.032	0.124	11.744	15.290	3.485	3.074	1.273	2.152	0.388	1.431	100.29
585-m4-1	0.854	31.175	30.334	0.009	0.364	12.073	15.493	4.796	3.123	0.054	2.000	0.187	0.894	101.36
585-m4-2	0.798	31.429	30.434	0.011	0.327	11.865	16.175	4.470	3.303	0.034	1.865	0.176	0.792	101.68
585-m4-3	0.781	31.719	30.532	0.007	0.293	11.810	15.912	4.164	3.275	0.068	1.948	0.191	0.984	101.68
585-m4-4	0.771	31.611	30.461	0.013	0.311	11.790	15.857	4.270	3.192	0.081	2.009	0.204	0.892	101.46
585-m5-1	0.740	30.056	30.608	0.021	0.201	12.030	15.108	3.559	3.301	1.239	2.169	0.170	1.414	100.62
585-m5-2	0.671	31.207	30.226	0.013	0.385	12.176	15.732	4.195	3.201	0.194	2.024	0.194	1.057	101.28
585-m5-3	0.630	30.260	30.595	0.020	0.207	12.041	15.308	3.043	3.090	1.182	2.190	0.190	1.565	100.32
585-m5-4	0.815	30.790	30.048	0.020	0.526	12.451	14.787	5.141	3.323	0.153	1.985	0.143	1.009	101.19
585-m6-1	1.387	28.328	30.891	0.049	0.103	11.104	15.300	4.469	3.119	1.529	1.848	0.426	1.468	100.02
585-m6-2	0.768	30.594	29.848	0.020	0.635	11.881	15.158	5.360	3.082	0.178	1.932	0.139	0.907	100.50
585-m6-3	0.440	31.273	29.900	0.025	0.524	11.336	17.992	3.541	3.010	0.460	1.576	0.133	0.781	100.99
585-m6-4	1.000	28.266	30.785	0.044	0.105	11.204	15.423	3.869	2.905	2.188	1.908	0.428	1.599	99.72
585-m7-1	1.132	29.911	31.018	0.041	0.124	11.035	14.920	4.168	3.099	1.527	1.985	0.544	1.505	101.01
585-m7-2	0.767	30.897	29.629	0.023	0.724	11.970	15.107	5.776	3.116	0.135	1.860	0.104	0.908	101.02
585-m7-3	0.770	31.189	30.291	0.011	0.374	11.361	16.710	4.288	3.055	0.145	1.857	0.189	1.047	101.29
585-m7-4	0.867	30.567	30.069	0.011	0.545	11.655	15.738	5.465	3.058	0.063	1.839	0.143	0.771	100.79
585-m8-1	0.811	31.165	30.249	0.022	0.495	12.286	15.155	5.219	3.195	0.125	2.015	0.172	0.966	101.88
585-m8-2	0.861	30.461	30.110	0.022	0.566	12.026	14.998	5.548	3.134	0.077	2.046	0.200	0.885	100.93
585-m8-3	0.746	30.564	29.770	0.022	0.702	12.209	14.991	5.820	3.090	0.081	1.896	0.109	0.960	100.96
585-m8-4	0.888	30.118	29.722	0.026	0.689	11.976	14.831	6.193	3.131	0.099	1.953	0.158	0.934	100.72
585-m9-1	0.774	30.317	30.117	0.018	0.363	12.230	15.482	4.428	3.146	0.494	2.044	0.143	1.191	100.75
585-m9-2	0.751	30.178	30.047	0.019	0.476	11.993	15.497	4.726	3.085	0.422	2.041	0.169	1.150	100.55
585-m9-3	0.998	29.692	30.876	0.024	0.112	11.763	15.695	4.192	3.186	0.576	2.013	0.290	1.208	100.63
585-m9-4	1.639	28.834	30.680	0.029	0.114	11.110	15.434	3.664	3.152	1.767	1.889	0.172	1.089	99.57
Sample 00TWG516A														
516A-m1-1	0.953	28.108	31.383	0.021	0.070	12.177	13.939	3.274	2.989	1.922	2.365	0.751	1.914	99.87
516A-m1-2	0.938	28.066	31.067	0.030	0.201	12.325	13.464	4.272	2.979	1.375	2.510	0.418	1.860	99.51

Analysis	CaO	Ce_2O_3	P_2O_5	PbO	SiO_2	Nd_2O_3	$La2O_3$	ThO_2	Pr_2O_3	Y_2O_3	Sm_2O_3	UO_2	Gd_2O_3	Total
516A-m1-3	0.977	27.478	31.618	0.019	0.780	12.016	13.173	3.412	3.004	2.246	2.462	0.735	1.942	99.86
516A-m1-4	0.902	28.535	31.199	0.018	0.076	11.969	13.844	3.074	3.022	1.871	2.357	0.736	1.678	99.28
516A-m2-1	0.990	28.999	31.012	0.024	0.102	12.158	13.889	3.511	3.048	1.574	2.267	0.664	1.619	99.86
516A-m2-2	1.078	28.114	31.332	0.025	0.119	12.297	13.233	3.729	2.998	2.015	2.412	0.819	1.784	99.96
516A-m3-1	1.067	28.057	31.178	0.021	0.079	12.113	13.343	3.815	3.122	2.086	2.338	0.706	1.730	99.66
516A-m3-2	1.048	28.673	31.061	0.029	0.116	12.294	13.515	3.730	3.023	1.805	2.424	0.709	1.768	100.20
516A-m3-3	1.073	28.558	31.690	0.023	0.160	12.171	13.520	3.854	3.061	1.733	2.310	0.703	1.636	100.49
516A-m4-1	1.099	27.794	31.419	0.027	0.418	11.897	13.168	3.995	3.031	2.146	2.408	0.758	1.680	99.84
516A-m4-2	1.097	28.274	30.878	0.027	0.108	12.228	13.252	4.058	3.053	1.881	2.342	0.655	1.829	99.68
516A-m4-3	1.059	28.406	30.429	0.022	0.072	12.043	13.605	3.749	2.907	1.815	2.399	0.681	1.829	99.02
516A-m4-4	1.062	27.377	31.488	0.021	2.019	11.871	12.933	3.851	2.881	2.484	2.351	0.664	1.741	100.74
516A-m4-5	1.072	28.367	30.973	0.021	0.079	11.937	13.438	3.936	2.984	2.090	2.410	0.705	1.799	99.81
516A-m6-1	1.032	28.413	31.386	0.028	0.109	12.198	13.423	3.700	2.958	1.746	2.317	0.703	1.782	99.80
516A-m6-2	1.019	28.217	31.298	0.026	0.117	12.093	13.549	3.526	3.111	1.913	2.458	0.723	1.731	99.78
516A-m6-3	1.035	27.890	31.777	0.019	1.155	11.743	13.477	3.711	3.080	2.299	2.326	0.657	1.703	100.87
516A-m7-1	1.230	27.488	31.241	0.033	0.257	11.870	13.154	4.523	3.129	1.964	2.360	0.701	1.884	99.83
516A-m7-2	1.122	27.622	31.337	0.027	0.207	12.269	13.150	4.079	3.090	1.958	2.465	0.685	1.922	99.93
516A-m7-3	1.094	28.098	31.381	0.027	0.239	12.264	13.272	3.975	2.959	1.934	2.407	0.644	1.761	100.06
516A-m7-4	1.052	27.811	31.601	0.021	0.275	12.151	13.437	3.737	2.999	1.967	2.416	0.662	1.801	99.93
516A-m8-1	1.108	27.672	31.728	0.029	0.709	11.744	13.376	3.892	2.901	2.195	2.287	0.728	1.725	100.09
516A-m8-2	1.086	28.319	31.329	0.027	0.114	12.283	13.430	3.853	3.099	1.977	2.496	0.804	1.935	100.75
516A-m8-3	0.855	29.845	30.444	0.028	0.190	12.494	14.183	3.248	3.114	0.960	2.403	0.446	1.659	99.87
516A-m9-1	1.052	28.154	31.601	0.030	0.141	12.212	13.562	3.708	3.077	1.790	2.356	0.717	1.823	100.22
516A-m9-2	1.050	28.200	31.399	0.024	0.244	11.991	13.581	3.821	3.097	1.863	2.321	0.642	1.772	100.01
516A-m9-3	1.124	28.057	30.946	0.026	0.163	11.752	13.347	4.002	2.899	1.898	2.399	0.747	1.686	99.05
516A-m9-4	0.995	27.967	30.810	0.026	0.162	12.415	13.260	3.593	3.144	1.691	2.558	0.651	2.005	99.28
Sample 00TWGwls														
wls-m1-1	0.716	29.720	30.550	0.018	0.172	11.860	15.316	2.917	2.966	1.725	2.142	0.394	1.551	100.05
wls-m1-2	0.616	29.512	30.592	0.019	0.152	12.353	14.745	2.466	3.167	1.794	2.264	0.362	1.486	99.53
wls-m1-3	0.665	29.711	30.824	0.014	0.154	11.934	14.963	2.325	3.194	1.761	2.102	0.383	1.427	99.46
wls-m1-4	1.206	27.837	30.752	0.033	0.344	11.544	13.949	5.054	2.954	2.137	2.049	0.429	1.575	99.86
wls-m2-1	0.736	28.304	30.795	0.038	0.216	12.062	13.975	3.109	3.087	2.409	2.251	0.424	1.938	99.34
wls-m2-2	0.726	28.638	30.650	0.038	0.210	12.204	13.869	3.072	3.051	2.365	2.331	0.429	1.839	99.42
wls-m2-3	0.727	28.870	30.869	0.042	0.202	12.238	13.926	3.043	3.140	2.394	2.298	0.424	1.995	100.17
wls-m2-4	0.711	28.697	30.787	0.041	0.227	12.147	13.879	3.127	3.063	2.333	2.338	0.394	1.785	99.53
wls-m3-1	0.736	28.451	30.886	0.045	0.206	11.899	14.458	3.154	3.008	2.245	2.251	0.413	1.814	99.57

Analysis	CaO	Ce_2O_3	P_2O_5	PbO	SiO_2	Nd_2O_3	$La2O_3$	ThO_2	Pr_2O_3	Y_2O_3	Sm_2O_3	UO_2	Gd_2O_3	Total
wls-m3-2	1.205	26.314	30.673	0.069	0.360	11.664	13.002	5.776	2.922	2.562	2.278	0.641	1.828	99.29
wls-m3-3	1.249	25.832	30.585	0.067	0.447	11.468	13.520	5.894	2.825	2.428	2.162	0.741	1.987	99.21
wls-m3-4	0.952	27.502	30.721	0.052	0.270	11.832	13.357	4.210	2.913	2.641	2.449	0.560	2.076	99.54
wls-m4-1	0.808	28.001	30.946	0.044	0.263	12.337	13.563	3.614	2.971	2.423	2.394	0.477	1.930	99.77
wls-m4-2	1.189	26.615	31.176	0.066	0.423	11.657	12.937	5.672	2.723	2.645	2.310	0.667	2.054	100.33
wls-m4-3	1.095	26.879	30.802	0.055	0.271	11.723	13.194	4.682	2.995	3.032	2.364	0.715	1.830	99.64
wls-m4-4	1.042	27.708	30.722	0.051	0.276	11.905	13.416	4.361	2.913	2.699	2.352	0.556	1.755	99.76
wls-m5-1	0.702	28.644	30.623	0.037	0.229	12.493	13.729	3.021	3.042	2.469	2.366	0.426	1.869	99.65
wls-m5-2	0.946	27.234	30.564	0.050	0.267	11.816	13.408	3.959	3.004	2.761	2.387	0.593	1.859	98.85
wls-m5-3	0.806	28.210	30.378	0.044	0.258	12.042	13.794	3.552	2.973	2.452	2.284	0.472	1.758	99.02
wls-m5-4	0.929	27.682	30.729	0.049	0.326	12.020	13.453	3.961	3.047	2.578	2.316	0.415	1.623	99.13
wls-m6-1	1.255	27.555	30.878	0.035	0.409	11.885	13.842	5.642	3.001	1.997	2.059	0.297	1.645	100.50
wls-m6-2	0.963	28.275	30.885	0.046	0.307	11.969	13.600	4.060	2.911	2.578	2.376	0.430	1.761	100.16
wls-m6-3	1.147	27.578	30.511	0.030	0.417	12.023	13.581	5.469	3.047	1.935	2.201	0.347	1.716	100.00
wls-m6-4	1.109	27.942	30.605	0.030	0.377	12.075	13.286	5.093	3.067	1.941	2.221	0.304	1.752	99.80
wls-m7-1	0.692	28.348	30.757	0.040	0.210	12.340	13.791	3.055	2.868	2.456	2.345	0.455	1.843	99.20
wls-m7-2	0.711	28.722	30.850	0.033	0.189	12.299	14.208	2.869	2.994	2.374	2.385	0.438	1.863	99.94
wls-m7-3	1.148	27.226	30.403	0.033	0.382	11.449	13.784	5.903	3.022	2.088	2.064	0.431	1.568	99.50
wls-m7-4	1.338	27.114	30.129	0.036	0.495	11.102	13.808	6.897	3.063	1.960	1.989	0.384	1.334	99.65
wls-m8-1	0.662	29.140	30.794	0.016	0.169	12.856	14.025	2.926	3.155	2.001	2.477	0.374	1.651	100.25
wls-m8-2	0.760	28.723	30.642	0.022	0.214	12.526	13.964	3.436	3.047	2.016	2.380	0.475	1.621	99.83
wls-m8-3	0.810	28.430	30.776	0.024	0.244	12.649	13.694	3.715	3.284	1.941	2.441	0.396	1.704	100.11
wls-m8-4	0.691	28.667	30.675	0.022	0.207	12.511	14.078	3.039	3.152	2.009	2.321	0.436	1.748	99.56
wls-m9-1	0.826	28.113	30.590	0.047	0.374	12.095	13.444	4.432	2.932	2.324	2.320	0.356	1.748	99.60
wls-m9-2	0.860	27.661	30.930	0.051	0.248	12.183	13.608	3.748	2.911	2.714	2.441	0.594	1.905	99.85
wls-m9-3	0.893	27.387	31.708	0.053	0.266	12.036	13.563	3.717	2.859	2.866	2.360	0.624	1.996	100.33
wls-m9-4	0.802	28.620	30.537	0.029	0.248	12.391	13.756	3.619	3.063	2.088	2.284	0.371	1.717	99.53
Sample 00TWG331														
331-m1-1	0.890	28.653	30.694	0.027	0.259	12.628	13.801	3.980	3.053	1.650	2.440	0.387	1.674	100.14
331-m1-2	0.887	28.574	30.788	0.025	0.246	12.524	13.931	3.693	3.118	1.661	2.458	0.497	1.708	100.11
331-m1-3	0.697	29.205	30.700	0.021	0.191	12.662	14.398	2.743	3.088	1.614	2.397	0.467	1.677	99.86
331-m1-4	0.630	29.458	30.774	0.018	0.182	12.833	14.353	2.516	3.257	1.523	2.381	0.407	1.579	99.91
331-m2-1	0.817	28.783	31.016	0.027	0.293	12.641	14.061	3.776	3.216	1.474	2.496	0.421	1.621	100.64
331-m2-2	0.788	28.723	30.580	0.021	3.786	12.599	13.762	3.713	3.077	1.445	2.367	0.368	1.496	102.73
331-m2-3	0.663	29.354	30.994	0.022	0.205	12.715	14.262	3.038	3.268	1.447	2.428	0.364	1.495	100.26
331-m2-4	0.915	28.374	30.732	0.032	0.229	12.421	13.903	4.040	3.155	1.870	2.362	0.525	1.690	100.25

Analysis	CaO	Ce_2O_3	P_2O_5	PbO	SiO_2	Nd_2O_3	$La2O_3$	ThO_2	Pr_2O_3	Y_2O_3	Sm_2O_3	UO_2	Gd_2O_3	Total
331-m3-1	1.031	28.517	30.399	0.031	0.259	12.211	13.485	4.530	2.968	1.803	2.380	0.590	1.622	99.83
331-m3-2	0.813	30.004	31.089	0.022	0.175	12.032	14.967	3.499	3.096	1.461	2.283	0.364	1.633	101.44
331-m3-3	0.767	29.215	30.912	0.024	0.146	12.630	14.176	3.237	3.144	1.699	2.440	0.485	1.690	100.57
331-m3-4	0.985	28.273	30.642	0.025	0.337	12.399	13.915	4.703	3.114	1.508	2.361	0.424	1.677	100.36
331-m4-1	0.721	29.546	30.469	0.021	0.181	12.563	14.604	3.094	3.145	1.495	2.376	0.436	1.449	100.10
331-m4-2	0.716	29.778	30.734	0.022	0.185	12.528	14.430	3.016	3.298	1.522	2.344	0.377	1.630	100.58
331-m4-3	0.895	28.510	30.843	0.027	0.290	12.453	13.895	4.298	3.036	1.460	2.328	0.378	1.537	99.95
331-m4-4	1.209	27.627	30.532	0.033	0.430	12.129	13.277	6.133	2.958	1.606	2.287	0.451	1.508	100.18
331-m5-1	0.964	28.152	31.409	0.032	0.232	12.543	13.873	4.211	3.231	1.739	2.418	0.475	1.621	100.90
331-m5-2	0.820	29.330	31.024	0.025	0.198	12.543	14.523	3.611	3.087	1.424	2.267	0.354	1.675	100.88
331-m5-3	0.882	29.082	31.047	0.026	0.206	12.391	14.415	4.004	3.082	1.524	2.360	0.398	1.589	101.01
331-m5-4	0.616	29.445	30.809	0.020	0.152	12.754	14.465	2.734	3.207	1.529	2.436	0.389	1.621	100.18
331-m6-1	0.889	28.476	30.692	0.029	0.577	12.301	13.862	4.181	3.062	1.592	2.375	0.430	1.730	100.20
331-m6-2	0.778	28.852	30.755	0.029	0.631	12.495	14.000	3.364	3.095	1.640	2.411	0.448	1.615	100.11
331-m6-3	1.038	27.934	30.841	0.030	0.348	12.361	13.482	4.439	3.062	1.842	2.462	0.667	1.719	100.23
331-m6-4	0.912	28.510	30.715	0.027	0.431	12.668	13.872	3.953	3.165	1.699	2.436	0.559	1.473	100.42
331-m7-1	0.702	29.592	30.826	0.025	0.121	12.838	14.370	2.692	3.091	1.717	2.503	0.428	1.641	100.55
331-m7-2	1.113	27.491	30.864	0.032	0.261	12.349	13.543	4.976	3.032	1.754	2.413	0.541	1.492	99.86
331-m7-3	1.341	26.713	30.761	0.042	0.290	12.018	13.023	6.053	3.096	1.961	2.347	0.697	1.696	100.04
331-m7-4	0.947	28.082	30.724	0.027	0.184	12.593	13.930	3.863	2.984	1.818	2.425	0.529	1.660	99.77
331-m8-1	0.875	28.506	31.135	0.022	0.222	12.639	13.982	3.889	3.155	1.497	2.348	0.431	1.536	100.24
331-m8-2	0.757	28.941	30.867	0.026	0.222	12.687	14.451	3.546	2.993	1.451	2.422	0.425	1.609	100.40
331-m9-1	1.360	27.130	30.561	0.040	0.418	11.731	13.448	7.039	3.023	1.511	2.215	0.515	1.547	100.54
331-m9-2	0.673	29.648	30.995	0.021	0.155	12.784	14.384	2.954	3.135	1.654	2.405	0.402	1.789	101.00
331-m9-3	1.064	27.892	30.933	0.032	0.318	12.308	13.603	5.288	3.127	1.579	2.363	0.461	1.578	100.55
331-m9-4	1.057	27.904	30.877	0.031	0.192	12.215	13.695	4.395	3.174	1.920	2.367	0.638	1.805	100.27
Sample 00TWG072B														
72B-m1-1	1.140	26.994	30.448	0.023	0.657	12.450	13.730	6.089	3.014	1.302	2.290	0.573	1.817	100.53
72B-m1-2	0.896	27.929	30.538	0.028	0.449	12.614	13.495	4.360	3.005	1.914	2.524	0.554	1.993	100.30
72B-m1-3	0.985	27.214	31.031	0.033	0.426	12.424	13.175	4.588	3.093	2.301	2.399	0.673	2.043	100.39
72B-m1-4	1.081	27.405	30.472	0.022	0.697	12.320	13.686	6.172	2.926	1.268	2.319	0.541	1.703	100.61
72B-m2-1	0.627	29.013	30.830	0.012	0.250	12.904	13.845	3.043	3.153	2.055	2.508	0.471	1.873	100.58
72B-m2-2	0.696	29.175	30.784	0.018	0.314	12.659	13.891	3.321	3.119	1.975	2.446	0.475	1.805	100.68
72B-m2-3	0.875	28.199	30.412	0.026	0.382	12.598	13.578	4.439	3.032	1.889	2.301	0.550	2.041	100.32
72B-m3-1	0.919	27.686	30.304	0.023	0.572	12.429	13.527	5.180	3.118	1.857	2.377	0.527	1.910	100.43
72B-m3-2	0.927	27.398	30.302	0.027	0.546	12.662	13.386	5.025	3.073	1.803	2.354	0.516	1.895	99.91

Analysis	CaO	Ce_2O_3	P_2O_5	PbO	SiO_2	Nd_2O_3	$La2O_3$	ThO_2	Pr_2O_3	Y_2O_3	Sm_2O_3	UO_2	Gd_2O_3	Total
72B-m3-3	0.803	28.383	30.696	0.019	0.426	12.653	13.761	4.388	2.924	1.835	2.408	0.482	1.854	100.63
72B-m3-4	0.652	29.116	30.610	0.015	0.334	12.599	14.082	3.063	3.099	1.974	2.386	0.366	1.761	100.06
72B-m4-1	0.998	28.053	30.733	0.052	0.402	12.282	13.579	4.693	2.858	1.862	2.392	0.516	1.698	100.12
72B-m4-2	0.972	28.748	30.536	0.034	0.419	12.099	14.603	4.768	3.126	1.018	2.347	0.503	1.798	100.97
72B-m4-3	0.803	29.272	30.635	0.028	0.272	12.865	14.324	3.639	3.219	0.969	2.331	0.524	1.823	100.70
72B-m4-4	0.921	27.936	30.960	0.026	0.547	12.682	13.884	4.937	3.127	1.662	2.394	0.549	1.827	101.45
72B-m5-1	0.771	28.509	31.019	0.028	0.239	12.596	14.019	3.392	3.045	1.648	2.471	0.563	2.064	100.36
72B-m5-2	0.808	28.760	31.259	0.028	0.238	12.731	14.103	3.502	3.128	1.571	2.449	0.583	2.022	101.18
72B-m5-3	0.784	29.060	30.767	0.022	0.215	12.306	14.648	3.510	3.288	1.327	2.430	0.496	1.904	100.76
72B-m5-4	0.925	28.966	31.047	0.029	0.257	12.238	14.460	3.963	3.050	1.662	2.210	0.544	1.723	101.07
72B-m6-1	0.958	28.300	30.812	0.039	0.311	11.895	14.602	4.714	2.962	1.470	2.245	0.486	1.886	100.68
72B-m6-2	0.841	27.807	31.027	0.021	0.311	12.456	13.614	3.952	3.300	2.214	2.537	0.611	2.035	100.73
72B-m6-3	0.935	27.720	31.105	0.030	0.227	12.271	13.530	4.028	3.110	2.413	2.375	0.617	1.785	100.15
72B-m6-4	0.821	27.610	30.884	0.026	0.265	12.277	14.063	3.921	2.963	1.889	2.439	0.548	1.904	99.61
72B-m7-1	0.639	29.417	30.707	0.026	0.145	12.605	14.490	2.603	3.099	1.757	2.479	0.570	1.867	100.40
72B-m7-2	0.802	28.351	30.368	0.030	0.330	12.483	13.737	3.715	3.072	2.258	2.479	0.612	2.007	100.24
72B-m7-3	0.843	28.542	30.507	0.030	0.211	12.446	13.962	3.484	3.141	2.137	2.250	0.605	1.805	99.96
72B-m7-4	0.900	28.048	30.407	0.020	0.454	12.688	13.836	4.497	3.031	1.644	2.386	0.577	1.944	100.43
72B-m8-1	0.954	27.889	30.748	0.027	0.296	12.476	13.446	4.191	3.054	2.365	2.340	0.697	1.906	100.39
72B-m8-2	0.978	28.005	30.542	0.032	0.277	12.362	13.541	4.343	3.080	2.427	2.456	0.625	1.906	100.57
72B-m8-3	0.942	27.981	30.985	0.049	0.250	12.709	13.539	4.211	3.116	2.041	2.550	0.557	1.796	100.73
72B-m8-4	0.955	28.202	30.673	0.050	0.245	12.570	13.607	4.207	3.103	1.984	2.469	0.557	1.722	100.34
72B-m9-1	0.900	28.435	30.475	0.024	0.321	12.451	13.632	4.260	3.045	1.769	2.448	0.656	1.886	100.30
72B-m9-2	0.984	28.045	30.884	0.035	0.226	12.183	13.356	4.312	2.955	2.429	2.358	0.677	1.881	100.33
72B-m9-3	0.924	28.387	30.929	0.029	0.166	12.296	13.965	3.791	3.062	2.111	2.258	0.598	1.738	100.25
72B-m9-4	1.025	28.051	30.695	0.033	0.192	12.298	13.472	4.326	3.043	2.333	2.232	0.600	1.755	100.06
Sample 00TWG488														
488-m1-1	0.794	28.353	30.691	0.027	0.235	11.239	16.200	3.518	2.959	2.001	2.083	0.558	1.409	100.07
488-m1-2	0.722	29.323	30.957	0.023	0.251	11.079	16.816	3.205	2.847	1.850	2.014	0.564	1.414	101.07
488-m1-3	0.883	28.805	30.941	0.028	0.237	10.967	16.917	3.339	3.035	1.874	1.979	0.562	1.310	100.88
488-m1-4	0.759	28.660	30.939	0.033	0.183	11.032	16.896	2.927	2.891	2.291	2.004	0.780	1.501	100.90
488-m1-5	0.936	27.788	30.846	0.025	0.472	10.597	17.194	4.760	2.974	1.885	1.864	0.519	1.334	101.19
488-m2-1	1.080	27.881	30.965	0.020	0.319	10.525	16.326	4.954	2.977	2.135	1.755	0.592	1.419	100.95
488-m2-2	1.249	26.834	30.939	0.038	0.242	11.541	13.996	4.432	2.933	2.949	2.225	1.036	1.935	100.35
488-m2-3	0.930	28.291	30.416	0.021	0.289	10.855	16.689	4.480	2.886	1.924	1.718	0.509	1.447	100.46
488-m2-4	0.997	28.365	30.812	0.019	0.315	10.702	16.566	4.550	2.775	1.925	1.768	0.563	1.376	100.73

Analysis	CaO	Ce_2O_3	P_2O_5	PbO	SiO_2	Nd_2O_3	$La2O_3$	ThO_2	Pr_2O_3	Y_2O_3	Sm_2O_3	UO_2	Gd_2O_3	Total
488-m3-1	0.007	0.000	0.552	0.000	0.122	0.000	0.000	0.007	0.072	0.020	0.010	0.021	0.000	0.81
488-m3-2	0.003	0.039	0.518	0.000	0.095	0.000	0.007	0.000	0.015	0.000	0.000	0.002	0.000	0.68
488-m3-3	0.011	0.000	0.530	0.000	0.123	0.011	0.000	0.000	0.000	0.015	0.000	0.017	0.000	0.71
488-m4-1	0.842	25.494	28.477	0.020	5.989	10.573	14.196	4.764	2.600	1.433	1.826	0.584	1.321	98.12
488-m4-2	1.492	25.508	30.049	0.047	5.324	10.218	14.522	5.939	2.802	1.835	1.830	0.560	1.496	101.62
488-m4-3	1.109	27.374	30.825	0.024	1.071	10.966	15.214	4.969	2.824	2.572	1.911	0.530	1.629	101.02
488-m4-4	1.151	27.023	30.778	0.026	3.320	10.965	14.776	5.478	2.884	2.063	2.047	0.513	1.566	102.59
488-m4-5	1.094	27.983	30.869	0.034	0.499	11.293	15.516	5.535	2.955	1.666	1.993	0.536	1.399	101.37
488-m5-1	0.955	27.259	30.456	0.032	0.339	11.817	15.164	4.541	3.181	2.103	2.292	0.632	1.850	100.62
488-m5-2	1.154	26.890	30.415	0.038	0.394	10.951	15.015	5.582	2.868	2.091	2.113	0.874	1.668	100.05
488-m5-3	0.835	28.220	30.379	0.027	0.347	11.287	15.876	4.302	2.895	1.712	2.194	0.469	1.625	100.17
488-m5-4	0.851	28.348	30.527	0.022	0.304	10.982	16.385	4.138	2.891	1.874	1.981	0.516	1.362	100.18
488-m5-5	0.768	27.592	29.837	0.019	2.856	10.561	15.671	3.183	2.840	1.733	1.854	0.569	1.469	98.95
Sample 99TWG537														
537-m1-1	0.807	31.465	31.000	0.024	0.126	13.311	15.008	3.562	3.409	0.183	2.277	0.195	0.925	102.29
537-m1-2	0.917	31.076	30.725	0.033	0.145	12.911	15.226	4.185	3.332	0.195	2.144	0.143	1.066	102.10
537-m1-3	0.864	31.017	30.978	0.027	0.117	13.199	14.955	3.952	3.275	0.258	2.244	0.172	1.177	102.24
537-m1-4	0.878	31.225	30.762	0.025	0.128	13.265	14.895	3.950	3.523	0.155	2.148	0.169	0.868	101.99
537-m1-5	0.769	31.570	30.619	0.033	0.178	12.953	15.144	3.543	3.267	0.115	2.239	0.319	0.995	101.74
537-m2-1	0.860	29.028	30.994	0.024	0.103	12.288	14.278	3.668	3.079	1.909	2.348	0.384	1.727	100.69
537-m2-2	0.884	29.911	30.581	0.043	0.289	13.027	14.742	4.374	3.323	0.084	2.358	0.576	1.101	101.29
537-m2-3	0.731	30.904	30.813	0.034	0.169	12.832	15.636	3.048	3.297	0.064	2.305	0.543	1.170	101.55
537-m2-4	0.887	29.889	30.632	0.045	0.218	13.114	14.885	3.940	3.295	0.059	2.437	0.694	1.186	101.28
537-m2-5	0.858	30.629	30.890	0.026	0.130	13.077	15.074	3.879	3.457	0.257	2.125	0.166	1.150	101.72
537-m3-1	0.673	31.022	30.325	0.030	0.210	13.410	15.481	3.028	3.416	0.023	2.213	0.369	0.849	101.05
537-m3-2	0.705	31.060	30.543	0.033	0.224	13.176	15.288	3.139	3.482	0.023	2.337	0.439	0.869	101.32
537-m3-3	0.932	29.695	30.674	0.018	0.139	13.001	14.419	3.747	3.332	0.683	2.509	0.366	1.742	101.26
537-m3-4	0.855	30.321	30.522	0.042	0.252	12.760	15.695	4.075	3.384	0.021	2.067	0.515	0.676	101.19
537-m3-5	0.827	29.743	30.768	0.032	0.135	13.150	14.455	3.713	3.390	0.490	2.487	0.295	1.816	101.30
537-m4-1	0.862	30.932	30.996	0.021	0.151	13.288	14.997	3.763	3.243	0.274	2.318	0.177	1.320	102.34
537-m4-2	0.873	31.175	30.909	0.024	0.132	13.181	15.199	3.939	3.250	0.187	2.047	0.159	0.979	102.05
537-m4-3	0.849	31.119	30.949	0.025	0.130	13.568	14.941	3.774	3.299	0.215	2.110	0.142	0.995	102.12
537-m4-4	0.788	28.749	30.755	0.015	0.141	12.928	14.027	3.508	3.141	1.459	2.702	0.312	2.299	100.82
537-m4-5	0.788	30.493	30.835	0.020	0.129	13.414	14.714	3.458	3.361	0.309	2.482	0.237	1.327	101.57
537-m5-1	0.800	30.783	30.506	0.039	0.252	12.991	15.130	3.624	3.432	0.109	2.279	0.522	1.066	101.73
537-m5-2	0.830	30.738	30.639	0.031	0.144	12.999	14.993	3.541	3.361	0.232	2.340	0.408	1.216	101.47

Analysis	CaO	Ce_2O_3	P_2O_5	PbO	SiO_2	Nd_2O_3	$La2O_3$	ThO_2	Pr_2O_3	Y_2O_3	Sm_2O_3	UO_2	Gd_2O_3	Total
537-m5-3	0.797	31.234	30.616	0.035	0.196	12.764	15.608	3.615	3.316	0.040	2.173	0.413	0.899	101.71
537-m5-4	0.650	31.156	30.718	0.029	0.174	13.179	15.333	2.779	3.493	0.144	2.365	0.488	1.169	101.68
537-m5-5	0.632	31.293	30.965	0.034	0.181	13.418	15.373	2.710	3.338	0.152	2.390	0.461	1.278	102.23
Sample 00TWG493														
493-m1-1	1.110	27.957	30.852	0.042	0.318	12.417	13.149	5.348	3.098	1.861	2.393	0.631	1.915	101.09
493-m1-2	0.816	29.198	31.204	0.026	0.182	12.558	13.972	3.420	3.210	1.531	2.376	0.575	1.685	100.75
493-m1-3	1.041	28.360	30.999	0.040	0.296	12.520	13.448	4.999	3.152	1.687	2.461	0.551	1.779	101.33
493-m1-4	0.873	28.963	31.384	0.031	0.184	12.945	13.716	3.697	3.166	1.584	2.441	0.609	1.764	101.36
493-m1-5	0.855	29.032	30.886	0.034	0.238	12.615	13.753	3.660	3.162	1.716	2.438	0.575	1.707	100.67
493-m2-1	1.101	28.566	30.482	0.039	0.387	11.873	13.517	5.399	2.921	1.666	2.276	0.529	1.796	100.55
493-m2-2	0.910	29.128	30.755	0.033	0.252	12.486	13.756	4.191	3.177	1.663	2.423	0.495	1.778	101.05
493-m2-3	0.871	29.052	30.824	0.033	0.239	12.524	13.755	3.978	3.100	1.713	2.460	0.570	1.837	100.96
493-m3-1	0.803	29.162	31.242	0.029	0.179	12.510	13.933	3.386	3.119	1.707	2.513	0.569	1.809	100.96
493-m3-2	1.047	28.725	31.146	0.038	0.249	12.128	13.851	4.778	3.018	1.632	2.289	0.605	1.772	101.28
493-m3-3	0.884	28.430	31.096	0.035	0.219	12.610	13.692	3.930	3.078	1.722	2.472	0.561	1.845	100.57
493-m3-4	1.069	28.343	30.833	0.040	0.254	12.397	13.364	4.911	2.968	1.843	2.380	0.614	1.690	100.71
493-m3-5	0.912	28.775	30.957	0.034	0.259	12.460	13.735	4.157	3.137	1.606	2.445	0.531	1.731	100.74
493-m4-1	0.895	28.809	31.142	0.029	0.231	12.570	13.845	3.880	3.075	1.737	2.455	0.564	1.740	100.97
493-m4-2	1.060	28.360	30.953	0.037	0.327	12.348	13.424	5.229	3.031	1.685	2.373	0.625	1.684	101.14
493-m4-3	0.792	29.261	31.353	0.033	0.207	12.951	13.965	3.548	3.108	1.694	2.521	0.567	1.688	101.69
493-m4-4	0.754	29.372	31.378	0.029	0.165	12.476	14.379	3.123	3.190	1.606	2.399	0.602	1.687	101.16
493-m4-5	0.903	28.884	31.165	0.034	0.216	12.666	13.792	3.936	3.175	1.667	2.531	0.566	1.847	101.38
493-m5-1	0.774	29.488	31.931	0.026	0.257	12.822	14.068	3.389	3.193	1.674	2.494	0.560	1.865	102.54
493-m5-2	0.837	29.063	31.057	0.030	0.513	12.471	14.019	3.612	3.146	1.676	2.419	0.541	1.666	101.05
493-m5-3	0.921	28.711	30.745	0.035	0.314	12.350	13.894	4.192	3.157	1.622	2.430	0.630	1.740	100.74
493-m6-1	0.722	29.384	31.058	0.029	1.253	12.801	13.972	3.147	3.214	1.617	2.477	0.505	1.704	101.88
493-m6-2	1.079	28.080	31.047	0.039	0.353	12.211	13.314	5.042	3.098	1.830	2.369	0.597	1.885	100.94
493-m6-3	0.889	26.919	29.632	0.033	10.225	11.837	12.756	3.881	2.913	1.587	2.291	0.586	1.587	105.14
493-m6-4	0.867	29.101	31.105	0.031	0.324	12.557	13.675	3.984	3.084	1.629	2.271	0.509	1.877	101.01
Sample 99TWG430														
430m-1	1.517	28.519	31.022	0.058	0.314	12.011	13.459	7.855	3.043	0.366	2.094	0.299	1.285	101.84
430m-2	0.917	30.197	30.706	0.054	0.426	11.767	14.947	4.894	3.118	0.289	2.068	0.704	1.151	101.24
430m-3	1.262	27.194	30.777	0.050	0.363	11.105	12.882	6.532	2.794	3.406	1.936	0.433	1.577	100.31
430m-4	1.181	27.242	31.040	0.047	0.383	11.277	12.961	6.390	2.979	3.281	2.002	0.441	1.688	100.91
430m-5	1.463	26.861	31.189	0.045	0.188	10.910	13.073	6.670	2.887	3.040	2.050	0.437	1.644	100.46

Analysis	CaO	Ce_2O_3	P_2O_5	PbO	SiO_2	Nd_2O_3	$La2O_3$	ThO_2	Pr_2O_3	Y_2O_3	Sm_2O_3	UO_2	Gd_2O_3	Total
430m-6	1.196	29.387	30.443	0.070	0.637	11.242	14.625	6.812	2.868	0.314	1.942	0.974	1.200	101.71
430m-7	1.192	27.209	31.157	0.045	0.270	11.062	12.936	5.966	2.773	3.676	2.003	0.404	1.583	100.28
430m-8	1.259	27.802	31.318	0.043	0.188	11.235	13.216	5.764	3.023	2.864	2.153	0.586	1.769	101.22
430m-9	1.185	28.249	30.919	0.051	0.260	11.266	13.826	5.761	2.960	2.191	2.008	0.553	1.445	100.67
430m-10	1.330	29.197	30.607	0.072	0.507	11.303	13.585	6.889	2.902	0.576	2.060	0.843	1.370	101.24
430m-11	1.044	29.931	31.128	0.039	0.131	11.792	14.353	4.664	3.044	0.941	2.350	0.346	1.806	101.57
430m-12	1.345	28.751	30.968	0.052	0.278	11.859	13.438	6.606	3.045	0.650	2.354	0.305	1.577	101.23
430m-13	1.347	29.052	31.048	0.058	0.170	11.878	13.798	5.746	2.880	0.600	2.344	0.677	1.675	101.27
430m-14	1.261	29.596	31.210	0.048	0.200	12.290	13.911	6.067	3.157	0.476	2.337	0.343	1.282	102.18
430m-15	1.289	29.536	31.223	0.047	0.193	12.194	13.896	5.938	3.208	0.484	2.297	0.418	1.415	102.14
430m-16	1.270	29.395	31.260	0.057	0.164	11.757	13.982	5.711	3.057	0.576	2.368	0.574	1.529	101.70
430m-17	1.317	29.318	31.341	0.051	0.146	11.746	13.972	5.658	3.142	0.638	2.318	0.645	1.735	102.03
430m-18	1.452	28.962	30.732	0.056	0.345	12.054	13.559	7.814	3.069	0.287	2.059	0.210	1.079	101.68
430m-19	1.217	27.915	31.563	0.044	0.147	10.955	13.216	5.400	3.009	3.242	2.029	0.502	1.646	100.89
430m-20	1.214	27.838	31.518	0.044	0.133	11.086	12.939	5.328	2.835	3.264	2.047	0.524	1.693	100.46
430m-21	1.237	28.915	31.467	0.052	0.098	11.370	14.003	5.223	2.945	0.975	2.400	0.568	1.943	101.20
430m-22	1.275	29.414	31.366	0.047	0.139	11.567	14.162	5.405	2.959	0.823	2.330	0.533	1.936	101.96
430m-23	1.285	29.046	31.572	0.057	0.125	11.585	14.087	5.481	2.976	0.845	2.453	0.549	2.047	102.11
430m-24	1.394	27.703	31.553	0.045	0.258	11.094	13.241	6.162	2.774	2.655	1.949	0.877	1.602	101.31
430m-25	1.242	29.016	31.339	0.040	0.151	11.581	14.259	5.694	3.083	1.205	2.139	0.409	2.069	102.23
Sample 99TWG431														
431a-1	1.051	27.450	31.978	0.045	0.102	11.549	13.310	4.710	2.976	3.968	2.235	0.340	1.884	101.60
431a-2	1.012	27.648	27.933	0.033	0.138	11.637	13.027	4.654	2.882	3.339	2.160	0.291	1.894	96.65
431a-3	0.724	24.648	36.233	0.048	1.301	10.175	13.964	2.593	2.540	4.290	1.957	0.386	1.549	100.41
431a-4	1.999	24.633	31.708	0.056	0.257	10.421	11.765	9.051	2.732	3.285	2.179	0.963	1.907	100.96
431a-5	1.737	26.027	31.654	0.048	0.231	11.174	12.643	8.028	2.920	2.622	2.094	0.746	1.609	101.53
431a-6	1.726	26.060	31.427	0.049	0.242	10.804	12.670	7.956	2.810	2.799	2.235	0.793	1.750	101.32
431a-7	1.559	26.788	31.220	0.044	0.188	11.066	13.098	6.415	2.929	2.417	2.159	1.125	1.732	100.74
431a-8	0.000	0.000	0.000	0.000	0.074	0.029	0.000	19.142	0.027	0.018	0.000	0.000	0.021	19.31
431a-9	0.000	0.045	0.000	0.001	0.106	0.000	0.000	18.019	0.086	0.007	0.000	0.000	0.000	18.26
431a-10	0.000	0.015	0.000	0.000	0.346	0.000	0.000	17.726	0.000	0.030	0.009	0.000	0.000	18.13
431a-11	1.106	27.931	31.691	0.041	0.092	11.297	13.702	4.831	3.033	3.029	2.100	0.505	1.880	101.24
431a-12	1.053	28.017	31.727	0.035	0.263	11.657	13.877	5.391	3.033	2.599	2.070	0.340	1.533	101.60
431a-13	1.067	28.839	31.552	0.056	0.182	11.914	14.184	4.928	2.954	1.412	2.363	0.491	1.687	101.63
431a-14	1.025	28.973	31.271	0.084	0.178	12.221	14.442	4.769	2.988	1.362	2.384	0.489	1.851	101.99
431a-15	1.031	29.115	31.550	0.055	0.177	11.899	14.512	4.719	3.134	1.353	2.245	0.471	1.687	101.95

Analysis	CaO	Ce_2O_3	P_2O_5	PbO	SiO_2	Nd_2O_3	$La2O_3$	ThO_2	Pr_2O_3	Y_2O_3	Sm_2O_3	UO_2	Gd_2O_3	Total
431a-16	1.024	28.878	31.520	0.054	0.168	11.853	14.547	4.910	3.113	1.471	2.233	0.498	1.844	102.11
431a-17	1.043	29.015	31.885	0.057	0.167	12.053	14.378	4.787	3.156	1.485	2.268	0.485	1.746	102.53
431a-18	1.033	28.828	31.770	0.063	0.178	12.146	14.446	4.762	3.067	1.438	2.336	0.491	1.774	102.33
431a-19	1.024	28.816	31.596	0.055	0.166	11.910	14.352	4.669	3.016	1.525	2.313	0.485	1.693	101.62
431a-20	1.166	29.374	31.203	0.044	0.492	12.426	14.299	5.216	3.189	0.569	2.245	0.376	1.254	101.85
431a-21	1.139	29.113	31.372	0.058	0.207	11.493	14.194	5.561	3.140	1.443	2.178	0.417	1.453	101.77
431a-22	1.256	29.841	31.367	0.050	0.149	12.276	14.373	5.778	3.163	0.451	2.107	0.432	1.264	102.51
431a-23	1.225	29.774	31.170	0.056	0.157	12.329	14.141	5.603	2.995	0.542	2.180	0.388	1.398	101.96
431a-24	1.137	27.872	31.714	0.046	0.219	11.580	12.923	5.462	3.095	3.478	2.178	0.454	1.544	101.70
431a-25	1.330	27.054	31.783	0.042	0.259	11.471	12.862	6.409	3.068	3.094	2.212	0.433	1.810	101.83
431a-26	1.369	27.768	31.578	0.036	0.314	11.463	13.640	7.022	3.026	1.797	2.111	0.383	1.422	101.93
431a-27	1.454	27.228	31.593	0.043	0.211	11.796	13.030	6.835	3.179	2.246	2.308	0.618	1.762	102.30
431a-28	1.341	28.695	31.450	0.047	0.216	11.894	13.944	6.049	3.131	1.322	2.117	0.560	1.397	102.16
431a-29	1.313	27.659	31.825	0.042	0.132	11.338	13.542	5.619	2.897	3.036	2.076	0.791	1.799	102.07
431b-1	1.315	29.399	31.332	0.056	0.223	11.580	13.714	5.746	3.119	1.408	2.132	0.453	1.542	102.02
431b-2	1.227	28.249	31.339	0.041	0.123	10.974	13.425	5.312	2.952	3.072	2.046	0.481	1.573	100.81
431b-3	1.156	28.777	31.075	0.041	0.186	11.437	13.593	5.218	3.074	2.367	2.002	0.458	1.660	101.04
431b-4	1.188	28.049	31.470	0.040	0.131	11.131	13.229	5.233	2.926	3.235	2.094	0.564	1.706	101.00
431b-5	1.198	29.637	30.983	0.052	0.164	12.124	14.351	5.561	3.240	0.659	1.970	0.347	1.285	101.57
431b-6	1.119	28.528	31.514	0.040	0.168	11.782	13.435	5.139	2.976	2.841	2.070	0.393	1.504	101.51
431b-7	1.145	28.075	31.911	0.039	0.170	11.402	13.543	5.276	2.925	2.997	2.063	0.418	1.526	101.49
431b-8	1.247	27.858	31.538	0.045	0.147	11.359	13.376	5.574	3.005	3.211	1.974	0.428	1.646	101.41
431b-9	0.988	30.940	30.993	0.048	0.308	12.091	14.523	4.932	3.235	0.416	2.035	0.509	1.086	102.10
431b-10	1.297	29.740	30.545	0.050	0.217	12.361	13.975	5.887	3.170	0.548	2.062	0.341	1.278	101.47
431b-11	1.141	28.247	31.255	0.042	0.145	11.428	13.466	4.919	3.163	3.169	2.001	0.393	1.722	101.09
431b-12	1.194	27.924	31.754	0.045	0.146	11.642	13.047	5.242	2.923	3.373	2.022	0.532	1.660	101.50
431b-13	1.286	27.732	31.451	0.045	0.186	11.236	13.051	5.794	2.863	3.072	2.018	0.418	1.687	100.84
431b-14	1.690	27.996	30.870	0.100	0.856	10.020	14.807	10.485	2.828	0.400	1.626	0.711	0.964	103.35
431b-15	1.229	28.623	31.767	0.065	0.233	11.682	13.714	6.038	3.006	1.566	2.126	0.264	1.519	101.83
431b-16	1.227	28.306	31.106	0.041	0.224	11.194	13.316	5.655	3.007	2.840	2.016	0.521	1.601	101.05
431b-17	1.207	29.605	30.987	0.063	0.446	11.897	13.723	5.950	3.059	0.853	2.234	0.611	1.410	102.05
431b-18	1.173	27.234	31.140	0.045	0.181	11.670	12.655	5.165	2.938	3.403	2.273	0.692	1.963	100.53
431b-19	1.123	28.188	31.616	0.042	0.182	11.159	13.049	4.671	3.011	3.267	2.144	0.749	1.800	101.00
431b-20	1.270	28.151	31.766	0.045	0.130	11.397	13.122	5.391	2.966	3.118	2.090	0.614	1.707	101.77
431b-21	0.798	22.101	0.002	0.049	0.390	9.275	0.167	5.974	2.362	0.018	1.493	0.001	0.608	43.24
431b-22	1.385	27.959	0.176	0.052	0.393	11.588	0.361	6.876	2.791	0.001	1.882	0.001	0.873	54.34
431b-23	0.007	0.026	0.007	0.000	31.464	0.006	0.000	0.038	0.021	0.015	0.000	0.050	0.000	31.63

Analysis	CaO	Ce_2O_3	P_2O_5	PbO	SiO_2	Nd_2O_3	$La2O_3$	ThO_2	Pr_2O_3	Y_2O_3	Sm_2O_3	UO_2	Gd_2O_3	Total
431b-24	0.008	0.022	0.155	0.000	31.102	0.049	0.017	0.015	0.000	0.157	0.000	0.169	0.000	31.69
431b-25	0.000	0.033	0.155	0.000	31.336	0.000	0.023	0.006	0.001	0.144	0.000	0.121	0.000	31.82
431b-26	0.006	0.000	0.097	0.000	31.145	0.000	0.034	0.034	0.006	0.119	0.000	0.130	0.000	31.57
431b-27	1.526	29.098	30.900	0.071	0.329	11.536	13.947	7.293	3.025	0.549	2.035	0.783	1.187	102.28
431b-28	0.006	0.066	0.043	0.000	31.733	0.031	0.007	0.000	0.000	0.126	0.000	0.021	0.000	32.03
431b-29	0.008	0.000	0.000	0.000	31.192	0.010	0.000	0.000	0.022	0.028	0.000	0.142	0.000	31.40
431b-30	0.000	0.000	0.006	0.000	31.779	0.016	0.000	0.045	0.074	0.136	0.025	0.027	0.000	32.11
431b-31	0.000	0.021	0.010	0.000	31.062	0.000	0.000	0.035	0.000	0.038	0.040	0.024	0.000	31.23
431b-32	0.008	0.000	0.000	0.000	31.221	0.016	0.048	0.005	0.022	0.000	0.000	0.182	0.000	31.50
431b-33	0.000	0.000	0.000	0.000	31.327	0.000	0.000	0.033	0.036	0.006	0.032	0.041	0.000	31.48

APPENDIX F

Monazite electron microprobe (EMP) chemical dating isochron plots and backscattered electron (BSE) images from metapelitic rocks of the Vernon area

Monazite electron microprobe chemical dating spot data histogram

Individual spot error = 10.1 Ma (2 sigma)

00TWG431 (n = 11)

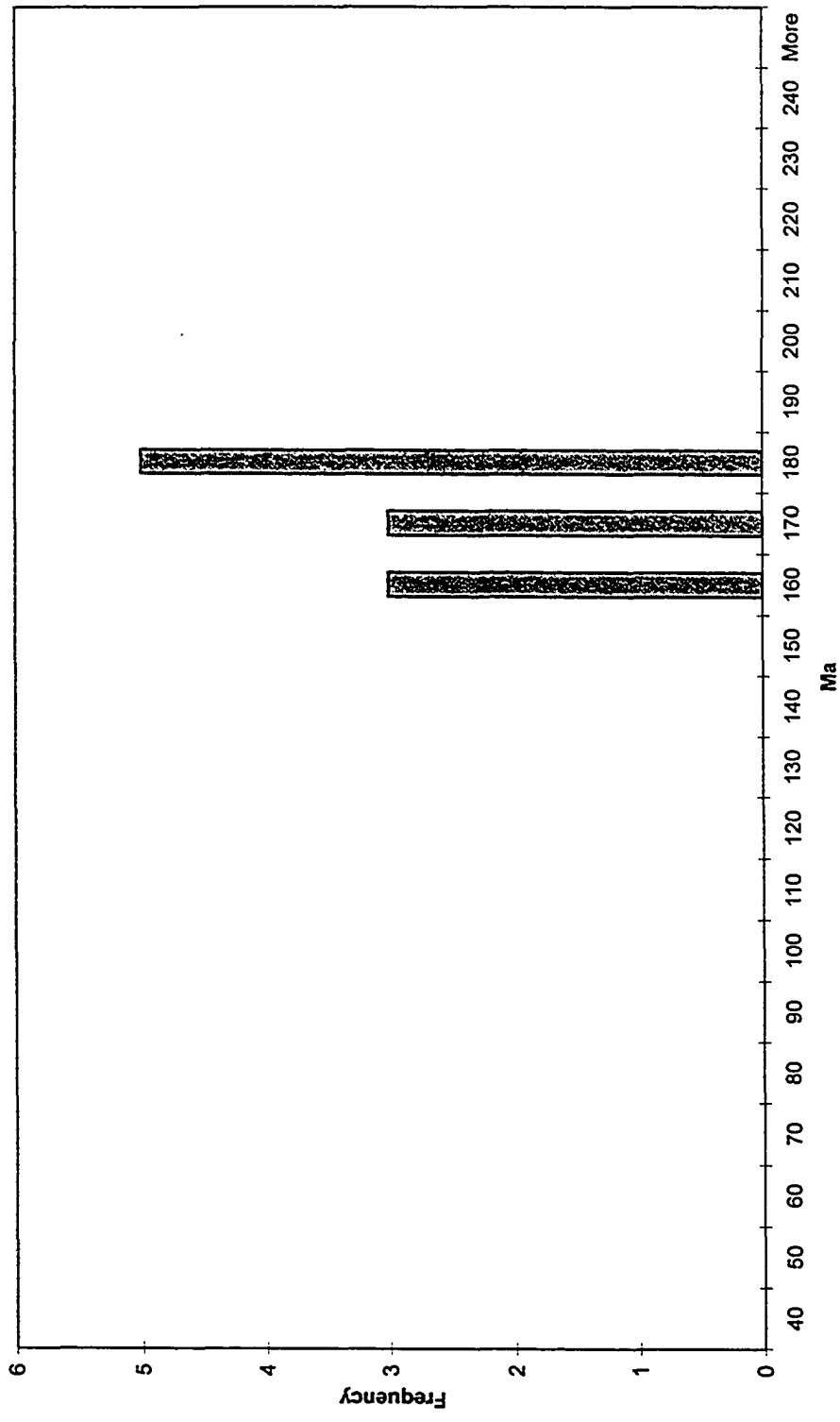

Sample 99TWG431: comparison of monazite chemical (EMP) age calculations

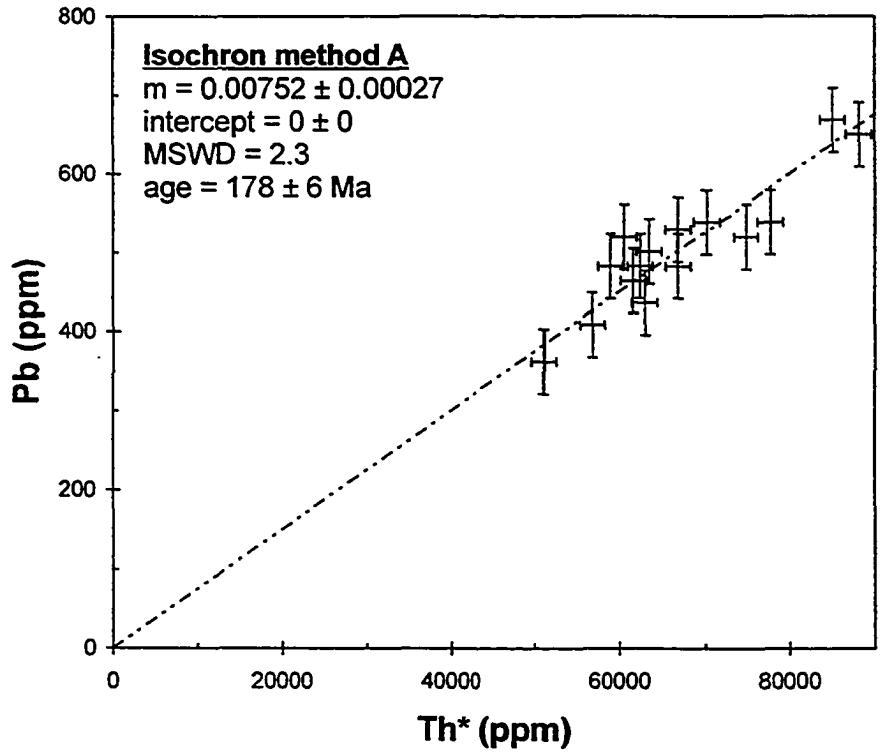

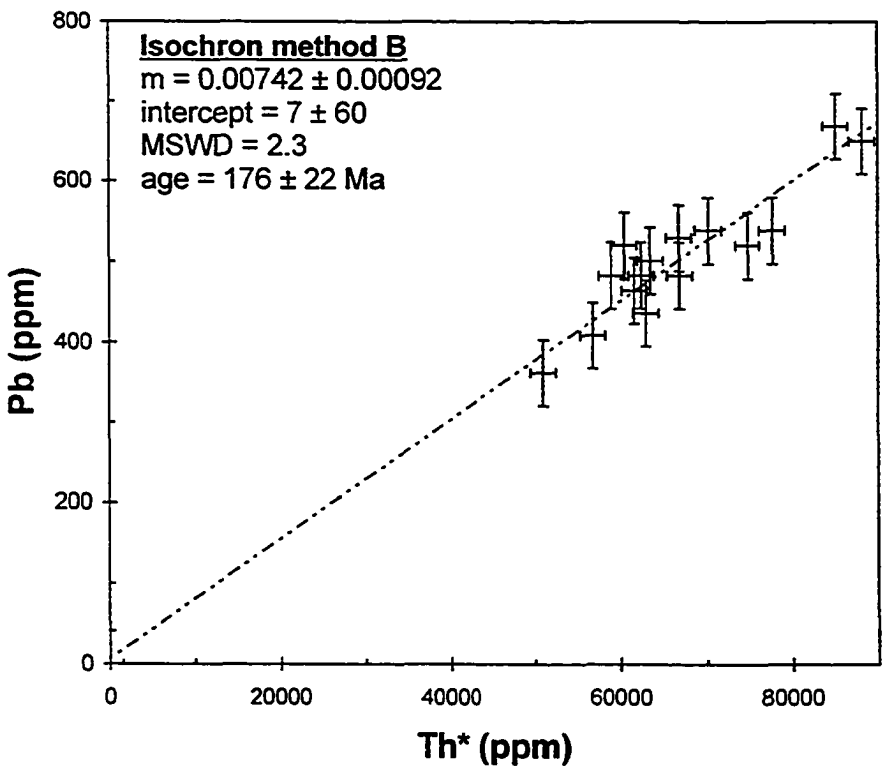

Monazite electron microprobe chemical dating spot data histogram

Individual spot error = 15.5 Ma (2 sigma)

99PG537 (n = 25)

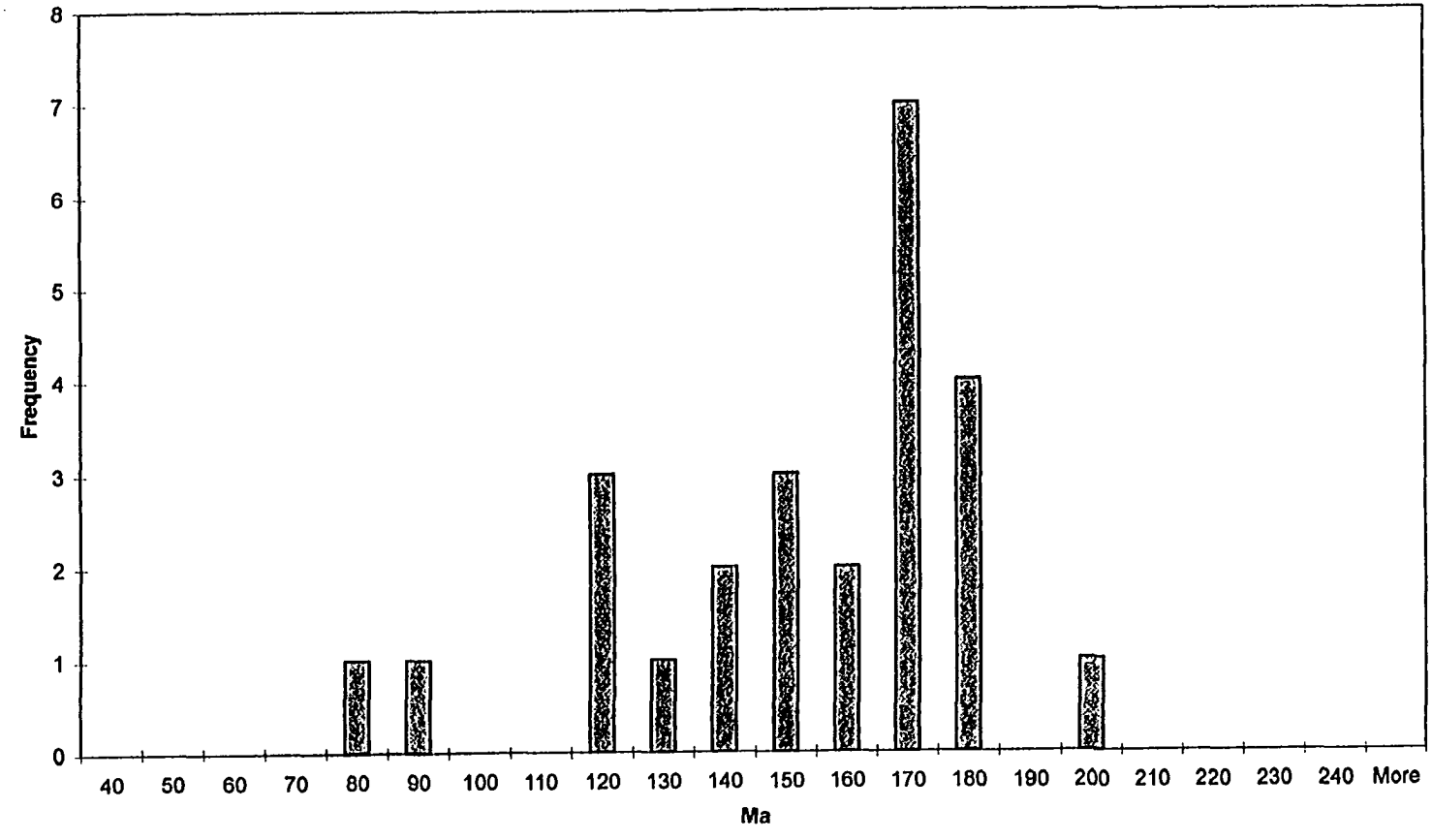

Sample 99TWG537 backscattered electron microprobe monazite images

Individual spot ages in brackets; spot error ± 15.5 Ma (2 sigma); ba: bad analysis

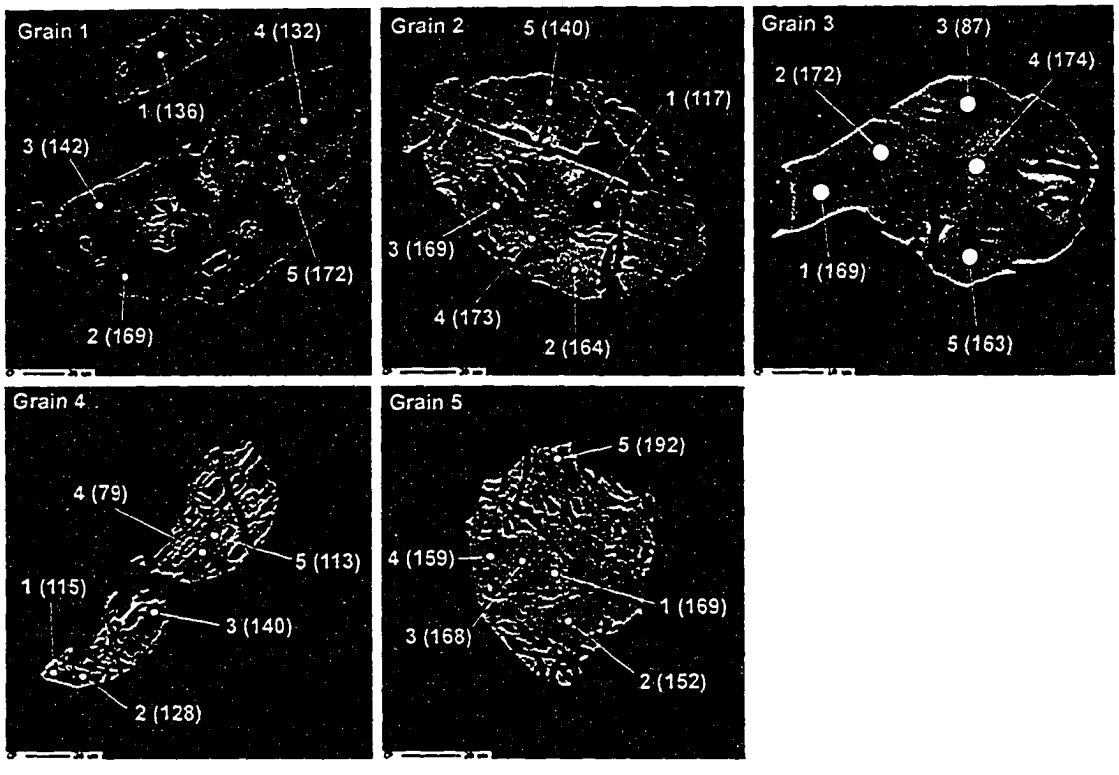

Sample 99TWG537: comparison of monazite chemical (EMP) age calculations

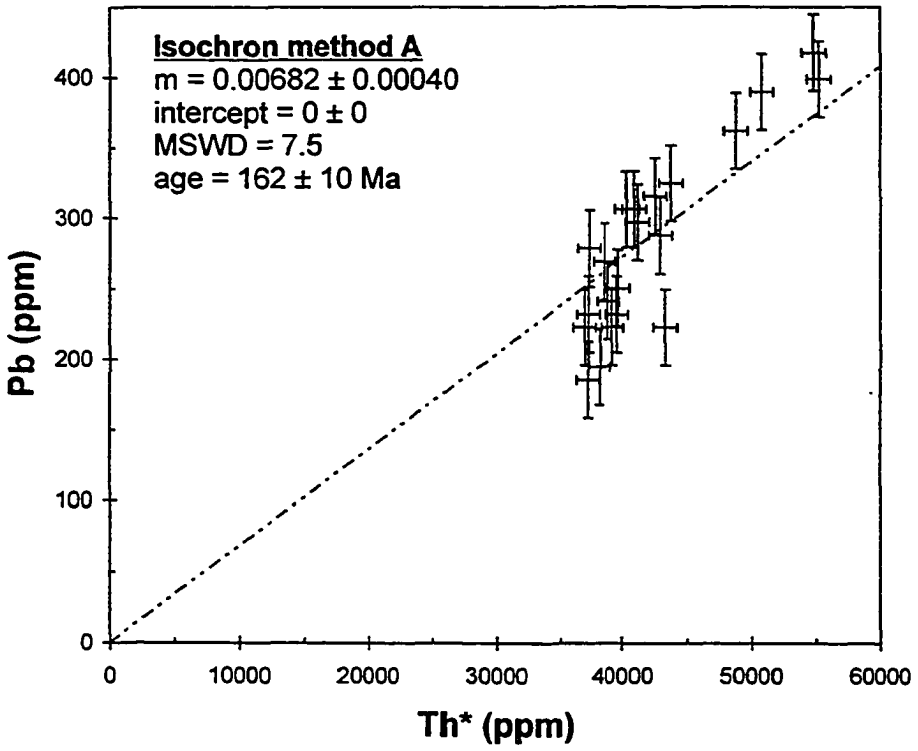

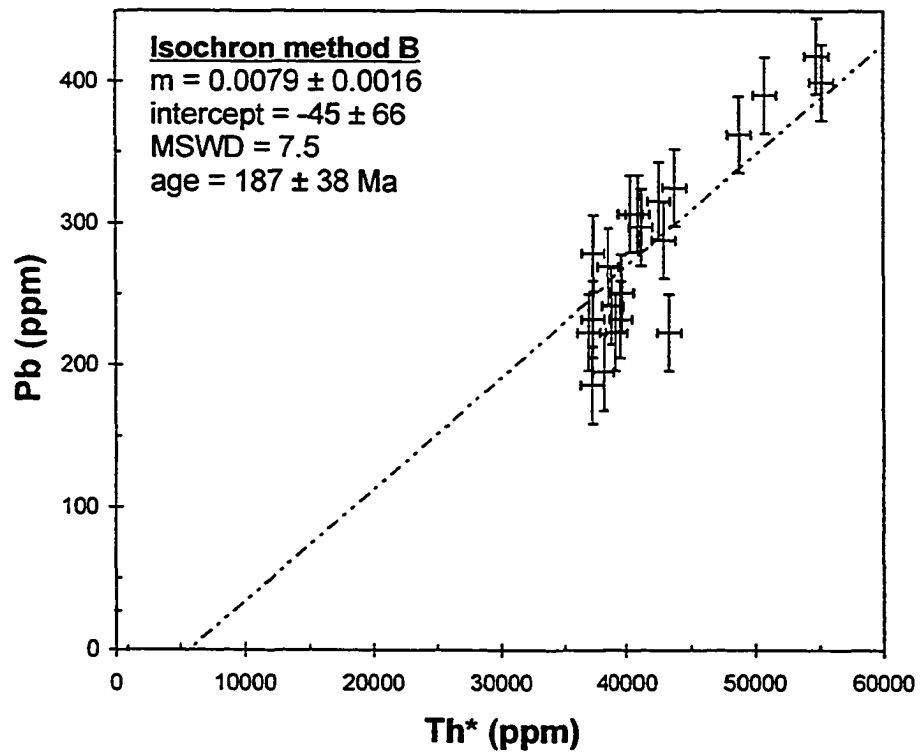

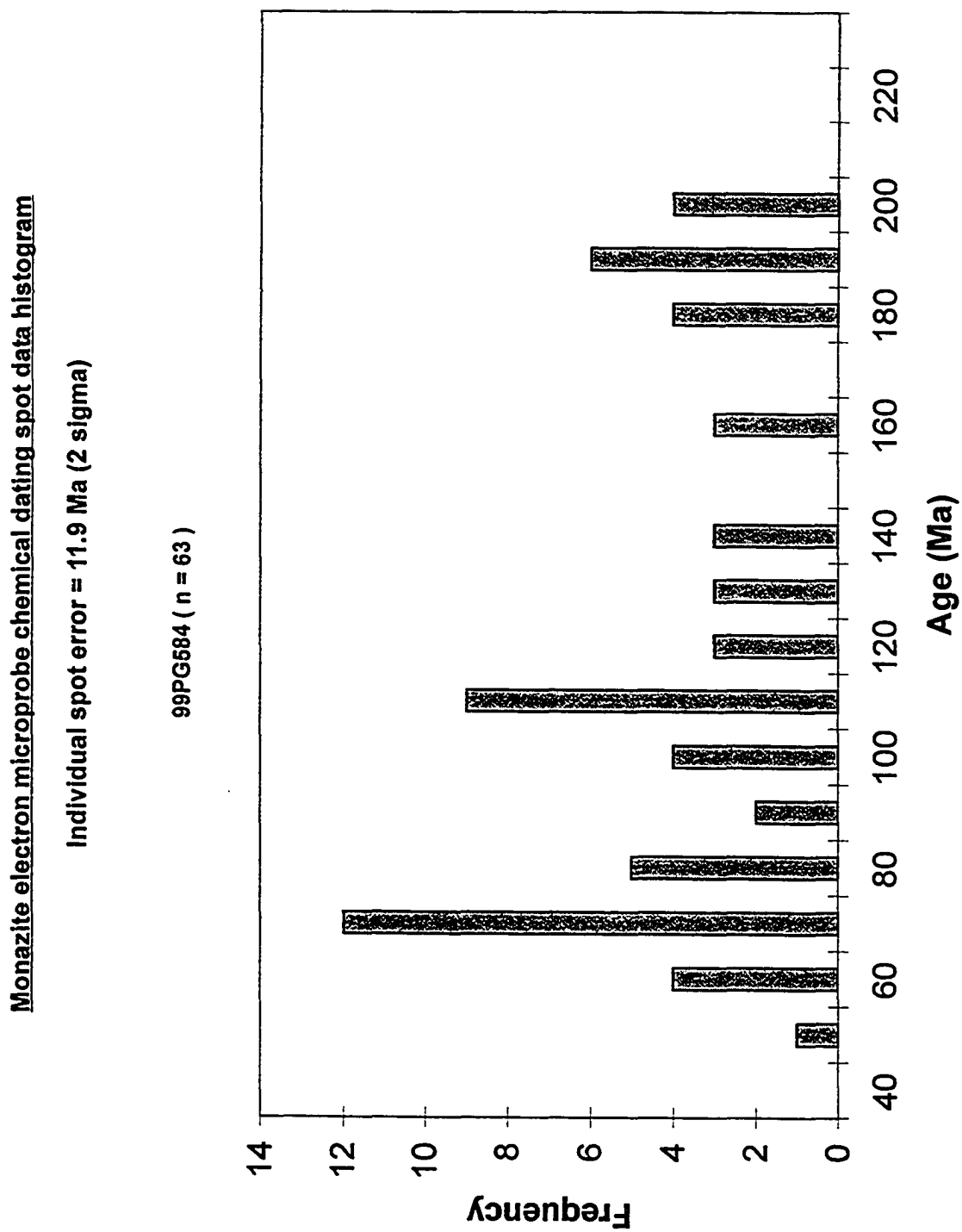

Sample 99TWG584 backscattered electron microprobe monazite images

Individual spot ages in brackets; spot error ± 11.9 Ma (2 sigma); ba: bad analysis

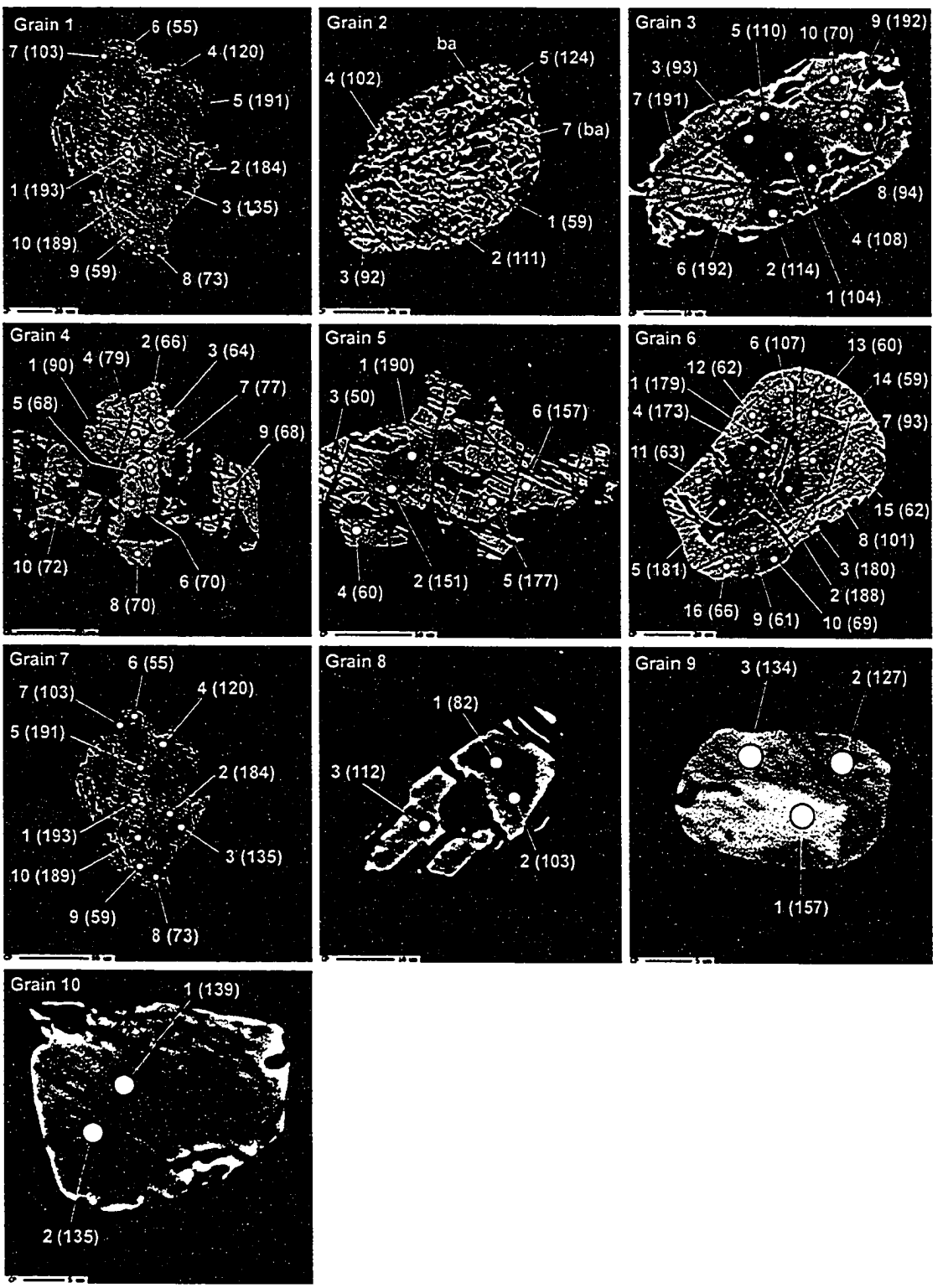

Sample 99TWG584: comparison of monazite chemical (EMP) age calculations

Popoulation # 1

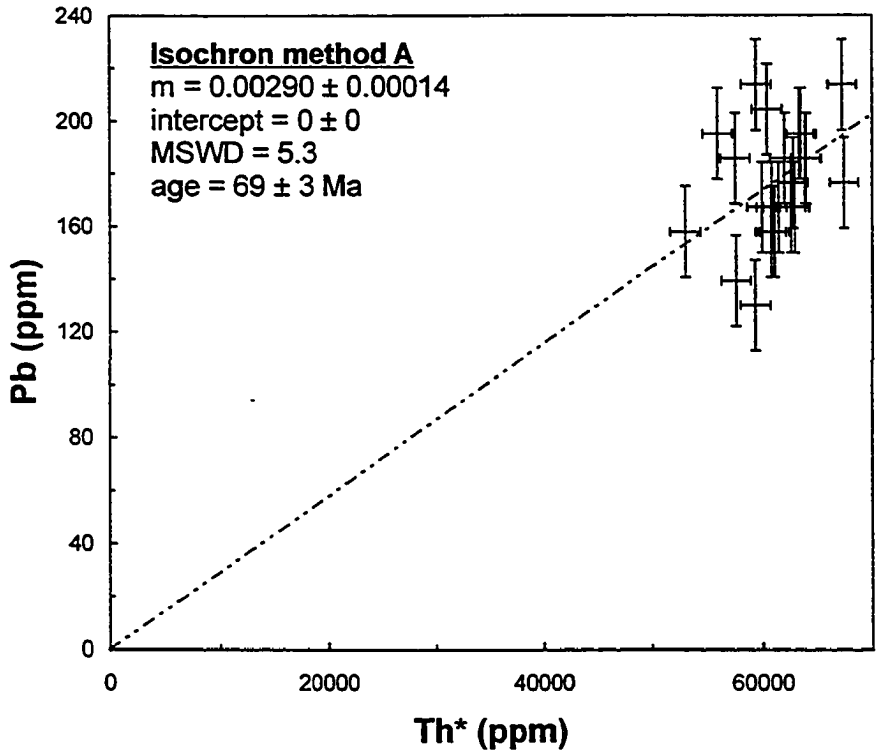

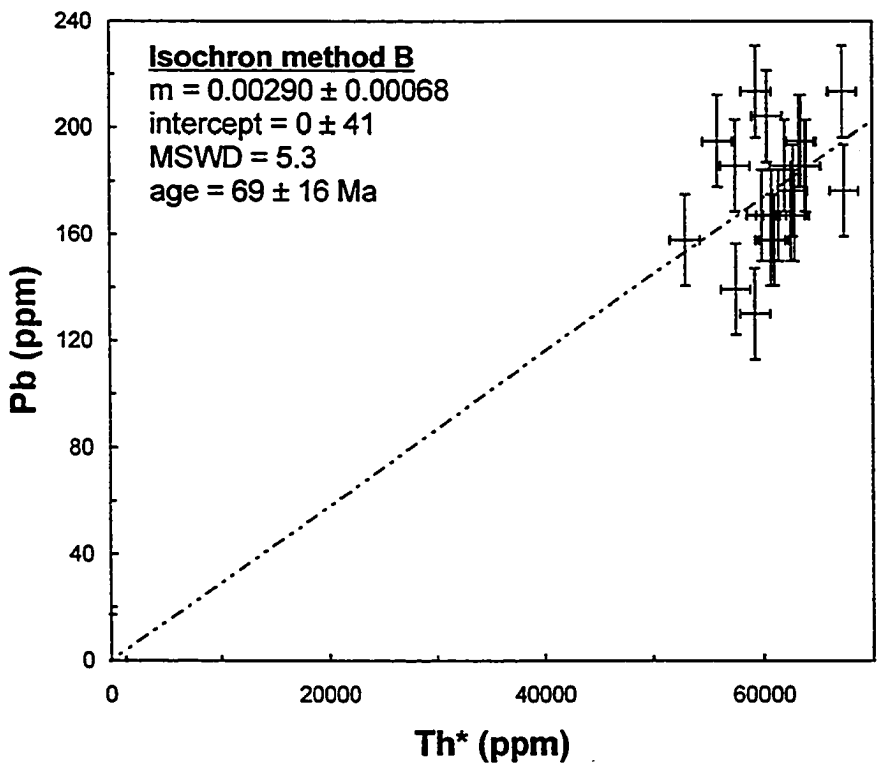

Sample 98TWG585: comparison of monazite chemical (EMP) age calculations

Population # 2

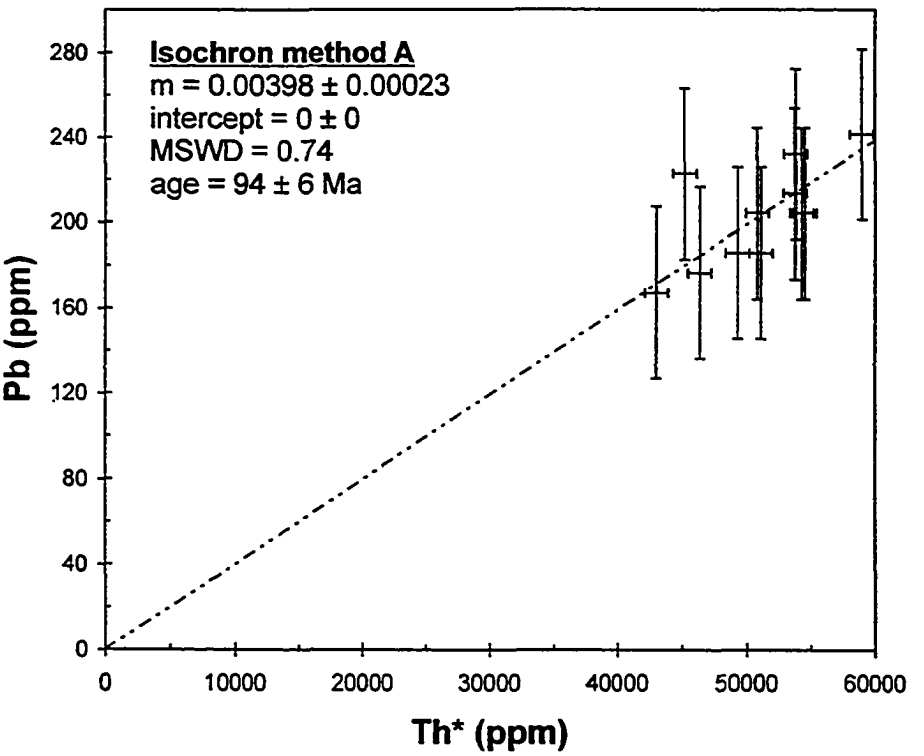

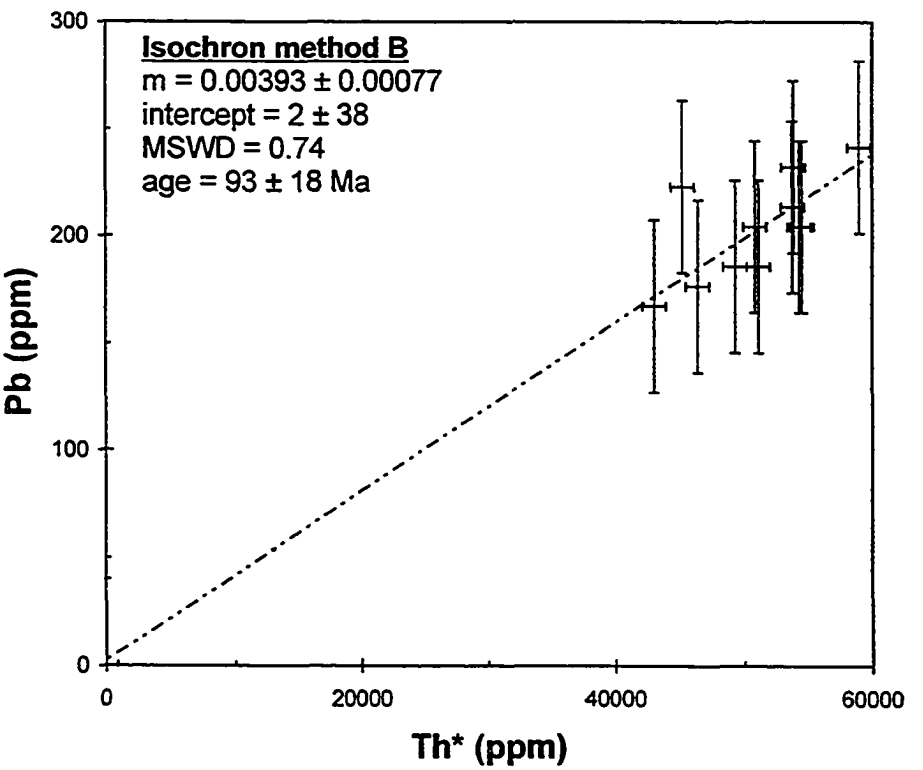

Sample 99TWG584: comparison of monazite chemical (EMP) age calculations

Population # 3

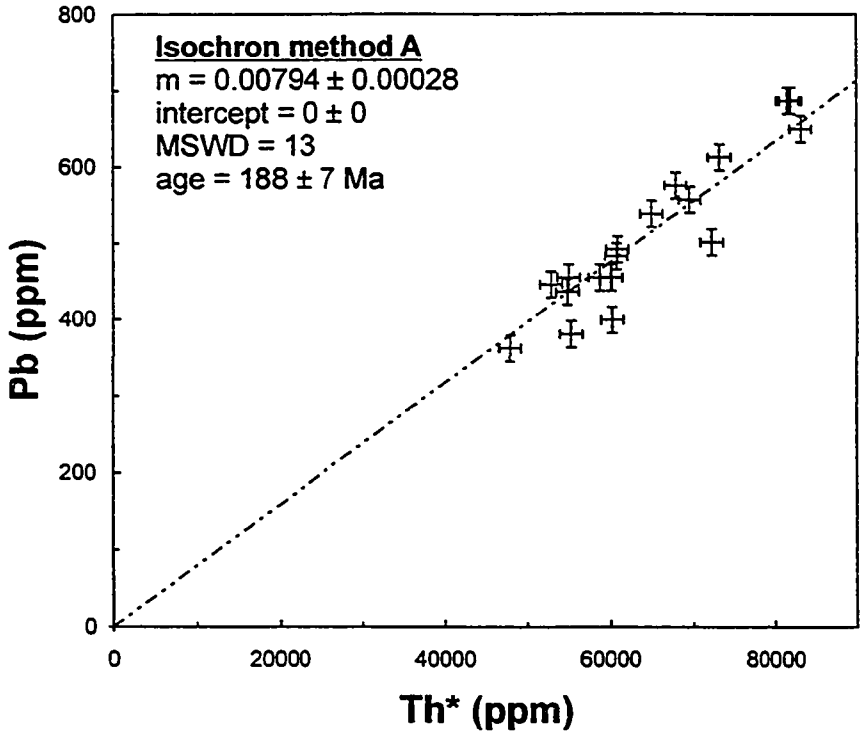

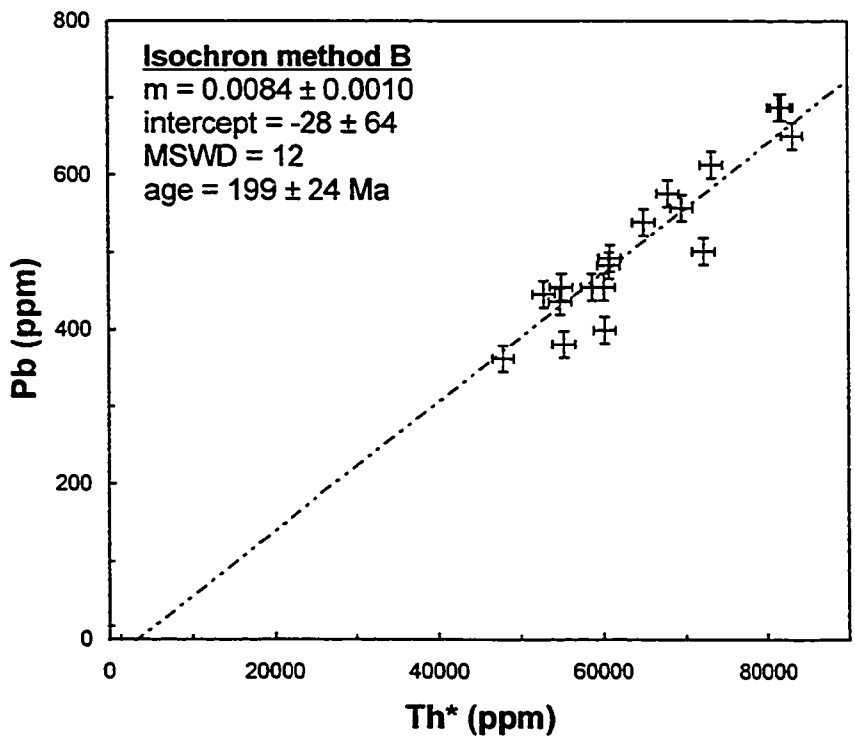

Monazite electron microprobe chemical dating spot data histogram

Individual spot error = 20.4 (2 sigma)

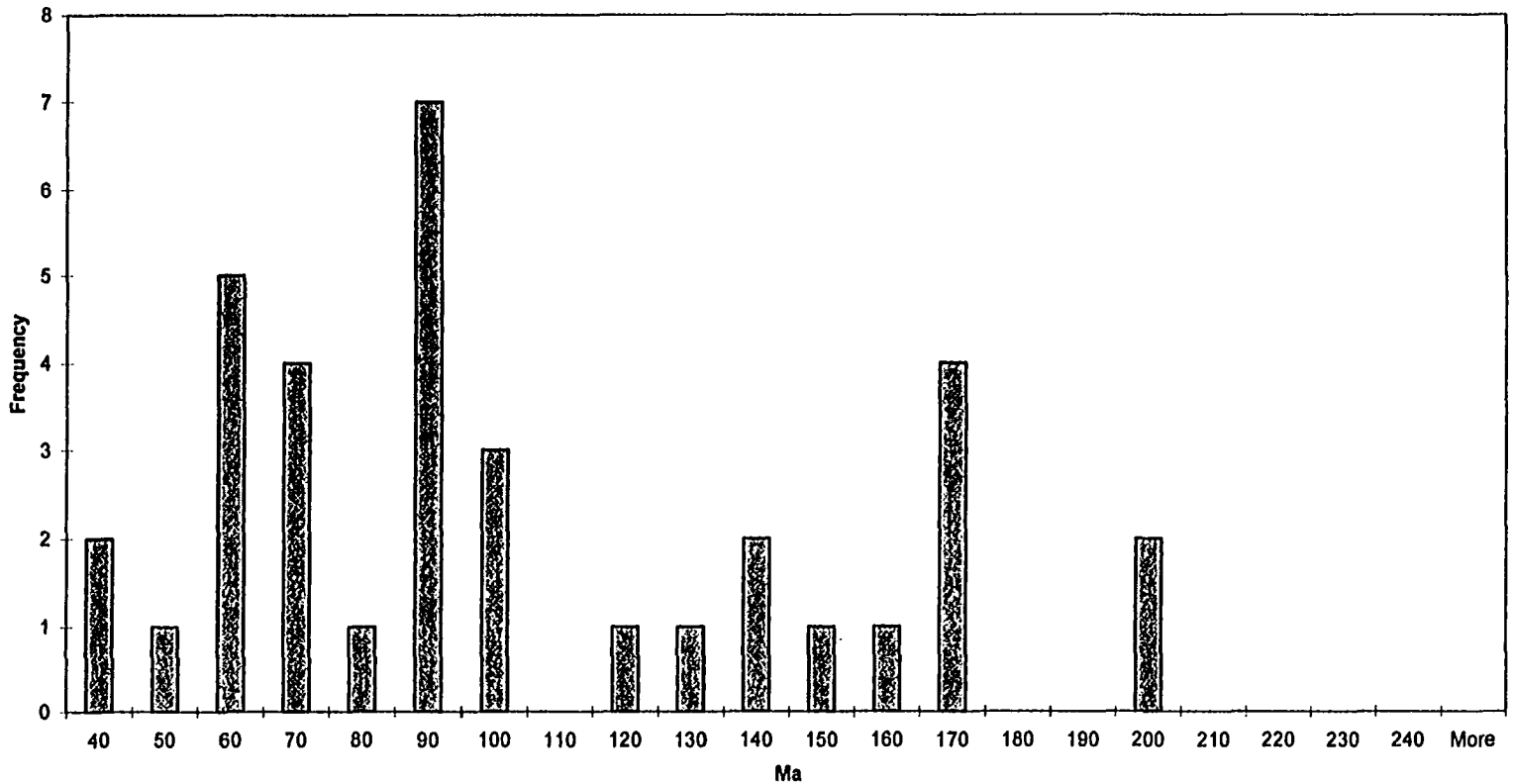

Sample 99TWG585 backscattered electron microprobe monazite images

Individual spot ages in brackets; spot error ± 20.4 Ma (2 sigma); ba: bad analysis

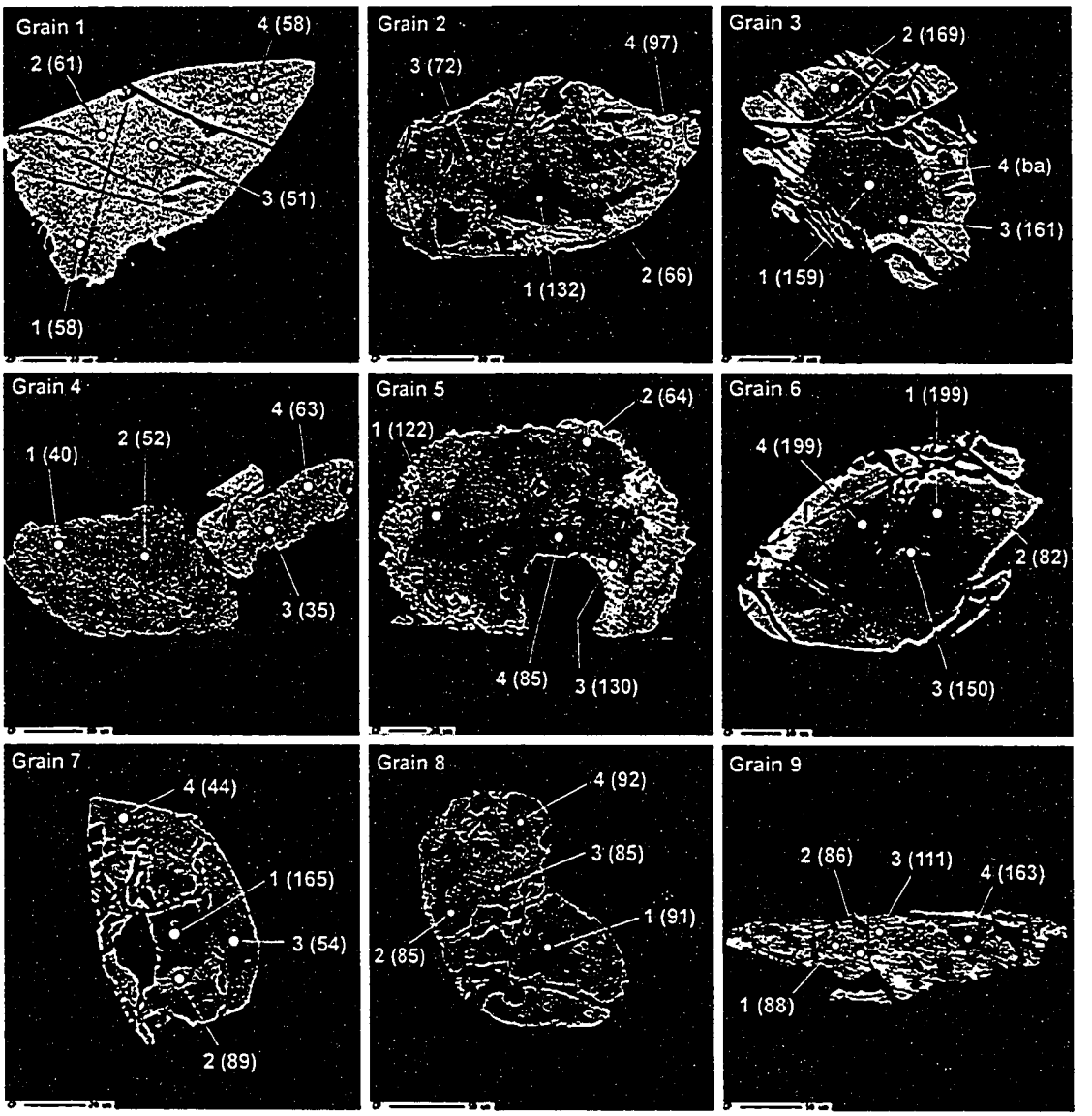

Sample 99TWG585: comparison of monazite chemical (EMP) age calculations

Population # 1

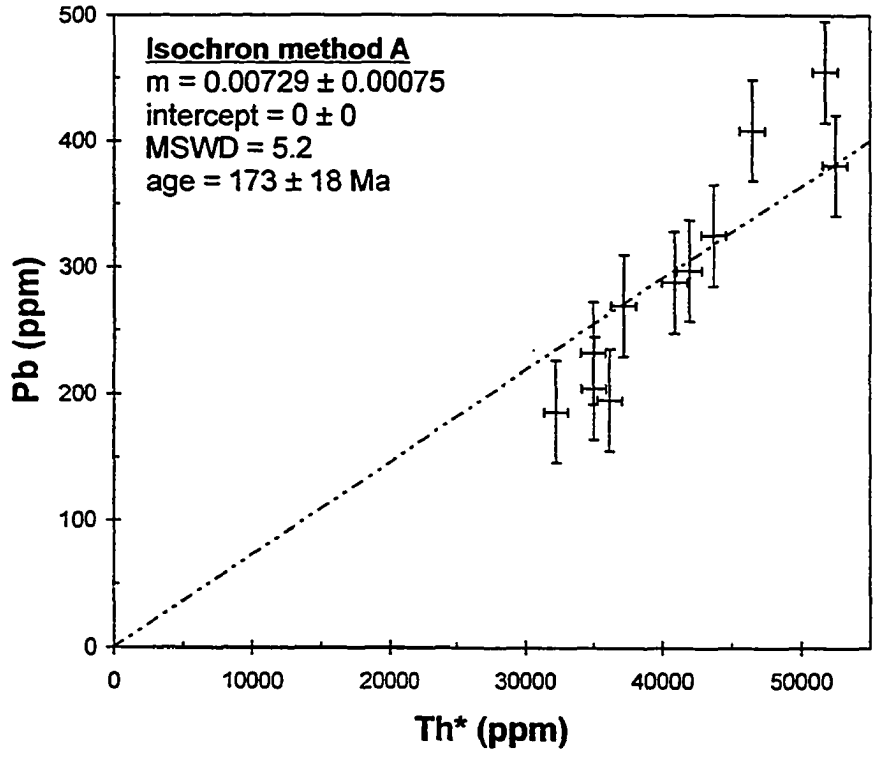

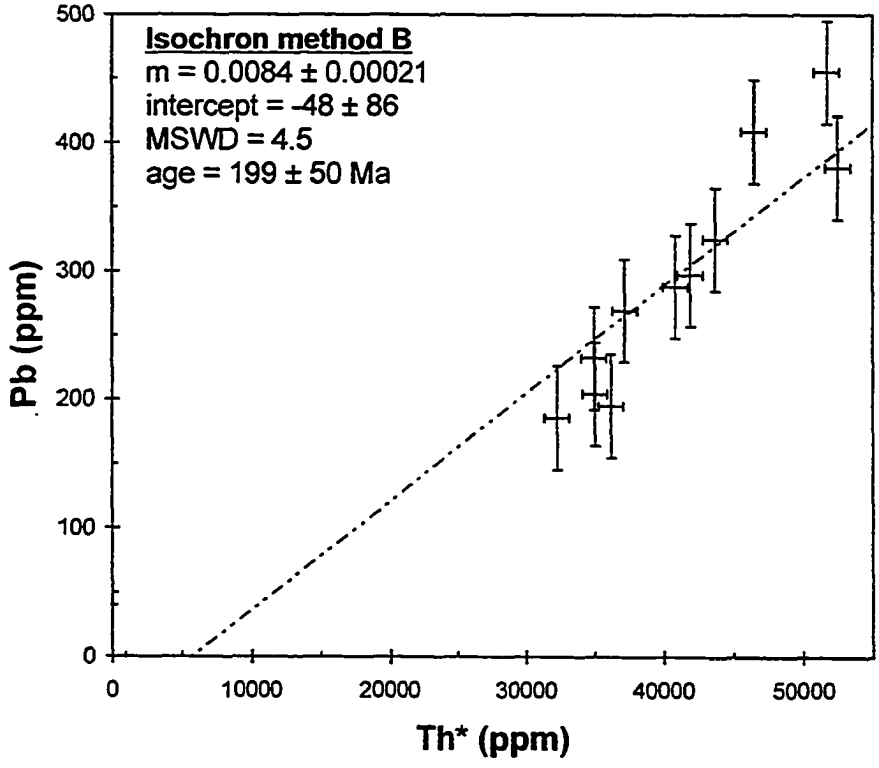

Sample 98TWG585: comparison of monazite chemical (EMP) age calculations

Population # 2

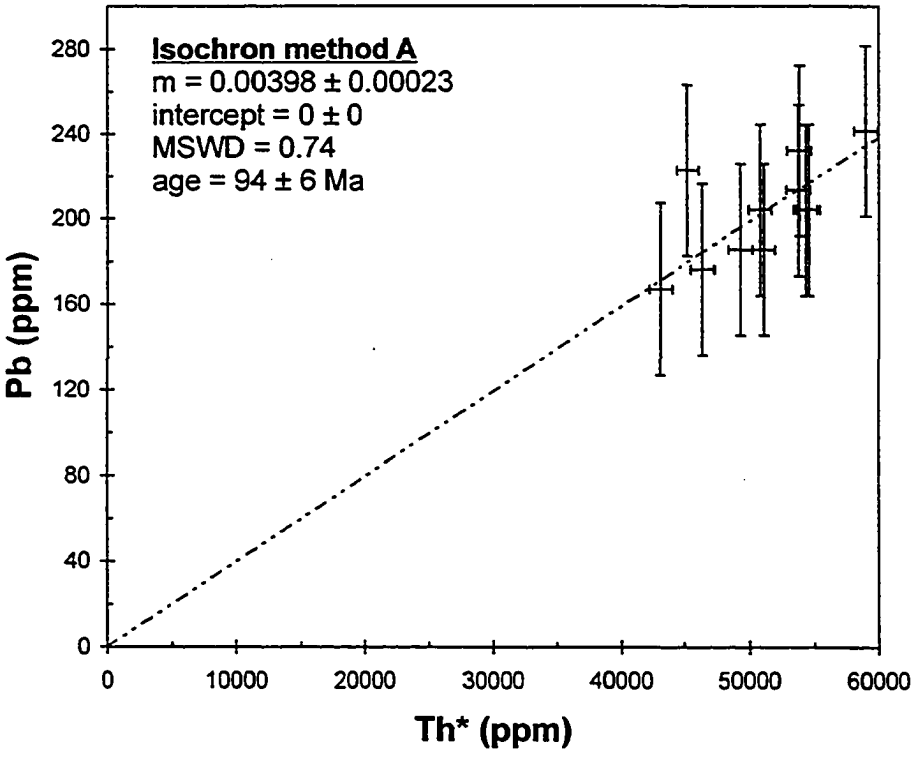

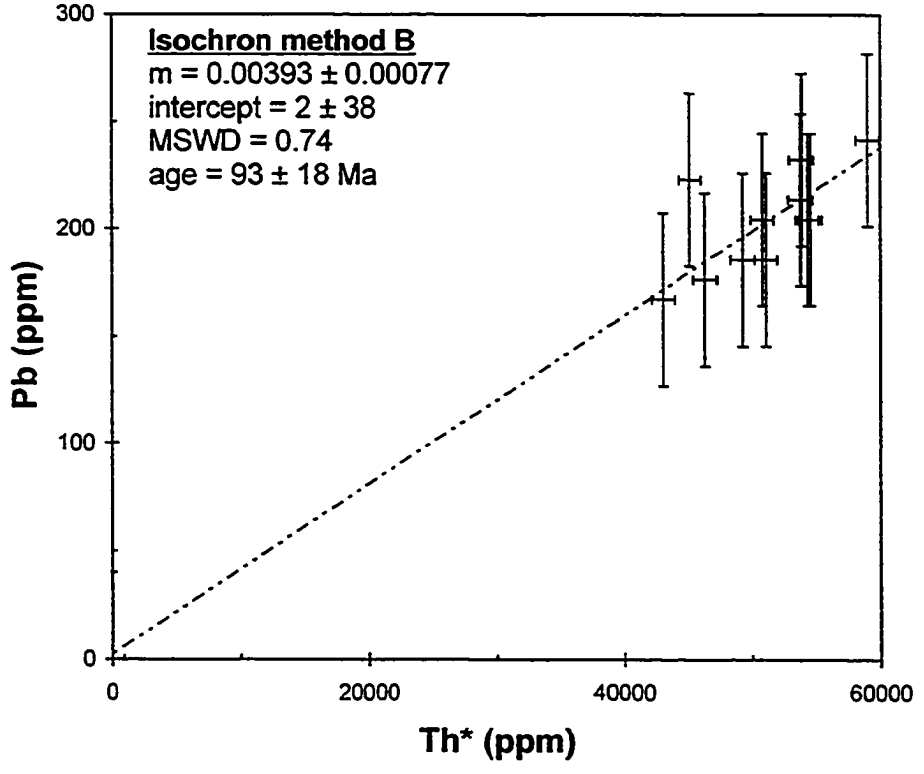

Sample 98TWG585: comparison of monazite chemical (EMP) age calculations

Popoulation # 3

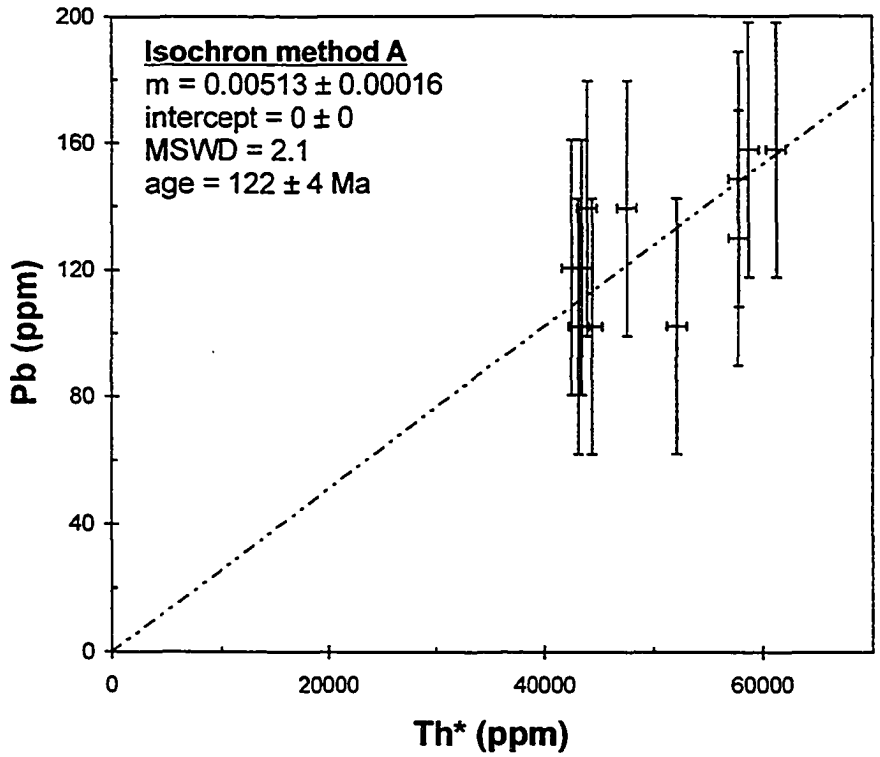

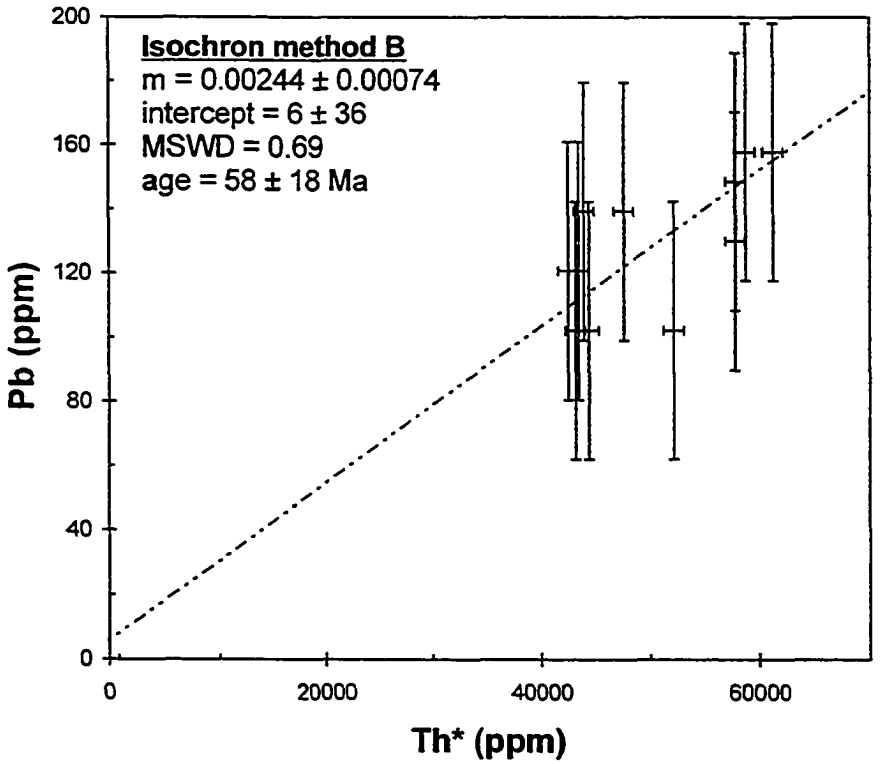

Monazite electron microprobe chemical dating spot data histogram

Individual spot error = 15.8 Ma (2 sigma)

00TWG391 (n = 17)

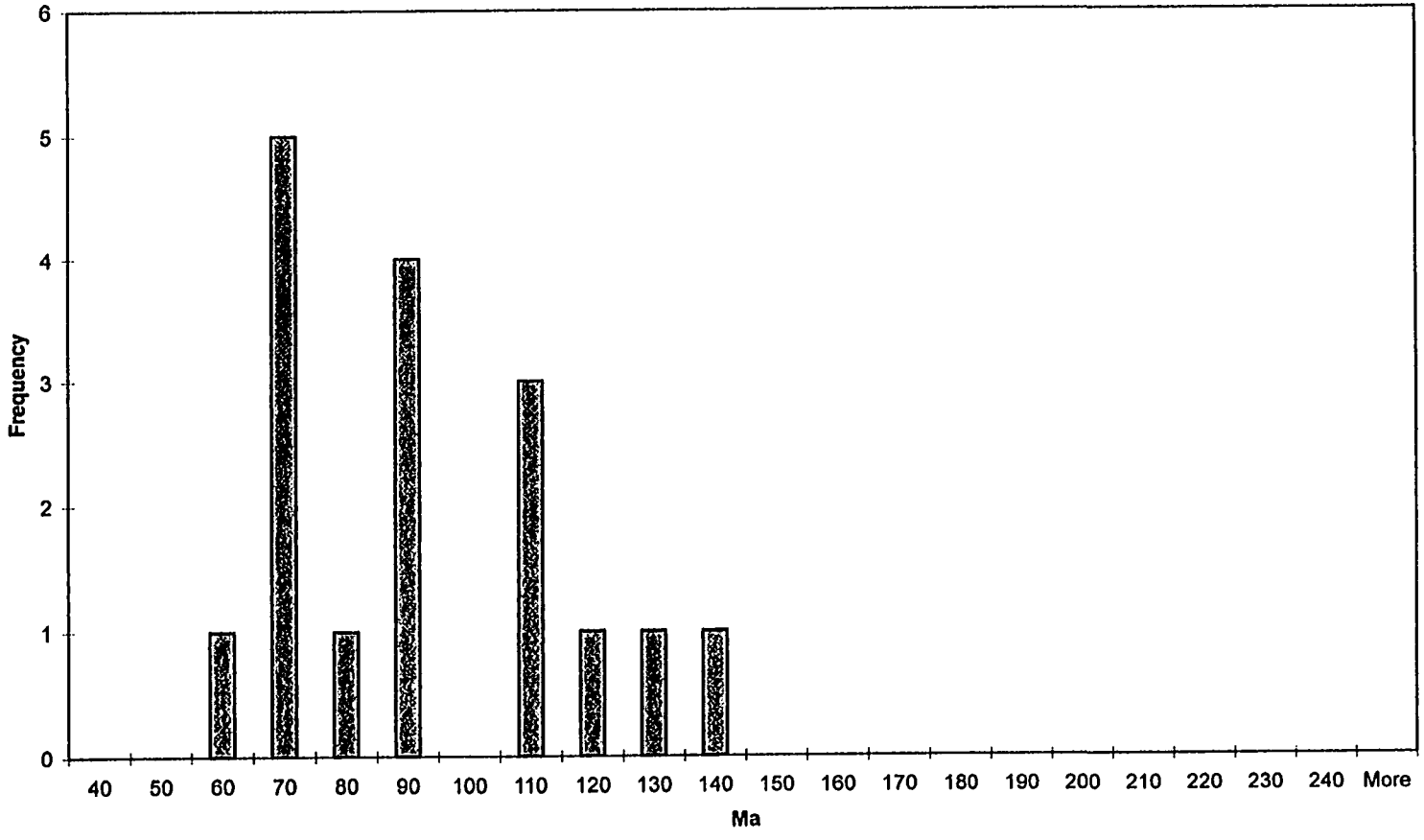

Sample 00TWG391 backscattered electron microprobe monazite images

Individual spot ages in brackets; spot error ± 15.8 Ma (2 sigma); ba: bad analysis

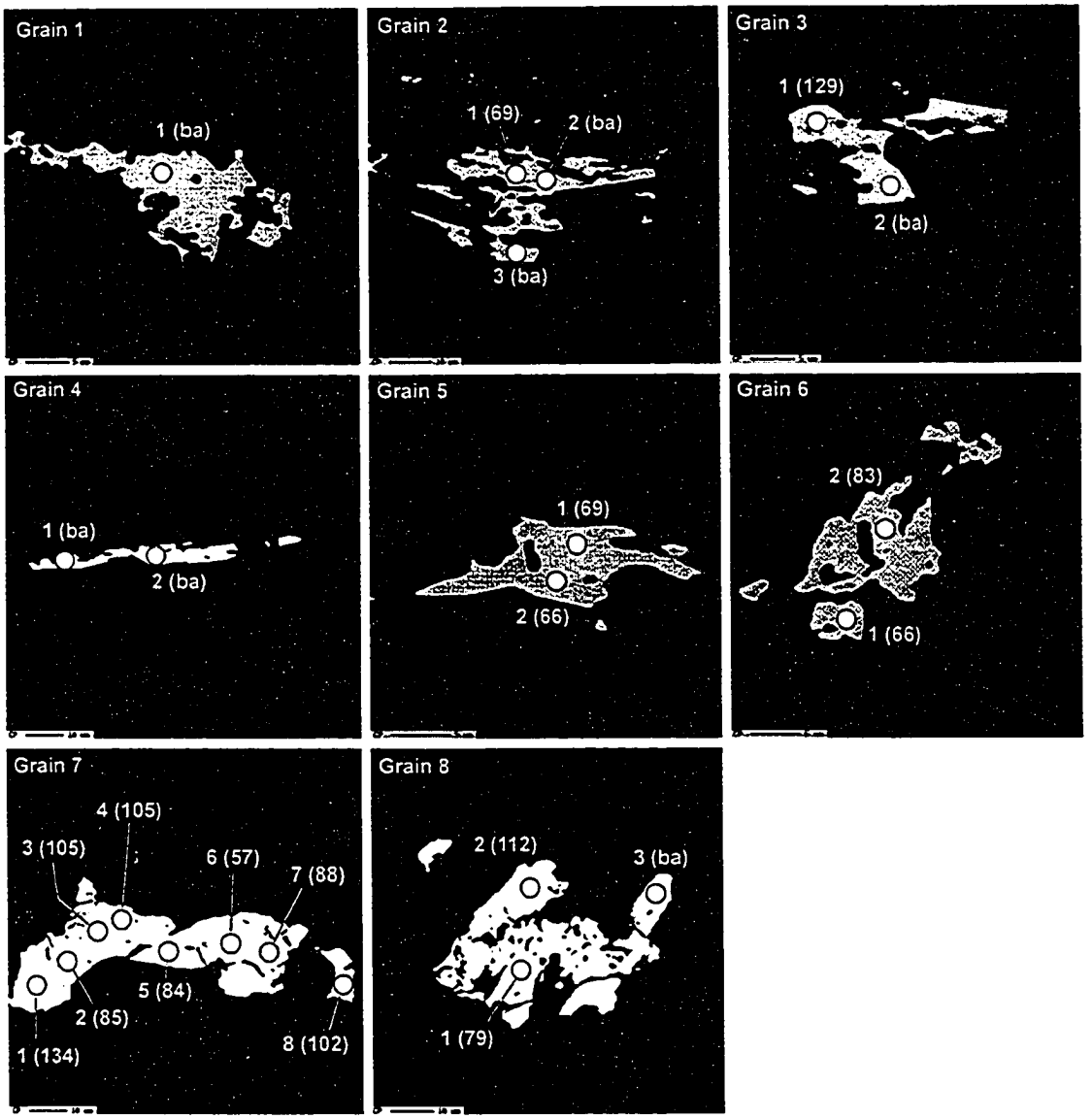

Sample 00TWG391: comparison of monazite chemical (EMP) age calculations

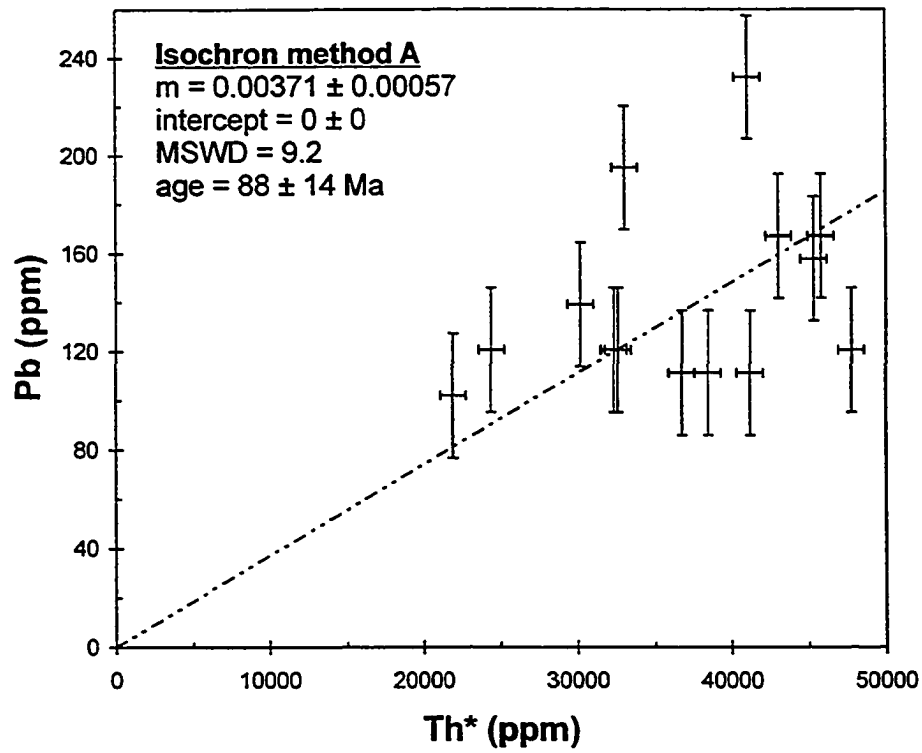

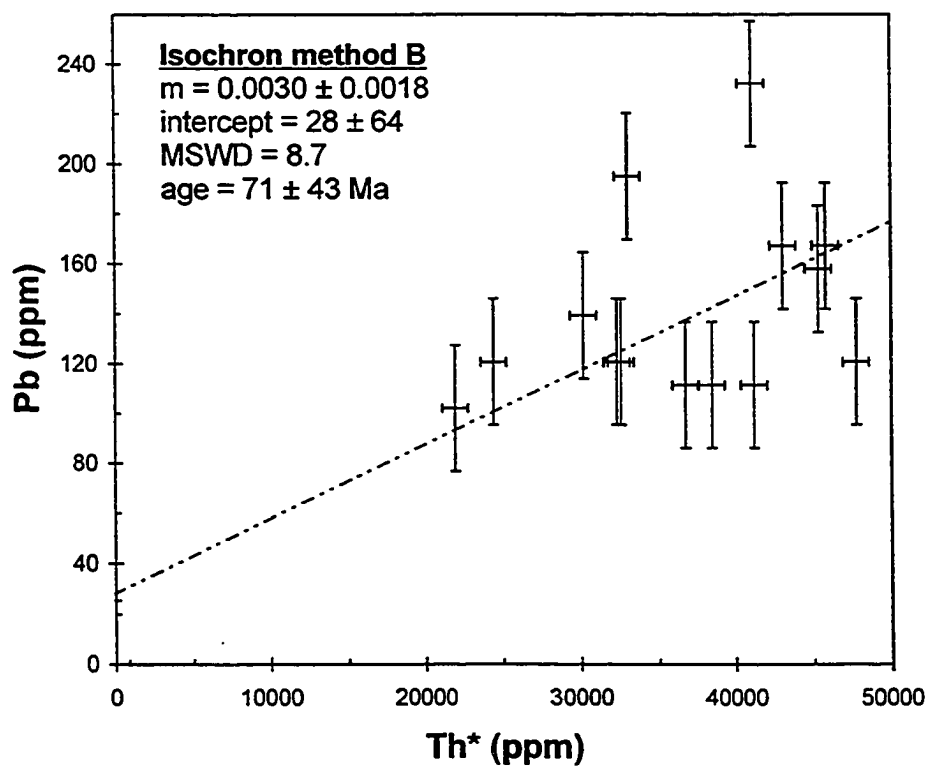

Monazite electron microprobe chemical dating spot data histogram

Individual spot error = 10.9 Ma (2 sigma)

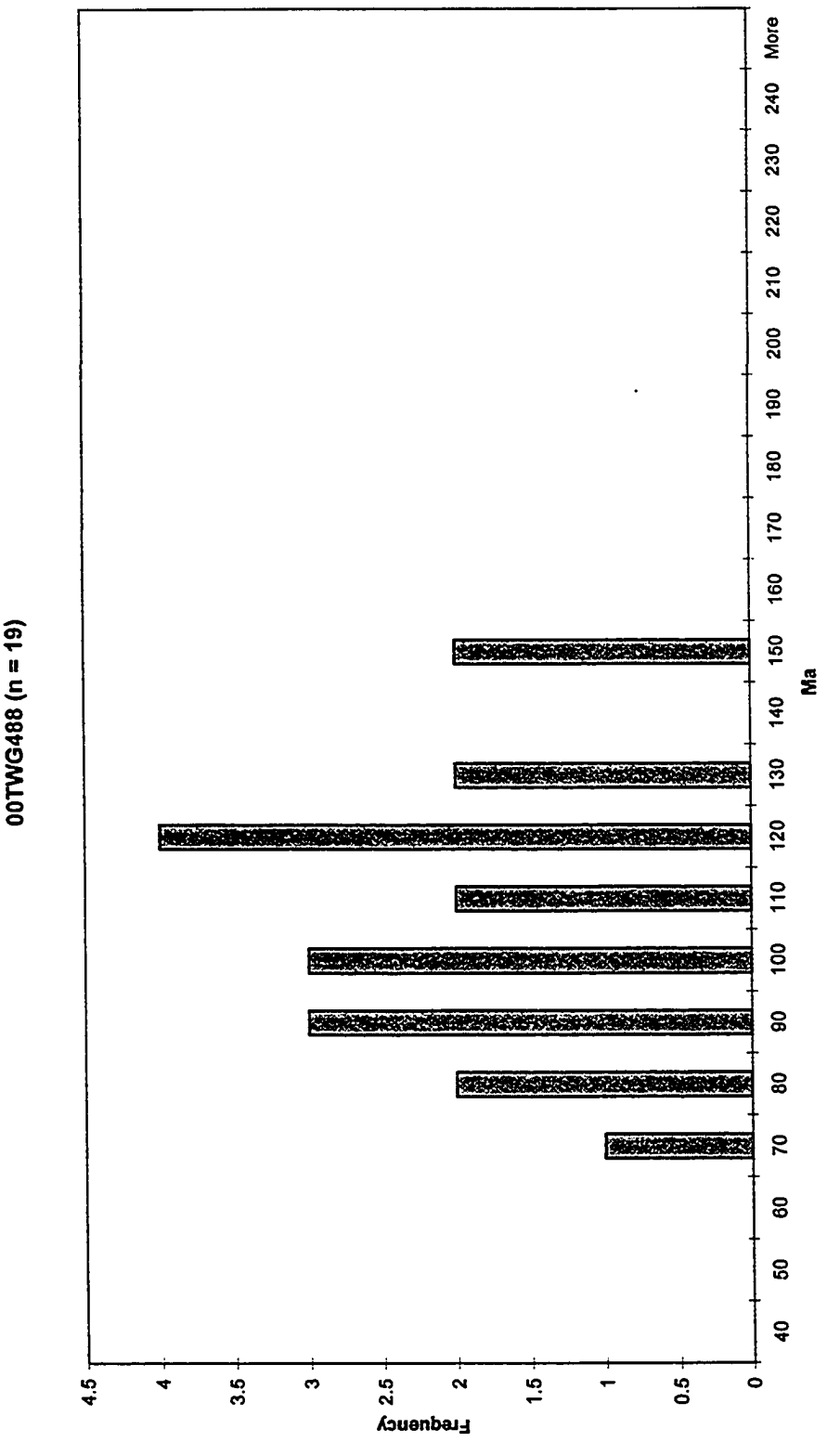

Sample 00TWG488 backscattered electron microprobe monazite images

Individual spot ages in brackets; spot error ± 10.9 Ma (2 sigma); ba: bad analysis

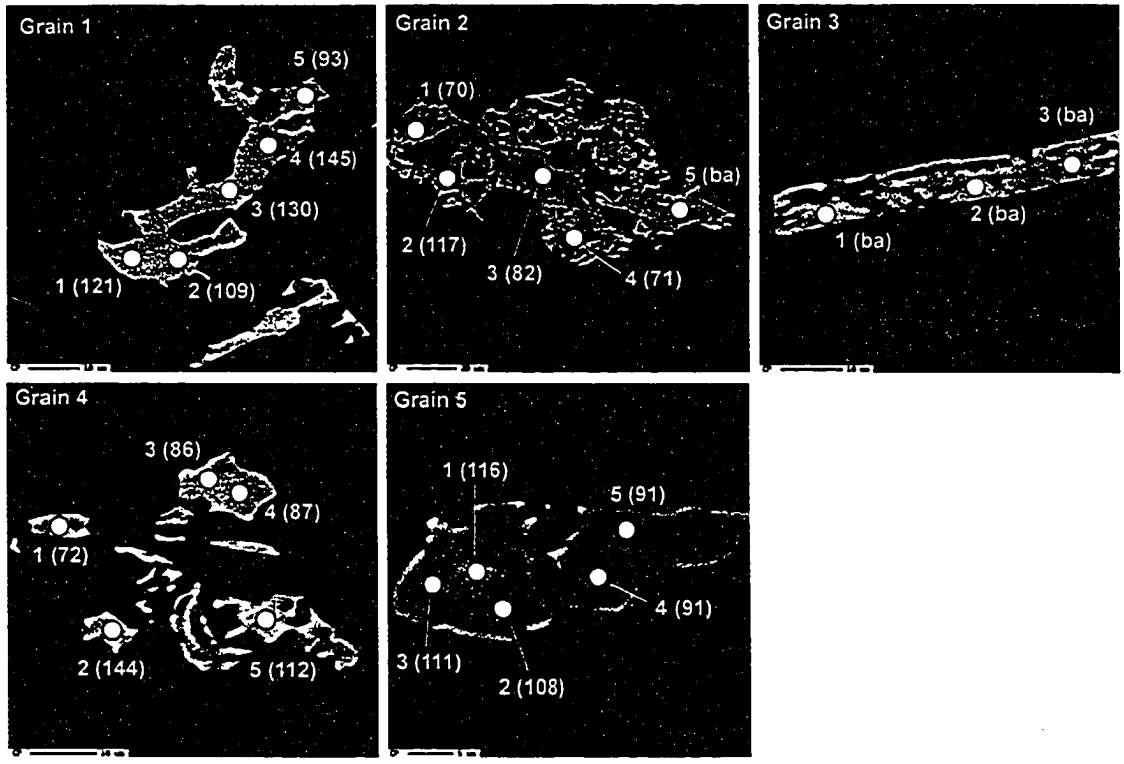

Sample 00TWG488: comparison of monazite chemical (EMP) age calculations

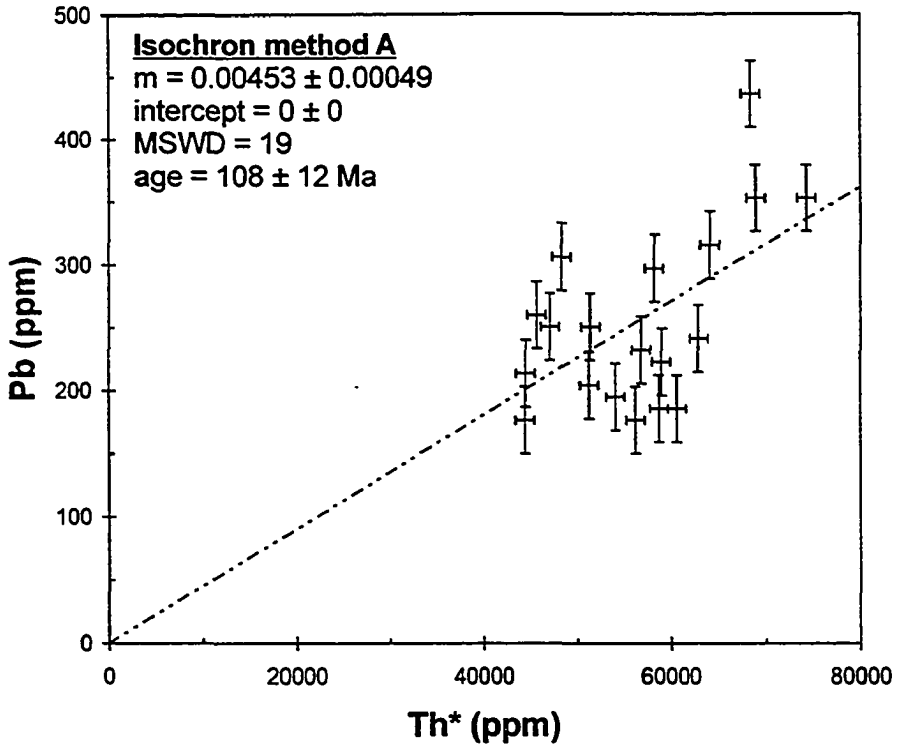

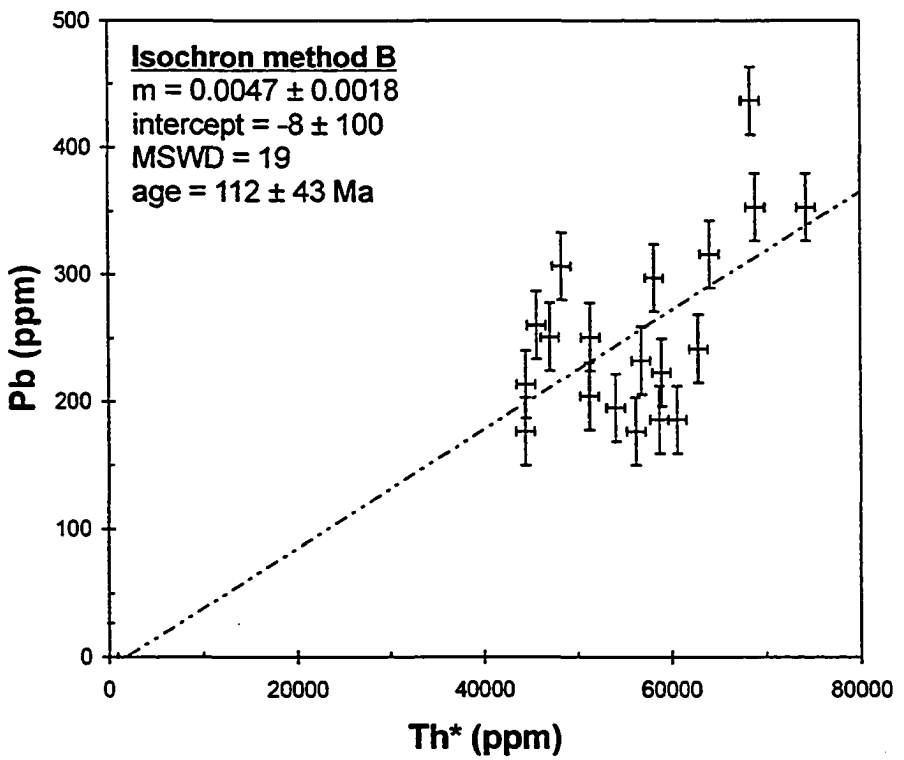

Monazite electron microprobe chemical dating spot data histogram

Individual spot error = 22.3 Ma (2 sigma)

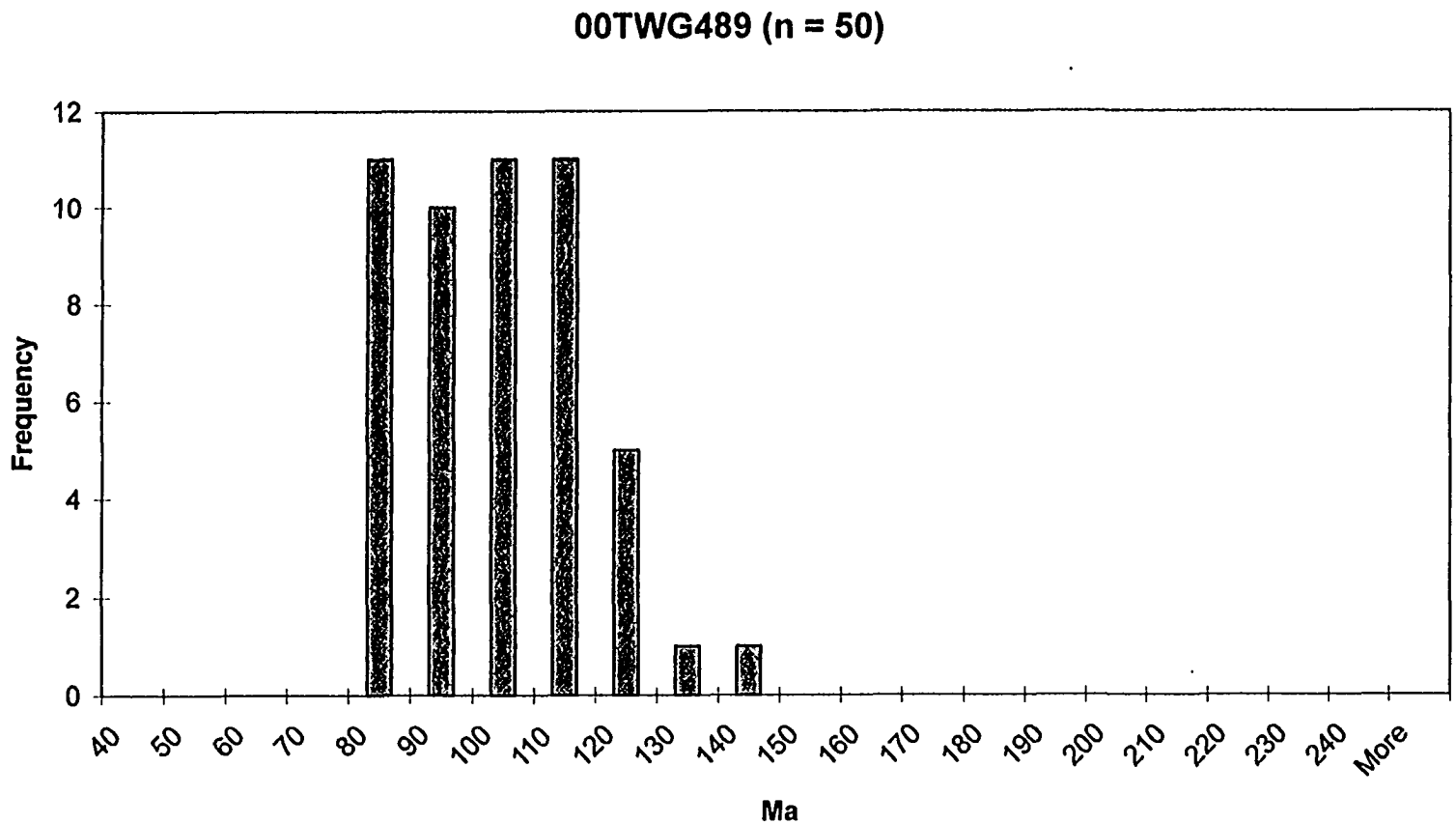

Sample 00TWG489 backscattered electron microprobe monazite images

Individual spot ages in brackets; spot error ± 22.3 Ma (2 sigma); ba: bad analysis

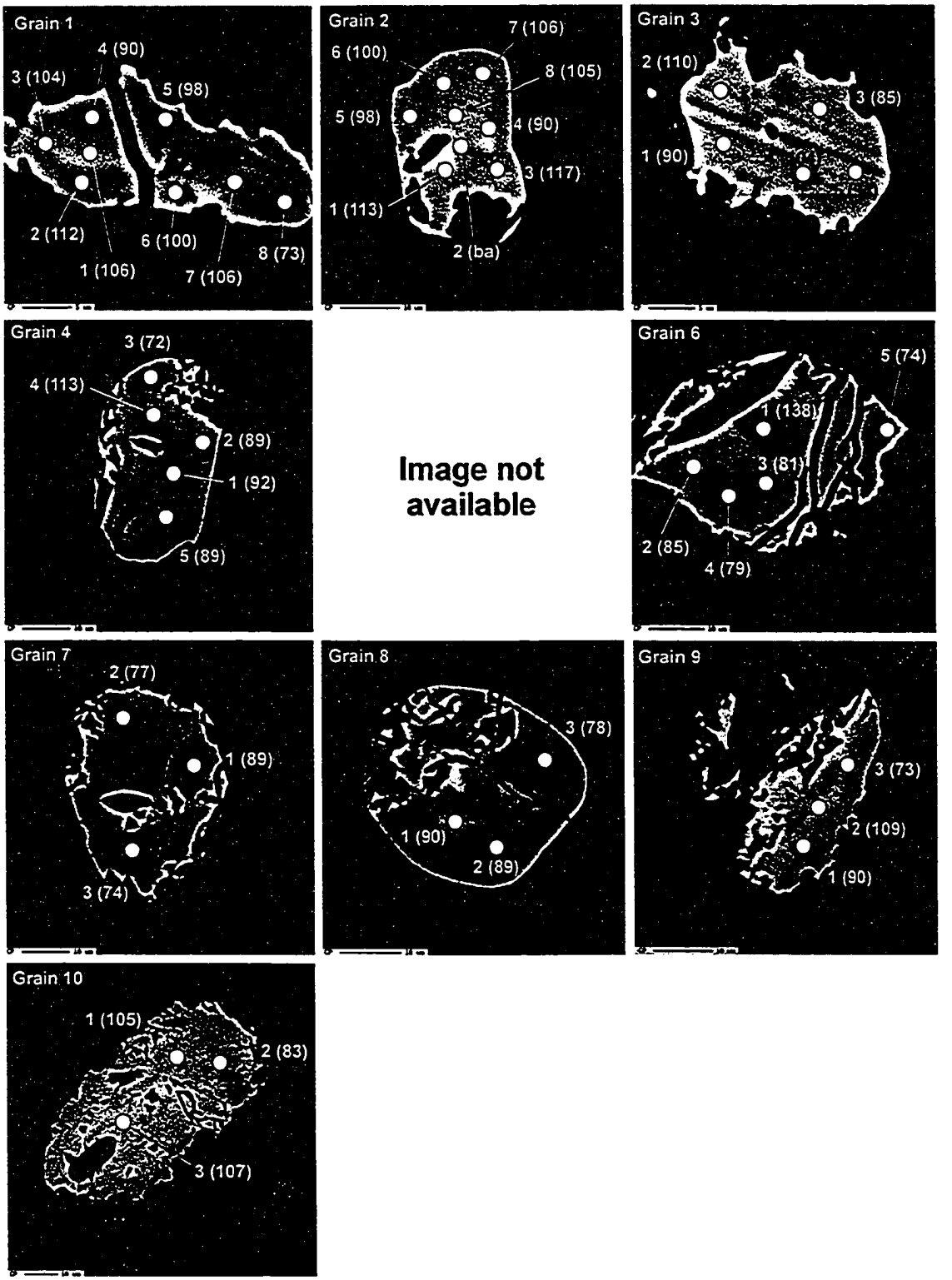

Sample 00TWG489: comparison of monazite chemical (EMP) age calculations

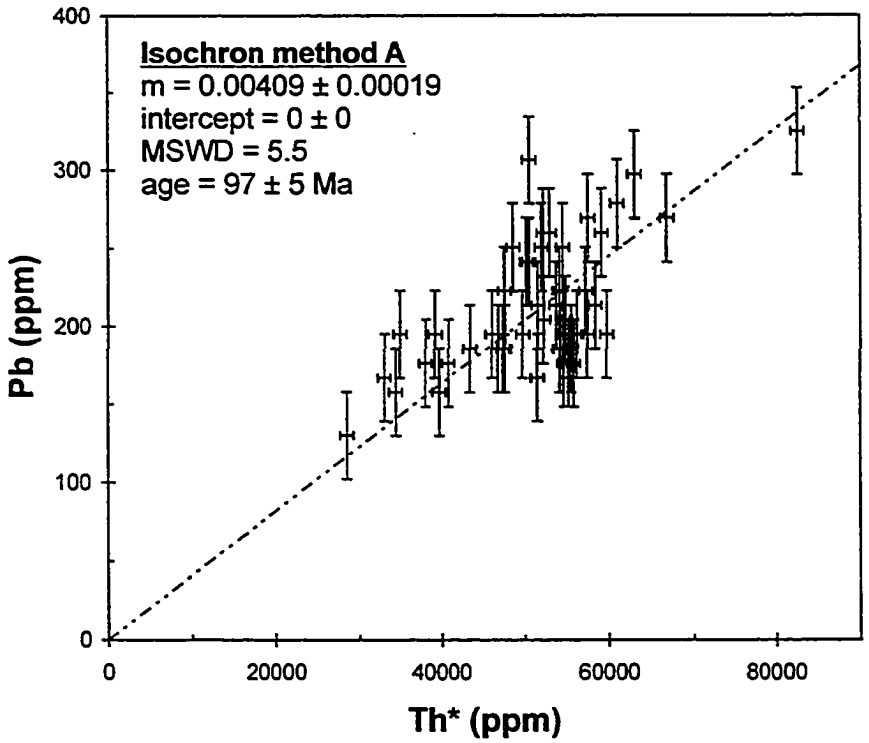

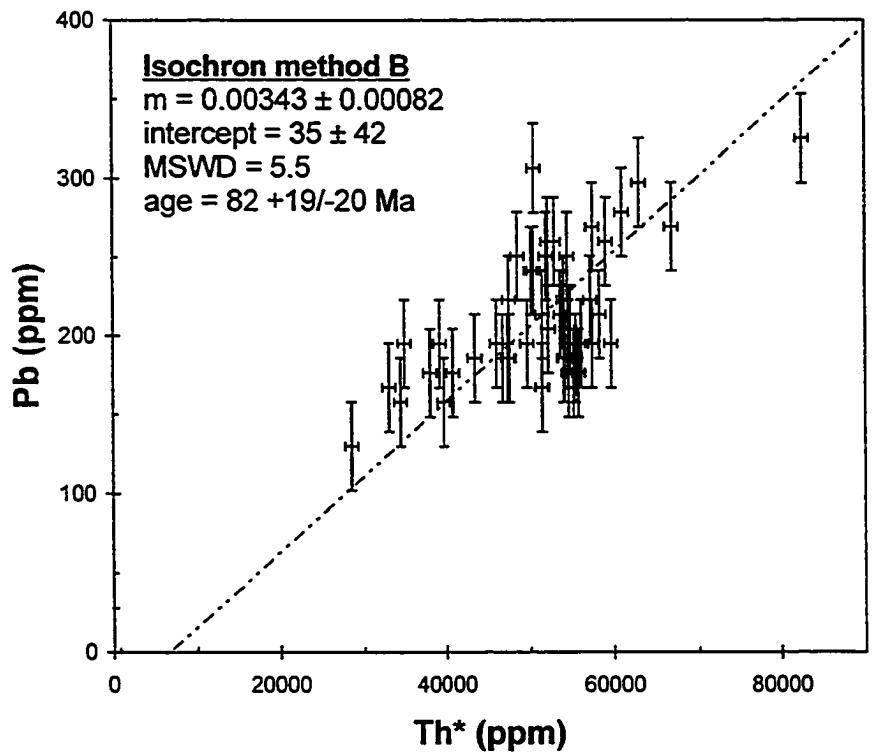

Monazite electron microprobe chemical dating spot data histogram

Individual spot error = 16.0 Ma (2 sigma)

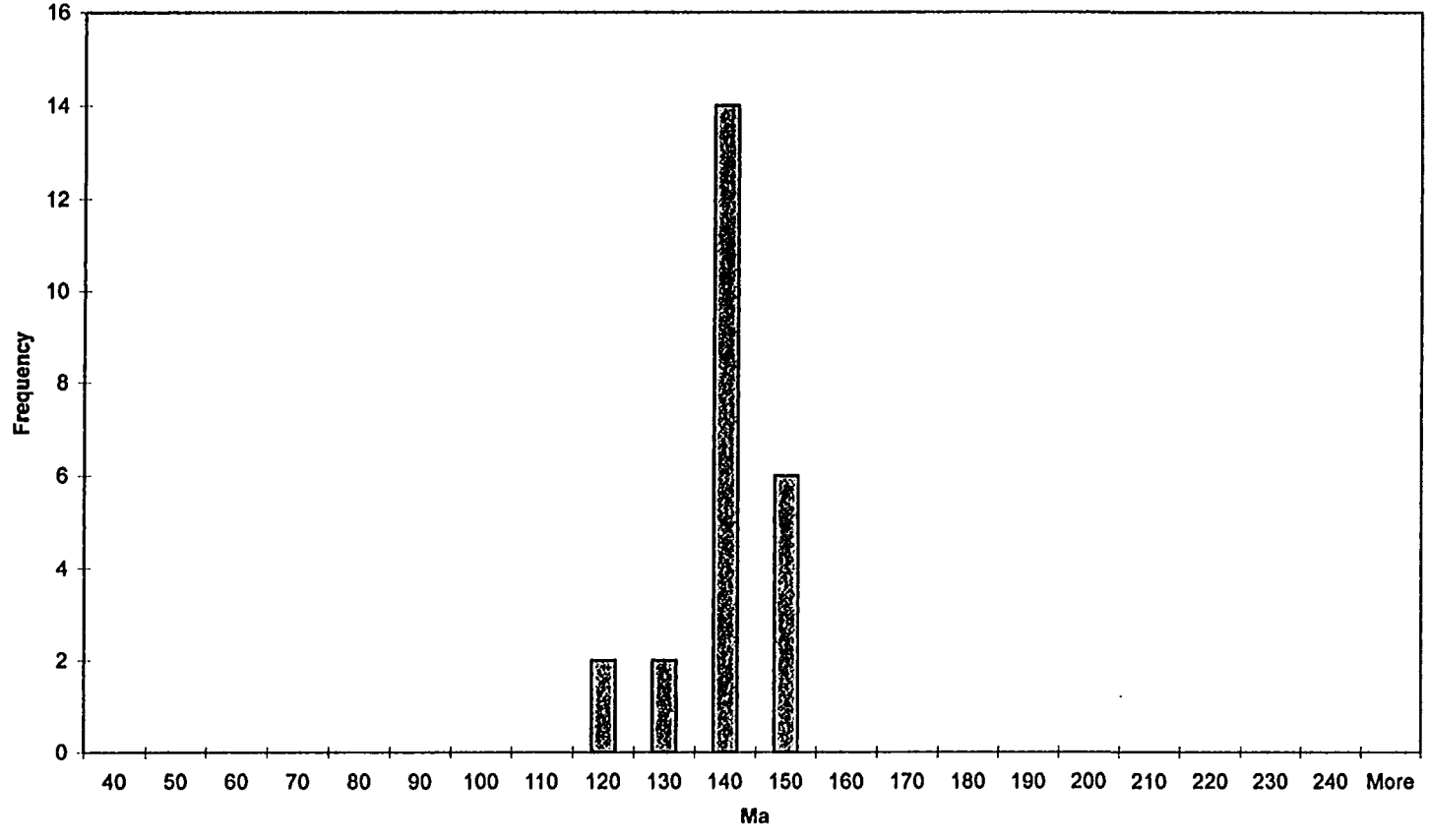

Sample 00TWG493 backscattered electron microprobe monazite images

Individual spot ages in brackets; spot error ± 16.0 Ma (2 sigma); ba: bad analysis

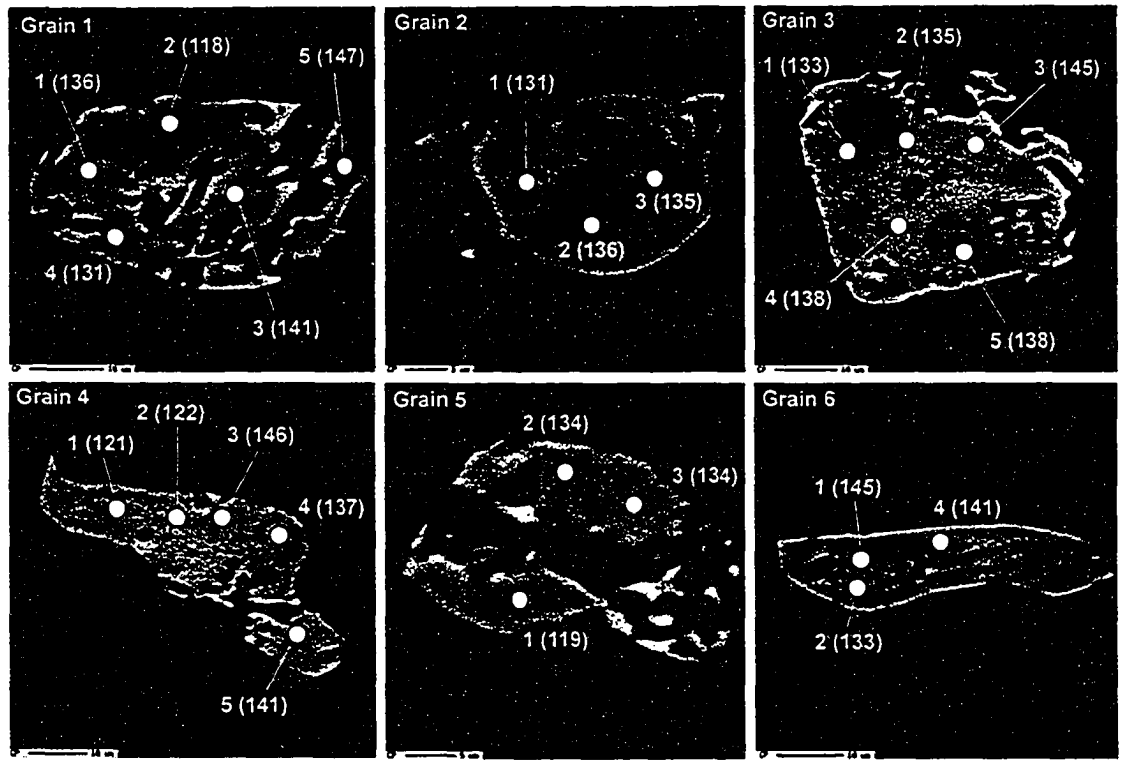

Sample 00TWG493: comparison of monazite chemical (EMP) age calculations

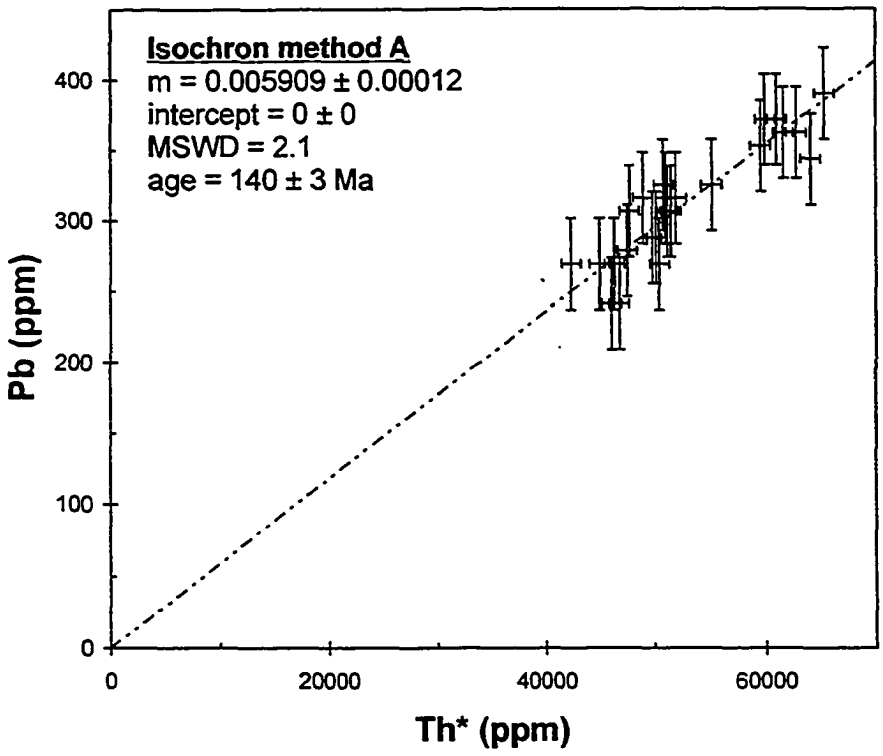

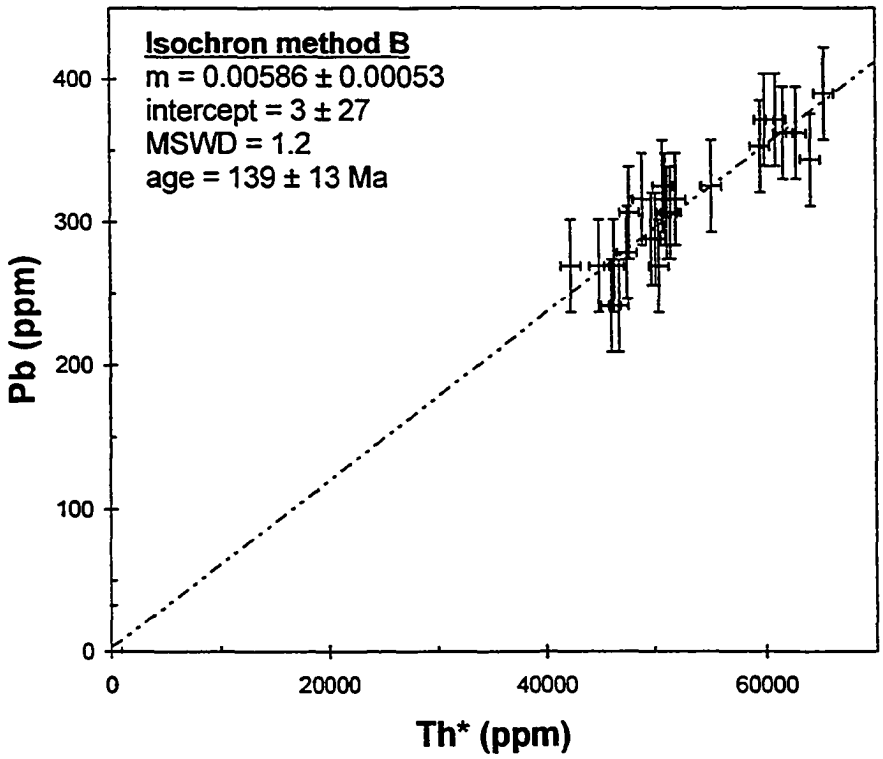

Monazite electron microprobe chemical dating spot data histogram

Individual spot error = 19.7 (2 sigma)

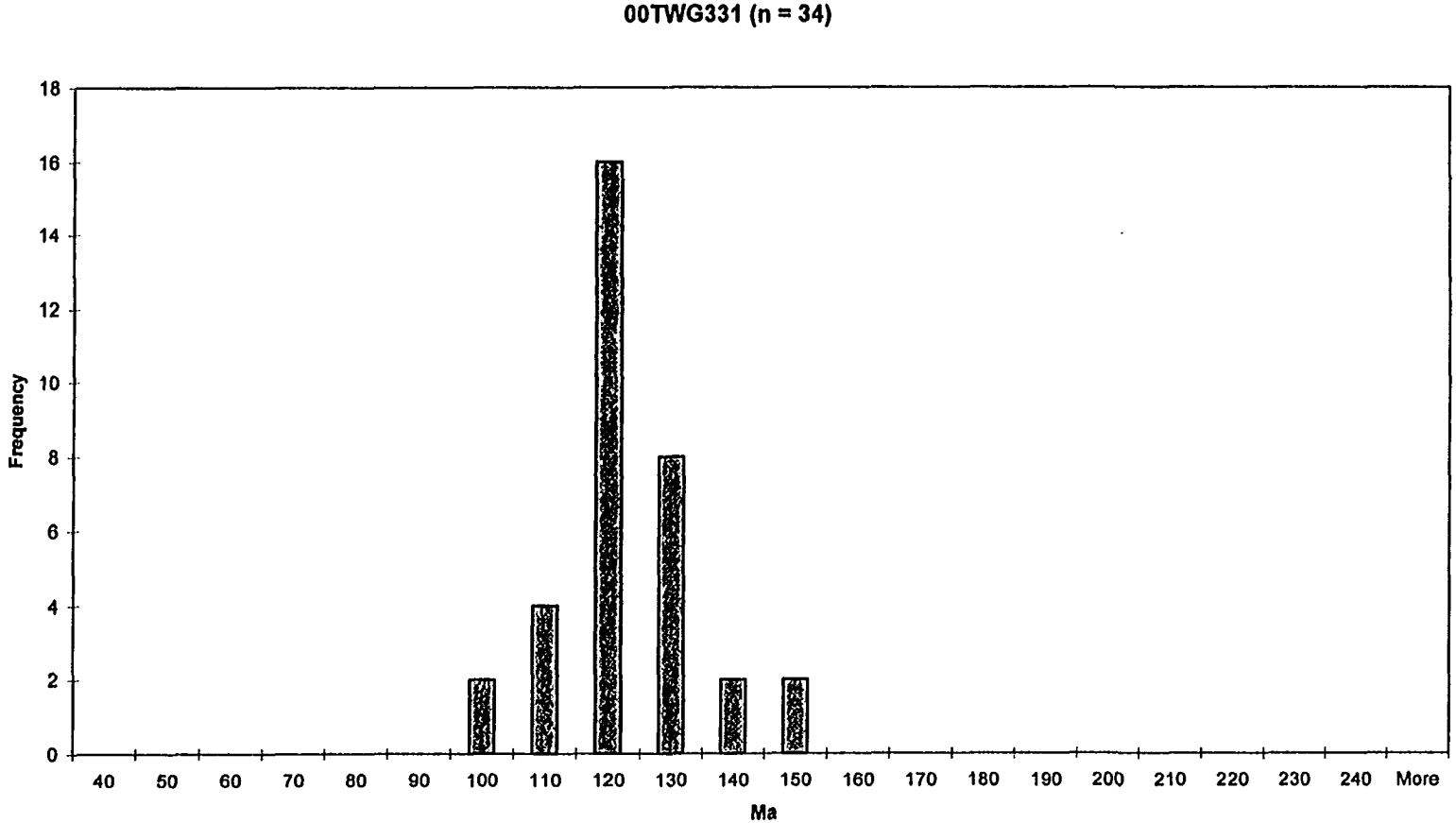

Sample 00TWG331 backscattered electron microprobe monazite images

Individual spot ages in brackets; spot error ± 19.7 Ma (2 sigma); ba: bad analysis

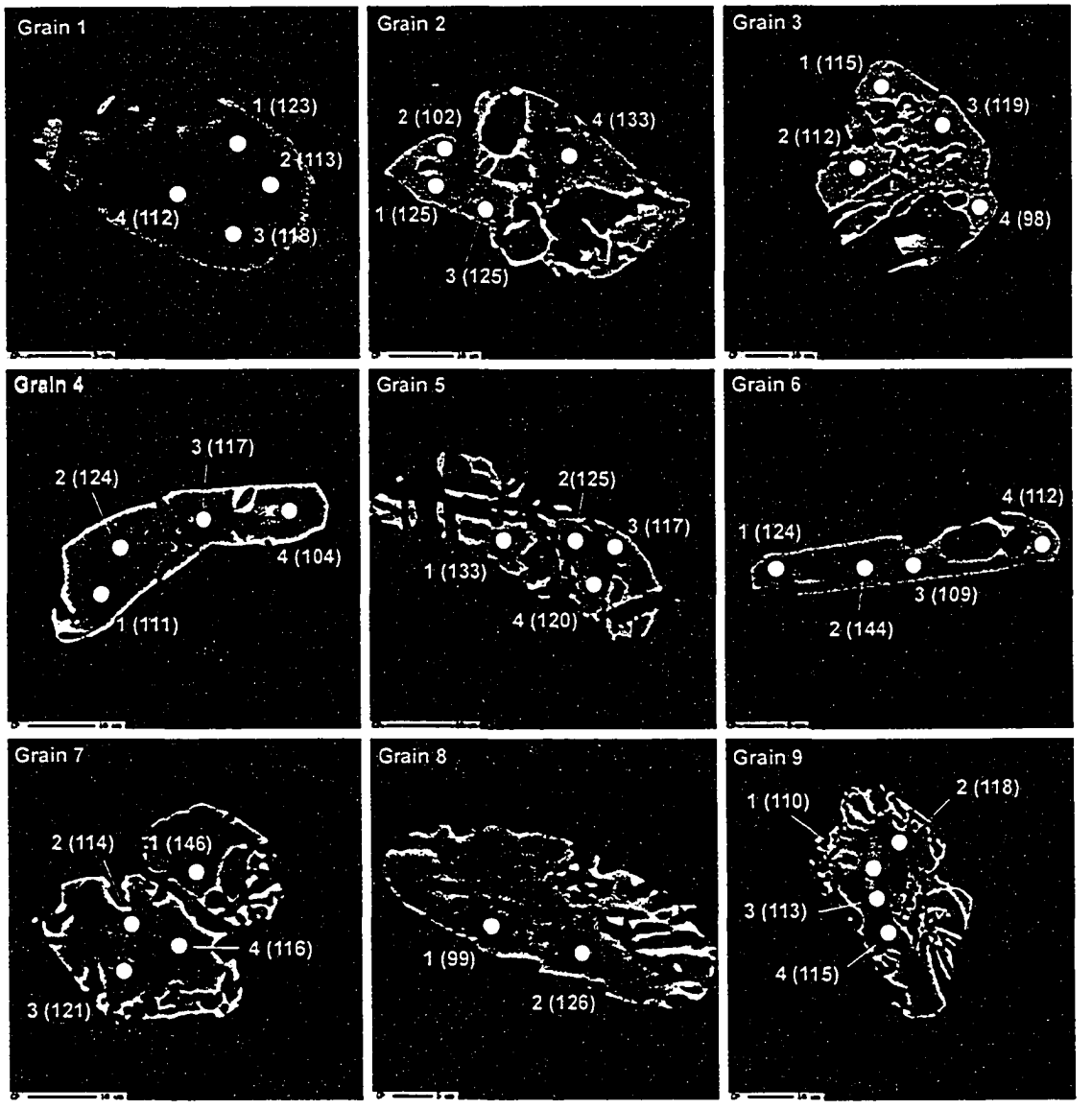

Sample 00TWG331: comparison of monazite chemical (EMP) age calculations

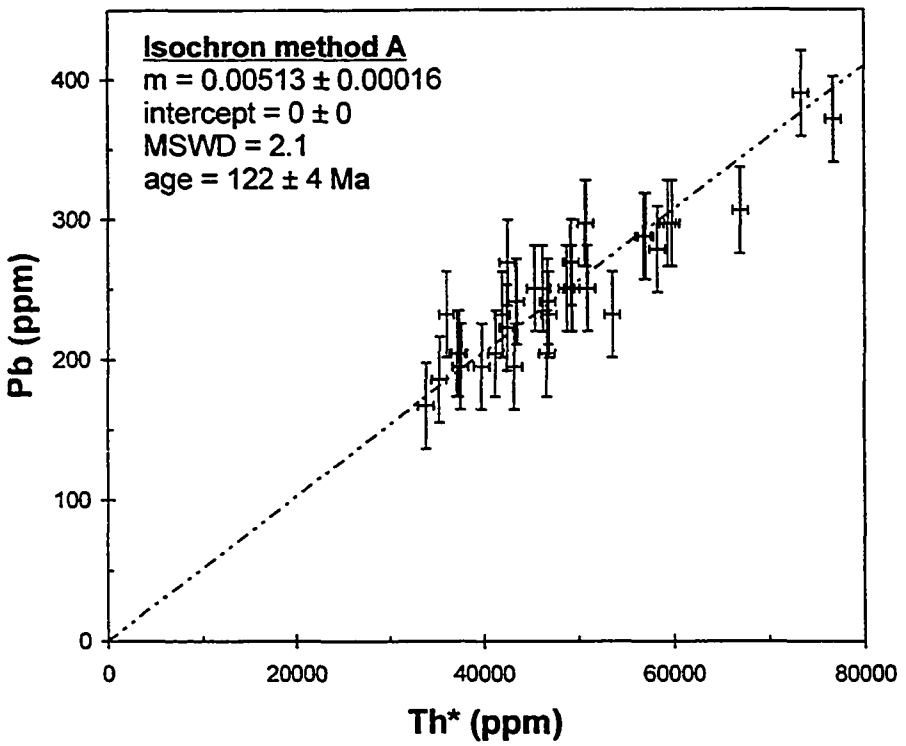

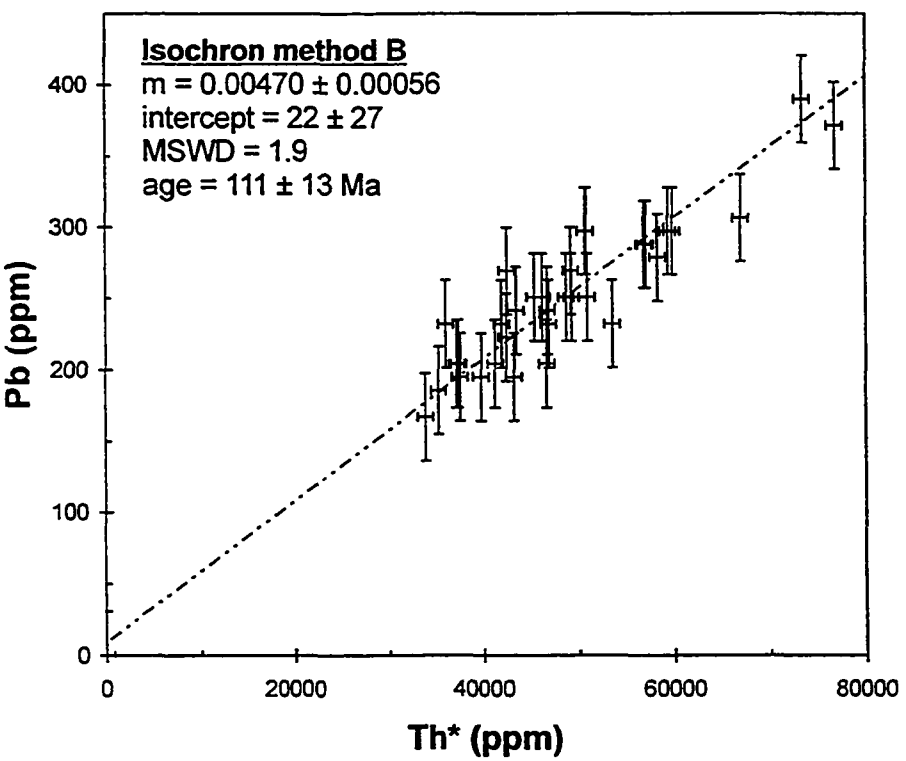

Monazite electron microprobe chemical dating spot data histogram

Individual spot error = 13.2 Ma (2 sigma)

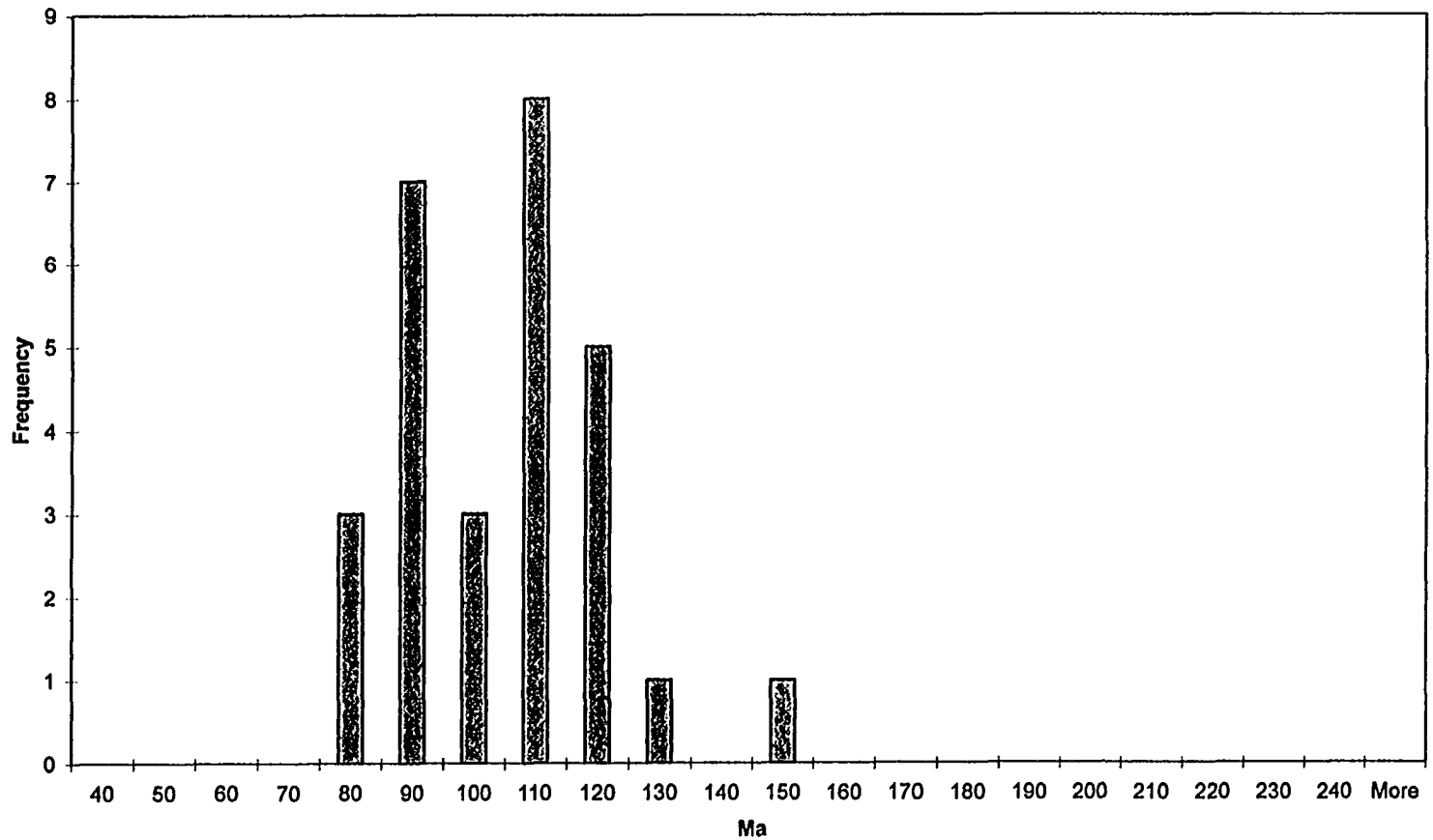

Sample 00TWG516 backscattered electron microprobe monazite images

Individual spot ages in brackets; spot error ± 13.2 Ma (2 sigma); ba: bad analysis

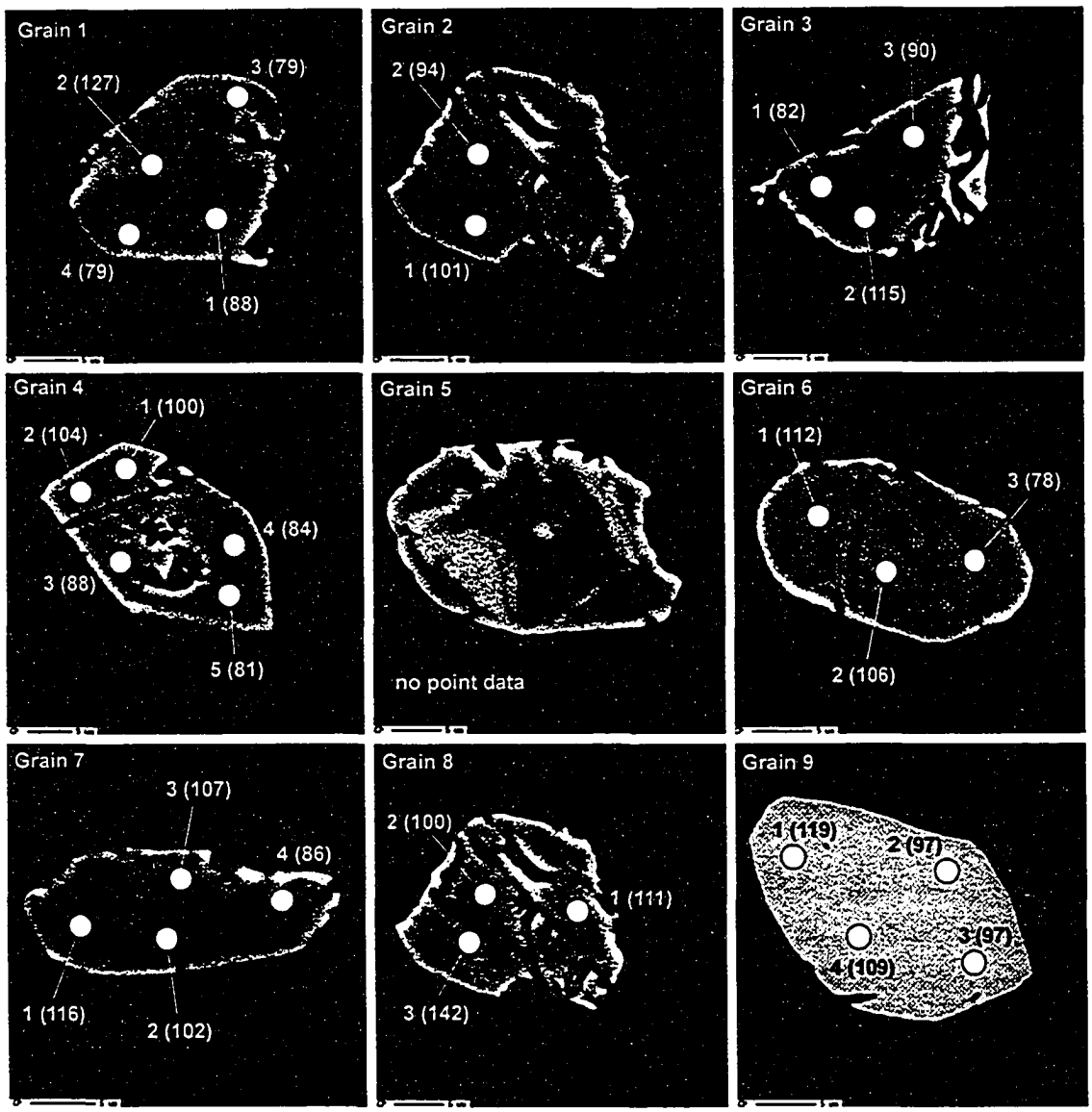

Sample 00TWG516: comparison of monazite chemical (EMP) age calculations

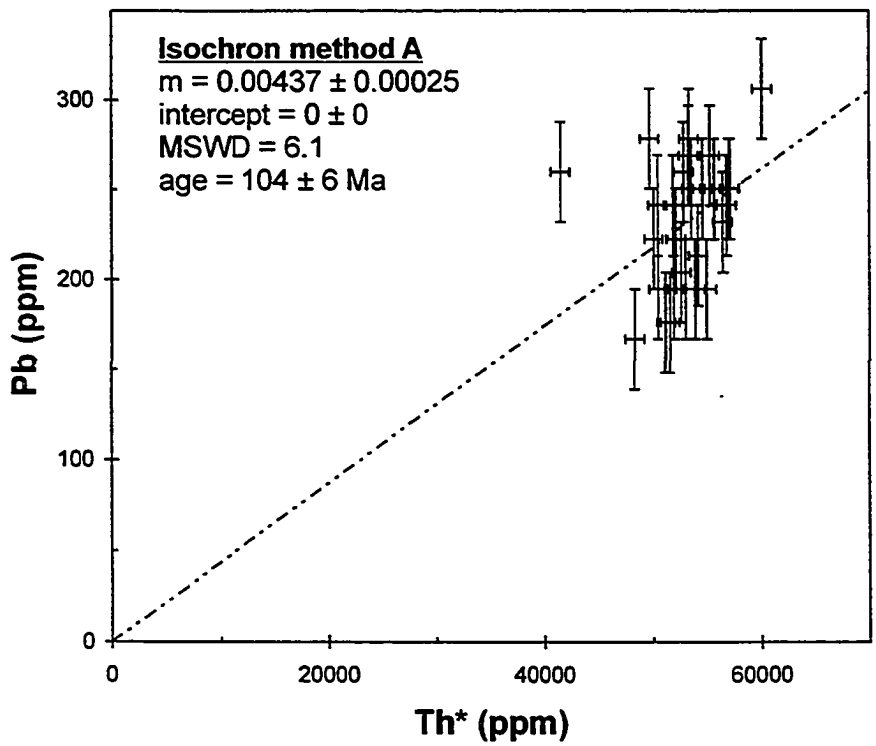

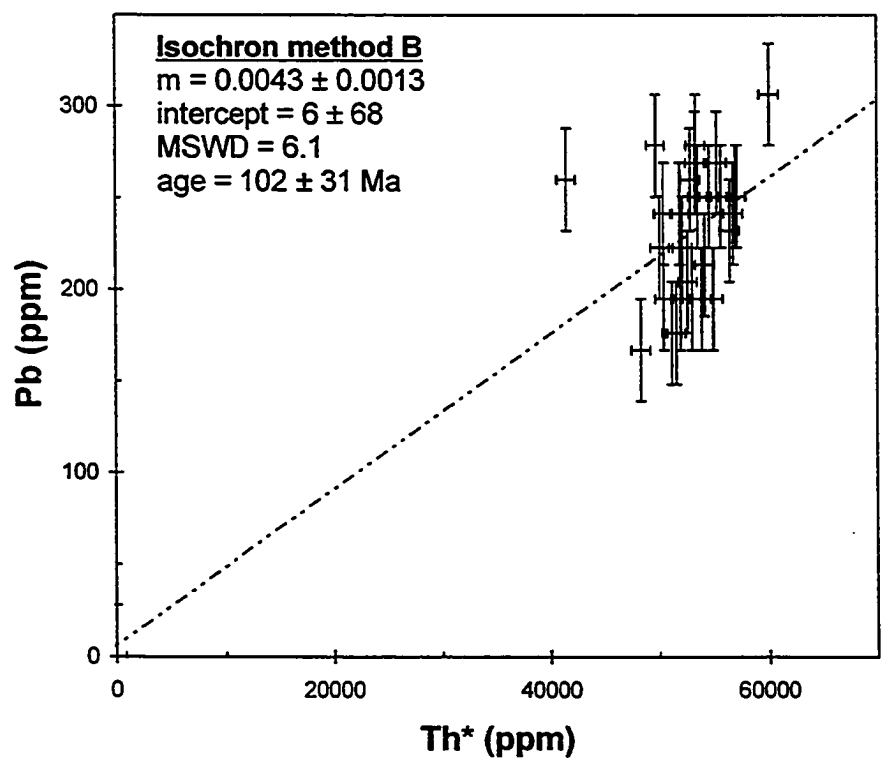

Monazite electron microprobe chemical dating spot data histogram

Individual spot error = 28.7 Ma (2 sigma)

00TWG328 (n = 32)

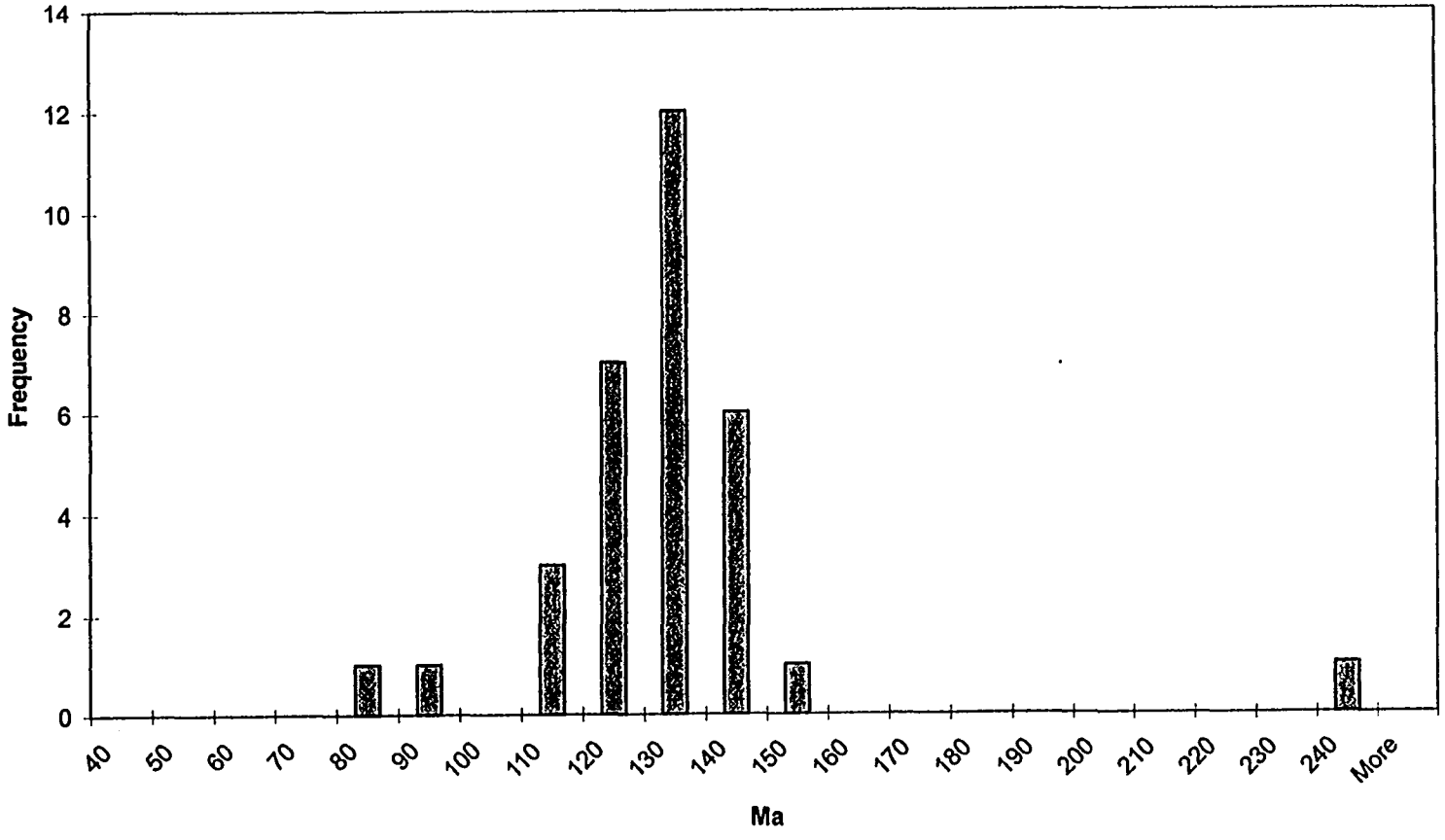

Sample 00TWG328: comparison of monazite chemical (EMP) age calculations

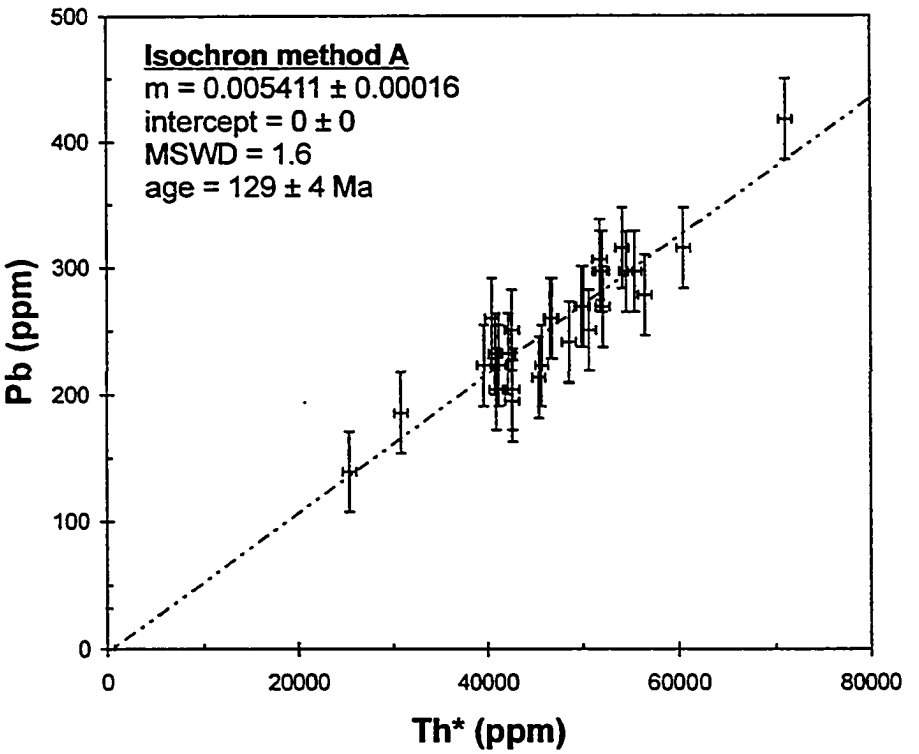

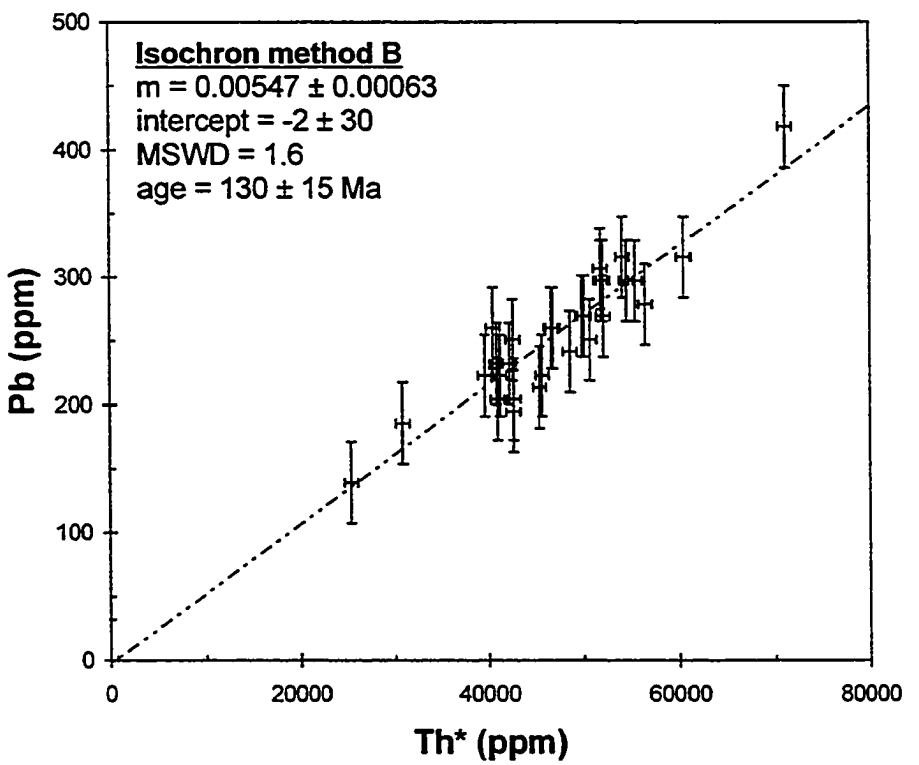

Monazite electron microprobe chemical dating spot data histogram

Individual spot error = 23.1 Ma (2 sigma)

00TWGWLS (n = 36)

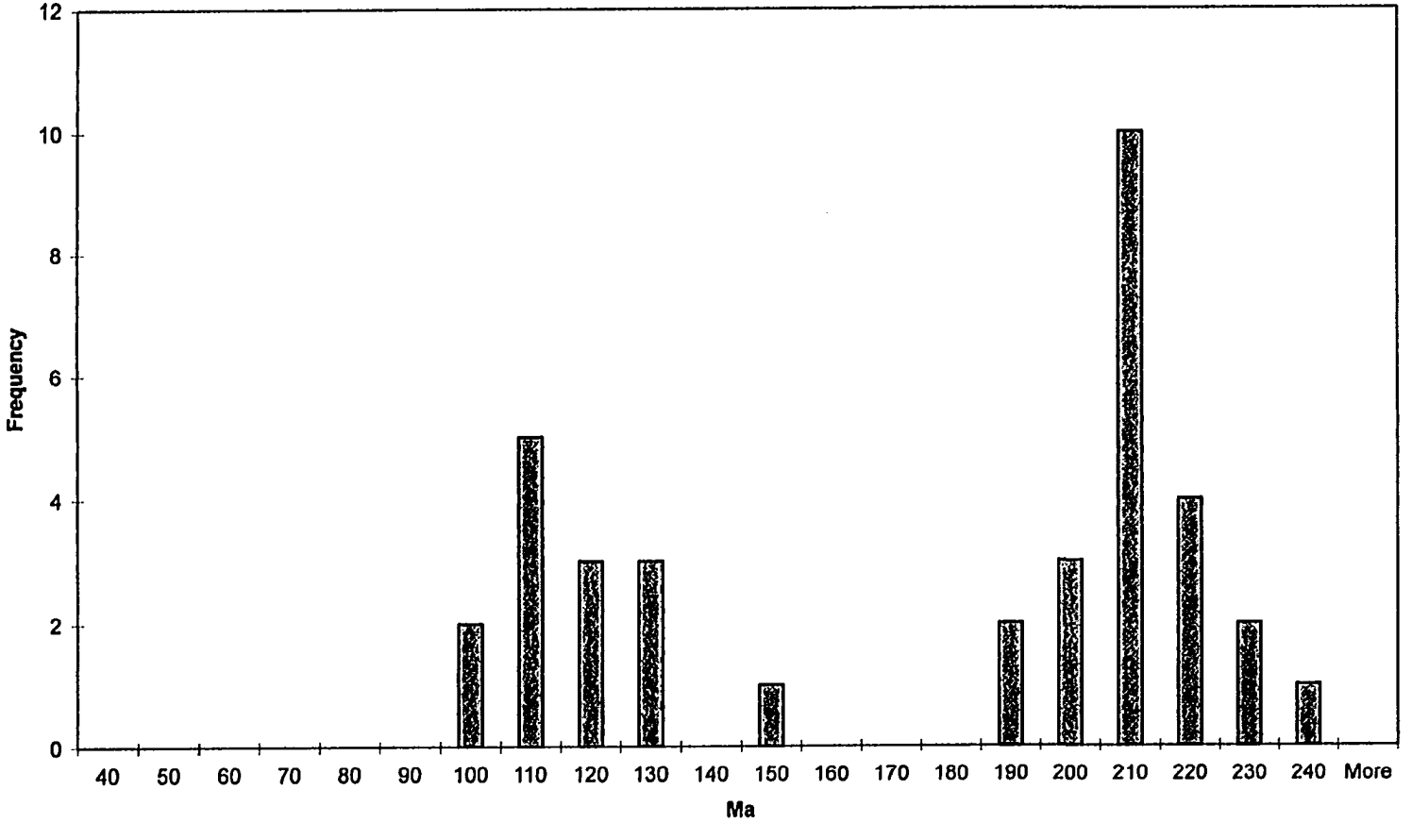

Sample 00TWGWLS backscattered electron microprobe monazite images

Individual spot ages in brackets; spot error ± 23.1 Ma (2 sigma); ba: bad analysis

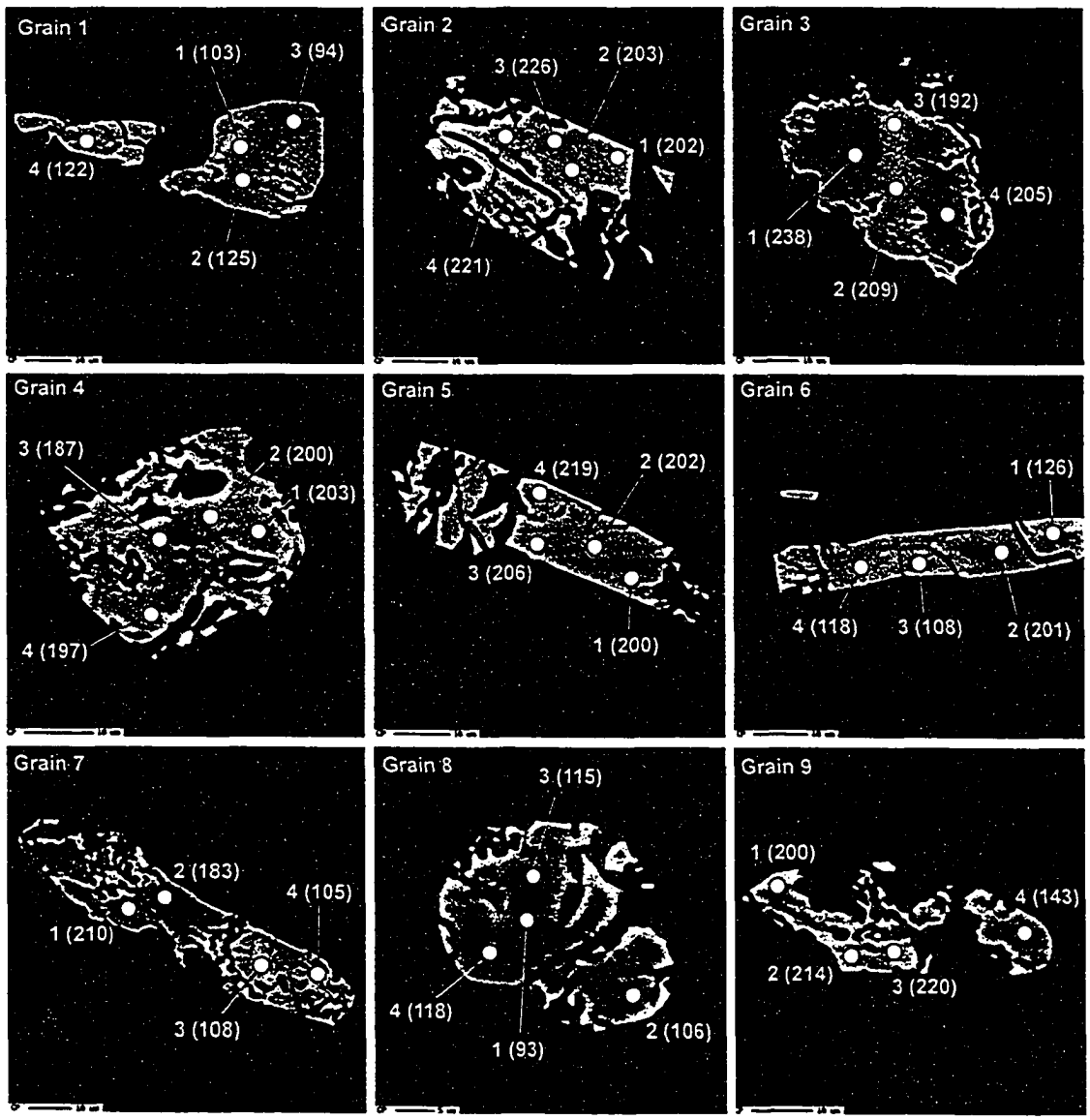

Sample 00TWGWLS: comparison of monazite chemical (EMP) age calculations

Population # 1

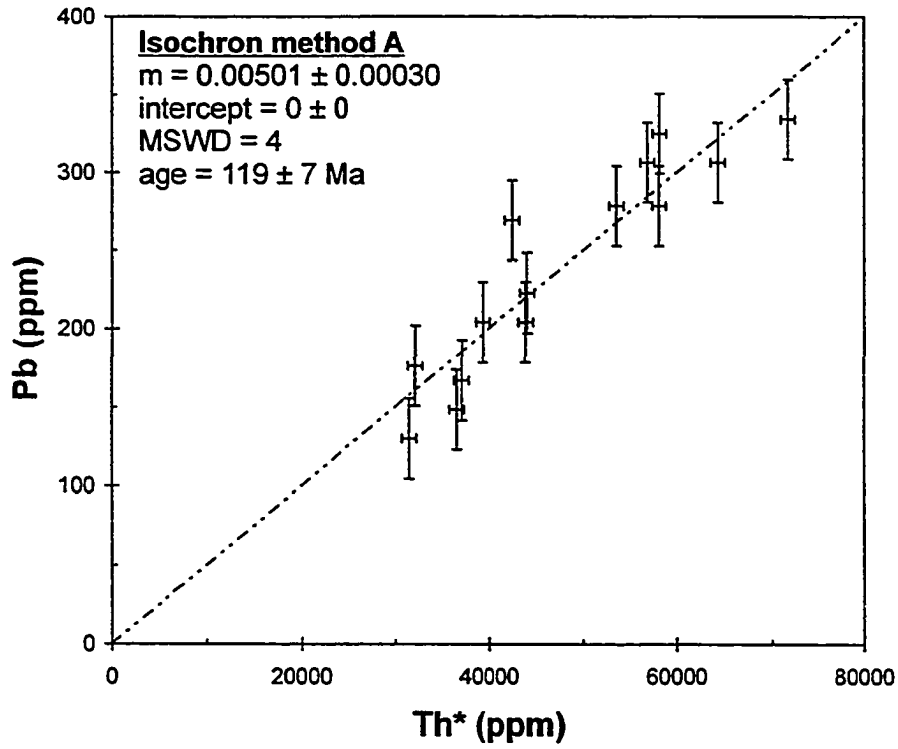

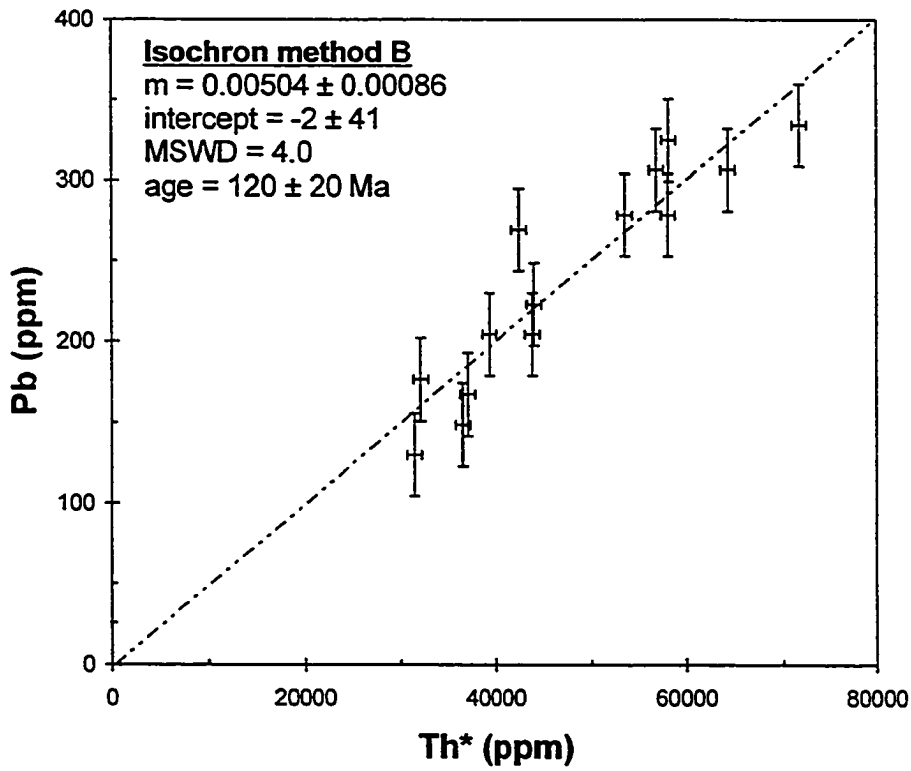

Sample 00TWGWLS: comparison of monazite chemical (EMP) age calculations

Population #2

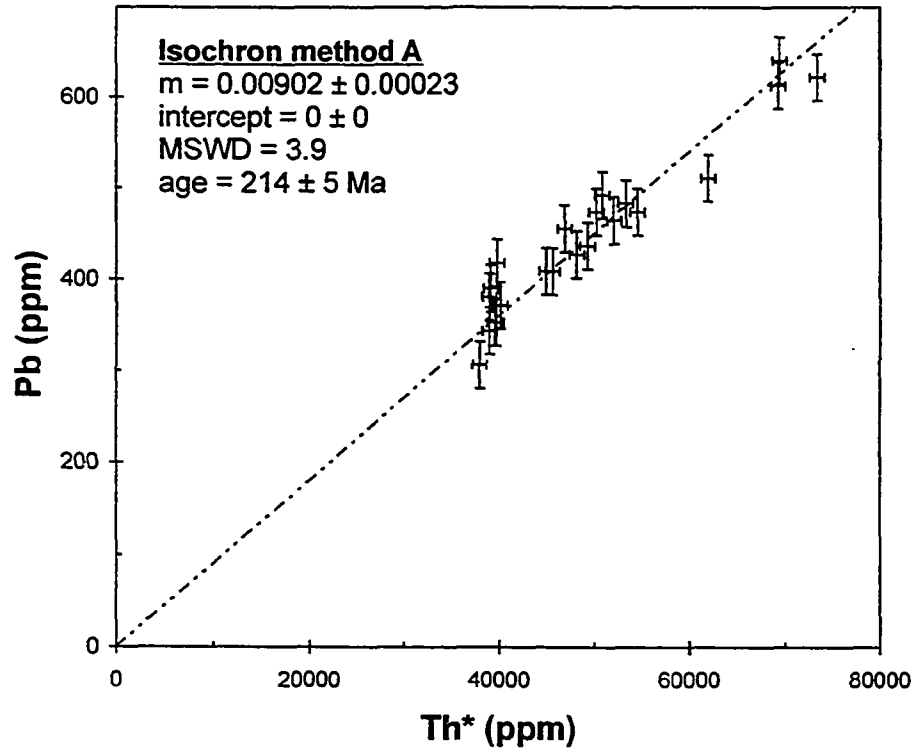

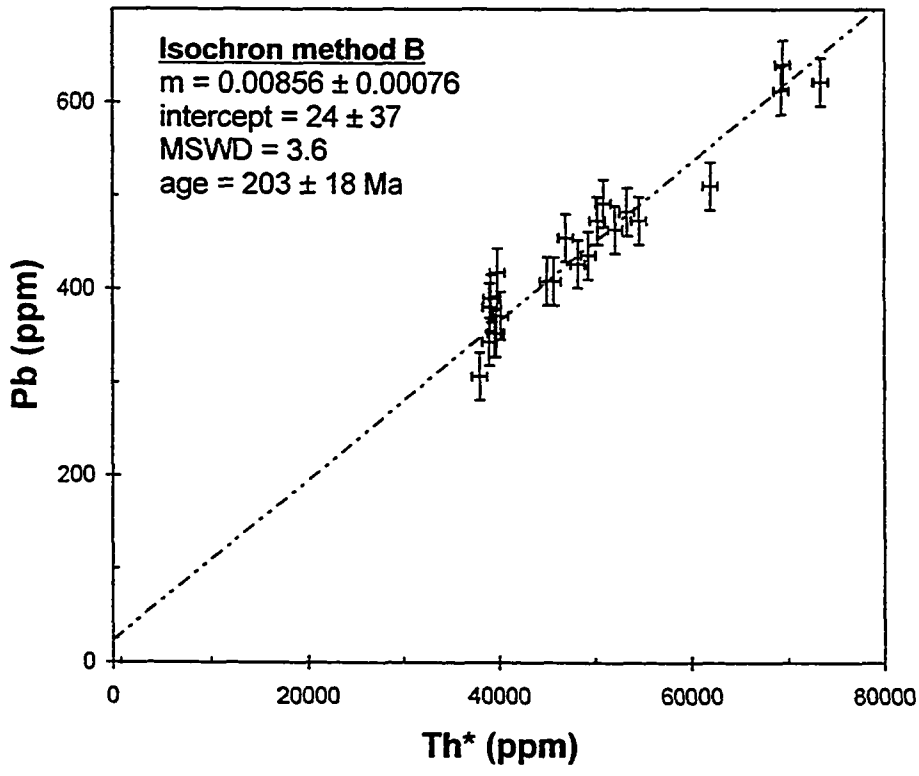

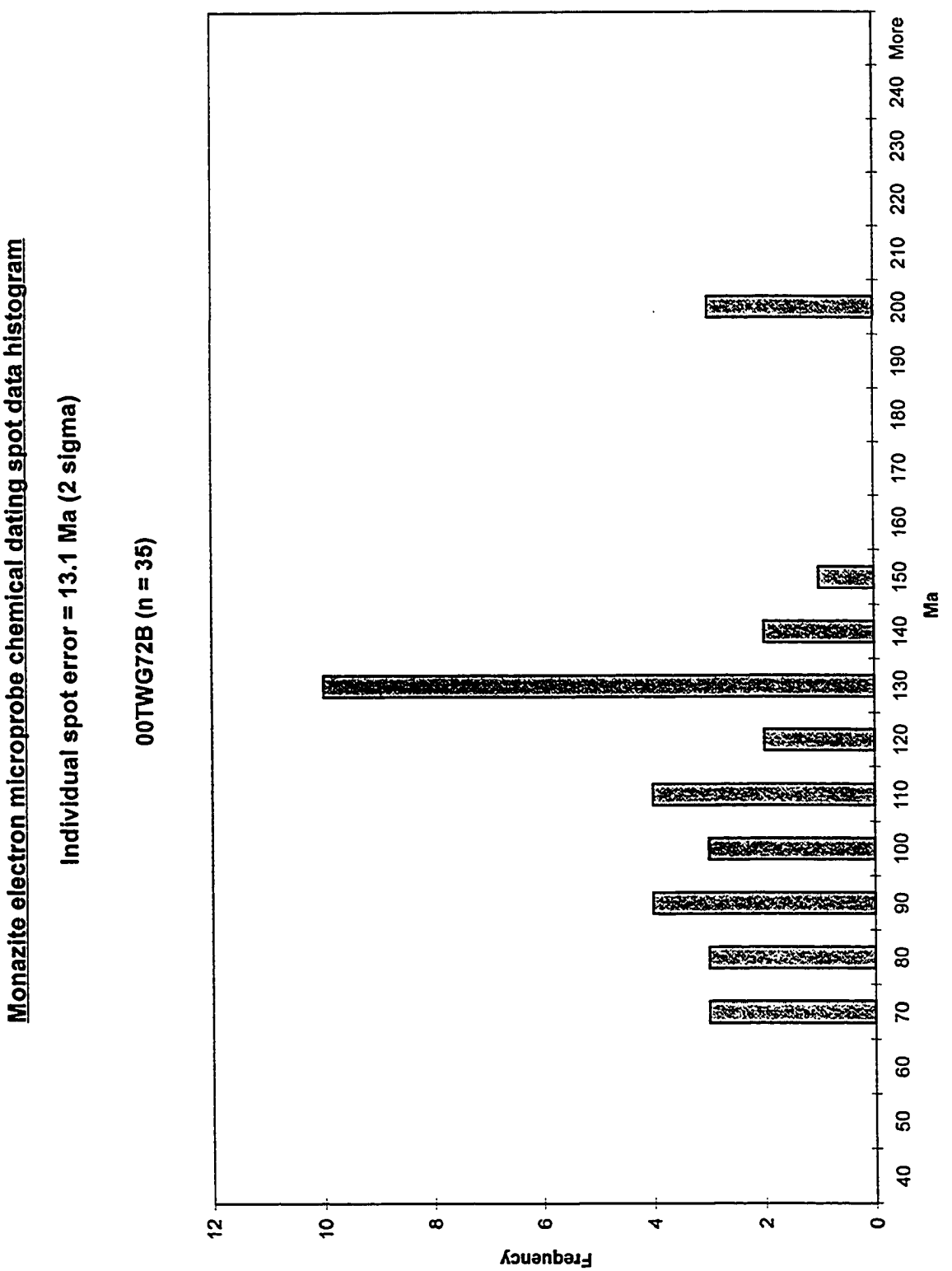

Sample 00TWG072B backscattered electron microprobe monazite images

Individual spot ages in brackets; spot error ± 13.1 Ma (2 sigma); ba: bad analysis

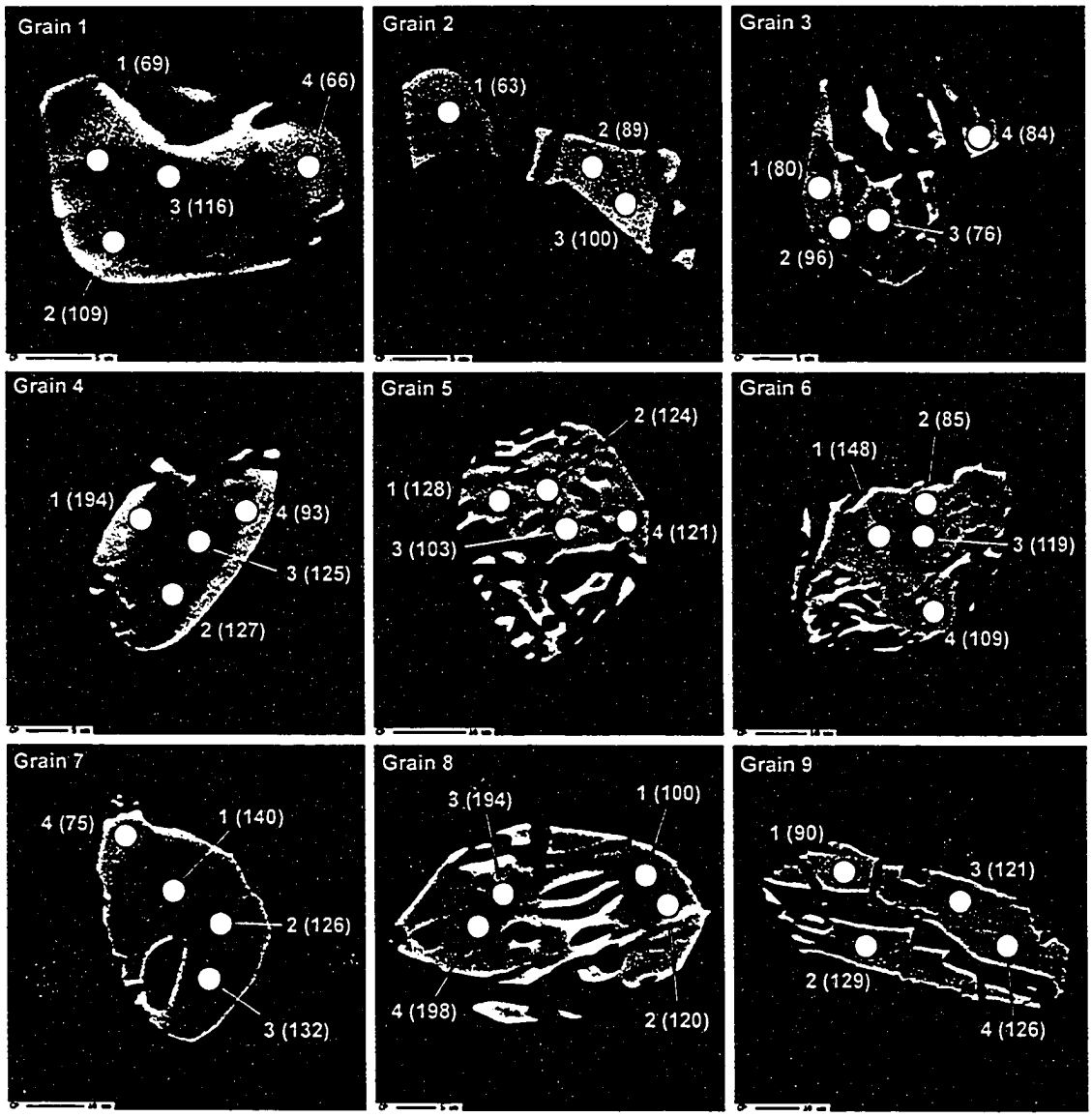

Sample 00TWG072: comparison of monazite chemical (EMP) age calculations

Population # 1

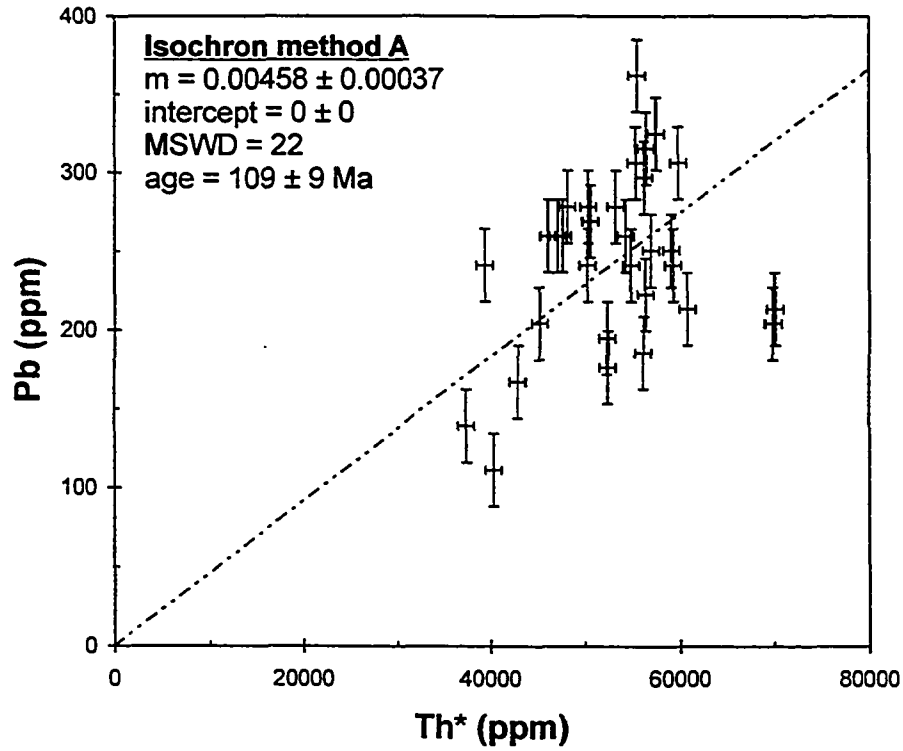

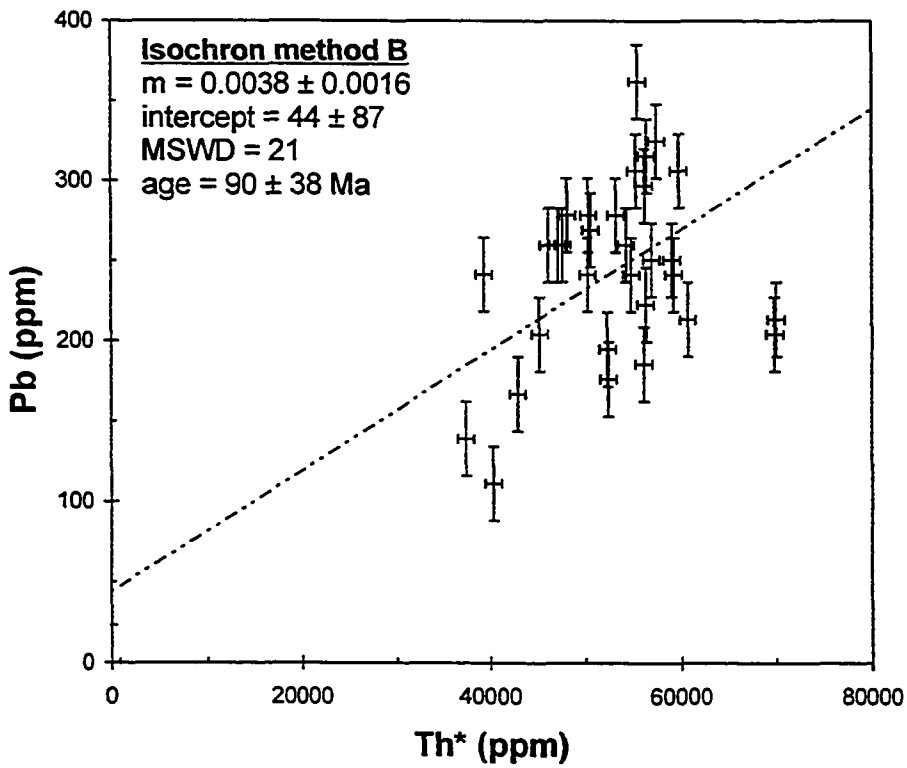

Sample 00TWG072: comparison of monazite chemical (EMP) age calculations

Population # 2

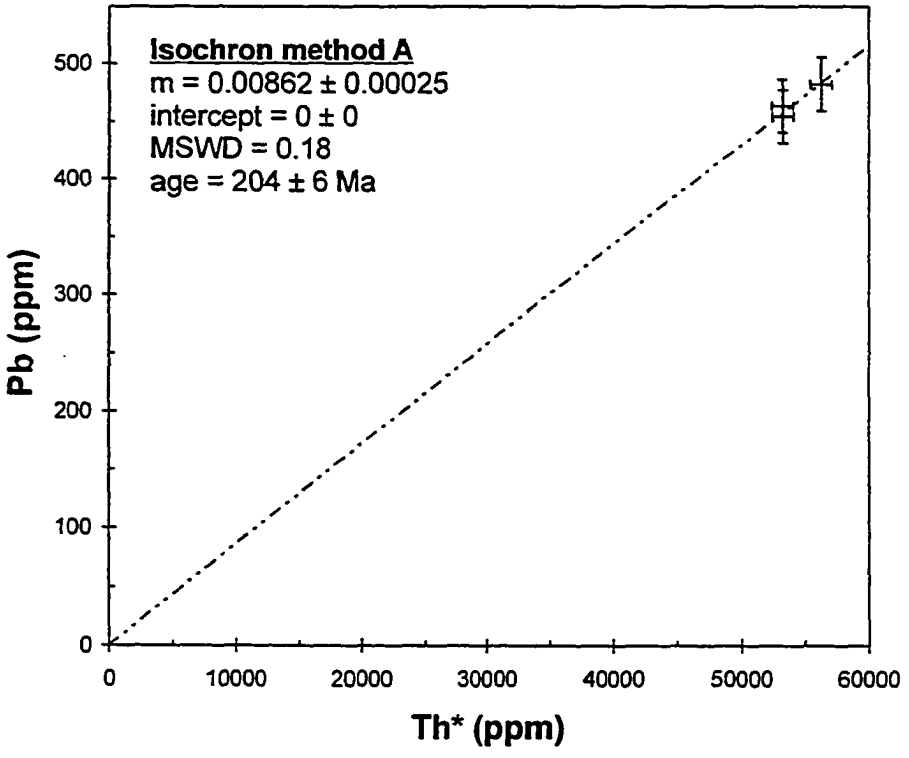

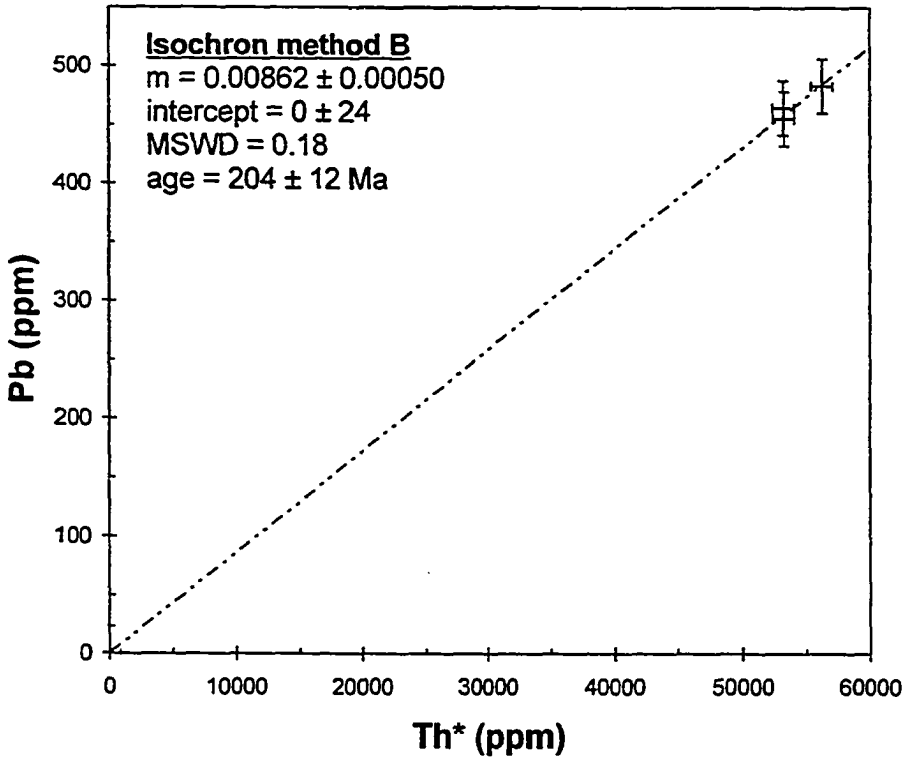

APPENDIX G

Selected backscattered electron (BSE) and cathodoluminescence (CL) images of zircon grains from geochronology samples

Granodiorite (M2), Cosens Bay pluton (page 1)

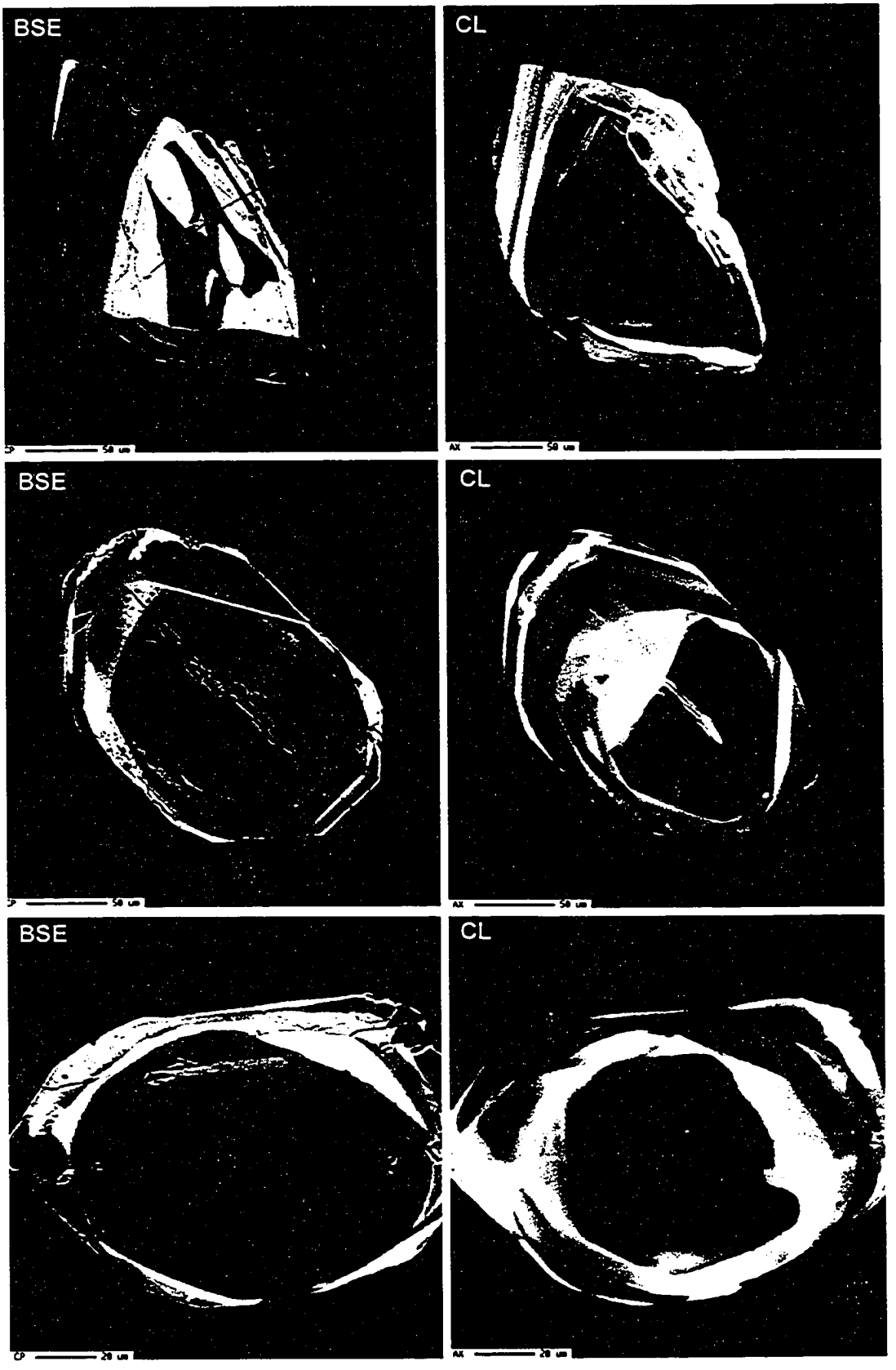

Granodiorite (M2), Cosens Bay pluton (page 2)

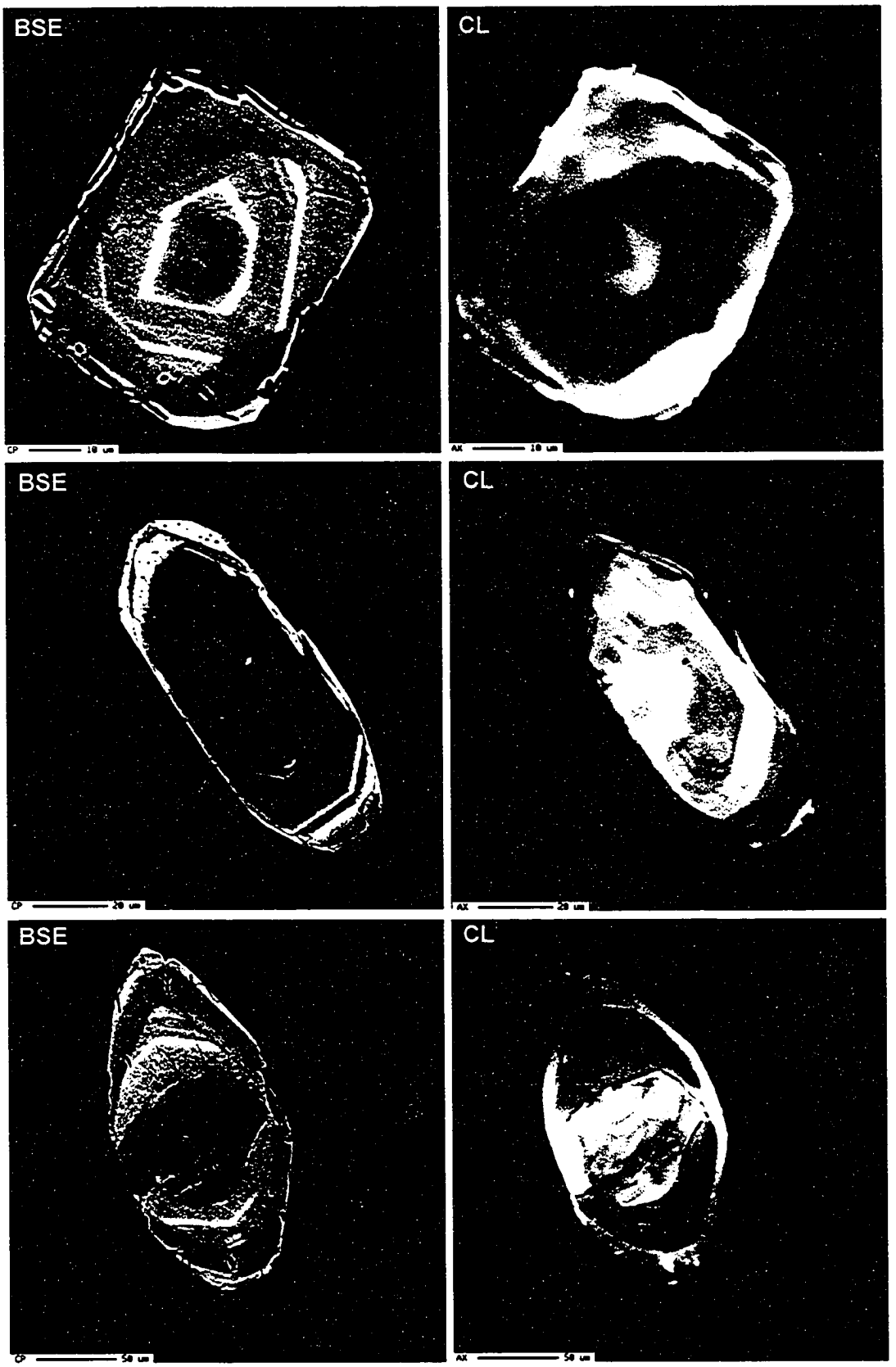

Diorite gneiss (M3), Aberdeen gneiss complex (page 1)

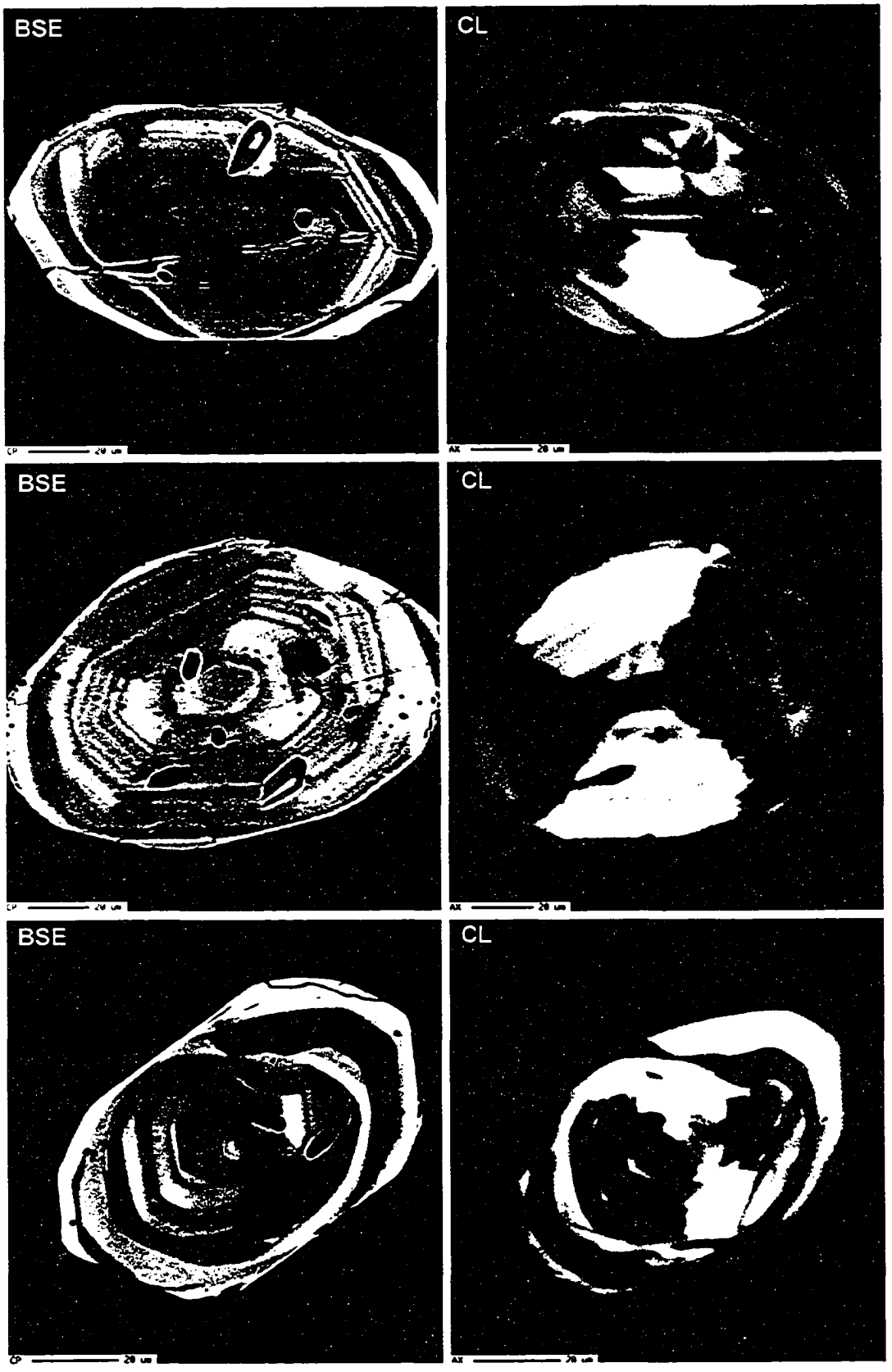

Diorite gneiss (M3), Aberdeen gneiss complex (page 2)

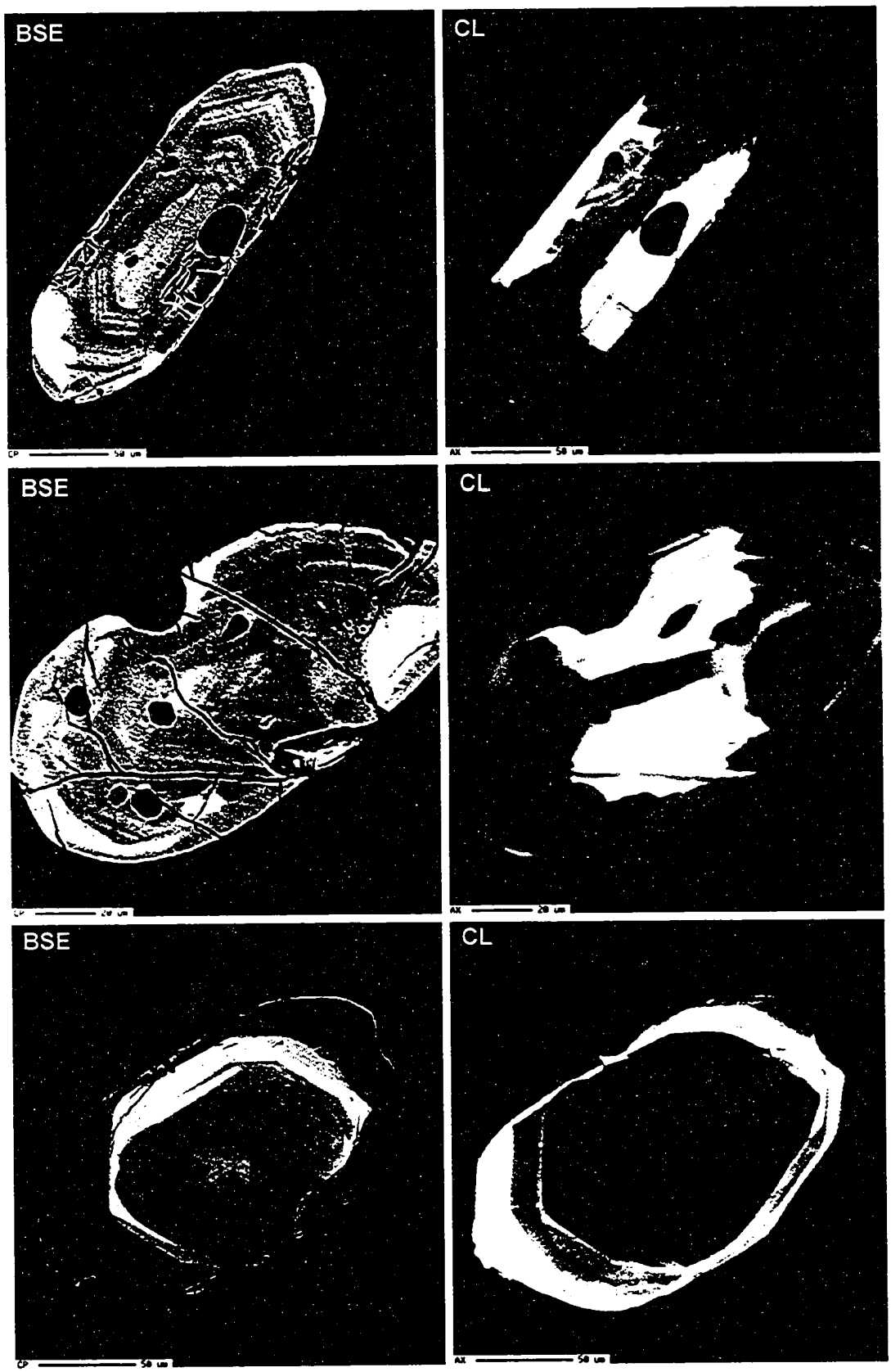

Migmatitic schist (M4), Aberdeen gneiss complex (page 1)

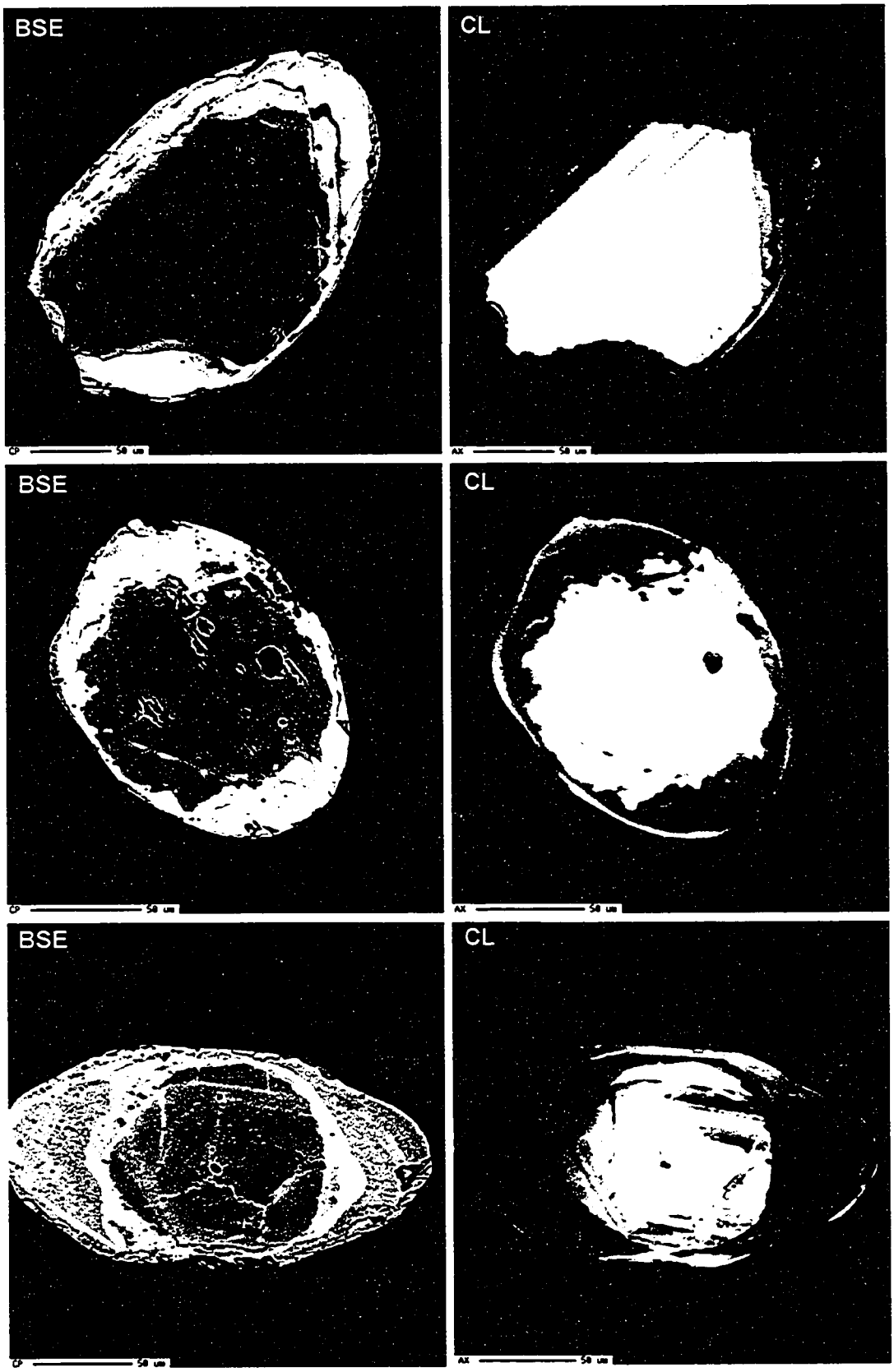

Migmatitic schist (M4), Aberdeen gneiss complex (page 2)

Tonalite gneiss (M6), Aberdeen gneiss complex (page 1)

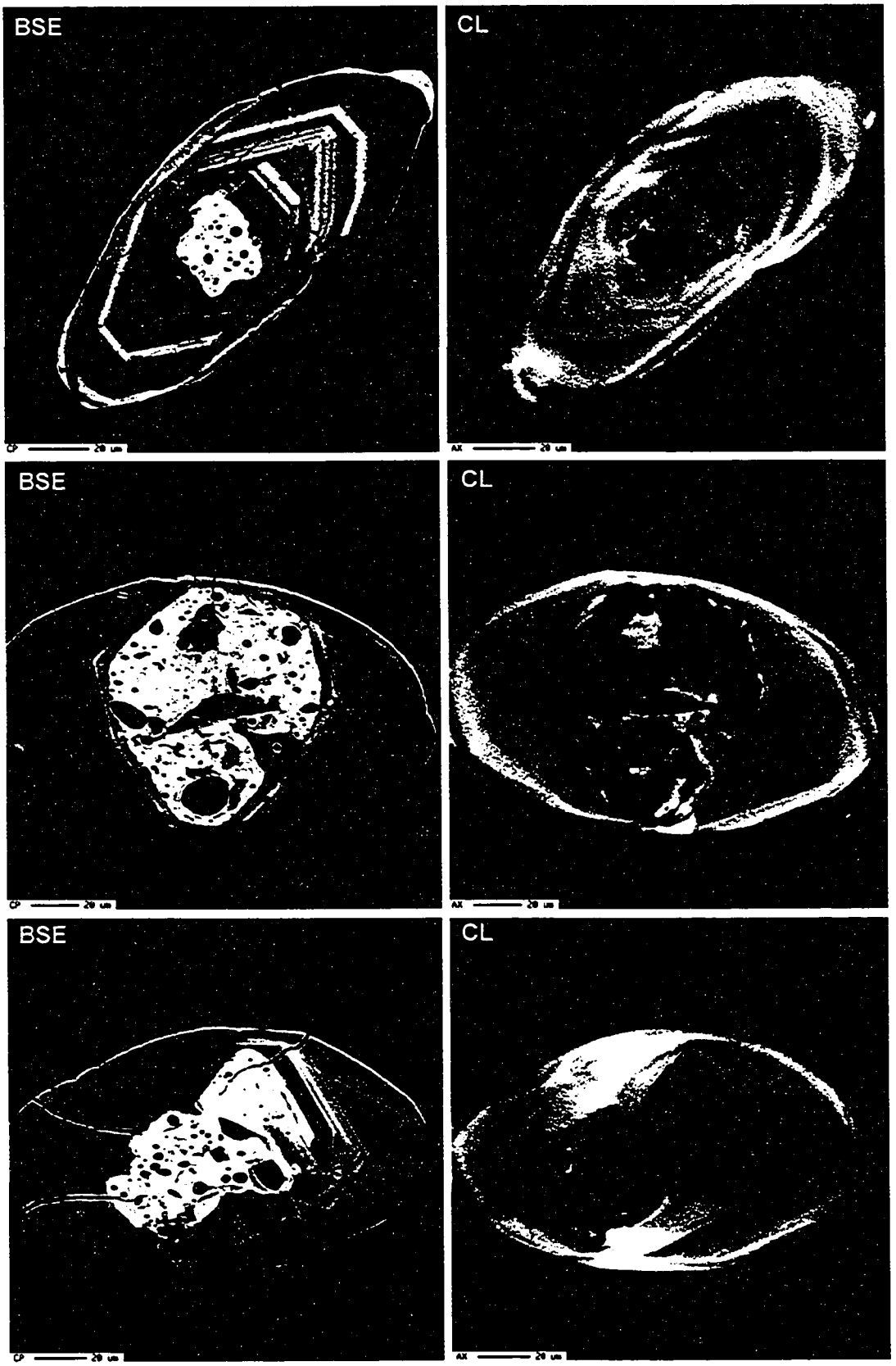

Tonalite gneiss (M6), Aberdeen gneiss complex (page 2)

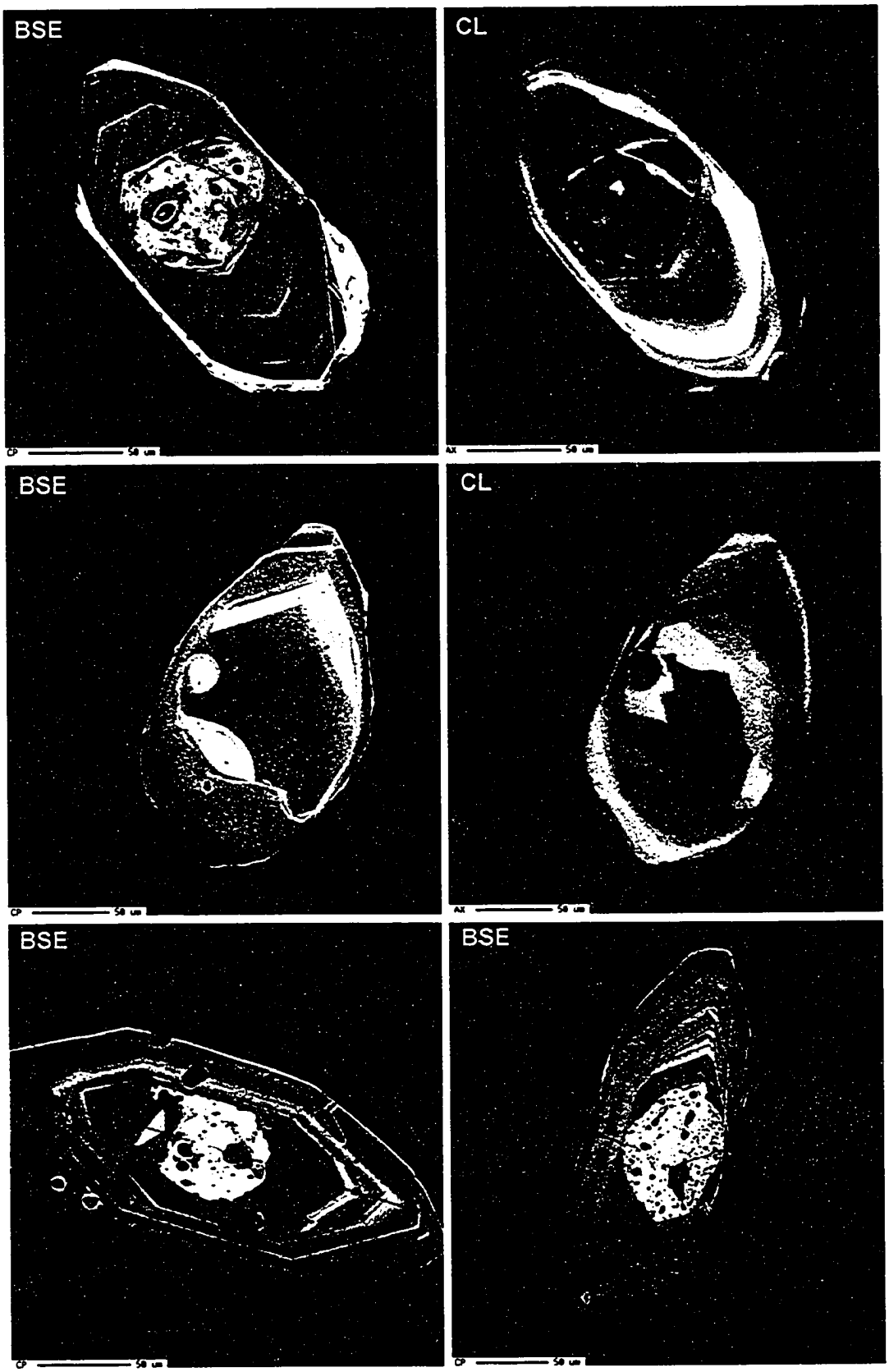

APPENDIX H

Thesis collection

Thesis collection data (page 1 of 1)

Sample	Rock Type	Rock Unit[a]	UTM Coordinates[b]	Significance[c]	Hand Sample	Thin-section
97PE-17	foliated granodiorite	Cosens Bay pluton (102 Ma)	334280E 5559720N	U-Pb isotopic dating (ID-TIMS)	X	X
98PG-181A	pelitic schist	Tsuius schist (Proterozoic?)	335265E 5554222N	Shear-sense (068°/15°)	X	X
99PG-537	migmatitic pelitic schist	Tsuius schist (Proterozoic?)	343725E 5559400N	Thermobarometry; monazite chemical dating	X	
99PG-584	migmatitic pelitic schist	Tsuius schist (Proterozoic?)	372900E 5603785N	Monazite chemical dating	X	
99PG-585	migmatitic pelitic schist	Tsuius schist (Proterozoic?)	372647E 5604833N	Thermobarometry; monazite chemical dating	X	
99PG680	mylonitic granite	Ladybird granite (55-62 Ma)	373400E 5590200N	Shear-sense (035°/20°)	X	X
99PG-769	monzonite	Nicklen Lake pluton (50 Ma)	351939E 5553138N	U-Pb isotopic dating (ID-TIMS)	X	X
00TWG039	tonalite gneiss	Aberdeen gneiss complex (232 Ma, 150 Ma)	360806E 5553415N	U-Pb isotopic dating (ID-TIMS)	X	X
00TWG072B	migmatitic pelitic schist	Silver Creek Formation (Devonian?)	378960E 5567540N	Thermobarometry; monazite chemical dating	X	X
00TWG328	pelitic schist	Silver Creek Formation (Devonian?)	408087E 5564744N	Monazite chemical dating	X	X
00TWG331	pelitic schist	Silver Creek Formation (Devonian?)	407130E 5565038N	Thermobarometry; monazite chemical dating	X	X
00WTG391	pelitic schist	Slocan Group (Upper Triassic to Lower Jurassic)	390827E 5576126N	Thermobarometry; monazite chemical dating	X	X
00TWG488	pelitic schist	Silver Creek Formation (Devonian?)	404011E 5572467N	Monazite chemical dating	X	X
00TWG489	pelitic schist	Silver Creek Formation (Devonian?)	405774E 5574020N	Monazite chemical dating	X	X
00TWG493	pelitic schist	Silver Creek Formation (Devonian?)	404043E 5572050N	Monazite chemical dating	X	X
00TWG516A	pelitic schist	Silver Creek Formation (Devonian?)	409877E 5567121N	Monazite chemical dating	X	X
00TWG608	psammite	Silver Creek Formation (Devonian?)	418918E 5553336N	Thermobarometry	X	X
01TWG023	mylonitic granite	Ladybird granite (55-62 Ma)	373431E 5590156N	Shear-sense (030°/13°)	X	X
01TWG058	mylonitic pelitic schist	Tsuius schist (Proterozoic?)	360378E 5609781N	Shear-sense (084°/19°)	X	X
01TWG074	migmatitic pelitic schist	Tsuius schist (Proterozoic?)	370618E 5614894N	Thermobarometry	X	X
01TWG117	mylonitic granite	Ladybird granite (55-62 Ma)	349807E 5580603N	Shear-sense (000°/55°)	X	X

Thesis collection data (page 2 of 2)

Sample	Rock Type	Rock Unit[a]	UTM Coordinates[b]	Significance[c]	Hand Sample	Thin-section
01TWG168	mylonitic granite	Ladybird granite (55-62 Ma)	349902E 5583235N	Shear-sense (342°/36°)	X	X
01TWG171	mylonitic pelitic schist	Silver Creek Formation (Devonian?)	350233E 5580532N	Shear-sense (000°/50°)	X	X
Whatshan Lake schist	pelitic schist	Silver Creek Formation (Devonian?)	411511E 5547671N	Thermobarometry; monazite chemical dating	X	X

[a] Map units are given as they appear in the legend for the maps in the back pocket.
[b] UTM Zone 11, North American 1983 datum (NAD 83).
[c] Orientation of oriented samples given according to right hand rule (strike/dip).